



MACQUARIE
University
SYDNEY · AUSTRALIA

A thesis submitted in total fulfilment of the requirements
for the degree of Doctor of Philosophy

Identification and characterization of a novel isoform of Fused in Sarcoma and its role in Amyotrophic Lateral Sclerosis

Marta Vidal Robau

(Master in Molecular Biology and Biomedicine)

MACQUARIE UNIVERSITY

Faculty of Medicine and Health Sciences

Department of Biomedical Sciences

June 2018

Contents

Contents	i
Abstract	ii
Declaration	iii
Preface	iv
Acknowledgements	v
Table of contents	vii
List of tables	xiii
List of figures	xiv
Publications and presentations	xvi
Abbreviations	xviii
Units of magnitude	xxvi

Abstract

The *fused in sarcoma (FUS)* gene is mutated in 4% of familial cases of Amyotrophic lateral sclerosis (ALS) and 1% of sporadic cases. Moreover, FUS immunoreactive inclusions are present in both ALS patients. Importantly, mutations in *FUS* account for a particularly aggressive, juvenile form of the disease. Hence, elucidating the pathological role of *FUS* in ALS is crucial for understanding the disease. While the mechanisms underlying neurodegeneration in ALS are not fully understood, defects in alternative splicing have been previously associated with ALS disease pathology. Additionally, alternative spliced forms of proteins linked to ALS, have also been implicated. This thesis focuses on the study of a newly identified, extracellular isoform of FUS, which was termed 'FUS^{EC}'. FUS^{EC} has a unique N-terminus sequence but shares its C-terminus with canonical FUS. For FUS, the most abundant ALS mutations are enriched at the C-terminus. Here it was confirmed FUS^{EC} expression at the mRNA and protein level. Furthermore, it was demonstrated it is *N*-glycosylated mostly with complex *N*-glycans, and this regulates its secretion. Also it was studied its intracellular localization and its potential normal functions. Finally, the role of FUS^{EC} in ALS was examined. FUS^{EC} bearing ALS mutations demonstrated inclusion formation, induction of ER stress and Golgi fragmentation and finally apoptosis, key cellular features of ALS. The discovery of a new alternatively spliced isoform of FUS provides novel insights into the pathogenic mechanisms implicated in ALS.

Declaration

I declare that the work presented in this thesis titled “Identification and characterization of a novel isoform of Fused in Sarcoma and its role in Amyotrophic Lateral Sclerosis” has not previously been submitted for a degree or diploma in any university. To the best of my knowledge and belief, this thesis contains no material previously published or written by another person except where due reference is made in the thesis itself. Unless otherwise acknowledged, this work was carried out by the author.

Signed

Marta Vidal

Date: 22/06/2018

Preface

The work described in this thesis was performed by the author, except where hereby stated. The author acknowledges the following people for assistance in performing the following experiments reported in this thesis:

Chapter 3

The primers for the positive control in PCR were designed by Dr Benjamin Heng, Macquarie University, Sydney. The human foetal primary neurons isolation was performed by Dr Benjamin Heng, Macquarie University, Sydney. Human Cerebrospinal fluid samples were kindly provided by Professor Gilles J Guillemin, Macquarie University, Sydney. Mass spectrometry was performed by Dr Albert Lee, Macquarie University, Sydney.

Chapter 4

HA and GFP FUS^{EC} constructs were designed with the help of Dr. Emily Don, Macquarie University, Sydney. Dr Edward S.X. Moh, carried out the glycomics studies at the Department of Molecular Science, Macquarie University, Sydney. The exosome isolation and characterization was performed by Amirmohammad Nasiri Kenari, La Trobe University, Melbourne. The mass spectrometry studies were performed by Dr Albert Lee and Flora Cheng, Macquarie University, Sydney.

Chapter 5

The mass spectrometry studies were performed by Dr Albert Lee and Flora Cheng, Macquarie University, Sydney. During the flow cytometry experiments the author was assisted by Dr Martin Ostrowski, Department of Science and Engineering, Macquarie University, Sydney.

Acknowledgements

I would like to thank everyone who has helped and accompanied me during my PhD journey.

Firstly, and foremost I would like to thank my supervisor, Associate Professor Julie Atkin. Your encouragement and constant support have been essential during this three-year journey, thank you for always having the door open. Your scientific advise and expertise has helped me tremendously during my PhD and writing the thesis. Special thanks to my co-supervisors Dr Audrey Ragagnin and Dr Albert Lee. I truly appreciate the time you took on providing suggestions for my experiments and thesis. Having you both as co-supervisors has truly enriched my PhD experience and I have learned a lot from you both.

I would also like to thank all the members from Julie Atkin's lab, actual and former: Cyril, Sina, Shafi, Audrey, Anna, Mariana, Emma, Sonam, Hamideh, Jess, Eric. Thanks for making the long hours in the lab easy, for the nice talks and encouraging words. In particular I would like to thank Reka, who has become a dear friend. Thank you for all the times shared, for knowing me so well and being such a big support especially in the last months of my PhD. Also, I would like to thank Vinod for transmitting his knowledge and enthusiasm in the early months here at Macquarie, you helped me settle in and made everything much easier.

Thanks to my friends, for helping me feel so close to them even though the long distance. Thanks to all my wonderful family and family-in-law, for caring for me and for believing in me. I am so grateful to my parents and sister, for always being so supportive and reminding me of the important things in life. For transmitting the philosophy of the need to challenge myself and the need for personal development.

And finally, a big thank you to my partner, Marc. I can't express how lucky I feel to have you by my side. Your unconditional love, patience, sense of humour and support has been crucial during this journey. You have made this possible.

Dedicated to my grandma- Rosenda- with love.

Table of contents

1. General introduction	1
1.1. Amyotrophic lateral sclerosis	2
1.1.1 Clinical features and symptoms of ALS.....	2
1.1.2 Epidemiology of ALS	3
1.1.3 Environmental factors	4
1.1.4 ALS and frontotemporal dementia (FTD) continuum.....	7
1.1.5 Genetics of ALS	7
SOD1	8
TARDBP	9
FUS	11
C9ORF72.....	11
1.1.6 Possible pathogenic mechanisms implicated in ALS.....	14
Protein misfolding and the formation of inclusions	14
Glutamate excitotoxicity.....	16
Mitochondrial impairment.....	17
Non-cell autonomous toxicity	19
Autophagy disruption	20
Dysfunction to RNA metabolism	21
The formation of stress granules	22
Impairment of cellular trafficking	25
ER stress and the UPR.....	27
ER stress and UPR activation in ALS	29
Golgi fragmentation.....	30
‘Prion-like’ mechanism or propagation of protein misfolding.	32
1.2 Fused in Sarcoma.....	34
1.2.1 Structure of FUS.....	34
Prion-like domain or Low complexity domain.....	35
RNA-recognition motif domain.....	36
Zinc finger domain	37

The arginine/glycine-rich domain	38
The PY nuclear localization signal	39
1.2.2 <i>Post-translational modifications of FUS</i>	39
Methylation	40
Phosphorylation	41
Ubiquitination	43
O-GlcNac	44
Acetylation	44
1.2.3 <i>The normal cellular functions of FUS</i>	45
DNA damage	45
Transcription	46
Splicing and mRNA processing	47
mRNA transport and local translation	48
1.3 The role of FUS in ALS	49
1.3.1 <i>Defects in RNP granules/liquid phase transition</i>	53
1.3.2 <i>Impaired DNA damage response</i>	54
1.3.3 <i>RNA-splicing defects</i>	55
1.4 Alternative splicing in ALS	57
1.4.1 <i>Alternative splicing: Definition, mechanism and regulators</i>	57
1.4.2 <i>Role of alternative splicing in neurodegenerative diseases</i>	60
1.4.3 <i>Aberrant alternative splicing in ALS</i>	62
1.4.4 <i>A novel splicing mechanism predicts many new protein isoforms</i>	63
1.5 Aims of this thesis	64
<i>Chapter 3: Identification of a novel extracellular isoform of FUS</i>	65
<i>Chapter 4: Characterization of FUS^{EC}</i>	65
<i>Chapter 5: Examining the role of FUS^{EC} in ALS</i>	65
2. Material and methods	66
2.1. Molecular biology	67
2.1.1. <i>LB medium</i>	67
2.1.2. <i>Transformation</i>	67
2.1.3. <i>Preparation of plasmids (small and large scale)</i>	67
2.1.4. <i>Glycerol stock</i>	68

2.1.5. DNA quantification.....	68
2.2. Mammalian cell culture techniques.....	68
2.2.1. Fetal calf serum (FCS)	68
2.2.2. Cell culture maintenance.....	68
2.2.3. Transfection.....	69
2.2.4. Long-term storage of cell lines.....	69
2.3. Protein chemistry methods	70
2.3.1. Conditioned media and lysate collection.....	70
2.3.2. Bicinchoninic acid (BCA) protein assay	70
2.3.3. SDS polyacrylamide gel electrophoresis (PAGE) and western blotting.....	70
2.3.4. Sample collection for immunoprecipitation (IP)	72
Cell lysate preparation for IP	72
Media preparation for IP.....	72
2.3.5. Immunoprecipitation with HA-magnetic beads.....	73
2.3.6. Immunoprecipitation with GFP trap	73
2.3.7. In-Gel Protease Digestion.....	73
2.3.8. Reverse Phase (C18) Liquid Chromatography Mass Spectrometry (RP-LC-MS/MS)	74
2.4. Microscopy	75
2.4.1. Fluorescent microscopy.....	75
2.4.2. Immunofluorescence microscopy	75
2.4.3. Confocal Microscopy and Image acquisition.....	76
2.4.4. Quantitative analysis	76
2.5. Statistical analysis.....	77
3. Identification of a novel extracellular isoform of FUS.....	78
3.1. Introduction	79
3.1.1. A novel predicted FUS isoform	80
3.1.2. The Classical and Non-Classical Secretory Pathways.....	82
The conventional secretory pathway	82
The Unconventional Secretory Pathway	84
3.2. Aims of this chapter.....	85
3.3. Material and methods	86
3.3.1. Foetal human primary neurons	86

3.3.2.	<i>RNA extraction and quantification</i>	86
3.3.3.	<i>RT-PCR and PCR</i>	87
3.3.4.	<i>Agarose gel electrophoresis and gel extraction of plasmid DNA</i>	88
3.3.5.	<i>Acetone precipitations</i>	88
3.3.6.	<i>Two Dimensional Gel Electrophoresis (2DGE)</i>	88
3.3.7.	<i>Human CSF samples</i>	89
3.4.	Results	90
3.4.1.	<i>FUS^{EC} is predicted to be a secreted protein</i>	90
3.4.2.	<i>FUS^{EC} novel isoform is expressed at mRNA level in HEK293T cells and in human primary neurons</i>	94
3.4.3.	<i>FUS^{EC} is found extracellularly, implying it is a secreted protein</i>	96
3.4.4.	<i>Optimization to detect FUS^{EC} in human CSF</i>	102
3.4.5.	<i>Characterization of a FUS^{EC} customised antibody</i>	103
3.5.	Discussion	105
	Implications and future perspective	110
	Conclusions	111
4.	Characterization of FUS^{EC}	112
4.1.	Introduction	113
4.1.1.	<i>Glycosylation of proteins</i>	113
	N-glycosylation process	114
	The role of protein glycosylation in neurodegenerative diseases	118
4.1.2.	<i>Protein secretion via exosomes</i>	119
	Extracellular vesicles	119
	Exosomes biogenesis and function	120
	Exosomes are implicated in the transmission of misfolded proteins in neurodegenerative disease	121
	The role of exosomes in ALS	121
4.2.	Aims of this chapter	122
4.3.	Material and methods	123
4.3.1.	<i>Vector and insert restriction enzyme digestion</i>	123
4.3.2.	<i>De-phosphorylation of the plasmid vector</i>	124
4.3.3.	<i>Ligation reaction</i>	124
4.3.4.	<i>Methods to confirm that cloning was successful: Digestion, agarose gel and_x</i>	

<i>Sequencing</i>	125
4.3.5. <i>PNGase F assay</i>	126
4.3.6. <i>Cells treatment with tunicamycin</i>	126
4.3.7. <i>Glycan analysis</i>	127
Porous graphitized carbon (PGC) liquid chromatography mass spectrometry (PGC-LC-MS).....	127
LTQ-Velos mass spectrometer.	127
Analysis and relative quantitation of N-glycans.....	128
4.3.8. <i>Exosomes isolation</i>	128
4.4. Results	129
4.4.1. <i>Design and generation of FUS^{EC} constructs</i>	129
4.4.2. <i>FUS^{EC} expresses in HEK293T cells and is secreted into the media</i>	133
4.4.3. <i>N-glycosylation regulates in part FUS^{EC} secretion</i>	136
4.4.4. <i>Glycomics analysis of FUS^{EC} reveals the presence of complex and sialylated glycans</i>	140
4.4.5. <i>FUS^{EC} is present in the media insoluble fraction but not in exosomes</i>	144
4.4.6. <i>Overexpressed FUS^{EC} was detected in the cytoplasm of HEK293T cells</i>	146
4.4.7. <i>Identification of FUS^{EC} binding partners</i>	149
4.4.8. <i>Antibody characterization</i>	152
4.5. Discussion.....	154
Implications and future perspective.....	159
Conclusions	160
5. Examining the role of FUS^{EC} in ALS	161
5.1. Introduction	162
The role of FUS loss of function or gain of toxic function mechanisms in ALS.	162
Mutant FUS activates ER stress and induces Golgi fragmentation.....	163
FUS aggregates are transmitted through a prion-like mechanism in ALS	163
5.2. Aims of this chapter.....	165
5.3. Material and methods	165
5.3.1. <i>Site-Directed Mutagenesis</i>	165
5.3.2. <i>Preparation of Insoluble Cell Fractions</i>	166
5.3.3. <i>Co-culture experiments</i>	166
5.3.4. <i>Flow cytometry</i>	167

5.4.	Results	167
5.4.1.	<i>Site directed mutagenesis to produce ALS-FUS^{EC} mutants.....</i>	167
5.4.2.	<i>ALS-associated FUS^{EC} mutants form more inclusions than WT FUS^{EC} in HEK293T cells.....</i>	169
5.4.3.	<i>Identifying potential binding partners of ALS linked mutant FUS^{EC} to provide insights into possible pathogenic mechanisms.</i>	172
5.4.4.	<i>ALS-FUS^{EC} mutants induce ER stress in HEK293T cells</i>	174
5.4.5.	<i>ALS-FUS^{EC} mutants localize more in the ER than WT-FUS^{EC}</i>	178
5.4.6.	<i>Cells overexpressing ALS mutant FUS^{EC} display fragmented cis-Golgi.....</i>	179
5.4.7.	<i>ALS-FUS^{EC} mutants induce apoptosis in HEK293T cells.</i>	182
5.4.8.	<i>Examining the secretion levels of ALS mutants and WT FUS^{EC} in HEK293T cells.....</i>	184
5.4.9.	<i>Examination of the cell-to-cell transfer ability of WT and ALS-FUS^{EC} mutants.....</i>	185
5.5.	Discussion.....	189
	Implications and future perspectives	196
	Conclusions	197
6.	General discussion	198
	Summary of the main findings of the thesis	199
	Identification and characterization of FUS ^{EC}	201
	The possible role of FUS ^{EC} in ALS	203
	Final conclusions	207
7.	References	209
8.	Appendix	257
8.1.	HA-FUS ^{EC} and GFP-FUS ^{EC} vector map.....	258
8.2.	GFP-FUS ^{EC} plasmid sequence	258
8.3.	HA-FUSEC plasmid sequence	261
8.4.	Uncropped western blots	263
8.6.	Flow cytometry results, Chapter 5.....	319
8.7.	Ethics	320

List of tables

Table 1.1 <i>FUS mutations in ALS colour coded according to the domains of Figure 1.3.....</i>	51
Table 2.1 <i>Primary antibodies used for immunoblotting</i>	71
Table 2.2 <i>Primary antibodies used for immunocytochemistry.....</i>	76
Table 3.1 <i>Characterization of FUS and FUSEC proteins.....</i>	82
Table 3.2 <i>Primers details used for PCR.....</i>	87
Table 3.3 <i>Details of healthy subjects for CSF studies.....</i>	89
Table 4.1 <i>Enzyme digestion reaction set up</i>	123
Table 4.2 <i>De-phosphorylation reaction set up.....</i>	124
Table 4.3 <i>Ligation reaction set up</i>	124
Table 4.4 <i>Primers used for Sanger sequencing confirmation</i>	125
Table 4.5 <i>Total assigned N-glycan composition from HA-FUS^{EC}.....</i>	142
Table 5.1 <i>Primers used for the mutagenesis.....</i>	166

List of figures

Figure 1.1 Mechanisms of pathogenesis in ALS.....	14
Figure 1.2 Schematic diagram of the domain structure of FUS, illustrating post-translational modifications (PTMs).....	35
Figure 1.3 FUS domain structure.....	50
Figure 1.4 Mutant FUS mechanisms in ALS.....	56
Figure 1.5 Alternative splicing give rise to multiple diverse proteins.....	58
Figure 1.6 Pre-mRNA splicing process.....	59
Figure 1.7 Schematic representation of constitutive splicing and the most common alternative splicing events.....	60
Figure 1.8 Representation of the novel alternatively splicing mechanism previously described for NCAPH2 gene.	64
Figure 3.1 Genomic organization of FUS and FUS ^{EC}	81
Figure 3.2 Cellular secretory pathways.....	85
Figure 3.3 Analysis of FUS ^{EC} protein sequence using bioinformatics tools that predict the presence of signal peptides	93
Figure 3.4 Detection of FUS ^{EC} mRNA in HEK293T cells and in human primary neurons using end point PCR.....	95
Figure 3.5 Detection of FUS ^{EC} in the media of HEK293T cells.....	97
Figure 3.6 LC-MS/MS confirms that FUSEC is present in the conditioned media of HEK293T cells s.	101
Figure 3.7 Detection of FUS ^{EC} in human CSF.	103
Figure 3.8 Examination of the specificity of the customized antibody designed specifically for FUS ^{EC} , AbGenscript #1	105
Figure 4.1 Simplified diagram of the N-glycosylation pathway, from the cytosolic face of the ER to the Golgi.....	117
Figure 4.2 Three types of N- glycans that compose mature glycoproteins, with the N-glycan core Man3GlcNAc2Asn: High Mannose, Hybrid and Complex. .	118
Figure 4.3 Schematic overview of FUS ^{EC} plasmids.. HA.....	131
Figure 4.4 Schematic representations of C-terminal HA- and GFP-tagged FUS ^{EC} proteins. Protein sequence for HA.....	132
Figure 4.5 AH-FUS ^{EC} is expressed in HEK293T cells and secreted in the soluble media fraction.....	134

Figure 4.6 GFP-FUS ^{EC} is expressed in HEK293T cells and secreted in the soluble media fraction.....	136
Figure 4.7 FUS ^{EC} is N-glycosylated.	139
Figure 4.8 HA- FUS ^{EC} is N-glycosylated with complex N-glycans.	141
Figure 4.9 FUS ^{EC} is secreted in the insoluble part of the media but not in exosomes.	146
Figure 4.10 Cytoplasmic distribution and subcellular localization of FUS ^{EC} ..	149
Figure 4.11 Identification of FUS ^{EC} binding partners.....	151
Figure 4.12 Examination of customized antibody against FUS ^{EC}	153
Figure 5.1 Design and site direct mutagenesis of FUS ^{EC} to produce R316G and P320L mutants.....	169
Figure 5.2 ALS-mutant FUS ^{EC} form inclusions..	172
Figure 5.3 Evaluation of the common putative binding partners of FUS ^{EC} mutants.....	174
Figure 5.4 Overexpression of FUS ^{EC} ALS-mutant induces ER stress in HEK293T cells.	177
Figure 5.5 ALS-linked FUS ^{EC} mutants associate more with ER than WT FUS ^{EC}	179
Figure 5.6 FUS ^{EC} ALS-mutants induces Golgi fragmentation in HEK293T cells..	182
Figure 5.7 Overexpression of ALS-mutants FUS ^{EC} induces apoptosis.....	183
Figure 5.8 Determining WT FUS ^{EC} and ALS-mutants secretion levels.....	185
Figure 5.9 Examination of uptake of GFP expressing FUS ^{EC} in HEK293T cells.	189
Figure 6.1 Schematic representation of the features of FUS ^{EC} identified in this thesis.	200
Figure 6.2 FUS ^{EC} is involved in molecular mechanisms related to ALS	206

Publications and presentations

Publications

The work presented in this thesis is included in the following manuscript in preparation:

Vidal, M., et al. (2018) ***“A novel extracellular isoform of FUS is involved in ALS.”*** [Manuscript in preparation].

The author has also contributed to the following publication the data of which are not covered by this thesis

Experimental papers:

- Ragagnin AMG, Sundaramoorthy V, Parakh S, Perri ER, Soo K, Vidal M, Jagaraj CJ, Shadfar S, Don EK, Yuan KC, Hogan A, Gwee S, Rayner S, Lee A, Williams KL, Chung RS, Blair IP, Laird AS & Atkin JD. (2018) ***“Rab1 rescues mutant cyclin F perturbation of ER homeostasis in ALS.”*** [Manuscript in preparation].
- Parakh S, Jagaraj CJ, Vidal M, Ragagnin AMG, Perri ER, Konopka A, Toth RP¹, Galper J, Blair IP, Thomas CJ, Walker AK, Yang S, Spencer DM, Atkin JD (2018) ***“ERp57 is protective against mutant SOD1-induced cellular pathology in amyotrophic lateral sclerosis”***. Human molecular genetics 27(8):1311-1331.

Review papers:

- Shahheydari H, Ragagnin A, Walker AK, Toth RP, Vidal M, Jagaraj CJ, Perri ER, Konopka A, Sultana JM, Atkin JD (2017) ***“Protein Quality Control and the Amyotrophic Lateral Sclerosis/ Frontotemporal Dementia Continuum”***. Frontiers in Molecular Neuroscience;10:119

Communications

Oral presentation

- Vidal M (2017) “ **Identification of a novel extracellular isoform of fused in sarcoma (FUS)**”. Oral presentation in the Australasian Neuroscience Society Annual Scientific meeting, Sydney, Australia.
- Vidal M, Lee A, Heng B, Ragagnin AMG, Sundaramoorthy V and Atkin JD (2017). “**Detection and characterization of a novel extracellular isoform of fused in sarcoma (FUS).**” 3 minutes pitch poster presentation at ComBio 2017, Adelaide, Australia.

Poster presentation at formal scientific meetings:

- Vidal M, Lee A, Heng B, Ragagnin AMG, Sundaramoorthy V and Atkin JD (2018). “ **Identification of a novel extracellular isoform of fused in sarcoma (FUS) and its role in ALS**”. Gordon Research Conference, Protein Folding dynamics, Galveston, USA.
- Vidal M, Lee A, Heng B, Ragagnin AMG, Sundaramoorthy V and Atkin JD (2018). “ **Identification of a novel extracellular isoform of fused in sarcoma (FUS) and its role in ALS**”. Gordon Research Seminar, Protein Folding dynamics, Galveston, USA.
- Vidal M, Lee A, Heng B, Ragagnin AMG, Sundaramoorthy V and Atkin JD (2017). “**Detection and characterization of a novel extracellular isoform of fused in sarcoma (FUS).**” ComBio, Adelaide, Australia.

Awards and Scholarships

Postgraduate Research Found (PGRF) 2018, Macquarie University

Macquarie University Research Excellence Scholarship (MQRES) 2015-2018

Abbreviations

2DGE	Two dimensional gel electrophoresis
aa	Amino acid
AD	Alzheimer's disease
AGO2	Argonaute-2
AGRF	Australian Genome Research Facility
ALG	Asparagine-Linked Glycosylation
ALS	Amyotrophic lateral sclerosis
ALS-PDC	ALS, PD and dementia complex
AMPA	α -amino-3-hydroxy-5-methyl-4-isoxazolepropionic acid receptor
APC	Adenomatous polyposis coli
ApoM	Apolipoprotein M
APP	Amyloid precursor protein
AR	Androgen receptor
ASK1	Apoptosis signal-regulating kinase 1
Asp	Asparagine
ATF	Activating transcription factor
ATM	Ataxia-telangiectasia mutated
ATP	Adenosine triphosphate
Bax	Bcl-2-associated_X_protein
BCA	Bicinchoninic acid
BDNF	Brain-Derived Neurotrophic Factor
BIM	Bcl2-interacting mediator of cell death
Bip	Binding immunoglobulin protein
BMAA	β -N-methylamino-L-alanine
Bp	Base pair
BSA	Bovine serum albumin
Ca ²⁺	Calcium
CAN	Acetonitrile
CCN5	Connective tissue growth factor/cysteine-rich 61/nephroblastoma overexpressed
CCND1	Cyclin D1

cDNA	Complementary DNA
CFHR4	CFH-related protein
CHMP2B	Charged multivesicular protein 2B
CHOP	CCAAT-enhancer-binding protein homologous protein
circRNAs	Circular RNAs
CLIP	Cross-linking immunoprecipitation
CNS	Central Nervous System
CO ₂	Carbone dioxide
ConA	Concanavalin A
COPII	Coat protein complexes II
CSF	Cerebrospinal fluid
CypB	Cyclophilin B
DCTN1	Dynactin subunit 1
DENN	Differentially expressed in neoplastic versus normal cells
dH ₂ O	Distillate water
DMEM	Dulbecco's modified eagle medium
DMSO	Dimethyl sulfoxide
DNA	Deoxyribonucleic acid
DNA-PK	DNA-dependent protein kinase
Dol-P	Dolichyphosphate-bound sugars
DPBS	Dulbecco's Phosphate-Buffered Saline
DPRs	Dipeptide repeat proteins
DR5	Death receptor 5
DSBs	Double-strand breaks
DsRed	Discosoma sp. red fluorescent protein
DTT	Dithiothreitol
<i>E. coli</i>	<i>Escherichia coli</i>
EAAT2	Excitatory amino acid transporter 2
ECC	EI Escorial Criteria
eIF2 α	Serine 51 of eukaryotic translation initiation factor 2 α
ELISA	Enzyme-linked immunosorbent assay
ER	Endoplasmic Reticulum
ERACS	ER-associated compartments

ERAD	Endoplasmic-reticulum-associated protein degradation
ERGIC	ER-Golgi intermediate compartment
ERp	Endoplasmic reticulum resident protein
ERQC	ER-protein quality control
ESCRT	Endosomal sorting complexes required for transport
EST	Expression sequence TAG
EV	Empty vector
EV	Extracellular vesicles
EWS	Ewing sarcoma breakpoint region 1
fALS	Familal ALS
FCS	Fetal calf serum
FGF	Fibroblast growth factor
FIG4	Factor-induced gene 4
FMRP	Fragile X mental retardation protein
FTD	Frontotemporal dementia
FTDP-17	Frontotemporal dementia with Parkinsonism linked to chromosome 17
FTLD	Frontotemporal lobar degeneration
FTLD-FUS	FTLD cases display FUS inclusions
FUS	Fused in Sarcoma
FUS ^{EC}	Extracellular isoform of Fused in Sarcoma
G3BP1	Ras GTPase-activating protein-binding protein 1
GABA	γ-aminobutyric acid
GADD153	DNA damage 153
Gal	Galactose
GalNac	N-acetylgalactosamine
GAPDH	Glyceraldehyde-3-Phosphate Dehydrogenase
GFP	Green Fluorescent Protein
GlcNAc	β-d-N-acetylglucosamine
GlcNAc ₂ -Man ₃	N-glycan core
GLT-1	Glutamate transporter 1
Glua1	Glutame A 1
GO	Gene ontology

GS-1	α -glucosidase I
HA	Hematoglutinin
HAT	Histone acetyltransferase
HD	Huntington disease
HDAC	Histone deacetylases
HDL	High density lipoprotein
HEK293T	Human embryonic kidneys 293T
HMM	Hidden Markov Model
hnRNP	Heterogeneous nuclear ribonucleoprotein 1
HR	Homologous recombination
IAA	Iodoacetamide
ICC	Immunocytochemistry
IDD	Intrinsically disordered domains
IEF	Isoelectric focusing
IgGs	Immunoglobulin G
ILV	Intra-luminal vesicles
IP	Immunoprecipitation
IPG	Immobilised pH gradient
iPSCs	Induced pluripotent stem cells
IRE-1	Inositol requiring kinase-1
JNK	Jun NH2 terminal kinase
KLD	Kinase, ligase, DpnI
LB	<i>Luria Bertani</i>
LC	Low complexity
LC-MS/MS	Liquid Chromatography Mass Spectrometry
LC3	Light chain 3
LIR	LC3- interacting region
LLO	Lipid linked oligosaccharides
LLPS	Liquid-liquid phase-state
LMN	Lower motor neurons
MAMs	Mitochondria-associated membranes
Man	Mannose
MAPS	Misfolding-associated protein secretion

MAPT	Microtubule Associated Protein Tau
mFUS	Mutant FUS
mGluR5	Metabotropic glutamate receptor 5
miRISC	microRNA-induced silencing complex
mRNA	Message RNA
MV	Microvesicles
MVB	Multivesicular bodies
MW	Molecular weight
N2A	Neuro-2a
<i>NCAPH2</i>	Non-SMC condensin II complex subunit H2
NEFL	Neurofilament Light Protein
NES	Nuclear export signal
NeuAc	<i>N</i> -acetylneuraminic acid
NHEJ	Non-homologous end joining
NLS	Nuclear Localisation Signal
NMD	Nonsense-mediated decay
NMJ	Neuromuscular junction
NMR	Nuclear magnetic resonance
NPC	Nuclear pore complex
Nrf2	Nuclear factor E2 related factor 2
Nuc	Nucleoporin
O-GalNAc	O-glycan structures
O.D.	Optical density
OGT	O-linked N-acetylglucosamine
OST	Oligosaccharyltransferase
PA	Physical activity
PAGE	Polyacrylamide gel electrophoresis
PAR	Poly (ADP-ribose)
PARP	Poly (ADP-ribose) polymerase
PBS	Phosphate buffer saline
PBs	Processing bodies
PCR	Polymerase chain reaction
PD	Parkinson disease

PDI	Protein Disulfide Isomerase
PERK	Protein kinase RNA like endoplasmic reticulum kinase
PGC	Porous graphitized carbon
PGKI	Phosphoglycerate kinase
PIKK	Phosphoinositide 3-kinase-like kinase
PNF1	Profilin-1
PNGase F	Peptide <i>N</i> -glycosidase F
PQC	Protein quality control
pre-mRNA	Precursor mRNA
PRMT	Protein arginine methyltransferase
PrP	Prion protein
PSMC4	26s protease regulatory subunit 6B
PTBP1	Polypyrimidine Tract Binding Protein 1
PTM	Post-translational modifications
PTPIP51	Mitochondrial resident tyrosine phosphatase-interacting protein-51
PUMA	p53 upregulated modulator of apoptosis
PY-NLS	Proline-tyrosine nuclear localization signal
Q-PCR	Quantitative polymerase chain reaction
QGSY-rich region	Glutamine-glycine-serine-tyrosine rich prion-like domain
RAN	Repeat-associated non ATG
RBP	RNA binding proteins
RBP _s	RNA binding proteins
RFP	Red fluorescent protein
RGG	Arginine-Glycine- Glycine -rich motif
RNA	Ribonucleic acid
RNAP3	RNA polymerase III
RNAPII	RNA polymerase II
RNP	Ribonucleoprotein
ROS	Reactive oxygen species
RRM	RNA recognition motif
rRNA	Ribosomal RNA
RT-PCR	Reverse transcriptase Polymerase Chain Reaction

S1R	Sigma-1 receptor
SAFB1	Scaffold attachment factor B
sALS	Sporadic ALS
SDS	Sodium dodecyl sulfate
SEM	Standard error of the mean
Ser	Serine
SFPQ	Splicing factor proline- and glutamine-rich
SGs	Stress granules
SNARE	Soluble <i>N</i> -ethylmaleimide-sensitive factor attachment protein receptors
snRNA	Small nuclear ribonucleic acid
snRNPs	Small nuclear ribonucleoproteins
SOD1	Superoxide dismutase 1
SP	Signal Peptide
SR	Serine/arginine
TAF15	TATA box-binding protein (TBP)-associated factor 15
TBP	TATA-binding protein
TBS	Tris-buffered saline
TBS-T	TBS tween-20
TDP-43	TAR DNA-binding protein 43
TERRA	Telomeric repeat-containing RNA
TFIID	Transcription Factor II D
TFIIIB	Transcription Factor IIIB
TGN	Trans Golgi Network
TIA-1	T-Cell-Restricted Intracellular Antigen-1
TM	Tunicamycin
TMH	Transmembrane helices
TNF	Tumour necrosis factor
TNPO1	Transportin
TRAF2	TNF receptor-associated factor 2
Trp	Tryptophan
TUBA4A	Tubulin Alpha 4a
Ub	Ubiquitin

UBA1	Ubiquitin-like modifier-activating enzyme 1
UBQLN2	Ubiquilin 2
UGGT1	UDP-Glc:glycoprotein glucosyltransferase 1
ULK1	Unc-51 like autophagy activating kinase 1
UMN	Upper motor neurons
UPR	Unfolded Protein Response
UPS	Ubiquitin-Proteasome System
USP19	Ubiquitin-specific protease 19
UT	Untreated
UTR	Untranslated region
UV light	Ultra violet light
VAPB	Vesicle-associated membrane protein-associated protein B
VCP	Valosin-containing protein
WT	Wild-Type
XBP1	X-box binding protein -1
ZnF	Zinc Finger
ΔNLS-FUS	FUS without a nuclear localization signal

Units of magnitude

C	celsius
Da	dalton/s
<i>g</i>	gravitational acceleration at the Earth's surface
g	gram/s
h	hour/s
k	kilo/s
L	litre/s
m	metre/s
m	milli
M	molar
min	minute/s
n	nano
n	number of units in a dataset
p	p-value
pl	isoelectric point
rpm	revolution/s per minute
s	second/s
SD	standard deviation
<i>t</i>	t-statistics
U	unit/s
V	volt/s
Vol	volume
X	magnification
μ	micro

1. ■ General introduction

1.1. Amyotrophic lateral sclerosis

Amyotrophic lateral sclerosis (ALS) is a fatal neurodegenerative disease that selectively affects upper and lower motor neurons of the brainstem, cortex and spinal cord [1]. ALS results in muscular weakness and with a rapid progression, it leads to paralysis and death, due to respiratory failure, usually within 3 to 5 years of diagnosis [2]. Most of ALS cases are classified as sporadic (sALS), with unknown aetiology, whereas 10% of cases are hereditary, termed familial ALS (fALS) [3]. Nonetheless, misfolded protein aggregates, forming motor neuronal inclusions are a common pathological hallmark of both sporadic and familial ALS, which clinically appear identical. The underlying pathophysiological mechanisms are still poorly understood and there is currently no effective treatment. In 2009, mutations in the Fused in Sarcoma (*FUS*) gene were first linked to familial ALS and to date more than 50 *FUS* mutations have been identified [4, 5]. In addition, *FUS* mutations were subsequently identified in a subset of sALS patients [6]. Interestingly, *FUS* mutations account for a particularly aggressive, juvenile form of disease [7-10]. Moreover, *FUS* immunoreactive inclusions are present in motor neurons of sALS, non-SOD1 fALS and 10% frontotemporal lobar degeneration (FTLD) patients [7, 11, 12]. This thesis focuses on the study of a novel, extracellular isoform of *FUS*, '*FUS*^{EC}'. It aims to characterise both WT and mutant forms of *FUS*^{EC}, thus broadening our knowledge of the *FUS* protein and its relationship to ALS.

1.1.1 Clinical features and symptoms of ALS

ALS is the most common adult onset motor neuron disorder. It is characterized by a progressive loss of both upper and lower motor neurons in the brain and spinal cord. ALS spreads progressively from an initial focal site of onset, leading to loss of control of the voluntary muscles, and death due to respiratory failure on average within 3 to 5 years from diagnosis [1]. The clinical features are heterogeneous, and can be categorised according to the site of onset, rate of progression and population of motor neurons lost, whether they are upper or lower [13]. The most common presentations of ALS are categorised as classical ALS (70%), ALS-FTD (5-15%), with isolated bulbar involvement or isolated

bulbar palsy (5%), and progressive spinal muscular atrophy, together with primary lateral sclerosis (10%) [14, 15].

There is currently no available reliable diagnostic biomarker, which leads to a 9-12 month delay in the diagnosis of ALS [16]. Since 1990, the El Escorial Criteria (ECC) have been used for the diagnosis of ALS [17], which focus on the clinical and electrophysiological evidence of lower and upper motor neuron degeneration, and the spread of clinical symptoms [17]. However, it was previously noted that the ECC is very restrictive and results in difficulties in the diagnosis of some cases of ALS. Hence these guidelines were updated more recently, and the 'Awaji Criteria' were proposed as an additional tool to increase the sensitivity of the ECC of probable or definite ALS cases [18, 19].

The targeting of upper motor neurons (UMN) in the motor cortex in ALS results in muscle stiffness, spasticity and hyperreflexia, whereas the involvement of lower motor neurons (LMN) in the brainstem and spinal cord leads to increased electrical irritability, spontaneous muscle twitching, weakness and finally motor neuron loss [15, 20]. These latter events translate into muscle denervation and ultimately, muscle atrophy [15, 20]. Additionally, in some studies it is reported that up to 85% of ALS patients will also experience sensory defects, although the underlying molecular mechanisms are not well understood [21].

ALS is characterized by a focal onset of symptoms, which spreads through adjacent anatomic regions, reflecting its clinical spread [22, 23]. Cross-sectional studies report that the spread of motor neuron degeneration is within, and between, the UMN and LMNs, which underlies the complex and heterogeneous clinical manifestation [22].

1.1.2 Epidemiology of ALS

The incidence and prevalence of ALS varies worldwide [24-26]. In Europe the incidence is recorded to be 2.6 individuals per 100,000 persons per year [27], whereas in China this number drops to 0.51-0.6 individuals per 100,000 [28]. Similarly, the prevalence in European populations is 6.9-9 people per 100,000/year [27, 29], and again in China this number drops to 1.97-3.04 individuals per 100,000 [28]. We can not eliminate the possibility that these

differences are due to reduced diagnosis in some remote Chinese populations. Interestingly, higher rates of ALS are found in people from the Kii Peninsula of Honshu Island, Japan, and from the Chamorro people of Guam [30, 31].

There are many factors that influence survival rate of ALS, including age of onset, presence of dementia, degree of diagnostic certainty, site of onset, body weight at the time of disease diagnosis, duration of treatment and gastrostomy [29, 32]. ALS mortality appears to be lower in highly ethnically “mixed” populations [25]. Studies of European populations have estimated that 70% of patients with ALS die within 3 years of the first appearance of symptoms [27]. In contrast, 5-10% of ALS patients survive more than 8 years [33] although this number can vary, depending on the inclusion criteria used in the analysis [28]. A recent study determined that ALS patients who took riluzole for more than 75% of disease duration survived 11 months longer than those patients that took riluzole for less than this period [32].

Gender is considered to be a risk factor for ALS, as the male: female incidence ratio is 1.6-2:1 [29, 34], although men and women are equally affected when the disease begins after the age of 70 years [35]. In European countries, the mean age of onset is 66.6 years [36] whereas in India, an earlier age of disease onset is observed, 46.2 years [37]. Nevertheless, ALS is often associated with aging because the age group with the highest prevalence is 70-79 years [29]. It has also been predicted that in the future, as the population ages, the incidence of ALS will increase 20% by 2040 in Europe [36] and across the globe, 69% by 2040 [38].

1.1.3 Environmental factors

Several environmental factors are hypothesized to contribute to the risk of ALS, such as smoking, exposure to toxins, physical activity, viral infection and head trauma [39].

Smoking has been considered as a risk factor for ALS for a long time, but there is still no clear evidence of its relationship to ALS. Systematic reviews of case-controlled and cohort studies evaluating smoking with the incidence of ALS, finds no strong association, but conclude that smoking is a risk factor for ALS in women [40, 41]. However no study has described a strong correlative

relationship between smoking and ALS [42]. Smoking has also been negatively associated with the median survival of ALS, independently of their respiratory status [43].

Exposure to some environmental toxins, including pesticides, organic solvents, environmental pollutants and heavy metals, are proposed to be risk factors for ALS [44-47]. One of the best studied examples, with substantial evidence linking it to ALS, is the toxin β -N-methylamino-L-alanine (BMAA). Elevated rates of ALS, PD and dementia complex (ALS-PDC), were reported in the Chamorro population in Guam [48], which has been associated with exposure to BMAA [48]. It has been suggested that BMAA, present in cycad seeds, undergoes biomagnification through the food chain [31, 49]. According to this hypothesis, animals consumed by the Guam population such as flying foxes, which are eaten traditionally by the Chamorro people, contain high concentration of BMAA [31, 49]. Consistent with this notion, high concentrations of BMAA are present in brains from ALS-PDC patients from Guam [50]. In addition, BMAA is a secondary metabolite produced by cyanobacteria, which possess a ubiquitous distribution in terrestrial and aquatic habitats, potentially expanding BMAA exposure to other regions. Supporting this hypothesis, high concentrations of BMAA were detected in the brains of ALS patients in Florida, where high concentrations of cyanobacteria are found [51]. However, there is no direct evidence of the effect of BMAA on humans; the only direct evidence comes from studies involving cell lines and animal models [52, 53]. Interestingly, recently a rat model with a single neonatal subcutaneous injection of 400 mg/kg BMAA developed neuropathology resembling ALS-PDC [52]. It has been further characterized that BMAA may become misincorporated into protein translation of L-serine [54].

Two controversial studies concluded that Gulf War veterans were twice as likely to develop ALS than non-veterans [55, 56]. Whilst the results of these studies were questioned because of the calculations used to determine the excess risk, the US Institute of Medicine issued a report confirming the association between military service and ALS [57]. This has been further confirmed by later studies [58, 59]. This predisposition to ALS is not exclusive to

military personnel from the Gulf war, because a Danish study identified 1.3 fold increase in ALS in Air Force and Marine personnel [60]. These findings suggest that the risk of ALS in military occupations could be due to exposure to environmental factors related to these specialities or to a predilection associated with physical aspects of military.

Premorbid fitness has also been proposed to be a risk factor of ALS, but this has not been conclusively determined. A review of case-controlled studies concluded that physical activity (PA) was not a risk factor for ALS; however there is some evidence suggesting a higher risk in athletes participating in professional football, although this is not clear [61]. Professional football players in Italy and the US, and professional cross-country skiers in Sweden, do have higher rates of ALS [62-64]. The first of these studies, studying the relationship between ALS and PA, detected a slightly decreased rate of death in ALS patients with previously high PA [65]. Additionally, a recent study of young Swedish men examined over 37 years did not identify any association between ALS and PA, but it did find that low muscle strength was a significant predictor of ALS, in contrast to high overall muscle strength [66]. The lack of relationship between ALS and PA was also confirmed by population-based studies, which implied that PA has a protective role instead [67, 68].

These results together with the lack of strong correlation between PA and ALS [65, 67] imply that PA is not a risk factor for ALS. Alternatively, it has been proposed that very physically active people are protected from common diseases, such as diabetes, cancer and cardiovascular disease, and are thus more likely to develop rare diseases such as ALS. Hence this notion provides a possible explanation as to why PA is implicated as a risk factor for ALS [69].

It has also been suggested that head trauma is the risk factor linking professional sports such as soccer to ALS [70]. A retrospective study on a Swiss population determined that head injuries were the only environmental factor predisposing to ALS [71]. On the contrary, a case-controlled study involving 300 cases and 300 controls found no relationship between ALS and sport or sport-related traumas [72]. Furthermore, a population-based study

suggested that sport related-trauma at earlier ages (before 55 years) was associated with ALS (odds ratio =1,2) but not later ages [73].

Environmental studies are complex and the numerous possible contributing factors are difficult to control. However, to date, there is not enough evidence to conclude that a single environmental factor is a strong risk factor for ALS, implying that a combination of several environmental factors together with a genetic predisposition could contribute to ALS.

1.1.4 ALS and frontotemporal dementia (FTD) continuum

Although classified as two different diseases at the beginning, it is now accepted that ALS and frontotemporal dementia (FTD) are clinically, genetically and pathologically linked forming a continuum disease spectrum. FTD is the second most common cause of dementia in patients younger than 65 after Alzheimer's disease [74]. FTD pathology includes atrophy of the frontal and temporal lobes, which translate in behavioural and language changes [75]. Approximately 50% of ALS patients develop cognitive and behavioural abnormalities and 13% have concomitant behavioural variant FTD [14]. Additionally, 15% of FTD patients display ALS clinical features [76, 77]. The overlap of ALS and FTD was confirmed by the discovery of common causes. These include mutations in *TARDBP*, *FUS*, *TANK-binding kinase -1 (TBK-1)*, *Ubiquilin2 (UBQLN2)*, *optineurin* and *cyclin F (CCNF)* [78]. Additionally, the identification of C9ORF72 repeat expansion as the major cause of fALS and FTD, has strengthened the notion that these diseases are extremes on a single disease continuum.

1.1.5 Genetics of ALS

Genetic studies allow identification of new ALS-associated genes that enable us to model the disease, identifying possible underlying pathways involved in neurodegeneration in ALS. The familial forms of ALS accounts for 5-10% of ALS cases [79]. The first identified gene linked to fALS in 2003 was superoxide dismutase 1 (SOD1), and currently there are approximately 30 genes associated with ALS [80]. In the next section a review of the most common

mutations associated with fALS: *SOD1*, *TARDBP*, *FUS* and *C9ORF72*, are presented [81].

SOD1

Mutations in *SOD1* were the first identified cause of ALS and population studies estimate that *SOD1* mutations account for approximately 20% of fALS and 1% of sALS cases [80, 82, 83]. It should be noted that *SOD1* is the most frequently mutated gene in the Chinese population, accounting for 25.3% of fALS and 1.6% of sALS [28, 84].

Almost 200 *SOD1* mutations have been linked to ALS (<http://alsod.iop.kcl.ac.uk/>), but only a small proportion of these have genetic evidence of pathogenicity [3]. Most of the identified mutations are point mutations that result in an autosomal dominant mode of inheritance [85, 86]. Additionally, some *SOD1* mutations have been linked to FTD [87, 88].

SOD1 mutations present high heterogeneity in their clinical presentation, disease course and phenotype. *SOD1* mutations A4V and G13R are associated with rapid disease progression compared to other mutations, particularly to two recently identified mutations in sALS, G73D and V120F, that display slower disease progression [84, 89-92]. Interestingly, the A4V mutation accounts for 40% of *SOD1* mutations in the US but it is rarely found in Europe [93]. In Norway there is a cluster of the *SOD1* H45R mutation that is related to longer survival rates [29], similar to the D90A mutation which presents a slower progression compared to others [94].

SOD1 encodes a 32 kDa homodimeric Cu/Zn-binding enzyme which is mainly localized in the cytoplasm, but it is also present in the mitochondria [95], peroxisomes [96] nucleus [97] and in the extracellular compartment [98]. *SOD1* is composed of eight β -antiparallel strands and two metal atoms that assist in catalysing the inactivation of superoxide anions to oxygen and hydrogen peroxide [99].

ALS mutations to *SOD1* can alter its structure in two ways. Mutations in the beta-barrel modify its structure with no alterations in metal content, or alternatively, mutations that affect the metal-binding site, result in lack of copper or zinc [100].

The pathogenic mechanism induced by mutant SOD1 in ALS was initially thought to be mediated by alterations in enzymatic activity [101]. However, later studies revealed that some SOD1 mutations maintain their enzymatic activity and no correlation between SOD1 mutant enzymatic activity and disease progression was observed [102-104]. Hence subsequently, a toxic gain of function mechanism was proposed to underlie SOD1 pathology in ALS. Moreover, this hypothesis was further confirmed when a mouse model lacking SOD1 presented no motor neuron phenotype before 6 months of age [105]. On the contrary, a SOD1 G93A mouse model developed motor deficits and degeneration of the neuromuscular junction at early stages, 80-90 days [106].

Whilst still not fully understood, additional studies have provided more evidence that a gain of toxic function of mutant SOD1 is involved in ALS. Mutations that lead to destabilization of the SOD1 structure promote oligomerization and aggregation [107, 108]. Mutant SOD1 cytoplasmic aggregates are found in fALS cases [80] and its wild-type (WT) counterpart in sALS spinal cords [109-113]. The underlying mechanism that drives SOD1 aggregation is still not fully understood. However, destabilization of the dimeric interface by ALS mutations can increase the tendency of SOD1 to unfold [114]. Furthermore, oxidation is thought to play a role in the misfolding and hence aggregation of WT SOD1 [109].

Aggregated and misfolded forms of SOD1 have been shown to trigger a wide range of cellular pathways linked to neurodegeneration, including ER and mitochondrial stress, proteasome and autophagy defects and ER-Golgi trafficking defects [95, 115-117]. Interestingly, SOD1 aggregates have been shown to seed assembly and to be transmissible among neurons in a prion-like fashion, thus transmitting ALS pathology to neighbouring cells [101, 115, 118-120].

TARDBP

TAR DNA-binding protein 43 (TDP-43) was firstly identified as the major component of ubiquitinated protein aggregates in affected neurons of ALS and FTLD patients in 2006 [121, 122]. Two years later, mutations in the gene encoding TDP-43, *TARDBP*, were directly linked to familial and sporadic ALS

and FTLT [123-125]. *TARDBP* mutations account for 3-6% of non-SOD1 fALS cases and 0-2% of sALS cases [124, 126-128]. To date, around 50 ALS mutations have been discovered in *TARDBP*, most of which are inherited missense mutations located at the C-terminus of the protein [128, 129].

TDP-43 inclusions are detected in 97% of ALS cases [130, 131] in affected brains and spinal cords, where it is abnormally hyperphosphorylated and ubiquitinated, together with the presence of a C-terminal TDP-43 fragment [121, 122]. Additionally, in neurons containing these aggregates, TDP-43 is mislocalized from the nucleus to the cytoplasm [121].

TDP-43 is a highly conserved RNA/DNA binding protein that is primarily found in the nucleus, and contains 414 amino acids (aa) encoded by six exons. It contains 2 RNA recognition motif (RRM) domains, a nuclear localization signal (NLS), a nuclear export signal (NES) and a C-terminal glycine rich region [132]. The normal functions of TDP-43 are still not fully understood, but it has been implicated in the entire process of messenger RNA (mRNA) biogenesis, in splicing regulation [133, 134], and in endosomal and mRNA trafficking and signalling in dendrites [135-138].

In its pathological form, TDP-43 is cleaved to form a C-terminal fragment containing the glycine rich domain, in selectively enriched affected cortical regions, but not in the spinal cord of ALS and FTD patients [139]. Full-length WT and mutants of TDP-43 are prone to aggregation under chronic oxidative stress conditions [140]. Additionally, an alternatively spliced form of TDP-43, produced from an alternative start codon, was found to be upregulated and aggregated in ALS patient tissue [141]. Moreover, TDP-43 has the capacity to autoregulate itself in a negative feedback loop, via binding to its own mRNA through the C-terminal domain [142]. Therefore, TDP-43 aggregation is a complex multifactorial process. In addition, as well as being ubiquitinated and hyperphosphorylated, TDP-43 is also acetylated and small ubiquitin-like modifier (SUMO)ylated in ALS and it is likely that alterations in all of these post-translational modifications will affect its aggregation propensity and toxicity [121, 122, 143, 144].

The neurodegenerative mechanism associated with pathological forms of TDP-43 are related to loss of function of nuclear TDP-43 and a gain of function of cytoplasmic aggregates. Depletion of nuclear TDP-43 in post-mortem human

brains is associated with alteration in the autoregulation of *TARDBP*, suggesting that loss of function also occurs in ALS patients [145]. Additionally, clearance of nuclear TDP-43 is associated with defects in its normal splicing functions [146, 147]. However, aggregation of TDP-43 has also been reported to trigger several cellular pathways leading to toxicity. TDP-43 aggregates are toxic in several different experimental models [148, 149]. Mice overexpressing TDP-43 with a defective NLS display accumulation of insoluble, cytoplasmic TDP-43 inclusions in the brain and spinal cord, in association with motor neuron loss and motor dysfunction, leading to death [150].

FUS

Similar to TDP-43, mutations in *FUS* are associated with both ALS and FTD. More than 50 mutations have now been identified in the *FUS* gene, accounting for 4-6% of fALS and 0.7-1.8% of sALS cases. Furthermore, 2% of sALS patients display FUS immunoreactive inclusions [151-155]. Mutations in *FUS* are rare in FTD patients, although a proportion of FTLD cases display FUS inclusions (FTLD-FUS) [156]. FUS is also an RNA/DNA binding protein involved in a wide range of cellular functions, from alternative splicing to DNA damage and repair [157-160]. However, the role of FUS in ALS pathology has not been studied in detail compared to TDP-43. The FUS protein structure, normal functions and its pathogenic pathways in ALS will be further explained in Section 1.2., page 34.

C9ORF72

An ALS and FTD risk locus was first identified on the chromosome 9p2, but no gene was identified [161]. Subsequently the retention of a large hexanucleotide (G₄C₂) non-coding repeat expansion in the first intron of *C9ORF72* was then linked to both ALS and FTD [161, 162].

The *C9ORF72* repeat expansion is the most common genetic cause of both ALS and FTD in caucasian population. In the Finnish population, the mutation in *C9ORF72* accounts for 46% of fALS, 21.2% sALS and 29.3% of FTD cases [162]. Whereas the cohorts analysed in the original studies identified

11.7% of familial FTD and 23.5 of fALS cases with mutations in this gene [161]. However, C9ORF72 repeat expansion accounts for rare FTD cases in Asian countries [163, 164].

A higher prevalence of female patients with C9ORF72 ALS is evident, with a risk ratio of 1.16, whereas, there is no sex difference in C9ORF72 FTD patients [165]. The clinical symptoms of C9ORF72 patients are heterogeneous among ALS and FTLD but also within the FTLD group. The clinical manifestation of C9ORF72 patients is quite heterogeneous, with different phenotypic characteristics compared to other ALS mutations.. The median survival rate from symptom onset was 3.2 years lower than TDP-43 carriers and longer than FUS carriers [166]. Males with spinal onset have particularly rapid progression of ALS [166-168].

C9ORF72 follows a process of unconventional repeat-associated non-ATG (RAN) translation [169]. The G₄C₂ repeats are translated into all six sense and antisense frames generating five RAN dipeptide repeat proteins (DPRs) [169]. A systematic review of studies of C9ORF72 patient inclusions revealed that a common theme was the high density of TDP-43 positive inclusions in the *substantia nigra*, whereas inclusions in the cerebellum were positive for sequestosome-1/p62 and DPRs, but negative for TDP-43 [170]. TDP-43, p62 and the DPRs were also often found in the hippocampus, but p62 and the DPRs were more abundant [170]. All five DPR proteins are found in the inclusions of ALS/FTS patient's brains together with p62, and the majority of these aggregates contain poly-GA [171, 172]. In healthy controls the G₄C₂ sequence is repeated 1 to 25 times, whereas in C9ORF72 ALS and FTD cases, this region is repeated fifty to several thousand times [173, 174], although the minimum number of repeats necessary for toxicity remains to be determined.

The normal function of C9ORF72 protein is not fully elucidated but bioinformatics studies have suggested that C9ORF72 contains a DEN domain [175, 176]. DEN domain-containing proteins are a highly conserved family of expressed in normal and neoplastic cell (DENN) proteins. This family of protein are related to Rab guanine-diphosphate/triphosphate exchange factors that activate Rab-GTPases. C9ORF72 has been related to the modulation of membrane trafficking and autophagy [177, 178].

Several pathogenic mechanisms have been implicated in C9ORF72 pathology. Firstly, reduced transcription of the mutant allele leads to loss of function of the C9ORF72 protein, referred to as haploinsufficiency [179]. Reduced transcription of C9ORF72 and associated protein levels were detected in C9ORF72 post-mortem tissue from fALS-FTD patients, confirming this notion [161, 180, 181]. This has also been demonstrated in animal models, where deletion or reduction of C9ORF72 expression promotes defective axon formation and motor-dysfunction [182-184]. However, there are also numerous C9ORF72 knock out animal models that do not develop ALS/FTD neurodegenerative phenotype, arguing against a unique role of haploinsufficiency in C9ORF72 underlying mechanism in these diseases [185-187].

Secondly, bidirectional transcription and generation of sense and antisense transcripts containing expanded G₄C₂ regions accumulate in nuclear RNA foci, conferring a possible toxic gain of function [188]. RNA foci have been detected in the frontal cortex and spinal cord of C9ORF72 patients [161]. Thus sequestering RNA-binding proteins impeding their normal function [189, 190].

The third mechanism linked to C9ORF72 is the repeat-associated non ATG (RAN) translation [191]. The accumulation of sense (polyGA, polyGP, polyGR) and antisense (polyPA, polyPR and polyGP) dipeptide repeat or RAN proteins was confirmed which are cytotoxic in cell models [169, 179, 188, 192-194]. They are thought to play a crucial role in the impairment of nucleocytoplasmic transport [195]. Overexpression of polyGR or polyPR induces the assembly of stress granules (SGs), and recently nucleocytoplasmic transport factors were found to localize within SGs, which leads to the impairment of these factors [195-197].

Interestingly, cell-to-cell transmission of DPRs has been demonstrated in cell models [198, 199]. However, treatment with antibodies against anti-GA blocked this transmission and aggregation, revealing a possible therapeutic strategy [199].

1.1.6 Possible pathogenic mechanisms implicated in ALS

There are now numerous pathophysiological mechanisms linked to ALS, which will be discussed in detail below (**Figure 1.1**).

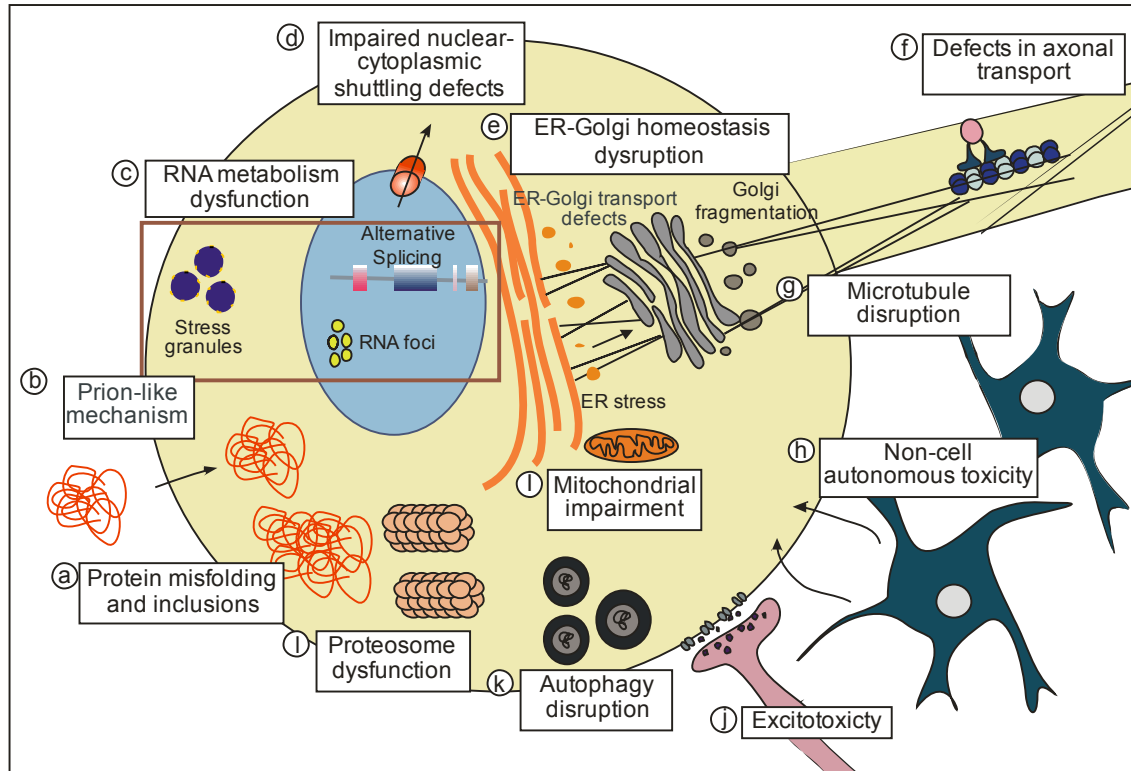


Figure 1.1 Mechanisms of pathogenesis in ALS (a) Misfolded proteins form intracellular inclusions. (b) Misfolded proteins are transmitted in a prion-like mechanism between cells (c) RNA binding proteins are mislocalized in the cytoplasm within SGs, and are cleared from the nucleus which impairs splicing activity. Additionally, RNA foci are formed by C9ORF72 repeats. (d) Impaired nucleo-cytoplasmic transport. (e) ER-Golgi homeostasis impairment: disruption of ER-Golgi trafficking, Golgi fragmentation and ER stress. (f) Disruption of axonal transport. (g) Inhibition of microtubule-based anterograde and retrograde transport. (h) Non-cell autonomous toxicity by non-neuronal cells. (i) Mitochondrial dysfunction. (j) Glutamate excitotoxicity. (k) Autophagy deregulation. (l) Inhibition of the UPS.

Protein misfolding and the formation of inclusions

Neurodegenerative diseases share a common pathological hallmark, the formation of protein inclusions containing aggregated, misfolded proteins, hence they are also termed ‘protein conformation disorders’. These disorders include Alzheimer’s disease (AD), Parkinson disease (PD), Huntington disease

(HD), Transmissible spongiform encephalopathy, as well as ALS. The population of neurons affected and the region of the brain involved confer the diverse clinical symptoms and progression of each disease [200].

In ALS, cytoplasmic inclusions are present in motor neurons and oligodendrocytes from the spinal cord and some brain regions (hippocampus and cerebellum) [201]. The ubiquitinated aggregates primarily detected in ALS patients are Lewy body-like hyaline inclusions or skein-like inclusions, which display randomly arranged filament morphology covered by fine granular structures [202, 203]. Additionally, small eosinophilic inclusions termed 'bunina bodies', and round hyaline inclusions are also present in ALS patients [204-207].

In fALS, the presence of inclusions containing the mutated proteins is an important characteristic. In sALS patients however, surprisingly, the misfolded inclusions contain WT versions of the same proteins associated with fALS. Ubiquitin-positive inclusions containing WT TDP-43 are the major hallmark of almost all ALS cases (97%), including sALS and fALS cases not involving SOD1 [121, 131, 208, 209]. In contrast, SOD1 hyaline-like inclusions and neurofilament inclusions are only present in SOD1 fALS cases, and in a subset of sALS cases [109, 210-212].

C9ORF72 fALS patients display TDP-43 positive inclusions in the anterior horn regions similar to other fALS cases. However, in addition, these patients also present with TDP-43 negative, p62 and ubiquilin-2 positive cytoplasmic and nuclear inclusions in the hippocampus, frontotemporal neocortex and cerebellum [213-216], as well as the DPRs [217-219]. Interestingly, C9ORF72 cases display mislocalization of phosphorylated TDP-43 in the frontal and motor cortex and in the spinal anterior horn, but only 4% of cases present inclusions positive for both [181].

FUS immunoreactive inclusions are present in non-SOD1 fALS and sALS motor neurons and these inclusions are also positive for TDP-43, p62 and ubiquitin in sALS cases, ALS/dementia, TDP-43 fALS, and non-SOD1 fALS [12, 220]. In contrast, the FUS inclusions present in mutant FUS fALS cases are negative for TDP-43 [221]. FUS inclusions are characterised by a skein-like and basophilic inclusion morphology in FUS-ALS and sALS motor neurons [12, 222-226].

Ciryam and colleagues recently proposed that the inclusions in ALS are formed by co-aggregation of supersaturated proteins, referring to proteins that are normally present in the cell at higher concentrations than predicted by their solubilities, and FUS, SOD1 and TDP-43 were all found to be supersaturated [227]. It is possible that reduced protein turnover, specifically in motor neurons, triggers the accumulation of such proteins, thus rendering them more sensitive to the formation of protein inclusions [227]. Accumulating evidence suggests that misfolded oligomers or small aggregated forms of these proteins are more likely to be toxic in ALS, rather than the large macroscopic aggregates or inclusions that are visible microscopically [228, 229].

Glutamate excitotoxicity

Excitotoxicity refers to over-activation of glutamate receptors, leading to neuron hyperpolarisation, and an increase in the concentration of calcium (Ca^{2+}) entering the cell. Motor neurons are especially vulnerable to deregulation of intracellular Ca^{2+} levels and excitotoxicity, because they express high levels of Ca^{2+} -permeable α -amino-5-methyl-3-hydroxisoxazolone-4-propionate (AMPA) receptors that lack the GluR2 subunit [230]. Hyperexcitability is a common documented phenomenon in both sporadic and familial cases of ALS, and in some cases of FTD [221, 231-235].

Glutamate levels are elevated in the cerebrospinal fluid (CSF) of sALS patients [236-239]. Under normal conditions, pre-synaptic neurons release glutamate into the synapse, where the levels of glutamate are tightly regulated. Both neurons and astrocytes have the capacity to release and take up glutamate to regulate this balance [240, 241]. Glutamate transporters are required to maintain glutamate homeostasis, but it has been suggested that in ALS this is impaired. Excitatory amino acid transporter 2 (EAAT2), which is expressed by astrocytes, has been the focus of extensive research in this area. Mice lacking glutamate transporter 1 (GLT-1) (homologous to EAAT2), display lethal spontaneous seizures, degeneration of hippocampal neurons and early death [242]. In sALS and fALS patients the function of EAAT2 is reduced [243-245], but clinical trials using Ceftriaxone, a compound that increases glutamate clearance via EAAT2 function, did not modify disease course [246].

It has been postulated that excitotoxicity could be induced by an imbalance of γ -aminobutyric acid (GABA) and glycine levels, leading to deregulated inhibition and excitation of synaptic transmission. In the brain, the majority of inhibitory interneurons use GABA, while inhibitory interneurons from the spinal cord use GABA and glycine as neurotransmitters [247]. Clinical neurophysiological studies of ALS patients have revealed dysfunctional cortical inhibition involvement in ALS [234, 248-251]. In ALS patients, in the motor cortex mRNA expression of the $\alpha 1$ GABA receptor was reduced, which was also recapitulated in G93A SOD1 transgenic mice [252, 253]. Accordingly to this, in Wobbler mice, a motor neuron mouse model that displays decreased motor neuron survival, loss of GABAergic neurons and reduced levels of GABA in the spinal cord were observed [254-256]. Similarly, in another animal model, the TDP-43 A315T mouse, impairment of GABAergic inhibition was observed [257]. Hence, besides to the loss of interneurons, disruption on cortical GABA signalling might be also involved in impairment of inhibitory circuits.

Riluzole was the first FDA-approved compound to treat ALS, which increases life expectancy by ~3 months [258]. It has been proposed that Riluzole alleviates neuronal excitability via pre-synaptic and post-synaptic mechanisms [259-261], by increasing glutamate uptake, modulating glutamate receptors and Na^+ and Ca^+ levels, and inhibiting GABA reuptake [262-265]. However, since Riluzole increases life expectancy only modestly, it remains to be determined whether glutamate excitotoxicity is a cause or a consequence of neurodegeneration.

Mitochondrial impairment

Mitochondria are the major organelles responsible for generating ATP via oxidative phosphorylation, and they are also involved in buffering of calcium levels, phospholipid biogenesis and apoptosis [266]. Several cellular manifestations related to mitochondria impairment are present in ALS, including defective oxidative phosphorylation, increased reactive oxygen species (ROS) production, defective calcium homeostasis, impaired mitochondrial dynamics, decreased ATP generation, and reduced mitophagy [267].

Neurons have high energy demands due to their specialised functions, and with their large size and long axonal terminals, motor neurons are particularly vulnerable to mitochondrial dysfunction. Recently, a second drug for ALS was approved: Edaravone [268, 269], which is thought to prevent lipid peroxidation, a mechanism that is associated with mitochondrial dysfunction [270, 271].

Abnormal mitochondrial structures and aberrant distribution have been reported in both sALS and fALS. Changes in mitochondrial density and distribution were detected in post-mortem spinal cord from sALS patients [272]. Conglomerates of aggregated dark mitochondria were present in synapses from anterior horn neurons of lumbar spinal cords from ALS patients [273]. Additionally, altered mitochondrial structures have been identified in skeletal muscle of ALS patients [274]. ALS related proteins, TDP-43, FUS, SOD1 and C9ORF72 associated poly-GR, localize or interact with mitochondria [208, 275-281]. Additionally, patient derived induced pluripotent stem cells (iPSCs), cell lines and animal models expressing TDP-43, FUS, SOD1 or C9ORF72, displayed damaged mitochondrial morphology [116, 276, 279, 281-288].

The endoplasmic reticulum (ER) and mitochondria associate and can mutually modulate their morphology and function via mitochondria-associated membranes (MAMs). The ER and mitochondria are physically related through MAMs, where ER-mitochondria communication takes place. Approximately 20% of the mitochondrial surface is highly associated to the ER membrane [289, 290]. Disrupted MAMs have emerged as a cause of mitochondrial dysfunction in ALS [290] and ALS-associated proteins impair MAMs in different ways. TDP-43 and FUS disrupt interaction of ER-localized VAMP-associated protein B/C (VAPB) and mitochondrial resident tyrosine phosphatase-interacting protein-51 (PTPIP51) via activation of GSK3 β [291, 292], which normally modulates ER-mitochondria association [291]. Disruption of this VAPB-PTPIP51 interaction by FUS and TDP-43 disrupts calcium exchange between ER and mitochondria, consequently decreasing ATP production [291, 292]. Sigma-1 receptor (S1R) is enriched in MAMs, and its function is to facilitate calcium delivery from the ER to mitochondria, and phospholipid exchange. Interestingly, S1R knockout mice displayed features of ALS [293] and loss of S1R exacerbated the ALS

phenotype in transgenic SOD1 G93A mice, and reduction of S1R activity led to axonal degeneration followed by cell death in human primary motor neurons [293-295]. Additionally, mutations in VAPB and S1R are present in a proportion of familial ALS cases [295, 296]. Furthermore, the MAM compartment transfers stress signals from the ER to mitochondria, mediated by the unfolded protein response (UPR) which is induced in ALS [297]. In addition, clearance of damaged mitochondria by autophagy, termed 'mitophagy' [298] is also inhibited in ALS, resulting in accumulation of damaged mitochondria [275, 299-301].

Non-cell autonomous toxicity

Growing evidence supports the idea that ALS pathology also involves non-neuronal cells such as astrocytes, microglia. Activated microglia is detected in brains of ALS patients [302, 303]. Additionally, postmortem studies on ALS patients brains, demonstrated that activated microglia, astrocytes and infiltrating T cells are localized in sites of motor neuron degeneration [304]. Furthermore protein aggregation and inclusions are also identified in astrocytes of ALS patients surrounding the motor neurons [305, 306]. Moreover, some ALS mutant genes are highly expressed in microglia such as C9ORF72, progranulin and TBK1 [307-310]. Confirming this notion, astrocytes cultured from both fALS and sALS patients induced toxicity causing neuronal death [311].

In SOD1 mice models it has been extensively reported the role of microglia in ALS neurodegeneration. The expression of mutants SOD1 in microglia was necessary to induce ALS phenotype [312]. According to this, extracellular SOD1 induces motor neuron toxicity through the activation of microglia which increases the release of ROS, pro-inflammatory cytokines and glutamate [313-315]. This cross talk among different cellular types gets even more complicated, implicating other cells than microglia and astrocytes. For instance, deregulation of miR 126-5p in myocytes of SOD1 G93A mice leads to upregulation of destabilizing factors facilitating axon degeneration and neuromuscular junction (NMJ) disruption [316]. More work is needed to elucidate the precise role of non-neuronal cells in ALS neurodegeneration.

Autophagy disruption

Initially the major function of autophagy was thought to be to provide nutrients under conditions of cell starvation, a process which is not selective. However, later autophagy was shown to possess cytoprotective functions, and its main role was determined to be elimination of unwanted proteins or organelles, a process known as selective autophagy. Autophagy is activated upon condition of ER stress, starvation, hypoxia, and protein aggregation among others [317]. A specific form of selective autophagy is induced by protein aggregates, termed 'aggrephagy'.

Optineurin is an autophagy receptor and mutations in optineurin account for 3% of fALS and 1% of sALS cases [318]. Similarly, TBK1 is a kinase that phosphorylates autophagy receptors p62 and optineurin, and TBK1 mutations are associated with 4% of fALS cases [319, 320]. Other autophagy related genes are found mutated in ALS, but in considerably lower frequency, these include: vesicle-associated membrane protein-associated protein B (VAPB) [153], Valosin-containing protein (VCP) [321, 322], ubiquilin 2 (UBQLN2) [323], Alsin [324], Charged multivesicular protein 2B (CHMP2B) [325], and Factor-induced gene 4 (FIG4) [326, 327].

Selective autophagy is necessary to ameliorate the accumulation of harmful material, such as protein aggregates [328]. Hence it is not surprising that impairment of autophagy has been proposed to be an underlying cause of ALS, and this has been described in cellular and animal models of ALS [329]. In addition, in sALS the presence of autophagosomes in association with protein inclusions has also been described [330]. Additionally, mutations in autophagy related genes have been associated with ALS [331]. Mutations in SQSTM1 or p62 are present in ALS and FTD cases [332-334], and an ALS mutant in the LIR domain of p62 has been tightly associated with autophagy disruption, as it reduced the affinity between p62 and LC3-II, interaction needed for the autophagosome formation [335]. The normal cellular function of C9ORF72 is associated with autophagy. Interaction of C9ORF72 with ULK1 and Rab proteins involved in autophagy initiation has been described, and C9ORF72 haploinsufficiency in cell lines and primary neurons leads to reduced autophagy

levels and increased p62 accumulation [336]. iPSCs derived from C9ORF72 patients displayed increased accumulation of p62 compared to controls, suggesting that autophagy was impaired [189]. In SOD1 G93A transgenic mice, increased LC3-II levels were reported in spinal cord motor neurons, representing an accumulation of autophagosomes [337].

ALS-associated FUS mutants have been shown to impair the early stages of autophagy [338]. Mutant FUS inhibits the formation of the autophagosome precursor, the omegasome, and early autophagosomes recruited less ATG9 and LC3-II, both of which are required for autophagosome enlargement, in neuronal cell lines [338]. Furthermore, mutant FUS SGs colocalize with autophagosomes, and inhibition of autophagy in primary neurons leads to accumulation of SGs containing FUS [339]. Several studies have suggested that autophagy induction inhibits the formation of SGs containing FUS, and increases survival in mice cortical neurons and in a *Drosophila* model of ALS [339, 340]. Additionally, FUS binds to RNAs of genes involved in autophagy or protein ubiquitination, such as *UBQLN1*, *UBQLN2*, *SQSTM1* and *VCP* [341-343]. Therefore, mutant FUS may also impair autophagy by disrupting regulation of mRNAs involved in this process.

Hence together these studies imply that dysfunction to autophagy is an important mechanism involved in ALS. Protein aggregation and reduced clearance of protein aggregates due to autophagy defects in ALS, probably combine to render motor neurons vulnerable to neurodegeneration.

Dysfunction to RNA metabolism

Since multiple mutations that cause ALS have been identified in RNA binding proteins (RBP), ALS has been described as a disease related to RNA dysfunction involving both loss and gain of functions of RNA binding proteins. Firstly, numerous RBP, including FUS and TDP-43, are present in cytoplasmic aggregates, accompanied by clearance or reduction of expression of each RBP from the nucleus [126, 344]. This may therefore result in splicing defects in the nucleus, which is further discussed in Chapter 3, section 3.1.3. Secondly, the involvement of RNA binding proteins in the formation of ribonucleoprotein (RNP) granules, and the aberrant phase transitions by ALS-associated mutant

RBPs is likely to confer a gain of toxicity (reviewed in the next section). Finally, the formation of RNA foci by the extended C9ORF72 repeat expansion is also likely to impact on cellular functions.

Major research efforts are focused on elucidating whether neurodegeneration by the C9ORF72 repeat expansion is driven by RNA toxicity, or toxic function of the DPRs. Expression of the sense RNA is toxic in rat primary neurons [345], and zebrafish C9ORF72 models expressing expanded sense and antisense RNAs developed a motor phenotype [346]. Hence, RNA foci may be an important therapeutic target, by designing antisense oligonucleotides targeting sense RNA strand or G-quadruplex binding molecules which target the sense-strand specific G-quadruplex RNA secondary structures [190, 196, 347, 348]. Importantly, RNA-targeting C9ORF72 repeats expansion have successfully reduced or eliminated RNA foci [349]. However, there is considerable evidence that the DPRs are also highly toxic, particularly the arginine-containing peptides [195, 345]. Hence, these findings combined with the lack of association of RNA foci with clinic-pathological features in C9ORF72 patients, suggests that C9ORF72 toxicity may be a complex mechanism involving both RNA foci and DPRs [350].

The formation of stress granules

SGs are a type of RNP granule that do not possess an enveloping membrane, but they maintain defined protein and RNA composition which is different from the cytosol. RNP granules include nucleoli [351], Cajal bodies [352], nuclear speckles and paraspeckles [351], processing bodies (PBs) [353], sites of DNA damage [354], as well as SGs [355]. Pathological inclusions colocalize with SGs markers in ALS and FTD patient tissues, in addition to cell culture models [138, 356-358].

SGs are spheroid or ellipsoid cytoplasmic structures, that dynamically assemble or disassemble in relation to cellular stress. SGs assembly is induced by heat shock, oxidative stress, hypoxia, mitochondrial dysfunction, glucose starvation, proteotoxic stress, viral infections or ER stress [359-362]. However, once the stress is resolved, the SGs disassemble. The purpose of SG formation

is thought to be inhibition of translation of specific mRNAs in specific subcellular compartments such as axon terminals and dendritic spines, when the cell is subjected to unfavourable conditions. SGs also exchange components with polysomes of PBs to prioritize translation or degradation of some mRNA transcripts, hence they are responsible for modulating the cellular proteome until the stress resolves [363].

The assembly of SGs is not fully understood; however it is likely to initiate from a pool of translationally inactive RNPs and mRNA [359, 364]. Additional RNB (RNA binding) proteins containing intrinsically disordered domains (IDD), such prion-like domains, are incorporated into SGs, such as T-Cell-Restricted Intracellular Antigen-1 (TIA-1), Ras GTPase-activating protein-binding protein 1 (G3BP1) and proteins that do not bind to mRNA, but are sequestered due to protein-protein interactions [360, 365].

SGs, and RNP granules in general, form reversible transient higher order structures that are separated from the cytoplasmic environment by the formation of a non-membranous liquid-liquid phase-state (LLPS). This feature allows the exchange of fluid components from the surrounding compartment. In these membrane-less phase separated droplets, proteins are concentrated approximately 100-fold when compared to the surrounding cytosol [360]. The formation of these condensate droplets is modulated by both multivalent forces among proteins and RNA, and by low affinity protein-protein interactions through IDD [366, 367]. While IDD and structural plasticity facilitate multivalent interactions, the RNA binding domains are critical for the interaction with specific mRNAs [368]. The ability of IDD to self-assemble is constantly regulated by chaperones, such as the heat shock proteins [369-371], and also by post-translational modifications such as phosphorylation and poly ADP-ribosylation [372, 373].

The formation of SGs has been suggested to be a key step in the production of pathological aggregates in ALS and FTD [374-376]. RBP involved in ALS, including FUS, TDP-43, heterogeneous nuclear ribonucleoprotein 1 (hnRNPA1), hnRNPA2/B1 and TIA1, can modify phase behaviour, promoting a more stable gelled state when mutated or post-translationally modified [354,

355, 368, 377-383]. The role of FUS in the modulation of LLPS will be reviewed in section 1.3.1 of this chapter.

Mutagenesis studies of TDP-43 revealed that an alpha-helical segment (320-340 amino acids) in the middle of the C-terminal domain, is necessary to condense and assemble TDP-43 into SGs [377, 380, 384, 385]. Furthermore, three tryptophan (Trp) residues in this domain, specifically Trp-334, are necessary for TDP-43 LLPS formation, with little contribution from the other two residues [384]. Cells expressing ALS-linked forms of TDP-43 and profilin-1 alter SGs morphology and assembly/disassembly [138, 380, 386, 387]. Since most of the ALS mutations are clustered at the C-terminal domain of TDP-43, it has been proposed that direct or indirect modulation of these key tryptophan residues is responsible for impairing SG dynamics [384].

C9ORF72 and DPRs localize in PBs and SGs upon stress stimuli, and the long isoform of C9ORF72 regulates SGs formation [388, 389]. RNA-RNA interactions also contribute to SG assembly attracting RBP, and the DPRs increase the propensity of RNA to assemble into SGs [390]. Additionally, the hexanucleotide repeat expansion G_4C_2 RNA adopts a G-quadruplex conformation, that seeds the assembly of RNA granules *in vitro* [391]. The length of the G_4C_2 repeat correlates with the degree of protein condensation *in vitro* in cells culture and in cell-free models [391]. PR repeats separate via a liquid-liquid phase transition, sequestering proteins involved in RNA metabolism [389]. PR₁₀₀ localizes in cytoplasmic SGs, which requires phosphorylated eIF2 α and G3BP1, and the resulting SGs displayed reduced dynamics and they were enriched for ALS-related proteins [389]. Additionally, it was shown that GR and PR DPRs further alter phase separation, towards a more rigid state of prion-like domain-containing proteins [392], through their interaction with prion-like domain of RBP (nhRNPA1, FUS, TIA-1) [389, 392].

SGs are thought to be a key factor for the formation of the inclusions characteristic of ALS and FTD. In ALS animal models, Ataxin-2 is a modifier of neurodegeneration. Interestingly, Ataxin-2 is an RBP involved in the regulation of SGs assembly [393]. Recent studies have focused on modulation of Ataxin-2 expression as a therapeutic target of ALS, with the aim of alleviating the transition of SGs to pathological aggregates [394].

Impairment of cellular trafficking

(i) Axonal transport

Efficient axonal transport is necessary for the maintenance and regeneration of neuronal axons and defects in axonal transport have been implicated in motor neuron diseases [395-397] and in early disease stages in ALS animal models [398, 399]. Axonal transport depends on molecular motor proteins such as kinesin, dynein and myosin [400] and recently, mutations within the C-terminal cargo domain of a kinesin family member, *KIF5A* were discovered in ALS [401]. *KIF5A* is responsible for the transport of RNA and RNP granules to neuronal dendrites and axons [401]. Similarly, other proteins involved in cytoskeleton functions, dynactin subunit 1 (DCTN1), profilin-1 (PNF1) [402], Tubulin Alpha 4a (TUBA4A) [402-407] are mutated in ALS.

Retrograde axonal transport defects were identified in G93A SOD1 pre-symptomatic mice [408, 409] and transport of different cargoes, such as mitochondria [286], neurofilaments [410] and vesicles [408], are disrupted in these animals. Axonal transport of mitochondrial and vesicles was also disrupted by the C9ORF72 DPRs, but not by RNA foci, in a *Drosophila* model [411].

Hence together this evidence suggests that axonal transport defects are common in ALS. Furthermore, inhibited axonal transport of mRNAs could be further affected by disruption of ER-Golgi trafficking and nucleocytoplasmic defects in ALS.

(ii) Trafficking in the soma

(a) Nuclear- cytoplasmic shuttling defects

Nuclear-cytoplasmic transport is a mechanism regulated by the nuclear pore complex (NPC). NPCs are formed by approximately 30 nucleoporins [412, 413] and they are composed of nucleoplasmic and cytoplasmic rings, with an inner ring complex. The central channel is composed of nucleoporins that possess prion-like domains that face the inner central channel, forming a selectively permeable phase separation mesh [414]. Small molecules, less than 30 kDa, can passively diffuse through the NPCs; however, larger molecules require nuclear transport receptors [415]. These receptors directly interact with the

prion-like domain network, guaranteeing efficient transport through the NPC. The majority of nuclear transport receptors are importins and exportins, which belong to the Karyopherin β family [416]. Interestingly, studies of yeast and *Drosophila* models of C9ORF72 have revealed that nuclear receptors are genetic modifiers of neurodegeneration [195, 196, 417, 418]. Moreover, poly-GR and PR cause defects in nucleocytoplasmic transport [419, 420]. Overexpression of cytoplasmic truncated TDP-43 also impaired nucleocytoplasmic transport [421]. Additionally, reduced expression or cytoplasmic mislocalization and aggregation of importins have been detected in brain and spinal cords of sALS, fALS and FTLD-FUS patients [11, 422-424]. Hence together these data imply that nucleocytoplasmic defects are a common and important mechanism in ALS and FTD.

It has been recently demonstrated that nuclear-cytoplasmic transport defects could be mediated by SGs assembly alterations. A study of poly-DPRs and cytoplasmic TDP-43 expression in human embryonic kidneys 293T (HEK293T) cells, revealed that nucleocytoplasmic transport factors were recruited into SGs [197]. Furthermore, SG assembly was concluded to be the underlying mechanism of disrupted nucleocytoplasmic transport, and treating C9ORF72 iPS-derived motor neurons with SG inhibitors resulted in recovery of nucleocytoplasmic transport defects [197]. Similarly, in a *Drosophila* model of C9ORF72, restoration of nucleocytoplasmic transport by inhibitors of SG assembly, was accompanied by inhibition of neurodegeneration [197]. Nevertheless, permanent stress granule inhibition could have a deleterious effect on cells since it regulates protein synthesis and it has been shown to compromise neuronal viability [425].

(b) ER-Golgi transport defects

Optimal ER-Golgi trafficking is essential for autophagy and axonal transport, as well as for proper function of the secretory pathway and the Golgi and ER organelles. ER-Golgi transport is inhibited in neuronal cells expressing mutant SOD1, TDP-43 or FUS [426]. However, expression of Rab1 restored ER-Golgi trafficking and prevented mutant SOD1-induced inclusion formation and apoptosis, implying that ER-Golgi trafficking is linked to neurodegeneration [426]. Furthermore, disruption of ER-Golgi trafficking by mutant SOD1 occurs in advance to ER stress, Golgi fragmentation, protein aggregation and apoptosis

[115]. C9ORF72 colocalize with different Rab family membranes, including Rab1, and C9ORF72 knock down has been linked to defective autophagy and endocytic trafficking [427].

Similarly, knockdown of TDP-43 in rat hippocampal neurons resulted in diminished endosomal transport [137]. Expression of TDP-43 ALS-mutants results in less efficient transport in rodent primary neurons compared to WT [135, 428, 429]. It has recently been proposed that this results from enhanced viscosity of axonal RNP granules due to mutations in TDP-43 [428].

ER stress and the UPR

The ER is an organelle with a crucial role in maintaining cellular homeostasis and function. It is responsible for the control of correct protein folding and processing of secretory proteins. ER stress results when homeostasis is perturbed by the accumulation of misfolded proteins within the ER. This leads to induction of the Unfolded Protein Response (UPR), a distinct set of signalling pathways that aim to resolve the load of misfolded proteins [430].

Misfolding of proteins can be triggered by alteration of the cellular redox state [431], nutrient deprivation [432], failure of protein post-translational modification [433], increased synthesis of secretory proteins and calcium imbalance [434]. Deregulation of the Endoplasmic-reticulum-associated protein degradation (ERAD) system, impairment of ER-Golgi transport and reduction of ER calcium levels, leading to inactivation of some ER-resident calcium binding chaperones, such as calreticulin, endoplasmic reticulum chaperonin (BiP) and Protein Disulfide Isomerase (PDI), can also trigger ER stress [435, 436].

The early phase of the UPR involves several cellular processes; i) inhibition of protein translation, ii) expansion of ER volume, iii) upregulation of ER chaperones that assist with protein misfolding, iv) increased activity of ERAD, which promotes the clearance of misfolded proteins from the ER by translocation to the cytosol, where they are degraded by the Ubiquitin-Proteasome System (UPS), and v) induction of macroautophagy [437, 438]. Overall, these events aim to resolve protein aggregation and accumulation within the ER, and thus restore cellular homeostasis [439]. However, if the UPR

cannot resolve these protein imperfections and ER stress is prolonged or severe, this can result in apoptosis [440]. During normal aging and under pathological conditions, ER stress can persist and the UPR shifts from having a protective role to becoming pro-apoptotic [441].

There are three major sensor proteins that detect the accumulation of misfolded proteins within the ER: protein kinase RNA like endoplasmic reticulum kinase (PERK), inositol requiring kinase-1 (IRE-1) and activating transcription factor 6 (ATF6) [442]. These sensors activate a signalling cascade, resulting in activation of transcription factors that inhibit protein synthesis and induce UPR genes. Under normal conditions the ER luminal domain of each UPR sensor protein binds to BiP, which maintains them in an inactive state [442]. BiP has a higher affinity for misfolded proteins than correctly folded proteins. Hence, under conditions of ER stress, it binds to misfolded proteins, resulting in its dissociation from each sensor protein [443]. This activates each UPR sensor resulting in initiation of the UPR cascade [443].

Activation of PERK leads to its dimerization and trans-phosphorylation [444], which results in further recruitment and phosphorylation of nuclear factor E2 related factor 2 (Nrf2) and serine 51 of eukaryotic translation initiation factor 2 α (eIF2 α) [445, 446]. Phosphorylation eIF2 α results in inhibition of protein synthesis and translation of specific transcription factors related to the UPR, such as activating transcription factor 4 (ATF4) [447]. Following activation, ATF4 translocates to the nucleus where it induces expression of specific genes encoding proteins involved in ERAD, ER chaperones [448], the antioxidant response and autophagy [449].

Activation of IRE1 results in auto-phosphorylation, which induces its RNase activity [437, 450]. This activity of IRE1 mediates the cleavage of ER associated mRNA causing their degradation and secondly, the cleavage of 26 base pairs from X-box binding protein -1 (XBP1) [451]. This leads to a change in reading frame in XBP1 mRNA, resulting in a potent bZIP transcription factor, spliced XBP1 [452]. Spliced XBP1 then translocates to the nucleus, where it controls the expression of genes encoding proteins involved in protein quality control (PQC), chaperones, and ERAD, as well as lipid synthesis to facilitate expansion of the volume of the ER [453].

Thirdly, activation of ATF6 by its dissociation from BiP exposes a Golgi localization sequence. Hence, under ER stress conditions, ATF6 translocates to the Golgi, where it is cleaved by two proteases (*site 1* and *site 2 proteases*) [454]. This produces the cytoplasmic domain of ATF6 that translocates to the nucleus, where it activates UPR genes [455, 456].

C/EBP homologous protein (CHOP), also known as DNA damage 153 (GADD 153), is a master regulator of the apoptotic pathway of the UPR. CHOP is downstream of both the PERK and ATF6 pathways, and in addition, the IRE1 pathway can induce expression of CHOP through XBP1 splicing [457, 458]. CHOP can induce expression of genes encoding pro-apoptotic proteins, including Bcl2-interacting mediator of cell death (BIM), p53 upregulated modulator of apoptosis (PUMA), Bcl-2-associated_X_protein (Bax) and Death receptor 5 (DR5) [458-460]. The IRE1 pathway also induces apoptosis through *Tumor necrosis factor* (TNF) receptor-associated factor 2 (TRAF2) and apoptosis signal-regulating kinase 1 (ASK1). This pathway activates extrinsic apoptosis, in which proteolytic activation of caspase-12/4 activates procaspase-9 to activate procaspase-3 [461]. At the same time, it also induces apoptosis through the upregulation of c-jun NH2 terminal kinase (JNK) [441].

ER stress and UPR activation in ALS

Induction of ER stress has been described in both sporadic and familial ALS. In sALS, most of the UPR proteins described before (eIF2 α , CHOP, ATF6, IRE1, PERK, Bip) and additionally PDI and Endoplasmic reticulum resident protein 57 (ERp57) were found upregulated in the spinal cord of patients [118, 462, 463]. UPR sensors, chaperones and apoptotic proteins were upregulated, in SOD1 G93A mice spinal cords, before symptom onset [464, 465], implying that ER stress is an early event in ALS pathology. Additionally, CHOP was upregulated in motor neurons and glia cells of the spinal cord in mutant SOD1 G93A transgenic mice [463].

In Neuro-2a (N2A) cell lines, induction of ER stress results in redistribution of WT and mutant TDP-43 to the cytoplasm [466]. In the same study, overexpression of WT and mutant TDP-43 lead to upregulation of ATF-6 and XBP1 and increased nuclear immunoreactivity for CHOP, indicating its

activation [466]. Moreover, TDP-43 and the UPR chaperone PDI co-immunoprecipitated from N2A cell lysates, and PDI was upregulated in spinal cords of A315T mutant TDP-43 mouse spinal cords [466]. Furthermore, overexpression of poly (GA) dipeptide repeat proteins, produced by non-ATG translation of the C9ORF72 repeat expansion, in neuronal culture increased neuronal death by triggering ER stress [171]. PDI is associated with protein misfolding in ALS, and overexpression of PDI and another ER chaperone, Erp57, are protective in neuronal cells expressing mutant SOD1 [467, 468].

Most of the proteins associated with ALS are not normally present within the ER. Hence, whilst it remains unknown how ER stress is triggered in ALS, several mechanisms have been postulated in relation to cytoplasmically localized ALS-associated proteins. These include indirect mechanisms whereby cytoplasmic SOD1 impairs ERAD or ER-Golgi transport, leading to accumulation of misfolded proteins within the ER and hence ER stress [115, 117, 119]. And also a direct mechanism for FUS and TDP-43 which were shown to induce ER-Golgi defects from the luminal side of the ER or its membrane, respectively [426].

Golgi fragmentation

Related to inhibition of ER-Golgi transport and ER stress, fragmentation of the neuronal Golgi apparatus has long been associated with ALS. The Golgi apparatus is an important cellular organelle responsible for the post-translational modification of proteins and lipids, as well as their sorting and trafficking. Proteins and lipids are first synthesized in the ER, from where they transit to the Golgi, where they are further modified by glycosylation, sulphation or proteolytic cleavage. From the Golgi, they are sorted and trafficked to their final destinations, such as the endo-lysosomal system, secretory granules or the plasma membrane [469]. In mammals, the Golgi apparatus is a stack of five to eight flattened membrane cisternae, which are inter-connected laterally by tubular structures that provide the characteristic ribbon morphology to the Golgi [470]. In neurons the Golgi is usually situated adjacent to the centrosome and it also extends to dendrites and axons. It consists of three functional

compartments, the *cis*-, media- and trans-Golgi network, and in neurites, it is present in Golgi outposts [471].

The structure of the Golgi is highly dynamic, and it can assemble and disassemble under physiological conditions. During mitosis, the Golgi is fragmented into vesicular and tubular structures that become dispersed in the cytoplasm to facilitate equal distribution to the resulting daughter cells [472]. However, this normal physiological mechanism can become pathological during disease conditions, and fragmentation of the Golgi then becomes irreversible [473]. Microtubule alterations [474, 475], or impaired secretory trafficking also leads to irreversible Golgi fragmentation [476]. This can subsequently lead to disruption of the secretory pathway, or perturbation of the post-translational modification and sorting of proteins.

Due to its central role in the secretory pathway, Golgi dysfunction in general can perturb cellular homeostasis that can lead to diseases such as ALS. Golgi fragmentation has been detected as an early event in animal models of ALS, prior to apoptosis, thus it has been implicated in the neurodegenerative process [477, 478]. In highly specialized cells such as neurons rely on this organelle for efficient transport in the cell body [479], which in turn may render them vulnerable to changes in Golgi morphology and function.

In ALS, Golgi fragmentation has been detected in motor neurons from the spinal cord, brainstem and cortex in both sporadic and familial ALS human motor neurons [480-483]. It has also been detected in transgenic mice models bearing ALS-mutant TDP-43 and SOD1 [474, 478, 484-487] and in cell lines and primary neurons overexpressing ALS-mutant Optineurin and VAPB respectively [318, 488, 489].

The molecular mechanism responsible for Golgi fragmentation is not fully understood; however, two mechanisms have been proposed. The first mechanism involves the alteration of microtubules [474, 475]. It has been shown in mouse models that Golgi fragmentation is caused by the disruption of polymerization of Golgi-nucleated microtubules [474, 475]. Secondly, Golgi fragmentation occurs when ER protein export is altered, or when vesicular trafficking from the Golgi is inhibited [115, 426, 490]. The formation of Golgi stacks requires continuous recycling of proteins from or to the ER, therefore

bidirectional vesicular transport with the ER is essential for Golgi organization [491, 492].

'Prion-like' mechanism or propagation of protein misfolding.

ALS has a focal site of onset with accentuated motor weakness in the spinal and bulbar regions that advances in an orderly and gradual manner through the anatomy during disease progression [22, 23, 493, 494]. The prion-like mechanism has been suggested to be a common pathological mechanism in neurodegenerative diseases such as prion diseases, Alzheimer's disease and ALS [495-499]. In this mechanism, misfolded aggregated proteins form seeds which serve as a template to trigger the aggregation of natively folded counterparts and are transmitted from cell to cell [500].

Prion-like domains are composed of polypeptide sequences rich in polar and aromatic residues, with no or few aliphatic and charged amino acids within their composition [375]. They are poor in terms of amino acid diversity, which is the reason why they are also named "Low complexity" (LC) domains. The prion-like or LC domains form self-templating fibrils spontaneously when isolated.. Proteins bearing these domains are implicated in a prion-like mechanism [23, 120, 375, 495, 501].

Misfolded proteins associated with ALS have been shown to serve as a template for replication of protein misfolding. When adding insoluble phosphorylated TDP-43 from post-mortem brain spinal cord tissue to human kidney HEK293T cells transfected with WT TDP-43, it induced its misfolding and this increased upon passaging the cells [502]. Furthermore, this was demonstrated using misfolded recombinant TDP-43 [503]. Similarly, adding detergent-insoluble fractions of ALS-disease brains to human neuroblastoma SH-SY5Y cells triggered the misfolding of intracellular TDP-43 in a seed dependent manner [504] and treatment of human glioblastoma U251 cells with ALS-FTD-CSF, but not ALS-CSF, resulted in mislocalization and aggregation of TDP-43 [505]. In addition, treatment of HEK293T cells with brain lysates from C9ORF72 mutation carriers resulted in poly-GA aggregation, demonstrating its seeding ability [199]. The seeding capacity of TDP-43 has been linked to the presence of a prion-like domain. Interestingly however, SOD1 doesn't possess

a prion-like domain, but its seeding ability has been demonstrated. Mutant SOD1 and misfolded WT SOD1 induced the misfolding on intracellular WT SOD1 in cell lines [119, 506]. Furthermore, the seeding potential of misfolded SOD1 has been demonstrated *in vivo*. Brain homogenates from symptomatic mutant SOD1 G93A transgenic mice were inoculated by sciatic nerve injection into asymptomatic mice from the same model, resulting in enhanced inclusion formation at 3 ± 0.2 months after injection and paralysis development [507]. This raises an interesting concept, where proteins without prion-like domains can act in the same manner than proteins with this specific domain.

Furthermore, these proteins have been implicated in a cell-to-cell transmission mechanism. Transmission of C9ORF72 DPRs to neurons was demonstrated in cells treated with either exosomes prepared from cells expressing DPRs or from incubation with conditioned media only. Interestingly, poly (PR)₅₀, one of the two most toxic DPRs, was significantly taken up from conditioned media only. These results suggest that C9ORF72 DPRs are transmitted via both exosome-dependent and independent mechanisms, however the specific mechanism mediating the uptake of DPRs remains unknown [198]. Similar results were obtained for TDP-43, although Feiler and colleagues demonstrated that more toxicity was observed in the receiving cells and cells preferentially took up exosomes containing TDP-43 compared to TDP-43 from conditioned media [504, 508]. Furthermore, SOD1 prion-like propagation has been demonstrated *in vitro*, and this was shown to induce ALS cellular features in the receiving cells [119]. So far, only SOD1 transmissibility has been demonstrated *in vivo*. However it has only been studied in mutant SOD1 transgenic mice, it has not yet been demonstrated in mouse lines expressing its wild type human form [507, 509].

Hence these data suggest that the spread of ALS is driven by a prion-like mechanism. However, more work is needed to elucidate the exact mechanism underlying ALS neurodegeneration, since it could be targeted with the goal to slow down or inhibit ALS progression.

1.2 Fused in Sarcoma

The *FUS* gene contains 15 exons and 14 introns, leading to the generation of 13 transcripts [510]. To date, two isoforms of *FUS* are listed on the curated Uniprot database (<https://www.uniprot.org/>): i) canonical FUS, which consists of 526 amino acids, and, ii) FUS isoform 2, a shorter version resulting from an alternate in-frame splice site in the 5' coding region, which generates a 525 amino acid protein [510, 511].

An additional transcript variant, containing 7 exons, has also been described, which omits exon 7, leading to a reading frame shift and a premature stop codon. This transcript is predicted to undergo nonsense-mediated decay (NMD), therefore no protein is annotated in Uniprot database. FUS binds to its own mRNA in exon 7 and flanking regions, thus repressing exon 7 splicing and therefore autoregulating its own expression [512].

FUS belongs to the FET protein family, composed of FUS, Ewing RNA-binding protein (EWS) and TATA-binding protein associated factor 2N (encoded by TAF15). All FET family members are fusion oncogenes that are ubiquitously expressed in the human body [513]. FET proteins have a conserved structure, containing a N-terminal glutamine-glycine-serine-tyrosine rich prion-like domain (QGSY-rich region), several arginine-glycine-glycine (RGG) domains, an RNA-recognition motif (RRM), zinc finger (ZnF) domain and a nuclear localization signal (NLS) (**Figure 1.2**). FUS is predominantly localized in the nucleus, but it normally has the ability to shuttle between the nucleus and the cytoplasm [514]. It has also been detected to be localized on dendritic spines upon neuronal stimuli [515, 516]. FUS has also been named '75kDa DNA-pairing protein' because of its 75 kDa apparent mobility in SDS-PAGE [517].

1.2.1 Structure of FUS

The domain structure of FUS is highly conserved among species. This conservation, which is common for all the FET family members, indicating their highly specialized functions.

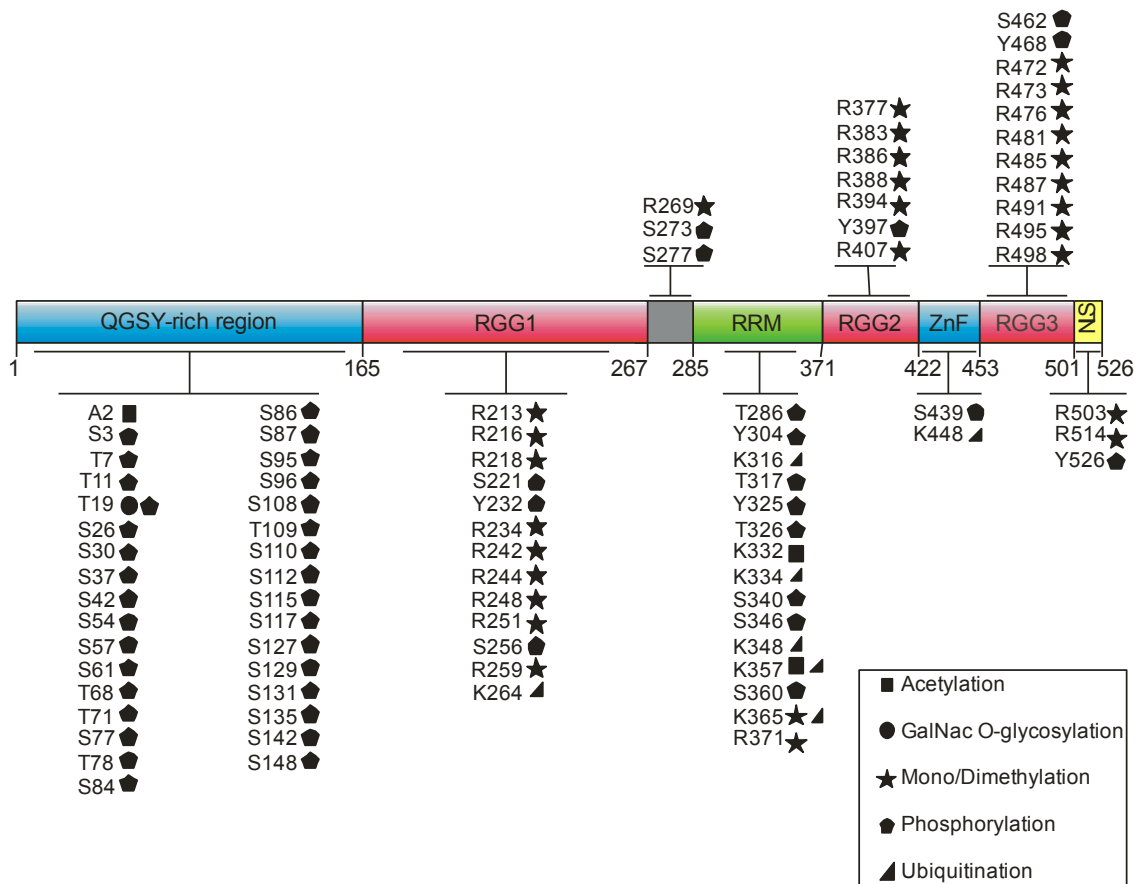


Figure 1.2 Schematic diagram of the domain structure of FUS, illustrating post-translational modifications (PTMs) Each symbol indicates the type and localization of each PTM. QGSY-rich region: Glutamine, Glycine, Serine Tyrosine-rich region; RGG: Arginine, glycine-rich region; RRM: RNA recognition motive; ZnF: Zinc finger domain; NLS: Nuclear localization signal.

Prion-like domain or Low complexity domain

When the human genome was analysed using an algorithm to detect prion domains, it uncovered 240 genes coding for proteins that possess a domain similar to the yeast prion domain. Approximately 30% of the proteins containing prion-like domains were annotated in the gene ontology (GO) molecular function as “RNA binding” and 33% were annotated as “DNA binding” proteins [518]. In a study using an algorithm trained to detect similar domains to the yeast prion-domain [519], out of 27,879 proteins FUS was ranked the 15th while TDP-43 69th [501].

The prion-like domain of FUS is intrinsically disordered and highly conserved [520-522]. It is mainly composed of serine, tyrosine, glycine and

glutamine residues and it also contains two charged residues. The FUS prion-like domain is composed of 24 tyrosine residues with a consensus motif of [S/G]-Y-[S/G], usually followed by one or two proline or glutamine residues [521].

The FUS prion-like domain is implicated in protein interaction, forming nuclear assemblies and RNP granules [127, 523]. *In vitro* experiments have suggested that the prion-like domain of FUS is required for its physiologically reversible phase separation, whereby it shifts from phase-separated liquid droplets to hydrogel droplets that possess amyloid fibrils structure [354, 368, 378, 524]. The latter structures were demonstrated to sequester other prion-like domain domains of other FUS molecules and prion-like domains from other RNA binding proteins, therefore acting like a scaffold for the formation of membrane-less organelles [378]. Under pathological conditions, these assemblies shift from a reversible conformation to a stable and irreversible fibrillar hydrogel, which are implicated in ALS and FTD pathology [371].

RNA-recognition motif domain

The RRM domain, which is responsible for binding to nucleic acid, is the most common RNA binding domain found in hnRNPs. FUS was initially also termed the 'hnRNP P2' protein, when discovered in myoxid liposarcoma [525]. Proteins containing RRM domains have important roles in RNA processing, splicing, export, stability, packaging and degradation [526]. A conventional conserved RRM domain has a $\beta 1$ - $\alpha 1$ - $\beta 2$ - $\beta 3$ - $\alpha 2$ - $\beta 4$ fold secondary structure. Interestingly, FUS lacks 2 aromatic residues with the $\beta 3$ fold that are responsible for conventional ring-stacking interaction between the RRM domain and nucleic acids [527]. Nuclear magnetic resonance (NMR) spectroscopy studies have revealed that FUS shares the classic secondary structure of RRM domains, but additionally it also contains an extended "KK-loop" between the $\alpha 1$ and $\beta 2$ folds, a common characteristic of the FET family [528]. Within this loop there are several conserved lysine residues that together with other positively charged residues define the nucleic acid binding site of FUS [528].

Nevertheless, the RRM domain of FUS has been demonstrated to bind nucleic acid [528, 529], even though its binding to RNA is very weak [528]. *In*

in vivo experiments determined that the RRM domain was dispensable for FUS RNA binding ability [514]. In contrast, in a *Drosophila* model, where 4 conserved phenylalanines from the RRM domain were mutated to leucines, the RNA binding capacity of FUS was abolished [357]. Subsequent studies that aimed to resolve these discrepancies revealed that combination of the RRM domain with an RGG domain displays a similar K_d to the RGG-Zn-RGG domain [529-531]. Both the RGG-RMM and RGG-Zn-RGG bound to DNA and RNA with the same affinity as full length FUS [529, 532]. A possible explanation for this will be discussed on RGG domain section.

It has been suggested that the RRM domain has an important role in conferring the toxicity of FUS in ALS. For example an *in vivo* study concluded that the RRM domain was required for FUS toxicity [533]. Later on, it was shown that the folded RRM domain has the ability to self-assemble spontaneously into amyloid fibrils *in vitro*, which explain its capacity to affect FUS toxicity in ALS [522].

In addition, the nuclear export sequence (NES) of FUS is located in the RRM domain. This short sequence (289 to 298 aa), was thought to target FUS from the nucleus to the cytoplasm through the NPC [534]. The NES activity of FUS is relatively weak and is probably negatively modulated by other domains, including RGG1 [535]. Consistent with this notion, a more recent study concluded that the NES of FUS was non-functional [536].

In conclusion, the ability of the RRM domain of FUS to bind DNA and RNA is not fully understood. However, since RRM domains are the most heavily translationally modified domains in human proteome [537], it is likely that the post-translational modifications (PTMs) of FUS play an important role in this aspect.

Zinc finger domain

The ZnF domain of FUS is a small protein motif in which one or more zinc ions are responsible for stabilization of the finger-like fold through cysteine and/or histidine residues. This domain was first identified to bind DNA but now is recognised to bind RNA and lipids as well [538]. All FET family members share

a conserved ZnF domain, where the zinc ion is coordinated through four conserved cysteine residues [510], but in FUS, it has been suggested that the ZnF domain plays a more important role in RNA recognition than the RRM domain [539]. In agreement with this idea, the ZnF domain was demonstrated to be necessary for SGs recruitment [540], where RNA is thought to act as a scaffold for RNA-binding proteins [390].

The arginine/glycine-rich domain

RGG/RG domains are the second most common RNA-binding domain in RNA binding proteins [541]. They are involved in multiple functions in RNA metabolism, protein-protein interactions and protein localization [542]. The FET family members possess a tri-RGG motif, containing three repeated RGG sequences of different length, interspaced by different domains [542]. The RGG/RG domain is the least conserved among FET family members.

The RGG/RG domains are intrinsically disordered, which is not surprising given that β -turns are the major structural component of RGGs [543]. The low complexity of RGG/RG domains is thought to provide a flexible and plastic conformation that guarantees recognition of a wide variety of RNAs. The first RGG1 domain of FUS contains an additional potential prion region, which is necessary for FUS aggregation [533]. This region also confers the DNA damage response capacity of FUS, because it contains the binding site for Poly (ADP-ribose) (PAR), and it also binds to G-quadruplex structures in telomeric DNA and non-coding telomeric RNA [158, 544].

As discussed above, it has been challenging to determine the domain responsible for the RNA binding capacity of FUS. A recent study concluded that the FUS RGG/RG domains co-operate with the other RNA binding domains of FUS to increase its affinity for RNA [545]. This finding is consistent with other studies which found that combination of RGG/RG with either the RRM or ZnF domain displayed the same binding capacity as full length FUS [529, 532].

In summary, the RGG domain of FUS is involved in a wide range of its functions. The relatively high proportion of arginine residues in this domain renders it susceptible to post-translational modifications that are likely to impact FUS's physiological and pathogenic functions.

The PY nuclear localization signal

Some of the functions of FUS are related to its ability to shuttle between the nucleus and cytoplasm. FUS binds to RNA in both the nucleus and cytoplasm, and it is involved in mRNA export and mRNA transit to neuronal dendrites [514, 515, 546]. FUS localization in the nucleus was predicted to be mediated by a non-classical R/H/KX₂₋₅ PY nuclear localization signal (PY-NLS) [547] and this was later confirmed experimentally [535, 548]. More recently, the RGG3 domain of FUS has also been implicated in its nuclear translocation [549].

The nuclear import of FUS involves recognition and binding of specific residues in the PY-NLS by Transportin (also known as Karyopherin β 2), which is responsible for translocating protein through the NPC [547, 548, 550]. The PY-NLS of FUS has been divided into specific different regions according to the nature of its interactions: Epitope I (⁵⁰⁸PGKM⁵¹¹), the hydrophobic motif, Epitope II (⁵¹⁴RGEHRQDRR⁵²²), composed of an arginine rich helical region, and Epitope III (⁵²¹RRERPYPY⁵²⁶), the PY fragment. The PY-NLS of FUS interacts with Transportin (TNPO1) via hydrophobic and electrostatic/polar interactions with the central helix sequence [551, 552]. The PY-NLS regions of other proteins bind to TNPO1 in their fully extended form, whereas FUS contains epitope II, an atypical central helical region, that is connected to epitopes I and III by short linker sequences [552].

The nuclear import of FUS is therefore essentially modulated by the interaction between FUS PY-NLS and TNPO1, hence any impairment of this interaction should alter the localization of FUS. In ALS, mutations in the C-terminal PY-NLS domain, as well as methylation and phosphorylation, disrupt this interaction [344, 548, 549, 553, 554]. Interestingly, the impairment of binding affinity between FUS and TNPO1 correlates with FUS mislocalization in the cytoplasm and the duration of ALS progression [548, 551].

1.2.2 Post-translational modifications of FUS

There are more than 200 possible protein PTMs [555], which are mostly catalysed by specific enzymes that recognize target sequences in specific

proteins. PTMs can affect the folding of a protein, its subcellular localization, its ligand binding capacity and its function.

FUS is subjected to a wide range of PTMs, including methylation, citrullination, phosphorylation, ubiquitination, O-GlcNAcylation and acetylation (**Figure 1.2**). Hence, it is likely that PTMs play an important role in the structure, localization and/or functions of FUS and importantly, PTMs fine-tune the pathogenic role of FUS in ALS.

Methylation

Methylation of lysines and arginines is a common protein modification carried out by methyltransferases. Arginine methylation has been implicated in the regulation of RNA processing, DNA damage and repair, protein translocation, gene transcription and signal transduction [556].

FUS has 20 sites of asymmetric dimethylation, and most of these are located at the C-terminal RGG3 domain [557]. Asymmetric dimethylation of some RNA binding proteins has been related to their nuclear-cytoplasmic shuttling [558]. Protein arginine methyltransferase 1 and 8 (PRMT1, PRMT8) bind to FUS and are responsible for its methylation [559-563].

Cytoplasmic FUS is found asymmetrically dimethylated in the inclusions of ALS-FUS patient spinal cord sections [549]. Whilst arginine residues in the RGG3 C-terminal domain of FUS are responsible for direct binding of FUS to TNPO1, [548, 549], hypomethylated FUS bound TNPO1 with high affinity, but this binding was very weak for asymmetrically methylated FUS [563]. Hence this finding implies that in ALS, nuclear import of FUS is impaired by disruption in binding to TNPO1 by mutations in the NLS. This would be further exacerbated by methylation of the RGG3 arginines, contributing to its cytoplasmic mislocalization and aggregation. Supporting this hypothesis, depletion of methylation, either by knock down of PRMT1, or by treatment with a global methyltransferase inhibitor, reduced cytoplasmic mislocalization and aggregation of ALS mutant FUS [282, 564]. However, prolonged treatment with high concentrations of a global methyltransferase inhibitor triggered intranuclear aggregation of mutant FUS [564].

In contrast to ALS, the pathological hallmark of FTLD is co-aggregation of FUS in FTLD-FUS patient's brains with TNPO1, TAF-15 and EWS [422, 565-567]. However, mutations in FUS are not considered causative of FTLD-FUS [568-570]. Recently, it was determined that in FTLD-FUS, cytoplasmic FUS is unmethylated and to a lesser extent, mono-methylated in these inclusions [563]. Monomethylated and unmethylated FUS display very strong affinity to TNPO1, further promoting co-aggregation of both proteins in pathological inclusions and further impairing nuclear transport of FUS [563].

Additionally, the hypomethylated state of FUS in FTLD has been recently linked to regulation of phase separation droplets [371, 571], a tightly regulated mechanism whereby methylation of arginines in the C-terminal domain of FUS modulates cation- π interactions with tyrosines from the N-terminal prion-like domain of FUS. These interactions regulate FUS assembly into more rigid structures [371]. Hypomethylated FUS assemblies were shown to display hydrogel-like structures, as determined by the increased presence of stiffer, non-spherical components, richer in antiparallel cross- β sheets, and increased hydrogen bonding [371]. It was further demonstrated that FUS hypomethylation was related to FTLD-FUS, RNP granule function [371].

Together these findings reveal that the methylation of FUS plays different roles in the pathology of FTLD and ALS. However, the effect of the methylation profile of FUS on its physiological functions remains unknown. One study demonstrated that FUS and PRMT1 act together to synergistically co-activate transcription, a process that is regulated by FUS methylation [559]. It remains to be determined if the other RNA/DNA binding functions of FUS are modulated by its methylation state.

Phosphorylation

Phosphorylation of FUS is involved in its nuclear-cytoplasmic shuttling, its response to DNA damage and regulation of its aggregation and phase-transition capacity. The N-terminal prion-like domain of FUS is highly phosphorylated, as it is rich in serine, threonine, glutamine, asparagine and

tyrosine residues. However, phosphorylation of FUS in its C-terminal domains has also been reported [572]. The first study describing the phosphorylation of FUS demonstrated that phosphorylation on serine 256, in the first RGG domain, prevented degradation of FUS by the proteasome [572].

Since FUS nuclear shuttling is mediated by the interaction of its NLS and TNPO1, it is not surprising that phosphorylation of the NLS is implicated in impairment of its nuclear import. Phosphorylation at the C-terminal residue Y526 by Src family kinases Fyn and c-Src, prevented its interaction with TNPO1 and lead to cytoplasmic accumulation [553].

Phosphorylation of the prion-like domain of FUS is also involved in its cellular localization, which is related to its function in DNA damage and repair. FUS was found to be phosphorylated at Ser42 by ATM (ataxia-telangiectasia mutated), a member of the phosphoinositide 3-kinase-like kinase (PIKK) family, as a response to induction of double-strand breaks (DSBs) by ionizing radiation [573]. However, another study reported conflicting findings, that DNA-dependent protein kinase (DNA-PK) is responsible for FUS phosphorylation, not ATM [574]. Subsequently, it was shown that induction of DNA damage in human astrocytes and primary neurons triggers phosphorylation of FUS at the N-terminus prion-like domain and this regulates the translocation of FUS into the cytoplasm [574]. According to this, a more recent paper found that inhibition of DNA-PK restored the nuclear localization of FUS [575].

In recent years, many studies have focused on identifying the mechanism underlying FUS aggregation and phase-separation. DNA-PK phosphorylation and phosphomimetic substitution in the prion-like domain delayed aggregation and phase separation of FUS in the presence of RNA or salt [576, 577]. DNA-PK impairs the ability of FUS to be incorporated into hydrogels [368] and FUS prion-like domain phosphorylation and phosphomimetics introduce electrostatic changes, which disrupted the nature of the prion-like domain [576]. Interestingly, this inhibited aggregation and cytotoxicity of FUS in a yeast model [576] and in addition to the 14 phosphorylation sites within the prion-like domain targeted by DNA-PK, other phosphorylation sites not targeted by DNA-PK were also identified, implying a role for other kinases [576].

Two recent studies aimed to determine the region of the prion-like domain involved in regulation of the phase separation of FUS, and the role of phosphorylation in this process. Whilst the two studies had differing conclusions as to the identity of the core sequence responsible for the assembly of FUS into fibrils, they both agreed that FUS fibril formation is controlled by phosphorylation of specific sites in this sequence. Murray and colleagues concluded that DNA-PK-mediated phosphorylation of residues 42-87 inhibits FUS hydrogel and droplet formation [578], whereas Luo and colleagues determined that phosphorylation of Ser42 is critical for amyloid fibril formation [579]. Nevertheless, the important role of FUS phosphorylation on key pathways implicated in ALS, including nucleocytoplasmic shuttling, DNA damage and phase transition, implies that this PTM may be an interesting therapeutic target.

Ubiquitination

Ubiquitination is a reversible post-translational modification whereby ubiquitin binds to lysine residues within a target protein. Whilst there are various types of ubiquitination, polyubiquitination is responsible for driving proteins for degradation via the proteasome and autophagy [580, 581].

FUS inclusions that are also immunopositive for ubiquitin are a common trait of several diseases affecting neurons, in the spinal cord in fALS, sALS [12], and in a subtype of FTLD, aFTLD-U [156, 569]. In motor neuronal cell lines, co-expression of mutant FUS with red fluorescent protein tagged (RFP)-ubiquitin resulted in 30% of FUS inclusions being positive for ubiquitin 72h post-transfection [582]. However, whilst the available evidence demonstrates that FUS inclusions are co-labelled with ubiquitin, there is little evidence for the direct ubiquitination of FUS itself.

The degradation of FUS is proteasome-dependent but rarely, independent of its ubiquitination status [572]. Similarly, ubiquitination of FUS was not detected in biochemical analyses of the insoluble fraction of two fALS patient spinal cords [583]. In contrast, mass spectrometry analyses identified ubiquitination of FUS predominantly in its C-terminal domains (residues: K264, K316, K334, K348, K357, K365, K448) but the ubiquitylation status and its

consequence to the function of FUS has not been characterised [584-588]. FUS also functions as a SUMO E3 ligase for Ebp1, promoting its SUMOylation (attachment of the SUMO proteins to lysine residues). Interestingly, the same study proposed that FUS is SUMOylated itself [589].

Further studies are therefore needed to confirm whether FUS is ubiquitinated, and to determine the role of ubiquitin in the function and degradation of FUS. Since SUMOylation can function as a secondary signal for marking proteins for ubiquitin-dependant degradation [590], the role of this PTM on the degradation of FUS should also be examined.

O-GlcNac

O-GlcNAcylation is a reversible and dynamic PTM of protein Ser/Thr residues, involving the addition of β -d-N-acetylglucosamine (GlcNAc) groups via an O-linkage. Mass spectrometry analysis revealed that FUS was O-GlcNAc glycosylated at residue T19 in HEK293 cell lines [591]. However, in contrast, surprisingly a more recent study failed to detect the presence of O-GlcNAc on FUS in different neuronal (Neuro2A, SH-SY5Y, A172) and non-neuronal (P19, HeLa, HEK 293T) cell lines by western blotting [592]. Moreover, FUS was found to be O-GlcNAcylated upon induction of oxidative stress, providing a possible explanation for the different findings obtained in these two studies [593].

Acetylation

Global protein acetylation is protective against Parkinson's disease and Alzheimer's disease protein aggregation [594, 595] on the contrary, in ALS, acetylated TDP-43 was detected in ALS patient spinal cords, where it impaired the RNA binding capacity of TDP-43 and promoted its hyper-phosphorylation and aggregation [144]. Importantly, proteins in ALS spinal cords were differentially acetylated compared to controls [596]. Mass-spectrometry studies of human biological samples have identified three possible acetylation sites in FUS, at residues A2, K332, and K357 [588, 597, 598]. However the function of this PTMs, and the acetylation profile of FUS under pathological conditions, has not been investigated. Inhibition of histone deacetylases (HDAC) 6 in motor

neurons from FUS ALS patients ameliorates impairment of axonal transport [599]. Whilst this could be linked to α -tubulin acetylation, it is possible that HDAC6 acts directly on mutant FUS. More studies are therefore needed to determine if FUS acetylation is involved in ALS.

In summary, these findings reveal that the major domains of FUS are subjected to numerous PTMs, particularly the prion-like domain and the RGG3 domain. These modifications can affect the localization and conformation of FUS, which has implications for ALS.

1.2.3 The normal cellular functions of FUS

DNA damage

FUS has been implicated in several DNA damage and repair processes. Fibroblast and lymphocytes from FUS $-/-$ mice lines were first shown to be sensitive to radiation and genomic instability [600, 601], implying that FUS functions in the repair of DNA damage and genomic integrity.

DSBs can normally be repaired by two major pathways: homologous recombination (HR) and nonhomologous end joining (NHEJ). FUS binds to duplex DNA and also to single-stranded DNA, an important process in HR [602, 603]. Baechtold and colleagues demonstrated that the formation of D-loops correlates with the concentration of FUS, and they identified that the C-terminal domain of FUS was responsible for this function [517]. Subsequently, it was demonstrated that the RRM domain also possesses DNA binding ability [528].

The most common pathway for DNA damage repair, particularly in neurons, is NHEJ. FUS is recruited to DSB sites together with PARP and HDAC1 [158, 604] during the early stages of DNA repair, since FUS localizes to these sites prior to recruitment of markers of DNA damage or proteins involved in DSB repair [604]. FUS is recruited to DNA damage foci in a PAR dependent manner, promoting DNA repair either by NHEJ or HR, downstream of PARP [158, 605]. Interestingly, it was later shown that PAR chains act as a seed for the formation of cytoplasmic FUS droplets in DNA damage associated compartments [605]. Therefore, this evidence links FUS to the formation of liquid droplets that would further recruit other DNA repair factors under

conditions of cellular stress [354]. Consistent with these findings, knockdown of FUS abolished the formation of γ H2AX foci, the most widely used marker of DNA damage, after DSBs [604]. RNA Binding Motif Protein 45 interacts with FUS and may negatively regulate the interaction between FUS and HDAC1, therefore preventing excessive recruitment of HDAC1 to sites of DNA damage [606]. DSBs are also related to transcriptional abnormalities that are associated with DNA damage. Recently, Furthermore, FUS depletion impaired the capacity to prevent or repair R loop-associated DNA damage [607].

The ends of chromosomes are protected by telomeres, repetitive sequences that shorten with aging and fold in G-quadruplex structures in the presence of Na^+ and K^+ . Expression of WT FUS resulted in shortening of telomere length by binding of its RGG3 domain to telomeric DNA and telomeric repeat-containing RNA (TERRA). This triggers the recruitment of histone-modifying enzymes which inhibit elongation of telomeres [544, 608]. Tyrosine and phenylalanine residues within the RGG3 domain of FUS are required for the formation and regulation of binary and ternary complexes with telomeric DNA and TERRA [609].

Transcription

FUS binds to RNA Polymerase II (RNA Pol II) and regulates its phosphorylation at the C-terminus [529, 610, 611]. Knockdown of WT FUS in human fibroblasts leads to aberrant accumulation of Ser-2 phosphorylation on RNA Pol II near the transcriptional start site, which also correlated with its altered nuclear distribution [612]. Additionally, FUS depletion perturbs back-splicing leading to the formation of circular RNAs (circRNAs), which regulate transcription by interacting with the RNA Pol II machinery [613]. In contrast, FUS can inhibit RNA3 activity by suppressing transcription of the 5S ribosomal RNA (rRNA) and small RNAs [614].

FUS binds to chromatin and this is required for regulation of transcription [523]. Additionally, FUS can function as a transcription factor by binding to various promoters [157, 615, 616]. FUS also interacts with RNPA2 and other transcription factors: IID (TFIID) and IIIB (TFIIIB) [527, 614, 617, 618]. FUS also

interacts with Androgen Receptor (AR), together with scaffold attachment factor B (SAFB1), which regulates ligand-dependent transcription [619].

Splicing and mRNA processing

FUS is known to bind to thousands of RNA within the cell [342, 620]. However, whilst numerous studies have tried to elucidate the target RNA motifs of FUS, the results have been conflicting. The first study that identified the RNA binding motifs of FUS found that recombinant FUS binds to GGUG motifs with nanomolar affinity [531]. An *in vitro* study using the recombinant RMM domain of FUS demonstrated that FUS binds to CGCGC motifs of RNA [621]. However, an NMR study determined that the ZnF domain of FUS binds to a GGUG motif, but no interaction was detected for the RRM domain [539]. Some CLIP-based studies have identified that FUS binds to GGU and GUGGU RNA motifs; although the enrichment of this binding was low [622, 623]. Several studies determined that FUS binds to GU-rich regions but no consensus motif was identified [512, 624].

A recent study in which RNA CLIP-sequence tags were normalized to Nascent-sequence tags, identified six combinations of motifs (UGUG, CUGG, UGGU, GCUG, GUGG, and UUGG) [625]. Other studies have found that FUS has a preference for RNA regions instead of specific motifs. FUS binding-sites were identified at 3' untranslated regions (UTR) of transcriptional targets and also in antisense RNA [342, 622, 623, 626]. However, a common finding amongst these studies is the affinity of FUS to bind to long introns, and to be enriched in the 5'UTR of long introns [622, 623]. This implies that FUS binding to RNA is quite promiscuous, and the involvement of several different domains of FUS in its RNA binding ability is consistent with this notion

Regardless of the specific RNA binding motifs, FUS has been widely implicated in RNA splicing. A CLIP-seq study in HeLa cells demonstrated that FUS regulates its own expression by binding to exon 7 [512]. Additionally, overexpression of WT and ALS-mutants FUS in *Drosophila* resulted in 90% down-regulation of FUS [627], confirming its auto regulation capacity.

Genome wide array studies have revealed that FUS regulates pre-mRNA splicing [620, 622, 623]. FUS interacts with splicing factors [628, 629], splicing

complexes [630] and small nuclear ribonucleoproteins (snRNPs) [617, 631, 632]. FUS also binds to SMN, a core protein involved in snRNPs biology. Recently a study involving human WT FUS expressed in mice, revealed that FUS and SMN function in a co-operative manner [631, 633, 634]. FUS also regulates RNAPII phosphorylation, a factor in the splicing cascade [610]. Additionally, FUS mediates the interaction between RNAPII and U1 snRNP, thus coupling transcription to splicing [159]. Furthermore, mRNA length is regulated by the binding position of FUS in the nascent RNA [624].

FUS co-purifies with micro RNA (miRNA) Drosha complexes and facilitates its recruitment to miRNA genes [635, 636]. FUS also promotes the biogenesis of miR-9, miR-132 and miR-134, which are involved in neuronal development and synaptic plasticity [636]. Furthermore, FUS interacts with argonaute-2 (AGO2), a component of the microRNA-induced silencing complex (miRISC), and it mediates microRNA gene silencing, which was also confirmed with its homologous counterpart in *C.elegans* [637]. Overexpression of WT FUS disrupted miRNA processing in the cytoplasm by triggering cellular stress [638]. In a recent study, a feed-forward regulatory loop between FUS and miR-141/200a was identified and in the same study, interestingly, miR-200a was also upregulated in Alzheimer's and Huntington's disease [639].

FUS is also involved in minor intron splicing, which is necessary for the correct splicing of a subset of mRNAs involved in muscle function, and postnatal maturation of spinal motor neurons [628]. Immunoprecipitation of FUS revealed that it binds to Mapt, Neurofilament Light Protein (NEFL), and NEFM [623] [640, 641]. Additionally, FUS expression regulates exon inclusion/exclusion of genes involved in neuronal development, neuronal function and neurodegeneration [620, 622]. This suggests that the splicing functions of FUS are closely related to the nervous system.

mRNA transport and local translation

The ability of FUS to shuttle between the nucleus and the cytoplasm is linked to the transport of mRNA to the cytoplasm [514]. In neurons, mRNA and proteins need to be transported over relatively long distances to reach the dendrites or axons, where they become translated or function respectively.

FUS has been linked to axonal transport by its association with motor proteins MyosinVA [642], Myosin VIO [643] and conventional kinesin [644]. FUS also associates with mRNA encoding the actin-stabilizing protein Nd1-L in mouse brains in response to glutamate receptor 5 (mGluR5) activation [515, 546, 645]. Furthermore, as well as its association with the transport machinery, FUS can also assemble into RNP [354, 368, 379]. FUS has been detected in synaptic spines, where it modulates local translation, affecting regulation and maturation of spine morphology [515, 646]. FUS knockdown mice present downregulation of AMPA receptor Glua1, which inhibited synaptic maturation [647]. Mice overexpressing human WT FUS displayed a progressive disruption of NMJ, and less Synaptophysin in the pre-synapse, indicating that overexpression of FUS impairs synaptic protein translation [648]. Recent super-resolution microscopy studies demonstrated that FUS localizes in axon terminals and co-localizes with Synaptophysin in rat hippocampal neurons [649]. Adenomatous polyposis coli (APC) target RNAs to cell protrusions, where they form APC-containing ribonucleoprotein complexes (APC-RNPs). FUS was detected in APC-RNPs where it modulated translation of mRNAs localized in these RNP complexes [646]. Similarly, a mass spectrometry study determined that FUS interacts with fragile X mental retardation protein (FMRP), a translational repressor that controls synaptic function [277]. Additionally, FUS has been purified from polyribosomes, further suggesting its has an active role in translation [650]. It is likely that any alterations in the phase separation properties of FUS would impact on its regulatory activities on translation and in its mRNA transport capacity, leading to axonal defects [411, 599].

1.3 The role of FUS in ALS

FUS mutations account for approximately 35% of juvenile fALS cases. Indeed, the overall average age of onset of FUS ALS (sALS and fALS) is 43.8 ± 17.2 years [651-654], which is younger than patients with C9ORF72, SOD1 or TDP-43 mutations [652]. Most FUS fALS cases display missense mutations that are inherited in a dominant fashion with incomplete penetrance [221] although one recessive mutation has been identified in 4 members of the same family [4]. *De novo* FUS mutations have also been identified in sALS cases, which are

associated particularly with early and bulbar onset forms of ALS [9, 655]. A comprehensive list of *FUS* mutations identified in ALS is displayed in **Table 1.1**, most of which are clustered at the C-terminus of FUS (**Figure 1.3**).

In *FUS*-associated ALS, the neuropathology observed in patient motor neurons is very diverse. Basophilic inclusions and round *FUS* immunoreactive cytoplasmic inclusions are detected in early onset cases of ALS, whereas for late onset cases, *FUS* immunoreactive inclusions are present in the cytoplasm of motor neurons and glial cells [7, 12, 226]. Together these data demonstrate that *FUS* inclusions display different morphologies in human patient tissues.

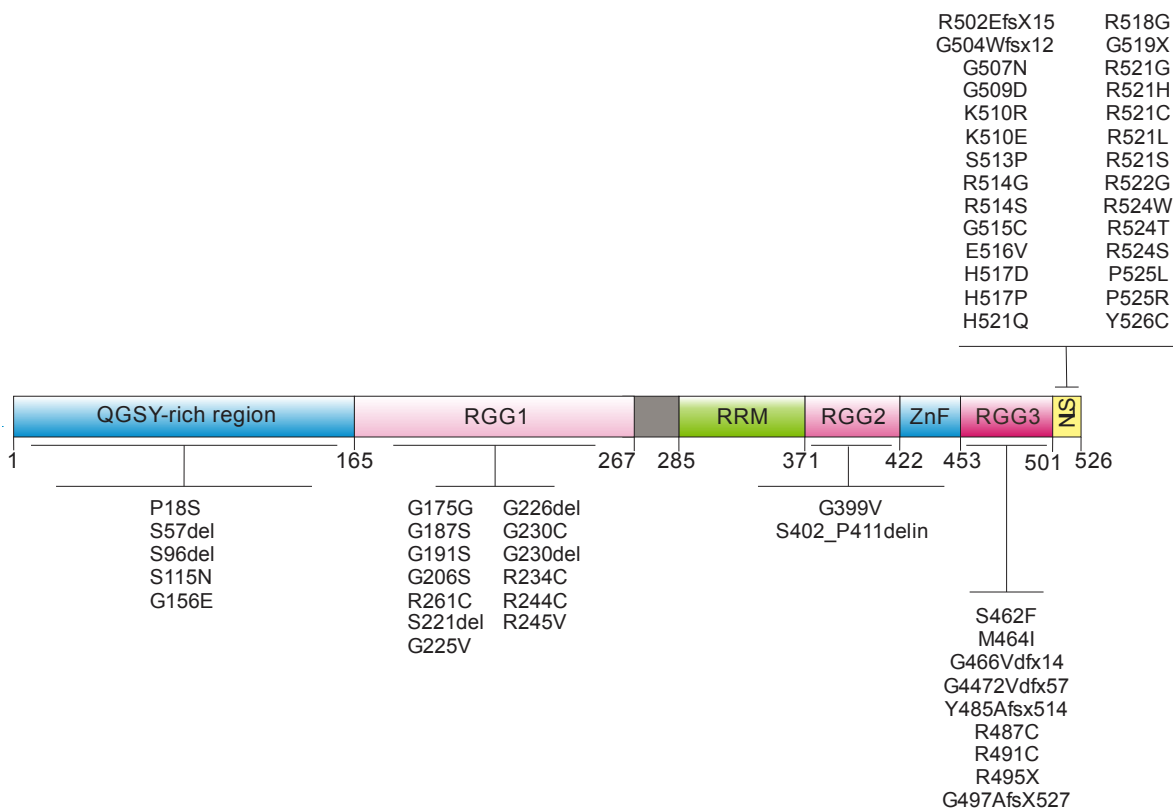


Figure 1.3 FUS domain structure with the mutations associated to ALS QGSY-rich region: Glutamine, Glycine, Serine Tyrosine-rich region; RGG: Arginine, glycine-rich region; RRM: RNA recognition motive; ZnF: Zinc finger domain; NLS: Nuclear localization signal.

Table 1.1 FUS mutations in ALS colour coded according to the domains of Figure 1.3.

Mutation	% of patients		Mean age of onset	Mean Duration (months)	Site of onset	Ref.
	fALS	sALS				
P18S	-	2/475	36,74	-	Limbs	[656]
S57del	0/80	1/145	80	10	Limbs	[656]
S96del	1/476	0/41	20s	216	NA	[657]
S115N	0/97	1/1192	60	27	Cervical	[658]
G156E	1/94	-	33	11	Bulbar	[151]
G175G	1/292	0/293	65	31	NA	[4]
G187S	0/32	1/168	79	14	Bulbar	[659]
G191S	1/45	0/964	43	108	Limbs	[152]
G206S	1/476	0/41	54	NA	NA	[657]
R216C	0/45	1/964	50	NA	NA	[152]
S221del	0/48	1/480	69	62	Bulbar	[660]
G225V	0/45	1/964	26	60	Limbs	[152]
G226del	-	1/454	62	5	Bulbar	[656]
G230C	0/45	1/964	65	NA	Limbs	[152]
G230del	0/9	1/249	59	NA	Limbs	[661]
R234C	0/45	1/964	40	120	Limbs	[152]
R234L	1/94	-	66	NA	Spinal	[151]
R244C	1/292	0/293	54	28.5	NA	[4]
R245V	0/5000	1/500	71	96	-	[662]
G399V	0/9	1/249	73	NA	Bulbar	[661]
S402_P411delinsGG	0/17	1/91	65	13	Bulbar	[663]
S462F	1/52	-	63	24	Limbs	[664]
M464I	-	1/1	74	24	Limbs	[665]
G466Vfdx14	0/17	1/91	20	22	Bulbar	[663]
G472Vfdx57	1/1	-	26	12	Limbs	[666]
Y485Afsx514	1/476	0/41	NA	18	NA	[657]
R487C	0/97	1/1192	80	36	Bulbar	[658]
R491C	0/500	1/500	65	84	Bulbar	[662]
R495X	3/647	3/1725	26.8	15	Limb / Bulbar	[356, 512, 657, 658,

						661]
G497AfsX527	1/276	0/41	29	14.3	Limbs	[657]
R502EfsX15	-	1/454	49	60	Limbs	[656]
G504Wfsx12	1/16	1/359	22.7	6	Limbs/NA	[661, 667]
G507N	0/87	4/2604	57.5	42	Limbs/NA	[6, 152, 668]
G509D	0/500	1/500	50	13	Limbs	[662]
K510R	3/580	0/133	48	84	Limb/NA	[669]
K510E	2/62	-	30.5	9	Limb/NA	[670]
S513P	1/40	-	60	NA	NA	[670]
R514G	1/198	-	NA	NA	NA	[5]
R514S	4/514	2/296	34.4	32	Limbs/NA	[4, 670, 671]
G515C	1/292	0/293	NA	NA	NA	[4, 153]
E516V	-	1/1	44	36	Limbs	[671]
H517D	1/15	-	42	>36	Bulbar	[154]
H517P	1/40	-	30	NA	NA	[670]
H517Q	1/292	0/293	45	168	NA	[4]
R518G	-	1/1523	46	NA	Limbs	[6]
G519X	-	1/454	20	12	Limbs	[656]
R521G	5/869	2/1093	45.9	26.9	Limbs, NA	[4, 151, 154, 221, 512, 657, 667, 672-674]
R521H	17/1605	3/4040	46.3	38.4	Limbs, cervical, NA	[4-6, 153, 656-658, 664]
R521C	33/1731	6/5757	39.4	32	Limbs, bulbar, NA	[4-6, 151-153, 221, 656-659, 664, 670, 672, 675]
R521L	3/667	1/731	41.8	29.7	Limbs	[153, 657, 660]
R521S	1/133	-	54	20	Limbs	[153]
R522G	1/292	0/293	28.5	25.1	NA	[4]
R524W	2/42	0/548	58	33.7	Limbs	[668]
R524T	1/292	0/293	61.6	32.9	NA	[4]
R524S	3/768	0/334	41	39	Limbs, NA	[4, 657]
P525L	4/891	9/1692	21, 10, 11	14	Limbs, bulbar, NA	[4, 7, 35, 225, 657, 660, 667, 672]
P525R	-	-	26	12	Limbs	[676]
Y526C	-	1/1	25	<12	Bulbar	[10]

NA= Not applicable

The pathological mechanisms induced by mutant FUS in ALS are thought to result from a combination of a gain of toxic function by cytoplasmic FUS aggregates, together with a loss of function by the partial clearance of nuclear FUS. Evidence for the existence of both mechanisms was provided by a study involving transgenic mice expressing ALS-linked R521G mutant FUS, that displayed evidence of DNA damage together with dendritic and synaptic abnormalities. Loss of the FUS-HDAC1 interaction due to sequestration of FUS into RNP complexes resulted in DNA damage, combined with stabilization of interactions between FUS and Brain-Derived Neurotrophic Factor (BDNF) mRNA, which impeded splicing of the latter leading to dendritic and synaptic impairment [677]. It is likely that misfolded FUS induces ALS by an intriguing and complex interplay between several different cellular mechanisms, including disruption to nucleo-cytoplasmic shuttling, impaired liquid:liquid phase separation, ER stress, Golgi fragmentation, altered DNA damage response and RNA defects, as discussed below. Chapter 5 describes in detail the mechanisms induced by mutant FUS that involve the ER-Golgi compartments; Golgi fragmentation, ER stress and disruption of ER-Golgi transport, as well as the prion-like mechanism. The remaining mechanisms will be discussed below (**Figure 1.4**).

1.3.1 Defects in RNP granules/liquid phase transition

FUS immunoreactive inclusions colocalize with SGs markers in fALS and FTD [548], in fALS FUS patients iPSCs [678] and in cell lines expressing ALS-associated mutant FUS [679]. Interestingly, in asymptomatic P525L FUS fALS fibroblasts, heat shock and DTT treatment resulted in the localization of FUS in SGs and delayed the disassembly of these SGs, suggesting SGs impairment might be an early disease event [680]. Under conditions of oxidative stress or heat shock, mutant FUS localizes to SGs and P-bodies [533, 548], whereas WT FUS accumulates in SGs only during osmotic stress, and not during oxidative stress, heat shock or ER stress [681, 682]. Similar to other RNA binding proteins with IDD domains, under stress conditions, FUS localizes to RNP complexes, and in physiological conditions it undergoes liquid-liquid phase transition. However, in ALS or FTD, the transition from LLPS to an irreversible

fibrillar hydrogel state of FUS is accelerated [354, 378, 379, 548]. Unlike TDP-43, the phase separation of FUS is not dependent on specific residues [371, 577], instead it is driven by valence interactions between the N and C-terminal domains [371]. PTMs of FUS affects its interactions and binding to chaperones such as TNPO1 via masking key residues of FUS responsible for this interaction, thus affecting FUS phase transition [370, 371, 571, 574, 576, 578, 683].

The propensity of mutant FUS to form a hydrogel state results in both a loss of function by sequestration of FUS, and also a gain of toxic function by sequestering several other proteins, therefore perturbing its normal function. Consistent with this notion, mutant FUS expressed in SH-SY5Y cells aggregates and colocalizes with eIF3, and recruits endogenous FUS upon sodium arsenite treatment [684]. Reduced protein synthesis was also detected in axonal termini of primary *Xenopus* retinal neurons overexpressing ALS/FTD mutant FUS, implying that the translational machinery was sequestered into RNP granules [379]. In FUS assemblies seeded by RNA, FUS prion-like domain binds to the C-terminal domain of RNAP2 [529]. hnRNP A1, hnRNP A2/B1 and SMN1 became sequestered into SGs containing mutant FUS in the absence of stress [684]. In a FUS transgenic *C. elegans* model, FUS irreversible hydrogels failed to release cargo such as SMN and STAU-1 [379].

Hence this evidence demonstrates that impaired SGs dynamics are important in FUS gain of function involved in ALS.

1.3.2 Impaired DNA damage response

DNA damage was detected in iPSCs-derived motor neurons bearing FUS mutations [685] and in motor neurons from FUS-ALS patients [604]. The role of WT FUS in the DNA damage response is modulated by its binding to HDAC1 and PARP1 [158, 604, 605, 677]. In an ALS-mutant R521C FUS mouse models, FUS-HDAC1 interactions involving the C-terminal domains of (RGG and PY-NLS) are disrupted by sequestration of WT FUS into cytoplasmic inclusions [677]. Hence it has been shown that mutations in the RGG and PY-NLS domains of FUS (R244C, R514S and R4521C) impair HDAC1 and FUS interactions, perturbing the normal cellular function of FUS in DSB repair in

primary neurons [604]. Additionally, FUS-ALS mutants triggered DNA-PK activation, which further enhanced cytoplasmic localization of FUS [575].

1.3.3 RNA-splicing defects

Under normal conditions, FUS regulates hundreds of genes [623]. In transgenic mice overexpressing mutant FUS more than 1000 introns were retained compared to animals overexpressing WT FUS [677]. In mouse embryonic motor neurons with null FUS or those expressing mutant P517L (the equivalent of human P525L), regulation of long non-coding RNA involved in motor neurons differentiation and maturation was different compared to those expressing WT FUS [686]. Similarly, knock down of FUS in SK-N-BE cells altered gene expression and RNA metabolism [687]. Overexpression of mutant FUS in U87 cells altered the alternative splicing properties of *MECP2* [688]. U11snRNP, a regulator of the minor spliceosome complex, was also retained in cytoplasmic aggregates formed by ALS FUS mutant P525L, which inhibited minor intron splicing in Hela cells [628].

Transcriptome analysis of small and long RNAs obtained from ALS-mutant motor neurons differentiated from embryonic stem cells from FUS transgenic mice, identified several deregulated miRNAs and their corresponding mRNA. This included miRNA-dependent deregulation of *Gria2*, which is involved in excitatory neurotransmission [689]. Additionally, FUS mutants have been linked to impaired gene silencing regulated by miRNAs [637]. HEK293T cells stably expressing mutant FUS R495X displayed increased mRNA and protein of *CAMK2N2* compared to WT FUS cells, by accumulation in the promoter region of its mRNA [616]. Hence this mechanism implies a gain in toxic function within the nucleus, consistent with studies in which overexpression of either WT or mutant FUS in the nucleus was toxic [612, 690]. This is not surprising since WT FUS is present in nuclear RNP granules such as paraspeckles and gems, and it binds to key proteins that compose these membrane-less compartments [634, 691, 692]. In addition, mutant FUS displayed enhanced binding to SMN and reduced binding to U1-snRNP; two key components of nuclear gems, hence these findings imply that ALS-mutant FUS disrupts gem formation [631, 693]. Additionally, another study reported

that SmB, a component of the U1 snRNP core particle, mislocalized in the cytoplasm together with mutant FUS in patient fibroblasts, and it coaggregated in SGs in HeLa cells [693]. Interestingly, loss of gems was a common trait detected in ALS patient fibroblasts bearing FUS or TDP-43 mutations [634]. Moreover, overexpression of mutant R522G FUS in SH-SY5Y cells led to the formation of cytoplasmic aggregates that further sequestered p.54nrb/NONO, an protein essential for paraspeckle formation [691]. Furthermore, NONO was detected in cytoplasmic and nuclear inclusions present in the spinal cord of FUS fALS patients [691]. The direct effect of mutant FUS on the formation of gems and paraspeckles is likely to indirectly effect splicing. Furthermore, since NONO, SMN and U1-snRNP have important roles in splicing [694], this will also directly impact on the regulation of splicing.

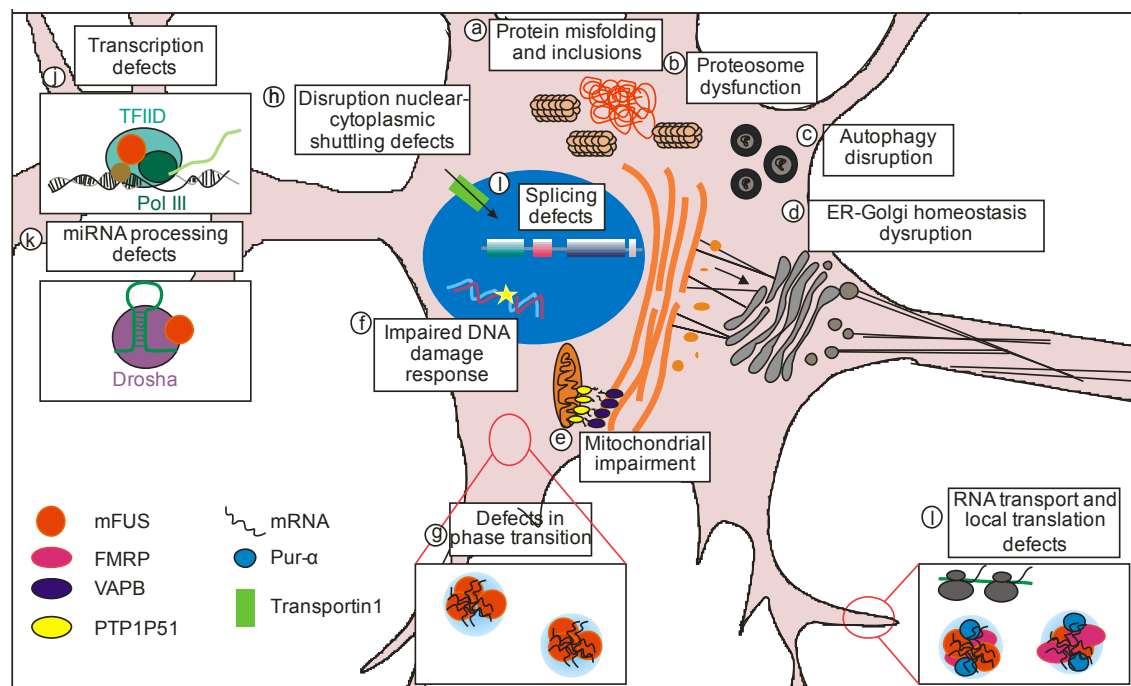


Figure 1.4 Mutant FUS mechanisms in ALS (a) Mutant FUS (mFUS) is mislocalized in the cytoplasm where it is misfolded and forms inclusions. mFUS induces proteasome dysfunction (b) and autophagy disruption (c). (d) mFUS perturbs ER-Golgi homeostasis, inhibiting ER-Golgi transport, leading to ER stress and Golgi fragmentation. (e) mFUS induces mitochondrial impairment by altering the interaction of VAPB and PTP1P51 in the MAM compartment. (f) mFUS displays impaired responses to DNA damage. (g) mFUS disrupts the reversible phase transition of SGs, promoting the formation of more rigid structures. (h) FUS nuclear translocation depends on its interaction with Transportin1, which is impaired by ALS mutant FUS and post-translational modifications at the C-terminus. (i) mFUS leads to defects in

splicing and impairment of binding to proteins involved in transcription (j) and miRNA processing (k). (l) Disruption of phase transition of RNP granules results in RNA transport and translation defects in specific subcellular compartments such as axons.

1.4 Alternative splicing in ALS

1.4.1 Alternative splicing: Definition, mechanism and regulators

Splicing is a highly dynamic and conserved process in which pre-mRNA is processed to mature mRNA. Constitutive splicing consists of intron removal and ligation of the majority of exons in the order in which they appear in the gene. Alternative splicing is a ubiquitous regulated process during gene expression that results in a single gene coding for multiple proteins (**Figure 1.5**). This results from deviation from the constitutive splicing system, and the inclusion or exclusion of specific exons from the final processed mRNA. Following translation of these alternatively spliced mRNAs, the resulting proteins can contain differences in their amino acid sequence and, hence biological function/s.

Genome-wide studies have estimated that 90-95% of human genes are alternatively spliced and mass spectrometry data has revealed that 37% of the ~20,000 human protein-coding genes generate multiple protein isoforms [695, 696]. Alternative splicing therefore increases the diversity of mRNA, and it produces diverse protein isoforms encoded by alternatively spliced genes. This can result in significant alterations to the properties of these proteins, such as changes in transactivation domains [697], protein binding capacity [698], or enzymatic activity [699]. Furthermore, alternative splicing can also modify the cellular localization of a protein by introducing either new localization signals [700], new post-translational modification sequences or new interaction sites [701]. All of these changes can modify the normal functions of a protein.

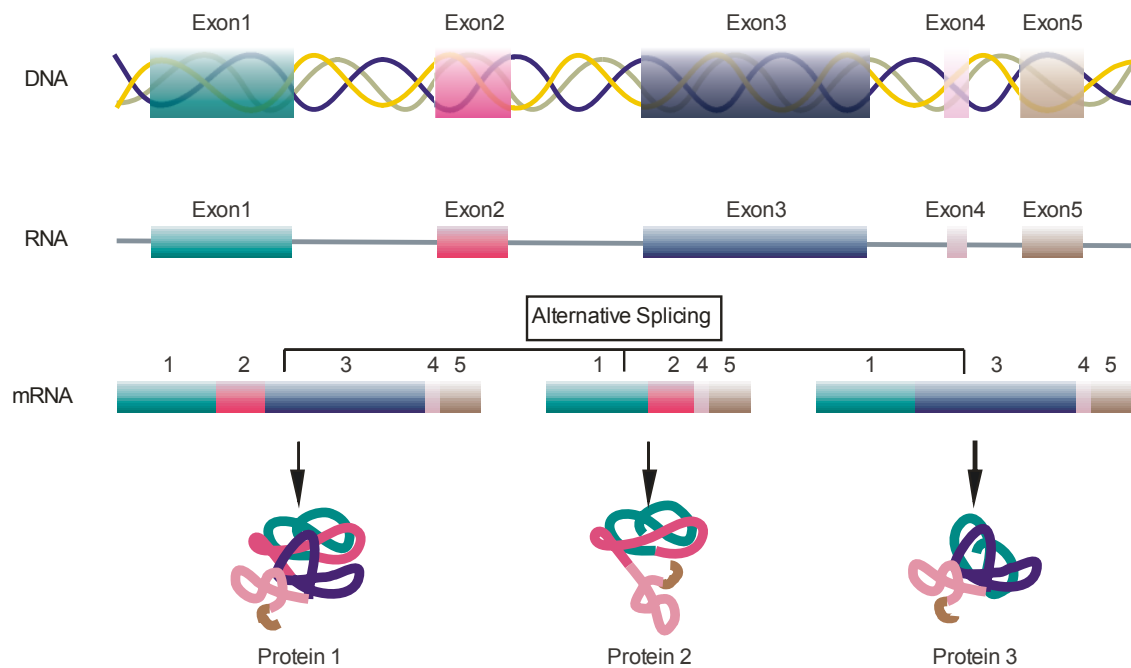


Figure 1.5 Alternative splicing give rise to multiple diverse proteins During alternative splicing, exons from precursor mRNA are differentially included. Hence, from a single gene multiple mRNA isoforms arise that translate into distinct proteins with varying characteristics.

The spliceosome machinery removes introns from the pre-mRNA by cleavage at conserved sequences, called splice sites, while the primary transcript is still being synthesised by RNAPII in the nucleus. Typically, the splice sites are located at the 5' and 3' of the intron and there is also a branch point located anywhere from 18-40 nucleotides upstream from the 3' end of an intron (**Figure 1.6**). The spliceosome complex, composed of at least 170 proteins and five snRNAs, recognizes these features, splice sites and branch points, and binds to the mRNA in an ordered manner [702]. Trans-acting splicing regulators, including RBPs, regulate the spliceosome machinery by binding directly or indirectly to cis-elements. The serine/arginine (SR)-rich protein family of RBPs that bind to exonic/ intronic sequences, are splicing enhancers [703, 704], while hnRNPs are recognized as splicing silencers [705]. Additionally, RBPs from other families have been implicated in the regulation of alternative splicing, such as FUS or TDP-43 [706].

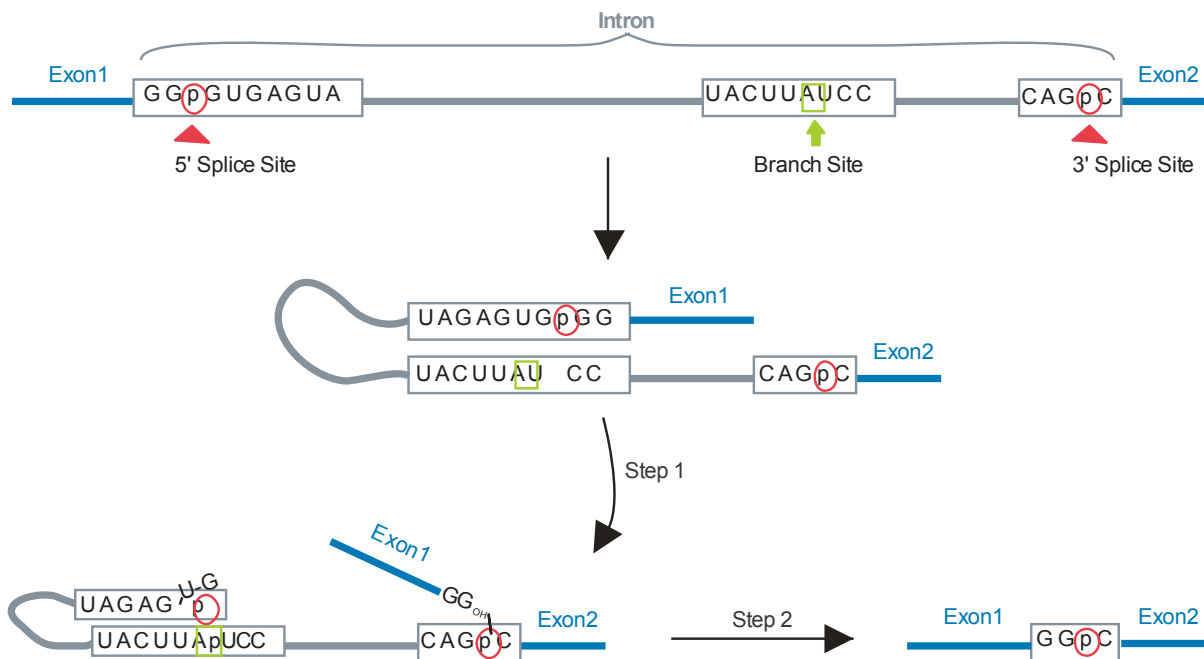


Figure 1.6 Pre-mRNA splicing process The splicing reaction is a two-step process. The first step involves the cleavage of the 5' splice site and the formation of the joined intron-exon. The second step is the cleavage of the 3' splice site and the union of both exons.

The basic mechanisms involved in alternative splicing are illustrated in **Figure 1.7**: a) mutually excluding exons, b) cassette exon inclusions/skipping, c) alternative 3' site, d) alternative 5' site, e) intron retention. In vertebrates and invertebrates the most prevalent alternative splicing mechanism is the cassette-type alternative exon [707]. While alternative 3' and 5' splice sites lead to subtle changes in the protein sequence, mutually excluding exons involves more complex changes [707].

Alternative splicing is regulated in a tissue-dependent manner, and it is also regulated during development and cellular differentiation, as well as by external stimuli [708-710]. Aberrant mechanisms of splicing, due to the presence of *cis*-element mutations or alterations in trans-acting splicing factors, are closely related to neurodegenerative diseases [711].

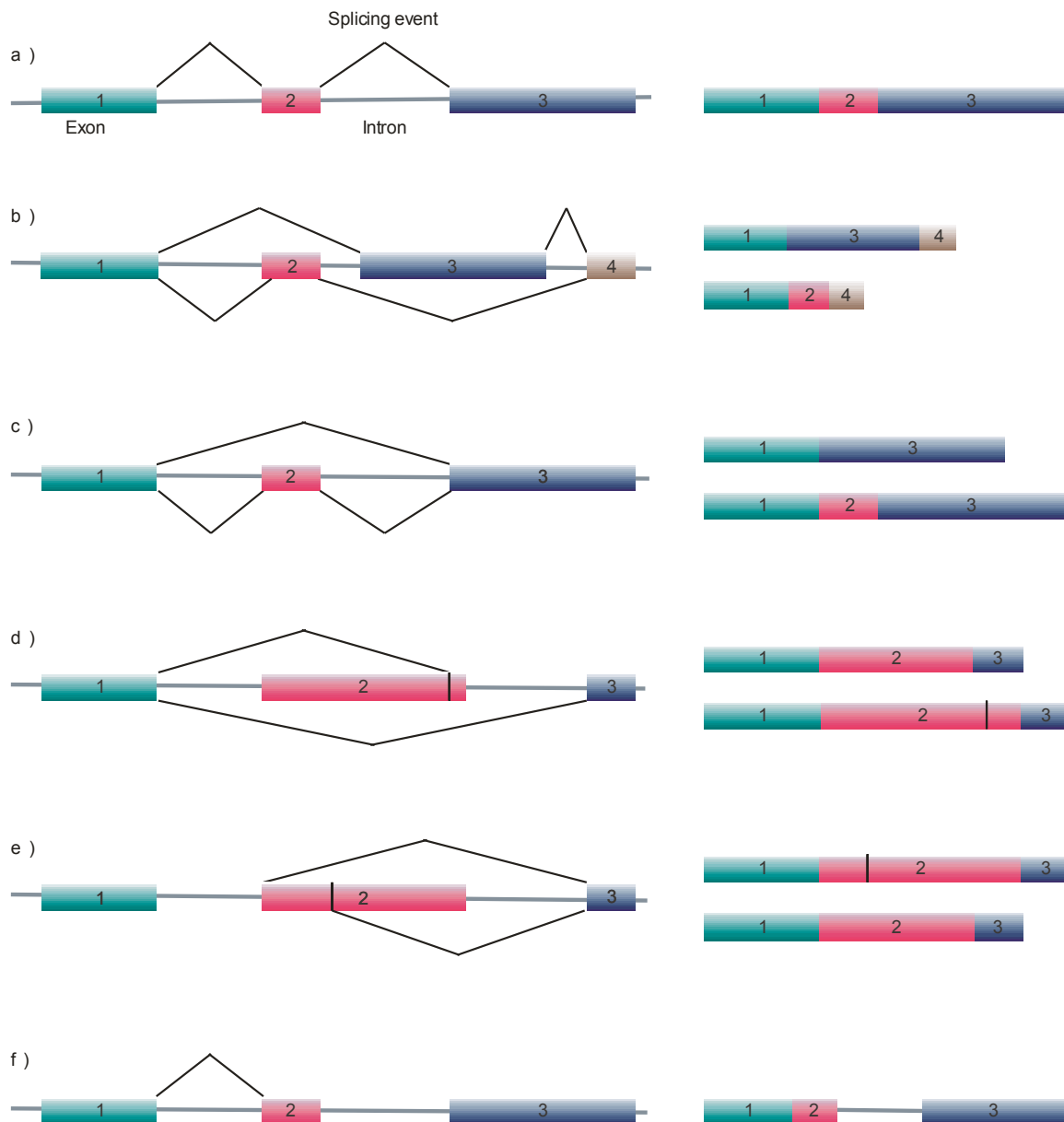


Figure 1.7 Schematic representation of constitutive splicing and the most common alternative splicing events (a) Constitutive splicing, (b-f) alternative splicing mechanisms: (b) mutually excluding exons, (c) cassette exon inclusions/skipping, (d) alternative 3' site, (e) alternative 5' site, (f) intron retention.

1.4.2 Role of alternative splicing in neurodegenerative diseases

The brain has one of the highest levels of alternative splicing activity amongst all tissues [712]. Alternative splicing is responsible for neuronal differentiation and plasticity, and disruption of alternative splicing has been linked to neurological, neurodevelopmental and neurodegenerative diseases [713, 714].

In neurological disorders, alternative splicing is affected by alterations in splicing factors that are only expressed in neurons, including Polypyrimidine Tract Binding Protein 1 (PTBP1), RBFOX proteins, and Nova1 [715]. Also, several neurological conditions have been linked to mutations that lead to faulty alternative splicing regulation, such as Alzheimer's disease, Huntington's disease, ALS and FTD [716]. Additionally, splicing regulators, SR proteins, hnRNPs and RBPs, are mutated, mis-localized and/or aggregated in neurological disorders which can impact their function in the nucleus, therefore impairing the regulation of alternative splicing [4, 5, 382].

Alpha-synuclein is a protein that is abundant in the human brain, which is strongly linked genetically and pathologically to synucleopathies (Parkinson's disease, dementia with Lewy bodies, multiple system atrophy). Alpha-synuclein is encoded by the *SNCA* gene, and alternative splicing of *SNCA* exon 5 or 3 (or both) results in the production of 4 distinct isoforms; the canonical form (AS140), as well as AS112, AS126, and AS98. The AS112 isoform was more prone to aggregation than full length alpha-synuclein and co-expression of both forms enhanced the toxicity of full length alpha-synuclein [717].

Similarly, alternative splicing of exon 2, 3 or 10 of the gene encoding Tau, *MAPT*, generates 6 distinct isoforms. These isoforms are distinguished by the number of microtubule binding repeat domains. Alternative splicing of exon 10 regulates the presence of the second microtubule binding repeat, resulting in either three (3R) or four (4R) of these binding motifs [718]. Mutations in *MAPT* result in inclusion of exon 10, which increases expression of the 4R isoform, associated with familial tauopathy FTDP-17 (frontotemporal dementia with parkinsonism linked to chromosome 17) [719]. A recent study showed that imbalance between 4R and 3R isoforms was enough to induce axonal transport defects in human neurons [720]. Interestingly, FUS and TDP-43 are thought to regulate the inclusion of exon 10 within *MAPT* [640, 721]. FUS interacts with Splicing factor proline- and glutamine-rich (SFPQ) and it regulates expression of the 3R and 4R isoforms of Tau. Knockdown of FUS and SFPQ in mice leads to an increase in the ratio of 4R: 3R, resulting in accumulation of phosphorylated tau, the development of FTLD-behaviours and neuronal loss [640]. Expression

of ALS-associated mutant TDP-43 promotes tau exon 10 inclusion more effectively than wild-type TDP-43 [721].

1.4.3 Aberrant alternative splicing in ALS

The normal cellular functions of FUS and TDP-43 involve splicing of mRNA. Even though both proteins share several structural and functional characteristics, studies to determine their alternatively spliced targets conclude that only approximately 10% of these targets overlap between the two proteins, suggesting that FUS and TDP-43 are involved in independent functions in relation to splicing [623, 722]. Interestingly, FUS and TDP-43 auto-regulate their own expression by alternative splicing, coupled to NMD [512, 723]. ALS-linked mutants of FUS and TDP-43 disrupt this autoregulatory mechanism [142, 512, 724-726]. This can trigger a vicious cycle, in which expression of each protein is enhanced by lack of autoregulation, which further increases cytoplasmic accumulation of either FUS or TDP-43 [512, 723].

Splicing changes were investigated by D'Erchia and collaborators using RNA-seq and MATS, a software tool implementing Bayesian multivariate analysis of transcript splicing [727]. Using 6 ALS patients and 5 age, sex and ethnicity matched control lumbar spinal cords, they identified more than 794 aberrant splicing events in genes predicted to be involved in neuronal function [727]. A second study that examined whole-genome exon splicing from 12 sALS patient and 10 control lumbar spinal cords, identified that 51.35 % of genes aberrantly spliced in ALS motor neurons were involved in cell adhesion [728]. Importantly, 21 common genes identified in these two studies were aberrantly spliced in ALS patients [727, 728]. Furthermore, defects in alternative splicing and polyadenylation were detected in the cerebellum of C9ORF72 ALS patients [729]. Additionally, the same study detected that the abnormally expressed genes in C9ORF72 patients were involved in neuronal development, protein localization, transcription and the UPR, whereas in sALS patients, the abnormally expressed genes were involved in calcium transport, synaptic transmission and oxidative phosphorylation [729]. A recent study reports that TDP-43 binds hnRNPA1 mRNA and modulates its splicing [146]. Depletion of nuclear TDP-43, as in ALS, leads to inclusion of a cassette exon in the

hnRNPA1 transcript and enhanced the levels of the hnRNPA1B isoform, which has a longer prion-like domain that increases protein aggregation and toxicity [146]. Interestingly, ALS patients with TDP-43 pathology also display cytoplasmic accumulation of hnRNPA1B [146]. Considering that TDP-43 and hnRNPA1 modulate a third of the transcriptome, this implies that splicing impairment is a key mechanism in ALS [146]. Furthermore, a shorter alternatively spliced variant of TDP-43 has also been reported. This isoform was shown to be upregulated in ALS patients and its overexpression in cell lines leads to neuronal death [141]. Hence together these studies point to an important role for alternative splicing in neurodegenerative diseases. This includes ALS, where important proteins implicated in pathophysiology are involved in the regulation of alternative splicing.

1.4.4 A novel splicing mechanism predicts many new protein isoforms

Bioinformatics tools have been widely used for both the prediction of new alternatively spliced variants and to study the functional consequences of alternative splicing. Automated methods to identify alternative splicing events conventionally regard genes as only having one single start codon, and they only normally consider alternative start codons when the canonical initiation codon is removed by splicing. However, recently, an unusual mechanism of alternative splicing was identified in which the N-terminal exon of a gene is translated into two reading frames. This new mechanism was first described for an alternatively spliced form of the mouse non-SMC condensin II complex subunit H2 (*NCAPH2*) gene [730]. The resulting new isoform lacks the last 17bp of the first exon. Whilst usually this event would change the reading frame downstream of the deleted region, translation from an alternative start codon within this region is able to rescue the reading frame, while shifting it upstream. The result is the production of a new protein isoform with a unique N-terminal sequence, which retains the same C-terminal sequence as its canonical counterpart (**Figure 1.8**).

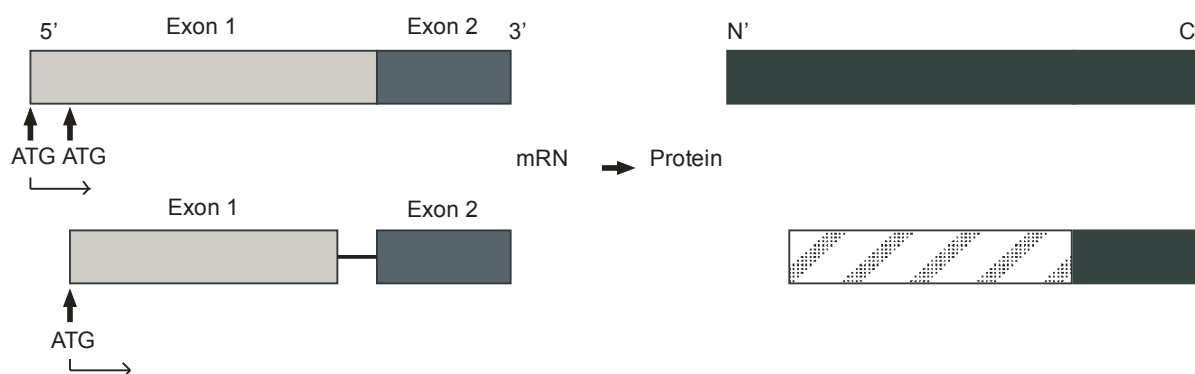


Figure 1.8 Representation of the novel alternatively splicing mechanism previously described for *NCAPH2* gene Schematic representation of the two alternatively spliced isoforms of *NCAPH2*. In the canonical variant the first exon becomes translated from the first start codon. In contrast, the alternatively spliced variant is translated from the second ATG, but it possesses a 17bp deletion at the end of the first exon. Hence the first exon is translated in a different reading frame to the canonical variant, but following the deleted sequence, the reading frame is restored and the remaining exons are the same for both isoforms.

Using publically available expressed sequence tags (EST) data, Wilson and colleagues predicted 2582 novel protein isoforms resulting from this unique and previously uncharacterised alternative splicing event [731]. Only two of these predicted proteins have been previously studied: otubain-1 and RNase κ-02; but expression of both of these proteins resulted in important cellular changes. The novel isoform of RNase κ-02 was shown to localized in the cytoplasm, whereas its canonical counterpart was predicted to be localized in the plasma membrane [732]. Similarly, the canonical form of Otubain-1 activates T-cells, while the novel alternatively spliced variant acts as a T-cell repressor [733]. Hence together these studies suggest that the unique amino terminus sequence of these new protein variants can induce important changes in protein localization and function.

1.5 Aims of this thesis

Alternative splicing defects are emerging as a central mechanism in ALS. And alternatively spliced forms of ALS related proteins are further implicated. The normal cellular functions of FUS involve alternative splicing, which is impaired in ALS. Furthermore, FUS autoregulates its own expression through alternative splicing. The hypothesis examined in this thesis was that an alternatively-

spliced isoform of the FUS protein is present in neuronal cells, where it plays essential physiological roles in neurobiology. Furthermore, the ALS-associated mutations in FUS^{EC} induce cellular dysfunction, leading to ALS pathogenesis. This hypothesis was addressed with the specific aims:

Chapter 3: Identification of a novel extracellular isoform of FUS

The aims of the studies described in this chapter were to confirm experimentally the expression of FUS^{EC} at the mRNA and protein level in human primary neurons and cell lines, and to confirm its predicted extracellular localization using different methods.

Chapter 4: Characterization of FUS^{EC}

The aim of the studies described in this chapter was to generate an overexpression system for FUS^{EC} to study its normal characteristics. Here it was examined its post-translational modifications, cellular localization and identified putative binding partners, to prove insights into its biological functions.

Chapter 5: Examining the role of FUS^{EC} in ALS

The aim of the studies described in Chapter 5 was to determine the effect of overexpressing WT and ALS-mutated FUS^{EC} in cell lines. Putative binding partners of ALS-mutated FUS^{EC} were examined to identify possible cellular features linked to pathophysiology, including ER stress, Golgi fragmentation, apoptosis and transmission of mutant FUS^{EC} from cell-to-cell.

Overall, this thesis focuses on identification and characterisation of a new isoform, FUS^{EC}. It provides insights into the normal physiological role of FUS^{EC} in biology and its pathogenic role in ALS.

2. ■ **Material and methods**

2.1. Molecular biology

2.1.1. **LB medium**

Luria Bertani (LB) broth was prepared diluting 20 g of LB Broth (Bacto Laboratories 240230) in 1 L of distillate water (dH₂O) and was autoclaved. The appropriate antibiotics were added (Ampicillin, Sigma) prior to be used as the liquid culture media for *Escherichia coli* (*E. coli*). A final concentration of 50 µg/mL was used for ampicillin, and the stock solutions was prepared at a concentration of 100 mg/mL in dH₂O, sterilized and stored at -20°C.

LB agar plates were used as the solid culture medium for *E.coli* in petri dishes. *LB* agar plates were prepared by dissolving 20 g of Agar (Agar, Sigma A1296-500G) in 1L of *LB* broth and the solution was autoclaved. After melting the *LB* agar, appropriate antibiotics were added and the *LB*-agar was poured into sterile petri dishes and plates were allowed to set and stored inverted at 4 °C.

2.1.2. **Transformation**

TOP10 competent cells (Invitrogen) or NEB 5-alpha competent (High Efficiency) (New England Biolabs, NEB) were thawed on ice. Approximately 2-5 µL of DNA (25-50 ng) was added to 50 µL of competent cells. The cells were incubated on ice for 30 min. Following heat shock treatment at 42°C for 30 sec, cells were placed on ice for 5 min. 250 µL of SOC media (Invitrogen) was added to 50 µL of cells and tubes were incubated at 37°C, horizontally shaking at 250 rpm for 1 h. Aliquots of 50-200 µL were spread on pre-warmed *LB* agar plates with the appropriate antibiotics. Plates were incubated at 37°C overnight.

2.1.3. **Preparation of plasmids (small and large scale)**

For isolation of the plasmid, 3 mL or 25 mL (mini or midi preparation respectively) of *LB* broth with the appropriate antibiotic was inoculated picking up a single cell colony from the appropriate plasmid and was incubated overnight at 37°C horizontally shaking at 250 rpm. The plasmid preparation was performed according to manufacturer's protocol and plasmid DNA was isolated using QIAprep Spin Miniprep Kit or QIAGEN PLASMID PLUS midi Kit. The DNA

was resuspended in 50 or 200 μL of nuclease-free H_2O , for small and large-scale isolation respectively, and stored at -20°C .

2.1.4. Glycerol stock

Glycerol stocks of fresh ~12 h bacterial cultures picked from single cell colonies were prepared by mixing 750 μL of the cultured media with 250 μL sterile glycerol, mixing and storing at -80°C .

2.1.5. DNA quantification

DNA was quantified by Nanodrop-2000 software (ThermoScientific). The concentration of DNA was analysed directly by using a Nanodrop ND-1000 spectrophotometer. A conversion of 1.0 optical density (O.D.) at 260 nm for double-stranded DNA = 50 ng/ μL was used to determine the original DNA concentration, and the A260/A280 ratio was used to assess the purity of DNA. Where $A_{260}/A_{280} < 1.85$ was considered satisfactorily pure for transfection experiments.

2.2. Mammalian cell culture techniques

2.2.1. Fetal calf serum (FCS)

FCS (Gibco) was removed from -20°C , allowed to thaw and was equilibrated to room temperature. FCS was then suspended in a 60°C water bath for 30 min with frequent mixing and was allowed to equilibrate. The heat-inactivated FCS was dispensed in 50 mL aliquots and stored at -20°C .

2.2.2. Cell culture maintenance

The immortalized neuronal cell line HEK293T cells were used throughout this study. The cells were maintained in Dulbecco's modified eagle medium high in glucose (DMEM) (Gibco) with 10% (v/v) heat activated FCS, incubated at 37°C with 5% CO_2 . To sub-culture the cells, they were washed with phosphate buffer saline (PBS, 3.2 mM Na_2HPO_4 , 0.5 mM KH_2PO_4 , 1.3 mM KCl, 135 mM NaCl,

pH 7.4) and treated with 1mL of Trypsin-EDTA (Gibco) with incubation for 2 min at 37 °C to detach the cells from the flask. The cells were resuspended in 5 mL of DMEM (Gibco) with 10% (v/v) FCS and centrifuged at 1000 g for 5 min. The medium was discarded and the cell pellet was resuspended in 1 mL of DMEM with 10% (v/v) FCS. Then, 10 μ L of cell suspension was mixed with 90 μ L of DMEM and cell counting was made with Scepter™ 2.0 Cell Counter (Merckmillipore). The number of cells was multiplied by dilution factor (10) to give cell number per mL. Cells were then plated into 24-well plates, 6-well plates or 50 cm² petri dishes as required and subcultured in a fresh T75 flask at a dilution factor of 1:10.

2.2.3. Transfection

HEK293T cells were transfected using Lipofectamine2000 (Invitrogen) and Opti-MEM (Invitrogen) according to the manufacturer's protocols, keeping constant the cell number and DNA amount per well between experiments. Cells were grown to 80% confluency and 0.5x10⁵ cells were plated out in 24-well plates transfected with 500ng plasmid DNA, 2x10⁵ cells were plated in 6-well plate and transfected with 2000ng plasmid DNA. The cells were incubated in a 37°C incubator with 5% CO₂ and observed post-transfection. Media was changed after 20 h post-transfection to Opti-MEM.

2.2.4. Long-term storage of cell lines

Low passage number cells were collected by trypsinisation in antibiotic-free DMEM with 10% (v/v) FCS. Approximately 1-2 million of cells were diluted per mL in 95 % (v/v) FCS 5% (v/v) Dimethyl sulfoxide (DMSO). Cells in freezing medium were dispensed in cryovials and cooled in an isopropanol-filled cryopresevative chamber at -80°C and then transferred to liquid nitrogen for long-term storage. To thaw the cells, cells were quickly warmed at 37°C, resuspended in 5 mL of DMEM with 10% (v/v) FBS, and to remove the DMSO cells were centrifuged at 1000 rpm (~200 g) for 5 min, supernatant was removed and cell pellet was resuspended in DMEM with 10% (v/v) FCS and immediately plated in T75 flasks in DMEM with 10% (v/v) FCS.

2.3. Protein chemistry methods

2.3.1. Conditioned media and lysate collection

Cells were plated and transfected, if needed, following manufacturers protocol. 20h post-transfection media was changed to Opti-MEM (low serum media). 48h post-transfection, media was kept and cells were washed in PBS and incubated with TN Buffer (50 mM Tris-HCl pH 7.5 and 150 mM NaCl with 0.1% (v/v) SDS, 1% (w/v) protease inhibitor cocktail (Sigma) and 1% (w/v) phosphatase inhibitor (Sigma)) for 15 min on ice. Cells were scrapped and samples were frozen at -20°C. Cell lysates were thawed on ice and centrifuged at 15000 rpm (~27600 g) for 15min. The protein concentration was determined from the supernatant using BCA protein assay (Thermo scientific) (section 2.3.2).

To process the media, 1 mL of harvested media was centrifuged at 1000 rpm for 5 min at 4°C twice to remove cell debris, following, the media was concentrated using Amicon Ultra-0.5 mL Centrifugal Filters for Protein Purification and Concentration (Merck Millipore Merck Ltd) by centrifugation at 15000 rpm (~27600 g) for 20 min at 4°C.

2.3.2. Bicinchoninic acid (BCA) protein assay

The BCA protein assay (Thermo scientific) was utilised to assess the protein concentration of cells, according to the manufacturer's protocol. The concentrations are compared to a BSA standard curve ranging from 0-2 mg/mL. The samples were diluted 1:10 with dH₂O, and the samples and standard curve were mixed with BCA reagents and incubated for 30 min at 37°C. All samples were done in duplicate in a 96 well plate and analysed on a Benchmark spectrometer (PHERstar FS) with an absorbance wavelength of 562 nm.

2.3.3. SDS polyacrylamide gel electrophoresis (PAGE) and western blotting

To performe SDS-PAGE electrophoresis, 20 µL of concentrated media or 20 µg of lysate protein samples were electrophoresed through 4-15% SDS-polyacrylamide gels (Bio-rad), unless otherwise specify it, with 2X SDS and

NuPAGE™ Sample Reducing Agent (10X) (ThermoFisher). Samples with loading buffer were first mixed and placed on a heat block for 5 min at 90°C and loaded on SDS-polyacrylamide gels. As a reference ladder for molecular weight assessment Precision Plus Protein™ Dual Color Standards (Bio-rad) was loaded. Proteins were electrophoresed at 100-150V and transferred to a nitrocellulose membrane and blocked in 5% (w/v) non-fatty milk in Tris-buffered saline pH 8.0 (TBS) tween-20 (TBS-T) for 30 min, then incubated with primary antibody (see **Table 2.1**) in 5% (w/v) non-fatty milk power in TBST at 4°C overnight.

Membranes were washed for 4 min, once with TBST and twice with TBS, and incubated at room temperature for 1 h with the correct secondary antibody (1:4000, HRP-conjugated goat anti rabbit, or HRP-conjugated goat anti mouse Chemicon) diluted in TBST. After repeating the washes, proteins were detected using ECL chemiluminescent reagent (Bio-rad) on Chemidoc XRS (Bio-rad). Membranes were stripped using Reblot Pluse solution (Chemicon), according to manufacturer's protocol and reprobed. Densitometry analysis was conducted using IMAGEJ software (v. 1.47; National Institutes of Health).

Alternatively, after incubation with the primary antibody, membranes were washed in PBS-T for 10 min three times. Membranes were incubated for 1 h at room temperature with fluorescently labelled IRDye 800 CW goat anti-rabbit IgG (1 : 10 000) or 680 WC IRDye CW goat anti-mouse IgG (1 : 10 000). Proteins were imaged using a Li-Cor Odyssey imaging system at the appropriate wavelength. Densitometry analysis was conducted using IMAGEJ software (v. 1.47; National Institutes of Health).

Table 2.1 Primary antibodies used for immunoblotting

Protein (Antigen)	Dilution	Species	Catalogue number and manufacturer
FUS	1:1000	Rabbit	ab23439, Abcam
HA	1:500	Mouse	H3663, Sigma
GFP	1:1000	Rabbit	P/N460705, ThermoFisher
GAPDH	1:4000	Mouse	CB1001, Merk Millipore
GAPDH	1:2000	Rabbit	G8795, Merk Millipore
Biotin con A	1:100	- *	B-1005, Vector Labs

GM130	1:1000	Mouse	610823, BD Transduction Lab
Nuc	1:100	Mouse	48373, Santa Cruz
Bcl-2	1:1000	Mouse	B9804, Sigma
Flotillin-1	1:500	Rabbit	Ab41927, Abcam
TSG 101	1:1000	Rabbit	Ab30871, Abcam
FUS ^{EC} customized antibody	1:500	Rabbit	Genscript

* streptavidin HRP

2.3.4. Sample collection for immunoprecipitation (IP)

Cell lysate preparation for IP

Cells were seeded in 50 cm² petri dish, in a density of 1×10^6 , and transfected following protocol in section 2.2.3. After 20 h transfection medium was changed to Opti-MEM, and after 24h cells were harvested. Medium was kept and the cell monolayer was washed with cold PBS and cells were scrapped in 1 mL of cold PBS. Cells were centrifuged at 1000 g for 5 min at 4°C. Supernatant was discarded and the pellet was resuspended in 400 μ L of lysis buffer (20 M Tris-HCl, 150 mM NaCl, 2 mM EDTA, 1% (v/v) NP40, pH 7.4) with 1% (w/v) protease and 1% (w/v) phosphatase inhibitors (Sigma). Samples were incubated for 30 min on ice, vortexing the cells every 10 min. After centrifugation at 14000 g for 10 min at 4°C, the supernatant was placed in a new tube, the BCA was performed from this fraction (section 2.3.2) and samples were kept at -20°C.

Media preparation for IP

8 mL of media were collected from a 50 cm² petri dish and 500 μ L of Opti-MEM with 1% protein inhibitor (Sigma) was added. Samples were centrifuged for 5 min at 1000 rpm (~120 g) at 4°C twice to remove cell debris. Media were concentrated with Amicon Ultra-15 mL Centrifugal Filters for Protein Purification and Concentration (Merckmillipore). The resulting volume was buffer exchanged three times with PBS and protease and phosphatase inhibitors and BCA was carried to determine the protein concentration.

2.3.5. Immunoprecipitation with HA-magnetic beads

Hematoglutinin (HA) tag is a widely use epitope tag of approximately 3 kDa. To performe IP of HA-tagged proteins, 25 μL of HA magnetic beads (ThermoFisher) were washed three times in 500 μL of TBS containing 0.05 % (v/v) Tween-20 detergent. 500 μg of protein from the lysate and concentrated media were added to 25 μL of HA magnetic beads and mixed well. Then, samples were incubated for 5 h at 4°C with mixing. The beads were collected with a magnetic stand and the supernatant was kept as control. Beads were washed again with 500 μL of TBS-T three times. Proteins were eluted from the beads with 2x SDS sample buffer, gently vortexed and boiled for 10 min at 95°C. The proteins were separated from the beads with the magnetic stand and loaded into 4-15% SDS-polyacrylamide gels (Bio-rad) and stained with Bio-safe Coomassie G-250 stain (Bio-rad).

2.3.6. Immunoprecipitation with GFP trap

The total volume of collected cell lysate or media was added to 25 μl of equilibrated GFP-Trap beads (ChromoTek) to a final volume of 500 μl . Samples were incubated for 2 h at 4°C constantly shaking. Beads were centrifuged at 2500 g for 2 min at 4°C. Supernatant was kept as control. Beads were resuspended in 500 μl of dilution buffer (10 mM Tris-HCl pH 7.5, 150 mM NaCl, 0.5Mm EDTA) and centrifuged at 2500 g for 2 min at 4°C and washes were repeated twice. 30-60 μl of 2x SDS-sample buffer was added to each sample and samples were boiled 10 min at 95°C to dissociate beads. Beads were collected by centrifugation at 2500 g for 2 min at 4°C and supernatant was loaded onto a 4-15% SDS-polyacrylamide gels (Bio-rad) and stained with Bio-safe Coomassie G-250 stain (Bio-rad).

2.3.7. In-Gel Protease Digestion

The regions of interest were excised from the 4-15% SDS-polyacrylamide gels (Bio-rad) and were washed in 100 mM ammonium bicarbonate (NH_4HCO_3), pH 7.8, and 50% (v/v) acetonitrile (ACN) in 50 mM NH_4HCO_3 for 10 min. Gel pieces were dehydrated in 100% (v/v) ACN and excess ACN was vacuum centrifuged. Gel pieces were then reduced with 10 mM 1,4-dithiotreitol DTT for 30 min at

50°C, and alkylated with 20 mM Iodoacetamide (IAA) for 45 min at room temperature in the dark. Digestion with trypsin (15 μ l at 12.5 ng/ μ l) or Glu-C (15 μ l at 100 ng/ μ l) was carried out overnight at 37°C, where excess buffer was aliquoted into a fresh tube. Tryptic or Glu-C peptides were extracted twice using 100 μ l of 50% ACN/2% formic acid, bath sonicated for 10 min each. Eluates from each extraction were pooled and dried to completion in a low-binding tube under vacuum centrifugation. Proteolytic peptides were desalted on a pre-equilibrated C₁₈ OMIX tip and eluted in 50 % (v/v) ACN, 0.1 % (v/v) formic acid, and dried under vacuum centrifugation.

2.3.8. Reverse Phase (C18) Liquid Chromatography Mass Spectrometry (RP-LC-MS/MS)

Peptides were resuspended in 0.1 % (v/v) formic acid (10 μ l) and separated on a NanoLC system (Thermo) employing a 60 min gradient (2%–50% v/v acetonitrile, 0.1% formic acid for 54 min, ramped up to 85% ACN for 5 mins) with a flow rate of 300nl/min. The peptides were eluted and ionized into either an Orbitrap Velos (Glu-C peptides) or a Q-Exactive mass spectrometer (tryptic peptides) (ThermoFisher). The electrospray source was fitted with an emitter tip of 10 μ m (New Objective, Woburn, MA) and maintained at 2.5 kV electrospray voltage. Precursor ions were selected for MS/MS fragmentation using a data-dependent “Top 10” method operating in FT-FT acquisition mode with CID (Orbitrap Velos) or HCD (Q-Exactive) fragmentation.

IT-MS on the Orbitrap Velos was carried out with a survey scan range between m/z 350 – 1800 Da with MS/MS threshold of 5000 ions for CID, with an isolation width of 2.0 Da and normalized collision energy of 30%. FT-MS analysis on the Q-Exactive was carried out with a 35,000 resolution and an AGC target of 1×10^6 ions in full MS; and MS/MS scans were carried out at 17,500 resolution, with an AGC target of 1×10^5 ions. Maximum injection times were set to 60 and 100 milliseconds respectively. The ion selection threshold for triggering MS/MS fragmentation was set to 25,000 counts and an isolation width of 2.0 Da was used to perform HCD fragmentation with normalised collision energy of 30%.

Spectra files were processed using the Proteome Discoverer 1.4 software (ThermoFisher) incorporating the Mascot search algorithm (Matrix Sciences, UK) using the UniProt/SwissProt human database, with the inclusion of the predicted protein sequence of FUS^{EC}. Peptide identifications were determined using a 30-ppm precursor ion tolerance and a 0.8-Da MS/MS fragment ion tolerance for IT-MS and CID fragmentation on the Orbitrap Velos, or 20-ppm precursor ion tolerance and a 0.1-Da MS/MS fragment ion tolerance for FT-MS and HCD fragmentation on the Q-Exactive. The parameters for searching were: (a) carbamidomethylation modification of cysteines, which was considered a static modification, while (b) oxidation of methionine, and (c) acetyl modification on N-terminal residues, were set as variable modifications, allowing for maximum three missed cleavages. The data was processed through Percolator for estimation of false discovery rates. Protein identifications were validated employing a q-value of 0.01. The low abundance of peptides corresponding to the unique N-terminal sequence of FUS^{EC} was also manually validated to verify that the MS2 ion series were correctly assigned.

2.4. Microscopy

2.4.1. Fluorescent microscopy

After transfection of HEK293T cells, conditioned medium was removed from the 24-well plate and cells were washed with PBS. Cells were fixed with freshly prepared 4% (w/v) paraformaldehyde and incubated in dark for 15 min. Then cells were washed again with PBS twice, treated with Hoechst 33528 stain (ThermoFisher) and incubated in the dark for 5 min and washed again twice with PBS. Slides were mounted on a drop of fluorescent mounting media (Dako) cells facing down, and let air-dry.

2.4.2. Immunofluorescence microscopy

To perform Immunocytochemistry (ICC), after fixation cells were permeabilized with 0.1% (v/v) Triton-X in PBS for 10 min and blocked with 3% (w/v) BSA in PBS for 30 min. After washing three times with PBS, cells were incubated at 4°C overnight with appropriate primary antibody (see **Table 2.2**) diluted in 1%

(w/v) BSA. Then cells were washed three times with PBS and the appropriate secondary antibody was added, and cells were incubated in the dark at room temperature for 1h (Alexa Fluor 568- conjugated rabbit anti-mouse IgG (1:250) or Alexa Fluor 568- conjugated mouse anti-rabbit IgG (1:250) or Alexa Fluor 488- conjugated rabbit anti-mouse IgG (1:250), Alexa Fluor 488-conjugated mouse anti- rabbit IgG (1:250)). After three washes, nuclei was stained with Hoechst stain and slides were mounted using Dako.

Table 2.2 Primary antibodies used for immunocytochemistry

Protein (Antigen)	Dilution	Species	Catalogue number, manufacturer
HA	1:500	Mouse	H3663, Sigma
HA	1:100	Rabbit	H6908, Sigma
GM130	1:50	Mouse	610823, BD Transduction Lab
FUS ^{EC} customized antibody	1:500	Rabbit	Genscript
XBP1	1:25	Rabbit	sc-7160, Santa Cruz
CHOP	1:50	Mouse	sc-7351 [B-3], Santa Cruz
Calnexin	1:100	Rabbit	22595, Abcam
Cleaved caspase-3	1:400	Rabbit	9661, Cell Signalling Technology

2.4.3. Confocal Microscopy and Image acquisition

Cells were then photographed with 63x/na=1.4 or 100x/na=1.46 objectives on a Zeiss LSM 880 inverted confocal laser-scanning microscope, equipped with a LSM-TPMT camera (Zeiss). In multichannel imaging, photomultiplier sensitivities and offsets were set to a level at which bleed through effects from one channel to another were negligible.

2.4.4. Quantitative analysis

The percentage of cells with FUS^{EC} inclusions, cells displaying nuclear immunoreactivity to CHOP or XBP1, cells with Golgi fragmentation and apoptotic cells, were quantified from at least 100 HEK293T cells per group expressing FUS^{EC} for 48h in n=3 independent experiments. For Golgi fragmentation analysis, only cells where the Golgi structure was clearly visible were analysed. Apoptotic nuclei were defined as condensed Hoechst-positive

structures under 5 μm in diameter or fragmented (multiple condensed Hoechst-positive structures per cell). Cells undergoing cell division were excluded from the analysis.

2.5. Statistical analysis

The experiments were performed at minimum three times on separate days with compulsory one blind experiment. Data are presented as mean value \pm standard error of the mean (SEM). Statistical comparisons between group means were performed using GraphPad Prism 6 software (Graph Pad software, Inc.). One-way or two-way ANOVA, followed by *post hoc* Tukey test for multiple comparisons was used, when justified. The significance threshold was set at $p=0.05$.

3. ■ Identification of a novel extracellular isoform of FUS

3.1. Introduction

Aberrations to alternative splicing in genes encoding proteins linked to ALS pathologically or genetically have been described [146, 619, 633, 734]. Pathogenic mutations in FUS and TDP-43 are causative of a proportion of familial ALS cases, and cytoplasmic inclusions containing these proteins are present in the brain and spinal cord of ALS patients [4, 5, 7, 12, 121, 122, 125]. FUS and TDP-43 are both RNA/DNA-binding proteins that share numerous functional and structural similarities. Both are involved in mRNA biogenesis including alternative splicing [735, 736]. The cytoplasmic aggregation of these proteins has been related to their mislocalization from the nucleus, leading to abnormalities in regulation of alternative splicing [737, 738]. Moreover, proteins involved in regulation of alternative splicing are sequestered into the cytoplasmic inclusions, further impairing their normal cellular functions in the nucleus [619, 721]. Furthermore, FUS and TDP-43 autoregulate their own expression by alternative splicing, while mutant ALS versions of these proteins evade this control system [142, 512, 724-726].

Interestingly, a shorter, alternatively spliced isoform of TDP-43 has been implicated in ALS [141]. This isoform is upregulated in ALS patient tissues, and its overexpression in cell lines led to the formation of cytoplasmic aggregates and cell death – key hallmark features of ALS pathogenesis [141]. Recently, a bioinformatics approach predicted the existence of a new isoform of FUS from a previously unrecognised splicing event, which surprisingly was predicted to be secreted [731]. With the emergence of recent findings indicating that the formation of alternatively spliced TDP-43 contributes to ALS, it was hypothesised that the new predicted alternatively spliced FUS isoform may also be relevant to ALS. Hence, the goal of the studies outlined in this chapter was i) to determine whether expression of the novel isoform of FUS can be confirmed experimentally, ii) to examine whether it is localized in the extracellular compartment, as predicted by Wilson and colleagues [731], and finally, iii) to determine whether it can be detected extracellularly, in human CSF.

3.1.1. A novel predicted FUS isoform

Novel isoforms of both TDP-43 and FUS were predicted to result from this unique alternative splicing mechanism. The new isoform of FUS skips exon 7, resulting in the deletion of 35 nucleotides. Because it is translated from an alternative start codon located at position 683 of the canonical sequence, the reading frame from exon 8 onwards in the C-terminal direction is rescued, resulting in a different reading frame downstream of the deletion site (**Figure 3.1a and 3.1b**). Following translation of this sequence, the resulting protein possesses a unique N-terminal sequence to canonical FUS (amino acids 1 to 61) (**Figure 3.1c and 3.1d**). This novel isoform was named, FUS^{EC}.

Since most protein localization signals are found at the N-terminus, using the software WoLF PSORT (<https://www.genscript.com/wolf-psort.html>), Wilson et al. studied the probable cellular localization of the novel predicted isoforms [731, 739]. The WoLF PSORT software calculates a 'pSort score', which predicts whether a protein is secreted or not by detecting signal sequences, transmembrane domains and cytoplasmic domains. Finally, WoLF PSORT compares the protein in question to proteins that have similar PSORT scores, and from this it predicts the probable cellular localization of the protein. Hence, Wilson et al. predicted that the novel FUS isoform, FUS^{EC}, localizes in the extracellular space rather than in the nucleus or cytoplasm [731].

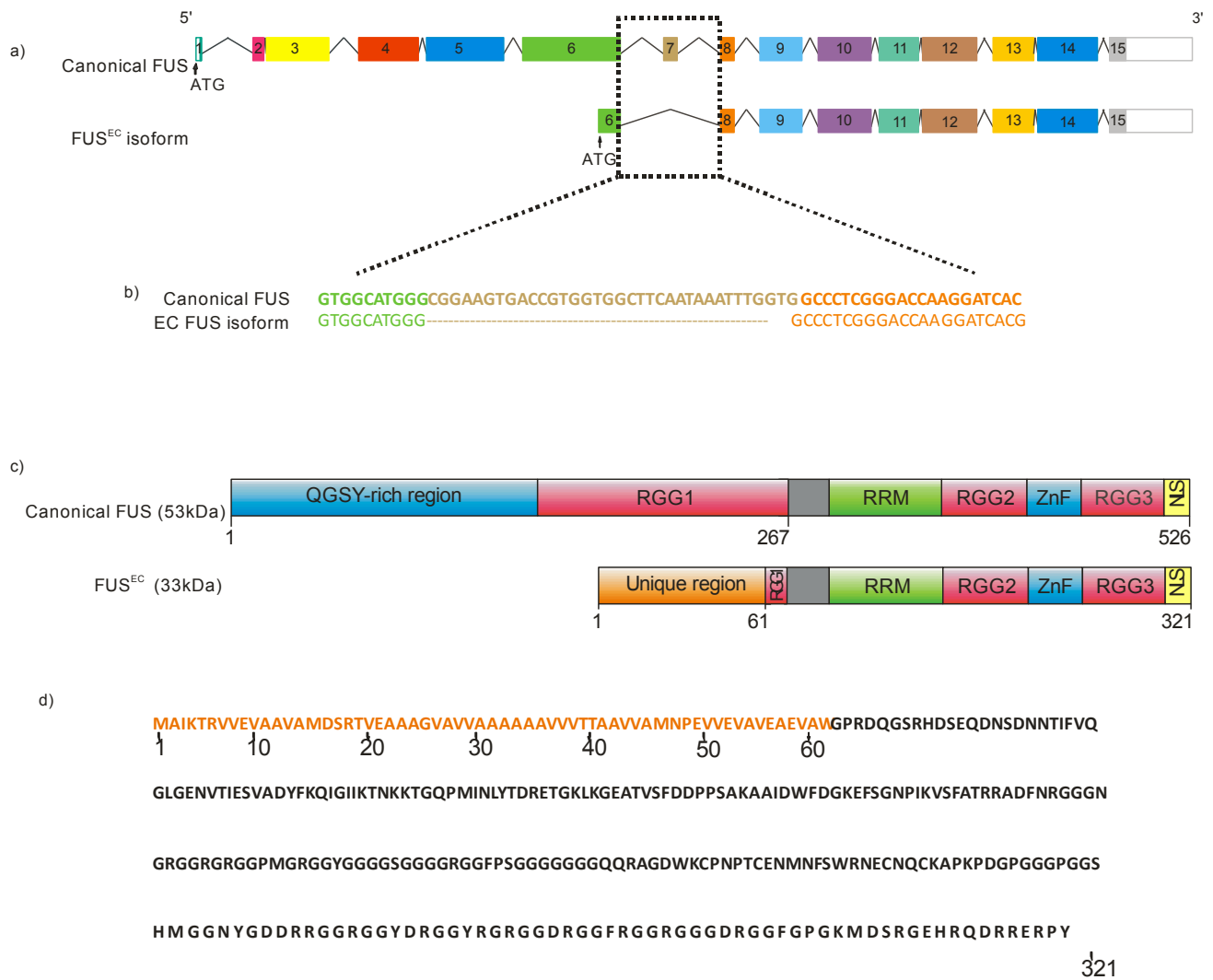


Figure 3.1 Genomic organization of *FUS* and *FUS^{EC}* (a) The human *FUS* mRNA (top) consists of 15 exons and is located on chromosome 16p11.2. The human *FUS^{EC}* mRNA, shown underneath, consists of 9 exons, including 8 common exons to *FUS* (exons 8-15). (b) Highlighted region of *FUS^{EC}* mRNA where exon 6 and 8 are joined. (c) Functional domains of *FUS* and *FUS^{EC}* proteins. The two proteins share C-terminal regions including the RNA-recognition motif (RRM, amino acids 285–371), two Arg-Gly-Gly (RGG)-repeat regions (amino acids 371–422 and 453–501) which is interrupted by a zinc-finger motif (ZnF) (amino acids 422–453) followed by a non-conventional nuclear localization signal (NLS) (amino acids 510–526). *FUS^{EC}* is lacking the N-terminal Q/G/S/Y-rich region (amino acids 1-165) present in canonical *FUS* but it possesses a unique N-terminal region (amino acids 1-61), followed by a few residues of the G-rich region compared to canonical *FUS* (amino acid 165–267). The majority of fALS-related mutations in *FUS* are found in the second RGG region and the NLS, and these areas are shared by both canonical *FUS* and *FUS^{EC}*. (d) Amino acid sequence of *FUS^{EC}*. The unique N-terminus sequence is highlighted in orange.

The canonical form of FUS is composed of 526 amino acids, with a calculated molecular weight of 53 kDa. On 1D SDS PAGE gels, FUS present within cellular lysates fractions has been observed to migrate between ~ 60-75 kDa depending on the sample type [530, 570, 612]. In contrast, the resulting novel isoform of FUS FUS^{EC} is predicted to contain 321 amino acids with a calculated molecular weight of 33 kDa (**Table 3.1**). FUS^{EC} is a smaller protein than canonical FUS because it lacks the QGSY-rich region and most of the first glycine rich domain (**Figure 3.1c**). In addition, the novel isoform FUS^{EC} has a unique N-terminal sequence consisting of 61 aa (**Figure 3.1d**).

Table 3.1 Characterization of FUS and FUS^{EC} proteins Molecular weight (MW), isoelectric point (pI) and localization. * MW of 53 kDa but runs higher on an SDS-PAGE gel. ** predicted values.

	FUS	FUS ^{EC}
MW (kDa)	53*	33**
pI	9.40	9.28**
Localization	Nuclear	Extracellular **

3.1.2. The Classical and Non-Classical Secretory Pathways

Secretion is the cellular process by which soluble and membrane protein cargoes are delivered to the extracellular space. The secretory pathway is necessary for many cellular events including growth, cell homeostasis, defence, neurotransmission, hormone release, structural maintenance and cytokines. There are two overall mechanisms of secretion, depending on whether proteins transit via the ER and Golgi compartments or not.

The conventional secretory pathway

The proteins that transit through the conventional secretory pathway usually carry a signal peptide (SP) at their N-terminus and/or transmembrane domain, which directs their translocation into the ER [740]. SPs are 15-30 aa sequences at the N-terminus of secretory or transmembrane proteins. There is no specific consensus sequence for this motif, but in general it has three common features: a positively charged N-terminus, a hydrophobic region and a C-terminal polar,

uncharged region. The consensus region dictates that residues -3 and -1 with respect to the cleavage site must be small, neutral amino acids. The translocation of both soluble proteins and membrane proteins can occur co-translationally [741], and this is the most common mechanism in mammals. On the other hand, translocation can also occur post-translationally, without the protein being folded [742]. The latter mechanism is the most common event for simpler organisms, but it has also been identified in mammals for specific proteins [742].

SPs are usually cleaved from the rest of the protein by signal peptidase complex during translocation across the ER membrane. The signal peptidase recognition site is the Ala-X-Ala motif (where X is any amino acid), located at the C-terminus of the signal peptide [743]. In the ER, proteins are synthesised, folded and partially glycosylated. For non-ER resident proteins that have been properly folded, they exit the ER via coat protein complexes II (COPII) vesicular mediated transport. After budding from the ER membrane, COPII vesicles fuse with the ER-Golgi intermediate compartment (ERGIC), which is a distinct organelle separate from the ER and cis-Golgi compartments [744]. The fusion of COPII vesicles with the ERGIC is a very well-orchestrated step that depends on the correct pairing of SNAREs on the vesicle surface and the acceptor membrane [745]. Microtubules are responsible for the transport of COPII vesicles from the ERGIC to the *cis*-Golgi.

From the ERGIC, the secretory protein cargo transits to the Golgi apparatus, an organelle composed of a set of stacked cisterna with different enzymatic contents and activity. Adjacent to the trans-Golgi, a tubular-compartment termed the 'trans-Golgi- network (TGN)' exists. Proteins are transported through the Golgi to the TGN via cisternal maturation. From the TGN proteins are sorted: a) in secretory vesicles, via constitutive secretion, which is a constant, non-regulated process, and b) in immature secretory granules, which accumulate in the cytoplasm. Upon external stimuli, they mature and are transported to the plasma membrane (**Figure 3.2**).

The Unconventional Secretory Pathway

The unconventional secretory route is composed of two major categories depending on whether the secreted protein possesses a signal peptide or not. The first route is for cytoplasmic proteins that lack a signal peptide, which can be secreted by one of three major mechanisms (Type I, II and III, detailed below), and secondly, proteins with a signal peptide and/or transmembrane domain (Type IV) (**Figure 3.2**). A common feature of both of these pathways is that both are induced by stress [746]. These pathways are discussed below;

In Type I secretion, proteins can directly cross the plasma membrane upon formation of a pore, which can be self-sustained or driven by inflammation [746, 747]. In contrast, Type II secretion involves the ABC transporter protein, and it has been described for the secretion of acylated peptides and yeast mating peptides [746]. Next, proteins secreted by the Type III mechanism follow an autophagosome and endosome-based process [748]. These proteins translocate directly across the autophagosome/endosome membrane, relying on these membrane-bound organelles that modify their normal function to assist in protein secretion. Finally, Type IV involves proteins with a signal peptide or/and transmembrane domain that are synthesised in the ER, but by-pass the Golgi on their route to the plasma membrane [749]. This process is independent of the classical COPII vesicular-mediated mechanism, and it is initiated upon induction of cellular stress, such as ER stress or mechanical stress [746].

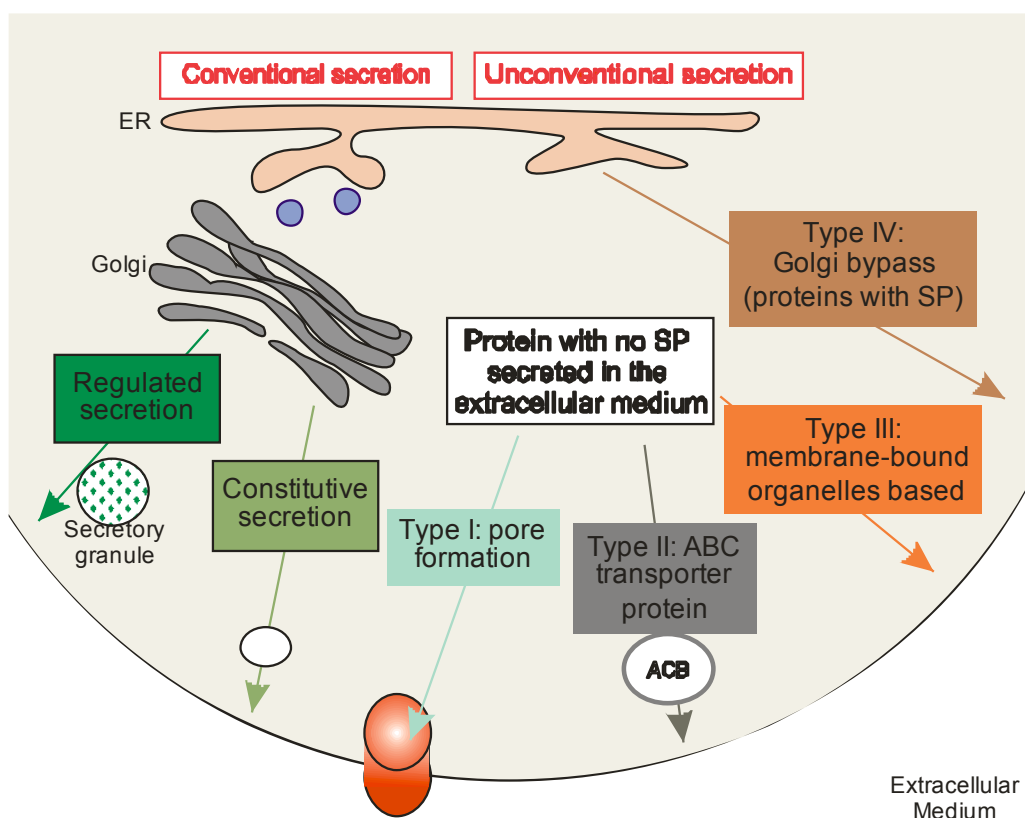


Figure 3.2 Cellular secretory pathways Proteins with a signal peptide are secreted through the conventional secretory pathway via the ER-Golgi network. It can be constitutive, when is non-regulated, or regulated. The unconventional secretory pathways include four different types. Proteins without signal peptide are secreted through: Type I which is dependent on the formation of a pore in the cytoplasmic membrane. Type II, where ABC transported proteins assist with the secretion. Type III when the secretion is mediated by membrane-bound organelles, such as autophagosome or endosome. Finally, proteins with a signal peptide can also be secreted through the unconventional secretory pathway by bypassing the Golgi, Type IV.

3.2. Aims of this chapter

Alternative splicing is a tightly regulated mechanism that is crucial for normal cellular function. Aberrant splicing plays an important role in ALS pathology and importantly, FUS and TDP-43 normally function as regulators of alternative splicing. Recently, a novel alternative splicing mechanism was described, which gives rise to more than 2000 predicted novel isoforms. Among them, an alternatively spliced isoform of FUS was predicted, which we have termed 'FUS^{EC}'. Therefore, the aim of this chapter was to identify the novel FUS isoform at both the mRNA level and at the protein level in

human primary neurons and in cell lines. Finally, since the original bioinformatics study by Wilson et al. [731] predicted the isoform to be extracellular, a second aim was to confirm this in cell lines and *in vivo*.

3.3. Material and methods

3.3.1. Foetal human primary neurons

Primary human foetal brain tissues were obtained from therapeutic terminations of 16 to 19-week-old fetuses. The primary neuronal culture work was approved by Macquarie University Human Ethics Committee (REF: 5201600719). Cortical tissue was dissected, cut into pieces under sterile conditions and digested using the Neuron Isolation kit (Miltenyi). Cortical neurons were plated in 24-well or 6-well culture plates coated with Matrigel (1/20 in Neurobasal) and maintained in Neurobasal medium supplemented with 1% (v/v) B-27 supplement (Thermo Fisher Scientific, Australia), 1% (v/v) Glutamax (Thermo Fisher Scientific, Australia), 1% (v/v) antibiotic Antimitotic (Thermo Fisher Scientific, Australia), and 0.5% (v/v) glucose. The cells were maintained at 37°C in a humidified atmosphere of 5% CO₂.

3.3.2. RNA extraction and quantification

RNA extraction from HEK293T cells and human primary neurons (8 days post-plating) was performed using an RNeasy mini kit (QIAGEN). Cells were lysed in RLT (RNA lysis buffer) buffer (QIAGEN), containing 1:100 β-mercaptoethanol to support the binding of RNA to the silica membrane. Extraction of RNA was performed following the manufacturers protocol and RNA was diluted in 20 µl of RNAase-free water and stored at -80 °C.

The concentration of RNA was analysed directly using a Nanodrop ND-1000 spectrophotometer and RNA was quantified with the Nanodrop 2000 software. A conversion of 1.0 A₂₆₀ = 50 ng/µl was used to determine the original RNA concentration, and A₂₆₀:A₂₈₀ and A₂₆₀:230 ratios were used to examine the purity of RNA. When readings of A₂₆₀>2.1:A₂₈₀>1.85 and A₂₆₀:230>1.8 were obtained, the RNA was considered to be satisfactorily pure.

3.3.3. RT-PCR and PCR

Reverse transcriptase Polymerase Chain Reaction (RT-PCR) was carried out following the “Invitrogen Superscript Vilo mastermix” (Invitrogen) protocol. The reaction was initiated with 2 µg of RNA mixed with 4 µl of SuperScript® VILO™ MasterMix (Invitrogen), and DEPC-treated water was added until a final volume of 20 µl was obtained. A negative control reaction with no RNA was included. Reactions were mixed gently and incubated in a Thermocycler (Thermo Scientific) as follows: 25°C for 10 min, 42°C for 90 min, and the reaction was terminated at 85°C for 15 min. cDNA was stored at -20°C until required. To amplify complementary DNA (cDNA) encoding endogenous FUS^{EC} (extracellular isoform of FUS), specific primers were designed (**Table 3.2**). The protocol from the manufacturer was followed. PCR reactions containing 4 µl of 5 X MyTaq Reaction buffer was mixed with 1 µl of 10 mM Forward primer and Reverse primers, 1 µl of template cDNA, 0.25 µl of MyTaq HS DNA polymerase (Bioline), in a total volume of 20 µl. A negative control reaction with no template cDNA was included, as well as two positive control reactions, to amplify two widely conservative and expressed genes, both the TATA-box binding protein (TBP) and the phosphoglycerate kinase I (PGKI) gene (see primers sequence in the **Table 3.2**). The cDNA was amplified in a Thermocycler (ThermoScientific) using an initiation denaturation temperature of 95°C for 1 min, followed by 30 cycles of denaturation at 95°C for 15 s, annealing at 60°C for 15 s and extension at 72°C for 10 s. Samples were loaded onto a 3% agarose gel and visualized to identify DNA bands of the expected size (200 bp).

Table 3.2 Primers details used for PCR

Primer Name	Primer sequence (5'-3')
FUS ^{EC} FP 1	ATGGCAATCAAGACCAGAGTGGT
FUS ^{EC} RP 1	ATCCTTGGTCCCGAGGGCCCCATG
TBP1 FP	GGGAGCTGTGATGTGAAGT
TBP1 RP	GGAGGCAAGGGTACATGAGA
PGK1 FP	TCACTCGGGGCTAAGCAGATT
PGK1 RP	CAGTGCTCACATGGCTGACT

3.3.4. Agarose gel electrophoresis and gel extraction of plasmid DNA

The DNA samples were mixed with 6x purple loading dye (New England Biolabs) and loaded onto a 1 % (w/v) agarose gel prepared in TAE buffer (40 mM Tris, 1 mM EDTA, 0.114 % v/v glacial acetic acid), and 0.1 % (v/v) Gel Red (Biotium) with 7 μ l of SYBER Safe was used as a size marker for electrophoresis, a 100 bp DNA ladder, hyperladder 1kb (Bioline) and easy ladder I (Bioline) were used to estimate the size of the DNA fragments. The gels were electrophoresed at 110 V for 1 h in TAE buffer and visualized under UV light using a ChemiDoc imaging system (Bio-rad). Target DNA fragments were excised from the gel and extraction of plasmid DNA was performed using QIAquick Gel Extraction Kit (QIAGEN) following manufacturer's protocol. The final DNA pellet was eluted in 30 μ l of MilliQ water and quantified using Nanodrop 2000 software and Sanger sequenced by the Australian Genome Research Facility using the primers specified.

3.3.5. Acetone precipitations

For protein acetone precipitation, 100 % acetone was pre-chilled at -80°C freezer, and 4 volumes of ice-cold acetone were added to the sample. Samples were incubated at -20°C overnight and centrifuged at 4000 xg for 10 min at 4°C. Supernatant was discarded and pellet was let to air dry.

3.3.6. Two Dimensional Gel Electrophoresis (2DGE)

To prepare the samples for 2DGE, 10 mL of conditioned medium from cultures of HEK293T cells was acetone precipitated, and the pellet was dissolved in 500 μ l of dilution buffer (7 M urea, 2 M thiourea and 4% CHAPS). The conditioned media pellet or 250 μ l of cell lysate was buffer exchanged (using centrifuge filter unit) in dilution buffer until the conductivity was < 300 μ S.cm⁻¹ (x4). Samples were diluted in 7 M urea, 2 M thiourea, 4 % (v/v) CHAPS, 40 mM Tris-HCL and reduced by adding DTT to a final concentration of 5 mM, followed by incubation for 1 h at room temperature. Next, to alkylate the samples, acrylamide was added to a final concentration of 10 mM, followed by incubation for 90 min at room temperature. Bromophenol blue was added to each sample as an

indicator for isoelectric focusing. Passive re-hydration was performed in a re-hydration tray with a 11 cm Immobilised pH gradient (IPG) 3-10 strip (Bio-rad) placed on top of the sample to allow passive rehydration for 5 h at room temperature.

Isoelectric focusing (IEF) was conducted on a Protean IEF Cell (Bio-Rad, MA, USA) with a current limit of 50 μ A per strip using the following program: 300 V for 5 h, a linear gradient to 8000 V for 8 h and 8000 V until 1000 kVh was reached. The strips were covered by mineral oil to control the temperature during IEF. Focused IPG-strips were briefly rinsed in Milli-Q water and equilibrated with 6 M urea, 2 % (w/v) SDS and 2 % (v/v) glycerol for 30 min at room temperature. The second dimension gel was run on 10-20 % Criterion Tris-HCl pre-cast gels (Bio-Rad, MA, USA) using the following conditions: 30 V for 10 min and 150 V for 90 min. 2DGE separated proteins were transferred to a nitrocellulose membrane and immunoblotting was performed using an anti-FUS antibody (Abcam #23439).

3.3.7. Human CSF samples

The use of human CSF samples was approved by Macquarie University Human Ethics Committee (REF: 5201600401). Cerebrospinal fluid samples from healthy subjects (n=4) were kindly donated by the Pitié-Salpêtrière Hospital in Paris, France (**Table 3.3**).

Table 3.3 Details of healthy subjects for CSF studies

	Age	Sex
Control 1	83	Male
Control 2	71	Female
Control 3	54	Female
Control 4	59	Female

3.4. Results

3.4.1. FUS^{EC} is predicted to be a secreted protein

To probe whether FUS^{EC} is an extracellular protein, as predicted by Wilson et al. [731], we first examined the predicted localization of the protein according to its sequence, using three different software programs: SignalP v4.1. [750], TMHMM [751] and Topcons [752]. Each of these programmes is specialized in predicting different proteins regions (signal peptides, transmembrane regions) or subcellular localization. Since there is no programme that combines these outputs, we decided to use these three programmes to compare their outputs and obtain a more reliable prediction.

SignalP v4.1 predicts the presence and localization of signal peptides from the primary sequence of a protein using two types of neural networks: SignalP-transmembrane (TM) and SignalP-noTM networks. Compared to SignalP-noTM network, SignalP-TM was trained with transmembrane domains as negative data and can thereby discriminate signal peptides from transmembrane regions. SignalP includes a decision scheme to automatically determine the network to be used. When SignalP-TM predicts four or more transmembrane regions, SignalP-TM is then used for the final prediction. The neural networks in SignalP produce three output scores for each position in the input sequence. The *C-score* (row cleavage site score) predicts the position of the cleavage signal peptide site. The *C-score* is high at the position immediately after the cleavage site (the first residue in the mature protein). The *S-score* (signal peptide score) assesses the presence or absence of a signal peptide within the primary sequence and it detects aas which constitute the signal peptide sequence. Finally the *Y-score* (combined cleavage site score) combines the *C-score* and the slope of the *S-score*, therefore identifying the cleavage site if the *C-score* has multiple peaks (where only one is the true cleavage site). The output shows the first 70 aa of the protein sequence, since signal peptides are usually found in this region. The threshold is calculated using Matthew's correlation coefficient.

The primary sequence of FUS^{EC} was analysed using SignalP-TM network (**Figure 3.3a**). The default threshold was used, 0.5. One peak in *C-score* (0.291) and *Y-score* (0.227) were detected at position 23. *S-score* was high at position 20 (0.258) and then dropped at position 28. However, no score reached the threshold (0.5), suggesting that FUS^{EC} does not have a cleavable signal peptide.

The choice of signal-TM network suggests that FUS^{EC} has transmembrane residues. Therefore, it was next analysed the FUS^{EC} protein sequence with TMHMM server 2.0 which predicts the presence of transmembrane domains within an aa sequence (**Figure 3.3b**). The results produced from TMHMM include a detailed specification of the number of transmembrane helices (TMH) regions. The number of residues composing the TMH and the probability that the N-terminus is cytoplasmic are then calculated [751]. Residues 1 to 21 in FUS^{EC} were predicted to be cytoplasmic, residues 21 to 44 were predicted to be TMH and residues 45 to 321 were predicted to be found extracellularly. Interestingly, the TMH predicted domain is localized within the first 60 aa, indicating that this domain could be a signal peptide.

We then used Topcons, which is a consensus prediction tool using five different topology prediction algorithms: Octopus [753], Philius [754], PolyPhobius [755], SCAMPI (multiple sequence mode) [756] and spoctopus [757]. These five algorithms are used as input to the Topcons Hidden Markov Model (HMM). When analysing FUS^{EC} protein sequence with this programme (**Figure 3.3c**), Philius predicted a signal peptide from residues 1 to 42 of FUS^{EC}. Polyphobius detected a transmembrane helix from aa 20 to 45. Both predicted that the rest of the protein (after residue 45) was extracellular. Octopus, SCAMPI and Scopopus predicted that the whole FUS^{EC} protein sequence was extracellular. Finally, Topcons consensus predicted that FUS^{EC} had a signal peptide from aa 1 to 22 and that the rest of the protein is extracellular, even though the reliability score was quite low, possibly due to the contradictory predictions calculated by the different algorithms (**Figure 3.3c**).

In conclusion, the software used in this study made different predictions. SignalP did not predict the presence of signal peptide within FUS^{EC}. A transmembrane helix at position 20-45 was predicted by both TMHMM and Polyphobius. Octopus, SCAMPI and Scioptopus predicted that the whole protein was extracellular. The presence of a signal peptide from residues 1-42 at the N-terminus of FUS^{EC} was predicted by Philius and the consensus Topcons. Due to the strong similarity between transmembrane helices and signal peptides (which consist of a core hydrophobic region that can form alpha helices), classifiers have limited ability to discriminate signal peptides from transmembrane helices. Therefore, it is possible that the bioinformatics tools which predicted a TMH (TMHMM and Polyphobius) were instead detecting a SP. However, a common prediction from all the bioinformatics tools used here was that the FUS^{EC} protein sequence is localized in the extracellular space, either in part, or entirely. Hence we next analysed the presence of FUS^{EC} in the extracellular space experimentally.

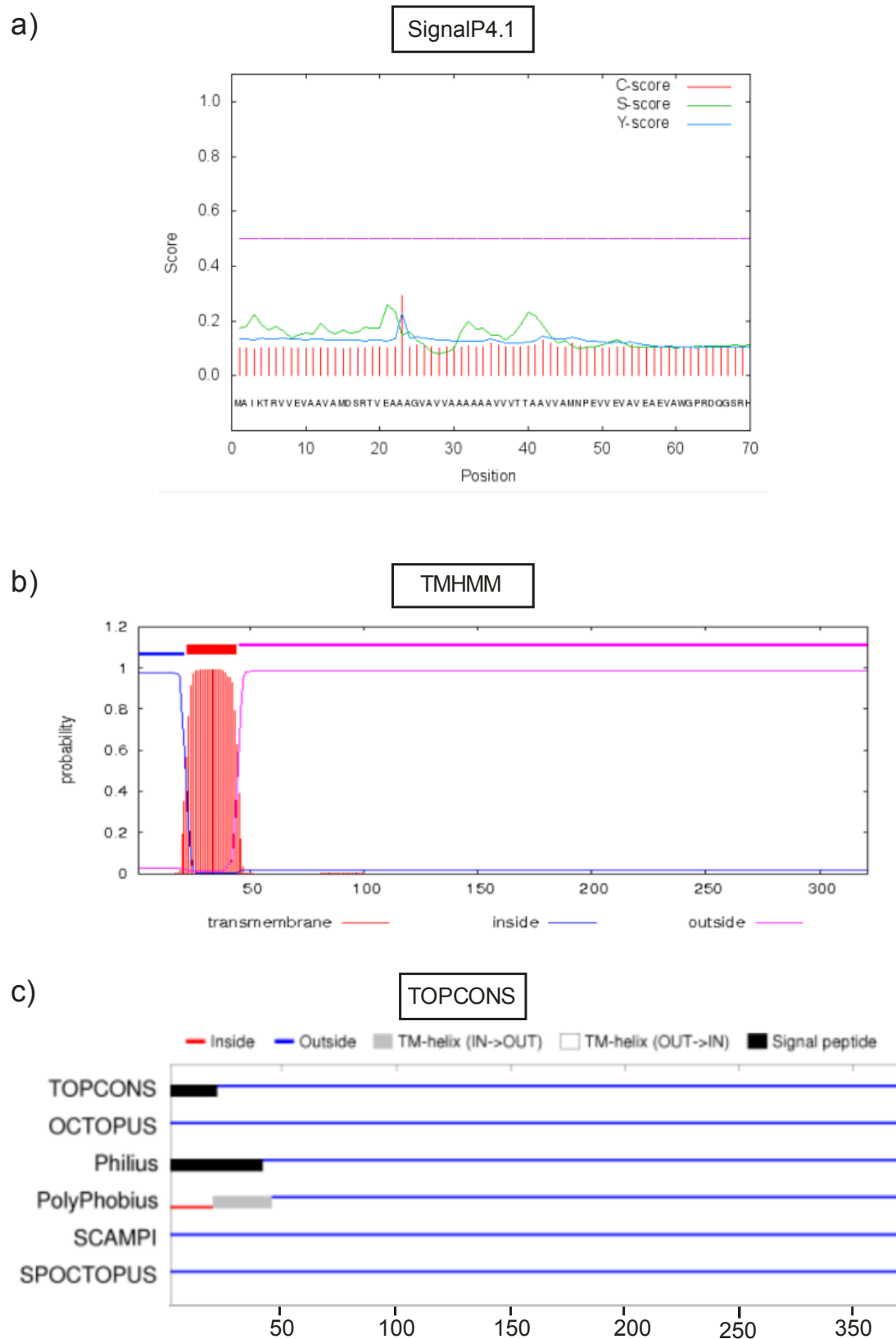


Figure 3.3 Analysis of FUS^{EC} protein sequence using bioinformatics tools that predict the presence of signal peptides a) Plot displaying the scores (C = cleavage, S = signal peptide, Y = combined) predicted for each amino acid by SignalP v4.1. (b) Plot displaying the prediction of a transmembrane region in FUS^{EC} using the TMHMMs Software. The Y axis represents the probability and the x axis the amino acid position,

on the top of the plot of the N-best predictions representing the most probable topology (c) Schematic diagram of the signal peptide and transmembrane domains of FUS^{EC} predicted using the TOPCONS consensus programmes. The TOPCONS consensus results are shown on the upper part of the figure.

3.4.2. FUS^{EC} novel isoform is expressed at mRNA level in HEK293T cells and in human primary neurons

Firstly, the aim was to confirm the presence of FUS^{EC} in cell culture studies. For this purpose, it was analysed whether the mRNA of FUS^{EC} was present in both untransfected HEK293T cells and in human primary neurons. We chose HEK293T cells as they are widely used cell line in transfection studies and have high levels of protein expression that will give sufficient material to study the biology better. While other cells such as SH-SY5Y, due to their low protein expression levels could make difficult the identification and characterization of FUS^{EC} protein at endogenous levels. Additionally, human primary neurons were used due to the relevance of FUS^{EC} to ALS. RNA was extracted from HEK293T cells and human primary neurons, and then it was reverse transcribed and amplified using specific primers for FUS^{EC}. A unique region in FUS^{EC} was selected to perform PCR, so that the presence of endogenous FUS^{EC} could be confirmed separate from the expression of canonical FUS. Specific primers were designed on the basis of the predicted sequence from Wilson et al. [731]. The forward primer binds at the alternative start codon in exon 6 and the reverse primer at the junction of exon 6 with 8, a unique region only found in FUS^{EC} (**Figure 3.4a**). A negative control for PCR was included, where no cDNA was added to the reaction. Primers for TATA-box binding protein gene (TBP) and Phosphoglycerate kinase I (PGKI), two ubiquitously expressed genes in human tissues, were used as positive controls [758, 759]. PCR of the cDNA from human primary neurons (**Figure 3.4b**) and HEK293T cells (**Figure 3.4c**) using the primers specific for FUS^{EC}, produced an amplicon of 200bp, corresponding to the expected size of the amplified region for FUS^{EC}. Sanger sequencing of DNA after extraction of the PCR product from the gel, confirmed the presence of the FUS^{EC} sequence (**Figure 3.4d**).

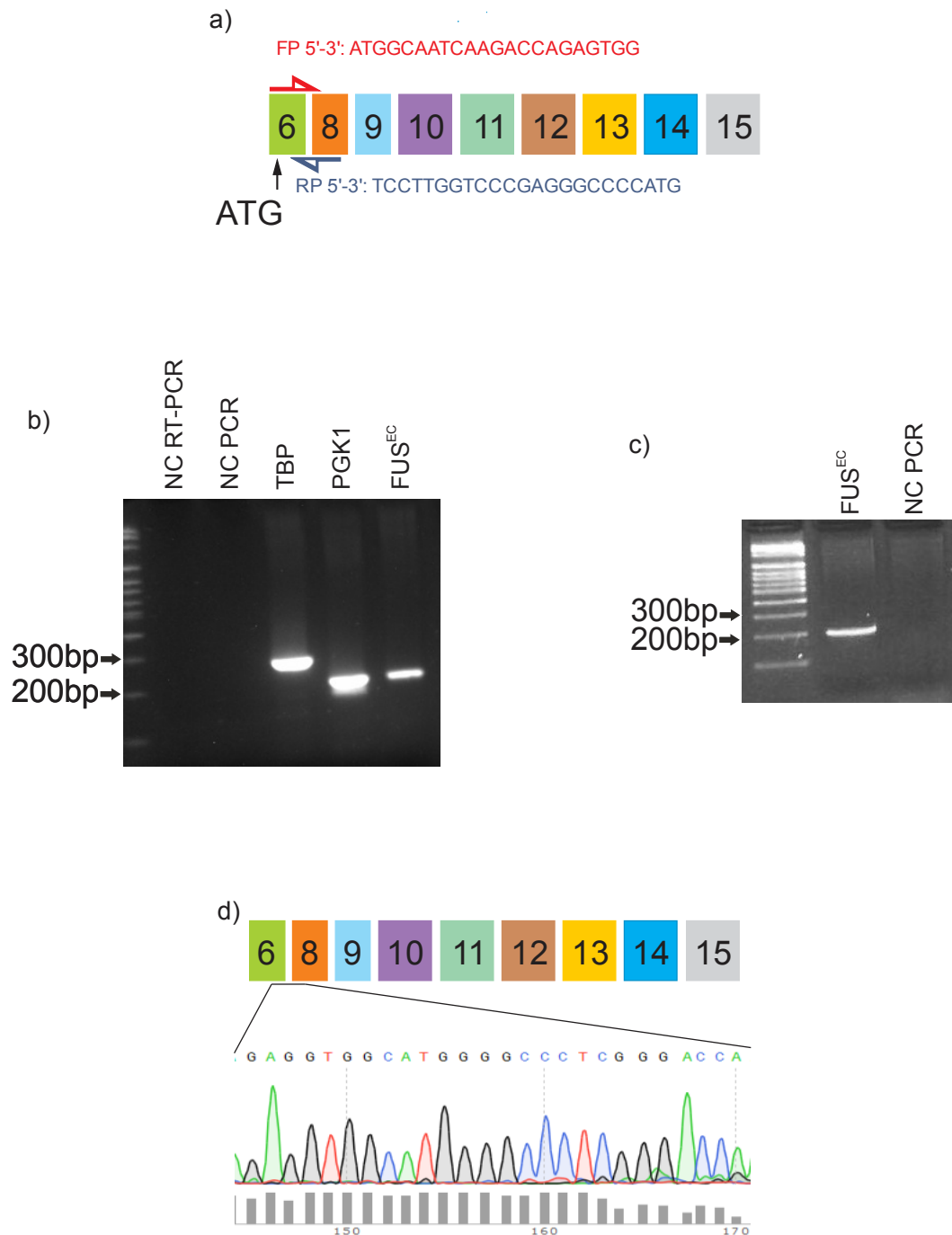


Figure 3.4 Detection of FUS^{EC} mRNA in HEK293T cells and in human primary neurons using end point PCR (a) Schematic diagram of the FUS^{EC} gene between exons 6 and 15. The red arrow indicates the position of the forward primer (FP) and the blue arrow illustrates the position of the reverse primer (RP) used for PCR. The FP and RP primers are used to specifically amplify FUS^{EC} from cDNA obtained from primary

neurons and HEK293T cells. (b-c) Agarose gel of the PCR products obtained from cDNA obtained by RT-PCR from RNA extracted from human primary neurons (b) and HEK293T cells (c). Lanes include negative controls for PCR reaction (NC PCR), two positive controls with primers for TATA-Box binding protein gene (*TBP*) and Phosphoglycerate kinase I gene (*PGKI*) and primers FP and RP used to detect FUS^{EC}. (d) DNA was extracted from the agarose gel and the sequence of the unique region of FUS^{EC} was analysed by Sanger sequencing.

3.4.3. FUS^{EC} is found extracellularly, implying it is a secreted protein

We then investigated expression of endogenous FUS^{EC} at the protein level in conditioned media of untreated HEK293T cells. For this purpose we used an anti-FUS antibody that binds to the C-terminus of FUS and therefore, it will identify both FUS isoforms, canonical FUS and FUS^{EC} (**Figure 3.5a**). Western blotting of the cell lysate and conditioned media fractions demonstrated the presence of a 75 kDa band in the lysate, corresponding to the expected size of canonical endogenous FUS, and a lower 40 kDa band in the concentrated media, representing endogenous FUS^{EC} (**Figure 3.5b**). Even though the predicted molecular weight of FUS^{EC} is 33 kDa, given that canonical FUS is known to run at a different mobility on SDS-PAGE than its predicted MW, this result implies that FUS^{EC} is secreted into the media of HEK293T cells. Glyceraldehyde 3-phosphate dehydrogenase (GAPDH) is an intracellular protein that was used as a control to detect cell lysis, which could account for the localization of normally cytoplasmic proteins in the media. However, GAPDH was hardly detected in the media, whereas it was present in the cell lysate fraction as expected. Together, with the absence of FUS^{EC} in the lysate these findings suggest that FUS^{EC} is not simply present in the media due to leakage from dead cells, thus implying that FUS^{EC} is actively secreted into the media.

To confirm that FUS^{EC} is located extracellularly and hence secreted, 2DGE of the conditioned media and lysate fraction from HEK293T cells was carried out. Western blotting was subsequently performed using an anti-C-terminal FUS antibody. A ~75 kDa band of pI ~9.40 was detected in the cell lysate, corresponding to the expected properties of canonical FUS (**Figure 3.5c**). In contrast, the conditioned media fraction contained multiple spots ~40

kDa in size, with a pI of ~9.28, corresponding to FUS^{EC}. Multiple spots representing a single protein are often observed due to post-translational modification, which can alter both the molecular weight and isoelectric point of the native protein (Figure 3.5d) [760]. Hence these data imply that FUS^{EC} is post-translationally modified.

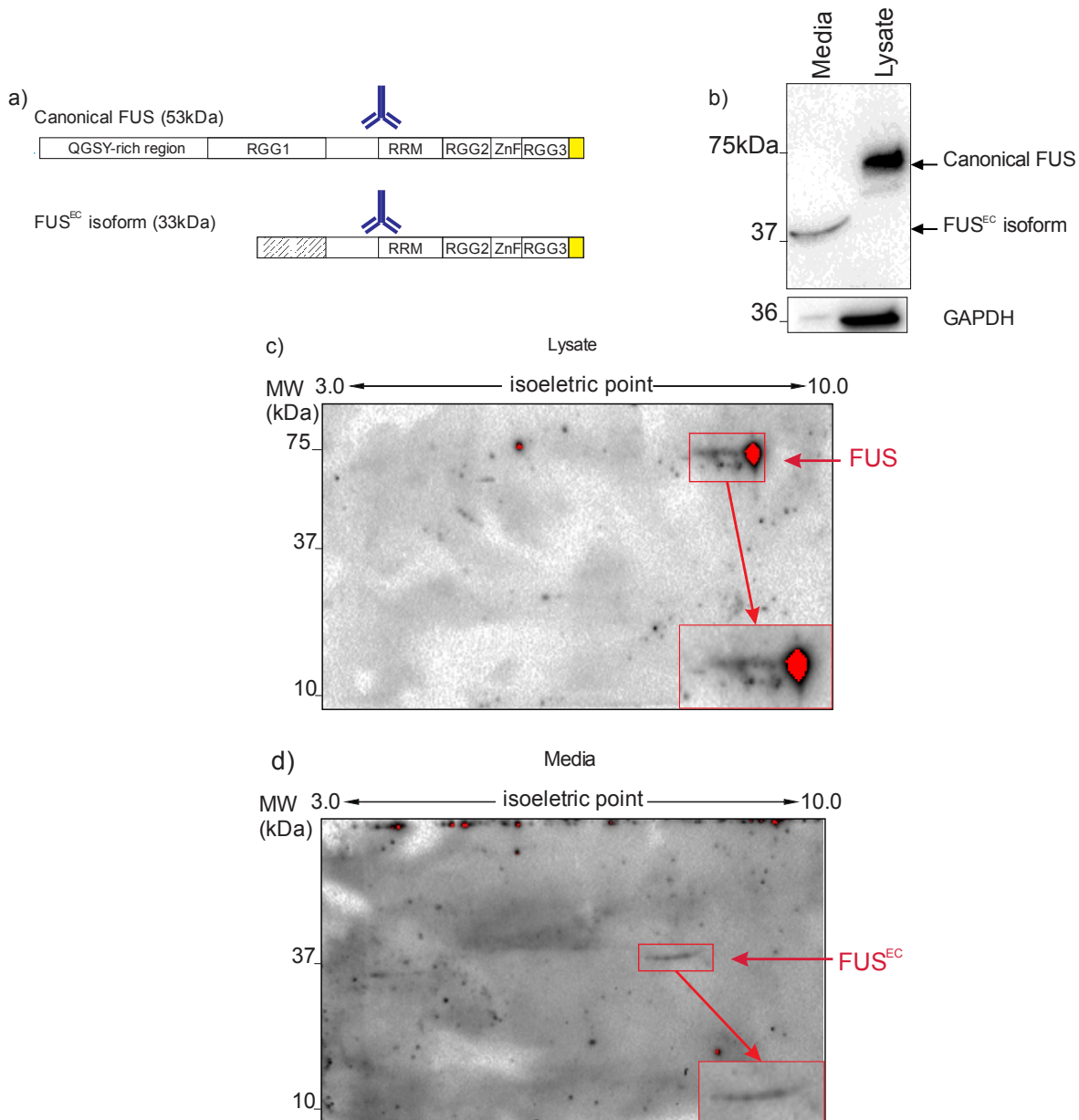


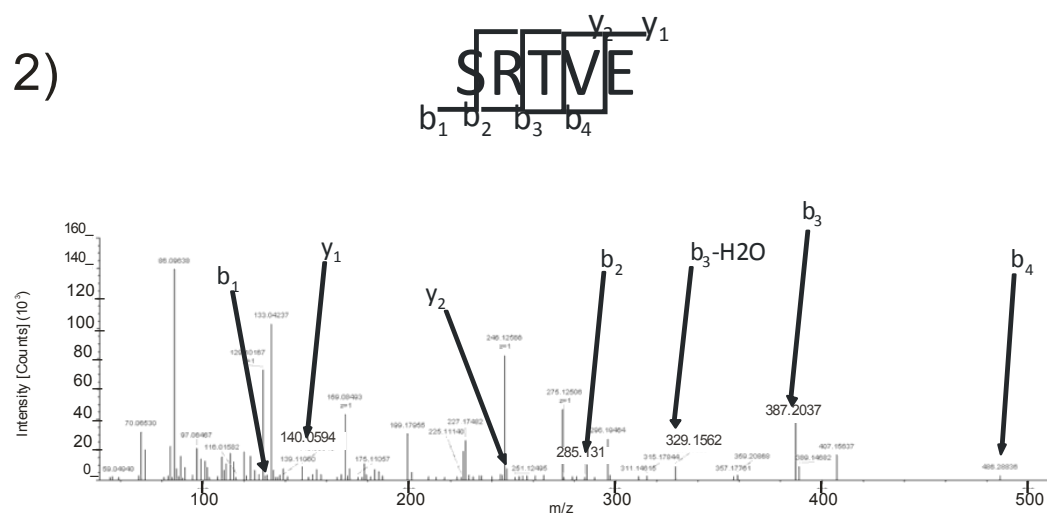
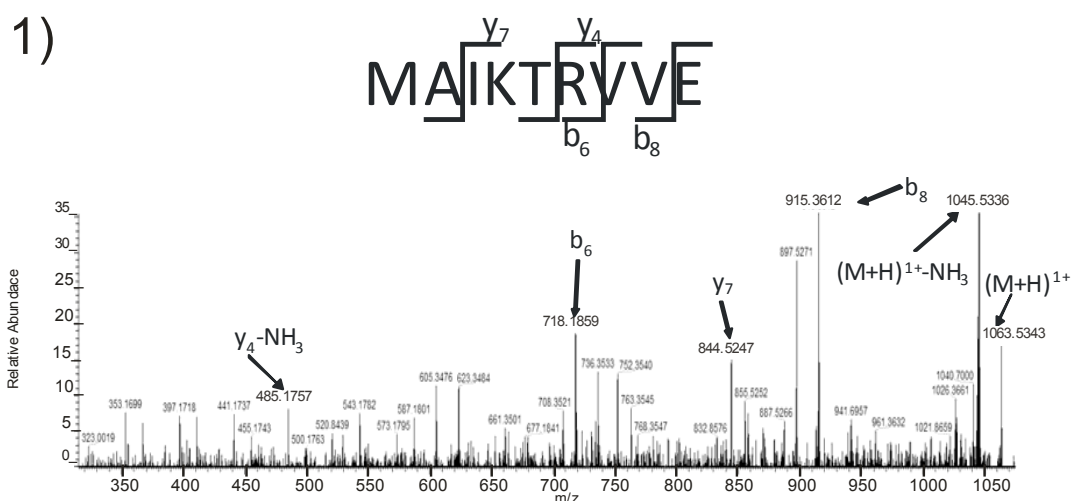
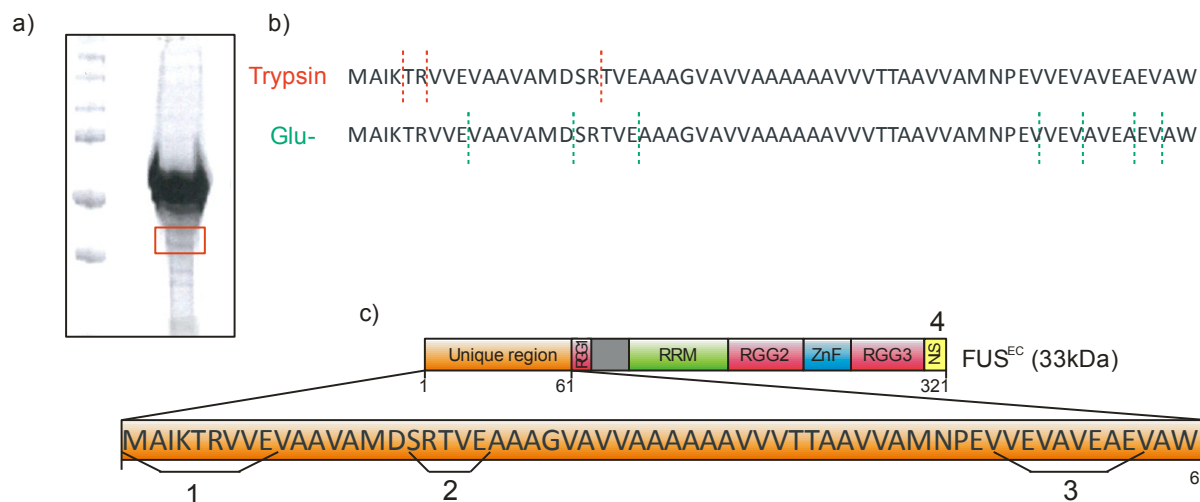
Figure 3.5 Detection of FUS^{EC} in the media of HEK293T cells (a) Schematic diagram representing where the anti-C-terminal FUS antibody used in this study binds to canonical FUS and FUS^{EC}. (b) Western blotting of HEK293T cell lysate and media fractions using the anti-C-terminal FUS antibody. GAPDH is shown as a loading control. Molecular weight markers are shown on the left. (c, d) Western blotting of 2DGE using the C-terminal FUS antibody of the (c) lysate, and (d) media of HEK293T cells. The horizontal dimension of each gel displays the predicted isoelectric point and

the vertical dimension illustrates separation of proteins based on MW. The position of canonical FUS and FUS^{EC} is indicated by a red frame.

Next, LC-MS/MS was performed to confirm that the 40 kDa protein detected in the conditioned medium of HEK293T cells was FUS^{EC}. For this purpose, we aimed to detect the presence of unique peptides from the N-terminal sequence of FUS^{EC} that are absent in canonical FUS. Media of untransfected cells was collected after 24 h in culture, and then concentrated using centrifugal filter unit. SDS-PAGE electrophoresis followed by Coomassie Blue staining was then performed to visualise the FUS^{EC} band. A band at ~40 kDa was excised from the gel and then analysed by LC-MS/MS (**Figure 3.6a**). Trypsin, which cleaves peptides at the C-terminus of lysine or arginine residues, is commonly used in LC-MS/MS studies to generate peptides for analysis. However, examination of the N-terminal protein sequence of FUS^{EC} revealed that digestion with Trypsin would generate either very short or very large peptides (**Figure 3.6b**). Unfortunately, this would make detection of FUS^{EC} difficult because only one conceivable proteolytic peptide (VVEVAAMDSR) could be generated for LC-MS/MS analysis. Hence, instead of Trypsin, we used an alternative protease: Endoproteinase Glu-C, to increase the likelihood of identifying more peptides (three) that are unique to FUS^{EC}. Endoproteinase Glu-C hydrolyses peptide bonds at the carboxyl side of Glutamic (E) and Aspartic (D) acid residues, thus generating peptides with a suitable length (7-35 amino acids) to be detected by LC-MS/MS (**Figure 3.6b**).

Using this approach, we verified 4 peptides present in the conditioned media that were present in FUS^{EC} and we confirmed these by manually inspecting the MS2 fragmentation based on the y/b ion series. Three peptides specific for FUS^{EC}, located in the unique N-terminal sequence, were identified (1: ¹MAIKTRVVE⁹, 2: ¹⁷SRTVE²¹, 3: ⁵⁰VVEVAVEAE⁵⁸) and one peptide from the C-terminus (4: ²⁹⁸RGGFGPGKMDSRGE³¹¹) which is also found in canonical FUS (**Figure 3.6c**). The FUS^{EC}-specific peptide sequence ¹MAIKTRVVE₉ was identified at m/z y₄ 485, y₇ 844, corresponding to RVVE and IKTRVVE respectively. Additionally, b₆ 718 and b₈ 915 were identified, representing part of this sequence: MAIKTR and MAIKTRVV respectively. The second peptide

unique for the N-terminus of FUS^{EC} identified was $_{17}\text{SRTVE}_{21}$, at m/z y_1 , 148 y_2 247, corresponding to E and VE respectively. Furthermore, m/z b_1 130 b_2 286 b_3 387 b_4 486, corresponding to S, SR, SRT AND STRV respectively was also detected. The third peptide identified from the unique N-terminal of FUS^{EC} was $_{50}\text{VVEVAVEAE}_{58}$, identified with m/z a_1 72, a_2 , 86, b_2 199, representing V, VV respectively plus ions y_1 148, y_6 618, y_7 746 representing the peptides E, VAVEAE and EVAVEAE respectively. Finally, the C-terminal peptide we identified that is common to both FUS^{EC} and canonical FUS was $_{298}\text{RGGFGPGKMDSRGE}_{311}$. Abundant ions were also detected with m/z a_1/b_1 129, a_2 169, a_3/b_3 226 a_6 544, b_{11} 1025, b_{10} 510, corresponding to the following peptides respectively; R, RG, RGG, RGGFGP, RGGFGPGK, RGGFGPGKM. In addition, ions with C charge with m/z y_1 148, y_2 205, y_3 361, y_6 814 were detected, corresponding to E, GE, RGE, MDSRGE respectively. Hence these mass spectrometry data confirm that the alternatively spliced isoform of FUS, FUS^{EC}, does indeed exist and it is expressed at sufficient levels to be detectable under endogenous conditions in conditioned media of HEK293T cells. Taken together, these results therefore confirm the discovery of a unique, extracellular FUS isoform (FUS^{EC}).



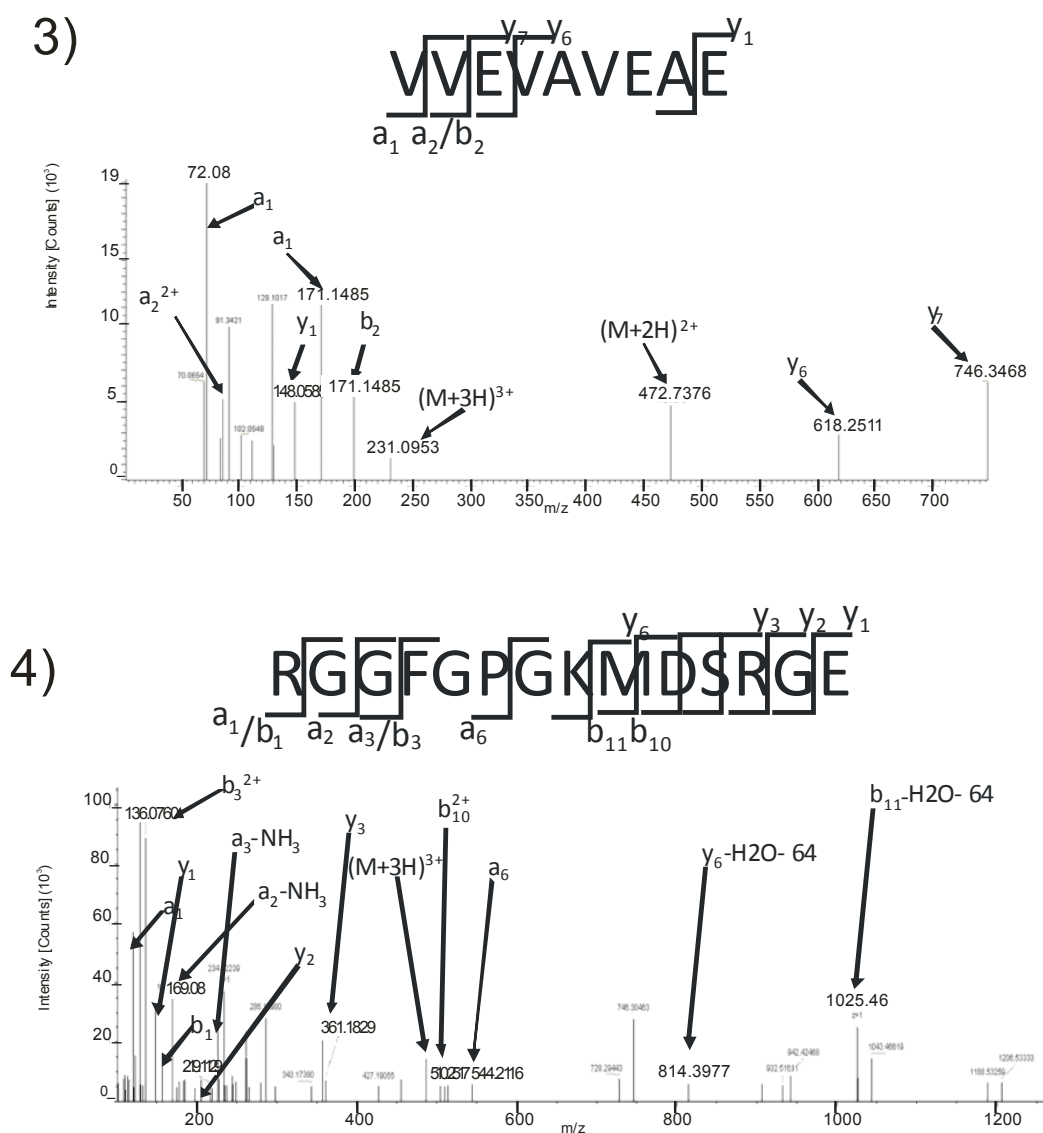


Figure 3.6 LC-MS/MS confirms that FUS^{EC} is present in the conditioned media of HEK293T cells (a) SDS-PAGE gel stained with Coomassie Blue. The conditioned medium prepared from HEK293T cells cultured for 24 h was concentrated and proteins were separated on a 4-15% SDS-PAGE gel. Following Coomassie blue staining, a band of the approximate expected size for FUS^{EC} (40 kDa) was excised and subjected to in-gel digestion, followed by LC-MS/MS. (b) Schematic representation of FUS^{EC} and peptides generated after Tryptic or Glu-C digestion. (c) Annotated spectrum of three different peptides generated from FUS^{EC} after Glu-C digestion. The peptide sequence is shown at the top of each spectrum, with the collision-induced fragmentation pattern. Peptide fragment ions with the N-terminus charge area are annotated by a, b, or c and by x, y or z if the charge is maintained on the C-terminus. The number of amino acid residues present in each fragment are indicated below. (1) MAIKTRVVE peptide (residues 1-9). (2) SRTVE peptide (residues 17-21). (3) VVEVAVEAE peptide (residues 50-58). (4) MS -spectrum of a peptide generated from the C-terminal NLS sequence of FUS^{EC} (RGGFGPGKMDSRGE, residues 298-311) after LC-MS/MS analysis.

3.4.4. Optimization to detect FUS^{EC} in human CSF

Since we confirmed that FUS^{EC} is present in human primary neurons and secreted by human cell lines, we next investigated whether FUS^{EC} is also present in the human CSF. CSF represents an *in vivo* extracellular compartment and it is the only extracellular fluid that is in contact with the central nervous system (CNS) because it originates from the ventricles and it surrounds the brain and spinal cord. Hence CSF is the perfect extracellular environment to examine for the presence of a secreted protein that is relevant to ALS.

CSF obtained from healthy patients was subjected to SDS-PAGE gel electrophoresis and western blotting was performed using an anti-C-terminal FUS antibody (**Figure 3.7a**). The cell lysate fraction from HEK293T cells was used as a positive control for antibody reactivity. Western blotting revealed the presence of a band at 50 kDa when using a short exposure, and several additional bands became visible under longer exposure (**Figure 3.7a**). However, none of the bands corresponded to the expected molecular weight of either canonical or FUS^{EC} (60-75 kDa and 40 kDa respectively). As CSF contains immunoglobulins (IgGs) [761, 762], we hypothesized that at least some of these bands were non-specific and could be due to cross reactivity of the secondary antibody with immunoglobulins present in CSF. To test this hypothesis, CSF samples were loaded onto a SDS-PAGE gel under reducing and non-reducing conditions and western blotting was performed using the C-terminal FUS antibody. A band at 60-75 kDa in the HEK293T cells lysate fraction was present, corresponding to canonical FUS, thus revealing that the antibody was capable of detecting FUS. However, blotting of the CSF samples revealed that whilst under reducing conditions, a band at 50 kDa was detected (**asterisk in Figure 3.7a**), under non-reducing conditions a single band of 250 kDa was present (**red arrow Figure 3.7a**). Given that IgG has a mobility of 250 kDa under non-reducing conditions (it has a MW of 150 kDa but runs around 250 kDa due to its glycosylation [763]) and at 50 kDa under reducing conditions, this suggests that the 50 kDa band corresponds to the heavy chain of IgG. To finally confirm that this band was due to unspecific binding of the

secondary HRP antibody with IgG, the membrane was incubated with the secondary HRP antibody only, without prior incubation with primary antibody. Again the band present at 50 kDa under reducing condition shifted to 250 kDa in non-reducing conditions, and no band was detected in the lysate from HEK923T cells (**Figure 3.7b**). Hence these data confirm that the band at 50 kDa detected in the CSF was probably the result of cross reactivity from the secondary HRP with IgG from CSF. Hence, from these data, it was not possible to confirm the presence of FUS^{EC} in the CSF from healthy human samples.

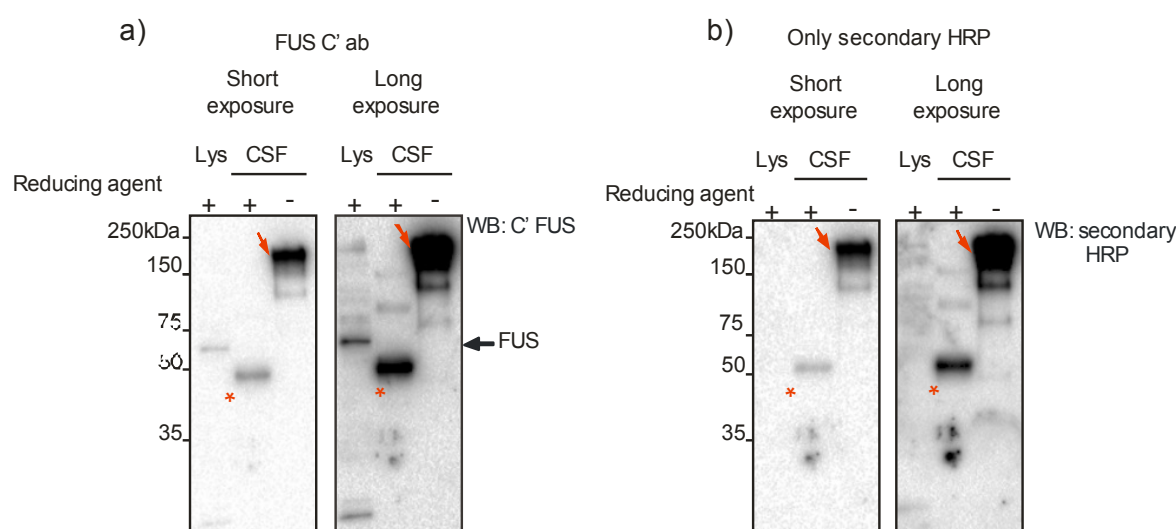


Figure 3.7 Detection of FUS^{EC} in human CSF (a) Western blotting of FUS in extracts prepared from human cerebrospinal fluid (CSF) under reducing or non-reducing conditions. HEK293T cell lysate (Lys) serves as a positive control of FUS expression. (b) Membranes were incubated with secondary HRP antibody and no primary anti-FUS antibody. Red asterisks indicated a ≈ 50 kDa band detected only under non-reducing conditions. Red arrows show unspecific bands around 150-250 kDa.

3.4.5. Characterization of a FUS^{EC} customised antibody

The next aim was to confirm expression of the novel isoform FUS^{EC} using a commercial antibody that was customized to be specific for the unique N-terminus of FUS^{EC}. This would provide additional evidence of the existence of FUS^{EC} by confirming the presence of the unique N-terminus sequence. Furthermore, the aim was to examine expression of FUS^{EC} in human tissues and CSF, using a customized antibody for future applications.

A rabbit polyclonal antibody was raised against a unique peptide at the N-terminus of FUS^{EC}: AVAMDSRTVEAAAGC, with the aim of detecting specifically the FUS^{EC} isoform and not the canonical version of FUS (**Figure 3.8a**). Validation of the customized antibody, which is referred to here as 'AbGenscript#1', was performed following guidelines published by The International Working Group for Antibody Validation [764].

First, the immunoreactivity of the new AbGenscript#1 antibody was compared to the anti-C-terminal FUS antibody (Abcam#23439) used previously (**Figure 3.5b**). Western blotting of conditioned media and lysate fractions from HEK293T cells revealed the presence of a band at ~140 kDa in the conditioned media under non-reducing conditions (without reducing agent) that shifted to 60 kDa in reducing conditions. Initially, reduction was not complete using NuPAGE reducing agent (which contains 500mM DTT) only because the 140 kDa band was retained following treatment. However, when the samples were subjected to stronger denaturing conditions (8 M urea and boiling for 15 minutes) most of the 140 kDa band disappeared and more 60 kDa was visualised (**Figure 3.8b**). This suggested that the AbGenscript#1 antibody was detecting a disulphide-bonded dimer/monomer form of a protein. Unfortunately, there was no band detected at 40 kDa, the expected size of FUS^{EC}. Hence, to confirm the expression of endogenous FUS^{EC} in the conditioned media sample used in this analysis, the western blot membrane was re-probed with the FUS C-terminal antibody used previously (Abcam #23439). As expected, this revealed the presence of a band at 40 kDa in the media samples and a band at 75 kDa in the lysate fraction, demonstrating that both FUS^{EC} and canonical FUS were present respectively (**Figure 3.8c**). This finding suggested that the customised antibody AbGenscript#1 did not recognize FUS^{EC} specifically. Further analyses of the customized antibody were performed using overexpressed FUS^{EC} (detailed in Chapter 4).

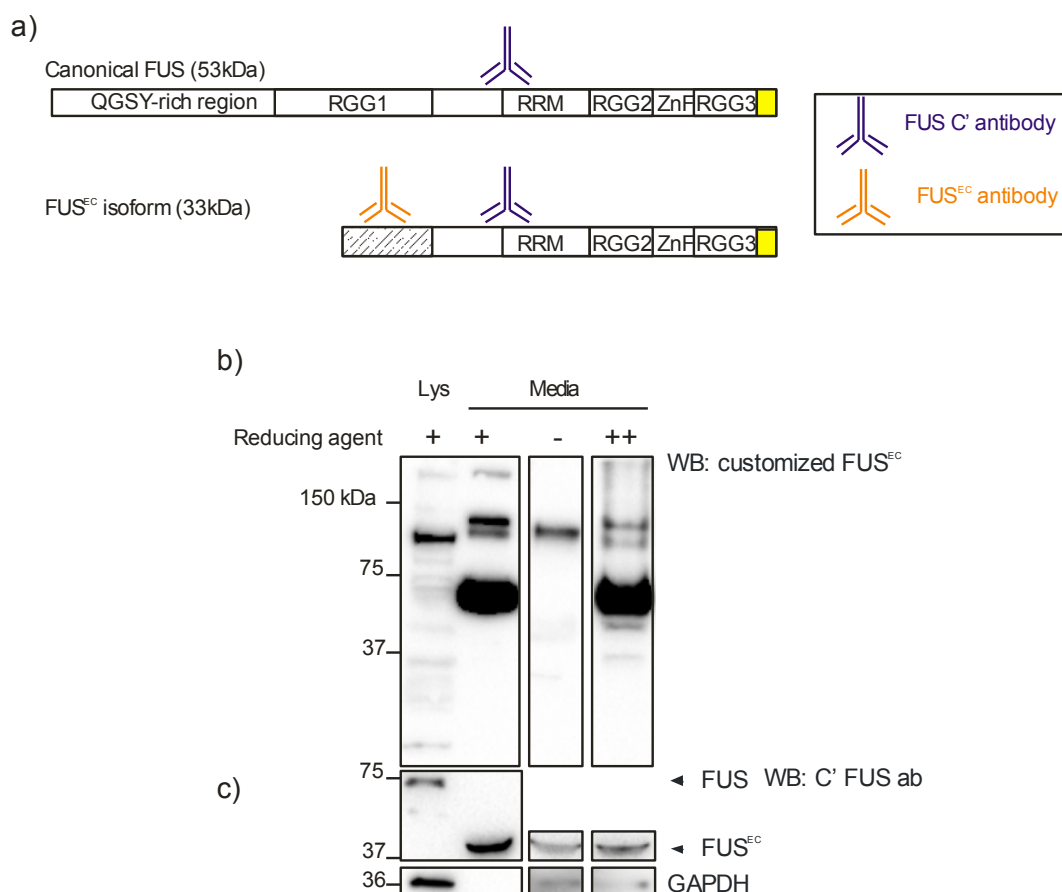


Figure 3.8 Examination of the specificity of the customized antibody designed specifically for FUS^{EC}, AbGenscript # 1 (a) Schematic diagram illustrating localization of the epitope of the anti-FUS C-terminus antibody (C'-FUS, blue) and the anti-FUS^{EC} customized antibody AbGenscript#1 (orange). (b) Western blotting of canonical FUS and FUS^{EC} in the lysate and conditioned media fractions of HEK293T cells under non-reducing, reducing or denaturing conditions using the AbGenscript#1 antibody. GAPDH was used as a loading control. (c) Western blotting of canonical FUS and FUS^{EC} in the lysate and conditioned media fractions of HEK293T cells under non-reducing, reducing or denaturing conditions using the C-terminal FUS antibody (Abcam #23439).

3.5. Discussion

This study provides the first experimental evidence for the existence of the predicted isoform of FUS, FUS^{EC}. Expression of the isoform was confirmed at both the mRNA and protein level in HEK293T cells and human primary neurons. The FUS^{EC} isoform is the result of a combination of an alternative start codon and exon skipping. LC-MS/MS analysis confirmed that FUS^{EC} shares the same C-terminal sequence with its canonical counterpart, but it contains a unique 61 amino acid sequence at its N-terminus. Interestingly, western blotting

and LC-MS/MS analysis of conditioned media demonstrated that this new isoform is secreted into the media of HEK293T cells. Hence this study demonstrates that FUS^{EC} is present in a completely new cellular location compared to the canonical form of FUS.

Wilson et al., predicted that FUS^{EC} was secreted, using the software WoLF PSORT. When analysing the protein sequence with several bioinformatics tools to identify the presence of a signal peptide in the current study, the results were not conclusive. WoLF PSORT predicts subcellular localization by sequence homology with known proteins. From the homologous proteins identified, 13 are extracellular and/or secreted, 12 with demonstrated cleavable signal peptide in the first 14-28 aa. Interestingly, the remaining protein, fibroblast growth factor 9 (FGF-9), is secreted but it possesses an atypical, non-cleavable signal sequence in its N-terminus [765]. FGF-9 belongs to the fibroblast growth factor (FGF) family, which comprises 22 homologous polypeptides that are involved in diverse biological activities. Most FGFs contain a cleavable signal peptide at the N-terminus and are also secreted. However, FGF-9, FGF-16 and FGF-20 are the exception, even though they are also secreted they contain an uncleavable bipartite signal sequence [766]. For FGF-16 and FGF-9, both a N-terminus and central hydrophobic domain were shown to be important for their secretion [766]. Even though they possess a SP without predictable cleavable site, both are glycosylated and secreted efficiently, and they translocate through the classical secretory pathway [767, 768]. Interestingly, when the sequence of FGF-16 was analysed with SignalP-HMM, a previous version of the SignalPv4.1 software used in this chapter, no cleavable SP was predicted [767], similar to FUS^{EC}. Therefore, this suggests that FUS^{EC} could have a SP that is not cleaved, but it efficiently targets FUS^{EC} to be secreted through the conventional secretory pathway via the ER-Golgi compartments.

Amplification of the cDNA from human primary neurons, with specific primers unique for FUS^{EC}, confirms that this alternatively spliced variant skips exon 7 and it possesses an alternative start codon upstream at position 683 of the canonical sequence. This is potentially important as FUS autoregulates its

expression by binding to exon 7 and its flanking regions [512]. Canonical FUS bearing ALS-associated mutations has been demonstrated to skip this autoregulation mechanism and likely exacerbates accumulation of mutant FUS in ALS [512]. Therefore, one could speculate that the FUS^{EC} isoform escapes this autoregulatory mechanism as it lacks exon 7 and thus may play a similar role as mutant canonical FUS.

At the protein level, the data demonstrated that FUS^{EC} is a secreted protein, and LC-MS/MS confirms that it contains a unique 61 aa sequence at the N-terminus and shares the same aa sequence with canonical FUS from aa residues 266 to 526. Peptide masses obtained in this study covered 37% of the unique N-terminal sequence of FUS^{EC} which corresponded to 11.5% of the total FUS^{EC} protein sequence covered. Additionally we identified 3 peptides from the unique N-terminus of FUS^{EC} plus one from its C-terminus. There is no standard minimum % of coverage or peptides identified generally accepted to estimate the confidence when identifying protein by LC-MS/MS. However, the only study determining this suggests that coverage of at least 20% of the protein sequence and the identification of four peptides should give confident results [769]. Whilst the percentage of protein sequence covered in this study was lower than this recommendation, taken together with the mRNA and the western blotting results, provides compelling evidence for the existence of FUS^{EC}. It is probable that the low percentage coverage obtained in this study was the result of the low abundance of endogenous FUS^{EC}. Furthermore, the low % coverage could also be due to incomplete digestion of FUS^{EC}, or alternatively due to the generation of peptides that were too small, too hydrophobic, or on the contrary, too large or hydrophilic. In addition, endoproteinase Glu-C also produces acidic peptides (with Glutamic acid at the C-terminus) which would confer FUS^{EC} with a negative charge and unfortunately because LC-MS/MS is analysed in positive ion mode, it prefers ionisation of positive charged species.

Furthermore, the LC-MS/MS results obtained in this study confirm that the SP of FUS^{EC} is not cleaved because the peptide sequences identified included the N-terminus. There are additional examples of secreted proteins that retain an uncleaved SP, including albumin, PAI-2 as well as FGF-9 and

FGF-16 [767, 770, 771]. If the SP of FUS^{EC} does remain uncleaved, it could be that this short sequence at the N-terminus of FUS^{EC} is instrumental in determining the unique functions of FUS^{EC}. In the examples of mature secreted proteins that retain their SP, the SP sequence gains additional specific functions [772-774]. For example, the N-terminal SP of secreted apolipoprotein (ApoM) protein is uncleaved, and it acts as an anchor for lipoproteins, and it is necessary for the formation of larger nascent high density lipoprotein (HDL) particles [774]. It is also possible that specific binding partners of FUS^{EC} target the unique N-terminal sequence and therefore recruit it into new molecular pathways, different from the canonical isoform of FUS.

FUS^{EC} shares its nuclear localization signal with canonical FUS, since the two proteins share the same C-terminus. However, when using western blotting by either 1D or 2D gel electrophoresis, no endogenous FUS^{EC} protein was detectable in the lysate fraction. The finding that a secreted protein is detectable in the lysate at the mRNA level but not at the protein level has been previously reported. Wang and colleagues showed that two secreted proteins, 14-3-3 protein and 22 kDa glycoprotein, were similarly expressed at the mRNA level intracellularly, but were barely detectable at the protein level [775]. It is possible that the intracellular levels of FUS^{EC} are so low they are not detectable by western blotting. However, in future studies this could be further investigated using immunocytochemistry, to determine whether FUS^{EC} is detectable within the cell. Although these experiments could not be performed in the current study due to the lack of availability of a FUS^{EC} specific antibody, this was further investigated in the studies described in next chapter using an overexpression system for FUS^{EC}.

Canonical FUS is an intracellular protein with the ability to shuttle between the nucleus and the cytoplasm. Proteins that can exist in both nuclear isoforms and extracellular isoforms have been reported previously. Clusterin is a molecular chaperone that can exist in three isoforms: pre-secretory, secretory and nuclear Clusterin. The two former isoforms display cytoprotective and anti-inflammatory activity, whilst the nuclear isoform promotes cellular death [776-778]. This suggests that these isoforms of clusterin display specialized functions

depending on their subcellular localization. In this study, FUS^{EC} was not detected intracellularly, implying that its main cellular function may be in the extracellular compartment, therefore playing a completely different role than its canonical counterpart.

GADPH was very faintly detected in the media, suggesting there was some leakage due to cell death. However the absence of FUS^{EC} in the lysate implies that it is actively secreted. This finding is highly relevant to ALS because actively secreted proteins (either via extracellular vesicles or in free form) have been implicated in ALS pathology. One of the best studied secreted proteins related to ALS is SOD1, which is secreted by astrocytes, fibroblasts, spinal cord cultures and NSC-34 cells, and additionally is detected in the CSF of ALS patients [98, 313, 779-781]. SOD1 has also been shown to be actively secreted via exosomes [780, 782-784], via the ER-Golgi pathway [98] and also passively due to cell death [496]. Extracellular mutant SOD1 can induce microgliosis and motor neuron death, while extracellular WT SOD1 suppressed extracellular inflammation [313]. Additionally, extracellular aggregated misfolded SOD1 or exosomal SOD1 has been implicated in the propagation of ALS [509, 785, 786]. Hence, secreted proteins in ALS can be involved in the cell-to-cell transmission of pathology that is implicated in ALS between neurons and other cell types.

I next tried to confirm the presence of FUS^{EC} in CSF, which represents an extracellular compartment *in vivo*. However, the results suggest that the 50 kDa band detected by the C-terminal FUS antibody is not specific and is due to cross-reactivity from the secondary antibody with proteins in CSF. Since albumin and immunoglobulins form more than 50-75% of the CSF proteome, they are likely to interfere with the immunoblotting experiments [761, 762]. It is also known that secondary HRP antibodies can cross-react with IgG from other species. Similar to the results, it was previously reported that the light chain of IgG from healthy human CSF was found to cross-react with an anti-TDP-43 antibody. This problem was overcome by depleting the IgG and albumin content of CSF samples [787]. In the future, the same approach could be used to determine whether FUS^{EC} is present in CSF. A further aim of this study was to validate FUS^{EC} expression in CSF using the specific customized antibody for

FUS^{EC} (AbGenscript#1). However, unfortunately this antibody was found not be specific for FUS^{EC}. Hence further studies are warranted to determine whether FUS^{EC} is expressed in human tissues samples such as CSF, as final step in the confirmation of its biological existence.

This study has several limitations and caveats that will now be discussed. In order to analyse the protein content of conditioned media, cells were incubated with Opti-MEM, a low serum media, to avoid high concentration of proteins from FBS that would interfere with the analysis. However, treating cells with this low serum media may affect cellular properties or induce cellular expression changes. A previous study using HT-1080 cells demonstrated that serum starvation did not change the expression of canonical FUS however, arguing against this possibility [513]. Hence, in future studies this needs to be determined for FUS^{EC} and for the cell types used in this study. A second major limitation of this study was the use of HEK293T cells, rather than the use of neuronal cell lines or primary neurons throughout. In future studies, ideally all the analyses described in this chapter should be repeated using primary neurons.

Implications and future perspective

The functions of FUS and its pathogenic mechanisms in ALS are still not fully understood. The discovery of a novel extracellular isoform of FUS provides further complexity to this issue. It is possible that FUS^{EC} shares functions with its canonical counterpart albeit in a completely different cellular compartment. Alternatively it could be that FUS^{EC} has new unique functions due to its novel extracellular localization, and to its unique N-terminal sequence. Therefore, understanding the normal cellular functions and properties of FUS^{EC} is a crucial step towards clarifying its role in FUS-related neurodegenerative diseases.

In the future it would also be interesting to determine whether FUS^{EC} expression is tissue specific, which would imply that it possesses specific functions in distinct tissues. Q-PCR from different human tissues would facilitate understanding of its expression patterns, which could be confirmed by western blotting. Another FET family member, EWS, also has a brain specific isoform,

and its expression differs throughout different stages of neuronal differentiation [788].

Conclusions

In conclusion, this chapter confirms the expression of a new isoform of FUS at both the mRNA and protein level in human primary neurons and cell lines. The splice variant is generated from skipping exon 7 and from the presence of an alternative start codon. This results in an alteration to the N-terminal protein sequence, and drives the protein, FUS^{EC}, to the extracellular compartment. The results presented in this chapter therefore provide a framework for future experiments to investigate the normal functions of FUS^{EC} and its role in ALS.

4. ■ **Characterization of FUS^{EC}**

4.1. Introduction

The pathogenic mechanisms that underlie ALS are not fully understood. It remains unclear whether neurodegeneration is related to the loss of normal cellular functions or a gain of toxic functions (or both) of proteins that aggregate in ALS. Therefore, it is important to characterise the normal cellular functions of WT FUS^{EC} under non-pathological conditions because this isoform has not been previously described and its structure and functions are unknown. These findings will also provide the baseline for further studies of FUS^{EC} and its role in ALS. Hence this chapter aims to characterise FUS^{EC} and its normal cellular functions, in particular, investigating how FUS^{EC} is secreted, where it is normally localized within the cell, and identifying its potential binding partners.

4.1.1. Glycosylation of proteins

Glycosylation is one of the most common and ubiquitous post-translational protein modifications. Glycoproteins are involved in many cellular functions including: cell-to-cell communication, microbial pathogenesis [789], tumour growth [790], anticoagulation [791], immune response [792] cell growth and metabolism [793], highlighting the potential importance of glycosylation. In the nervous system, glycosylation is involved in neuronal development [794], synaptic transmission [795], modulating neuronal ion channels [796] and membrane excitability [797].

There are four major types of glycosylation in mammals: N-linked glycosylation, O-linked glycosylation, C-linked mannosylation and glypiation [798]. O/N-linked glycosylation is the most commonly studied types of protein glycosylation. O-linked glycosylation begins at the Golgi apparatus where an N-acetylgalactosamine (GalNAc) residue is transferred to the side chain of a serine or threonine residue, which can extend to become an 8 core O-glycan structure [799]. O-linked glycosylation that incorporates these core O-glycan structures (O-GalNAc) is often a characteristic of mucin-like glycoproteins that constitute epithelial secretion. O-linked glycosylation also exists on nucleocytosolic proteins through covalent attachment of O-linked N-acetylglucosamine (O-GlcNAc) to Ser/Thr residues by the O-GlcNAc Transferase (OGT), which are mostly involved in signal transduction [800, 801].

Moreover, O-linked glycosylation does not appear to have a consensus sequence by which we can predict potential sites of O-glycosylation.

N-glycosylation is the co-translational process that attaches an oligosaccharide chitobiose *N*-glycan core (Man₃-GlcNAc₂) to the amine nitrogen of an asparagine residue in the consensus motif N-X-S/T, where X can be any amino acid except proline [802, 803]. *N*-glycosylation assists in protein folding during ER translational process [804].

N-glycosylation process

N-glycosylation begins at the cytoplasmic face of the ER and finishes in the ER lumen. The precursors for *N*-glycans are lipid linked oligosaccharides (LLO) that are derived primarily through metabolism and they enter the pathway as nucleotide-activated sugars; UDP-GlcNAc and GDP-Man. These nucleotide sugars are substrates for elongation of the glycan in the cytoplasm, and in the ER lumen, which are converted to dolichyphosphate-bound sugars (Dol-P); Dol-P-Man and Dol-P-Glc [804].

On the cytoplasmic side of the ER, asparagine-Linked glycosylation (ALG) genes encode glycosyltransferases, which control the assembly process (**Figure 4.1**, Step a). The first step of the process is performed by ALG7 *N*-glucosamine-phosphate transferase, which adds the first GlcNAc-P to Dol-P, forming an ER-membrane anchored lipid dolichol phosphate (Dol-P) [805, 806]. ALG7 is the target of Tunicamycin, an inhibitor of *N*-glycosylation that is commonly used to induce ER stress [807]. The final cytoplasmic phase involves the transfer of additional carbohydrate residues: a second GlcNAc, and 5 mannose residues, generating a Man₅GlcNAc₂-P-P-Dol tetradecaoligosaccharide [808, 809].

The process continues in the luminal side of the ER (**Figure 4.1**, Step b). The translocation of the lipid-linked Man₅GlcNAc₂ oligosaccharide across the membrane is protein dependent and independent of ATP [810]. In the lumen of the ER, biosynthesis of the LLO continues, where four mannose and three glucose residues are added by ER luminal-oriented mannosyl and glucosyl transferases, forming Glc₃Man₉GlcNAc₂-P-P-Dol [804, 811]. The resulting oligosaccharide structure is considered a completely assembled LLO, which is usually highly conserved in eukaryotes. Oligosaccharyltransferase (OST), a

membrane bound enzyme, catalyses the formation of a covalent *N*-glycosidic linkage between the LLO and the side-chain amide of the Asp residue of the polypeptide, while it emerges into the lumen [812, 813]. The LLO substrate is highly specific, whereas the polypeptide acceptor of OST can vary, although it must contain the consensus sequence [813]. Furthermore, there are additional constraints on the polypeptide, such as the presence of the glycosylation site within flexible domains such as those containing potential loops or turns domains and the presence of proline residues. In addition, some *N*-glycosylation sites are located in defined secondary structures such as β -sheets. Two-thirds of the potential *N*-glycosylation sites are used as substrates by OST [814, 815].

Once the *N*-glycan is properly added to the protein to form the glycoprotein, it then undergoes a series of folding checkpoints. These determine whether the glycoprotein is correctly folded, and if so, it is driven further along the ER-Golgi pathway and hence its final localization. Alternatively, if it is aberrantly folded, it is targeted for degradation. The first checkpoint is controlled by α -glucosidase I (GS-1), which cleaves the terminal glucose of the LLO [816, 817]. This step inhibits rebinding of the glycoprotein to OST, and promotes its binding to malectin, which binds preferentially to misfolded proteins and targets them to ERAD [818]. Secondly, GS-II removes the second last glucose, leading to a glycan that binds to ER lectin-like chaperones, such as calnexin and calreticulin, that together with Erp57 and cyclophilin B (CypB) constitute the calnexin/ calreticulin cycle which supports the folding of the protein to its native state [819, 820]. GS-II carries out a second de-glycosylation step, preventing the glycoprotein binding to calnexin and calreticulin [820]. This also drives the glycoprotein to the last checkpoint, controlled by UDP-Glc:glycoprotein glucosyltransferase 1 (UGGT1), which forms the last step of the calnexin/calreticulin cycle [821]. UGGT1 binds to the glycoprotein *N*-glycan and if it is properly folded, it will progress to the ER-Golgi trafficking pathway. However, if it is not correctly folded, it will be re-glycosylated and re-enter the calnexin/calreticulin cycle again [822]. There is an additional battery of chaperones; BiP, Grp94, Grp170 and a series of enzymes; PDI, ERp57, ERp59 and ERp72, that assist in folding and disulphide bond formation of the protein, during this folding cycle [817].

At this point if glycoproteins are properly folded they will be transported to the Golgi via COPII vesicles, upon receptor recognition of the glycan chain, receptors such as ERGIC-53 [823], or if not degraded by ERAD [824]. However, instead of progressing to either the Golgi or ERAD, glycoproteins can be retained in the ER, where they may become susceptible to aggregation. These glycoprotein aggregates can be transported out of the ER via 'EDEMosomes', involving a vesicular system linked to ERAD [825]. Alternatively, aggregates form juxtanuclear structures, ER-protein quality control (ERQC) compartments and ER-associated compartments (ERACS) that are thought to maintain ER homeostasis by segregating ER aggregates [826].

In the *cis*-Golgi, an intermediate oligosaccharide is formed, Man₅GlcNAc₂ (high mannose), which precedes the formation of more complex *N*-glycans, which takes place in the intermediate and trans-Golgi (**Figure 4.1** Step c). Trans-Golgi branching of the mature glycan takes place by galactosidases and GlcNAc transferases, which add N-acetylglucosamine (GlcNAc) and galactose (Gal) residues. Additionally, some glycans also have fucose attached to the Asp residue adjacent to GlcNAc. Finally, the most important step for capping of the oligosaccharide is the addition of sialic acid, fucose, Gal and/or GalNAc, which results in three types of glycoproteins: high mannose, hybrid and complex (**Figure 4.2**). At this point, proteins are sorted to one of three destinations: the plasma membrane, endosomes, or if proteins are misfolded, they are recognized by quality control systems in the Golgi, and they are delivered to the lysosome for degradation [827].

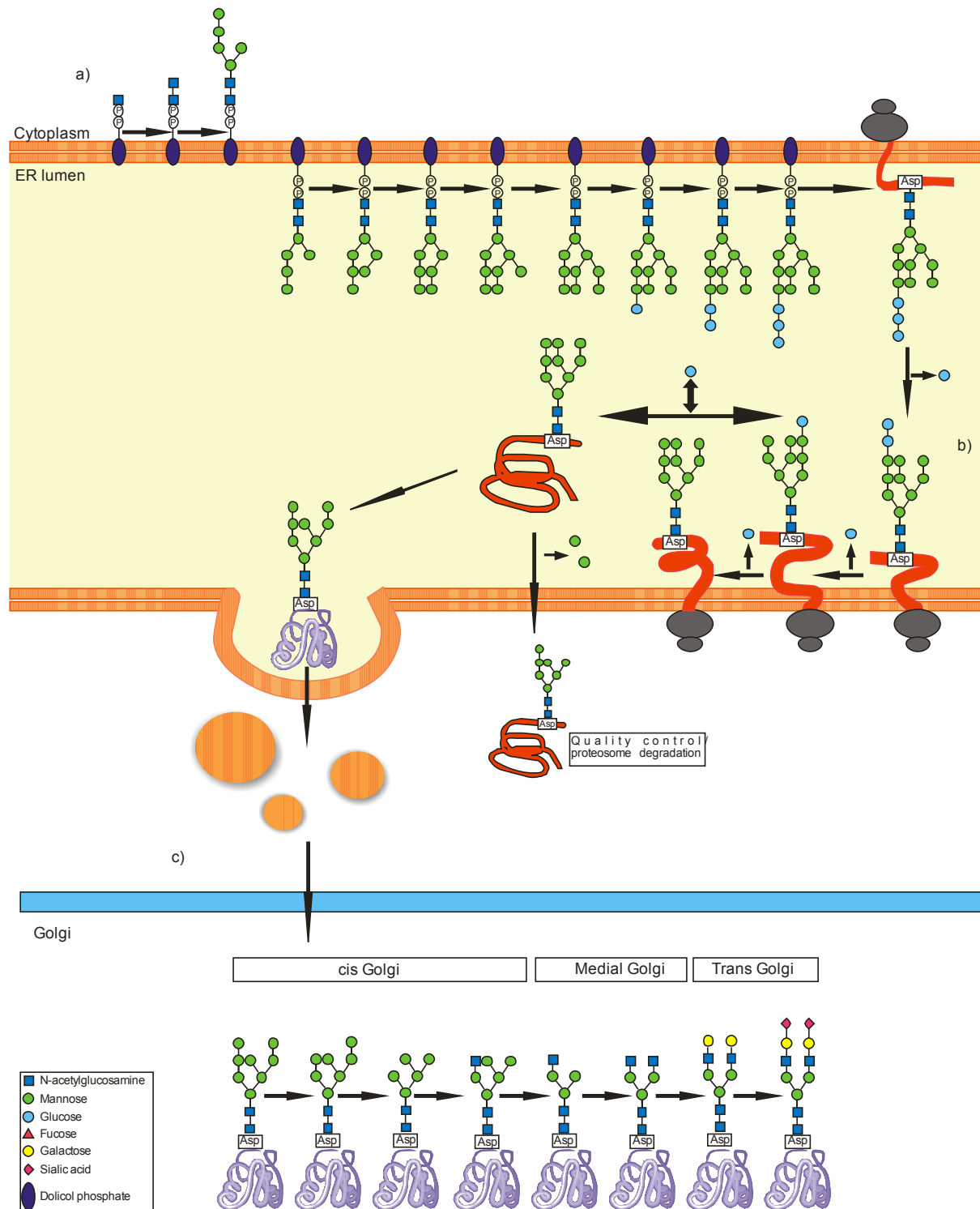


Figure 4.1 Simplified diagram of the *N*-glycosylation pathway, from the cytosolic face of the ER to the Golgi. (a) At the cytoplasmic face of the ER, dolichol (blue oval) phosphate (Dol-P) receives GlcNAc-1-P, to generate Dol-P-P-GlcNAc, which becomes further extended to Dol-P-P-GlcNAc₂Man₅. The glycolipid is translocated through the ER membrane to the luminal side. In the ER lumen four mannose residues and three glucose residues are added. The mature Dol-P-P-glycan is transferred to Asn-X-Ser/Thr sequons while the protein is being synthesised. (b) At this point, the

glycoprotein is subjected to several folding checkpoints, where glucosidases remove three glucose residues, ER mannosidase removes a mannose residue, and calnexin and calreticulin assist in folding of the protein. (c) If the glycoprotein is detected as properly folded, it will be transported to the Golgi via COPII vesicles. In the *cis*-Golgi, mannose residues are removed until Man₅GlcNAc₂Asn is formed. GlcNAc transferases are located in the medial Golgi, where the first branching of the *N*-glycan begins. In the trans-Golgi, galactosyltransferase and sialyltransferase are responsible for attachment of sialic acid and galactose residues, to generate the mature glycoprotein.

N-glycosylation can impact on protein folding, disulphide bond formation and the final localization of proteins. *N*-glycosylation has a critical role in the development of the nervous system. Studies from human congenital disorder of glycosylation are tightly related to neurological abnormalities [797].

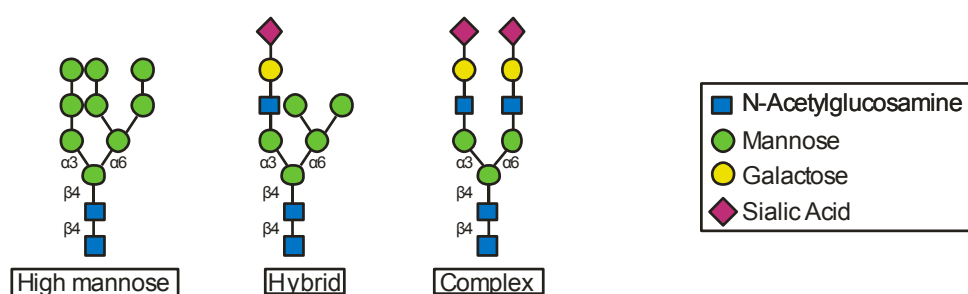


Figure 4.2 Three types of *N*- glycans that compose mature glycoproteins, with the *N*-glycan core Man₃GlcNAc₂Asn: High Mannose, Hybrid and Complex.

The role of protein glycosylation in neurodegenerative diseases

Several misfolded proteins linked to neurodegeneration are known to be glycosylated. Amyloid precursor protein (APP) is glycosylated (both O- and N-) in the CSF and this PTM is involved in its secretion in cell lines [828-830]. Tau glycosylation affect its phosphorylation status, such that aberrant *N*-glycosylation of Tau leads to its hyperphosphorylation and amyloidogenesis [831, 832]. AD patients display specific differences in their glycome compared to controls and other non-AD neurodegenerative disease patients in serum and CSF samples [833, 834], and other studies have revealed alterations in sialylation of glycoproteins in the CSF of AD patients [835, 836].

In ALS, high levels of sialylated glycans and low levels of core fucosylated glycans were detected in the serum of ALS patients compared to healthy controls [837]. A more recent study concluded that the CSF of ALS patients contained higher levels of specific monosialylated diantennary *N*-glycans than that of controls [838]. Additionally, reduced protein O-glycosylation was detected in motor neurons from the spinal cord of mutant transgenic mice [839]. While differences in N- and O-linked glycosylation have been identified from secreted biofluids, another ALS protein FUS was identified to be dynamically O-GlcNAcylated in the cell during stress granule formation upon oxidative stress [593].

In summary, this evidence demonstrates that glycosylation is implicated in neurodegenerative diseases. The glycosylation status of specific proteins involved in neurodegenerative conditions can affect their pathogenic capacity, but more broadly, glycomics profiles may have potential as biomarkers also. However, this field is relatively unexplored, hence further studies are required to determine the implication of glycosylation on the secretion of proteins involved in ALS.

4.1.2. Protein secretion via exosomes

Extracellular vesicles

Extracellular vesicle (EV) research has been a growing field for the last 10 years [840]. It has been particularly under the spotlight in relation to neurodegenerative diseases, where it is considered to be a promising new tool for diagnostics and therapeutics. EVs contain heterogeneous content, including RNA, proteins and lipids [841]. Therefore, EV are implicated in a wide range of cellular functions, although these are not completely understood.

Extracellular vesicles can be divided according to their size and origin. Exosomes are a small type of EV, typically 50-200 nm in size, that originate from the trafficking of multivesicular bodies (MVB) from the cytosol to the cell surface [842]. Microvesicles (MV), or ectosomes, are larger EVs, of size 100-1000 nm that are derived from the plasma membrane, and become released as

a response to specific stimuli [842]. Finally, apoptotic bodies are released during cell death and are usually larger still, of size 500-4000 nm [843]. Due to the heterogeneity in their size, identification and characterization of the different EV's can be particularly challenging.

Exosomes biogenesis and function

The biogenesis of exosomes is a complex process that involves several different mechanisms once thought to be independent of each other. However more recent studies have revealed that they are interconnected. Exosome biogenesis begins with the formation of endocytic vesicles from the plasma membrane. This is followed by the maturation of endosomes into multivesicular bodies (MVB), and the generation of intra-luminal vesicles (ILV) in the MVB [844]. Finally, exosomes are produced when the ILVs fuse with the plasma membrane and release into the extracellular space.

The first mechanism identified, which is also the most characterized process, employs the endosomal-sorting complex required for transport (ESCRT) machinery. Four different protein complexes compose ESCRT, which assists in sorting protein cargo in the endosomal membrane as well as in the formation of intraluminal vesicles [845]. This process was first identified from proteomic studies that detected TSG101 and ALIX within exosomes, two proteins from the ESCRT complex [846]. Another family of proteins implicated in exosome biogenesis and cargo selection are tetraspanins, transmembrane proteins that are enriched in exosomes. Expression of tetraspanins CD9, CD82, and CD63 affects the secretion of exosomes [847]. Lastly, lipids are also important in exosomal transport since they are able to modulate membrane curvature, fission and fusion and therefore exosome formation and cargo selection [847, 848].

Exosome composition is complex as it is dependent on cell type and the state of cellular homeostasis, and the mechanism of biosynthesis also influences its cargo. Additionally, PTMs of proteins can determine the selection of cargo, including SUMOylation, phosphorylation and glycosylation, particularly the attachment of complex *N*-glycans [849, 850].

After maturation, a MVB can follow one of two fates. It can fuse with the lysosome, where its contents are degraded and recycled [851]. Alternatively, it

can fuse with the plasma membrane, releasing the newly formed exosome into the extracellular compartment [844].

Exosomes can be taken up by the receiving cells by one of several different mechanisms. Exosomes can fuse directly with the plasma membrane of the target cell, and release their cargo into the cytosol of the receiving cell [852]. Secondly, transmembrane proteins within the exosomal membrane can be recognized by membrane receptors of the target cell, thus promoting fusion [852]. Lastly, exosomes can be internalized by the receiving cell, from where they are targeted to lysosomes for degradation or transcytosis [853].

Exosomes were first thought to be simply a mechanism to remove unwanted proteins by the cell. It is now known however, that under normal conditions, exosomes are involved in many cellular functions, including cell migration and invasion, immunity and cell-to-cell communication, and they also function to protect their cargo, whether protein, lipid, or particularly, circulating RNA and microRNA [854]. Exosomes are implicated in the pathogenesis of several diseases, and it has also been suggested that they may therefore be potential therapeutic targets for disorders such as cancers, auto-immune syndromes, infectious diseases, as well as neurodegenerative diseases including ALS [855-858].

Exosomes are implicated in the transmission of misfolded proteins in neurodegenerative disease

Exosomes were first linked to neurodegenerative diseases when the prion protein (PrP^C) and its misfolded form (PrP^{Sc}) were shown to be within these vesicles [859-861]. Later on, it was shown that exosomal release and uptake of PrP^{Sc} induces misfolding of PrP^C and transmission of prion pathology *in vitro* and *in vivo* [859, 861-863]. Additionally, MVB was identified as the major cellular location for the conversion of PrP^C to pathogenic PrP^{Sc} prior to exosomal release, highlighting the importance of these vesicles in pathology [864].

The role of exosomes in ALS

Several misfolded proteins that aggregate in ALS have been shown to be released via exosomes. SOD1 was the first protein in ALS to be identified in

exosomes, and it is now established that the prion-like mechanism of SOD1 is in part exosome dependent [506, 782, 783]. TDP-43 has also been detected in exosomes from either cultured cells or CSF from ALS patients, and it has been demonstrated that TDP-43 transmits among cells, and is taken up from microvesicles [504, 508]. Also, exosomal TDP-43 obtained from CSF from ALS/FTD patients efficiently induced the misfolding of endogenous TDP-43 in U251 cells [505]. Similarly, C9ORF72 DPRs transmission has been demonstrated in an exosome dependent and independent manner in NSC-34 cells [198]. Finally, WT and ALS-mutant FUS was detected in exosomes obtained from transfected SH-SY5Y cells, although its role in exosomes still remains unknown [630]. In addition to misfolded proteins, other exosomal cargo might be involved in ALS. MicroRNA cargo is involved in the alteration of microglial in ALS [865] and monocyte activation is triggered by exosomal TDP-43 [866] both studies were performed in cell lines.

Hence together this evidence suggests that exosomes are a vehicle which may be a potential mechanism for the release of ALS-linked proteins to the extracellular environment, where they are implicated in cell-to-cell transmission of misfolded proteins and ultimately ALS cellular pathology.

4.2. Aims of this chapter

Proteins are secreted through different mechanisms. *N*-glycosylation can direct proteins through the classical secretory pathway, and interestingly, whilst *N*-glycosylation is relatively unexplored in ALS, it is implicated in other neurodegenerative diseases such as Alzheimer's disease [833].

The previous chapter described the discovery of a new isoform of FUS, FUS^{EC}, which has the unusual property of being secreted. In the studies outlined in this chapter, an overexpression system for this isoform was generated, with the aim of confirming its extracellular localization and further characterising its properties. The further aims of the studies outlined in this chapter were to examine the mechanisms by which FUS^{EC} is secreted, focusing on the modification of FUS^{EC} by *N*-glycosylation as a driver of its secretion, and the presence of FUS^{EC} in extracellular vesicles, because these two

mechanisms are implicated in neurodegenerative diseases. Finally, to provide insights into the possible normal functions of FUS^{EC}, its extra/intracellular binding partners were examined. Therefore overall this chapter aimed to characterise the normal characteristics and functions of FUS^{EC}.

4.3. Material and methods

4.3.1. Vector and insert restriction enzyme digestion

Hematoglutinin (HA)-FUS and green fluorescent protein (GFP)-FUS (canonical form) was purchased from Genscript in pcDNA3.1 (+) vector and codon optimized. All plasmid sequences were confirmed by Sanger sequencing in forward and reverse direction.

HA-WT-FUS^{EC} (6,566 bp) in pMAT-vector was purchased from Invitrogen, and GFP-WT-FUS^{EC} (7,313 bp) strings from Geneart (Invitrogen). Both constructs were designed with Geneious software and codon optimized. HA-WT-FUS^{EC} and GFP-WT-FUS^{EC} fragments were cloned into pcDNA3.1 (+) vector between BamHI and EcoRV restriction enzyme sites. Restriction enzymes were purchased from New England Biolabs. For cloning, NEB 5-alpha competent E.Coli cells (High Efficiency) were purchased from New England Biolabs.

DNA isolated from transformed competent cells were digested to isolate DNA sequences and plasmids for ligation. The restriction enzyme digestion reactions for cloning of the -GFP and -HA tagged constructs of EC-WT-FUS-isoform were prepared as follows:

Table 4.1 Enzyme digestion reaction set up

Reagent	Amount
Plasmid DNA	2-3 µg
Restriction EcoRV	1 µl (10units)
Restriction BamHI	1 µl (10units)
10xbuffer (Multicore)	3 µl
Pure water	Up to 30 µl
TOTAL VOLUM	30 µl

The reaction was incubated at 37°C for 3 h.

4.3.2. De-phosphorylation of the plasmid vector

In order to prevent self-ligation of the empty vector (pcDNA3.1. (+)), de-phosphorylation of the 5' phosphate was performed setting up the following reaction:

Table 4.2 De-phosphorylation reaction set up

Reagent	Amount
Plasmid vector DNA	39 μ l
Antarctic Phosphatase (NEB)	6 μ l
10x Antarctic Phosphatase buffer	5 μ l
Pure water	Up to 50 μ l
TOTAL VOLUME	50 μ l

The reaction was incubated for 15 min at 37°C. Next samples were run on agarose gel, and DNA was extracted following protocol in Chapter 3 Section 3.3.4.

4.3.3. Ligation reaction

To insert the HA/GFP-WT-FUS^{EC} sequence into pcDNA3.1 (+) digested vector, the following ligation reaction was set up:

Table 4.3 Ligation reaction set up

Component	Ligation reaction 1:3 molar ratio	Negative control
Vector DNA	25 μ g	25 μ g
Insert DNA	75 μ g	-
10x ligase buffer (Promega)	1 μ l	1 μ l
T4 DNA ligase (Promega)	1 μ l	1 μ l
Pure water	Up to 10 μ l	Up to 10 μ l
TOTAL VOLUME	10 μ l	10 μ l

Samples were mixed and quickly centrifuged at 1000 g, and the reaction was incubated overnight at 16°C in a Thermocycler (Thermo Fisher). 10 μ l of

either the ligation or negative control reactions was used to transform 50 μ l of NEB 5-alpha competent *E. Coli.* cells (High Efficiency) (New England Biolabs).

4.3.4. Methods to confirm that cloning was successful: Digestion, agarose gel and Sequencing

10 single colonies were selected from the *LB* agar plate containing *E. Coli.* from the ligation reactions, inoculated into *LB* broth and plasmid miniprep DNA was prepared to determine whether cloning of HA/GFP-FUS^{EC} into pcDNA.3.1(+) was successful. Firstly, a diagnostic digestion reaction was performed. For HA-FUS^{EC} constructs (6,566 bp) the following enzymes were used: PstI and XhoI for the first reaction generating a 1,470 and 5,096 bp fragment. For the second reaction XhoI and Bgl II were used, producing a 1,942 and 4,624 bp fragment. For the GFP-.FUS^{EC} constructs (7,313 bp) NruI and BamH1 were used and produced a 721 and 6,592 bp fragment. Secondly, BamH1 and NotI were used, producing a 1,766 and 5,547 bp fragments. The samples that presented the expected results from the diagnose digestion were send for Sanger sequencing. Sequencing samples were prepared by mixing 500-1000 μ g of miniprep plasmid DNA with 1 μ l of 10 mM primers (**Table 4.4**) and the reaction mix was made up to 12 μ l with water. Sequencing was performed at the Australian Genome Research Facility (AGRF) by using Sanger sequencing method. The results were analysed using Basic Local Alignment Search Tool (BLAST, NCBI) and the chromatographs were analysed by using FinchTV.Ink software to determine the accuracy of the sequence.

Table 4.4 Primers used for Sanger sequencing confirmation

Primer Name	Primer sequence (5'-3')
FUS ^{EC} FP 1	CAAATTAATCATGGCTGTCC
FUS ^{EC} RP 1	TGGCTATGAACCCAGAGGTC
FUS ^{EC} FP 2	ATGGCAATCAAGACCAGAGTGG
HA RP	CTTGTACAGCTCGTCCATGC
GFP RP	CGTAATCTGGAACATCGTATGG

4.3.5. PNGase F assay

Cells were plated on a 50 cm² petri dish and transfected with Lipofectamine 2000. After 20h transfection, cells were washed with PBS and the media was changed to Opti-MEM. The media and cells were collected after 48h post-transfection and the lysates were collected as per IP. Protease inhibitors were added to 8 mL of conditioned media, which was centrifuged at 1000 rpm (~230 g) for 5 min at 4°C twice to discard the cell debris. Proteins were acetone precipitated by adding 4 volumes of ice cold acetone followed by incubation overnight at -20°C. Samples were centrifuged at 4000 rpm (~4000 g) for 10 min and pellets were resuspended in 500 µl of PBS+1 % protease inhibitor (Sigma). Then samples were buffer exchanged three times with PBS containing 1% protease inhibitors, and the protein concentration was determined using a BCA assay.

A Peptide *N*-glycosidase F (PNGase F) (NEB) assay was carried using 100 µg of total protein from the media and lysate fractions following the manufacturers protocol. Briefly, proteins were denatured with Glycoprotein Denaturing buffer (10X) by heating samples at 100°C for 10 min. The reactions were chilled on ice and centrifuged at 1000 g. To neutralize SDS, 2 µl of 10% (v/v) NP-40 was added to the reaction, as well as the Glycobuffer 2 (10X).

Finally, 500 units of PNGase F were added and samples were incubated for 3h at 37°C. The reactions were stopped using SDS-PAGE sample buffer and 20 µg of protein was loaded onto an 8 % SDS-PAGE gel to analyse the glycosylation state by mobility shift. Control samples were treated identically but without the addition of PNGase F.

4.3.6. Cells treatment with tunicamycin

HEK293T cells were plated in a 6 well plate and transfected with HA-tagged FUS^{EC} constructs following the protocol in the Chapter 2, section 2.2.3. At 24 h post-transfection, the media was replaced with Opti-MEM and tunicamycin (2.5 mg/mL diluted in DMSO) was added to the cells in the treatment group (10⁻¹-0.1-0.01 µl /ml), and 4 µl of DMSO was added to the control cells. Conditioned media and cell lysate were collected 24 h after changing the media and western blotting was performed as previously described.

4.3.7. Glycan analysis

HA-FUS^{EC} captured by IP (Chapter 2, section 2.3.5) was eluted 4 times, using 25 μ l of 2 mg/mL HA-peptide by 15 min incubation at 37 °C. The eluates were combined and concentrated using Amicon ultra centrifugal filter unit with 10 kDa (Millipore), washing three times with 0.5 mL of 100 mM ammonium bicarbonate. The concentrate was then collected, and 50% of the sample was dot-blotted onto a PVDF membrane. Glycan release and clean up, was carried out as per Jensen 2012 Nature Protocols [867]. Approximately 4 μ l of Rapid PNGaseF (NEB) at 1x working concentration, was used for glycan release followed by overnight incubation at 37 °C. Following overnight incubation, the samples were bath sonicated for 5 min and the samples containing released *N*-glycans were collected.

Porous graphitized carbon (PGC) liquid chromatography mass spectrometry (PGC-LC-MS)

Chromatographic separation of reduced *N*-glycans was carried out on an Ultimate 3000 LC instrument using a Hypercarb porous graphitized carbon (100 mm x 2.1 mm, 3 μ m particle size) column with mobile phases: 10 mM ammonium bicarbonate aqueous solution (solvent A) and 10 mM ammonium bicarbonate aqueous solution with 70% acetonitrile (solvent B) with a flow rate of 4 μ l /min. The gradient program for elution of *N*-glycans was as follows: 0 min, 2.6% B for 8 mins; linear increase up to 13.5% B for 2 min; linear increase up to 33% B for 45 min; linear increase up to 64% B for 15 min; linear increase up to 98% B for 1 min; held at 98% B for 5min; and then equilibrated at 2.6% B for 7 min, before the next injection—giving a total LC run time of 83 min.

LTQ-Velos mass spectrometer.

The Thermo Scientific linear ion trap (LTQ) was performed as per Ashwood 2018 JASMS [868]. Glycans were analyzed according to following MS conditions: *m/z* 580–2000, 3 microscans, *m/z* 0.25 resolution (FWHM), 5×10^4 automatic gain control (AGC) and 50 ms accumulation time and MS/MS conditions: *m/z* 0.35 resolution (FWHM); 2×10^4 AGC, 300 ms accumulation

time, 2 *m/z* window and top five data-dependent acquisition. For ion trap HCD, nitrogen was used as the collision gas. HCD subjected ions to 30–37.5% NCE with a default charge state of 2 and an activation time of 2 ms.

Analysis and relative quantitation of *N*-glycans

Mass spectrometry ions were detected over the time range of 10–45 mins were deconvoluted within the mass range of *m/z* 500–3000 and searched for putative *N*-glycan composition using Glycomod (<http://www.expasy.ch/tools/glycomod>). Compositions that were determined to be *N*-glycan structures based on published observations curated in the Unicarbkb database were then quantified manually by area under curve (AUC) measurements of the extracted ion chromatogram of *m/z* values corresponding to *N*-glycans, with a maximum peak width of 1 min. Peak areas of glycan compositions detected with multiple charge states were combined for analysis and the relative quantitation of specific *N*-glycan structures were calculated as a percentage of all *N*-glycans identified within each sample.

4.3.8. Exosomes isolation

To prevent cross contamination from exosomes present in FCS, exosomes were depleted from heat inactivated FCS by ultracentrifugation at 100,000 g for 16 h at 4°C.

Exosome-depleted FCS 10% (v/v) was added to DMEM for experiments involving the collection and isolation on exosomes secreted from HEK293T cells. Cells were seeded in a T175 flask, after 24 h cells were transfected with HA-FUS^{EC} constructs (Chapter 2, section 2.2.3). After 24 h post transfection, the cells were lifted with trypsin and resuspended in exosome-depleted media. Then, cells were seeded in exosome-depleted media in a T175 flask to 80 to 90% confluency and incubated for two days to allow maximal yield of exosome production from HEK293T cells.

The conditioned media was collected from each flask and centrifuged at 2000 g for 10 min to clear the cell debris and whole cells. The supernatant was centrifuged at 10,000 g for 30 min at 4°C in 60 mL screw top polycarbonate tube (Beckman Coulter) to remove larger vesicles. The remaining supernatant

was then ultracentrifuged at 100, 000 g for 70 min at 4°C to pellet exosomes on a 45 Ti rotor (Beckman Coulter).

The supernatant was discarded and the exosomes were resuspended with filtered (0.2 µm) Dulbecco's Phosphate-Buffered Saline (DPBS) (Dulbecco's Phosphate-Buffered Salines, Gibco® Thermo Fisher Scientific).

A washing step was conducted by resuspending the exosome pellet and performing another ultracentrifugation at 100, 000 g for 70 minutes at 4°C. The exosome pellet was resuspended in 150 to 200 µl of filtered (0.2µm) DPBS depending on the size of the exosome pellet. Exosomes were stored at -20°C and -80°C for short and long storage, respectively.

4.4. Results

4.4.1. Design and generation of FUS^{EC} constructs

In the previous chapter we identified a novel extracellular isoform of FUS (FUS^{EC}) in human neuronal cells. To further study and characterize this new protein, a mammalian expression vector for FUS^{EC} was designed and generated.

To build a HA-tagged FUS^{EC} (HA-FUS^{EC}) construct, a synthetic gene was purchased from Invitrogen in the PMA-t vector. It was then inserted into the pcDNA3.1 (+) vector, between BamHI and EcoRV restriction enzymes sites. For the GFP-tagged FUS^{EC} (GFP-FUS^{EC}) construct, string DNA fragments were purchased from Invitrogen and cloned into the pcDNA3.1 (+) vector, between BamHI and EcoRV restriction enzymes sites (supplementary data).

HA and GFP tagged FUS^{EC} constructs were designed with the software Geneious. The original FUS^{EC} sequence was codon optimized (HA vector: **Figure 4.3b**; GFP vector: **Figure 4.3c**) to ensure a high level of protein expression. The tags were placed at the C-terminus in order to avoid affecting the N-terminal sequence. FUS constructs tagged at the C-terminus have been used in other publications [533, 869]. In **Figure 4.4a,b**, the amino acid sequence for HA and GFP C-terminal tag FUS^{EC} is detailed, colour-coded to FUS proteins domains (**Figure 4.4c and d**).

While human influenza hemagglutinin (HA) tag is a 9 amino acid small peptide that it is unlikely to have any effect on the protein sequence and structure, it requires the use of a secondary Alexa Fluor to be visualized under the microscope, with the risk of detecting unspecific binding. In contrast, a green fluorescent protein (GFP)-tagged construct has the advantage of being directly visualized by fluorescent microscopy, but the 238 amino acid peptide (26.9 kDa) can potentially affect the folding, localization or function of the protein [870]. Therefore, we used both HA- and GFP-tagged constructs together in this study to provide additional confidence in the results we obtained.

a) HA-FUS^{EC} Sequence codon optimized

GGATCCACCATGGCCATCAAGACCAGAGTGGTGGAAAGTGGCCGCCGTGGCCATGG
 ATAGCAGAACAGTTGAAGCTGCTGCTGGCGTGGCAGTGGTTGCTGCTGCCGCTGC
 TGCAGTGGTGGTTACAACAGCTGCTGTGGTGGCCATGAATCCCGAGGTGGTGGAA
 GTTGCCCGTGGAAAGCCGAAGTTGCTTGGGCGCCTAGAGATCAGGGCAGCAGACAC
 GATAGCGAGCAGGACAACAGCGACAACAACACCATCTTCGTGCAAGGCCTGGGCG
 AGAACGTGACCATTGAGAGCGTGGCCGACTTCAAGCAGATCGGCATCATCAAG
 ACGAACAAGAAAACCGGGCAGCCCATGATCAACCTGTACACCGACAGAGAGACAG
 GCAAGCTGAAGGGCGAAGCCACCGTGTCTTCGACGATCCTCCATCTGCCAAGGC
 CGCCATCGATTGGTTTCGACGGCAAAGAGTTTCAGCGGCAACCCCATCAAGGTGTCC
 TTTGCCACCAGACGGGCCGACTTCAATAGAGGCGGCGGAAATGGTAGAGGCGGAC
 GTGGAAGAGGTGGCCCTATGGGAAGAGGCGGATATGGTGGCGGAGGATCTGGCG
 GAGGTGGCAGAGGCGGTTTTCTAGCGGAGGTGGTGGCGGCGGAGGACAACAAC
 GAGCTGGCGATTGGAAGTGCCCCAATCCTACCTGCGAGAACATGAACCTCAGCTGG
 CGGAACGAGTGCAACCAGTGCAAGGCTCCTAAGCCTGATGGACCAGGTGGCGGA
 CCTGGCGGATCTCACATGGGAGGAAATTACGGCGACGATCGGAGAGGTGGACGCG
 GCGGTTATGACAGAGGCGGCTATAGAGGACGCGGAGGCGATCGCGGAGGATTCAG
 AGGTGGAAGAGGCGGCGGAGATAGAGGCGGATTTGGCCCTGGCAAGATGGACTCT
 AGAGGCGAGCACCGGGCAGGACAGAAGAGAGAGGCCTTACTACCCCTACGACGTGC
 C C G A T T A C G C C T G A G A T A T C

b) GFP-FUS^{EC} Sequence codon optimized

GGATCCACCATGGCCATCAAGACCAGAGTGGTGGAAAGTGGCCGCCGTGGCCATGG
 ATAGCAGAACAGTTGAAGCTGCTGCTGGCGTGGCAGTGGTTGCTGCTGCCGCTGC
 TGCAGTGGTGGTTACAACAGCTGCTGTGGTGGCCATGAATCCCGAGGTGGTCGAA
 GTTGCCCGTGGAAAGCCGAAGTTGCTTGGGCGCCCTAGAGATCAGGGCAGCAGACAC
 GATAGCGAGCAGGACAACAGCGACAACAACACCATCTTCGTGCAAGGCCTGGGCG
 AGAACGTGACCATTGAGAGCGTGGCCGACTACTTCAAGCAGATCGGCATCATCAAG
 ACGAACAAAGAAAACCGGGCAGCCCATGATCAACCTGTACACCGACAGAGAGACAG
 GCAAGCTGAAGGGCGAAGCCACCGTGTCTTCGACGATCCTCCATCTGCCAAGGC
 CGCCATCGATTGGTTCGACGGCAAAGAGTTCAGCGGCAACCCCATCAAGGTGTCC
 TTTGCCACCAGACGGGCGGACTTCAATAGAGGCGGCGGAAATGGTAGAGGCGGAC
 GTGGAAGAGGTGGCCCTATGGGAAGAGGCGGATATGGTGGCGGAGGATCTGGCG
 GAGGTGGCAGAGGCGGTTTTCTAGCGGAGGTGGTGGCGGCGGAGGACAACAAC
 GAGCTGGCGATTGGAAGTGCCCCAATCCTACCTGCGAGAACATGAACTTCAGCTGG
 CGGAACGAGTGCAACCAGTGCAAGGCTCCTAAGCCTGATGGACCAGGTGGCGGA
 CCTGGCGGATCTCACATGGGAGGAAATTACGGCGACGATCGGAGAGGTGGACGCG
 GCGGTTATGACAGAGGCGGCTATAGAGGACGCGGAGGCGATCGCGGAGGATTGAG
 AGGTGGAAGAGGCGGCGGAGATAGAGGCGGATTGGCCCTGGCAAGATGGACTCT
 AGAGGCGAGCACCGGCGAGGACAGAAGAGAGAGGCGCTTACATGGTGTCCAAAGGC
 GAGGAACTGTTACCGGCGTGGTGGCCATTCTGGTGGAACTGGACGGGGATGTGA
 ACGGCCACAAGTTTAGCGTTAGCGGCGAAGGCGAAGGGGATGCCACATACGGA
 GCTGACCCTGAAGTTTATCTGCACCACCGGCAAGCTGCCCGTGCCTTGGCCTACAC
 TTGTGACCACACTGACCTACGGCGTGCAGTGCTTCAGCAGATACCCCGACCATATG
 AAGCAGCACGACTTCTTCAAGAGCGCCATGCCTGAGGGCTACGTGCAAGAGCGGA
 CCATCTTCTTTAAGGACGACGGCAACTACAAGACCAGGGCCGAAGTGAAGTTCGAG
 GGCGACACCCTGGTCAACCGGATCGAGCTGAAAGGCATCGATTTCAAAGAGGACG
 GCAACATCCTGGGCCACAAGCTCGAGTACAACCTACAACCTCCACAACGTGTACATC
 ATGGCCGACAAGCAGAAAAACGGCATCAAAGTGAACCTCAAGATCCGGCACAACAT
 CGAGGACGGCTCTGTGCAGCTGGCCGATCACTACCAGCAGAACACACCCATCGGA
 GATGGCCCTGTCTGTGCTGCTGCAACCACTACCTGAGCACACAGAGCGCCCTGA
 GCAAGGACCCCAACGAGAAGAGGGATCACATGGTGTGCTGCTGGAATTCGTGACCGC
 CGCTGGCATCACACTCGGCATGGACGAACTGTACAAAGGCGGAGGCAGAAGCGGC
 AACTCCAGACCTCTGGAACCACTGGATAGCGCTGCCCTCTAAATATC

Figure 4.3 Schematic overview of FUS^{EC} plasmids.. HA (a) and GFP (b) plasmid sequence between the EcoRV and BamHI restriction enzymes sites (in red).

a) HA-FUS^{EC} protein sequence

MAIKTRVVEVA AVAMDSRTVEAAAGVAVVAAAAA VVTTAAV VAMNPEVVEVAEAEVA PRDQGSR
HDSEQDNSDNN IFVQGLGENVTIESVADYFKQIGIIKTNKKTGQPMINLYTDRETGKLKGEATVSFDDF
AKAAIDWFDGKEFSGNPIKVSFATRADFNRRGGNGRGGRRGGPMGRGGYGGGSGGGGRGGFP
GGGGGGGQQRAGDWKCPNPTCENMNF SWRNECNQCKAPKPPGGGPGGSHMGGNYGDDRRGGF
GGYDRGGYRGRGGDRGGFRGGRGGRGGDRGGFGPGKMDSRGEHRQDRRERPYYPYDVPDYA

b) GFP-FUS^{EC} protein sequence

MAIKTRVVEVA AVAMDSRTVEAAAGVAVVAAAAA VVTTAAV VAMNPEVVEVAEAEVA PRDQGSR
HDSEQDNSDNN IFVQGLGENVTIESVADYFKQIGIIKTNKKTGQPMINLYTDRETGKLKGEATVSFDDF
AKAAIDWFDGKEFSGNPIKVSFATRADFNRRGGNGRGGRRGGPMGRGGYGGGSGGGGRGGFP
GGGGGGGQQRAGDWKCPNPTCENMNF SWRNECNQCKAPKPPGGGPGGSHMGGNYGDDRRGGF
GGYDRGGYRGRGGDRGGFRGGRGGRGGDRGGFGPGKMDSRGEHRQDRRERPYVSKGEELFTGVVPIL
VELDGDVNGHKFSVSGEGEDATYGKLT LKFICTTGKLPVPWPTLVTTLT YGVQCFSRYPDHMKQHD
KSAMPEGYVQERTIFFKDDGNYKTRAEVKFEGDTLVNRIELKGIDFKEDGNILGHKLEYNNSHNVYIMAD
KQKNGIKVNFKIRHNIEDGSVQLADHYQQNTPIGDGPVLLPDNH YLSTQSALSKDPNEKRDH MVLL
A A G I T L G M D E L Y K

c)

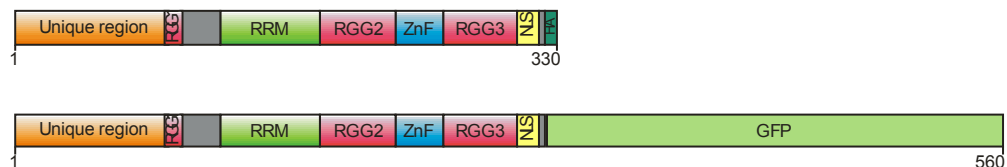


Figure 4.4 Schematic representations of C-terminal HA- and GFP-tagged FUS^{EC} proteins. Protein sequence for HA (a) and GFP (b) FUS^{EC} colour coded for the different domains. (C) Protein structure of FUS^{EC} with its domains and the C-terminal tags for HA and GFP. HA-FUS^{EC} is a 330 aa protein and GFP-FUS^{EC} is 560 aa protein.

4.4.2. FUS^{EC} expresses in HEK293T cells and is secreted into the media

The next step was to confirm the expression of HA and GFP tagged FUS^{EC} protein using these constructs. To analyse the expression of HA-FUS^{EC}, HEK293T cells were transfected with either pcDNA3.1 (+) empty vector (EV) or HA-FUS or HA-FUS^{EC} plasmids, and the conditioned media and lysate fractions were collected 48h post-transfection. Western blotting of the lysate prepared from transfected cells using an anti-HA antibody revealed the presence of a band at ~60 kDa, corresponding to HA-FUS in the lysate. HA-FUS^{EC} was also detected in the cell lysate and it migrated at ~33 kDa (**Figure 4.5a**). No bands were detected in untransfected cells or in cells expressing empty vector.

Proteins in the conditioned media of transfected cells were concentrated using a centrifugal filter unit, loaded onto an SDS-PAGE gel and Western blotted using an anti-HA antibody. The GAPDH band intensity was increased in the medium of cells expressing HA-FUS or HA-FUS^{EC}, and it appeared similar in cells expressing EV only compared to untransfected cells, thus suggesting that the transfection was toxic, leading to cell death. However, Western blotting with an anti-HA antibody revealed no bands in untransfected cells or cells expressing empty vector. In addition, no band was detected in cells expressing HA-FUS, indicating that FUS was not secreted. A sharp band at ~33 kDa, together with a smear around 40-50 kDa, was detected in the medium, corresponding to HA-FUS^{EC}, indicating that HA-FUS^{EC} was secreted (**Figure 4.5b**).

Expression of the constructs was further confirmed by immunocytochemistry using an anti-HA antibody for HA-FUS and HA-FUS^{EC} transfected cells (**Figure 4.5c**). Both HA-FUS and HA-FUS^{EC} were expressed efficiently as detected using an anti-HA antibody. HA-FUS was localized in the nucleus, as expected, while HA-FUS^{EC} was localized in the cytoplasm. These intriguing localization differences will be further investigated and discussed in section 4.4.6. of this chapter.

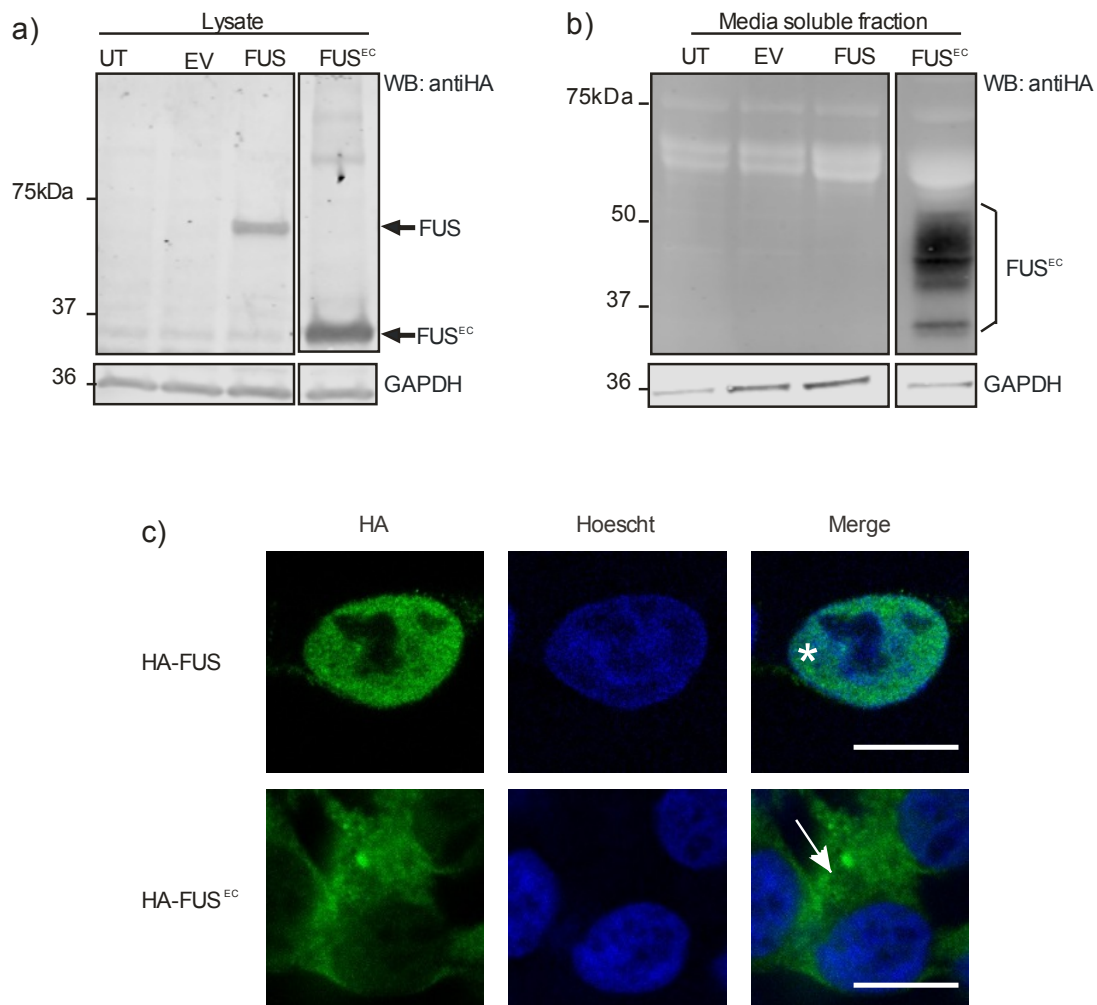


Figure 4.5 AH-FUS^{EC} is expressed in HEK293T cells and secreted in the soluble media fraction. (a) Western blotting of HA-FUS, HA- FUS^{EC} and empty vector (EV). GAPDH is shown as a loading control. (b) Western blotting for the media of HA-FUS, HA- FUS^{EC} and empty vector in transfected HEK293T cells. (c) HEK293T cells overexpressing HA tag FUS and FUS^{EC} were fixed and stained with an anti-HA antibody (green). Nuclei were stained with Hoechst (blue). Asterisk: nuclear localization, arrow: cytoplasmic localisation. Scale bar: 10 μm.

The same studies were performed with GFP-FUS and GFP-FUS^{EC}. HEK293T cells were transfected with GFP vector alone, GFP-FUS or GFP-FUS^{EC}. After 48h of transfection, cell lysates and conditioned media were collected. Western blotting for the lysate of transfected cells revealed the presence of a ≈ 26 kDa band in the GFP transfected cells, corresponding to GFP. GFP-FUS was detected at approximately 90 kDa, corresponding to the approximate MW of FUS tagged with GFP. Additionally, in the GFP-FUS^{EC}

transfected cells a band at ≈ 70 kDa was detected, corresponding to GFP-FUS^{EC} (**Figure 4.6a**).

The conditioned media from the transfected cells was concentrated, loaded into SDS-PAGE gels and Western blotting using an anti-GFP antibody was performed. In GFP transfected cells, a ≈ 26 kDa band was detected. GFP-FUS expressing cells displayed a band of 90 kDa, a sharp band at ≈ 50 kDa and a smear at ≈ 70 kDa, together with a 26 kDa band, probably corresponding to incomplete translated GFP (**Figure 4.6b**). These results suggest that GFP alone is secreted, as previously described [871-873], which would explain why canonical FUS is detected in the media of transfected cells when tagged with GFP. Finally, fluorescent microscopy analyses of GFP-FUS and GFP-FUS^{EC} transfected cells was performed, confirming the expression of both plasmids (**Figure 4.6c**).

Together these results suggest that HA and GFP-tagged plasmids encoding FUS and FUS^{EC} express well, and the resulting proteins migrate at the expected molecular weight when analysed by Western blotting. Additionally, they demonstrate that GFP itself becomes secreted, which may affect the tagged FUS^{EC}. Hence in the subsequent studies presented in this chapter, the HA-tagged FUS^{EC} constructs were used preferentially, unless a fluorescent tag was required for specific experimental proposes.

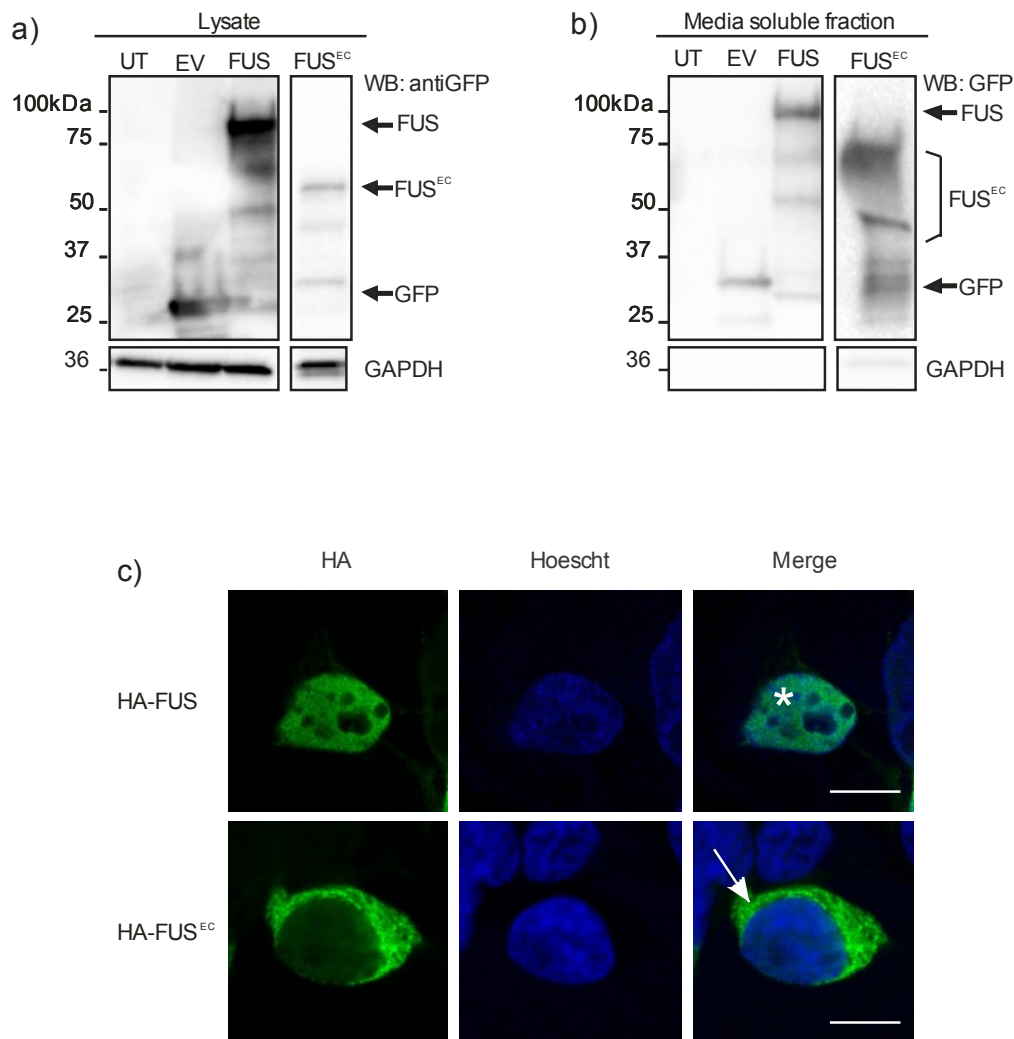


Figure 4.6 GFP-FUS^{EC} is expressed in HEK293T cells and secreted in the soluble media fraction. (a) Western blotting of GFP-FUS, GFP- FUS^{EC} and empty vector (EV). GAPDH is shown as a loading control. (b) GFP immunoblotting of GFP alone, GFP-FUS and GFP-FUS^{EC} HEK293T transfected cells. (c) HEK293T cells overexpressing GFP tag FUS and FUS^{EC} were fixed. Nuclei were stained with Hoechst (blue). Asterisk: nuclear localization, arrow: cytoplasmic localisation. Scale bar: 10 μm.

4.4.3. N-glycosylation regulates in part FUS^{EC} secretion

N-glycosylation is an important post-translational modifications that drives proteins through the secretory pathway [804]. The detection of several bands corresponding to HA-FUS^{EC} in the medium of HEK239T cells (33-50 kDa; Fig. 4.5b, 4.6b) suggested that overexpressed FUS^{EC} could be glycosylated.

The potential *N*-glycosylation sites of FUS^{EC} were first analysed using the NetNGlyc 1.0 server [874]. Three potential *N*-glycosylated sites were predicted at Asparagines 79, 90 and 232, localized in the RRM and ZnF domains of FUS^{EC} (**Figure 4.7a, 4.7b**).

To further study the *N*-glycosylated status of FUS^{EC}, HEK293T cells were transfected with the WT HA-FUS^{EC} construct for 48h. The conditioned media was collected, concentrated, and then treated with PNGase F, an amidase enzyme, which cleaves between the innermost GlcNAc and asparagine residues of high mannose, hybrid, and complex oligosaccharides [875], and thus removes the entire *N*-glycosyl oligosaccharide chain. The enzyme treated media was then subjected to SDS-PAGE and Western blotting was performed using an anti-HA antibody. These analyses revealed the presence of a smear of approximately 40-50 kDa in the untreated media. However, in the PNGaseF - treated media, a thick, sharp band was detected of ~33 kDa, consistent of removal of *N*-linked oligosaccharides by PNGaseF. As a positive control, the same blot was probed for concanavalin A (ConA), a plant lectin that recognises α -mannose residues that are found on the *N*-glycan core (GlcNAc₂-Man₃) structure (**Figure 4.7c**). The sample treated with PNGaseF had less reactivity to ConA compared to the untreated sample, confirming that the change in MW was due to the de-glycosylation by PNGaseF. Hence these data imply that FUS^{EC} is *N*-glycosylated.

We next examined the effect of tunicamycin treatment on FUS^{EC} secretion. If *N*-glycosylation is involved in secretion of FUS^{EC}, we would expect to see less secretion upon tunicamycin treatment. HEK293T cells were transfected with HA-FUS^{EC} constructs, and at 24h post-transfection, cells were treated overnight with either vehicle only (DMSO) or with tunicamycin at various concentrations (0.01, 0.1, 1 or 10 μ g/ml). The medium was collected and subjected to SDS-PAGE and Western blotting using an anti-HA antibody was performed. In cells treated with vehicle, the 33 kDa band and the 40-50 kDa smear were present as expected. In contrast, the intensity of the upper band was less in cells treated with tunicamycin and was almost undetectable in the cells treated at 10 μ g/ml. The 33 kDa band was present in all treatment groups

and appeared to increase upon tunicamycin treatment, demonstrating that there was a fraction of secreted FUS^{EC} that is not glycosylated (**Figure 4.7d**). The intensity of the GAPDH band increased when cells were treated with 10 $\mu\text{g/mL}$ tunicamycin, suggesting that some cells lyse at this concentration, leading to release of cytoplasmic proteins into the media. This was not surprising because it has been previously reported that the inhibition of *N*-glycosylation by tunicamycin triggers ER stress and ultimately cell death [876]. Together, these results demonstrate that FUS^{EC} is *N*-glycosylated and this post-translational modification affects its secretion. However, there is a proportion of secreted FUS^{EC} that does not depend on its glycosylation, hence implying that a second secretory mechanism may exist such as exosome-mediated secretion, which will be further investigated in section 4.4.5.

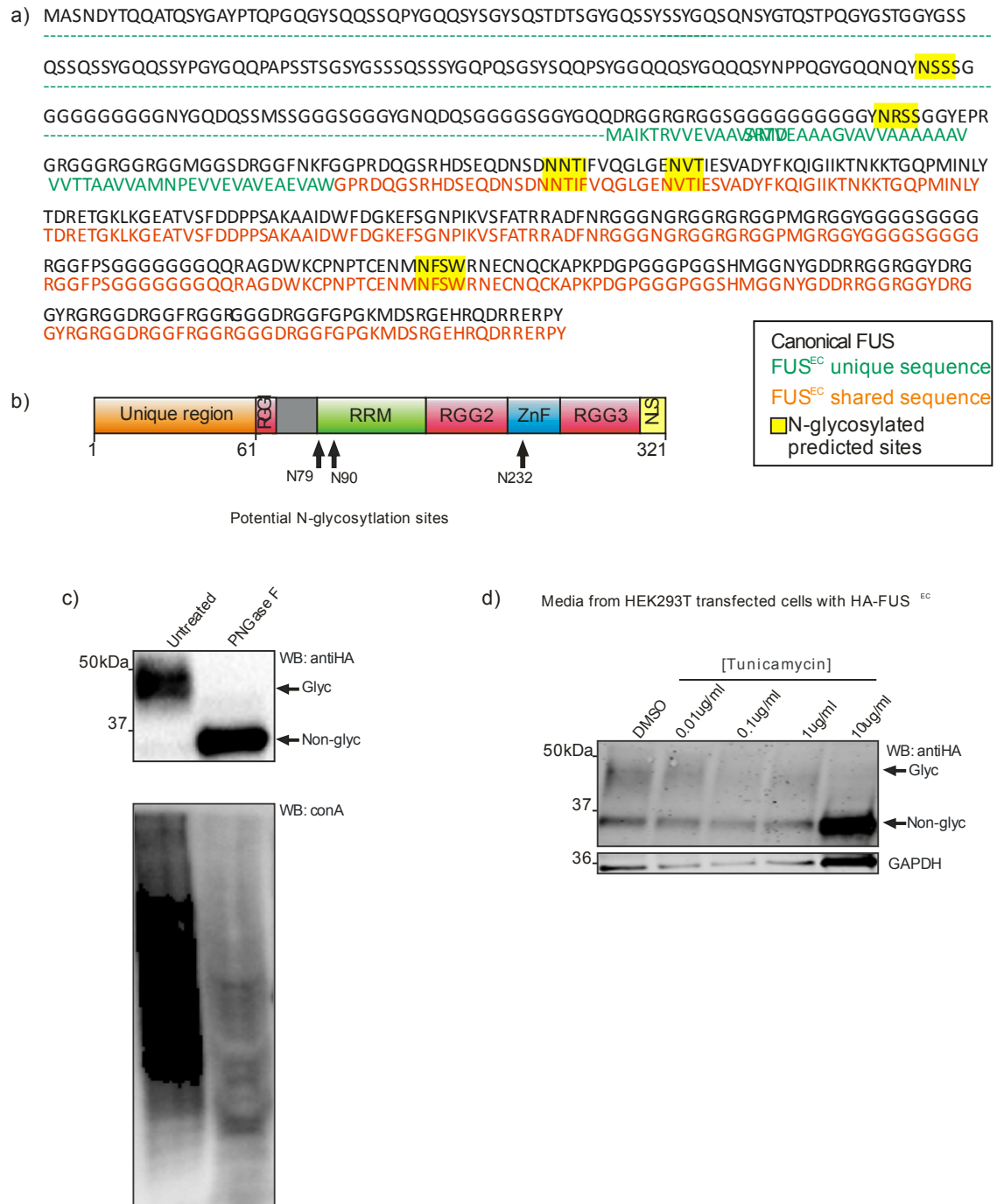


Figure 4.7 FUS^{EC} is N-glycosylated. (a) Protein sequence of canonical FUS (black) and FUS^{EC} (common sequence with FUS in green and unique sequence of FUS^{EC} in orange). N-glycosylation sites predicted with NetNGlyc1.0 Server are highlighted in yellow. (b) Schematic diagram of FUS^{EC} protein structure showing the location of the predicted N-glycosylated sites (N79, N90, N232). (c) Conditioned media from HEK293T cells expressing HA-FUS^{EC} was prepared for PNGaseF assay. Western blotting for HA, and conA of samples treated and not treated with PNGaseF. ConA was used as a positive control for de-glycosylation. (d) Western blotting of FUS^{EC} using an anti-HA antibody in HEK293T cells treated with vehicle only (DMSO) or tunicamycin (0.01, 0.1, 1 or 10 μ g/ml). GAPDH was used as control for cell lysis.

4.4.4. Glycomics analysis of FUS^{EC} reveals the presence of complex and sialylated glycans

We next examined the *N*-glycan structures attached to FUS^{EC} using LC-MS/MS analysis. For this purpose, HA-FUS^{EC} was immunoprecipitated from the media of HEK293T transfected cells. A fraction (20% of the IP) of the pulled-down protein was loaded onto a SDS-PAGE gel, and electrophoresis was performed. The gel was then stained with Coomassie blue. The major band detected in the gel was of MW 40-50 kDa, corresponding to the expected size for glycosylated FUS^{EC} (**Figure 4.8a**). For the glycomics analysis, the glycans from the immunoprecipitated material were released by PNGase F treatment, separated and detected using porous graphitized carbon-LC-ESI-MS/MS.

Glycan profiling of FUS^{EC} revealed a mixture of high mannoses, hybrids and complex structures. From this analysis, the proposed structures of the glycans were predicted, according to their elution times, as represented in the **Table 4.5**. Of all the *N*-glycans that were identified from the IP, 88.5% of the *N*-glycans detected were composed of complex structures (See **Figure 4.2**. as a reference), and 84% contained sialic acids on either or both of the $\alpha(1-3)$ mannose or $\alpha(1-6)$ mannose arms of the *N*-glycan core. Bi-, tri- and tetra-antennary complex structures were also detected (**Figure 4.8b**).

In conclusion, these data confirm that FUS^{EC} is *N*-glycosylated. They also reveal that FUS^{EC} is mostly composed of complex *N*-glycans, which are known to be attached to the protein in the Golgi apparatus. These data therefore imply, that FUS^{EC} is secreted through the classical ER-Golgi pathway [877].

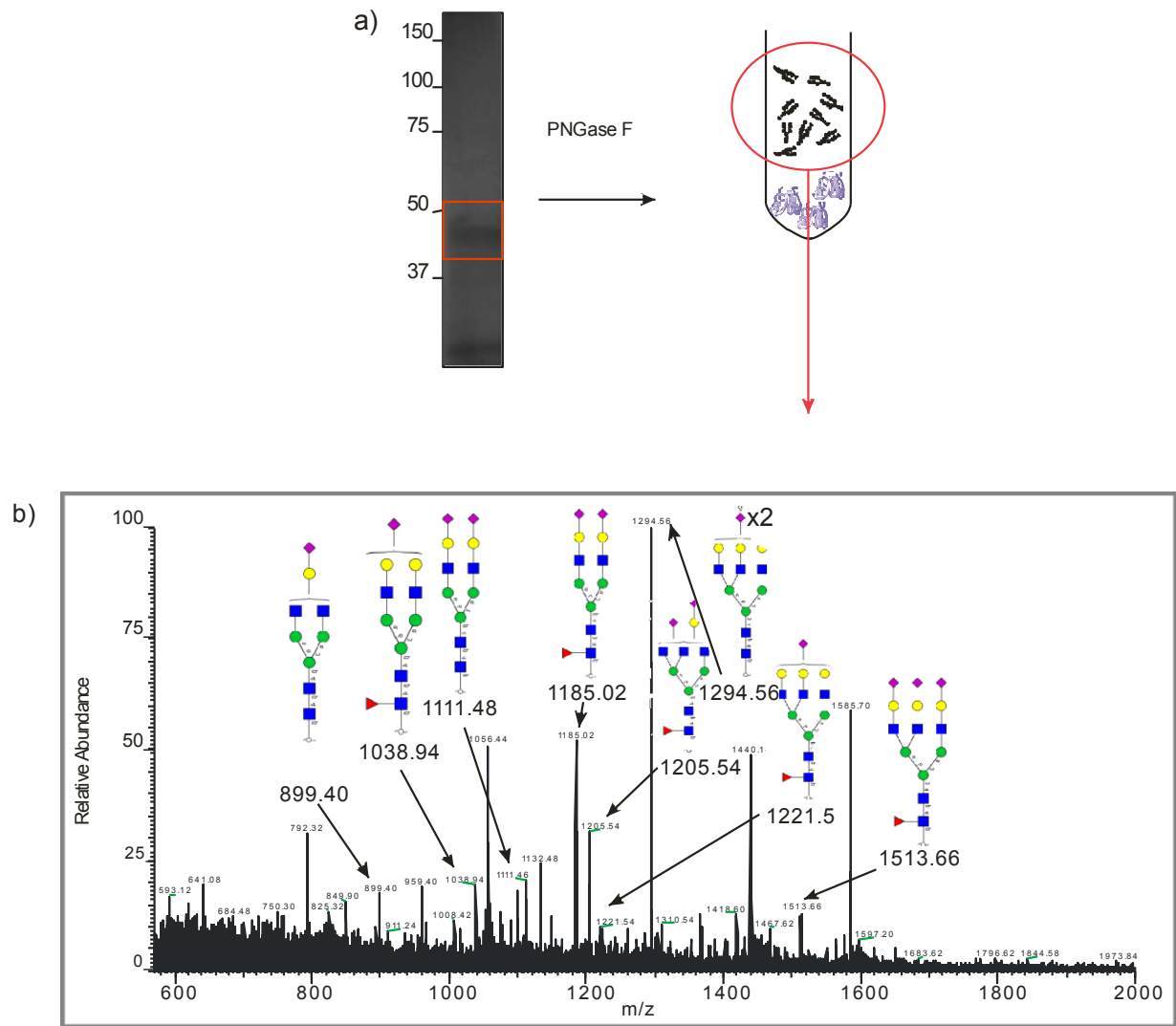


Figure 4.8 HA- FUS^{EC} is N-glycosylated with complex N-glycans. (a) The immunoprecipitated HA-FUS^{EC} fraction from transfected cells was loaded into an SDS PAGE gel, a 40-50 kDa band was excised and treated with PNGase F. (b) Average MS from N-glycans from HA-FUS^{EC} of the retention time (26 -30 min) window.

Table 4.5 Total assigned *N*-glycan composition from HA-FUS^{EC}.

	Mass	MH-	Composition	Time	Area	Relative %
High mannose	1235.52	1235.52	(Hex)2 + (Man)3(GlcNAc)2	20	5375	4.92
	698.28	1397.56	(Hex)3 + (Man)3(GlcNAc)2	16.6	1507	1.38
	1397.6	1397.6	(Hex)3 + (Man)3(GlcNAc)2	16.6	714	0.65
	779.32	1559.64	(Hex)4 + (Man)3(GlcNAc)2	16.5	1630	1.49
	1559.68	1559.68	(Hex)4 + (Man)3(GlcNAc)2	16.5	350	0.32
	860.34	1721.68	(Hex)5 + (Man)3(GlcNAc)2	16.6	1668	1.53
	941.38	1883.76	(Hex)6 + (Man)3(GlcNAc)2	16.6	1359	1.24
Complex glycans	731.3	1463.6	(HexNAc)2 (Deoxyhexose)1 + (Man)3(GlcNAc)2	20.8	3230	2.96
	1463.7	1463.7	(HexNAc)2 (Deoxyhexose)1 + (Man)3(GlcNAc)2	20.8	721	0.66
	832.86	1666.72	(HexNAc)3 (Deoxyhexose)1 + (Man)3(GlcNAc)2	16.1	952	0.87
	832.86	1666.72	(HexNAc)3 (Deoxyhexose)1 + (Man)3(GlcNAc)2	20.2	1595	1.46
	832.86	1666.72	(HexNAc)3 (Deoxyhexose)1 + (Man)3(GlcNAc)2	22.7	431	0.39
	884.88	1770.76	(Hex)1 (HexNAc)2 (NeuAc)1 + (Man)3(GlcNAc)2	17.5	646	0.59
	913.9	1828.8	(Hex)1 (HexNAc)3 (Deoxyhexose)1 + (Man)3(GlcNAc)2	17	1217	1.11
	913.9	1828.8	(Hex)1 (HexNAc)3 (Deoxyhexose)1 + (Man)3(GlcNAc)2	18.2	358	0.33
	913.9	1828.8	(Hex)1 (HexNAc)3 (Deoxyhexose)1 + (Man)3(GlcNAc)2	26.4	439	0.4
	934.4	1869.8	(HexNAc)4 (Deoxyhexose)1 + (Man)3(GlcNAc)2	23.7	1151	1.05
	937.4	1875.8	(Hex)2 (HexNAc)1 (Deoxyhexose)1 (NeuAc)1 + (Man)3(GlcNAc)2	18.9	688	0.63
	957.88	1916.76	(Hex)1 (HexNAc)2 (Deoxyhexose)1 (NeuAc)1 + (Man)3(GlcNAc)2	20	641	0.59
	957.88	1916.76	(Hex)1 (HexNAc)2 (Deoxyhexose)1 (NeuAc)1 + (Man)3(GlcNAc)2	21.6	1356	1.24
	966.42	1933.84	(Hex)2 (HexNAc)2 (Deoxyhexose)2 + (Man)3(GlcNAc)2	18.9	3058	2.8
	966.42	1933.84	(Hex)2 (HexNAc)2 (Deoxyhexose)2 + (Man)3(GlcNAc)2	23.7	571	0.52
	966.42	1933.84	(Hex)2 (HexNAc)2 (Deoxyhexose)2 + (Man)3(GlcNAc)2	25.8	281	0.26
	966.42	1933.84	(Hex)2 (HexNAc)2 (Deoxyhexose)2 + (Man)3(GlcNAc)2	30.8	149	0.14
	1038.94	2078.88	(Hex)2 (HexNAc)2 (Deoxyhexose)1 (NeuAc)1 + (Man)3(GlcNAc)2	23.5	4517	4.13
	1038.94	2078.88	(Hex)2 (HexNAc)2 (Deoxyhexose)1 (NeuAc)1 + (Man)3(GlcNAc)2	30.6	775	0.71
	1047.46	2095.92	(Hex)3 (HexNAc)2 (Deoxyhexose)2 + (Man)3(GlcNAc)2	19.8	1215	1.11
	1059.46	2119.92	(Hex)1 (HexNAc)3 (Deoxyhexose)1 (NeuAc)1 + (Man)3(GlcNAc)2	16	1532	1.4
	1059.46	2119.92	(Hex)1 (HexNAc)3 (Deoxyhexose)1 (NeuAc)1 + (Man)3(GlcNAc)2	18.2	262	0.24
	1059.46	2119.92	(Hex)1 (HexNAc)3 (Deoxyhexose)1 (NeuAc)1 + (Man)3(GlcNAc)2	21	306	0.28
	1059.46	2119.92	(Hex)1 (HexNAc)3 (Deoxyhexose)1 (NeuAc)1 + (Man)3(GlcNAc)2	21.9	897	0.82
	1059.46	2119.92	(Hex)1 (HexNAc)3 (Deoxyhexose)1 (NeuAc)1 + (Man)3(GlcNAc)2	23.8	543	0.5
	1059.46	2119.92	(Hex)1 (HexNAc)3 (Deoxyhexose)1 (NeuAc)1 + (Man)3(GlcNAc)2	29	280	0.26
	1067.42	2135.84	(Hex)2 (HexNAc)3 (NeuAc)1 + (Man)3(GlcNAc)2	15	737	0.67
	1111.48	2223.96	(Hex)2 (HexNAc)2 (NeuAc)2 + (Man)3(GlcNAc)2	18	9018	8.26
	1111.48	2223.96	(Hex)2 (HexNAc)2 (NeuAc)2 + (Man)3(GlcNAc)2	24.5	1182	1.08

Complex glycans	1112	2225	(Hex)2 (HexNAc)2 (Deoxyhexose)2 (NeuAc)1 + (Man)3(GlcNAc)2	22.2	305	0.28
	1132.5	2266	(Hex)1 (HexNAc)3 (Deoxyhexose)2 (NeuAc)1 + (Man)3(GlcNAc)2	17.3	428	0.39
	1132.5	2266	(Hex)1 (HexNAc)3 (Deoxyhexose)2 (NeuAc)1 + (Man)3(GlcNAc)2	21	502	0.46
	1132.5	2266	(Hex)1 (HexNAc)3 (Deoxyhexose)2 (NeuAc)1 + (Man)3(GlcNAc)2	27.9	444	0.41
	1140.5	2282	(Hex)2 (HexNAc)3 (Deoxyhexose)1 (NeuAc)1 + (Man)3(GlcNAc)2	16.9	736	0.67
	1140.5	2282	(Hex)2 (HexNAc)3 (Deoxyhexose)1 (NeuAc)1 + (Man)3(GlcNAc)2	21.3	549	0.5
	1148.48	2297.96	(Hex)3 (HexNAc)3 (NeuAc)1 + (Man)3(GlcNAc)2	21.3	2050	1.88
	1148.48	2297.96	(Hex)3 (HexNAc)3 (NeuAc)1 + (Man)3(GlcNAc)2	23.8	359	0.33
	1184.5	2370	(Hex)2 (HexNAc)2 (Deoxyhexose)1 (NeuAc)2 + (Man)3(GlcNAc)2	21.5	####	9.88
	1184.5	2370	(Hex)2 (HexNAc)2 (Deoxyhexose)1 (NeuAc)2 + (Man)3(GlcNAc)2	25	113	0.1
	1184.5	2370	(Hex)2 (HexNAc)2 (Deoxyhexose)1 (NeuAc)2 + (Man)3(GlcNAc)2	28.6	790	0.72
	1184.5	2370	(Hex)2 (HexNAc)2 (Deoxyhexose)1 (NeuAc)2 + (Man)3(GlcNAc)2	34.3	372	0.34
	1205.04	2411.08	(Hex)1 (HexNAc)3 (Deoxyhexose)1 (NeuAc)2 + (Man)3(GlcNAc)2	20.5	4028	3.69
	1205.04	2411.08	(Hex)1 (HexNAc)3 (Deoxyhexose)1 (NeuAc)2 + (Man)3(GlcNAc)2	21.5	320	0.29
	1205.04	2411.08	(Hex)1 (HexNAc)3 (Deoxyhexose)1 (NeuAc)2 + (Man)3(GlcNAc)2	27.3	553	0.51
	1213.02	2427.04	(Hex)2 (HexNAc)3 (NeuAc)2 + (Man)3(GlcNAc)2	15.3	470	0.43
	1213.02	2427.04	(Hex)2 (HexNAc)3 (NeuAc)2 + (Man)3(GlcNAc)2	27.3	139	0.13
	1221.5	2444	(Hex)3 (HexNAc)3 (Deoxyhexose)1 (NeuAc)1 + (Man)3(GlcNAc)2	25.8	686	0.63
	1221.5	2444	(Hex)3 (HexNAc)3 (Deoxyhexose)1 (NeuAc)1 + (Man)3(GlcNAc)2	31.8	387	0.35
	1286.08	2573.16	(Hex)2 (HexNAc)3 (Deoxyhexose)1 (NeuAc)2 + (Man)3(GlcNAc)2	16.4	1739	1.59
	1286.08	2573.16	(Hex)2 (HexNAc)3 (Deoxyhexose)1 (NeuAc)2 + (Man)3(GlcNAc)2	20.3	327	0.3
	1294.06	2589.12	(Hex)3 (HexNAc)3 (NeuAc)2 + (Man)3(GlcNAc)2	20	1933	1.77
	1294.06	2589.12	(Hex)3 (HexNAc)3 (NeuAc)2 + (Man)3(GlcNAc)2	22.3	616	0.56
	1294.06	2589.12	(Hex)3 (HexNAc)3 (NeuAc)2 + (Man)3(GlcNAc)2	27.1	1079	0.99
	1294.06	2589.12	(Hex)3 (HexNAc)3 (NeuAc)2 + (Man)3(GlcNAc)2	29.9	521	0.48
	1294.06	2589.12	(Hex)3 (HexNAc)3 (NeuAc)2 + (Man)3(GlcNAc)2	33.4	779	0.71
	1294.06	2589.12	(Hex)3 (HexNAc)3 (NeuAc)2 + (Man)3(GlcNAc)2	38.5	412	0.38
	1367.1	2735.2	(Hex)3 (HexNAc)3 (Deoxyhexose)1 (NeuAc)2 + (Man)3(GlcNAc)2	23.8	844	0.77
	1367.1	2735.2	(Hex)3 (HexNAc)3 (Deoxyhexose)1 (NeuAc)2 + (Man)3(GlcNAc)2	31.4	491	0.45
	1367.1	2735.2	(Hex)3 (HexNAc)3 (Deoxyhexose)1 (NeuAc)2 + (Man)3(GlcNAc)2	36.7	327	0.3
	959.38	2880.14	(Hex)3 (HexNAc)3 (NeuAc)3 + (Man)3(GlcNAc)2	25.6	818	0.75
	959.38	2880.14	(Hex)3 (HexNAc)3 (NeuAc)3 + (Man)3(GlcNAc)2	32	2202	2.02
	959.38	2880.14	(Hex)3 (HexNAc)3 (NeuAc)3 + (Man)3(GlcNAc)2	38.5	279	0.26
	1439.64	2880.28	(Hex)3 (HexNAc)3 (NeuAc)3 + (Man)3(GlcNAc)2	19.1	479	0.44
	1439.64	2880.28	(Hex)3 (HexNAc)3 (NeuAc)3 + (Man)3(GlcNAc)2	25.6	2285	2.09
	1439.64	2880.28	(Hex)3 (HexNAc)3 (NeuAc)3 + (Man)3(GlcNAc)2	28.9	329	0.3
	1439.64	2880.28	(Hex)3 (HexNAc)3 (NeuAc)3 + (Man)3(GlcNAc)2	32.1	6400	5.86
	1439.64	2880.28	(Hex)3 (HexNAc)3 (NeuAc)3 + (Man)3(GlcNAc)2	38.5	869	0.8
	1512.68	3026.36	(Hex)3 (HexNAc)3 (Deoxyhexose)1 (NeuAc)3 + (Man)3(GlcNAc)2	22.4	267	0.24
	1512.68	3026.36	(Hex)3 (HexNAc)3 (Deoxyhexose)1 (NeuAc)3 + (Man)3(GlcNAc)2	28.7	363	0.33
	1512.68	3026.36	(Hex)3 (HexNAc)3 (Deoxyhexose)1 (NeuAc)3 + (Man)3(GlcNAc)2	35.1	177	0.16
	1512.68	3026.36	(Hex)3 (HexNAc)3 (Deoxyhexose)1 (NeuAc)3 + (Man)3(GlcNAc)2	36.3	258	0.24
	1549.7	3100.4	(Hex)4 (HexNAc)4 (Deoxyhexose)1 (NeuAc)2 + (Man)3(GlcNAc)2	31.5	231	0.21
	1549.7	3100.4	(Hex)4 (HexNAc)4 (Deoxyhexose)1 (NeuAc)2 + (Man)3(GlcNAc)2	32.8	258	0.24
	1549.7	3100.4	(Hex)4 (HexNAc)4 (Deoxyhexose)1 (NeuAc)2 + (Man)3(GlcNAc)2	36.8	281	0.26
	1056.44	3171.32	(Hex)3 (HexNAc)3 (NeuAc)4 + (Man)3(GlcNAc)2	23.5	1267	1.16
	1056.44	3171.32	(Hex)3 (HexNAc)3 (NeuAc)4 + (Man)3(GlcNAc)2	30.1	1497	1.37
	1056.44	3171.32	(Hex)3 (HexNAc)3 (NeuAc)4 + (Man)3(GlcNAc)2	38.5	361	0.33
	1585.22	3171.44	(Hex)3 (HexNAc)3 (NeuAc)4 + (Man)3(GlcNAc)2	23.5	1099	1.01
	1585.22	3171.44	(Hex)3 (HexNAc)3 (NeuAc)4 + (Man)3(GlcNAc)2	30.1	966	0.88
	1585.22	3171.44	(Hex)3 (HexNAc)3 (NeuAc)4 + (Man)3(GlcNAc)2	38.5	200	0.18

Complex glycans	1129.84	3391.52	(Hex)4 (HexNAc)4 (Deoxyhexose)1 (NeuAc)3 + (Man)3(GlcNAc)	36	305	0.28
	1129.84	3391.52	(Hex)4 (HexNAc)4 (Deoxyhexose)1 (NeuAc)3 + (Man)3(GlcNAc)	37.4	448	0.41
	1129.84	3391.52	(Hex)4 (HexNAc)4 (Deoxyhexose)1 (NeuAc)3 + (Man)3(GlcNAc)	38.7	267	0.24
	1695.26	3391.52	(Hex)4 (HexNAc)4 (Deoxyhexose)1 (NeuAc)3 + (Man)3(GlcNAc)	36	250	0.23
	1695.26	3391.52	(Hex)4 (HexNAc)4 (Deoxyhexose)1 (NeuAc)3 + (Man)3(GlcNAc)	37.4	419	0.38
	1695.26	3391.52	(Hex)4 (HexNAc)4 (Deoxyhexose)1 (NeuAc)3 + (Man)3(GlcNAc)	38.7	259	0.24
	1226.86	3682.58	(Hex)4 (HexNAc)4 (Deoxyhexose)1 (NeuAc)4 + (Man)3(GlcNAc)	35.6	337	0.31
	1226.86	3682.58	(Hex)4 (HexNAc)4 (Deoxyhexose)1 (NeuAc)4 + (Man)3(GlcNAc)	37.2	1302	1.19
	1840.94	3682.88	(Hex)4 (HexNAc)4 (Deoxyhexose)1 (NeuAc)4 + (Man)3(GlcNAc)	35.6	112	0.1
	1840.94	3682.88	(Hex)4 (HexNAc)4 (Deoxyhexose)1 (NeuAc)4 + (Man)3(GlcNAc)	37.2	209	0.19

Abbreviations: Hex: hexose, HexNAc: N-acetylhexoseamine, NeuAc: N-acetylneuraminic acid, Man: mannose, GlcNAc: N-Acetylglucosamine

4.4.5. FUS^{EC} is present in the media insoluble fraction but not in exosomes

The results described in section 4.4.3. imply that FUS^{EC} is secreted via a mechanism independent from its *N*-glycosylation. Hence, it was next examined the mechanisms of FUS^{EC} secretion further by investigating whether FUS^{EC} is present in the insoluble fraction of the media. If so, this would imply that FUS^{EC} is present within extracellular vesicles, or alternatively, in an aggregated form. Conditioned media from HEK293T cells transfected with WT HA-FUS^{EC}, was collected after 24h of transfection. The insoluble fraction of the media was isolated by ultracentrifugation at 100,000 g for 1 h. Western blotting using an anti-HA antibody revealed the presence of a band at 33 kDa, corresponding to the expected size for non-glycosylated HA-FUS^{EC} (**Figure 4.9a**). These results suggest that the 33 kDa band in the media corresponding to FUS^{EC} may also be secreted via extracellular vesicles or as aggregates.

Hence, it was next investigated whether FUS^{EC} was present within exosomes. Exosomes were isolated from the media of HA-FUS^{EC} HEK293T transfected cells. Nanoparticle tracking analysis demonstrated that isolated particles presented exosome-like characteristics, with size ranging from 50 to 200 nm. This was confirmed by electron microscopy analysis (**Figure 4.9b**). Additionally, whole-cell lysate and exosome isolated samples were treated to SDS-PAGE gel and Western blotting for different exosome markers, as well as

negative controls and anti-HA antibody, was performed. HA immunoblotting revealed the presence of a band at 38 kDa in the lysate samples, but no bands were detected in the exosome preparation samples. The integrity of the exosome samples was confirmed by immunoblotting using two exosomal markers, tsg-101 and flotillin-1, , whereas no detectable GM130 (a marker of the Golgi apparatus) or Bcl-2 (a marker of apoptotic membranes) were present indicating little contamination or cell death. However, immunoblotting for a nuclear marker, Nuc (nucleoporin), revealed the presence of some nuclear material in the exosome preparation, even though this was less than in the lysate (**Figure 4.9c**).

These preliminary results suggest that HA-FUS^{EC} is not present within exosomes, however these experiments require further optimisation and repetition as well as different exosome preparations to confidently rule out that HA-FUS^{EC} is not secreted in an exosome-dependent manner. This experiment was only performed once, hence it needs repetition and optimization to improve the exosomes purity.

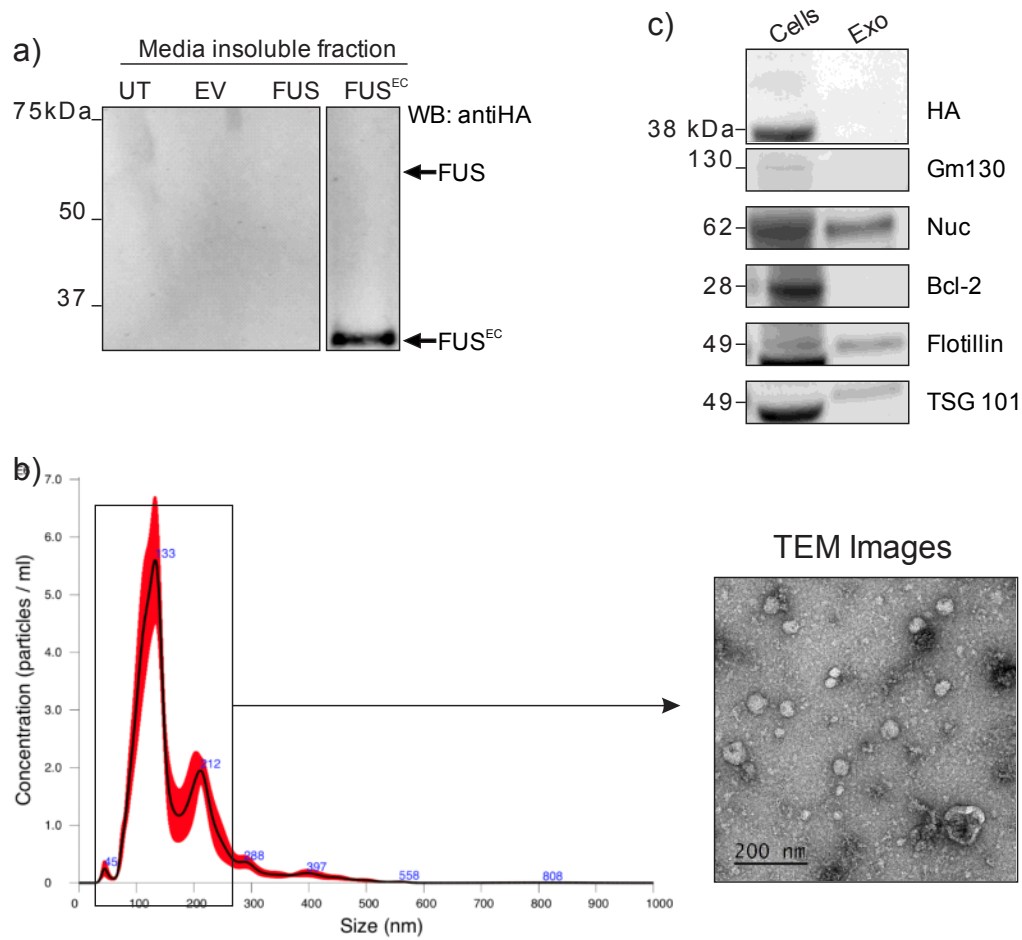


Figure 4.9 FUS^{EC} is secreted in the insoluble part of the media but not in exosomes (a) Western blot analysis for the secretion of HA tag constructs in the insoluble part of the conditioned media after 1 h ultracentrifugation at 100,000 g (n=3). Exosomes were isolated from the conditioned media of HA-FUS^{EC} transfected cells (n=1). (b) Nanoparticle tracking analysis from the isolated fraction of the media of HA-FUS^{EC} transfected cells. Transmission electron microscopy image of exosomes (Scale bar: 200 nm). (c) Western blotting of the whole cell lysate and the isolated exosome fraction with anti-HA antibody and a panel of antibodies to determine the purity of exosome fraction.

4.4.6. Overexpressed FUS^{EC} was detected in the cytoplasm of HEK293T cells

Since in section 4.4.2 we were able to detect cytoplasmic FUS^{EC} by Western blotting and microscopy, the next aim was to examine the localization of FUS^{EC} intracellularly. HEK293T cells were transfected with FUS^{EC} constructs for 48h. Cells were fixed and immunocytochemistry was performed using an anti-HA antibody.

FUS^{EC} was present in the nucleus, either diffuse or as punctiform structures (**Figure 4.10a** and **4.10b**), but this was only present in 10 % of cells expressing HA-FUS^{EC} (**Figure 4.10f**). A proportion of 14% of cells displayed both nuclear and cytoplasmic diffuse FUS^{EC} (**Figure 4.10c** and quantification in **4.10f**). Diffuse cytoplasmic FUS^{EC} was present in 13% of transfected cells. Cytoplasmic FUS^{EC} formed small punctiform or large inclusions in 61% of cells (**Figure 4.10d** and **4.10e** and quantification in **4.10f**). Additionally, immunocytochemistry with anti-HA, anti-calnexin (ER) and anti-GM130 (*cis*-Golgi) antibodies demonstrated that FUS^{EC} partially colocalized with the ER (**Figure 4.10g**) and the Golgi (**Figure 4.10h**) compartments.

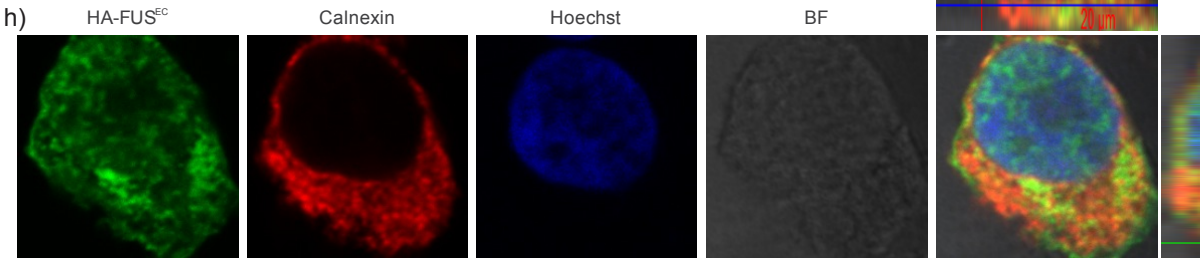
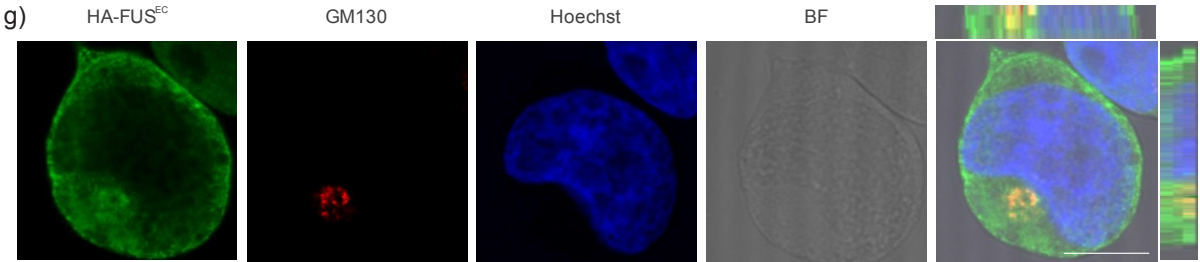
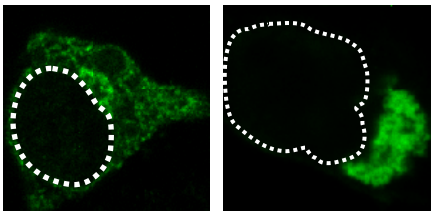
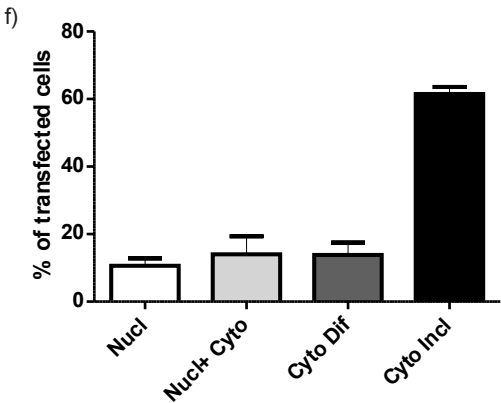
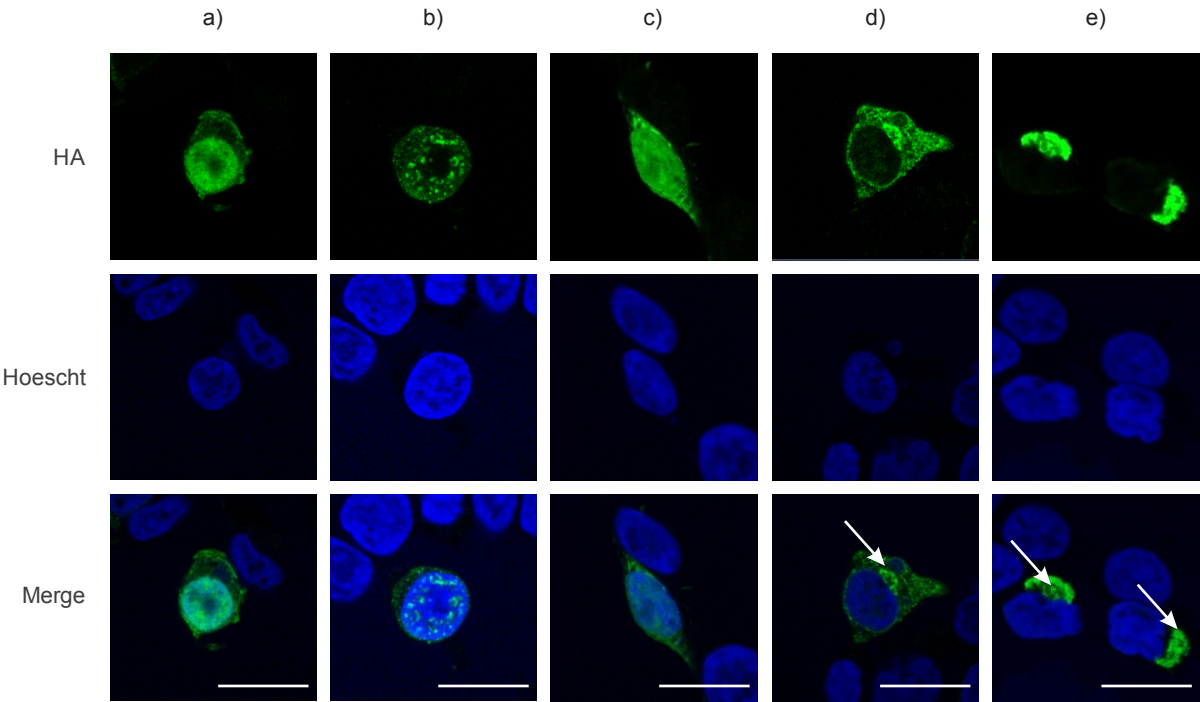


Figure 4.10 Cytoplasmic distribution and subcellular localization of FUS^{EC} (a) HEK293T cells were transfected with HA-FUS^{EC} constructs, fixed and stained with an anti-HA antibody (green) and Hoechst for nuclei (blue). Morphological pattern for FUS^{EC} localized in a-b the nucleus c-e the cytoplasm. Higher magnification images are provided for the cells containing cytoplasmic aggregates. Arrows: cytoplasmic aggregates. (f) Quantification of the cellular localization of HA-FUS^{EC} transfected cells. (g-h) Confocal z-stack images from HEK293T cells overexpressing HA-FUS^{EC} (green) and immunolabelled with anti-GM130 (Golgi) (g) or anti-calnexin (endoplasmic reticulum) (h) antibodies (red). Nucleus was stained with Hoechst (blue). Scale bar: 20 μ m.

4.4.7. Identification of FUS^{EC} binding partners

In order to elucidate the normal functions of FUS^{EC} the next aim was to identify its normal putative interacting partners within the cell, as well as in the conditioned media.

For this purpose, empty vector or WT-HA-FUS^{EC} were overexpressed in HEK293T cells. At 48h post-transfection, lysate and media were collected and processed as in Chapter 2, section 2.3.1. Next, HA magnetic beads were used to immunoprecipitate FUS^{EC} from transfected cell populations, and from untransfected cells as a control. 10% of the immunoprecipitated material of each sample was loaded onto a SDS-PAGE gel and immunoblotting using anti-HA or anti-GFP antibodies was performed. In the lysate, a band at 33 kDa was detected in cells expressing HA-FUS^{EC}, while no band was detected in the untransfected samples, confirming that the immunoprecipitation was specific. In the conditioned media samples, bands at 33kDa and approximately 40-50kDa were precipitated, corresponding to non-glycosylated and glycosylated FUS^{EC} respectively. No band was detected in the untransfected samples as expected (**Figure 4.11a**).

Next, the rest of each immunoprecipitation reaction was subjected to SDS-PAGE. Electrophoresis was performed for 3 mins (1 cm into the gel) so ensure that the proteins all had entered the gel, followed by staining with Coomassie Blue. The entire stained 1cm protein fraction was excised and in-gel digested with trypsin. LC-MS/MS analysis identified a number of interacting proteins from all immunoprecipitated samples. Those proteins identified in

untreated and empty vector samples were subtracted from the list of binding partners of FUS^{EC}. We established specific criteria that proteins must be identified in at least two replicates to be considered as a potential binding partner (all the proteins identified are listed in the appendix 8.2).

In the lysate samples 144 interacting partners were identified. GO molecular function analysis revealed that 36.4% (52) of the FUS^{EC} interacting proteins are involved in protein and nucleic acid binding functions. Of these 55.8% (29) were characterised as nucleic acid binding proteins (**Figure 4.11b**). Two examples of interacting partners identified under this category are: TDP-43 and matrin-3. In the media, 369 proteins were identified and in this case 39.3% (145) were protein and nucleic acid binding proteins, and 48.5% (70) of these were characterised as having nucleic acid binding function (**Figure 4.11c**). Again Matrin-3 was identified to bind extracellular FUS^{EC}.

These results identify potential interacting partners of FUS^{EC}, suggesting a potential role of FUS^{EC} in DNA/RNA processing.

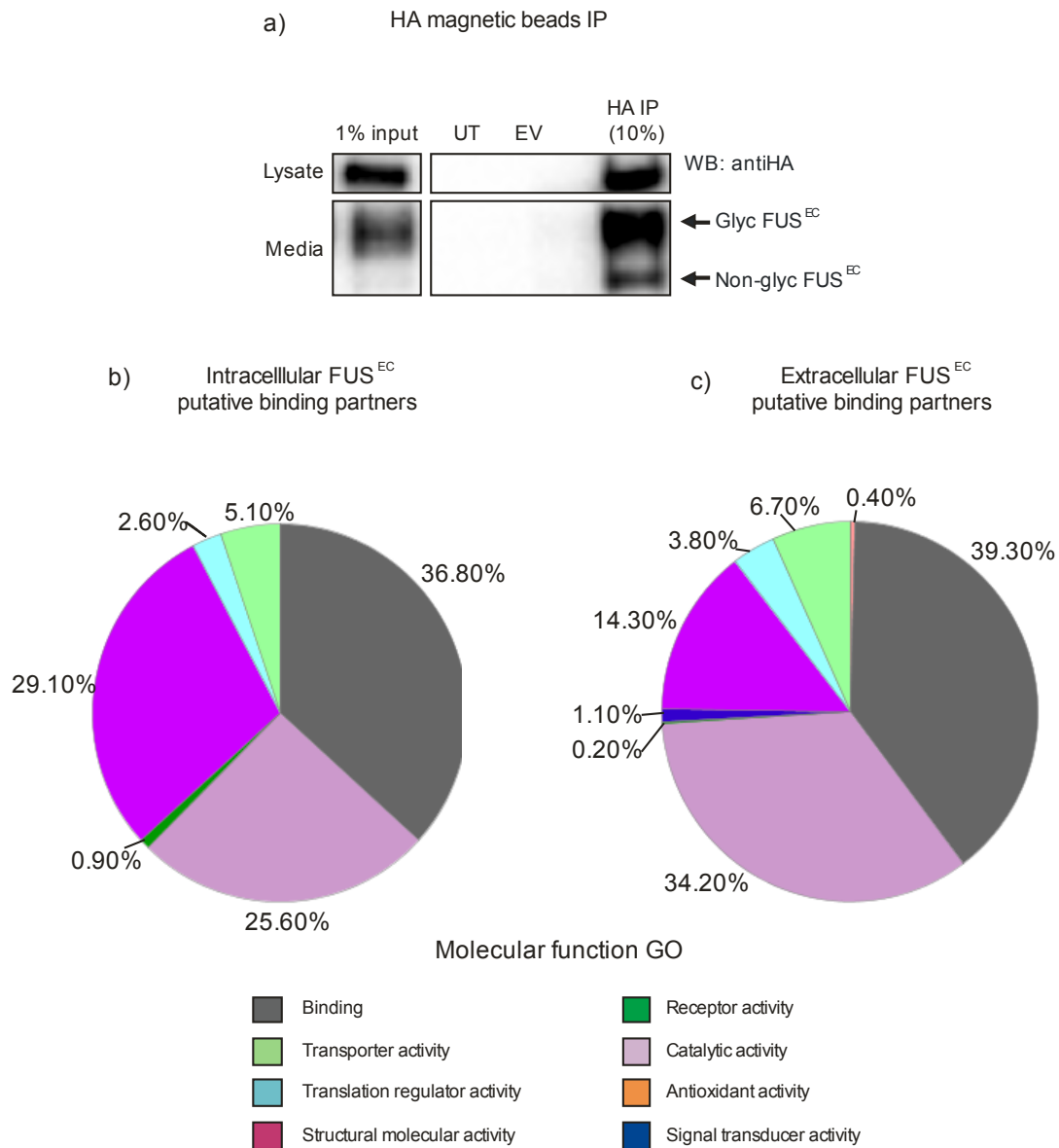


Figure 4.11 Identification of FUS^{EC} binding partners. HEK293T cells were transfected with HA tagged-FUS^{EC} or empty vector (EV) as a control. Lysates and media was collected and prepared for immunoprecipitation with HA magnetic beads. (a) SDS-PAGE electrophoresis and immunoblotting for the pulled down protein from the lysate and media with HA magnetic beads probed for HA antibody. (b) Gene ontology (GO) annotations for the potential putative binding partners of FUS^{EC} in the lysate. (c) GO annotations for the potential putative binding partners of FUS^{EC} in the media.

4.4.8. Antibody characterization

In the previous chapter a customized antibody specific for FUS^{EC} was purchased commercially, with the aim of examining its expression in human tissue. However, characterization of the antibody using endogenous FUS^{EC} expressed in non-transfected cells, suggested that the antibody was not capable of detecting the protein. Hence in the experiments described in this section, the antibody was further investigated using the overexpression system for FUS^{EC} described above.

The specificity of the customized antibody was next examined by overexpressing HA-tagged FUS^{EC} in HEK293T cells, followed by a Western blotting using an anti-HA antibody. This confirmed expression of FUS^{EC} in both the cell lysate (band at 33 kDa) and conditioned media (one band at 33kDa, and the second band at 40-50 kDa) fractions. However, immunoblotting using the FUS^{EC} customized antibody revealed a band at ≈100 kDa in both the lysate and the media. Furthermore, an additional band of approximately 70 kDa was detected in the medium. Hence, the bands detected by the anti-HA antibody did not correspond to those detected by the customized antibody (**Figure 4.12a**).

Secondly, the specificity of the antibody was also studied by immunocytochemistry. GFP-FUS^{EC} was overexpressed in HEK293T cells and cells were fixed at 48h post-transfection. Immunocytochemistry using the FUS^{EC} customized antibody (red), and colocalization of the red signal with GFP, were analysed by confocal microscopy. Unfortunately, however, there was no colocalization between GFP-FUS^{EC} and the customized antibody signal, further suggesting that this antibody could not detect FUS^{EC} (**Figure 4.12b**). To confirm this notion, proteins binding to the customized antibody were next examined by IP of the media of transfected HEK293T cells. LC-MS/MS analysis revealed that FUS^{EC} was not enriched by the customised antibody, because the only peptides detected from the mass spectrometry were the IgG heavy and light chains of the customised antibody (**Figure 4.12c**).

These results confirmed that the commercial customised antibody was not capable of detecting FUS^{EC}. Since the customized antibody was raised

using a specific unique peptide present at the N-terminus of FUS^{EC}, instead of using native FUS^{EC} as an antigen, it is possible that the epitope of the customised antibody is masked due to the structural conformation of FUS^{EC}.

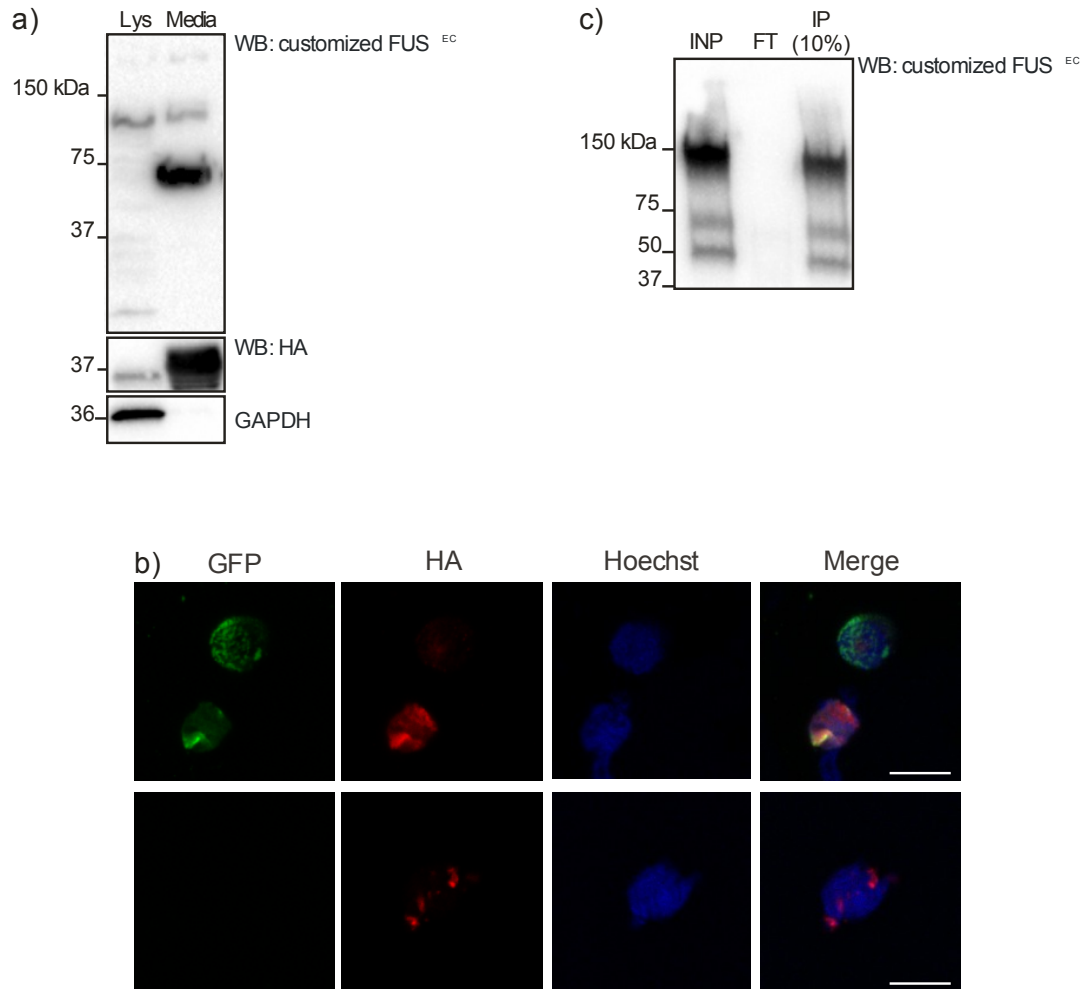


Figure 4.12 Examination of customized antibody against FUS^{EC} (a) Western blotting of cell lysate and media from HEK293T cells transfected with HA-FUS^{EC} construct. Immunoblotting with anti-HA antibody to confirm HA-FUS^{EC} expression (middle panel). Blot was probed using an anti-FUS^{EC} customized antibody (top panel). GAPDH was used as a loading control and a marker for cell lysis. (b) HEK293T cells overexpressing GFP tagged FUS^{EC} were fixed and immunocytochemistry using an anti-FUS^{EC} customized antibody (red) and GFP-FUS^{EC} (green) was performed. Nuclei were stained with Hoechst (blue). Scale bar: 20 μm. (c) Immunoprecipitation of the conditioned media of HEK293T cells using FUS^{EC} customized antibody, and immunoblotting with the same antibody. INP: Input, FT: Flow through, IP: Immunoprecipitated sample.

4.5. Discussion

Since FUS^{EC} has never been studied experimentally before, it was imperative to examine its normal characteristics, including its cellular localization, post-translational modifications and normal cellular function. In the results presented in this chapter, an overexpression system was established that allowed the confirmation of the unique extracellular localization of FUS^{EC}. It was demonstrated that FUS^{EC} is *N*-glycosylated and inhibition of glycosylation using tunicamycin affected its secretion. We further characterized the *N*-glycan structure of FUS^{EC} and concluded that FUS^{EC} is mainly composed of complex *N*-glycans. After ultracentrifugation, FUS^{EC} was localized within the insoluble part of the media, but not in exosomes. Additionally, FUS^{EC} was detectable intracellularly, where it was found to localize in the cytoplasm, and partially colocalized within membranous organelles such as the Golgi and ER compartments. Finally, we identified intracellular and extracellular candidate binding partners of FUS^{EC} that may assist in determining the biological function of the isoform in the future.

Previous results from this thesis suggested that FUS^{EC} displays posttranslational modifications. In the 2DGE gels (**Figure 3.9b**, Chapter 3), FUS^{EC} was detected as a train of protein isoforms corresponding to the expected molecular weight. These data suggest that this represents the same protein containing different PTMs (such as *N*-glycosylation) which change the isoelectric point of the protein. In the first blot (**Figure 3.9b**, Chapter 3), FUS^{EC} displayed an apparent MW of 40 kDa, even though, according to its primary protein sequence, it was predicted to possess a MW of 33 kDa. When overexpressing the HA and GFP constructs, a thick band resembling a smear was detected.

Several predominant proteins linked to neurodegenerative diseases are *N*-glycosylated, such as APP and Tau [828, 829, 831]. Additionally, glycomics alterations have been detected in serum and CSF samples of ALS patients compared to controls [837, 838]. Interestingly, the results in this chapter reveal that FUS^{EC} is *N*-glycosylated, and this modulates in part its secretion. To

conclusively determine if *N*-glycosylation is essential for the secretion of FUS^{EC} additional experiments are needed. Firstly, the experiments reported in this chapter should be repeated on endogenous FUS^{EC} to confirm that these results are not due to the overexpressing system used. Additionally, future studies could focus on mutation of the FUS^{EC} predicted *N*-glycosylated sites (for example, to Asp which is the amino acid most closely related to Asn) and examine its effect on secretion. A similar study was performed on extracellular SOD3, where mutation of the consensus *N*-glycosylated site impaired its secretion [878].

Additionally, in this chapter, it was demonstrate that FUS^{EC} colocalizes partially with markers of the ER and Golgi, consistent with its secretion through the classical secretory pathway. The results from the glycomics studies further confirm this finding, because most of the glycans detected on FUS^{EC} are complex and only become added to glycoproteins that have been transported to the Golgi apparatus for further protein folding (**Figure 4.8**). To confirm that FUS^{EC} is secreted through this route, further studies could examine the effect of brefeldin A and nocodazole (which are inhibitors of ER to Golgi protein transport and microtubule polymerization respectively) on the secretion of FUS^{EC}. A similar approach was taken previously to demonstrate that SOD1 secretion was brefelidin A sensitive, which implied that secretions was through the conventional secretory route [879]. The secretion of FUS^{EC} through the classical route is relevant to ALS, since accumulating evidences implicate disruption of protein trafficking as a key pathogenic mechanism in ALS [115, 426]. Moreover, FUS^{EC} localizes partially within the ER and Golgi organelles, therefore it could have a direct effect on their morphology and function.

Moreover, it was also determined that non-glycosylated FUS^{EC} was secreted in the insoluble part of the media, implying that it is secreted within exosomes or in an aggregated form. However in this chapter preliminary studies suggested that HA-FUS^{EC} is *not* secreted by an exosome-dependent manner, although further replication of the experiments is needed to conclusively rule out this hypothesis. Due to time constraints, we could not determine whether FUS^{EC} was secreted in an aggregated form. It would be

interesting to perform a filter trap assay with the media, as previously carried out on SOD1 aggregates [782], to investigate the possible scenario that FUS^{EC} is secreted as an aggregate. SOD1 has been shown to be secreted within exosomes, passively upon cell death, as well and through the conventional ER-Golgi secretory pathway [98, 782]. Similarly, the data presented in this chapter suggest that a similar pathway may also be relevant for FUS^{EC}.

Canonical FUS has the ability to shuttle between the nucleus and the cytoplasm but it is mainly localized within the nucleus. Microscopy analysis of over-expressed FUS^{EC} revealed that a small proportion of FUS^{EC} is found within the nucleus, similar to its canonical counterpart. This is not surprising because FUS^{EC} retains the NLS of canonical FUS at its C-terminus. However, what is more surprising is that most intracellular FUS^{EC} was localized in the cytoplasm, and this was more obvious for ALS-associated mutant forms of canonical FUS, not WT [880]. CCN5 (connective tissue growth factor/cysteine-rich 61/nephroblastoma overexpressed), a secreted member of the CNN family of growth factors, was also shown to unexpectedly translocate in a similar way. Even though the CCN5 protein contains a secretory signal peptide and thus is secreted predominantly, it also bears a NLS, which allows CCN5 to exist in both the nucleus and the cytoplasm [881]. It could be hypothesized that when FUS^{EC} is targeted to the ER-Golgi pathway, this interferes somehow with its targeting to the nucleus. It will be interesting to further study the function of the NLS in FUS^{EC} in future studies by performing site directed mutagenesis to remove it.

It was initially surprising that WT FUS^{EC} forms aggregates similar to those formed by mutant canonical FUS, where the ALS linked mutants mislocalize to the cytoplasm and aggregate [582, 880, 882]. However, the mechanism by which FUS forms inclusions in ALS is still controversial. Some evidence implies that the presence of a mutation is enough to drive the aggregation of FUS, regardless of its cellular localization [883]. On the contrary, it has been proposed that the subcellular localization of FUS rather than the presence of mutations *per se* drives its aggregation. In SH-SY5Y cells and primary hippocampal neurons, over-expression of FUS ALS-associated mutants

and artificial NLS truncation lead to its diffuse cytoplasmic localization. However, increasing concentration of FUS drove the formation of large compact aggregates from small granule-like microaggregates in a concentration dependent manner [884], implying that the accumulation of FUS drives its aggregation. In a yeast model, high levels of overexpressed WT FUS led to its cytoplasmic localization and aggregation, which was linked to the presence of the inefficient NLS in yeast [533]. In contrast, when expression of WT FUS was restricted to the nucleus, aggregation was inhibited [533]. Similarly, WT FUS tagged with NES was mislocalized to the cytoplasm, where it formed inclusions [885], implying that its cytoplasmic expression drives aggregation. Additionally, WT FUS forms inclusions in sALS and non-SOD1 fALS in addition to ALS/dementia and FTD cases [12, 156]. Interestingly, a 35 kDa isoform of TDP-43 was found to be up-regulated in ALS patient spinal cords, which aggregates and induces neuronal cell death in primary neurons [141]. Furthermore, overexpression of WT TDP-43 in NSC-34 and primary cortical neurons induces cell death [886]. Similarly, overexpression of WT TDP-43 in neuronal stem/progenitors and iPS, induced apoptosis [887]. Hence, overexpression of ALS-WT proteins can cause the formation of aggregates and toxicity. As FUS^{EC} lacks exon 7, it can be hypothesized that the levels of FUS^{EC} are not autoregulated in the same way as canonical FUS. The lack of exon 7 in FUS^{EC} may increase its expression levels, predisposing it to form aggregates. Consistent with this hypothesis, splicing of FUS exon 7 is regulated by binding to its own mRNA in exon 7 and the associated flanking regions. Furthermore, ALS mutations that lead to the mislocalization of FUS in the cytoplasm have this autoregulatory ability impaired [512]. Hence, it could be hypothesized that WT FUS^{EC} expression is deregulated and that mislocalized FUS^{EC} in the cytoplasm is toxic by itself. Additionally, it is possible that the use of a protein overexpression system in itself promoted the aggregation of FUS^{EC} within the cell, due to overwhelming of the protein quality control pathway. In future, this could be overcome by studying the endogenous protein or by the use of a stable cell line, with lower levels of protein expression compared to a transient system.

This chapter also aimed to identify extracellular and intracellular binding partners of FUS^{EC}. Gene Ontology analysis identified putative intracellular binding partners of WT FUS^{EC} that belong to DNA/RNA binding proteins, hence this suggests that FUS^{EC} may have similar functions to its canonical counterpart, which is also implicated in those pathways. This is not surprising as FUS^{EC} shares the same C-terminus of FUS and retains four domains (the RRM, two RGG and a ZnF) involved in DNA/RNA binding [888]. Interestingly, two of the putative binding partners of FUS^{EC} include TDP-43 and matrin-3 which are known to also bind canonical FUS and they are mutated and form inclusions in ALS [619, 630, 889]. Additionally, matrin 3 and TDP-43 coaggregate in inclusions in motor neurons from sALS [890].

Interestingly, the putative binding partners of FUS^{EC} from the extracellular media of transfected cells were enriched in DNA/RNA binding proteins based on GO analysis. These observations agree with a previous study that performed LC-MS/MS on the conditioned media from HMC-1 cells, which concluded that RNA binding proteins composed 27% (high density fraction) and 17.3% (low density fraction) of the total proteome in the media [891]. This is highly interesting because RNB proteins associate and form ribonucleoprotein complexes with extracellular RNA [892, 893], although this mechanism remains poorly understood. Additionally, matrin 3 was also identified as a putative binding partner of FUS^{EC} in the conditioned media. Surprisingly, matrin3 has been detected in extracellular vesicles from HEK293T cells and in a neuroblastoma cell line [894, 895]. In the future, it could be investigated whether FUS^{EC} is present in other extracellular vesicles, different from exosomes, such as microvesicles.

There are several limitations of this study that should be noted. The first is the use of transient transfection, which results in high levels of expression of proteins, which may not be reminiscent of the physiological conditions of FUS^{EC}. Therefore, these studies have to be repeated under endogenous conditions. In future studies the putative binding partners identified for FUS^{EC} should be verified by Western blotting and immunocytochemistry. Moreover, given that the customised antibody did not react against FUS^{EC}, further studies

in this area would be enhanced by the availability of a much more specific customised antibody. Future studies could then focus on performing immunoprecipitations using a specific customised antibody, to enrich endogenous FUS^{EC} for improved characterisation that is more relevant to the humans. The advantage of this approach is that the use of an over-expression system is avoided; and the binding partners are therefore capable of binding to FUS^{EC} under physiological and diseased conditions. In future studies, a second customized antibody will be raised by immunising with more than one peptide, thus increasing the chance of the antibody being specific. Raising an antibody against the whole FUS^{EC} protein is not ideal, as this approach has the risk of detecting the C-terminus, which will also react against canonical FUS.

Additionally, FUS^{EC} localization within the ER and Golgi organelles should be confirmed with other techniques such as subcellular fractionation. FUS^{EC} Golgi localization could be further confirmed with electron microscopy, since it allows the discrimination among aggresomes and Golgi, which sometimes are difficult to differentiate when studying an overexpressed protein [896].

Implications and future perspective

In ALS, there is a need to identify biomarkers that aid in the diagnosis and progression of disease. However, detection of specific proteins in body fluids (CSF, serum) can be difficult due to their low abundance. In the future we could take advantage of the *N*-glycosylated nature of FUS^{EC}. Enriching the CSF or serum samples for *N*-glycosylated proteins prior to proteomics profiling would reduce the noise of the sample as these biofluids are often contaminated by high concentrations of albumin and IgG. Additionally, glycoproteins are abundant in the CSF [897] and therefore in the future, the study of the glycomic profile of FUS^{EC} in healthy controls and ALS patients may identify differences between the two populations, which may aid future studies examining possible biomarkers of ALS. This approach has been adopted for other neurodegenerative diseases such as Parkinson's disease [898].

Conclusions

In summary, the results described in this chapter confirm that FUS^{EC} is secreted via the classical secretory pathway, transiting through the ER and Golgi compartments. Furthermore, they reveal that *N*-glycosylation of FUS^{EC} is linked to its secretion. Impairment of ER, Golgi and ER-Golgi trafficking are important pathogenic mechanisms associated with ALS, presenting the possibility that ALS-mutant forms of FUS^{EC} may also have a role in ALS. Studies investigating this notion are presented in Chapter 5.

5. ■ Examining the role of FUS^{EC} in ALS

5.1. Introduction

In the previous chapters, we characterised the novel extracellular isoform of FUS in terms of which unique features of FUS^{EC} distinguishes itself from the canonical FUS. The purpose of the studies described in this chapter was to examine the pathogenic mechanisms induced by ALS-associated mutant forms of FUS^{EC} expressed in cell lines.

ER stress and Golgi fragmentation are two well defined cellular mechanisms that have been detected at early disease stages in ALS rodent models [478, 485, 487, 899]. As FUS^{EC} is secreted via the classical secretory pathway, it was then examined whether ALS mutant forms of FUS^{EC}, bearing similar mutations in the C-terminus as canonical FUS, trigger pathogenic mechanisms associated with these organelles, including Golgi fragmentation and ER stress.

In the recent years, increasing evidence supports a common mechanism driving neurodegeneration in ALS, involving i) the formation of protein aggregates or seeds (a process called nucleation) which are then converted to pathological molecules and ii) their propagation in a self-templating manner. This mechanism leads to a subsequent increase in aggregate size and the release of seeds to the extracellular space where they are taken up by the neighbouring cells. Wild-type and mutant forms of SOD1, TDP-43 were shown to propagate through a 'prion-like' mechanism [120, 504, 508, 900]. In this study, it was therefore hypothesized that FUS^{EC} is transmitted from cell-to-cell by a similar process and transmits ALS pathology from neuron to neuron.

The role of FUS loss of function or gain of toxic function mechanisms in ALS

In healthy subjects, FUS predominantly localizes in the nucleus, whereas in ALS patients with FUS mutations, FUS is redistributed to the cytoplasm of affected cells, where it accumulates and aggregates [4, 5]. FUS immunoreactive cytoplasmic inclusions are observed in sporadic and familial ALS, [12]. Over-expression of FUS bearing ALS mutants R521G or P525L in cell lines or animal models leads to the formation of cytoplasmic aggregates [282, 283, 551]. Furthermore, FUS mislocalization in the cytoplasm leads to a partial loss of nuclear protein [5, 901]. This loss of FUS in the nucleus can impair alternative splicing and/or transcription, whereas dysfunction of FUS in the cytoplasm, especially in the dendritic spines of neurons, can cause mRNA destabilization [902]. Therefore, FUS loss of function can lead to the pathogenesis of

ALS [687, 903]. Moreover, the overexpression of exogenous FUS without a nuclear localization signal (Δ NLS-FUS) provokes progressive motor deficits and neuronal loss in the motor cortex of transgenic mice [904]. In this model, endogenous FUS expression, nuclear localization, and splicing activity were not altered, indicating that mislocalized FUS is sufficient for proteinopathy and activates ER stress [904]. In another mice model, mice overexpressing mutant FUS presented loss of motor neurons and synaptic changes leading to denervation, whereas selective elimination of FUS in motor neurons does not lead to a motor phenotype [283]. These results indicate that FUS loss and gain of function mechanism are likely involved in the pathogenesis of ALS.

Mutant FUS activates ER stress and induces Golgi fragmentation

Cytoplasmic mutant FUS bearing the R521C FUS mutation was shown to induce XBP1 splicing and CHOP activation in NSC-34 cells, and FUS colocalized with PDI in ALS patient spinal cords [880]. FUS transgenic mice lacking the NLS presented higher phosphorylation of eIF2 α in spinal motor neurons compared to control mice, suggesting induction of ER stress [905]. Furthermore, over-expression of ALS-associated FUS mutants R521H and R521C induces Golgi fragmentation in NSC-34 cells [906]. Transgenic rats overexpressing R521C FUS mutants displayed Golgi fragmentation although they had a phenotype resembling FTLD [907]. Disruption of Golgi apparatus is linked to disrupted vesicular trafficking and secretion. A direct mechanism has been described for this, whereby FUS localization in the ER lumen was associated with disruption to ER-Golgi trafficking in a Rab1 dependent manner [426].

Altogether, this evidence suggests that in ALS, mutant FUS gains a toxic function that leads to disruption of ER-Golgi trafficking, which triggers ER stress and Golgi fragmentation. Since in the previous chapter it was shown that FUS^{EC} is secreted by the classical secretory pathway, it should transit the ER-Golgi compartments. Hence, it was hypothesized that mutant FUS^{EC} has a deleterious effect on these organelles

FUS aggregates are transmitted through a prion-like mechanism in ALS

Misfolded proteins may induce toxicity by impairing ER-Golgi function and the protein degradation pathway [115, 119, 426, 908]. Additionally, mutated RBP can alter the

phase transition of RNA granules, sequestering other proteins and impairing their normal function [207, 356, 360]. Finally, protein aggregates can be transmitted from cell-to-cell in a prion-like fashion, inducing toxic effects to neighbouring cells [505, 507, 909, 910].

FUS contains a prion-like glutamine/asparagine rich domain at the N-terminus that shares similarities with yeast prion protein [539, 579]. Purified FUS can easily aggregates *in vitro* and this domain is important for amyloid-like fiber polymerization in cell-free models of RNA granule formation [378]. Moreover, FUS RGG-Zn-RGG domain also forms fibres 10-15 nm wide and 100 nm or longer, composed of 49% beta-sheets and 33% random colloids [529] and the RRM domain has the capacity to irreversibly self-assemble into amyloid fibrils [522]. The fact that small amounts of recombinant G156E mutant FUS can induce the misfolding of WT FUS into amyloid-like aggregates *in vitro* [883] strongly suggests that FUS has a self-templating seeding ability shared by prion-like proteins.

Prion-like proteins are transmitted from cell to cell, and have a deleterious effect on the receiving cells. The role of FUS in relation to prion-like spread in ALS in particular, is poorly understood. Both mutant and WT FUS have been reported within exosomes from SH-SY5Y and N2A cell lines but, to date, this is the only evidence of extracellular forms of FUS, it was in cells overexpressing FUS not endogenous conditions [630]. One study described the uptake of FUS in *Drosophila* primary neurons using flow cytometry and confocal microscopy, but these results need to be further validated in other systems [911]. Additionally, it is not known whether mutant FUS uptake induces ALS pathology in the receiving cells [911]. Another study demonstrated that treating primary spinal cord cultures with conditioned medium from WT or mutant FUS-expressing cells induced the misfolding of endogenous SOD1, however no uptake of FUS was detected [912]. It should also be noted that the authors did not provide evidence that FUS was secreted into the media in either of these studies, although conditioned medium was used as the transmission method. Together these data therefore indicate that the cell-to-cell transmission of FUS is poorly characterised in comparison to other proteins linked to ALS.

5.2. Aims of this chapter

The existence of a novel isoform of FUS, that shares some features with canonical FUS, but which also display unique properties, such as its extracellular localization, can lead to new investigations that aim to elucidate the role of this protein in ALS. The first aim of the studies described in this chapter was to identify the binding partners of WT and ALS-mutant forms of FUS^{EC}, given that both loss and gain-of-function mechanisms are associated with FUS-ALS. The second aim was to determine whether FUS^{EC} is involved in cellular mechanisms already implicated in FUS-associated ALS: inclusion formation, ER stress, Golgi fragmentation and apoptosis. Next, due to the unique cellular localization of FUS, the third aim was to determine whether ALS-associated mutant FUS^{EC} is secreted differently to WT, and also whether it can be transmitted amongst cells. Overall these studies aimed to determine whether mutant forms of FUS^{EC} imply a gain of toxic function, having a role in ALS pathology.

5.3. Material and methods

5.3.1. Site-Directed Mutagenesis

Constructs encoding HA/GFP-WT-FUS^{EC} were purchased from Genscript. Primers were designed using NEBaseChanger™ software, and known ALS mutations were incorporated using their sequence in the ALS mutation database (www.alsod.iop.kcl.ac.uk). Primers were purchased from Sigma (**Table 5.1**). Mutagenesis was carried using a Q5® Site-Directed Mutagenesis Kit (New England Biolabs) following the manufacturer's protocol. Briefly, 20 ng of template DNA was used for the exponential amplification PCR reaction; 30 cycles elongation was performed using a temperature gradient, with a final step of 72°C for 195 s, which was dependent on plasmid length. The KLD (kinase, ligase, DpnI) enzyme treatment was performed for 30 min at room temperature to phosphorylate and ligate the DNA and DpnI degrades the template DNA.

DH5- α ultra-competent E.Coli cells (High Efficiency) (New England Biolabs) were transformed with ligated DNA. After inoculation of a single colony into *LB* broth, a miniprep of plasmid DNA was performed. Identification of positive colonies, with incorporation of the successful mutations, was confirmed by Sanger Sequencing. The primers used for sequencing are the same used on Chapter 4 **Table 4.4**.

Table 5.1 Primers used for the mutagenesis

Primer Name	Primer sequence (5'-3')
P320L FP	CAGGGAGAGGCTGTATTAATGGC
P320L RP	CGATCCTGTCTGTGCTCAC
R316G FP	CCGGCAGGACGGAAGAGAGAGGC
R316G RP	TGCTCGCCTCTAGAGTCCATC

5.3.2. Preparation of Insoluble Cell Fractions

HEK293T cells were seeded in 6-well plates, at a density of 2×10^5 cells/ mL and cultured for 24 h to 80% confluence at 37°C in a humidified atmosphere of 5% CO₂ in DMEM (Gibco) supplemented with 10% (v/v) heat-inactivated FBS. Cells were then transfected with lipofectamine 2000 (Invitrogen). 48-hours post-transfection, cells were washed with PBS and lysed on ice for 15 min in 200 μ l of cold TN buffer with protease and phosphatase inhibitors (1:1000) and PMSF (1:500). The cell lysates were then frozen at -20°C until required. Samples were thawed on ice, probe sonicated (10s, Setting 3) and centrifuged at 45,000 rpm (~100,000 g) for 30 min at 4°C. The supernatant, representing the Triton-X 100 soluble fraction, was retained and a BCA assay was performed to determine its protein concentration. The pellet was then washed with TN buffer and sonicated and centrifuged as previously. The supernatant was discarded and the pellet was re-solubilised in 50 μ l of lysis buffer composed of 50 mM Tris-HCl, 150 mM NaCl (pH 7.6) and 2% (w/v) SDS, followed by incubation on ice for 5 min, probe sonication (10s, Setting 3), and centrifugation at 45,000 rpm (~100,000 g) for 30 min at 22°C. According to quantification of the soluble fractions, volumes corresponding to ~20 μ g of insoluble protein were loaded onto an 8.5% SDS polyacrylamide gel.

5.3.3. Co-culture experiments

HEK293T cells were first plated into 50 cm² petri dishes, at a density of 1×10^6 cells/ ml. After 24h, two populations of cells were transfected with either Discosoma sp. red fluorescent protein (DsRed) vector alone or GFP-tagged constructs encoding empty vector, GFP-WT-FUS^{EC}, GFP-R316G-FUS^{EC}, or GFP-P320L-FUS^{EC}. After 24h post-transfection, DsRed and GFP-tagged FUS^{EC} expressing cells were lifted and mixed in a

proportion of 1:1 and plated in 6-well plates or 24-well plates to be analysed by flow cytometry and microscopy respectively.

5.3.4. Flow cytometry

For flow cytometry analysis, the cells in 6-well plates were harvested, washed with PBS and transferred to an eppendorf tube for analysis. Flow cytometry was performed with a CytoFLEX flow cytometer (Beckman Coulter). Two lasers were used for this experiment: blue (488 nm) and yellow-green (561 nm). All parameters were set to log¹⁰ for acquisition.

5.4. Results

5.4.1. Site directed mutagenesis to produce ALS-FUS^{EC} mutants

Site directed mutagenesis was performed to introduce two ALS causative mutations into the HA- and GFP-tagged constructs encoding FUS^{EC}. The R521G mutant was chosen because it is one of the most common mutations in FUS-associated ALS, and the P525L mutant was selected because it is related to particularly aggressive, juvenile cases of ALS [8, 672, 913]. Both mutations are localized in the NLS at the C-terminus of FUS, and both have been previously shown to disrupt the import of FUS into the nucleus from the cytoplasm (**Figure 5.1a**) [548]. The R521G mutation in canonical FUS sequence corresponds to R317G in FUS^{EC}, and the P525L mutation corresponds to P320L in FUS^{EC}. Primers were designed, and mutagenesis was performed using HA-FUS^{EC} and GFP-FUS^{EC} as a template. In the R316G mutant, an arginine at position 316 is replaced by a glycine (**Figure 5.1b**), which is caused by the substitution of an adenine to a guanine in the DNA sequence (**Figure 5.1c**). In the P320L mutant, there is a substitution at of a proline with leucine at position 320 (**Figure 5.1b**) that results from replacement of a cytosine to a thymine in the DNA sequence (**Figure 5.1c**). Sanger sequencing confirmed incorporation of the desired mutations in each case, for both HA- and GFP-tagged constructs (**Figure 5.1d**) in both strands. HA-FUS^{EC} constructs were used in all experiments described in this chapter, except where indicated, when a

a)

Unique region RRM RGG2 ZnF RGG3 NS

1 330

R316G P320L

b) MAIKTRVVEVAAVAMDSTRVEAAAGVAVAAAAAAVVTTAAVVAAMNPEVVEVAVEAEVAADPRDQGSR
HDSEQDNSDNN¹TIFVQGLGENVTIESVADYFKQIGIIKTNKKTGQPMINLYTDRETGKLGKGEATVSFDDP
AKAAIDWFDGKEFSGNPIKVSFATR²ADFNRRGGNGRGGRRGGPMGRGGYGGGGSGGGGRGGFPS
GGGGGGGQQR³AGDWKCPNPTCENMNF⁴SWRNECNQCKAPK⁵PD⁶PGGGPGGSHMGGNYGDDRRGGR
GGYDRGGYRGRGGDRGGFRGGRGG⁷DRGGFGPGK⁸MDSRGEHRQD⁹RRER¹⁰PY¹¹YPYDV¹²PDYA

GGATCCACCATGGCCATCAAGACCAGAGTGGTGGAAGTGGCCGCGGCGCCATG
ATAGCAGAACAGTTGAAGCTGCTGCTGGCGTGCCAGTGTTGCTGCTGCCGCTG
TGCAGTGGTGGTTACAACAGCTGCTGTGGTGCCATGAATCCCGAGGTGGTCTGA
GTTGCCGTGGAAGCCGAAGTTGCTTGGGCGCCTAGAGATCAGGGCAGCAGACAC
GATAGCGAGCAGGACAACAGCGACAACAACACCATCTTCGTGCAAGGCCCTGGGCG
AGAACGTGACCATTGAGAGCGTGGCCGACTACTTCAAGCAGATCGGCATCATCAAC
ACGAACAAGAAAACCGGGCAGCCCATGATCAACCTGTACACCGACAGAGAGACAG
GCAAGCTGAAGGGCGAAGCCACCGTGTCTTCGACGATCCTCCATCTGCCAAGGC
CGCCATCGATTGGTTCGACGGCAAAGAGTTACAGCGGCAACCCCATCAAGGTGTCC
TTTGCCACCAGACGGGGCCGACTTCAATAGAGGGCGGCGAAATGGTAGAGGCGGA
GTGGAAGAGGTGGCCCTATGGGAAGAGGCGGATATGGTGGCGGAGGATCTGGC
GAGGTGGCAGAGGCGGTTTTCTAGCGGAGGTGGTGGCGGCGGAGGACAACA
GAGCTGGCGATTGGAAGTGCCCCAATCCTACCTGCGAGAACATGAACCTCAGCTG
CGGAACGAGTGCAACCAAGTCAAGGCTCCTAAGCCTGATGGACCAGGTGGCGGA
CCTGCGGATCTCATATGGGAGAAATTACGGCGACGATCGGAGAGGTGGACGC
CGCGTTATGACAGAGGCGGCTATAGGAGACGCGGAGGCGATCGCGGAGGATTCA
AGGTGGAAGAGGCGGCGGAGATAGAGGCGGATTTGGCCCTGGCAAGATGGACTCT
AGAGGCGAGCACCGGCGAGGACAGAGAGAGAGGCGCTTACTACCCCTACGACGTG
CCCGATTACGCCTGAGATATC

900 910 920 930 940

G A G G C G A G C A C C C G A C G A G G A A A G A A C C T T A T C A T G T G T C C A A A G G

Figure 5.1 Design and site direct mutagenesis of FUS^{EC} to produce R316G and P320L mutants. (a) Schematic diagram of HA-FUS^{EC} illustrating the position of the two ALS mutations, R316G and P320L. (b) HA-FUS^{EC} protein sequence, with the different domains colour coded, and the amino acids mutated in R316G and P320L highlighted in black (c) HA-FUS^{EC} nucleotide sequence, which is colour coded to present the protein domains. Highlighted in black are the codons mutated in P320L and R316G FUS^{EC}. (d) Sanger sequencing results confirmed the substitution in R316G and P320L mutants. The red square highlights the successful substitution of the required nucleotides. Sanger sequencing confirm the replacement of proline with leucine in the P320L mutant and substitution of arginine for glycine in the R316G mutant.

5.4.2. ALS-associated FUS^{EC} mutants form more inclusions than WT FUS^{EC} in HEK293T cells

Firstly, expression of the ALS-associated mutant FUS^{EC} and WT was compared. HEK293T cells were transfected with empty vector or HA-tagged constructs encoding either WT or mutant (R316G and P320L) FUS^{EC}. The supernatant (soluble fraction) was analysed by SDS-PAGE, followed by immunoblotting using an anti-HA antibody. The pellets were retained for further experiments to isolate insoluble protein aggregates (see below). The blots were then stripped and re-probed using an anti-GAPDH antibody as a loading control. Western blotting revealed the presence of a band of the expected size for FUS^{EC}, approximately 33 kDa, in lysates from cells transfected with HA-tagged WT or mutants R316G and P320L (**Figure 5.2a**), confirming that each construct properly expresses FUS^{EC} protein. Expression levels of WT and mutant FUS^{EC} were similar (**Figure 5.2b**).

FUS-immunoreactive inclusions are a common pathological hallmark of mutant FUS fALS, non-SOD1 fALS, and sALS patient motor neurons [12]. Hence, it was next examined whether overexpression of ALS-mutant FUS^{EC} in HEK293T cells leads to the aggregation and misfolding of FUS^{EC}. For this purpose, pellets obtained from cells expressing FUS^{EC} after lysis were further washed and solubilized with 2% SDS. SDS-PAGE and immunoblotting of these fractions using an anti-HA antibody revealed the presence of HA-FUS^{EC} WT and mutants in the insoluble fraction and formation of high molecular proteins (**Figure 5.2c**). Quantification of these bands revealed there was no statistical difference between HA-FUS^{EC} bearing R316G and P320L mutations and those expressing WT (**Figure 5.2d**). However mutant R316G displayed a trend to be more insoluble and form slightly more high molecular species than WT. This blot was also stripped and re-probed for GAPDH as a control to confirm that the soluble and insoluble cell fractions were correctly separated. The lack of GAPDH in the insoluble

fraction, but its presence in the soluble fractions as expected, confirmed that the fractions were successfully separated (**Figure 5.2c**).

Next, it was assessed whether over-expression of WT and ALS-mutants HA-FUS^{EC} resulted in the presence of inclusions in HEK293T cells. Cells expressing FUS^{EC} for 48 h were fixed and processed for immunocytochemistry using an anti-HA antibody and Hoechst stain to visualise the nuclei. Cells were examined using confocal microscopy and the percentage of cells with inclusions was quantified from at least 100 transfected cells (**Figure 5.2e**). Inclusions were defined as protein aggregates visible under a light microscope [468, 914]. Surprisingly, WT FUS^{EC} formed inclusions in 61% cells, in contrast to WT canonical FUS which normally forms few inclusions in cell culture [880] and it is mainly nuclear (**Figure 4.5 and 4.6**). However, a significantly ($p < 0.01$) higher proportion of cells expressing FUS^{EC} mutants formed inclusions compared to those expressing WT (74% of cells expressing R316G and 73% of cells expressing P320L) (**Figure 5.2f**). Together these results reveal that HA-FUS^{EC} bearing ALS mutations forms more inclusions than WT FUS^{EC}.

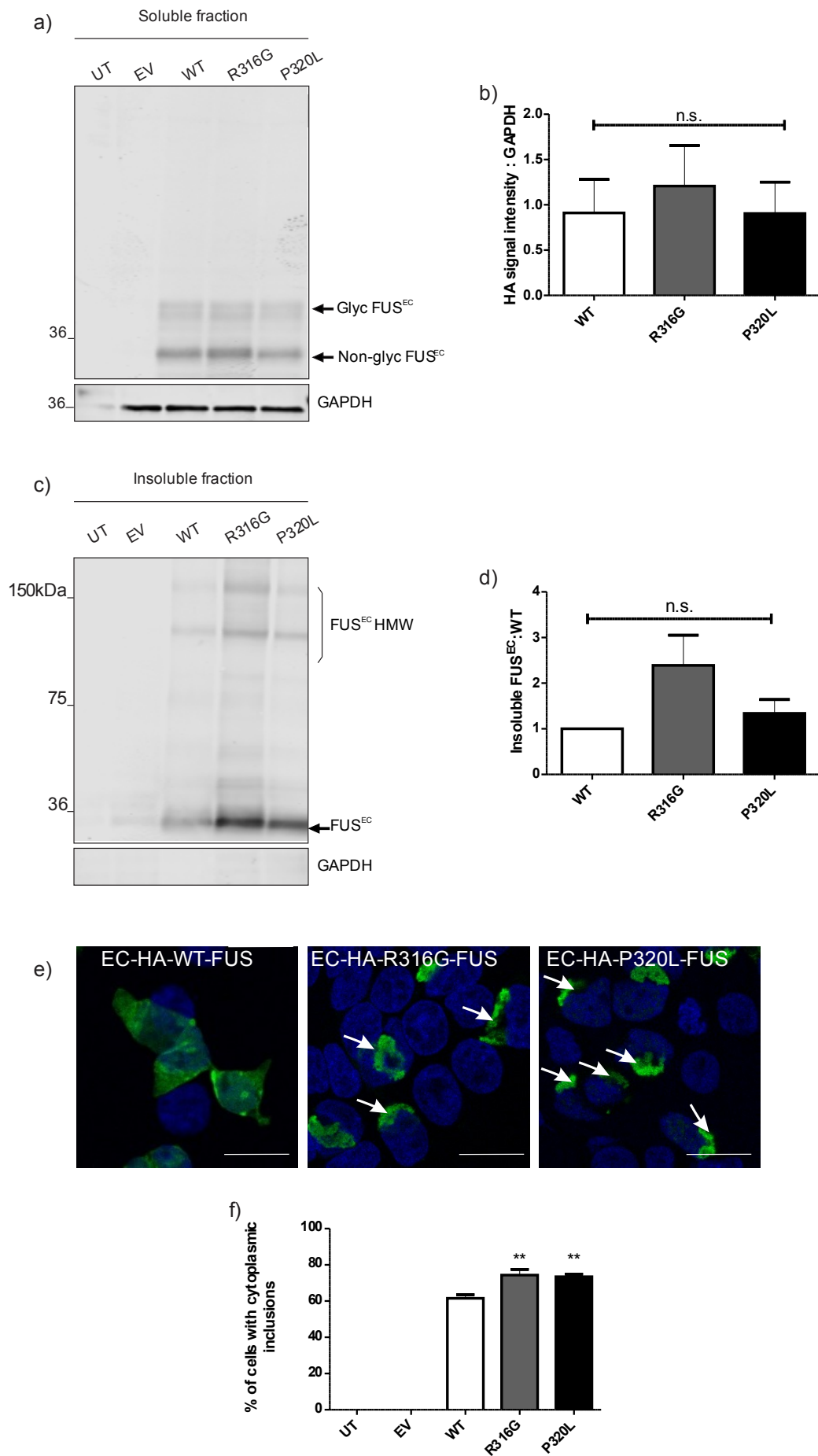


Figure 5.2 ALS-mutant FUS^{EC} form inclusions. (a) Immunoblotting of soluble lysates from HEK293T cells expressing untreated (UT), empty vector (EV), wild type (WT) or mutants (R316G and P320L) HA-FUS^{EC}. Western blotting using an anti-HA antibody, and GAPDH was used as a loading control. (b) Quantification of the relative intensity of FUS^{EC} in the blots in (a), normalized to GAPDH (n=5). (c) Western blotting of the detergent insoluble cell lysate fractions for the same samples. The membrane was immunoblotted using an anti-HA antibody, and GAPDH is shown as a control to confirm efficient separation of the insoluble fractions. (d) Quantification of FUS^{EC} band intensity in (c) normalized to WT (n=5). (e) Fluorescent confocal microscopy images of FUS^{EC} and Hoechst in HEK293T cells expressing HA-FUS^{EC}. Scale bar: 20 μ m. White arrows indicate aggregates. (f) Quantification of the percentage of cells expressing HA-FUS^{EC} with FUS^{EC} inclusions. Mean \pm SEM, n=3. **p<0.01 compared to WT. One way ANOVA followed by *post hoc* Tukey's test.

5.4.3. Identifying potential binding partners of ALS linked mutant FUS^{EC} to provide insights into possible pathogenic mechanisms.

To gain insights into possible pathogenic gain of toxic mechanisms induced by mutant FUS^{EC}, proteins that bind to mutant FUS^{EC} in the intracellular and extracellular cellular fractions were examined and compared to the putative binding partners of WT- FUS^{EC} identified in Chapter 4, section 4.4.7. This approach should also provide insights into which proteins are co-aggregated in mutant FUS^{EC} inclusions, as described in the previous section.

HEK293T cells were transfected with wild type HA-FUS^{EC}, mutant HA-FUS^{EC} R316G and P320L or empty vector control. After 48 h, the conditioned media and lysate fractions were collected and immunoprecipitation with HA magnetic beads was performed to pull down putative FUS^{EC} binding partners. Samples were loaded onto an SDS-PAGE gel, electrophoresis was performed for 5 min to run the proteins into the gel and the gel was then stained with Coomassie blue to fix the proteins. The entire lane was excised in each case, and proteomic analysis was performed to identify proteins that may bind to WT and mutant FUS^{EC} (all the proteins identified are listed in the appendix 8.2). High confidence hits were those proteins identified in at least in two replicate experiments, and proteins identified in the control samples (empty vector and untreated) were subtracted from the list of possible binding proteins identified.

For the lysate samples, 90 proteins (13.7%) were pulled down by both WT and the two mutants, indicating they may be shared binding partners. In contrast 97 proteins (14.8%) were found to be common between both the two mutants but not present in WT, as shown in the Venn Diagram (**Figure 5.3a**) [915]. Gene ontology (GO) [916] analysis was performed to determine the biological functions of the proteins linked to

FUS^{EC} mutants exclusively (**Figure 5.3b**). A selection of the identified proteins are listed in **Figure 5.3c**.

Three proteins involved in the ER quality control system were pulled down for both FUS^{EC} mutants but not for WT: namely calnexin, PDIA3 and PDIA1 [917]. Calnexin is an ER transmembrane molecular chaperone involved in the calnexin/calreticulin cycle, which is responsible for interacting with newly synthesized glycoproteins in the ER, thus assisting with nascent protein folding and ER quality control [918]. PDIA3 (also known as Erp57) and PDIA1 are two protein disulphide isomerases whose expression is induced in response to ER stress conditions, triggering the UPR. Both are chaperones localized mainly in the ER, which modulate the formation of disulphide bonds, thus facilitating protein folding [455]. Additionally, Erp57 is a key component of the calnexin/calreticulin cycle [919].

In addition, some unique FUS^{EC} mutant (R316G and P320L) interacting proteins identified were involved in the protein degradation pathway, such as ubiquitin-like modifier-activating enzyme 1 (UBA1), 26s protease regulatory subunit 6B (PSMC4) and VCP. Furthermore, several actin binding proteins were found to interact with WT FUS^{EC} and both mutants. However, Cofilin-1, a non-motor-actin binding protein that has been linked to several pathways implicated in ALS [909, 920], was bound only to both FUS^{EC} mutants and not WT. Finally, R316G -FUS^{EC}, but not P320L or WT, pulled down G3BP1. Interestingly, G3BP1 is a core protein necessary for stress granule assembly [921].

These results suggest that proteins involved in the UPR induction and linked to proteasome degradation are potential interacting partners of mutant FUS^{EC}, but not WT. These data suggests that these pathways are altered in HEK293T cells overexpressing R316G and P320L ALS-mutants, hence this gave us confidence to further study this pathway in cells overexpressing FUS^{EC} mutants. These mechanisms were then investigated in more detail.

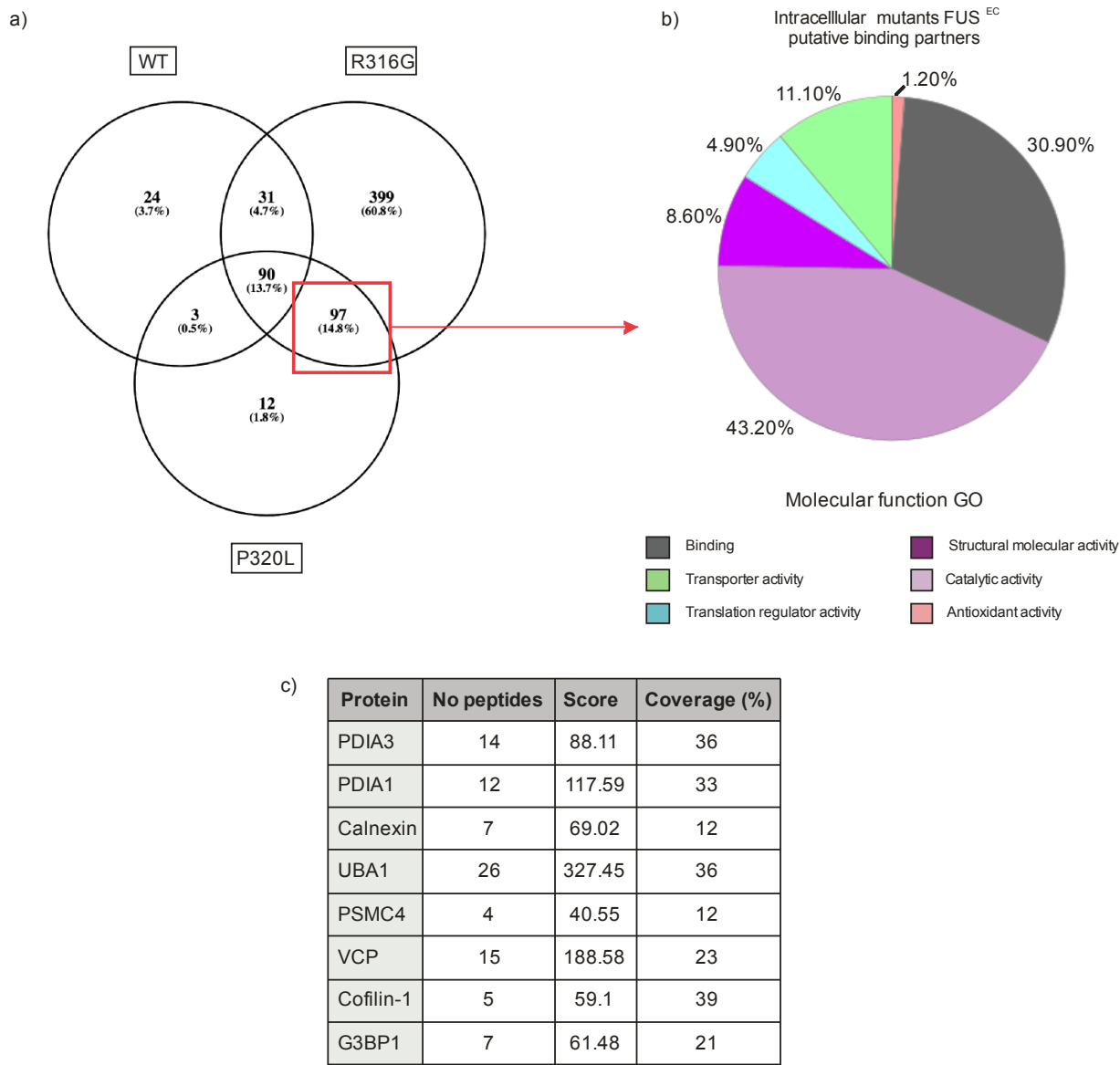


Figure 5.3 Evaluation of the common putative binding partners of FUS^{EC} mutants (a) Venn diagram comparing the proteins pulled down by FUS^{EC} WT and R316G and P320L mutants (b) Gene ontology analysis of the molecular function for the proteins pulled down uniquely by both ALS mutants. (c) List of some of the potential binding partners identified for FUS^{EC} mutants.

5.4.4. ALS-FUS^{EC} mutants induce ER stress in HEK293T cells

In the previous chapter, it was demonstrated that FUS^{EC} partially co-localizes with ER and Golgi markers (section 4.4.6). Additionally, the putative binding partners of the FUS^{EC} mutants identified above implied that the UPR and dysfunction of the proteasome system may be induced by ALS mutant of FUS^{EC}. Additionally, our laboratory has previously shown that R521C and R521H mutant canonical FUS induces ER stress in neuronal cell lines [880]. Hence, it was next examined whether

overexpression of FUS^{EC} WT and mutants induces ER stress in cell culture. For the ER stress experiments, as in our previous studies, rather than Western blotting, immunocytochemistry assays were used so that only transfected cells were included in the analysis [467, 880]. These assays are used for the purposes of analysing individual transfected cells only, so that outcomes are not dependent on transfection efficiency. This is in contrast to Western blotting which quantifies the population as a whole, (transfected and untransfected), where untransfected cells can mask changes in expression of ER stress markers, which occur primarily in transfected cells.

XBP1 was used as an ER stress marker, where cells with nuclear immunoreactivity to XBP1 were considered as undergoing ER stress. Activation of IRE1 results in splicing of XBP1, which generates a transcription factor that translocates to the nucleus when the UPR is activated [456]. For this purpose, immunocytochemistry using anti-HA and anti-XBP1 antibodies was performed in HEK293T cells overexpressing empty vector, HA-tagged WT FUS^{EC} and HA-tagged FUS^{EC} mutants after 72h post-transfection (**Figure 5.4a**). Untreated and empty vector transfected cells displayed mostly cytoplasmic XBP1 expression, with only 22% and 26% cells respectively displaying nuclear immunoreactivity. Overexpression of WT FUS^{EC} resulted in a significantly increased proportion of cells displaying nuclear localization of XBP1 (40 %, $p < 0.5$) compared to untreated cells, although there was no statistical difference to cells expressing empty vector only. However, a significantly greater proportion of cells overexpressing R316G and P320L mutant FUS^{EC} was detected (60% and 54% respectively, $p < 0.01$) compared to untreated cells or those expressing empty vector alone (22.53% and 26.05% respectively), although only mutant R316G had significant higher levels of ER stress compared to WT. As a positive control for ER stress, untransfected cells were also treated with tunicamycin (TM) (1 μ g/ml), which inhibits the first step of *N*-glycosylation of proteins in the ER, thus inducing ER stress [922]. Approximately 38 % of cells treated with TM displayed activated XBP1 (**Figure 5.4b**). No HA immunoreactivity was detected in control cells incubated with secondary antibody only (no primary antibody), demonstrating that the signal obtained from the transfected cells was specific.

Secondly, nuclear immunoreactivity to CHOP was also used as an ER stress marker, as described previously [467, 880]. During prolonged or unresolved ER stress conditions, in the pro-apoptotic phase of the UPR downstream of the IRE1, PERK and ATF6 pathways. CHOP becomes activated and translocates to the nucleus [458]. Cells

were transfected with empty vector or plasmids encoding HA-tagged WT and mutants FUS^{EC} as above. ER stress were identified when CHOP was localized in the nucleus of cells that displayed immunoreactivity to the HA tag (**Figure 5.4c**). No HA immunoreactivity was detected in control cells incubated with secondary antibody only (no primary antibody), demonstrating that the signal obtained from the transfected cells was specific.

In untreated cells or cells expressing empty vector, only a few cells displayed nuclear CHOP immunoreactivity, indicating little activation of the UPR (5% and 9% respectively). In contrast, significantly more cells over-expressing WT HA-tagged FUS^{EC} displayed nuclear CHOP immunoreactivity (29%, $p < 0.05$) compared to control untransfected cells, indicating induction of ER stress. However, nuclear CHOP activation was detected in a significantly greater percentage of cells expressing R316G (67%) and P320L (61%) ($p < 0.001$ and $p < 0.01$ respectively) FUS^{EC} mutants in comparison to WT FUS^{EC}, indicating that FUS^{EC} mutants induce more ER stress than WT. Furthermore, the R316G mutant expressing cells presented significantly higher levels of ER stress when treated with TM (45 % cells with nuclear CHOP, $p < 0.05$) while mutant P320L levels were similar (**Figure 5.4d**), indicating that they are more sensitive to ER stress.

Together these results indicate that ER stress is induced by overexpression of both WT and mutant FUS^{EC}, and hence FUS^{EC} is capable of inducing the UPR. However, more ER stress was induced by ALS-related mutant FUS^{EC} compared to WT FUS^{EC}, consistent with previous studies involving canonical mutant FUS [880].

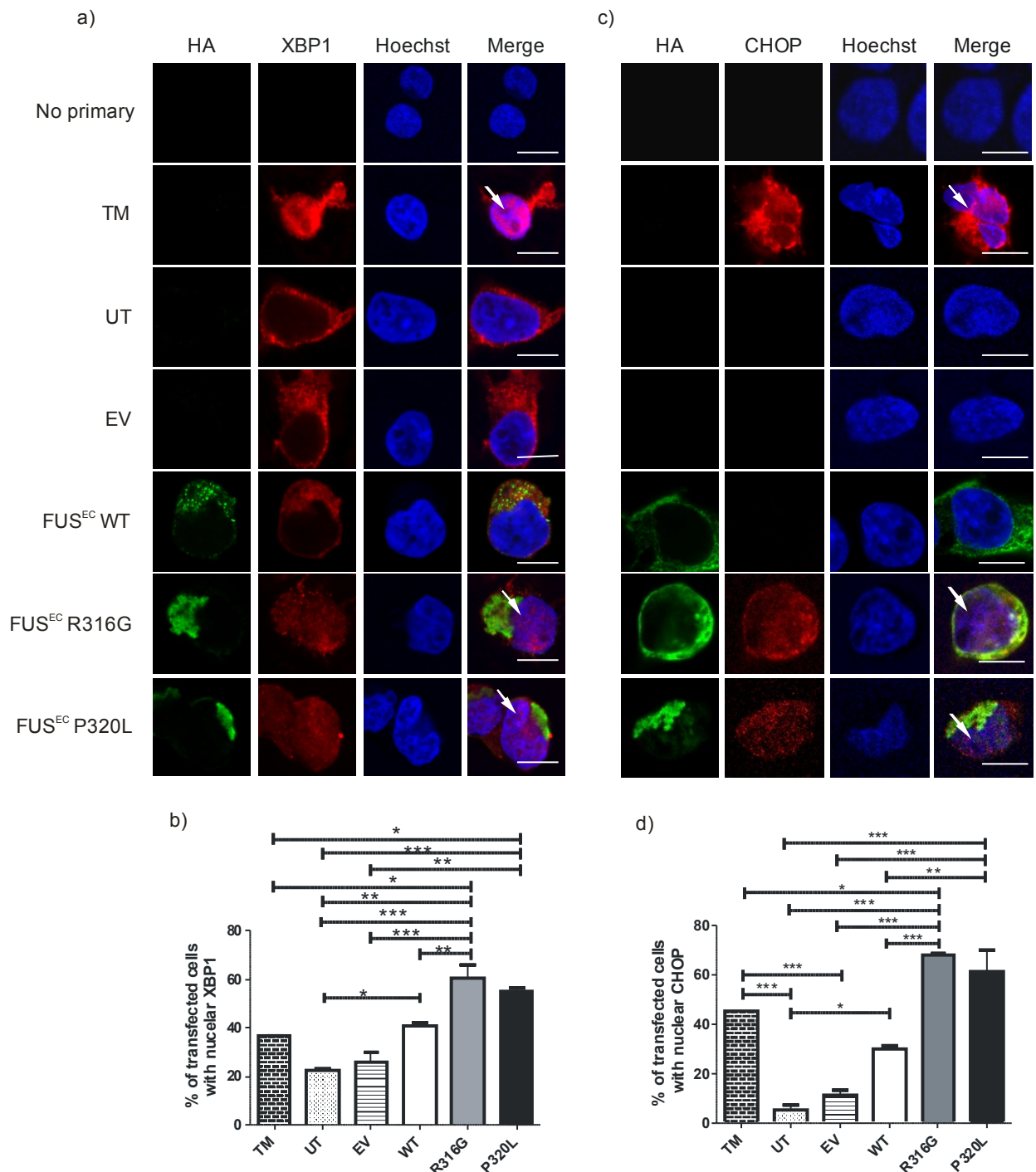


Figure 5.4 Overexpression of FUS^{EC} ALS-mutant induces ER stress in HEK293T cells. (a) Fluorescent confocal microscopy images of FUS^{EC} (HA), XBP1 and Hoechst in untransfected HEK293T cells (UT), cells expressing empty vector (EV) or HA-FUS^{EC}. White arrows show cells with nuclear activated XBP1. Scale bar: 10 μ m (b) Quantification from images in (a) of the percentage of HA-FUS^{EC} transfected cells with nuclear XBP1. Mean \pm SEM, n=3. *p<0.05, **p<0.01, ***p<0.001. (c) Fluorescent confocal microscopy images of FUS^{EC} (HA), CHOP and Hoechst in UT, cells expressing EV or HA-FUS^{EC}. White arrows indicate cells with nuclear CHOP. As a positive control for ER stress, cells were treated with 1 μ g/mL of Tunicamycin (TM). Scale bar: 10 μ m. (d) Quantification of the percentage of transfected cells with nuclear CHOP. Mean \pm SEM, n=3. *p<0.05, **p<0.01, ***p<0.001. One way ANOVA followed by a *post hoc* Tukey's test.

5.4.5. ALS-FUS^{EC} mutants localize more in the ER than WT-FUS^{EC}

Our laboratory previously showed that ALS mutant canonical FUS localizes more in the ER compared to the WT [426]. In Chapter 4, it was demonstrated that WT FUS^{EC} was localized at least partially within the ER, and since FUS^{EC} ALS-mutants induce ER stress, we next hypothesized that the mutants may localize more in the ER than WT. This would explain how mutant FUS^{EC} perturbs this organelle more than WT. To estimate the degree of localization of WT and mutant FUS^{EC} with the ER, HA-tagged constructs were over-expressed in HEK293T cells. Calnexin, a 570 residue protein that resides in the ER membrane [923], was used as a marker of the ER. After 48h post-transfection, cells were fixed and immunocytochemistry using anti-HA and anti-calnexin antibodies was performed. The cells were then examined by confocal microscopy. Z-stack confocal analysis revealed that both WT and mutant FUS^{EC} partially colocalized with calnexin (**Figure 5.5a**), indicating that both proteins associate with the ER. Quantification of the degree of colocalization using Mander's coefficient demonstrated that R316G (0.53, $p < 0.1$) and P320L (0.58, $p < 0.001$) FUS^{EC} colocalized significantly more with the ER than WT FUS^{EC} (0.38, **Figure 5.5b**). Hence, these data indicate that FUS^{EC} mutants are retained more in the ER compared to WT.

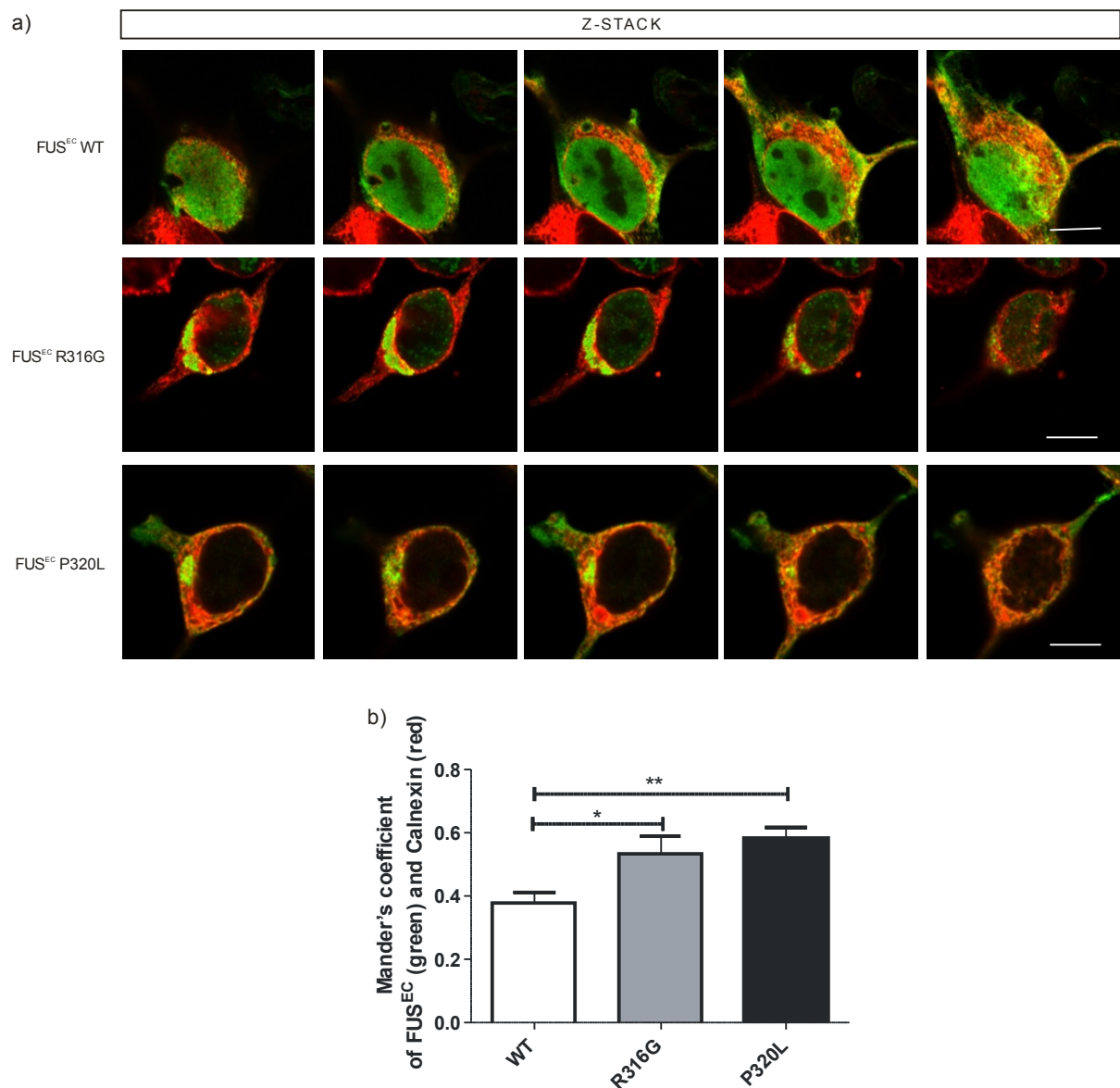


Figure 5.5 ALS-linked FUS^{EC} mutants associate more with ER than WT FUS^{EC}. (a) Z-series of merge fluorescent confocal microscopy images of FUS^{EC} (HA in green) and calnexin (red) in cells expressing WT or mutant HA-FUS^{EC}. Scale bar: 10 μ m. (b) Colocalization of FUS^{EC} and calnexin was quantified using Mander's coefficient. Mean \pm SEM, n=3. *p<0.05, **p<0.01. One way ANOVA followed by *post hoc* Tukey's test.

5.4.6. Cells overexpressing ALS mutant FUS^{EC} display fragmented cis-Golgi

In Chapter 4, it was demonstrated that WT FUS^{EC} partially colocalizes with GM130, a marker of the *cis*-Golgi apparatus. Given that Golgi fragmentation is a well reported feature of ALS biology, it was next assessed whether mutant FUS^{EC} overexpression led

to fragmentation of the Golgi apparatus in HEK293T cells. Cells were transfected with either empty vector, HA-tagged WT or mutant FUS^{EC}. After 72h post-transfection, cells were fixed and immunocytochemistry was performed using an anti-HA antibody to detect FUS^{EC} expression, and an anti-GM130 antibody as a Golgi marker. Cells were examined using confocal microscopy and the proportion of cells expressing FUS^{EC} with fragmented Golgi was quantified (**Figure 5.6a**). Golgi fragmentation was identified by the presence of condensed punctate Golgi structures in comparison to a compact, perinuclear ribbon morphology of the normal Golgi (**Figure 5.6a**). A small proportion of untreated cells (15%) or cells transfected with empty vector (8%) displayed fragmented Golgi. Slightly more cells (22%) expressing WT FUS^{EC} displayed fragmented Golgi compared to controls, but the difference was not statistically significance. The proportion of cells with fragmented Golgi was significantly increased in cells expressing R316G (55,83 %, $p<0.05$) and P320L (60,20 %, $p<0.05$) (**Figure 5.6b**) compared to WT. Hence these results reveal that overexpression FUS^{EC} ALS mutants trigger Golgi fragmentation in HEK293T cells.

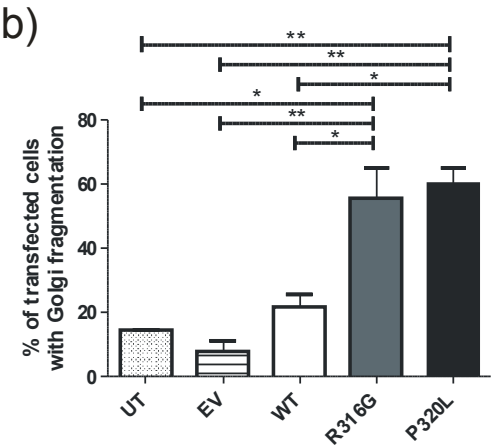
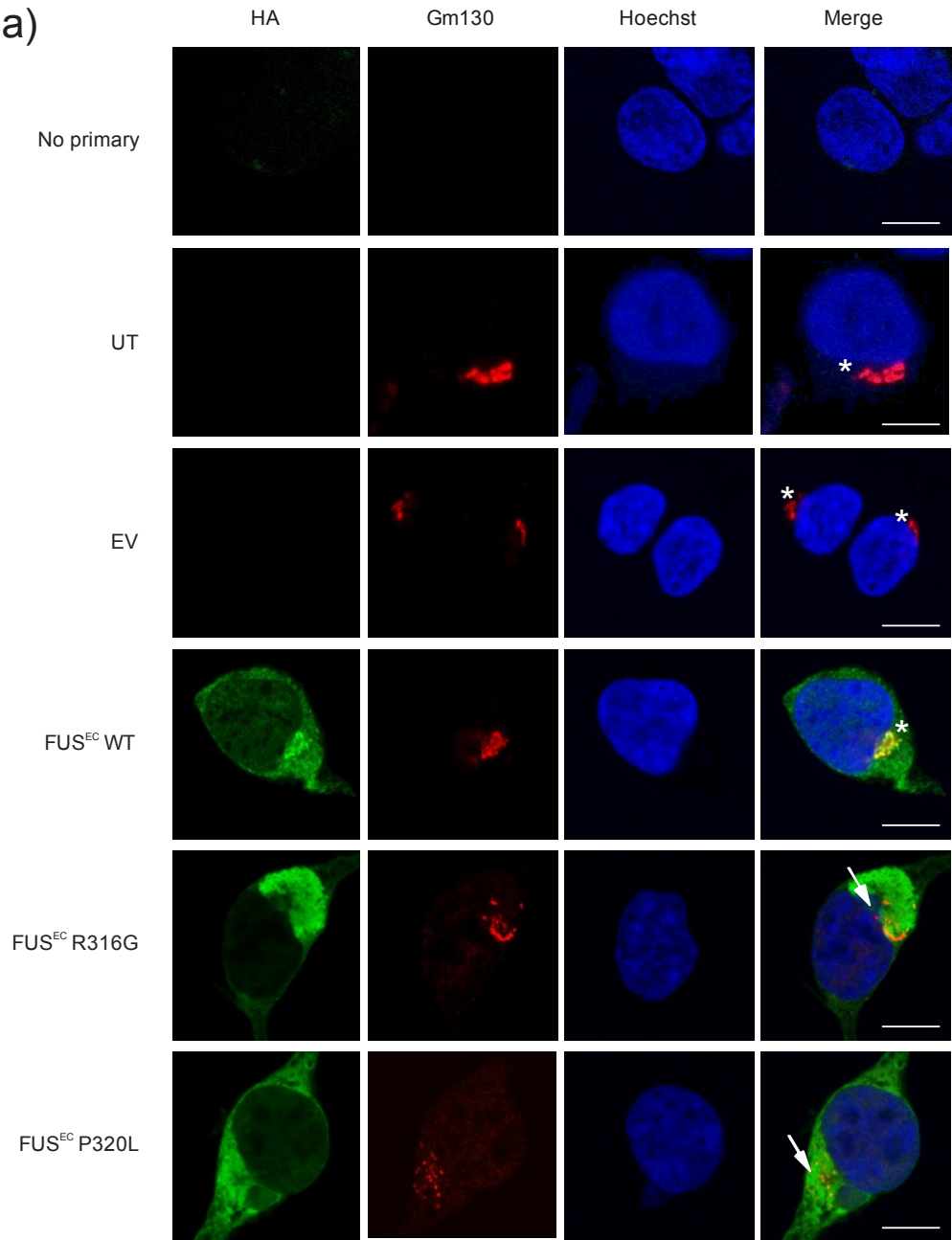


Figure 5.6 FUS^{EC} ALS-mutants induces Golgi fragmentation in HEK293T cells. (a) Fluorescent microscopy images of FUS^{EC} (HA), GM130 and Hoechst in untransfected HEK293T cells (UT), cells expressing empty vector (EV) or HA-FUS^{EC}. Asterisks, intact Golgi; arrows, fragmented Golgi. Scale bar: 10 μ m. (b) Quantification of the percentage of HA-FUS^{EC} transfected cells with fragmented Golgi. Mean \pm SEM, n=3. *p<0.05, **p<0.01. One way ANOVA followed by *post hoc* Tukey's test.

5.4.7. ALS-FUS^{EC} mutants induce apoptosis in HEK293T cells.

Since prolonged ER stress and Golgi fragmentation lead to apoptosis [490], and in ALS motor neurons are thought to die by apoptosis [924-926], it was next examined whether overexpression of FUS^{EC} triggers apoptotic cell death, using two specific markers.

Activated cleaved caspase-3 was used as the first marker of apoptosis, as in previous studies [914] (**Figure 5.7a**). Immunocytochemistry using anti-HA and anti-cleaved caspase-3 antibodies revealed that few cells expressing empty vector (2%) or untransfected cells (6%) expressed activated caspase-3. More cells expressing WT FUS^{EC} displayed activated caspase-3 (19%) compared to control cells, but this difference did not reach statistical significance (**Figure 5.7b**). However, a greater proportion of cells with activated caspase-3 were detected in populations expressing FUS^{EC} mutants (R316G: 49% and P320L: 37%, p<0.01) compared to WT FUS^{EC} cells, untreated or empty vector controls. Positive control cells treated with TM displayed high levels of apoptotic nuclei (80%), as expected.

Secondly, the number of cells with apoptotic nuclei was quantified according to their nuclear morphology, as in previous studies [467]. Cells were transfected with empty vector only or WT and mutant HA-tagged FUS^{EC} constructs for 72h. Cells were fixed and processed for immunochemistry using an anti-HA antibody to identify cells expressing FUS^{EC} and the nuclei were stained using Hoechst. Apoptotic nuclei were identified by condensed chromatin and fragmented morphology (**Figure 5.7c**). Few untreated cells and cells expressing empty vector or WT FUS^{EC} displayed apoptotic nuclei (5%, 4% and 10% respectively). However, significantly more cells expressing FUS^{EC} mutants were undergoing apoptosis (R316G: 34%, p<0.01; P320L: 29 %, p<0.001) compared to WT. As expected, a major proportion of positive control cells treated with Tunicamycin displayed apoptotic nuclei (70%, **Figure 5.7d**). Hence, together these data reveal that overexpression of ALS-linked mutant FUS^{EC}, but not WT FUS^{EC}, induces apoptotic cell death in HEK293T cells.

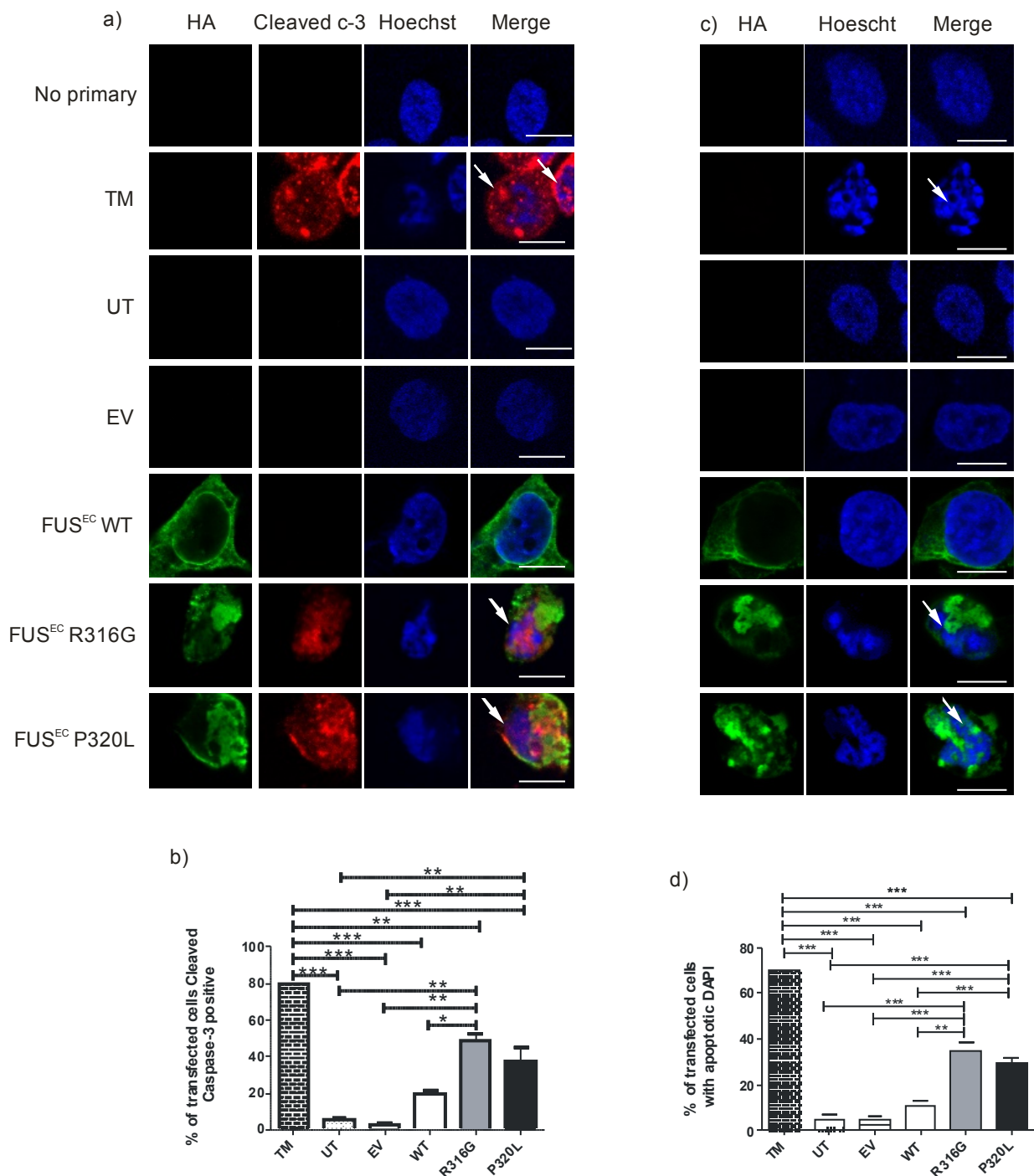


Figure 5.7 Overexpression of ALS-mutants FUS^{EC} induces apoptosis. (a) Fluorescent confocal microscopy images of FUS^{EC} (HA), cleaved caspase-3 and Hoechst in untransfected HEK293T cells (UT), cells expressing empty vector (EV) or HA-FUS^{EC}. White arrows indicate cells with activated cleaved caspase-3. Scale bar: 10 μ m. (b) Quantification of the percentage of HA-FUS^{EC} transfected cells with activated caspase-3 immunoreactivity. (c) Fluorescent confocal microscopy images of FUS^{EC} (HA) and Hoechst in UT and cells expressing EV or HA-FUS^{EC}. White arrows show apoptotic nuclei. As a positive control, cells were treated with 1 μ g/mL of Tunicamycin (TM). Scale bar: 10 μ m. (d) Quantification of the percentage of HA-FUS^{EC}

transfected cells with apoptotic nuclei. Mean \pm SEM, n=3. ***p<0.001, **p<0.01, *p<0.05. One way ANOVA followed by *post hoc* Tukey's test.

5.4.8. Examining the secretion levels of ALS mutants and WT FUS^{EC} in HEK293T cells

ALS-linked FUS^{EC} mutants accumulate in the ER and induce significantly more Golgi fragmentation compared to WT FUS^{EC}. Hence, it was next hypothesised that secretion of the mutants could be altered compared to WT given that both the ER and Golgi are organelles involved in secretion. Secretion of WT and mutant FUS^{EC} was next investigated in HEK293T cells transfected with empty vector or HA tagged constructs. After 24h post-transfection, the media was replaced with Opti-MEM, a reduced serum media, and cells were incubated for 24h before collection of the conditioned media. Conditioned media was centrifuged at 1,000 rpm (~200 g) twice to pellet the cell debris and the supernatant was concentrated using a centrifugal filter unit. Identical volumes (20 μ l) of concentrated medium were subjected to SDS-PAGE, followed by staining of the membrane using red Ponceau to confirm that the samples had been equally loaded. Immunoblotting using an anti-HA antibody revealed the presence of two bands in the medium of FUS^{EC} expressing cells, presumably representing the two glycoforms of FUS^{EC}. A 33 kDa band was detected, which is the expected MW for non-glycosylated FUS^{EC}, and a much thicker band of approximately 50 kDa, which as described in Chapter 4, is expected to be a glycosylated form of FUS^{EC} (**Figure 5.8a**). These bands were quantified using densitometry. Quantification of the total secreted FUS^{EC} demonstrated that there was no significant difference between groups (**Figure 5.8b**). When the glycosylated and non-glycosylated forms of FUS^{EC} were quantified separately, neither the 33 kDa band (**Figure 5.8c**) nor the 50 kDa (**Figure 5.8d**) band were different when compared to WT. Whilst the results were not statistically significant however, there appeared to be a trend suggesting that the mutants are secreted more than WT FUS^{EC}.

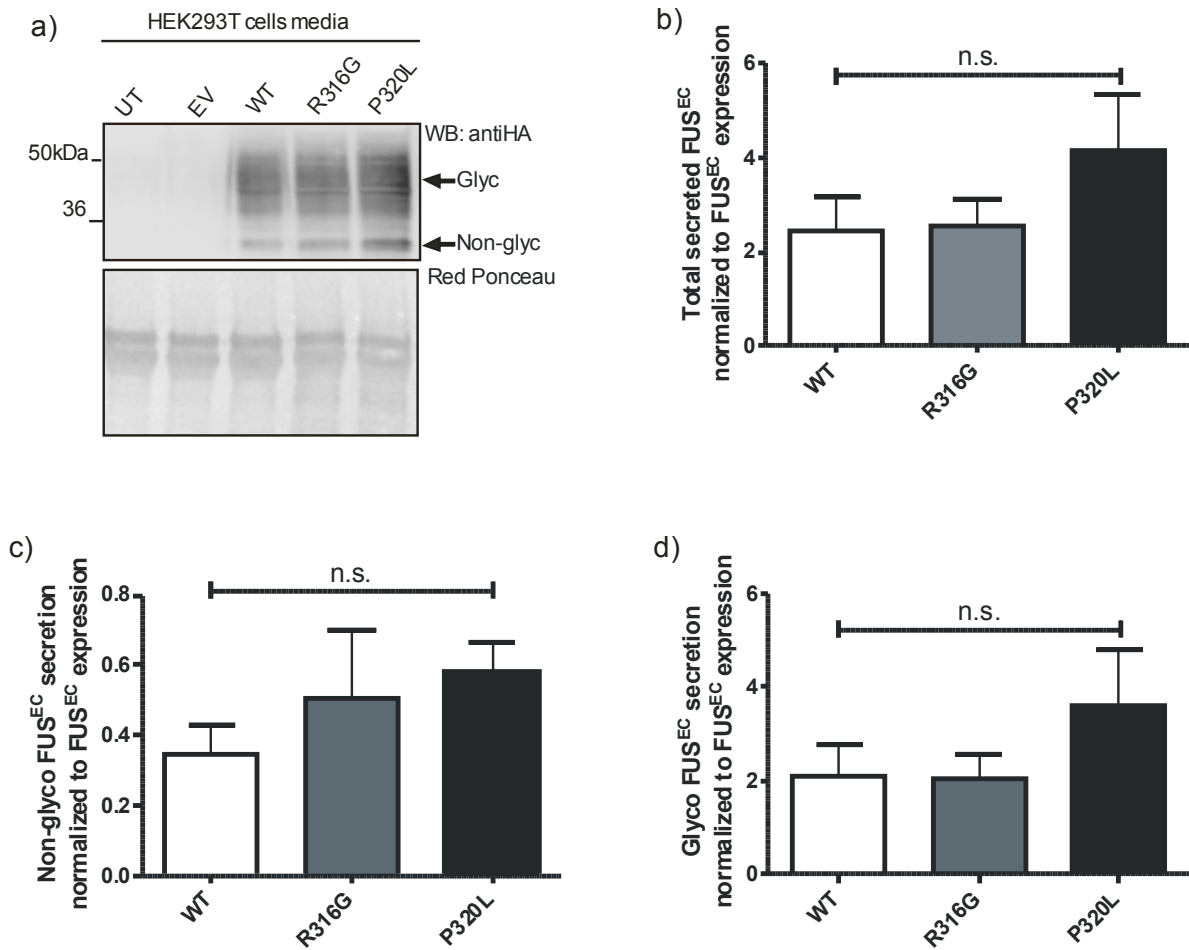


Figure 5.8 Determining WT FUS^{EC} and ALS-mutants secretion levels. (a) Western blotting of the conditioned media from untreated cells (UT), cells expressing empty vector (EV), WT or mutant HA-FUS^{EC}. Membrane was probed for anti-HA antibody, and red Ponceau staining was used as a loading control. (b) Relative intensity of total HA-FUS^{EC} normalized to protein expression levels in the lysate. (c) Relative intensity of non-glycosylated HA-FUS^{EC} normalized to protein expression levels in the lysate. (d) Relative intensity of glycosylated HA-FUS^{EC} normalized to protein expression levels in the lysate. Mean \pm SEM, $n=6$. One way ANOVA with *post hoc* Tukey's test.

5.4.9. Examination of the cell-to-cell transfer ability of WT and ALS-FUS^{EC} mutants

The mechanism underlying the spread of ALS is unknown and the transmission of canonical FUS has been poorly characterised. Additionally, Cofilin-1, a putative interacting partner of the FUS^{EC} mutants identified here, has been implicated in the uptake of SOD1 [909]. Hence it was next investigated whether FUS^{EC} can be transmitted amongst cells through a prion-like mechanism, using a co-culture experiment. Several approaches were undertaken to test this hypothesis. Firstly, 1 mL

of conditioned media from cells expressing HA-FUS^{EC} was directly added to untransfected cells for 24h, as previously described for SOD1 [782] and TDP-43 [508]. Fluorescent microscopy and Western blotting of the receiving cells were then performed to determine the eventual uptake of HA-FUS^{EC}. However, these studies revealed none of the cells were immunofluorescent for HA-FUS^{EC} (data not shown). It is possible that the levels of FUS^{EC} secreted into conditioned media were too low to be transmitted, similar to TDP-43 and C9ORF72 [199, 502, 927]. Alternatively, it is possible that the capacity of transmitted FUS^{EC} in cells was too low to be detected by microscopy. The same experiment was performed by concentrating 5 mL of media, but similar results were observed.

Next, a different approach was undertaken. As overexpressed FUS^{EC} was also detected in the cell lysate, untransfected cells were incubated with cell lysate fractions prepared from FUS^{EC} transfected cells. This method was previously used to demonstrate the uptake of SOD1 and TDP-43 [928]. Untreated cells were incubated with lysate from cells expressing WT and mutant HA-FUS^{EC} for 24h and then fixed in paraformaldehyde. However, immunocytochemistry using an anti-HA antibody revealed no cells were immunopositive for HA-FUS^{EC}, implying that there was no uptake (data not shown).

Recently a novel co-culture method was used to examine the transmission of TDP-43 and C9ORF72 DPRs [198, 199, 502, 927, 928]. Smethurst and colleagues used this approach to demonstrate the uptake of phosphorylated TDP-43, following their initial studies that failed to detect uptake using conditioned media only [502]. Ultimately the co-culture experimental approach was chosen next because it is arguably the most biologically relevant when studying cell-to-cell natural transmission of proteins. For these experiments, two groups of HEK293T cells were used. The first group were transfected with DsRed empty vector only, as a marker of acceptor cells. The second population were transfected with constructs encoding GFP empty vector, or GFP-tagged WT or FUS^{EC} mutants. After 24 h post-transfection, both cell populations were trypsinised, washed in PBS and mixed together in a ratio of 1:1: DsRed:GFP-expressing cells and re-plated in either 6 well plates for flow cytometry analysis or 24 well plates for microscopy analysis (**Figure 5.9a**). After 24h, cells were lifted and washed with PBS and analysed using a CytoFLEX flow cytometer. Untransfected cells were used as a control to identify the cell population on density plots. Cells expressing

GFP or DsRed only were used as positive controls to assess the autofluorescence threshold of HEK293T cells. Unfortunately, due to the high fluorescent intensity of DsRed, the voltage of the flow cytometer was found not to be suitable and the results were therefore not conclusive (Flow cytometry results are added in the appendix 8.4).

For the microscopy analysis, 24h following co-culture, cells were fixed and the nuclei were stained with Hoechst. Confocal microscopy was used to examine the cells for the presence of both DsRed and GFP. At least 200 cells were scored for each treatment group (**Figure 5.9b**). These studies revealed that GFP only (1.89%) appeared to be taken up by a larger proportion of cells than either GFP WT (1.31%) or R316G (0.85%) mutant FUS^{EC}. However, in contrast, P320L was taken up by a significantly greater proportion of cells than WT or R316G (2.73%, $p < 0.01$, $p < 0.001$ respectively) (**Figure 5.9c**). These data suggest that more FUS^{EC} mutant P320L was taken up compared to WT and R316G mutants, but this was less than the GFP empty vector alone.

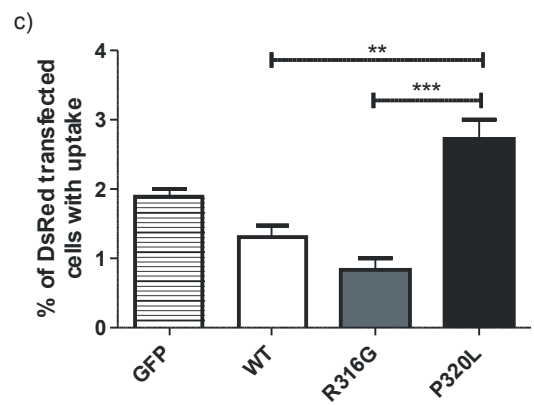
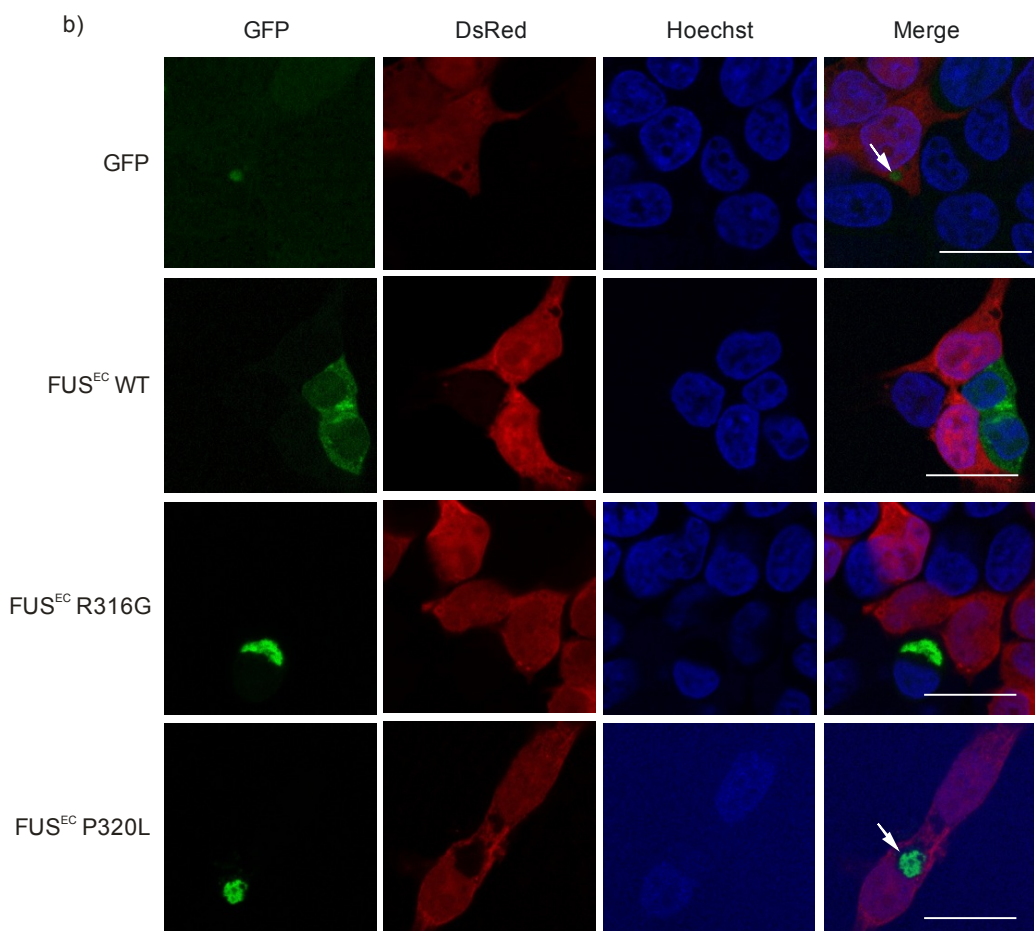
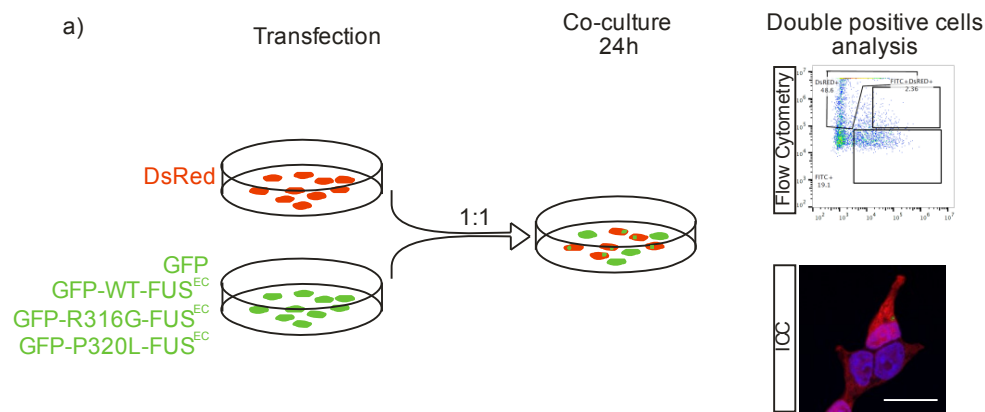


Figure 5.9 Examination of uptake of GFP expressing FUS^{EC} in HEK293T cells. (a) Schematic diagram to illustrate the experiment design. Two populations of HEK293T cells were used, expressing either DsRed or GFP, WT or mutant GFP- FUS^{EC} separately. At 24h post-transfection cells were harvested and re-plated mixed together at a ratio of DsRed: GFP of 1:1. Cells were co-cultured and after 24h, cells were analysed by flow cytometry and microscopy to detect cells positive for DsRed and GFP. (b) Representative fluorescent microscopy images of DsRed and GFP constructs expressing cells after 24h co-culture. White arrows indicate double positive cells. Scale bar: 20 μ m. (c) Quantification of the percentage of DsRed cells with GFP uptake. Mean \pm SEM, n=3. *p<0.05. One way ANOVA with *post hoc* Tukey's test.

5.5. Discussion

In the studies described in the current chapter, it was investigated whether FUS^{EC} is involved in cellular pathogenic mechanisms implicated in ALS, given that the C-terminus of its canonical counterpart is retained, and many of the ALS linked mutants are clustered in this region. Over-expression of two ALS mutants of FUS^{EC} in cell lines resulted in the formation of more inclusions than WT FUS^{EC}, a known pathological hallmark of ALS. It was also identified proteins that function in the UPR and proteasome degradation as uniquely binding to ALS-mutant FUS^{EC}. Additionally, the mutants FUS^{EC} triggered ER stress, Golgi fragmentation and more apoptosis than WT FUS^{EC}, events that resemble mechanisms associated with neurodegeneration in ALS. Moreover, it was found that mutant FUS^{EC} (R316G and P320) localizes more in the ER than WT FUS^{EC}. Finally, preliminary data was presented implying that mutant P320L - FUS^{EC} may be involved in the transmission of FUS in a 'prion-like' fashion, although further experiments are necessary to confirm this.

A key hallmark of ALS is the aggregation of misfolded proteins, leading to the formation of protein inclusions [207]. It is well established that mutant forms of the proteins involved in ALS form inclusions in fALS patients, and in animal models and cell lines, overexpression of ALS mutants also leads to the formation of inclusions [7, 150, 344, 929, 930]. In the studies presented in the current chapter, immunocytochemistry revealed that mutant FUS^{EC} formed more inclusions compared to WT. Similarly, although not statistically significant, mutant FUS^{EC} appeared to be more abundant in the Triton-X insoluble cell pellet of transfected cells, and formed slightly more high molecular species than WT. Since inclusion formation has been linked to ER stress, Golgi fragmentation and ultimately apoptosis [115, 318, 482, 484, 487, 906, 931], these results suggest that FUS^{EC} mutants are also involved in these mechanisms that are already well defined in ALS.

It could be hypothesized that the ALS-mutants possess a different *N*-glycosylation profile than WT FUS^{EC} and this can affect their aggregation propensity, which has been demonstrated for other proteins [932, 933]. Additionally, *N*-glycosylation can enhance protein stability and hence decrease the tendency of misfolded proteins to aggregate [934]. For example, Neuroserpin undergoes aberrant polymerization in the ER in a neurological disorder: familial encephalopathy with Neuroserpin inclusion bodies [932]. Interestingly, altering the *N*-glycosylation profile of WT Neuroserpin, results in the formation of aggregates [932, 935]. The prion protein is *N*-glycosylated, and there is evidence to suggest that *N*-glycosylation negatively modulates its aggregation propensity. A recent study determined that synthetic prion protein (PrP) variants modified with *N*-glycan mimics reduced the propensity for PrP to form fibrils [936]. Similarly, an in vitro study using peptides derived from PrP demonstrated that *N*-glycosylation decelerated the fibril formation rate [933]. However the *N*-glycosylation profile does not have any effect of prion infectivity [937, 938]. Another example is the protein tau, which also has important roles in neurodegenerative diseases. Tau is O-GlcNacylated such that increasing tau O-GlcNac in tau transgenic mice (by treating the mice with O-GlcNacase) leads to a reduction in tau aggregation and ameliorated neuronal cell loss [939]. Studying the *N*-glycosylated profile of mutant versus WT FUS^{EC} would elucidate whether this mechanism is also involved in FUS^{EC} aggregation which may have further implications for disease onset and progression.

The identification of potential ALS-mutant FUS^{EC} interacting partners may elucidate possible gain of toxic function mechanisms of these mutants. Some of the interacting partners of mutants FUS^{EC} detected in this study are involved in the UPR response, such Calnexin, PDI and ERp57 [940, 941]. Additionally, mutations in PDI and ERp57 are risk factors for ALS [942]. ERp57 is up-regulated in prion disease and in cellular models of Parkinson's disease [943, 944]. In ALS, ERp57 has been shown to be up-regulated in spinal cord of sALS patients and patients with the SOD1 G93A mutation [118]. ERp57 colocalized with phosphorylated TDP-43 in sALS spinal cord [467]. Additionally, PDI colocalizes with FUS, TDP-43 and SOD1 inclusions in ALS patients tissues [880, 945]. Secondly, some binding partners are involved in the proteasome pathway, such as UBA1, VCP, PSMD1, suggesting that the cells overexpressing mutant FUS^{EC} had this pathway impaired. This is consistent with the presence of misfolded mutant FUS^{EC}. Interestingly, UBA1, VCP and PMSD12 were demonstrated to bind to

P525L canonical FUS [946]. Further experiments are needed to confirm the effect of mutant FUS^{EC} on proteasome function.

An interesting novel binding partner of mutant FUS^{EC} identified from this study was Cofilin-1. Cofilin-1 is an actin-binding factor that regulates actin assembly and disassembly. C9ORF72 binds to Cofilin-1 regulating its phosphorylation and ultimately regulating actin-binding dynamics, which was suggested to play a role in C9ORF72 loss of function in ALS [920]. Intriguing, SOD1 aggregates were shown to penetrate inside cells following a prion-like mechanism, using cofilin-1 to remodel actin [909]. Even though a direct interaction between SOD1 and Cofilin-1 has not been examined, this is exciting evidence that could further relate mutant FUS^{EC} to similar uptake mechanism. And finally, G3BP1 was identified as a possible binding partner of FUS^{EC} R316G, which functions in a well-established pathogenic mechanism of FUS in the formation of stress granules [678, 947]. FUS localizes into SGs under stress conditions, and FUS mutations have been linked to the disruption of phase transition, leading to an irreversible liquid-to-solid phase that matures into pathological aggregates [354, 360, 524, 681]. Interestingly, VCP, which was also found to interact with both FUS^{EC} mutants in this study, is involved in clearance of SGs by autophagy [948], suggesting the localization of at least mutant R316G FUS^{EC} in SG. Hence future studies are warranted to confirm this interaction and to determine the domains of FUS^{EC} involved in this mechanism.

ER stress was examined using a marker of early UPR, XBP1, and a marker of the later UPR, CHOP. Both markers were significantly increased in cells overexpressing FUS^{EC} mutants. Interestingly, overexpression of spliced XBP1 is linked to an increase in general protein secretion, through the up-regulation of genes involved in the secretory pathway and expansion of the rough ER [949]. Furthermore, two apoptotic markers, CHOP nuclear immunoreactivity and the presence of condensed nuclei, were significantly increased in cells overexpressing ALS-mutants FUS^{EC}, suggesting that irreversible ER stress triggered the apoptotic phase of UPR.

It has also been reported previously that overexpression of WT forms of known ALS proteins can display pathologic features [109]. In this study, 61% of cells expressing WT FUS^{EC} formed inclusions, and additionally, more of these cells presented induced ER stress when compared to untreated cells. On the contrary, there was no difference in the proportion of WT FUS^{EC} cells undergoing apoptosis compared

to untreated controls. NSC-34 cells expressing transfected with WT canonical FUS displayed induced splicing of XBP1, similarly to the present study, but CHOP activation was not detected in the this study [880]. Overexpression of WT FUS leads to its cytoplasmic mislocalization in primary neurons [947], the formation of inclusions and it has also been shown to be toxic in yeast and mice models of ALS [882, 950]. In animal models, overexpression of WT FUS leads to induced neonatal death in a slightly less profound manner than mutant FUS overexpression [951]. Over-expression of WT TDP-43 in NSC-34 cells led to the formation of 15% inclusions after 72h transfection [927]. Moreover, overexpression of WT TDP-43 displayed up-regulated CHOP, XBP1 activation and increased caspase-12 in Neuro2A cells and SH-SY5Y cells [466, 952]. Similarly, extracellular misfolded WT SOD1 impaired ER-Golgi transport and triggered ER stress and Golgi fragmentation in SH-SY5Y cells [119]. Hence these data together show that overexpression of WT versions of proteins involved in ALS can display toxic features. However, overexpression of pathogenic mutant forms of these ALS proteins, exacerbates toxic features.

Previous studies from our laboratory have demonstrated that the degree of canonical FUS mislocalized in the cytoplasm correlates with ER stress [880]. Moreover, canonical and mutant forms of FUS were previously detected in the ER [426]. In the same study, the higher degree of ER localization of mutant FUS compared to WT was associated with impairment of ER-Golgi transport, a condition that is also known to trigger ER stress [426]. The results presented in this chapter show that FUS^{EC} mutants localize more in the ER than WT. Taking into account what is already known for canonical FUS, one could speculate that FUS^{EC} mutants induce ER stress more directly than WT, since they colocalize more with ER marker calnexin. However, the link between ER localization of FUS^{EC} and ER stress induction remains to be fully defined. In future studies it would be worthwhile to investigate whether cytoplasmic localization of FUS^{EC} affects ER homeostasis. SOD1 was detected in the ER, therefore linking it to direct activation of ER stress [465, 908]. However, subsequent studies concluded that it was localized in the cytoplasm, at the ER membrane, where it induced ER stress by its interaction with Derlin-1 [117] or by inhibiting ER-Golgi transport [426]. The ER localization of FUS^{EC} needs to be confirmed by complementary methods, such as subcellular fractionation followed by western blotting, and also using a fluorescence protease protection assay [426]. These studies should also examine whether mutant FUS^{EC} is aggregated and misfolded in the ER. Whilst WT and mutant SOD1 localized

with the ER and microsome fractions, only mutant SOD1 had the propensity to aggregate in the ER-Golgi pathway in transgenic mutant SOD1 mice [465, 908].

Golgi fragmentation has been linked to other pathological mechanisms in ALS such as ER stress and protein aggregation [318, 490]. Golgi morphology is dependent on efficient vesicular trafficking between the ER and Golgi compartments. Since it was found that mutant FUS^{EC} induced ER stress, it was next investigated if Golgi morphology was also altered. Golgi fragmentation has been detected in sALS and fALS motor neurons [478, 481, 482] and by overexpression of mutant FUS mutant in cell lines [906]. In this chapter, it was also shown that mutant FUS^{EC} induces greater levels of Golgi fragmentation than WT, consistent with the induction of ER stress. The integrity of the ER and Golgi compartments depends on efficient vesicular trafficking between these two organelles. Disruption to ER-Golgi trafficking has been demonstrated for ALS proteins: TDP-43, FUS and SOD1 [426]. It would therefore be interesting to examine whether FUS^{EC} has a similar effect on ER-Golgi trafficking in future studies.

In this study there was no statistically significant difference between secretion of the FUS^{EC} mutants compared to WT, although a trend towards increased secretion was apparent, specifically for P320L FUS^{EC}. In these experiments, the amount of secreted protein detected in each case was quite variable among different replicates, which may explain why statistical significance was not reached. Further studies are therefore required to probe this further. The generation of stable cell lines with inducible expression of FUS^{EC} WT or mutants that could overcome this limitation and reduce the experimental variability would be worthwhile

However a feasible explanation for the increased tendency of the mutants to be secreted more is that this could be a protective process, in that the cell releases misfolded proteins in an attempt to alleviate their burden within the cell. This is consistent with the finding that proteasome inhibition in NIH3T3 cells increased the secretion of mSOD1 [313]. Filter trap assays of conditioned media of GFP-SOD1, WT and mutants, revealed that more aggregated SOD1 is released for mutant SOD1 when compared to WT [782]. Interestingly, a recently described unconventional secretory route, misfolding-associated protein secretion (MAPS), has been linked to the processing of other proteins that aggregate in ALS, including SOD1 and TDP-43, and also other misfolded proteins linked to neurodegenerative diseases, α -synuclein, tau and ataxin3 [953, 954]. The mechanism underlying MAPS is still unclear, but has been demonstrated to be regulated by Ubiquitin-specific protease 19 (USP19) [953]. Hence,

future studies could examine whether FUS^{EC} is secreted through this pathway. To this end, knockout or overexpression of USP19 and examination of the effect on FUS^{EC} secretion could be performed [953]. In addition, secretion of another protein linked to neurodegeneration, tau, was found to correlate with Golgi fragmentation [955], a condition it was also demonstrated is induced by mutant FUS^{EC}. In contrast, there is also evidence that secretion of ALS-associated mutant SOD1 is impaired compared to WT in NSC-34 transfected cells, leading to aggregation and neurodegeneration [98]. In this study it was found that more mutant FUS^{EC} than WT associated with the ER-Golgi compartments, which would imply that mutant FUS^{EC} should be secreted more. Additionally, it could be that conditions triggered by FUS^{EC} mutants increase FUS^{EC} secretion through an alternative route different from the ER-Golgi, such as MAPS.

In this study it was also examined whether FUS^{EC} WT and mutants could transmit amongst cells in a 'prion-like' fashion. There have been a number of methods used to show how proteins can be transmitted among neurons, thus implicating them in the spread of neurodegenerative disease in a prion-like fashion. The most widely accepted method to demonstrate that a protein propagates in a prion like fashion would be an *in vivo* experiment. Unfortunately because of lack of time we were not able to do this here.

In this study, different concentrations of conditioned media from FUS^{EC} transfected cells and the lysate fractions were used as the transmission vehicle for FUS^{EC}, but no transmission of FUS^{EC} among cells was detected with these protocols. Both methods had the limitations of missing the possibility that the protein could be transmitted through direct cell-to-cell contact. Finally, a co-culture experiment design was used. This method overcomes some of the limitations that were encountered previously and it allows detection of protein transmission among cells by multiple methods such as: through exosomes, free in the media, or via cell-to-cell contact. The microscopy results revealed that mutant P320L is taken up more than WT and mutant R316G. These results need to be confirmed with another alternative approach. Unfortunately, the flow cytometry analysis developed during this study was not conclusive due to the high fluorescent intensity of DsRed cells, making the measurements inconclusive. These experiments should be optimised and repeated in the future to generate more conclusive results. Additionally, a cell viability dye should be used as a control since death cells display high levels of autofluorescence, hence this can be detected as false positive.

It was surprising that DsRed expressing cells were able to take up GFP only to such a high extent compared to WT or R316G FUS^{EC}, this is an important technical limitation of this study. However it is possible that a longer incubation time would overcome this problem in future studies. However GFP is known to be secreted [871] as it is shown in the previous chapter. Another study demonstrated that when inoculated into mice, untagged WT or mutant SOD1 was less susceptible to transmission in the inoculated mice spinal axis, in contrast to the yellow fluorescent protein (YFP) tagged versions of the same proteins, suggesting that the fluorescent tag could affect uptake or spread of misfolded proteins [509]. YFP is a genetic mutant of GFP, in which threonine at position-203 is replaced for tyrosine, hence it is highly similar to GFP [956]. Furthermore it should be noted that neither this study, nor many of the studies that use GFP tagged proteins for co-culture experiments, include YFP or GFP empty vector only as a control [509, 927].

For PrP, it has been proposed that transmission between cells is dependent on protein conformation. Westergard and colleagues examined the cell-to-cell transmission of C9ORF72 DPRs, and demonstrated that PR repeatedly displayed different mechanisms of transmission compared to other DPRs [198]. Similarly, different SOD1 mutants possess different transmissibility properties [509]. These findings suggest that in ALS the different misfolded protein mutants display different transmissibility properties, which may explain why the P320L FUS^{EC} mutant was more easily taken up. In contrast, the R316G mutant was not taken up as readily. Additionally this mutant was also found to have the trend to be secreted more than WT or R316G. Interestingly, fALS patients bearing the P525L FUS mutation (corresponding to P320L in FUS^{EC}) displayed rapid and aggressive disease progression compared to other FUS mutations [8, 672, 913].

Most of the previous studies investigating uptake and transmissibility of misfolded proteins linked to ALS, have described low rates of transmissibility between cells: TDP-43 [502, 927] and C9ORF72 [199]. Similar findings were obtained in this study, where P320L -FUS^{EC} give -approximately 2.73% of transmission between cells. However, even low transmission rates are likely to be relevant to pathology given that these proteins are capable of inducing toxicity. Clearly, here more experiments are needed to confirm the uptake of FUS^{EC}, and to determine if the uptake of mutant or WT FUS^{EC} induces misfolding of the endogenous FUS^{EC} and toxicity in the receiving cells.

In addition, other characteristics of prion-like proteins need to be examined for FUS^{EC}. In future studies the seeding ability of FUS^{EC} could be tested. These investigations could focus on whether overexpression of FUS^{EC} (preferably tagged to facilitate its detection) and subsequent secretion into conditioned medium leads to misfolding of its endogenous, untagged counterpart in recipient cells. Related to this idea, it would also be interesting to examine whether overexpression of ALS-associated mutant FUS^{EC} leads to sequestration and misfolding of endogenous, FUS^{EC} or canonical FUS. Further experiments are also needed to confirm the cell-to-cell transmission of FUS^{EC}.

It is important to note the limitations of this study. Firstly, the use of cell lines and transient transfections. Transient transfection results in high protein levels of expression that may not be physiological, therefore leading to a different phenotype not directly relevant to the disorder. Future studies would benefit from the use of an inducible, stable expression system to improve experimental reproducibility. Furthermore, the findings obtained in this study would ideally be confirmed in more physiological systems, either primary neurons, organotypic cultures or animal models. In particular, the prion-like mechanism of transmission of FUS^{EC} would benefit from more physiologically relevant systems. The protocol used here involving co-culture experiments, is arguably more relevant than using conditioned media only applied to cells, to replicate the transmission of proteins between cells. However a better methodology would be to examine the transmission of FUS^{EC} in animal models.

Finally, the binding partners identified in **Figure 5.3**, should be further validated, and also binding partners of endogenous FUS^{EC} need to be examined and compared to these, to make sure that the presence of the HA tag, or the high levels of overexpression, are not identifying false, non-native binding partners. However this requires the use of an antibody specific for FUS^{EC}. When this thesis was completed however, an anti-FUS^{EC} antibody was not available, despite the purchase of a customised antibody commercially.

Implications and future perspectives

The precise mechanism by which FUS induces motor neuron degeneration is still not fully understood. The identification of a novel extracellular isoform of FUS, which induces cellular features previously linked to FUS-ALS, is likely to be relevant to our future understanding of pathogenic mechanisms in ALS. Future experiments are

warranted to fully understand the role of FUS^{EC} in ALS and to examine whether these two FUS proteins - the canonical form and FUS^{EC} isoform - act together in a co-operative manner, or they have independent functions.

Conclusions

The findings in this chapter reveal that FUS^{EC} bearing ALS mutants, R316G and P320L, trigger cellular mechanisms involved in ALS. The results showed that both mutants form more inclusions than WT FUS^{EC} and they also localize more in the ER, enhancing ER stress, Golgi fragmentation and ultimately cellular apoptosis. Additionally, it was shown that FUS^{EC} mutant P320L is taken up by neighbouring cells, highlighting its potential role in the spread of ALS pathology.

6. ■ General discussion

Summary of the main findings of the thesis

The first part of this thesis (Chapters 3 and 4) presents the first evidence for the existence of a novel extracellular FUS isoform (FUS^{EC}), and its characterization of its function (**Figure 6.1**). Wilson and colleagues predicted this novel isoform through bioinformatics tools [731] and this thesis has experimentally confirmed its existence. In the studies presented in the first chapter, the expression of the isoform was confirmed at the mRNA and protein level in human primary neurons and HEK293T cells. Additionally, it was confirmed, using multiple techniques that FUS^{EC} is found in the extracellular environment. In the studies presented in Chapter 4, it was further determined that FUS^{EC} is secreted in part through the classical ER-Golgi secretory pathway. It was also demonstrated that FUS^{EC} is *N*-glycosylated and contains mostly complex *N*-glycans that regulates its secretion. Consistent with these findings, overexpressed WT FUS^{EC} colocalizes partially with ER and Golgi markers. In addition, in only a small proportion of transfected cells, WT FUS^{EC} localized in the nucleus, in contrast to WT canonical FUS, which is found predominantly in the nucleus [4, 5]. A number of putative binding partners of WT FUS^{EC} from cells lysates were identified and determined by GO to be involved in nucleic acid binding proteins suggesting that FUS^{EC} might also play a role in this pathway, similar to canonical FUS [342, 514, 532]. Interestingly, binding partners that mapped to nucleic acid binding were also identified from extracellular FUS^{EC} immunoprecipitations suggesting a completely new role that is different to the canonical FUS. Furthermore, it was demonstrated that overexpressing WT FUS^{EC} leads to the formation of cytoplasmic inclusions, implying that FUS^{EC} may be toxic when overexpressed in cells similar to the role of TDP-43 isoform in ALS patients [141].

In Chapter 5 the role of FUS^{EC} in ALS was investigated. Since FUS^{EC} shares the C-terminal sequence with canonical FUS, where most of ALS-mutations are clustered, they should also be present in FUS^{EC} [4, 5]. We identified putative binding partners unique to ALS-mutants FUS^{EC}, mutants R316G and P320L (corresponding to mutants R521G and P525L in canonical FUS), distinct from those binding to WT FUS^{EC}. Analysis revealed proteins involved in the UPR and proteosomal function, suggesting an impairment of this pathway which corresponded to higher inclusion formation in cells expressing FUS^{EC} mutants compared to WT. It was further confirmed that overexpression of mutant FUS^{EC} induced ER stress, Golgi fragmentation and apoptosis

when overexpressed in HEK293T cells. Finally, preliminary data obtained in this thesis suggested that mutant FUS^{EC} has the ability to be transmitted from cell-to-cell (**Figure 6.2**).

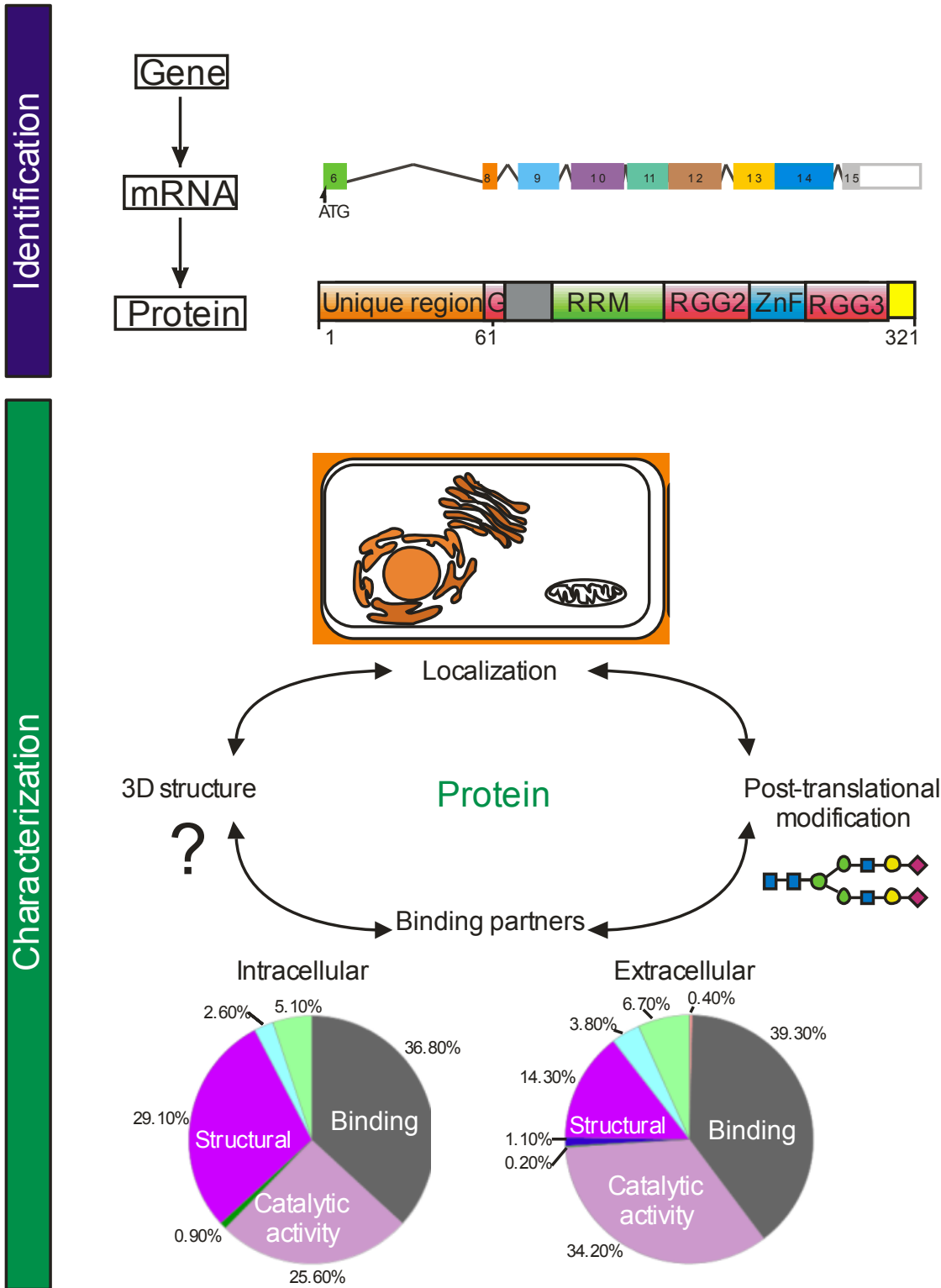


Figure 6.1 Schematic representation of the features of FUS^{EC} identified in this thesis. This thesis has confirmed the expression of FUS^{EC} at the mRNA and protein level in human neuronal

cell lines and in HEK293T cells. Furthermore it has characterized its cellular localization, its *N*-glycosylation profile and identified putative binding partners in the intra/extracellular compartment. Future studies could focus on the examining of its three dimensional (3D) structure.

Identification and characterization of FUS^{EC}

The findings obtained in Chapter 3 demonstrated that FUS^{EC} has 61 unique amino acids at its N-terminal but it shares 260 amino acids at the C-terminus with canonical FUS. Hence FUS^{EC} shares 5 entire domains with canonical FUS: the RRM domain, two RGG domains, the ZnF and the NLS. The RRM domain and the RGG-ZnF-RGG domains are involved in RNA and DNA binding [528, 538] and the NLS is responsible for its translocation to the nucleus with the assistance of the third RGG domain [548, 549].

Canonical FUS is localized mainly in the nucleus, where it is involved in functions including alternative splicing, transcription regulation, formation of RNP complexes and the DNA damage response [160, 523, 636, 735]. These functions are linked to its capacity to bind directly to RNA and DNA, and also to bind to proteins that regulate these processes such as snRNPs, SMN, DROSHA, PARP and HDAC1 [604, 605, 617, 631, 632, 634-636]. Additionally, upon certain stimuli, FUS has the ability to relocate to the axons and dendritic spines to transport mRNA thus facilitating local translation in these specific subcellular compartments [515, 546]. These functions are important for synapse formation, neuronal plasticity, differentiation and proliferation [515, 546]. Furthermore, canonical FUS has specific functions in the cytoplasm, including RNA stability, translation, and degradation [341].

The C-terminal shared domains between canonical FUS and FUS^{EC} provide some clues about the possible intracellular functions of FUS^{EC}. When localized in the nucleus or cytoplasm, FUS^{EC} may perform similar functions to canonical FUS, related to mRNA processing including splicing and mRNA transport. This possibility was supported by the findings of this study where putative binding partners of WT FUS^{EC} were identified. Most of these were RNA/DNA binding proteins, such as Matrin-3 and TDP-43, which are mainly nuclear resident RNA binding proteins [888, 957]. Hence this implies that FUS^{EC} is involved in nuclear mRNA processing and transport to the cytoplasm. However, FUS^{EC} lacks the first 266 amino acids of canonical FUS, hence it

lacks the QGSY-rich domain and the intrinsically disordered first glycine-rich domain [543]. Both of these domains have prion-like characteristics and are involved in transcriptional regulation, protein-protein interactions, and regulation of FUS phase separation [127, 523]. While FUS^{EC} retains most of the domains responsible for the DNA damage response [158, 958], FUS recruitment to DNA sites has been tightly linked to its phosphorylation at the N-terminal prion-like domain upon DNA damage [574]. Hence in future studies the ability of FUS^{EC} in the DNA damage response should be investigated [573, 574].

The functions of FUS^{EC} in the extracellular environment remain intriguing. In this thesis we identified putative interacting partners of extracellular FUS^{EC} that suggest DNA/RNA binding functions in that subcellular compartment. More work is needed to determine the specific functions of FUS^{EC} extracellularly. An interesting area of future research would be to examine whether FUS^{EC} is associated with the export of exRNA. exRNA has been shown to be secreted via RNP complexes and extracellular vesicles, hence FUS^{EC} may be a constituent of RNP complexes or may be located within extracellular vesicles. Whilst in this thesis it was concluded that FUS^{EC} is not present in exosomes, it remains to be elucidated whether FUS^{EC} is present in microvesicles, where, interestingly, matrin-3, an extracellular FUS^{EC} putative binding partner, has been identified [959, 960]. Furthermore, the binding of extracellular FUS^{EC} with RNA could be investigated using the technique iCLIP, which has been used previously to identify RNA targets of FUS and TDP-43 [622, 736]. iCLIP combines CLIP-seq and immunoprecipitation and have been optimized recently, so that it now is more efficient and accurate than previous [961, 962].

FUS functions are tightly regulated by its PTMs. This thesis presented evidence that FUS^{EC} is *N*-glycosylated, with two potential *N*-glycosylated sites identified in the RRM domain (N79, N90) and one in the ZnF domain (N232). In contrast, *N*-glycosylation of canonical FUS has not been demonstrated to date. FUS PTMs include methylation in the RGG3 domain [557], which is involved in the regulation of its binding to TRPO1, and could thus impact its nuclear import. Similarly, phosphorylation of residues in the PY-NLS region are implicated in disruption of this interaction [535, 553], leading to cytoplasmic FUS accumulation. Therefore, FUS^{EC} nuclear localization could be also mediated by its phosphorylation and methylation status at its C-terminus.

This study has provided some clues to the possible functions of FUS^{EC}. The spatial conformation of proteins has a critical effect on its function. Hence in future studies the three-dimensional structure of FUS^{EC} should be elucidated to have a better understanding of the protein and its functions.

The possible role of FUS^{EC} in ALS

This thesis presents evidence that WT FUS^{EC}, and to a greater extent ALS-mutant FUS^{EC}, are involved in cellular pathological features that have been shown to be a common trait among other ALS related proteins, including TDP-43, SOD1 and C9ORF72 as well as canonical FUS [115, 119, 171, 485, 487, 880, 952, 963]. These processes include ER stress, Golgi fragmentation and apoptosis.

This new evidence regarding FUS^{EC} has raised new questions however. Undoubtedly the prion-like domain plays a critical role in canonical FUS pathology in ALS. However, is it possible that FUS^{EC}, which lacks this domain, be involved in similar pathways and has similar toxic effects to canonical FUS within the cell. The FUS prion-like domain is important due to its self-assembly capacity and the formation of cross-beta filament-containing hydrogels in vitro [378]. Indeed, some studies have demonstrated that these regions are required for canonical FUS aggregation [964] and localization into stress granules [378]. However, the C-terminal region (423-526) of canonical FUS promoted the aggregation of large macroscopic aggregates in vitro [533] and according to this study, the FUS RRM domain was required for cytotoxicity [533]. Hence future studies are needed to determine the role of FUS^{EC} inclusions in its structure and function and to examine the role of the unique N-terminal sequence of FUS^{EC} in its folding.

An important role of canonical FUS toxicity in ALS is the abnormal entrapment of RNA-binding proteins and RNA in the inclusions, which impairs RNA regulation and axonal transport [965, 966]. It has been proposed that the underlying pathophysiologic mechanism in ALS is impairment of FUS phase transition by mutant canonical FUS, which promotes the formation of irreversible solid RNP granules, such as SGs [354, 379]. Recently, it has been shown for the first time that persistent SGs transit to pathological inclusions that induce neuronal cell death [967]. Hence it is important to determine whether FUS^{EC} would have a similar role to canonical FUS in this manner. This thesis presents some evidence to suggest that FUS^{EC} could be a component of

SGs. Firstly, a number of potential binding partners of FUS^{EC} were nucleic acid binding proteins including, TDP-43 that is known to modulate SGs formation [968]. Additionally, Matrin-3 was also identified and proteins involved in RNA stress granule formation were consistently identified as major Matrin-3 interacting partners [957]. Additionally, the data reveal that mutant FUS^{EC}, R316G, possibly binds to G3BP1, a stress granule component. Furthermore, it also revealed that both FUS^{EC} mutants potentially bind to VCP, which is localized in SGs under stress conditions, which regulates their clearance [948]. The prion-like domain of canonical FUS has been suggested to be responsible for driving FUS assembly into reversible liquid phase [378, 521, 529]. However, is this domain important for the irreversible assembly of SGs, which may underlie the formation of inclusions in ALS? It is important to note that ALS mutant proteins without a prion-like domain, such as SOD1, have been shown to interact with G3BP1, localize to SGs and impair their dynamics [969]. Cytoplasmic mislocalization is a common prerequisite of SGs formation. Additionally, the RGG-ZnF-RGG domain of FUS is necessary for the recruitment of canonical FUS into stress granules [540]. Another study demonstrated that the RGG domains of FUS, also present in FUS^{EC}, were prone to phase separate in the presence of a molecular crowder [389]. Furthermore, the RRM domain of FUS, although intrinsically folded, is able to self-assemble irreversibly into amyloid fibrils [522]. Hence, although FUS^{EC} is missing the prion-like domain, this evidence suggests that FUS^{EC} could be a component of SGs. Future studies to determine FUS^{EC} localization in SGs are therefore warranted. Additionally, it will be interesting to study whether mutant FUS^{EC} impairs SGs dynamics similar to other ALS related proteins and/or whether FUS^{EC} is the main driver of RNP granule formation and/or whether it is passively pulled down by RBP complexes.

Extracellular proteins have been implicated in the orderly spread of ALS pathology in a prion-like mechanism [507, 508]. This thesis presents preliminary evidence that mutant FUS^{EC} could be transmitted from cell-to-cell, but this should be further confirmed with additional techniques and with a more biologically relevant disease model. More work is therefore needed to confirm the transmissibility of FUS^{EC} and to investigate the prion-like properties of FUS^{EC}. In future studies, in the first experiments, it would be important to elucidate if FUS^{EC} has the ability to self-assemble similar to canonical FUS [522, 578]. Next it could be investigated whether FUS^{EC} inclusions have amyloid like properties by examining their reactivity to thioflavin S or Congo red and to test their resistance to proteinase K.

It is also worthwhile to study the possible involvement of WT and mutant FUS^{EC} in the non-cell autonomous mechanism involved in ALS. Altered functions of non-neuronal cells have been implicated in ALS/FTD, affecting disease onset, progression and neurodegeneration [970, 971]. Canonical FUS is ubiquitously expressed in the CNS and FUS inclusions have been detected in glia and astrocytes of ALS/FTD patients [4, 12, 972]. Interestingly, microglia activated by extracellular mutant SOD1 induces motor neuron degeneration [313, 314]. It would be interesting to determine whether glia and astrocytes also exhibit the cell-to-cell transmission of FUS^{EC}, and examine whether these cells are implicated in its spread. It should also be examined whether FUS^{EC} normal extracellular functions involves the communication among cells, for example through the transfer of exRNA that as has been described before for other protein [973] and if this is altered in ALS mutants.

Finally, future studies should also focus on determining the mechanism underlying alternative splicing regulation of FUS^{EC}. The normal functions of canonical FUS include alternative splicing, and FUS has been shown to autoregulate its protein levels through alternative splicing and NMD [512]. Hence it would be interesting to examine whether canonical FUS regulates FUS^{EC} expression. Similarly, also whether the alternative splicing defects seen in FUS ALS lead to altered expression of FUS^{EC}.

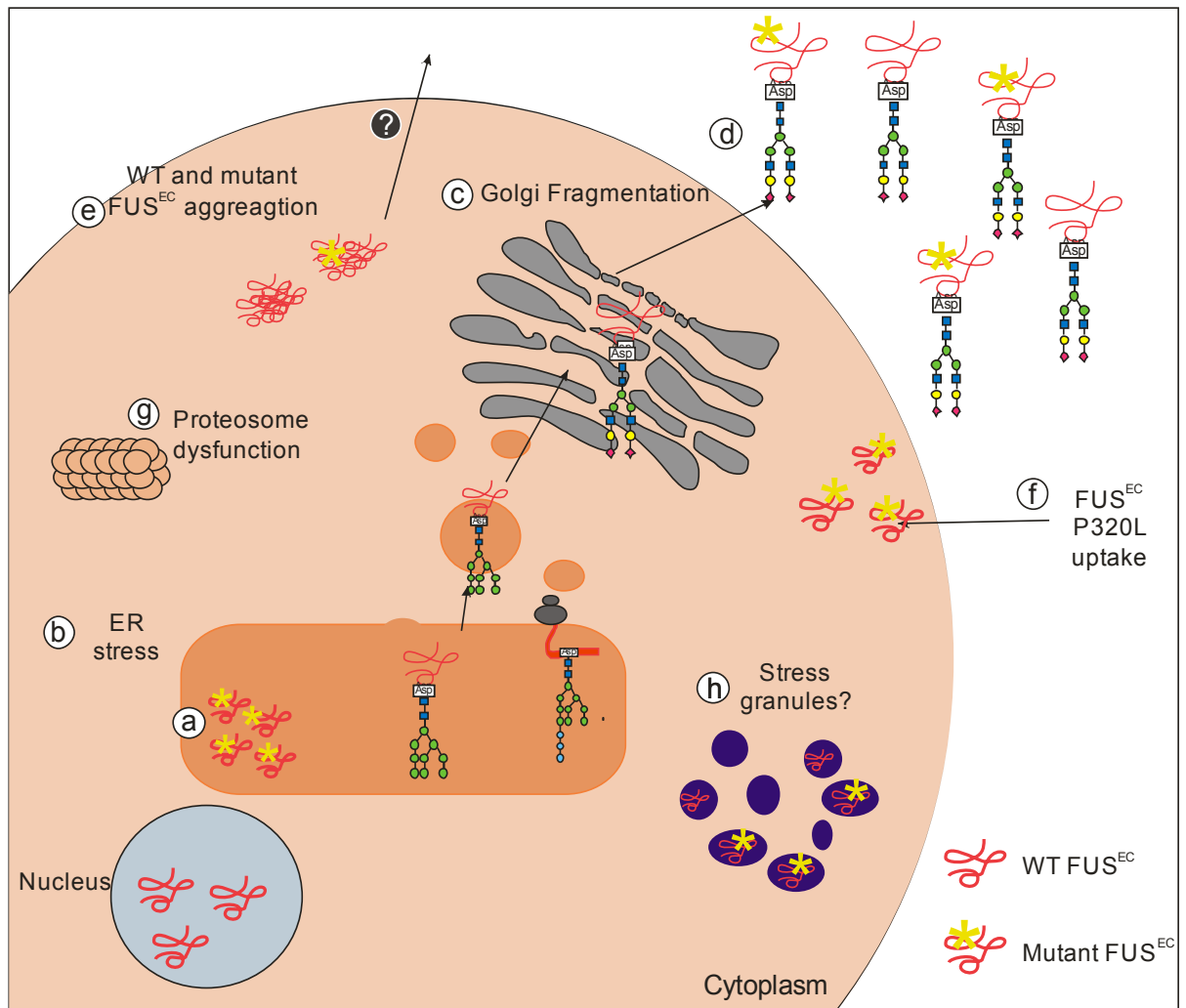


Figure 6.2 FUS^{EC} is involved in molecular mechanisms related to ALS (a) Mutant FUS^{EC} (P230L and R316G) localizes more in the ER and also induce more of ER stress (b) and Golgi fragmentation than WT FUS^{EC} (c), triggering apoptosis. FUS^{EC} is N-glycosylated and secreted through the classic secretory pathway (d). However a second secretory mechanism, implying aggregates or extracellular vesicles other than exosomes (e), is also implicated and needs to be further investigated. (f) Preliminary data demonstrated that P230L is capable of transmitting from cell-to-cell. The putative binding partners identified in this study suggest that overexpression of mutant FUS^{EC} could lead to proteasome dysfunction (g), and localize within stress granules (h). However this needs to be experimentally confirmed.

It is important to mention some caveats to this study. The studies presented in this thesis are based on the use of cell culture models overexpressing FUS^{EC}. Although this model allows us to better study FUS^{EC} characteristics and effects on ALS cellular features, it has also some limitations. Transient transfection results in high levels of protein expression, which may not be at physiological levels, and thus not related to the disease. Hence, in future studies stable and inducible expression of FUS^{EC} or the use of CRISPR/Cas9 technology could help to obtain protein levels closer to physiological

conditions. Additionally, these studies should be verified using more relevant models. FUS^{EC} expression and the studies of FUS^{EC} N-glycosylation should be confirmed in human tissue samples, such as CSF. Given the limitations of investigations into a complex disease in cell culture, it will be important in future studies to further investigate the role of FUS^{EC} in ALS using *in vivo* models or ALS patients iPSCs. Additionally, the expression of FUSEC should be studied in ALS patient and control samples to validate its biological relevance to pathology

Final conclusions

ALS is the most common motor neuron disorder with adult onset. FUS is linked pathologically and genetically to both familial and sporadic cases of ALS. Importantly, FUS mutations are linked to an aggressive, juvenile form of ALS. However, the role of FUS in ALS remains largely unknown in comparison to TDP-43. The body of work presented in this thesis confirms the discovery of a new extracellular FUS isoform, FUS^{EC}, and describes normal characteristics and functions of FUS^{EC}. Importantly, it also presents evidence of its potential role in ALS. This new evidence raises several questions and further work is needed to determine the unique role of FUS^{EC} under normal conditions and importantly, in ALS neurodegeneration in ALS.

It is likely that the results presented in this thesis will have further implications in our understanding of ALS and also opens up important new avenues of research focused on FUS^{EC}, such as determining the unique function of FUS^{EC} in the extracellular compartment under normal conditions and in ALS.

Highlights of this thesis

- A novel isoform of FUS has been identified, termed 'FUS^{EC}'.
- FUS^{EC} is an extracellular protein that is *N*-glycosylated with complex *N*-glycans, and this regulates its secretion.
- The vast majority of potential intra- and extracellular binding partners of WT FUS^{EC} are RNA/DNA binding proteins.
- Overexpression of FUS^{EC} bearing ALS mutations triggers cellular features characteristic of ALS: inclusion formation, ER stress, Golgi fragmentation and apoptosis.
- Potential binding partners of mutant FUS^{EC} are proteins involved in the UPR, proteasome function and stress granule formation.
- Preliminary evidence implies that ALS-mutant P320L FUS^{EC} is transmitted among cells.

7. ■ **References**

1. Cleveland, D.W. and J.D. Rothstein, *From Charcot to Lou Gehrig: deciphering selective motor neuron death in ALS*. Nat Rev Neurosci, 2001. **2**(11): p. 806-19.
2. Rowland, L.P. and N.A. Shneider, *Amyotrophic lateral sclerosis*. N Engl J Med, 2001. **344**(22): p. 1688-700.
3. Renton, A.E., A. Chio, and B.J. Traynor, *State of play in amyotrophic lateral sclerosis genetics*. Nat Neurosci, 2014. **17**(1): p. 17-23.
4. Kwiatkowski, et al., *Mutations in the FUS/TLS gene on chromosome 16 cause familial amyotrophic lateral sclerosis*. Science, 2009. **323**: p. 5.
5. Vance C, R.B., Hortobágyi T, De Vos KJ, Lumi Nishimura, Sreedharan Jemeen, Hu X, Smith B, Ruddy D, Wright P, Ganesaingan J, Williams KL, Tripathi V, Al-Saraj S, Al-Chalabi A, Leigh PN, Blair IP, Nicholson G, Bellerocche J, Gallo JM, Miller CC, Shaw CE, *Mutations in FUS, an RNA processing protein, Cause Familial Amyotrophic Lateral Sclerosis Type 6*. Science, 2009. **323**: p. 4.
6. Lai, S.L., et al., *FUS mutations in sporadic amyotrophic lateral sclerosis*. Neurobiol Aging, 2011. **32**(3): p. 550.e1-4.
7. Bäumer, D., et al., *juvenile ALS with basophilic inclusions is a FUS proteinopathy with FUS mutations*. Neurology, 2010. **75**: p. 8.
8. Conte, A., et al., *P525L FUS mutation is consistently associated with a severe form of juvenile amyotrophic lateral sclerosis*. Neuromuscul Disord, 2012. **22**(1): p. 73-5.
9. Hubers, A., et al., *De novo FUS mutations are the most frequent genetic cause in early-onset German ALS patients*. Neurobiol Aging, 2015. **36**(11): p. 3117.e1-6.
10. Corcia, P., et al., *A novel mutation of the C-terminal amino acid of FUS (Y526C) strengthens FUS gene as the most frequent genetic factor in aggressive juvenile ALS*. Amyotroph Lateral Scler Frontotemporal Degener, 2017: p. 1-4.
11. R., T., et al., *Transportin 1 accumulates in FUS inclusions in adult - onset ALS without FUS mutation*. Neuropathology and Applied Neurobiology, 2013. **39**(5): p. 580-584.
12. Deng, H.X., et al., *FUS-immunoreactive inclusions are a common feature in sporadic and non-SOD1 familial amyotrophic lateral sclerosis*. Ann Neurol, 2010. **67**(6): p. 739-48.
13. Westeneng, H.J., et al., *Prognosis for patients with amyotrophic lateral sclerosis: development and validation of a personalised prediction model*. Lancet Neurol, 2018.
14. van Es, M.A., et al., *Amyotrophic lateral sclerosis*. Lancet, 2017. **390**(10107): p. 2084-2098.
15. Swinnen, B. and W. Robberecht, *The phenotypic variability of amyotrophic lateral sclerosis*. Nat Rev Neurol, 2014. **10**(11): p. 661-70.
16. Al-Chalabi, A. and O. Hardiman, *The epidemiology of ALS: a conspiracy of genes, environment and time*. Nat Rev Neurol, 2013. **9**(11): p. 617-28.
17. Brooks, B.R., et al., *El Escorial revisited: Revised criteria for the diagnosis of amyotrophic lateral sclerosis*. Amyotroph Lateral Scler Other Motor Neuron Disord, 2000. **1**(5): p. 293-299.
18. Costa, J., M. Swash, and M. de Carvalho, *Awaji criteria for the diagnosis of amyotrophic lateral sclerosis: a systematic review*. Arch Neurol, 2012. **69**(11): p. 1410-6.
19. Li, D.W., et al., *The Awaji criteria increases the diagnostic sensitivity of the revised El Escorial criteria for amyotrophic lateral sclerosis diagnosis in a Chinese population*. PLoS One, 2017. **12**(3): p. e0171522.
20. Brown, R.H. and A. Al-Chalabi, *Amyotrophic Lateral Sclerosis*. New England Journal of Medicine, 2017. **377**(2): p. 162-172.
21. Tao, Q.-Q., Q. Wei, and Z.-Y. Wu, *Sensory nerve disturbance in amyotrophic lateral sclerosis*. Life Sciences, 2018. **203**: p. 242-245.

22. Ravits, J., P. Paul, and C. Jorg, *Focality of upper and lower motor neuron degeneration at the clinical onset of ALS*. *Neurology*, 2007. **68**(19): p. 1571-5.
23. Ravits, J.M. and A.R. La Spada, *ALS motor phenotype heterogeneity, focality, and spread: deconstructing motor neuron degeneration*. *Neurology*, 2009. **73**(10): p. 805-11.
24. Henry, K.A., et al., *Geographic Variation of Amyotrophic Lateral Sclerosis Incidence in New Jersey, 2009–2011*. *American Journal of Epidemiology*, 2015. **182**(6): p. 512-519.
25. Chio, A., et al., *Global epidemiology of amyotrophic lateral sclerosis: a systematic review of the published literature*. *Neuroepidemiology*, 2013. **41**(2): p. 118-30.
26. Marin, B., et al., *Variation in worldwide incidence of amyotrophic lateral sclerosis: a meta-analysis*. *Int J Epidemiol*, 2017. **46**(1): p. 57-74.
27. Hardiman, O., et al., *The changing picture of amyotrophic lateral sclerosis: lessons from European registers*. *J Neurol Neurosurg Psychiatry*, 2017. **88**(7): p. 557-563.
28. Liu, X., et al., *The epidemiology and genetics of Amyotrophic lateral sclerosis in China*. *Brain Res*, 2018.
29. Nakken, O., et al., *Assessing amyotrophic lateral sclerosis prevalence in Norway from 2009 to 2015 from compulsory nationwide health registers*. *Amyotroph Lateral Scler Frontotemporal Degener*, 2018. **19**(3-4): p. 303-310.
30. Kurtzke, J.F., *Epidemiology of amyotrophic lateral sclerosis*. *Adv Neurol*, 1982. **36**: p. 281-302.
31. Cox, P.A., S.A. Banack, and S.J. Murch, *Biomagnification of cyanobacterial neurotoxins and neurodegenerative disease among the Chamorro people of Guam*. *Proc Natl Acad Sci U S A*, 2003. **100**(23): p. 13380-3.
32. Mandrioli, J., et al., *Riluzole and other prognostic factors in ALS: a population-based registry study in Italy*. *J Neurol*, 2018. **265**(4): p. 817-827.
33. Rooney, J., et al., *Survival analysis of irish amyotrophic lateral sclerosis patients diagnosed from 1995-2010*. *PLoS One*, 2013. **8**(9): p. e74733.
34. Mehta, P., et al., *Prevalence of Amyotrophic Lateral Sclerosis - United States, 2014*. *MMWR Morb Mortal Wkly Rep*, 2018. **67**(7): p. 216-218.
35. Chio, A., et al., *Prognostic factors in ALS: A critical review*. *Amyotroph Lateral Scler*, 2009. **10**(5-6): p. 310-23.
36. Rosenbohm, A., et al., *Epidemiology of amyotrophic lateral sclerosis in Southern Germany*. *J Neurol*, 2017. **264**(4): p. 749-757.
37. Nalini, A., et al., *Clinical characteristics and survival pattern of 1,153 patients with amyotrophic lateral sclerosis: experience over 30 years from India*. *J Neurol Sci*, 2008. **272**(1-2): p. 60-70.
38. Arthur, K.C., et al., *Projected increase in amyotrophic lateral sclerosis from 2015 to 2040*. *Nat Commun*, 2016. **7**: p. 12408.
39. Bozzoni, V., et al., *Amyotrophic lateral sclerosis and environmental factors*. *Funct Neurol*, 2016. **31**(1): p. 7-19.
40. Alonso, A., G. Logroscino, and M.A. Hernan, *Smoking and the risk of amyotrophic lateral sclerosis: a systematic review and meta-analysis*. *J Neurol Neurosurg Psychiatry*, 2010. **81**(11): p. 1249-52.
41. Alonso, A., et al., *Association of smoking with amyotrophic lateral sclerosis risk and survival in men and women: a prospective study*. *BMC Neurology*, 2010. **10**(1): p. 6.
42. Wang, H., et al., *Smoking and risk of amyotrophic lateral sclerosis: a pooled analysis of 5 prospective cohorts*. *Arch Neurol*, 2011. **68**(2): p. 207-13.
43. Calvo, A., et al., *Influence of cigarette smoking on ALS outcome: a population-based study*. *J Neurol Neurosurg Psychiatry*, 2016. **87**(11): p. 1229-1233.

44. Sutedja, N.A., et al., *Exposure to chemicals and metals and risk of amyotrophic lateral sclerosis: a systematic review*. Amyotroph Lateral Scler, 2009. **10**(5-6): p. 302-9.
45. Seals, R.M., et al., *Occupational formaldehyde and amyotrophic lateral sclerosis*. Eur J Epidemiol, 2017. **32**(10): p. 893-899.
46. Su, F.C., et al., *Association of Environmental Toxins With Amyotrophic Lateral Sclerosis*. JAMA Neurol, 2016. **73**(7): p. 803-11.
47. Dickerson, A.S., et al., *Amyotrophic lateral sclerosis and exposure to diesel exhaust in a Danish cohort*. Am J Epidemiol, 2018.
48. Bradley, W.G. and D.C. Mash, *Beyond Guam: the cyanobacteria/BMAA hypothesis of the cause of ALS and other neurodegenerative diseases*. Amyotroph Lateral Scler, 2009. **10 Suppl 2**: p. 7-20.
49. Banack, S.A. and P.A. Cox, *Biomagnification of cycad neurotoxins in flying foxes: implications for ALS-PDC in Guam*. Neurology, 2003. **61**(3): p. 387-9.
50. Murch, S.J., P.A. Cox, and S.A. Banack, *A mechanism for slow release of biomagnified cyanobacterial neurotoxins and neurodegenerative disease in Guam*. Proc Natl Acad Sci U S A, 2004. **101**(33): p. 12228-31.
51. Pablo, J., et al., *Cyanobacterial neurotoxin BMAA in ALS and Alzheimer's disease*. Acta Neurol Scand, 2009. **120**(4): p. 216-25.
52. Scott, L.L. and T.G. Downing, *A Single Neonatal Exposure to BMAA in a Rat Model Produces Neuropathology Consistent with Neurodegenerative Diseases*. Toxins (Basel), 2017. **10**(1).
53. Tan, V.X., et al., *Neurotoxicity of the Cyanotoxin BMAA Through Axonal Degeneration and Intercellular Spreading*. Neurotox Res, 2018. **33**(1): p. 62-75.
54. Dunlop, R.A., et al., *The non-protein amino acid BMAA is misincorporated into human proteins in place of L-serine causing protein misfolding and aggregation*. PLoS One, 2013. **8**(9): p. e75376.
55. Horner, R.D., et al., *Occurrence of amyotrophic lateral sclerosis among Gulf War veterans*. Neurology, 2003. **61**(6): p. 742-9.
56. Coffman, C.J., et al., *Estimating the occurrence of amyotrophic lateral sclerosis among Gulf War (1990-1991) veterans using capture-recapture methods*. Neuroepidemiology, 2005. **24**(3): p. 141-50.
57. Affairs, D.o.V., *Presumption of service connection for amyotrophic lateral sclerosis. Final rule*. Fed Regist, 2009. **74**(212): p. 57072-4.
58. Weisskopf, M.G., et al., *Prospective study of military service and mortality from ALS*. Neurology, 2005. **64**(1): p. 32-7.
59. Cragg, J.J., N.J. Johnson, and M.G. Weisskopf, *Military Service and Amyotrophic Lateral Sclerosis in a Population-based Cohort: Extended Follow-up 1979-2011*. Epidemiology, 2017. **28**(2): p. e15-e16.
60. Seals, R.M., et al., *Amyotrophic Lateral Sclerosis and the Military: A Population-based Study in the Danish Registries*. Epidemiology, 2016. **27**(2): p. 188-93.
61. Hamidou, B., et al., *Epidemiological evidence that physical activity is not a risk factor for ALS*. Eur J Epidemiol, 2014. **29**(7): p. 459-75.
62. Chio, A., et al., *Severely increased risk of amyotrophic lateral sclerosis among Italian professional football players*. Brain, 2005. **128**(Pt 3): p. 472-6.
63. Lehman, E.J., et al., *Neurodegenerative causes of death among retired National Football League players*. Neurology, 2012. **79**(19): p. 1970-1974.
64. Fang, F., et al., *Amyotrophic lateral sclerosis among cross-country skiers in Sweden*. Eur J Epidemiol, 2016. **31**(3): p. 247-53.
65. Gallo, V., et al., *Physical activity and risk of Amyotrophic Lateral Sclerosis in a prospective cohort study*. Eur J Epidemiol, 2016. **31**(3): p. 255-66.

66. Aberg, M., et al., *Risk factors in Swedish young men for amyotrophic lateral sclerosis in adulthood*. J Neurol, 2018. **265**(3): p. 460-470.
67. Huisman, M.H., et al., *Lifetime physical activity and the risk of amyotrophic lateral sclerosis*. J Neurol Neurosurg Psychiatry, 2013. **84**(9): p. 976-81.
68. Pupillo, E., et al., *Physical activity and amyotrophic lateral sclerosis: a European population-based case-control study*. Ann Neurol, 2014. **75**(5): p. 708-16.
69. Visser, A.E., et al., *Multicentre, cross-cultural, population-based, case-control study of physical activity as risk factor for amyotrophic lateral sclerosis*. J Neurol Neurosurg Psychiatry, 2018.
70. Piazza, O., A.L. Siren, and H. Ehrenreich, *Soccer, neurotrauma and amyotrophic lateral sclerosis: is there a connection?* Curr Med Res Opin, 2004. **20**(4): p. 505-8.
71. Feddermann-Demont, N., et al., *Prevalence of potential sports-associated risk factors in Swiss amyotrophic lateral sclerosis patients*. Brain Behav, 2017. **7**(4): p. e00630.
72. M., V., et al., *Amyotrophic lateral sclerosis and sports: a case-control study*. European Journal of Neurology, 2005. **12**(3): p. 223-225.
73. Seals, R.M., et al., *Physical Trauma and Amyotrophic Lateral Sclerosis: A Population-Based Study Using Danish National Registries*. Am J Epidemiol, 2016. **183**(4): p. 294-301.
74. Arvanitakis, Z., *Update on frontotemporal dementia*. Neurologist, 2010. **16**(1): p. 16-22.
75. Cairns, N.J., et al., *Neuropathologic diagnostic and nosologic criteria for frontotemporal lobar degeneration: consensus of the Consortium for Frontotemporal Lobar Degeneration*. Acta Neuropathol, 2007. **114**(1): p. 5-22.
76. Ringholz, G.M., et al., *Prevalence and patterns of cognitive impairment in sporadic ALS*. Neurology, 2005. **65**(4): p. 586-90.
77. Wheaton, M.W., et al., *Cognitive impairment in familial ALS*. Neurology, 2007. **69**(14): p. 1411-7.
78. Shahheydari, H., et al., *Protein Quality Control and the Amyotrophic Lateral Sclerosis/Frontotemporal Dementia Continuum*. Front Mol Neurosci, 2017. **10**: p. 119.
79. Byrne, S., et al., *Rate of familial amyotrophic lateral sclerosis: a systematic review and meta-analysis*. Journal of Neurology, Neurosurgery & Psychiatry, 2011. **82**(6): p. 623-627.
80. Rosen, T.S., David Patterson, Danise A. Figlewicz, Peter Sapp, Afif Hentati, Deirdre Donaldson, Jun Goto, Jeremiah P. O'Regan, *Mutations in Cu/Zn superoxide dismutase gene are associated with familial amyotrophic lateral sclerosis*. Nature, 1993. **362**: p. 4.
81. Cirulli, E.T., et al., *Exome sequencing in amyotrophic lateral sclerosis identifies risk genes and pathways*. Science, 2015. **347**(6229): p. 1436-1441.
82. Gurney, M., et al., *Motor neuron degeneration in mice that express a human Cu,Zn superoxide dismutase mutation*. Science, 1994. **264**(5166): p. 1772-1775.
83. Scrutton, N., et al., *Cooperativity induced by a single mutation at the subunit interface of a dimeric enzyme: glutathione reductase*. Science, 1992. **258**(5085): p. 1140-1143.
84. Wei, Q., et al., *Analysis of SOD1 mutations in a Chinese population with amyotrophic lateral sclerosis: a case-control study and literature review*. Sci Rep, 2017. **7**: p. 44606.
85. Bunton-Stasyshyn, R.K., et al., *SOD1 Function and Its Implications for Amyotrophic Lateral Sclerosis Pathology: New and Renascent Themes*. Neuroscientist, 2015. **21**(5): p. 519-29.
86. Saccon, R.A., et al., *Is SOD1 loss of function involved in amyotrophic lateral sclerosis?* Brain, 2013. **136**(Pt 8): p. 2342-58.

87. Nakamura, M., et al., *A truncating SOD1 mutation, p.Gly141X, is associated with clinical and pathologic heterogeneity, including frontotemporal lobar degeneration.* Acta Neuropathol, 2015. **130**(1): p. 145-57.
88. Katz, J.S., et al., *Combined fulminant frontotemporal dementia and amyotrophic lateral sclerosis associated with an I113T SOD1 mutation.* Amyotroph Lateral Scler, 2012. **13**(6): p. 567-9.
89. Kim, M.J., et al., *Rapid Progression of Sporadic ALS in a Patient Carrying SOD1 p.Gly13Arg Mutation.* Exp Neurol, 2016. **25**(6): p. 347-350.
90. Niu, Q., et al., *The G41D mutation in the superoxide dismutase 1 gene is associated with slow motor neuron progression and mild cognitive impairment in a Chinese family with amyotrophic lateral sclerosis.* J Neurol Neurosurg Psychiatry, 2016. **87**(7): p. 788-9.
91. Cudkowicz, M.E., et al., *Epidemiology of mutations in superoxide dismutase in amyotrophic lateral sclerosis.* Ann Neurol, 1997. **41**(2): p. 210-21.
92. Pan, L., et al., *Different human copper-zinc superoxide dismutase mutants, SOD1G93A and SOD1H46R, exert distinct harmful effects on gross phenotype in mice.* PLoS One, 2012. **7**(3): p. e33409.
93. Andersen, P.M., *Amyotrophic lateral sclerosis associated with mutations in the CuZn superoxide dismutase gene.* Curr Neurol Neurosci Rep, 2006. **6**(1): p. 37-46.
94. Luigetti, M., et al., *Heterozygous SOD1 D90A mutation presenting as slowly progressive predominant upper motor neuron amyotrophic lateral sclerosis.* Neurol Sci, 2009. **30**(6): p. 517-20.
95. Deng, H.-X., et al., *Conversion to the amyotrophic lateral sclerosis phenotype is associated with intermolecular linked insoluble aggregates of SOD1 in mitochondria.* Proceedings of the National Academy of Sciences, 2006. **103**(18): p. 7142-7147.
96. Islinger, M., et al., *Hitchhiking of Cu/Zn superoxide dismutase to peroxisomes--evidence for a natural piggyback import mechanism in mammals.* Traffic, 2009. **10**(11): p. 1711-21.
97. Tsang, C.K., et al., *Superoxide dismutase 1 acts as a nuclear transcription factor to regulate oxidative stress resistance.* Nat Commun, 2014. **5**: p. 3446.
98. Turner, B.J., et al., *Impaired extracellular secretion of mutant superoxide dismutase 1 associates with neurotoxicity in familial amyotrophic lateral sclerosis.* J Neurosci, 2005. **25**(1): p. 108-17.
99. Kaur, S.J., S.R. McKeown, and S. Rashid, *Mutant SOD1 mediated pathogenesis of Amyotrophic Lateral Sclerosis.* Gene, 2016. **577**(2): p. 109-118.
100. Seetharaman, S.V., et al., *Immature copper-zinc superoxide dismutase and familial amyotrophic lateral sclerosis.* Exp Biol Med (Maywood), 2009. **234**(10): p. 1140-54.
101. Bowling, A.C., et al., *Superoxide dismutase activity, oxidative damage, and mitochondrial energy metabolism in familial and sporadic amyotrophic lateral sclerosis.* J Neurochem, 1993. **61**(6): p. 2322-5.
102. Borchelt, D.R., et al., *Superoxide dismutase 1 subunits with mutations linked to familial amyotrophic lateral sclerosis do not affect wild-type subunit function.* J Biol Chem, 1995. **270**(7): p. 3234-8.
103. Corson, L.B., et al., *Chaperone-facilitated copper binding is a property common to several classes of familial amyotrophic lateral sclerosis-linked superoxide dismutase mutants.* Proceedings of the National Academy of Sciences, 1998. **95**(11): p. 6361-6366.
104. Marklund, S.L., et al., *Normal binding and reactivity of copper in mutant superoxide dismutase isolated from amyotrophic lateral sclerosis patients.* J Neurochem, 1997. **69**(2): p. 675-81.

105. Reaume, A.G., et al., *Motor neurons in Cu/Zn superoxide dismutase-deficient mice develop normally but exhibit enhanced cell death after axonal injury*. Nat Genet, 1996. **13**(1): p. 43-7.
106. Frey, D., et al., *Early and selective loss of neuromuscular synapse subtypes with low sprouting competence in motoneuron diseases*. J Neurosci, 2000. **20**(7): p. 2534-42.
107. Chattopadhyay, M., et al., *Initiation and elongation in fibrillation of ALS-linked superoxide dismutase*. Proceedings of the National Academy of Sciences, 2008. **105**(48): p. 18663-18668.
108. Cozzolino, M., et al., *Cysteine 111 affects aggregation and cytotoxicity of mutant Cu,Zn-superoxide dismutase associated with familial amyotrophic lateral sclerosis*. J Biol Chem, 2008. **283**(2): p. 866-74.
109. Bosco, D.A., et al., *Wild-type and mutant SOD1 share an aberrant conformation and a common pathogenic pathway in ALS*. Nat Neurosci, 2010. **13**(11): p. 1396-403.
110. Orrell, R.W., et al., *Familial amyotrophic lateral sclerosis with a point mutation of SOD-1: intrafamilial heterogeneity of disease duration associated with neurofibrillary tangles*. J Neurol Neurosurg Psychiatry, 1995. **59**(3): p. 266-70.
111. Shibata, N., et al., *Intense superoxide dismutase-1 immunoreactivity in intracytoplasmic hyaline inclusions of familial amyotrophic lateral sclerosis with posterior column involvement*. J Neuropathol Exp Neurol, 1996. **55**(4): p. 481-90.
112. Inoue, K., et al., *Familial amyotrophic lateral sclerosis with a point mutation (G37R) of the superoxide dismutase 1 gene: a clinicopathological study*. Amyotroph Lateral Scler Other Motor Neuron Disord, 2002. **3**(4): p. 244-7.
113. Ohi, T., et al., *Familial amyotrophic lateral sclerosis with His46Arg mutation in Cu/Zn superoxide dismutase presenting characteristic clinical features and Lewy body-like hyaline inclusions*. J Neurol Sci, 2004. **225**(1-2): p. 19-25.
114. Hough, M.A., et al., *Dimer destabilization in superoxide dismutase may result in disease-causing properties: structures of motor neuron disease mutants*. Proc Natl Acad Sci U S A, 2004. **101**(16): p. 5976-81.
115. Atkin, J.D., et al., *Mutant SOD1 inhibits ER-Golgi transport in amyotrophic lateral sclerosis*. J Neurochem, 2014. **129**(1): p. 190-204.
116. Vande Velde, C., et al., *Misfolded SOD1 associated with motor neuron mitochondria alters mitochondrial shape and distribution prior to clinical onset*. PLoS One, 2011. **6**(7): p. e22031.
117. Nishitoh, H., et al., *ALS-linked mutant SOD1 induces ER stress- and ASK1-dependent motor neuron death by targeting Derlin-1*. Genes Dev, 2008. **22**(11): p. 1451-64.
118. Atkin, J.D., et al., *Endoplasmic reticulum stress and induction of the unfolded protein response in human sporadic amyotrophic lateral sclerosis*. Neurobiol Dis, 2008. **30**(3): p. 400-7.
119. Sundaramoorthy, V., et al., *Extracellular wildtype and mutant SOD1 induces ER-Golgi pathology characteristic of amyotrophic lateral sclerosis in neuronal cells*. Cell Mol Life Sci, 2013. **70**(21): p. 4181-95.
120. Grad, L.I., E. Pokrishevsky, and N.R. Cashman, *Intercellular Prion-Like Conversion and Transmission of Cu/Zn Superoxide Dismutase (SOD1) in Cell Culture*. Methods Mol Biol, 2017. **1658**: p. 357-367.
121. Neumann, M., et al., *Ubiquitinated TDP-43 in frontotemporal lobar degeneration and amyotrophic lateral sclerosis*. Science, 2006. **314**(5796): p. 130-133.
122. Arai, T., et al., *TDP-43 is a component of ubiquitin-positive tau-negative inclusions in frontotemporal lobar degeneration and amyotrophic lateral sclerosis*. Biochem Biophys Res Commun, 2006. **351**(3): p. 602-11.
123. Kabashi, E., et al., *TARDBP mutations in individuals with sporadic and familial amyotrophic lateral sclerosis*. Nat Genet, 2008. **40**(5): p. 572-4.

124. Sreedharan, J., et al., *TDP-43 mutations in familial and sporadic amyotrophic lateral sclerosis*. Science, 2008. **319**(5870): p. 1668-72.
125. Gitcho, M.A., et al., *TDP-43 A315T mutation in familial motor neuron disease*. Ann Neurol, 2008. **63**(4): p. 535-8.
126. Buratti, E., *Functional Significance of TDP-43 Mutations in Disease*. Adv Genet, 2015. **91**: p. 1-53.
127. Lagier-Tourenne, C., M. Polymenidou, and D.W. Cleveland, *TDP-43 and FUS/TLS: emerging roles in RNA processing and neurodegeneration*. Hum Mol Genet, 2010. **19**(R1): p. R46-64.
128. Daoud, H., et al., *Contribution of TARDBP mutations to sporadic amyotrophic lateral sclerosis*. J Med Genet, 2009. **46**(2): p. 112-4.
129. Lagier-Tourenne, C. and D.W. Cleveland, *Rethinking ALS: the FUS about TDP-43*. Cell, 2009. **136**(6): p. 1001-4.
130. Maekawa, S., et al., *TDP-43 is consistently co-localized with ubiquitinated inclusions in sporadic and Guam amyotrophic lateral sclerosis but not in familial amyotrophic lateral sclerosis with and without SOD1 mutations*. Neuropathology, 2009. **29**(6): p. 672-83.
131. Mackenzie, I.R., et al., *Pathological TDP-43 distinguishes sporadic amyotrophic lateral sclerosis from amyotrophic lateral sclerosis with SOD1 mutations*. Ann Neurol, 2007. **61**(5): p. 427-34.
132. Cohen, T.J., V.M. Lee, and J.Q. Trojanowski, *TDP-43 functions and pathogenic mechanisms implicated in TDP-43 proteinopathies*. Trends Mol Med, 2011. **17**(11): p. 659-67.
133. Fiesel, F.C. and P.J. Kahle, *TDP-43 and FUS/TLS: cellular functions and implications for neurodegeneration*. Febs j, 2011. **278**(19): p. 3550-68.
134. De Conti, L., et al., *TDP-43 affects splicing profiles and isoform production of genes involved in the apoptotic and mitotic cellular pathways*. Nucleic Acids Res, 2015. **43**(18): p. 8990-9005.
135. Alami, N.H., et al., *Axonal transport of TDP-43 mRNA granules is impaired by ALS-causing mutations*. Neuron, 2014. **81**(3): p. 536-543.
136. Ishiguro, A., et al., *TDP-43 binds and transports G-quadruplex-containing mRNAs into neurites for local translation*. Genes Cells, 2016. **21**(5): p. 466-81.
137. Schwenk, B.M., et al., *TDP-43 loss of function inhibits endosomal trafficking and alters trophic signaling in neurons*. Embo j, 2016. **35**(21): p. 2350-2370.
138. Liu-Yesucevitz, L., et al., *ALS-linked mutations enlarge TDP-43-enriched neuronal RNA granules in the dendritic arbor*. J Neurosci, 2014. **34**(12): p. 4167-74.
139. Igaz, L.M., et al., *Enrichment of C-terminal fragments in TAR DNA-binding protein-43 cytoplasmic inclusions in brain but not in spinal cord of frontotemporal lobar degeneration and amyotrophic lateral sclerosis*. Am J Pathol, 2008. **173**(1): p. 182-94.
140. White, A., et al., *TDP-43 aggregation during chronic oxidative stress is mediated by c-Jun N-terminal kinase and can be inhibited by a potentially therapeutic metallo-complex*. Alzheimer's & Dementia: The Journal of the Alzheimer's Association, 2011. **7**(4): p. S118.
141. Xiao, S., et al., *Low molecular weight species of TDP-43 generated by abnormal splicing form inclusions in amyotrophic lateral sclerosis and result in motor neuron death*. Acta Neuropathol, 2015. **130**(1): p. 49-61.
142. Ayala, Y.M., et al., *TDP-43 regulates its mRNA levels through a negative feedback loop*. Embo j, 2011. **30**(2): p. 277-88.
143. Seyfried, N.T., et al., *Multiplex SILAC analysis of a cellular TDP-43 proteinopathy model reveals protein inclusions associated with SUMOylation and diverse polyubiquitin chains*. Mol Cell Proteomics, 2010. **9**(4): p. 705-18.

144. Cohen, T.J., et al., *An acetylation switch controls TDP-43 function and aggregation propensity*. Nat Commun, 2015. **6**: p. 5845.
145. Koyama, A., et al., *Increased cytoplasmic TARDBP mRNA in affected spinal motor neurons in ALS caused by abnormal autoregulation of TDP-43*. Nucleic Acids Res, 2016. **44**(12): p. 5820-36.
146. Deshaies, J.E., et al., *TDP-43 regulates the alternative splicing of hnRNP A1 to yield an aggregation-prone variant in amyotrophic lateral sclerosis*. Brain, 2018. **141**(5): p. 1320-1333.
147. Prpar Mihevc, S., et al., *TDP-43 aggregation mirrors TDP-43 knockdown, affecting the expression levels of a common set of proteins*. Sci Rep, 2016. **6**: p. 33996.
148. Zhang, Y.J., et al., *Aberrant cleavage of TDP-43 enhances aggregation and cellular toxicity*. Proc Natl Acad Sci U S A, 2009. **106**(18): p. 7607-12.
149. Johnson, B.S., et al., *A yeast TDP-43 proteinopathy model: Exploring the molecular determinants of TDP-43 aggregation and cellular toxicity*. Proc Natl Acad Sci U S A, 2008. **105**(17): p. 6439-44.
150. Walker, A.K., et al., *Functional recovery in new mouse models of ALS/FTLD after clearance of pathological cytoplasmic TDP-43*. Acta Neuropathol, 2015. **130**(5): p. 643-60.
151. Ticozzi, N., et al., *Analysis of FUS gene mutation in familial amyotrophic lateral sclerosis within an Italian cohort*. Neurology, 2009. **73**(15): p. 1180-5.
152. Corrado, L., et al., *Mutations of FUS gene in sporadic amyotrophic lateral sclerosis*. J Med Genet, 2010. **47**(3): p. 190-4.
153. Millicamps, S., et al., *SOD1, ANG, VAPB, TARDBP, and FUS mutations in familial amyotrophic lateral sclerosis: genotype-phenotype correlations*. J Med Genet, 2010. **47**(8): p. 554-60.
154. Tsai, C.P., et al., *FUS, TARDBP, and SOD1 mutations in a Taiwanese cohort with familial ALS*. Neurobiol Aging, 2011. **32**(3): p. 553.e13-21.
155. Ling, S.C., M. Polymenidou, and D.W. Cleveland, *Converging mechanisms in ALS and FTD: disrupted RNA and protein homeostasis*. Neuron, 2013. **79**(3): p. 416-38.
156. Seelaar, H., et al., *Frequency of ubiquitin and FUS-positive, TDP-43-negative frontotemporal lobar degeneration*. J Neurol, 2010. **257**(5): p. 747-53.
157. Tan, A.Y., et al., *TLS/FUS (translocated in liposarcoma/fused in sarcoma) regulates target gene transcription via single-stranded DNA response elements*. Proc Natl Acad Sci U S A, 2012. **109**(16): p. 6030-5.
158. Mastrocola, A.S., et al., *The RNA-binding protein fused in sarcoma (FUS) functions downstream of poly(ADP-ribose) polymerase (PARP) in response to DNA damage*. J Biol Chem, 2013. **288**(34): p. 24731-41.
159. Yu, Y. and R. Reed, *FUS functions in coupling transcription to splicing by mediating an interaction between RNAP II and U1 snRNP*. Proc Natl Acad Sci U S A, 2015. **112**(28): p. 8608-13.
160. Efimova, A.D., et al., *[The FUS protein: Physiological functions and a role in amyotrophic lateral sclerosis]*. Mol Biol (Mosk), 2017. **51**(3): p. 387-399.
161. DeJesus-Hernandez, M., et al., *Expanded GGGGCC hexanucleotide repeat in noncoding region of C9ORF72 causes chromosome 9p-linked FTD and ALS*. Neuron, 2011. **72**(2): p. 245-56.
162. Renton, A.E., et al., *A hexanucleotide repeat expansion in C9ORF72 is the cause of chromosome 9p21-linked ALS-FTD*. Neuron, 2011. **72**(2): p. 257-68.
163. Kim, E.J., et al., *Clinical and genetic analysis of MAPT, GRN, and C9orf72 genes in Korean patients with frontotemporal dementia*. Neurobiol Aging, 2014. **35**(5): p. 1213.e13-7.

164. Tsai, C.P., et al., *A hexanucleotide repeat expansion in C9ORF72 causes familial and sporadic ALS in Taiwan*. Neurobiol Aging, 2012. **33**(9): p. 2232.e11-2232.e18.
165. Curtis, A.F., et al., *Sex differences in the prevalence of genetic mutations in FTD and ALS: A meta-analysis*. Neurology, 2017. **89**(15): p. 1633-1642.
166. Chio, A., et al., *Clinical characteristics of patients with familial amyotrophic lateral sclerosis carrying the pathogenic GGGGCC hexanucleotide repeat expansion of C9ORF72*. Brain, 2012. **135**(Pt 3): p. 784-93.
167. Rooney, J., et al., *C9orf72 expansion differentially affects males with spinal onset amyotrophic lateral sclerosis*. J Neurol Neurosurg Psychiatry, 2017. **88**(4): p. 281.
168. Hübers, A., et al., *Polymerase chain reaction and Southern blot-based analysis of the C9orf72 hexanucleotide repeat in different motor neuron diseases*. Neurobiology of Aging, 2014. **35**(5): p. 1214.e1-1214.e6.
169. Ash, P.E., et al., *Unconventional translation of C9ORF72 GGGGCC expansion generates insoluble polypeptides specific to c9FTD/ALS*. Neuron, 2013. **77**(4): p. 639-46.
170. Schipper, L.J., et al., *Prevalence of brain and spinal cord inclusions, including dipeptide repeat proteins, in patients with the C9ORF72 hexanucleotide repeat expansion: a systematic neuropathological review*. Neuropathol Appl Neurobiol, 2016. **42**(6): p. 547-60.
171. Zhang, Y.J., et al., *Aggregation-prone c9FTD/ALS poly(GA) RAN-translated proteins cause neurotoxicity by inducing ER stress*. Acta Neuropathol, 2014. **128**(4): p. 505-24.
172. Mori, K., et al., *Bidirectional transcripts of the expanded C9orf72 hexanucleotide repeat are translated into aggregating dipeptide repeat proteins*. Acta Neuropathol, 2013. **126**(6): p. 881-93.
173. Muller, K., et al., *Comprehensive analysis of the mutation spectrum in 301 German ALS families*. J Neurol Neurosurg Psychiatry, 2018.
174. Ng, A.S.L. and E.K. Tan, *Intermediate C9orf72 alleles in neurological disorders: does size really matter?* J Med Genet, 2017. **54**(9): p. 591-597.
175. Zhang, D., et al., *Discovery of Novel DENN Proteins: Implications for the Evolution of Eukaryotic Intracellular Membrane Structures and Human Disease*. Front Genet, 2012. **3**: p. 283.
176. Levine, T.P., et al., *The product of C9orf72, a gene strongly implicated in neurodegeneration, is structurally related to DENN Rab-GEFs*. Bioinformatics, 2013. **29**(4): p. 499-503.
177. Farg, M.A., et al., *C9ORF72, implicated in amyotrophic lateral sclerosis and frontotemporal dementia, regulates endosomal trafficking*. Human Molecular Genetics, 2014.
178. Sellier, C., et al., *Loss of C9ORF72 impairs autophagy and synergizes with polyQ Ataxin - 2 to induce motor neuron dysfunction and cell death*. The EMBO Journal, 2016. **35**(12): p. 1276-1297.
179. Shi, Y., et al., *Haploinsufficiency leads to neurodegeneration in C9ORF72 ALS/FTD human induced motor neurons*. Nat Med, 2018. **24**(3): p. 313-325.
180. Belzil, V.V., et al., *Reduced C9orf72 gene expression in c9FTD/ALS is caused by histone trimethylation, an epigenetic event detectable in blood*. Acta Neuropathol, 2013. **126**(6): p. 895-905.
181. Saberi, S., et al., *Sense-encoded poly-GR dipeptide repeat proteins correlate to neurodegeneration and uniquely co-localize with TDP-43 in dendrites of repeat-expanded C9orf72 amyotrophic lateral sclerosis*. Acta Neuropathol, 2018. **135**(3): p. 459-474.
182. Therrien, M., et al., *Deletion of C9ORF72 results in motor neuron degeneration and stress sensitivity in C. elegans*. PLoS One, 2013. **8**(12): p. e83450.

183. Ciura, S., et al., *Loss of function of C9orf72 causes motor deficits in a zebrafish model of amyotrophic lateral sclerosis*. Ann Neurol, 2013. **74**(2): p. 180-7.
184. Yeh, T.H., et al., *C9orf72 is essential for neurodevelopment and motility mediated by Cyclin G1*. Exp Neurol, 2018. **304**: p. 114-124.
185. Atanasio, A., et al., *C9orf72 ablation causes immune dysregulation characterized by leukocyte expansion, autoantibody production, and glomerulonephropathy in mice*. Sci Rep, 2016. **6**: p. 23204.
186. Sudria-Lopez, E., et al., *Full ablation of C9orf72 in mice causes immune system-related pathology and neoplastic events but no motor neuron defects*. Acta Neuropathol, 2016. **132**(1): p. 145-7.
187. Sullivan, P.M., et al., *The ALS/FTLD associated protein C9orf72 associates with SMCR8 and WDR41 to regulate the autophagy-lysosome pathway*. Acta Neuropathol Commun, 2016. **4**(1): p. 51.
188. Zu, T., et al., *RAN proteins and RNA foci from antisense transcripts in C9ORF72 ALS and frontotemporal dementia*. Proc Natl Acad Sci U S A, 2013. **110**(51): p. E4968-77.
189. Almeida, S., et al., *Modeling key pathological features of frontotemporal dementia with C9ORF72 repeat expansion in iPSC-derived human neurons*. Acta Neuropathol, 2013. **126**(3): p. 385-99.
190. Donnelly, C.J., et al., *RNA toxicity from the ALS/FTD C9ORF72 expansion is mitigated by antisense intervention*. Neuron, 2013. **80**(2): p. 415-28.
191. Zu, T., et al., *Non-ATG-initiated translation directed by microsatellite expansions*. Proc Natl Acad Sci U S A, 2011. **108**(1): p. 260-5.
192. Mori, K., et al., *The C9orf72 GGGGCC repeat is translated into aggregating dipeptide-repeat proteins in FTL/ALS*. Science, 2013. **339**(6125): p. 1335-8.
193. Chang, Y.J., et al., *The Glycine-Alanine Dipeptide Repeat from C9orf72 Hexanucleotide Expansions Forms Toxic Amyloids Possessing Cell-to-Cell Transmission Properties*. J Biol Chem, 2016. **291**(10): p. 4903-11.
194. Freibaum, B.D. and J.P. Taylor, *The Role of Dipeptide Repeats in C9ORF72-Related ALS-FTD*. Frontiers in Molecular Neuroscience, 2017. **10**(35).
195. Freibaum, B.D., et al., *GGGGCC repeat expansion in C9orf72 compromises nucleocytoplasmic transport*. Nature, 2015. **525**(7567): p. 129-33.
196. Zhang, K., et al., *The C9orf72 repeat expansion disrupts nucleocytoplasmic transport*. Nature, 2015. **525**(7567): p. 56-61.
197. Zhang, K., et al., *Stress Granule Assembly Disrupts Nucleocytoplasmic Transport*. Cell, 2018.
198. Westergard, T., et al., *Cell-to-Cell Transmission of Dipeptide Repeat Proteins Linked to C9orf72-ALS/FTD*. Cell Rep, 2016. **17**(3): p. 645-652.
199. Zhou, Q., et al., *Antibodies inhibit transmission and aggregation of C9orf72 poly-GA dipeptide repeat proteins*. EMBO Mol Med, 2017. **9**(5): p. 687-702.
200. Shantanu, S., et al., *VEGF alleviates ALS-CSF induced cytoplasmic accumulations of TDP-43 and FUS/TLS in NSC-34 cells*. J Chem Neuroanat, 2017. **81**: p. 48-52.
201. Al-Chalabi, A., et al., *The genetics and neuropathology of amyotrophic lateral sclerosis*. Acta Neuropathol, 2012. **124**(3): p. 339-52.
202. Robinson, J.L., et al., *TDP-43 skeins show properties of amyloid in a subset of ALS cases*. Acta Neuropathol, 2013. **125**(1): p. 121-31.
203. Lin, W.L. and D.W. Dickson, *Ultrastructural localization of TDP-43 in filamentous neuronal inclusions in various neurodegenerative diseases*. Acta Neuropathol, 2008. **116**(2): p. 205-13.
204. Kimura, T., et al., *Bunina bodies in motor and non-motor neurons revisited: a pathological study of an ALS patient after long-term survival on a respirator*. Neuropathology, 2014. **34**(4): p. 392-7.

205. Mori, F., et al., *Co-localization of Bunina bodies and TDP-43 inclusions in lower motor neurons in amyotrophic lateral sclerosis*. Neuropathology, 2014. **34**(1): p. 71-6.
206. Fujita, Y., et al., *Different clinical and neuropathologic phenotypes of familial ALS with A315E TARDBP mutation*. Neurology, 2011. **77**(15): p. 1427-31.
207. Blokhuis, A.M., et al., *Protein aggregation in amyotrophic lateral sclerosis*. Acta Neuropathol, 2013. **125**(6): p. 777-94.
208. Sasaki, S., et al., *Alterations in subcellular localization of TDP-43 immunoreactivity in the anterior horns in sporadic amyotrophic lateral sclerosis*. Neurosci Lett, 2010. **478**(2): p. 72-6.
209. Tan, C.F., et al., *TDP-43 immunoreactivity in neuronal inclusions in familial amyotrophic lateral sclerosis with or without SOD1 gene mutation*. Acta Neuropathol, 2007. **113**(5): p. 535-42.
210. Shibata, N., et al., *Immunohistochemical study on superoxide dismutases in spinal cords from autopsied patients with amyotrophic lateral sclerosis*. Dev Neurosci, 1996. **18**(5-6): p. 492-8.
211. Jiang, H., et al., *Familial amyotrophic lateral sclerosis with an I104F mutation in the SOD1 gene: Multisystem degeneration with neurofilamentous aggregates and SOD1 inclusions*. Neuropathology, 2017. **37**(1): p. 69-77.
212. Forsberg, K., et al., *Novel antibodies reveal inclusions containing non-native SOD1 in sporadic ALS patients*. PLoS One, 2010. **5**(7): p. e11552.
213. Brettschneider, J., et al., *Pattern of ubiquitin pathology in ALS and FTLN indicates presence of C9orf72 hexanucleotide expansion*. Acta Neuropathol, 2012. **123**(6): p. 825-39.
214. Al-Sarraj, S., et al., *p62 positive, TDP-43 negative, neuronal cytoplasmic and intranuclear inclusions in the cerebellum and hippocampus define the pathology of C9orf72-linked FTLN and MND/ALS*. Acta Neuropathol, 2011. **122**(6): p. 691-702.
215. Cykowski, M.D., et al., *Phosphorylated TDP-43 (pTDP-43) aggregates in the axial skeletal muscle of patients with sporadic and familial amyotrophic lateral sclerosis*. Acta Neuropathologica Communications, 2018. **6**(1): p. 28.
216. Davidson, Y.S., et al., *Immunohistochemical detection of C9orf72 protein in frontotemporal lobar degeneration and motor neurone disease: patterns of immunostaining and an evaluation of commercial antibodies*. Amyotroph Lateral Scler Frontotemporal Degener, 2018. **19**(1-2): p. 102-111.
217. Mori, K., et al., *hnRNP A3 binds to GGGGCC repeats and is a constituent of p62-positive/TDP43-negative inclusions in the hippocampus of patients with C9orf72 mutations*. Acta Neuropathol, 2013. **125**(3): p. 413-23.
218. Simon-Sanchez, J., et al., *The clinical and pathological phenotype of C9orf72 hexanucleotide repeat expansions*. Brain, 2012. **135**(Pt 3): p. 723-35.
219. Lee, Y.B., et al., *C9orf72 poly GA RAN-translated protein plays a key role in amyotrophic lateral sclerosis via aggregation and toxicity*. Hum Mol Genet, 2017. **26**(24): p. 4765-4777.
220. Keller, B.A., et al., *Co-aggregation of RNA binding proteins in ALS spinal motor neurons: evidence of a common pathogenic mechanism*. Acta Neuropathol, 2012. **124**(5): p. 733-47.
221. Blair, I.P., et al., *FUS mutations in amyotrophic lateral sclerosis: clinical, pathological, neurophysiological and genetic analysis*. J Neurol Neurosurg Psychiatry, 2010. **81**(6): p. 639-45.
222. Matsuoka, T., et al., *An autopsied case of sporadic adult-onset amyotrophic lateral sclerosis with FUS-positive basophilic inclusions*. Neuropathology, 2011. **31**(1): p. 71-6.

223. Kusaka, H., S. Matsumoto, and T. Imai, *Adult-onset motor neuron disease with basophilic intraneuronal inclusion bodies*. Clin Neuropathol, 1993. **12**(4): p. 215-8.
224. Fujita, Y., et al., *Numerous FUS-positive inclusions in an elderly woman with motor neuron disease*. Neuropathology, 2011. **31**(2): p. 170-6.
225. Huang, E.J., et al., *Extensive FUS-immunoreactive pathology in juvenile amyotrophic lateral sclerosis with basophilic inclusions*. Brain Pathol, 2010. **20**(6): p. 1069-76.
226. Mackenzie, I.R., et al., *Pathological heterogeneity in amyotrophic lateral sclerosis with FUS mutations: two distinct patterns correlating with disease severity and mutation*. Acta Neuropathol, 2011. **122**(1): p. 87-98.
227. Ciryam, P., et al., *Spinal motor neuron protein supersaturation patterns are associated with inclusion body formation in ALS*. Proc Natl Acad Sci U S A, 2017. **114**(20): p. E3935-e3943.
228. Brotherton, T.E., et al., *Localization of a toxic form of superoxide dismutase 1 protein to pathologically affected tissues in familial ALS*. Proc Natl Acad Sci U S A, 2012. **109**(14): p. 5505-10.
229. Witan, H., et al., *Heterodimer formation of wild-type and amyotrophic lateral sclerosis-causing mutant Cu/Zn-superoxide dismutase induces toxicity independent of protein aggregation*. Hum Mol Genet, 2008. **17**(10): p. 1373-85.
230. Van Damme, P., et al., *GluR2 deficiency accelerates motor neuron degeneration in a mouse model of amyotrophic lateral sclerosis*. J Neuropathol Exp Neurol, 2005. **64**(7): p. 605-12.
231. Wainger, B.J. and M.E. Cudkowicz, *Cortical Hyperexcitability in Amyotrophic Lateral Sclerosis: C9orf72 Repeats*. JAMA Neurol, 2015. **72**(11): p. 1235-6.
232. Geevasinga, N., et al., *Cortical Function in Asymptomatic Carriers and Patients With C9orf72 Amyotrophic Lateral Sclerosis*. JAMA Neurol, 2015. **72**(11): p. 1268-74.
233. Bae, J.S., et al., *Cortical excitability differences between flexor pollicis longus and APB*. Neuroscience Letters, 2013. **541**: p. 150-154.
234. Vucic, S., G.A. Nicholson, and M.C. Kiernan, *Cortical hyperexcitability may precede the onset of familial amyotrophic lateral sclerosis*. Brain, 2008. **131**(Pt 6): p. 1540-50.
235. Vucic, S. and M.C. Kiernan, *Chapter 45 - Utility of transcranial magnetic stimulation in delineating amyotrophic lateral sclerosis pathophysiology*, in *Handbook of Clinical Neurology*, A.M. Lozano and M. Hallett, Editors. 2013, Elsevier. p. 561-575.
236. Rothstein, J.D., et al., *Abnormal excitatory amino acid metabolism in amyotrophic lateral sclerosis*. Ann Neurol, 1990. **28**(1): p. 18-25.
237. Rothstein, J.D., et al., *Excitatory amino acids in amyotrophic lateral sclerosis: an update*. Ann Neurol, 1991. **30**(2): p. 224-5.
238. Shaw, P.J., et al., *CSF and plasma amino acid levels in motor neuron disease: elevation of CSF glutamate in a subset of patients*. Neurodegeneration, 1995. **4**(2): p. 209-16.
239. Spreux-Varoquaux, O., et al., *Glutamate levels in cerebrospinal fluid in amyotrophic lateral sclerosis: a reappraisal using a new HPLC method with coulometric detection in a large cohort of patients*. J Neurol Sci, 2002. **193**(2): p. 73-8.
240. Danbolt, N.C., D.N. Furness, and Y. Zhou, *Neuronal vs glial glutamate uptake: Resolving the conundrum*. Neurochem Int, 2016. **98**: p. 29-45.
241. Malarkey, E.B. and V. Parpura, *Mechanisms of glutamate release from astrocytes*. Neurochemistry International, 2008. **52**(1): p. 142-154.
242. Tanaka, K., et al., *Epilepsy and exacerbation of brain injury in mice lacking the glutamate transporter GLT-1*. Science, 1997. **276**(5319): p. 1699-702.
243. Fray, A.E., et al., *The expression of the glial glutamate transporter protein EAAT2 in motor neuron disease: an immunohistochemical study*. Eur J Neurosci, 1998. **10**(8): p. 2481-9.

244. Rothstein, J.D., et al., *Selective loss of glial glutamate transporter GLT-1 in amyotrophic lateral sclerosis*. Ann Neurol, 1995. **38**(1): p. 73-84.
245. Sasaki, S., T. Komori, and M. Iwata, *Excitatory amino acid transporter 1 and 2 immunoreactivity in the spinal cord in amyotrophic lateral sclerosis*. Acta Neuropathol, 2000. **100**(2): p. 138-44.
246. Rosenblum, L.T. and D. Trotti, *EAAT2 and the Molecular Signature of Amyotrophic Lateral Sclerosis*. Adv Neurobiol, 2017. **16**: p. 117-136.
247. Do-Ha, D., Y. Buskila, and L. Ooi, *Impairments in Motor Neurons, Interneurons and Astrocytes Contribute to Hyperexcitability in ALS: Underlying Mechanisms and Paths to Therapy*. Mol Neurobiol, 2018. **55**(2): p. 1410-1418.
248. Enterzari-Taher, M., et al., *Abnormalities of cortical inhibitory neurons in amyotrophic lateral sclerosis*. Muscle Nerve, 1997. **20**(1): p. 65-71.
249. Ziemann, U., et al., *Impaired motor cortex inhibition in patients with amyotrophic lateral sclerosis. Evidence from paired transcranial magnetic stimulation*. Neurology, 1997. **49**(5): p. 1292-8.
250. Zanette, G., et al., *Changes in motor cortex inhibition over time in patients with amyotrophic lateral sclerosis*. J Neurol, 2002. **249**(12): p. 1723-8.
251. Karandreas, N., et al., *Impaired interhemispheric inhibition in amyotrophic lateral sclerosis*. Amyotroph Lateral Scler, 2007. **8**(2): p. 112-8.
252. Petri, D., et al., *GABAA-receptor activation in the subthalamic nucleus compensates behavioral asymmetries in the hemiparkinsonian rat*. Behav Brain Res, 2013. **252**: p. 58-67.
253. Petri, S., et al., *The cellular mRNA expression of GABA and glutamate receptors in spinal motor neurons of SOD1 mice*. J Neurol Sci, 2005. **238**(1-2): p. 25-30.
254. Nieto-Gonzalez, J.L., et al., *Reduced GABAergic inhibition explains cortical hyperexcitability in the wobbler mouse model of ALS*. Cereb Cortex, 2011. **21**(3): p. 625-35.
255. Moser, J.M., P. Bigini, and T. Schmitt-John, *The wobbler mouse, an ALS animal model*. Molecular Genetics and Genomics, 2013. **288**(5): p. 207-229.
256. Bonanno, G., et al., *Release of [³H]d-aspartate induced by K⁺-stimulation is increased in the cervical spinal cord of the wobbler mouse: a model of motor neuron disease*. Neurochemistry International, 2009. **55**(5): p. 302-306.
257. Zhang, W., et al., *Hyperactive somatostatin interneurons contribute to excitotoxicity in neurodegenerative disorders*. Nat Neurosci, 2016. **19**(4): p. 557-559.
258. Bensimon, G., L. Lacomblez, and V. Meininger, *A Controlled Trial of Riluzole in Amyotrophic Lateral Sclerosis*. New England Journal of Medicine, 1994. **330**(9): p. 585-591.
259. Geevasinga, N., et al., *Riluzole exerts transient modulating effects on cortical and axonal hyperexcitability in ALS*. Amyotroph Lateral Scler Frontotemporal Degener, 2016. **17**(7-8): p. 580-588.
260. Doble, A., *The pharmacology and mechanism of action of riluzole*. Neurology, 1996. **47**(6 Suppl 4): p. 233S-241S.
261. Wokke, J., *Riluzole*. The Lancet, 1996. **348**(9030): p. 795-799.
262. Dall'Igna, O.P., et al., *Riluzole increases glutamate uptake by cultured C6 astroglial cells*. Int J Dev Neurosci, 2013. **31**(7): p. 482-6.
263. Lamanauskas, N. and A. Nistri, *Riluzole blocks persistent Na⁺ and Ca²⁺ currents and modulates release of glutamate via presynaptic NMDA receptors on neonatal rat hypoglossal motoneurons in vitro*. Eur J Neurosci, 2008. **27**(10): p. 2501-14.
264. Kretschmer, B.D., U. Kratzer, and W.J. Schmidt, *Riluzole, a glutamate release inhibitor, and motor behavior*. Naunyn Schmiedeberg's Arch Pharmacol, 1998. **358**(2): p. 181-90.

265. Jaiswal, M.K., *Riluzole But Not Melatonin Ameliorates Acute Motor Neuron Degeneration and Moderately Inhibits SOD1-Mediated Excitotoxicity Induced Disrupted Mitochondrial Ca²⁺ Signaling in Amyotrophic Lateral Sclerosis*. *Frontiers in Cellular Neuroscience*, 2017. **10**(295).
266. Osellame, L.D., T.S. Blacker, and M.R. Duchen, *Cellular and molecular mechanisms of mitochondrial function*. *Best Pract Res Clin Endocrinol Metab*, 2012. **26**(6): p. 711-23.
267. Smith, E.F., P.J. Shaw, and K.J. De Vos, *The role of mitochondria in amyotrophic lateral sclerosis*. *Neurosci Lett*, 2017.
268. Sawada, H., *Clinical efficacy of edaravone for the treatment of amyotrophic lateral sclerosis*. *Expert Opin Pharmacother*, 2017. **18**(7): p. 735-738.
269. Rothstein, J.D., *Edaravone: A new drug approved for ALS*. *Cell*, 2017. **171**(4): p. 725.
270. Yamamoto, Y., *Plasma marker of tissue oxidative damage and edaravone as a scavenger drug against peroxyl radicals and peroxynitrite*. *J Clin Biochem Nutr*, 2017. **60**(1): p. 49-54.
271. Ademowo, O.S., et al., *Lipid (per) oxidation in mitochondria: an emerging target in the ageing process?* *Biogerontology*, 2017. **18**(6): p. 859-879.
272. Delic, V., et al., *Discrete mitochondrial aberrations in the spinal cord of sporadic ALS patients*. *J Neurosci Res*, 2018.
273. Sasaki, S. and M. Iwata, *Ultrastructural study of synapses in the anterior horn neurons of patients with amyotrophic lateral sclerosis*. *Neuroscience Letters*, 1996. **204**(1): p. 53-56.
274. Chung, M.J. and Y.L. Suh, *Ultrastructural changes of mitochondria in the skeletal muscle of patients with amyotrophic lateral sclerosis*. *Ultrastruct Pathol*, 2002. **26**(1): p. 3-7.
275. Davis, S.A., et al., *TDP-43 interacts with mitochondrial proteins critical for mitophagy and mitochondrial dynamics*. *Neurosci Lett*, 2018. **678**: p. 8-15.
276. Deng, J., et al., *FUS Interacts with HSP60 to Promote Mitochondrial Damage*. *PLoS Genet*, 2015. **11**(9): p. e1005357.
277. Blokhuis, A.M., et al., *Comparative interactomics analysis of different ALS-associated proteins identifies converging molecular pathways*. *Acta Neuropathol*, 2016.
278. Wang, W., et al., *The inhibition of TDP-43 mitochondrial localization blocks its neuronal toxicity*. *Nature Medicine*, 2016. **22**: p. 869.
279. Higgins, C.M., et al., *Mutant Cu, Zn superoxide dismutase that causes motoneuron degeneration is present in mitochondria in the CNS*. *J Neurosci*, 2002. **22**(6): p. Rc215.
280. Lopez-Gonzalez, R., et al., *Poly(GR) in C9ORF72-Related ALS/FTD Compromises Mitochondrial Function and Increases Oxidative Stress and DNA Damage in iPSC-Derived Motor Neurons*. *Neuron*, 2016. **92**(2): p. 383-391.
281. Ruxandra, D., et al., *C9orf72 Hexanucleotide Expansions Are Associated with Altered Endoplasmic Reticulum Calcium Homeostasis and Stress Granule Formation in Induced Pluripotent Stem Cell - Derived Neurons from Patients with Amyotrophic Lateral Sclerosis and Frontotemporal Dementia*. *STEM CELLS*, 2016. **34**(8): p. 2063-2078.
282. Tradewell, M.L., et al., *Arginine methylation by PRMT1 regulates nuclear-cytoplasmic localization and toxicity of FUS/TLS harbouring ALS-linked mutations*. *Hum Mol Genet*, 2012. **21**(1): p. 136-49.
283. Sharma, A., et al., *ALS-associated mutant FUS induces selective motor neuron degeneration through toxic gain of function*. *Nat Commun*, 2016. **7**: p. 10465.
284. Hong, K., et al., *Full-length TDP-43 and its C-terminal fragments activate mitophagy in NSC34 cell line*. *Neuroscience Letters*, 2012. **530**(2): p. 144-149.

285. Magrane, J., et al., *Abnormal mitochondrial transport and morphology are common pathological denominators in SOD1 and TDP43 ALS mouse models*. Hum Mol Genet, 2014. **23**(6): p. 1413-24.
286. De Vos, K.J., et al., *Familial amyotrophic lateral sclerosis-linked SOD1 mutants perturb fast axonal transport to reduce axonal mitochondria content*. Hum Mol Genet, 2007. **16**(22): p. 2720-2728.
287. Wang, W., et al., *The ALS disease-associated mutant TDP-43 impairs mitochondrial dynamics and function in motor neurons*. Hum Mol Genet, 2013. **22**(23): p. 4706-19.
288. Onesto, E., et al., *Gene-specific mitochondria dysfunctions in human TARDBP and C9ORF72 fibroblasts*. Acta Neuropathologica Communications, 2016. **4**(1): p. 47.
289. Csordas, G., et al., *Structural and functional features and significance of the physical linkage between ER and mitochondria*. J Cell Biol, 2006. **174**(7): p. 915-21.
290. Lau, D.H.W., et al., *Disruption of ER-mitochondria signalling in fronto-temporal dementia and related amyotrophic lateral sclerosis*. Cell Death Dis, 2018. **9**(3): p. 327.
291. Stoica, R., et al., *ER-mitochondria associations are regulated by the VAPB-PTPIP51 interaction and are disrupted by ALS/FTD-associated TDP-43*. Nat Commun, 2014. **5**: p. 3996.
292. Stoica, R., et al., *ALS/FTD-associated FUS activates GSK-3beta to disrupt the VAPB-PTPIP51 interaction and ER-mitochondria associations*. EMBO Rep, 2016.
293. Bernard-Marissal, N., et al., *Dysfunction in endoplasmic reticulum-mitochondria crosstalk underlies SIGMAR1 loss of function mediated motor neuron degeneration*. Brain, 2015. **138**(Pt 4): p. 875-90.
294. Mavlyutov, T.A., et al., *Lack of sigma-1 receptor exacerbates ALS progression in mice*. Neuroscience, 2013. **240**: p. 129-34.
295. Watanabe, S., et al., *Mitochondria-associated membrane collapse is a common pathomechanism in SIGMAR1- and SOD1-linked ALS*. EMBO Mol Med, 2016. **8**(12): p. 1421-1437.
296. Nishimura, A.L., et al., *A mutation in the vesicle-trafficking protein VAPB causes late-onset spinal muscular atrophy and amyotrophic lateral sclerosis*. Am J Hum Genet, 2004. **75**(5): p. 822-31.
297. van Vliet, A.R. and P. Agostinis, *Mitochondria-Associated Membranes and ER Stress*. Curr Top Microbiol Immunol, 2018. **414**: p. 73-102.
298. Okamoto, K. and N. Kondo-Okamoto, *Mitochondria and autophagy: Critical interplay between the two homeostats*. Biochimica et Biophysica Acta (BBA) - General Subjects, 2012. **1820**(5): p. 595-600.
299. Smith, E.F., P.J. Shaw, and K.J. De Vos, *The role of mitochondria in amyotrophic lateral sclerosis*. Neuroscience Letters, 2017.
300. Kim, Nam C., et al., *VCP Is Essential for Mitochondrial Quality Control by PINK1/Parkin and this Function Is Impaired by VCP Mutations*. Neuron, 2013. **78**(1): p. 65-80.
301. Xie, Y., et al., *Endolysosomal Deficits Augment Mitochondria Pathology in Spinal Motor Neurons of Asymptomatic fALS Mice*. Neuron, 2015. **87**(2): p. 355-370.
302. Corcia, P., et al., *Molecular imaging of microglial activation in amyotrophic lateral sclerosis*. PLoS One, 2012. **7**(12): p. e52941.
303. Turner, M.R., et al., *Evidence of widespread cerebral microglial activation in amyotrophic lateral sclerosis: an [11C](R)-PK11195 positron emission tomography study*. Neurobiol Dis, 2004. **15**(3): p. 601-9.
304. Engelhardt, J.I. and S.H. Appel, *IgG reactivity in the spinal cord and motor cortex in amyotrophic lateral sclerosis*. Arch Neurol, 1990. **47**(11): p. 1210-6.
305. Kato, S., et al., *Pathological characterization of astrocytic hyaline inclusions in familial amyotrophic lateral sclerosis*. Am J Pathol, 1997. **151**(2): p. 611-20.

306. Kato, S., et al., *New consensus research on neuropathological aspects of familial amyotrophic lateral sclerosis with superoxide dismutase 1 (SOD1) gene mutations: inclusions containing SOD1 in neurons and astrocytes*. Amyotroph Lateral Scler Other Motor Neuron Disord, 2000. **1**(3): p. 163-84.
307. Freischmidt, A., et al., *Haploinsufficiency of TBK1 causes familial ALS and frontotemporal dementia*. Nat Neurosci, 2015. **18**(5): p. 631-6.
308. Cruts, M., et al., *Null mutations in progranulin cause ubiquitin-positive frontotemporal dementia linked to chromosome 17q21*. Nature, 2006. **442**(7105): p. 920-4.
309. Pickering-Brown, S.M., et al., *Mutations in progranulin explain atypical phenotypes with variants in MAPT*. Brain, 2006. **129**(Pt 11): p. 3124-6.
310. Gass, J., et al., *Mutations in progranulin are a major cause of ubiquitin-positive frontotemporal lobar degeneration*. Hum Mol Genet, 2006. **15**(20): p. 2988-3001.
311. Haidet-Phillips, A.M., et al., *Astrocytes from familial and sporadic ALS patients are toxic to motor neurons*. Nat Biotechnol, 2011. **29**(9): p. 824-8.
312. Pramatarova, A., et al., *Neuron-specific expression of mutant superoxide dismutase 1 in transgenic mice does not lead to motor impairment*. J Neurosci, 2001. **21**(10): p. 3369-74.
313. Urushitani, M., et al., *Chromogranin-mediated secretion of mutant superoxide dismutase proteins linked to amyotrophic lateral sclerosis*. Nat Neurosci, 2006. **9**(1): p. 108-18.
314. Zhao, W., et al., *Extracellular mutant SOD1 induces microglial-mediated motoneuron injury*. Glia, 2010. **58**(2): p. 231-43.
315. Roberts, K., et al., *Extracellular aggregated Cu/Zn superoxide dismutase activates microglia to give a cytotoxic phenotype*. Glia, 2013. **61**(3): p. 409-19.
316. Maimon, R., et al., *miR126-5p Downregulation Facilitates Axon Degeneration and NMJ Disruption via a Non-Cell-Autonomous Mechanism in ALS*. J Neurosci, 2018. **38**(24): p. 5478-5494.
317. Dikic, I. and Z. Elazar, *Mechanism and medical implications of mammalian autophagy*. Nat Rev Mol Cell Biol, 2018.
318. Fifita, J.A., et al., *A novel amyotrophic lateral sclerosis mutation in OPTN induces ER stress and Golgi fragmentation in vitro*. Amyotroph Lateral Scler Frontotemporal Degener, 2017. **18**(1-2): p. 126-133.
319. Tohnai, G., et al., *Frequency and characteristics of the TBK1 gene variants in Japanese patients with sporadic amyotrophic lateral sclerosis*. Neurobiol Aging, 2018. **64**: p. 158.e15-158.e19.
320. Gomez-Tortosa, E., et al., *Familial primary lateral sclerosis or dementia associated with Arg573Gly TBK1 mutation*. J Neurol Neurosurg Psychiatry, 2017. **88**(11): p. 996-997.
321. Abramzon, Y., et al., *Valosin-containing protein (VCP) mutations in sporadic amyotrophic lateral sclerosis*. Neurobiol Aging, 2012. **33**(9): p. 2231.e1-2231.e6.
322. Johnson, J.O., et al., *Exome sequencing reveals VCP mutations as a cause of familial ALS*. Neuron, 2010. **68**(5): p. 857-64.
323. Daoud, H., et al., *UBQLN2 mutations are rare in French and French-Canadian amyotrophic lateral sclerosis*. Neurobiol Aging, 2012. **33**(9): p. 2230.e1-2230.e5.
324. Yang, Y., et al., *The gene encoding alsin, a protein with three guanine-nucleotide exchange factor domains, is mutated in a form of recessive amyotrophic lateral sclerosis*. Nat Genet, 2001. **29**(2): p. 160-5.
325. Cox, L.E., et al., *Mutations in CHMP2B in lower motor neuron predominant amyotrophic lateral sclerosis (ALS)*. PLoS One, 2010. **5**(3): p. e9872.
326. Bertolin, C., et al., *New FIG4 gene mutations causing aggressive ALS*. Eur J Neurol, 2018. **25**(3): p. e41-e42.

327. Osmanovic, A., et al., *FIG4 variants in central European patients with amyotrophic lateral sclerosis: a whole-exome and targeted sequencing study*. Eur J Hum Genet, 2017. **25**(3): p. 324-331.
328. Zaffagnini, G. and S. Martens, *Mechanisms of Selective Autophagy*. J Mol Biol, 2016. **428**(9 Pt A): p. 1714-24.
329. Nguyen, D.K.H., R. Thombre, and J. Wang, *Autophagy as a Common Pathway in Amyotrophic Lateral Sclerosis*. Neurosci Lett, 2018.
330. Sasaki, S., *Autophagy in spinal cord motor neurons in sporadic amyotrophic lateral sclerosis*. J Neuropathol Exp Neurol, 2011. **70**(5): p. 349-59.
331. Ramesh, N. and U.B. Pandey, *Autophagy Dysregulation in ALS: When Protein Aggregates Get Out of Hand*. Front Mol Neurosci, 2017. **10**: p. 263.
332. Fecto, F., et al., *SQSTM1 mutations in familial and sporadic amyotrophic lateral sclerosis*. Arch Neurol, 2011. **68**(11): p. 1440-6.
333. Rea, S.L., et al., *SQSTM1 mutations--bridging Paget disease of bone and ALS/FTLD*. Exp Cell Res, 2014. **325**(1): p. 27-37.
334. Teyssou, E., et al., *Mutations in SQSTM1 encoding p62 in amyotrophic lateral sclerosis: genetics and neuropathology*. Acta Neuropathol, 2013. **125**(4): p. 511-22.
335. Goode, A., et al., *Defective recognition of LC3B by mutant SQSTM1/p62 implicates impairment of autophagy as a pathogenic mechanism in ALS-FTLD*. Autophagy, 2016. **12**(7): p. 1094-104.
336. Webster, C.P., et al., *The C9orf72 protein interacts with Rab1a and the ULK1 complex to regulate initiation of autophagy*. Embo j, 2016. **35**(15): p. 1656-76.
337. Morimoto, N., et al., *Increased autophagy in transgenic mice with a G93A mutant SOD1 gene*. Brain Research, 2007. **1167**: p. 112-117.
338. Soo, K.Y., et al., *ALS-associated mutant FUS inhibits macroautophagy which is restored by overexpression of Rab1*. Cell Death Dis, 2015. **1**: p. 15030.
339. Ryu, H.H., et al., *Autophagy regulates amyotrophic lateral sclerosis-linked fused in sarcoma-positive stress granules in neurons*. Neurobiol Aging, 2014. **35**(12): p. 2822-31.
340. Marrone, L., et al., *Isogenic FUS-eGFP iPSC Reporter Lines Enable Quantification of FUS Stress Granule Pathology that Is Rescued by Drugs Inducing Autophagy*. Stem Cell Reports, 2018. **10**(2): p. 375-389.
341. Colombrita, C., et al., *TDP-43 and FUS RNA-binding proteins bind distinct sets of cytoplasmic messenger RNAs and differently regulate their post-transcriptional fate in motoneuron-like cells*. J Biol Chem, 2012. **287**(19): p. 15635-47.
342. Hoell, J.I., et al., *RNA targets of wild-type and mutant FET family proteins*. Nat Struct Mol Biol, 2011. **18**(12): p. 1428-31.
343. Heidelberger, J.B., et al., *Proteomic profiling of VCP substrates links VCP to K6-linked ubiquitylation and c-Myc function*. EMBO Rep, 2018. **19**(4).
344. Vance, C., et al., *ALS mutant FUS disrupts nuclear localization and sequesters wild-type FUS within cytoplasmic stress granules*. Hum Mol Genet, 2013. **22**(13): p. 2676-88.
345. Wen, X., et al., *Antisense proline-arginine RAN dipeptides linked to C9ORF72-ALS/FTD form toxic nuclear aggregates that initiate in vitro and in vivo neuronal death*. Neuron, 2014. **84**(6): p. 1213-25.
346. Swinnen, B., et al., *A zebrafish model for C9orf72 ALS reveals RNA toxicity as a pathogenic mechanism*. Acta Neuropathol, 2018. **135**(3): p. 427-443.
347. Sareen, D., et al., *Targeting RNA foci in iPSC-derived motor neurons from ALS patients with a C9ORF72 repeat expansion*. Sci Transl Med, 2013. **5**(208): p. 208ra149.
348. Simone, R., et al., *G-quadruplex-binding small molecules ameliorate C9orf72 FTD/ALS pathology in vitro and in vivo*. EMBO Mol Med, 2018. **10**(1): p. 22-31.

349. Batra, R., et al., *Elimination of Toxic Microsatellite Repeat Expansion RNA by RNA-Targeting Cas9*. Cell, 2017. **170**(5): p. 899-912.e10.
350. DeJesus-Hernandez, M., et al., *In-depth clinico-pathological examination of RNA foci in a large cohort of C9ORF72 expansion carriers*. Acta Neuropathol, 2017. **134**(2): p. 255-269.
351. Feric, M., et al., *Coexisting Liquid Phases Underlie Nucleolar Subcompartments*. Cell, 2016. **165**(7): p. 1686-1697.
352. Neugebauer, K.M., *Special focus on the Cajal Body*. RNA Biol, 2017. **14**(6): p. 669-670.
353. Kroschwald, S., et al., *Promiscuous interactions and protein disaggregases determine the material state of stress-inducible RNP granules*. Elife, 2015. **4**: p. e06807.
354. Patel, A., et al., *A Liquid-to-Solid Phase Transition of the ALS Protein FUS Accelerated by Disease Mutation*. Cell, 2015. **162**(5): p. 1066-77.
355. Molliex, A., et al., *Phase Separation by Low Complexity Domains Promotes Stress Granule Assembly and Drives Pathological Fibrillization*. Cell, 2015. **163**(1): p. 123-33.
356. Bosco, D.A., et al., *Mutant FUS proteins that cause amyotrophic lateral sclerosis incorporate into stress granules*. Hum Mol Genet, 2010. **19**(21): p. 4160-75.
357. Daigle, J.G., et al., *RNA-binding ability of FUS regulates neurodegeneration, cytoplasmic mislocalization and incorporation into stress granules associated with FUS carrying ALS-linked mutations*. Hum Mol Genet, 2013. **22**(6): p. 1193-205.
358. McDonald, K.K., et al., *TAR DNA-binding protein 43 (TDP-43) regulates stress granule dynamics via differential regulation of G3BP and TIA-1*. Hum Mol Genet, 2011. **20**(7): p. 1400-10.
359. Anderson, P. and N. Kedersha, *RNA granules*. J Cell Biol, 2006. **172**(6): p. 803-8.
360. Fan, A.C. and A.K. Leung, *RNA Granules and Diseases: A Case Study of Stress Granules in ALS and FTL D*. Adv Exp Med Biol, 2016. **907**: p. 263-96.
361. White, J.P. and R.E. Lloyd, *Regulation of stress granules in virus systems*. Trends Microbiol, 2012. **20**(4): p. 175-83.
362. Kimball, S.R., et al., *Mammalian stress granules represent sites of accumulation of stalled translation initiation complexes*. Am J Physiol Cell Physiol, 2003. **284**(2): p. C273-84.
363. Kedersha, N., et al., *Stress granules and processing bodies are dynamically linked sites of mRNP remodeling*. J Cell Biol, 2005. **169**(6): p. 871-84.
364. Mokas, S., et al., *Uncoupling stress granule assembly and translation initiation inhibition*. Mol Biol Cell, 2009. **20**(11): p. 2673-83.
365. Kedersha, N.L., et al., *RNA-binding proteins TIA-1 and TIAR link the phosphorylation of eIF-2 alpha to the assembly of mammalian stress granules*. J Cell Biol, 1999. **147**(7): p. 1431-42.
366. Shin, Y. and C.P. Brangwynne, *Liquid phase condensation in cell physiology and disease*. Science, 2017. **357**(6357).
367. Uversky, V.N., *Intrinsically disordered proteins in overcrowded milieu: Membrane-less organelles, phase separation, and intrinsic disorder*. Curr Opin Struct Biol, 2017. **44**: p. 18-30.
368. Han, T.W., et al., *Cell-free formation of RNA granules: bound RNAs identify features and components of cellular assemblies*. Cell, 2012. **149**(4): p. 768-79.
369. Gilks, N., et al., *Stress granule assembly is mediated by prion-like aggregation of TIA-1*. Mol Biol Cell, 2004. **15**(12): p. 5383-98.
370. Guo, L., et al., *Nuclear-Import Receptors Reverse Aberrant Phase Transitions of RNA-Binding Proteins with Prion-like Domains*. Cell, 2018. **173**(3): p. 677-692.e20.
371. Qamar, S., et al., *FUS Phase Separation Is Modulated by a Molecular Chaperone and Methylation of Arginine Cation-pi Interactions*. Cell, 2018. **173**(3): p. 720-734.e15.

372. Leung, A.K., et al., *Poly(ADP-ribose) regulates stress responses and microRNA activity in the cytoplasm*. Mol Cell, 2011. **42**(4): p. 489-99.
373. Reineke, L.C., et al., *Casein Kinase 2 Is Linked to Stress Granule Dynamics through Phosphorylation of the Stress Granule Nucleating Protein G3BP1*. Mol Cell Biol, 2017. **37**(4).
374. Aguzzi, A. and M. Altmeyer, *Phase Separation: Linking Cellular Compartmentalization to Disease*. Trends Cell Biol, 2016. **26**(7): p. 547-558.
375. King, O.D., A.D. Gitler, and J. Shorter, *The tip of the iceberg: RNA-binding proteins with prion-like domains in neurodegenerative disease*. Brain Res, 2012. **1462**: p. 61-80.
376. Ramaswami, M., J.P. Taylor, and R. Parker, *Altered ribostasis: RNA-protein granules in degenerative disorders*. Cell, 2013. **154**(4): p. 727-36.
377. Conicella, A.E., et al., *ALS Mutations Disrupt Phase Separation Mediated by alpha-Helical Structure in the TDP-43 Low-Complexity C-Terminal Domain*. Structure, 2016. **24**(9): p. 1537-49.
378. Kato, M., et al., *Cell-free formation of RNA granules: low complexity sequence domains form dynamic fibers within hydrogels*. Cell, 2012. **149**(4): p. 753-67.
379. Murakami, T., et al., *ALS/FTD Mutation-Induced Phase Transition of FUS Liquid Droplets and Reversible Hydrogels into Irreversible Hydrogels Impairs RNP Granule Function*. Neuron, 2015. **88**(4): p. 678-90.
380. Schmidt, H.B. and R. Rohatgi, *In Vivo Formation of Vacuolated Multi-phase Compartments Lacking Membranes*. Cell Rep, 2016. **16**(5): p. 1228-1236.
381. St George-Hyslop, P., et al., *The physiological and pathological biophysics of phase separation and gelation of RNA binding proteins in amyotrophic lateral sclerosis and fronto-temporal lobar degeneration*. Brain Res, 2018.
382. Kim, H.J., et al., *Mutations in prion-like domains in hnRNPA2B1 and hnRNPA1 cause multisystem proteinopathy and ALS*. Nature, 2013. **495**(7442): p. 467-473.
383. Martinez, F.J., et al., *Protein-RNA Networks Regulated by Normal and ALS-Associated Mutant HNRNPA2B1 in the Nervous System*. Neuron, 2016. **92**(4): p. 780-795.
384. Li, H.R., et al., *TAR DNA-binding protein 43 (TDP-43) liquid-liquid phase separation is mediated by just a few aromatic residues*. J Biol Chem, 2018. **293**(16): p. 6090-6098.
385. Lim, L., et al., *ALS-Causing Mutations Significantly Perturb the Self-Assembly and Interaction with Nucleic Acid of the Intrinsically Disordered Prion-Like Domain of TDP-43*. PLoS Biol, 2016. **14**(1): p. e1002338.
386. Figley, M.D., et al., *Profilin 1 associates with stress granules and ALS-linked mutations alter stress granule dynamics*. J Neurosci, 2014. **34**(24): p. 8083-97.
387. Khalfallah, Y., et al., *TDP-43 regulation of stress granule dynamics in neurodegenerative disease-relevant cell types*. Sci Rep, 2018. **8**(1): p. 7551.
388. Maharjan, N., et al., *C9ORF72 Regulates Stress Granule Formation and Its Deficiency Impairs Stress Granule Assembly, Hypersensitizing Cells to Stress*. Mol Neurobiol, 2017. **54**(4): p. 3062-3077.
389. Boeynaems, S., et al., *Phase Separation of C9orf72 Dipeptide Repeats Perturbs Stress Granule Dynamics*. Mol Cell, 2017. **65**(6): p. 1044-1055.e5.
390. Van Treeck, B., et al., *RNA self-assembly contributes to stress granule formation and defining the stress granule transcriptome*. Proc Natl Acad Sci U S A, 2018. **115**(11): p. 2734-2739.
391. Fay, M.M., P.J. Anderson, and P. Ivanov, *ALS/FTD-Associated C9ORF72 Repeat RNA Promotes Phase Transitions In Vitro and in Cells*. Cell Rep, 2017. **21**(12): p. 3573-3584.
392. Lee, K.H., et al., *C9orf72 Dipeptide Repeats Impair the Assembly, Dynamics, and Function of Membrane-Less Organelles*. Cell, 2016. **167**(3): p. 774-788.e17.

393. Kaehler, C., et al., *Ataxin-2-like is a regulator of stress granules and processing bodies*. PLoS One, 2012. **7**(11): p. e50134.
394. Becker, L.A., et al., *Therapeutic reduction of ataxin-2 extends lifespan and reduces pathology in TDP-43 mice*. Nature, 2017. **544**: p. 367.
395. Chevalier-Larsen, E. and E.L.F. Holzbaur, *Axonal transport and neurodegenerative disease*. Biochimica et Biophysica Acta (BBA) - Molecular Basis of Disease, 2006. **1762**(11): p. 1094-1108.
396. Hirokawa, N., S. Niwa, and Y. Tanaka, *Molecular Motors in Neurons: Transport Mechanisms and Roles in Brain Function, Development, and Disease*. Neuron, 2010. **68**(4): p. 610-638.
397. Millecamps, S. and J.P. Julien, *Axonal transport deficits and neurodegenerative diseases*. Nat Rev Neurosci, 2013. **14**(3): p. 161-76.
398. Williamson, T.L. and D.W. Cleveland, *Slowing of axonal transport is a very early event in the toxicity of ALS-linked SOD1 mutants to motor neurons*. Nat Neurosci, 1999. **2**(1): p. 50-6.
399. Gibbs, K.L., et al., *Inhibiting p38 MAPK alpha rescues axonal retrograde transport defects in a mouse model of ALS*. Cell Death Dis, 2018. **9**(6): p. 596.
400. Hirokawa, N., S. Niwa, and Y. Tanaka, *Molecular motors in neurons: transport mechanisms and roles in brain function, development, and disease*. Neuron, 2010. **68**(4): p. 610-38.
401. Nicolas, A., et al., *Genome-wide Analyses Identify KIF5A as a Novel ALS Gene*. Neuron, 2018. **97**(6): p. 1268-1283.e6.
402. Daoud, H., et al., *Mutation analysis of PFN1 in familial amyotrophic lateral sclerosis patients*. Neurobiol Aging, 2013. **34**(4): p. 1311.e1-2.
403. Munch, C., et al., *Heterozygous R1101K mutation of the DCTN1 gene in a family with ALS and FTD*. Ann Neurol, 2005. **58**(5): p. 777-80.
404. Stockmann, M., et al., *The dynactin p150 subunit: cell biology studies of sequence changes found in ALS/MND and Parkinsonian syndromes*. J Neural Transm (Vienna), 2013. **120**(5): p. 785-98.
405. Smith, B.N., et al., *Novel mutations support a role for Profilin 1 in the pathogenesis of ALS*. Neurobiol Aging, 2015. **36**(3): p. 1602.e17-27.
406. Rademakers, R. and M. van Blitterswijk, *Excess of rare damaging TUBA4A variants suggests cytoskeletal defects in ALS*. Neuron, 2014. **84**(2): p. 241-3.
407. Smith, B.N., et al., *Exome-wide rare variant analysis identifies TUBA4A mutations associated with familial ALS*. Neuron, 2014. **84**(2): p. 324-31.
408. Bilsland, L.G., et al., *Deficits in axonal transport precede ALS symptoms in vivo*. Proc Natl Acad Sci U S A, 2010. **107**(47): p. 20523-8.
409. Zhang, F., et al., *Interaction between familial amyotrophic lateral sclerosis (ALS)-linked SOD1 mutants and the dynein complex*. J Biol Chem, 2007. **282**(22): p. 16691-9.
410. Zhang, B., et al., *Neurofilaments and orthograde transport are reduced in ventral root axons of transgenic mice that express human SOD1 with a G93A mutation*. J Cell Biol, 1997. **139**(5): p. 1307-15.
411. Baldwin, K.R., et al., *Axonal transport defects are a common phenotype in Drosophila models of ALS*. Hum Mol Genet, 2016. **25**(12): p. 2378-2392.
412. Hoelz, A., E.W. Debler, and G. Blobel, *The structure of the nuclear pore complex*. Annu Rev Biochem, 2011. **80**: p. 613-43.
413. Cronshaw, J.M., et al., *Proteomic analysis of the mammalian nuclear pore complex*. J Cell Biol, 2002. **158**(5): p. 915-27.

414. Bestembayeva, A., et al., *Nanoscale stiffness topography reveals structure and mechanics of the transport barrier in intact nuclear pore complexes*. Nat Nanotechnol, 2015. **10**(1): p. 60-64.
415. Kim, H.J. and J.P. Taylor, *Lost in Transportation: Nucleocytoplasmic Transport Defects in ALS and Other Neurodegenerative Diseases*. Neuron, 2017. **96**(2): p. 285-297.
416. Cautain, B., et al., *Components and regulation of nuclear transport processes*. Febs j, 2015. **282**(3): p. 445-62.
417. Chai, N. and A.D. Gitler, *Yeast screen for modifiers of C9orf72 poly(glycine-arginine) dipeptide repeat toxicity*. FEMS Yeast Res, 2018. **18**(4).
418. Kramer, N.J., et al., *CRISPR-Cas9 screens in human cells and primary neurons identify modifiers of C9ORF72 dipeptide-repeat-protein toxicity*. Nat Genet, 2018. **50**(4): p. 603-612.
419. Jovicic, A., et al., *Modifiers of C9orf72 dipeptide repeat toxicity connect nucleocytoplasmic transport defects to FTD/ALS*. Nat Neurosci, 2015. **18**(9): p. 1226-9.
420. Boeynaems, S., et al., *Drosophila screen connects nuclear transport genes to DPR pathology in c9ALS/FTD*. Sci Rep, 2016. **6**: p. 20877.
421. Woerner, A.C., et al., *Cytoplasmic protein aggregates interfere with nucleocytoplasmic transport of protein and RNA*. Science, 2016. **351**(6269): p. 173-176.
422. Neumann, M., et al., *Transportin 1 accumulates specifically with FET proteins but no other transportin cargos in FTL-D-FUS and is absent in FUS inclusions in ALS with FUS mutations*. Acta Neuropathol, 2012. **124**(5): p. 705-16.
423. Nishimura, A.L., et al., *Nuclear import impairment causes cytoplasmic trans-activation response DNA-binding protein accumulation and is associated with frontotemporal lobar degeneration*. Brain, 2010. **133**(Pt 6): p. 1763-71.
424. Chou, C.C., et al., *TDP-43 pathology disrupts nuclear pore complexes and nucleocytoplasmic transport in ALS/FTD*. Nat Neurosci, 2018. **21**(2): p. 228-239.
425. Arimoto-Matsuzaki, K., H. Saito, and M. Takekawa, *TIA1 oxidation inhibits stress granule assembly and sensitizes cells to stress-induced apoptosis*. Nat Commun, 2016. **7**: p. 10252.
426. Soo, K.Y., et al., *Rab1-dependent ER-Golgi transport dysfunction is a common pathogenic mechanism in SOD1, TDP-43 and FUS-associated ALS*. Acta Neuropathol, 2015. **130**(5): p. 679-97.
427. Farg, M.A., et al., *C9ORF72, implicated in amyotrophic lateral sclerosis and frontotemporal dementia, regulates endosomal trafficking*. Hum Mol Genet, 2014. **23**(13): p. 3579-95.
428. Gopal, P.P., et al., *Amyotrophic lateral sclerosis-linked mutations increase the viscosity of liquid-like TDP-43 RNP granules in neurons*. Proc Natl Acad Sci U S A, 2017. **114**(12): p. E2466-e2475.
429. Liu-Yesucevitz, L., et al., *ALS-Linked Mutations Enlarge TDP-43-Enriched Neuronal RNA Granules in the Dendritic Arbor*. The Journal of Neuroscience, 2014. **34**(12): p. 4167-4174.
430. Wang, M. and R.J. Kaufman, *Protein misfolding in the endoplasmic reticulum as a conduit to human disease*. Nature, 2016. **529**(7586): p. 326-35.
431. Fra, A., E.D. Yoboue, and R. Sitia, *Cysteines as Redox Molecular Switches and Targets of Disease*. Front Mol Neurosci, 2017. **10**: p. 167.
432. Malhotra, J.D. and R.J. Kaufman, *The endoplasmic reticulum and the unfolded protein response*. Semin Cell Dev Biol, 2007. **18**(6): p. 716-31.
433. Walsh, G. and R. Jefferis, *Post-translational modifications in the context of therapeutic proteins*. Nat Biotechnol, 2006. **24**(10): p. 1241-52.

434. Torres, M., et al., *Abnormal calcium homeostasis and protein folding stress at the ER: A common factor in familial and infectious prion disorders*. Commun Integr Biol, 2011. **4**(3): p. 258-61.
435. Hetz, C. and S. Saxena, *ER stress and the unfolded protein response in neurodegeneration*. Nat Rev Neurol, 2017. **13**(8): p. 477-491.
436. Coe, H. and M. Michalak, *Calcium binding chaperones of the endoplasmic reticulum*. Gen Physiol Biophys, 2009. **28 Spec No Focus**: p. F96-f103.
437. Hetz, C., *The unfolded protein response: controlling cell fate decisions under ER stress and beyond*. Nat Rev Mol Cell Biol, 2012. **13**(2): p. 89-102.
438. Kouroku, Y., et al., *ER stress (PERK/eIF2alpha phosphorylation) mediates the polyglutamine-induced LC3 conversion, an essential step for autophagy formation*. Cell Death Differ, 2007. **14**(2): p. 230-9.
439. Walter, P. and D. Ron, *The unfolded protein response: from stress pathway to homeostatic regulation*. Science, 2011. **334**(6059): p. 1081-6.
440. Xiang, C., et al., *The role of endoplasmic reticulum stress in neurodegenerative disease*. Apoptosis, 2017. **22**(1): p. 1-26.
441. Oakes, S.A. and F.R. Papa, *The role of endoplasmic reticulum stress in human pathology*. Annu Rev Pathol, 2015. **10**: p. 173-94.
442. Hughes, D. and G.R. Mallucci, *The unfolded protein response in neurodegenerative disorders - therapeutic modulation of the PERK pathway*. Febs j, 2018.
443. Rutkowski, D.T., et al., *Adaptation to ER stress is mediated by differential stabilities of pro-survival and pro-apoptotic mRNAs and proteins*. PLoS Biol, 2006. **4**(11): p. e374.
444. Cui, W., et al., *The structure of the PERK kinase domain suggests the mechanism for its activation*. Acta Crystallogr D Biol Crystallogr, 2011. **67**(Pt 5): p. 423-8.
445. Rajesh, K., et al., *Phosphorylation of the translation initiation factor eIF2alpha at serine 51 determines the cell fate decisions of Akt in response to oxidative stress*. Cell Death Dis, 2015. **6**: p. e1591.
446. Cullinan, S.B., et al., *Nrf2 is a direct PERK substrate and effector of PERK-dependent cell survival*. Mol Cell Biol, 2003. **23**(20): p. 7198-209.
447. Pakos-Zebrucka, K., et al., *The integrated stress response*. EMBO Rep, 2016. **17**(10): p. 1374-1395.
448. Halperin, L., J. Jung, and M. Michalak, *The many functions of the endoplasmic reticulum chaperones and folding enzymes*. IUBMB Life, 2014. **66**(5): p. 318-26.
449. Hetz, C. and B. Mollereau, *Disturbance of endoplasmic reticulum proteostasis in neurodegenerative diseases*. Nat Rev Neurosci, 2014. **15**(4): p. 233-49.
450. Maurel, M., et al., *Getting RIDD of RNA: IRE1 in cell fate regulation*. Trends Biochem Sci, 2014. **39**(5): p. 245-54.
451. Calfon, M., et al., *IRE1 couples endoplasmic reticulum load to secretory capacity by processing the XBP-1 mRNA*. Nature, 2002. **415**(6867): p. 92-6.
452. Joshi, A., et al., *Molecular mechanisms of human IRE1 activation through dimerization and ligand binding*. Oncotarget, 2015. **6**(15): p. 13019-35.
453. Acosta-Alvear, D., et al., *XBP1 controls diverse cell type- and condition-specific transcriptional regulatory networks*. Mol Cell, 2007. **27**(1): p. 53-66.
454. Ye, J., et al., *ER stress induces cleavage of membrane-bound ATF6 by the same proteases that process SREBPs*. Mol Cell, 2000. **6**(6): p. 1355-64.
455. Schroder, M. and R.J. Kaufman, *ER stress and the unfolded protein response*. Mutat Res, 2005. **569**(1-2): p. 29-63.
456. Yoshida, H., et al., *XBP1 mRNA is induced by ATF6 and spliced by IRE1 in response to ER stress to produce a highly active transcription factor*. Cell, 2001. **107**(7): p. 881-91.

457. Harding, H.P., et al., *Perk is essential for translational regulation and cell survival during the unfolded protein response*. Mol Cell, 2000. **5**(5): p. 897-904.
458. Nishitoh, H., *CHOP is a multifunctional transcription factor in the ER stress response*. J Biochem, 2012. **151**(3): p. 217-9.
459. Kim, I., W. Xu, and J.C. Reed, *Cell death and endoplasmic reticulum stress: disease relevance and therapeutic opportunities*. Nat Rev Drug Discov, 2008. **7**(12): p. 1013-30.
460. Oyadomari, S. and M. Mori, *Roles of CHOP/GADD153 in endoplasmic reticulum stress*. Cell Death Differ, 2004. **11**(4): p. 381-9.
461. Zhang, K. and R.J. Kaufman, *The unfolded protein response: a stress signaling pathway critical for health and disease*. Neurology, 2006. **66**(2 Suppl 1): p. S102-9.
462. Ilieva, E.V., et al., *Oxidative and endoplasmic reticulum stress interplay in sporadic amyotrophic lateral sclerosis*. Brain, 2007. **130**(Pt 12): p. 3111-23.
463. Ito, Y., et al., *Involvement of CHOP, an ER-stress apoptotic mediator, in both human sporadic ALS and ALS model mice*. Neurobiol Dis, 2009. **36**(3): p. 470-6.
464. Atkin, J.D., et al., *Induction of the unfolded protein response in familial amyotrophic lateral sclerosis and association of protein-disulfide isomerase with superoxide dismutase 1*. J Biol Chem, 2006. **281**(40): p. 30152-65.
465. Kikuchi, H., et al., *Spinal cord endoplasmic reticulum stress associated with a microsomal accumulation of mutant superoxide dismutase-1 in an ALS model*. Proceedings of the National Academy of Sciences, 2006. **103**(15): p. 6025-6030.
466. Walker, A.K., et al., *ALS-associated TDP-43 induces endoplasmic reticulum stress, which drives cytoplasmic TDP-43 accumulation and stress granule formation*. PLoS One, 2013. **8**(11): p. e81170.
467. Parakh, S., et al., *ERp57 is protective against mutant SOD1-induced cellular pathology in amyotrophic lateral sclerosis*. Hum Mol Genet, 2018. **27**(8): p. 1311-1331.
468. Walker, A.K., et al., *Protein disulphide isomerase protects against protein aggregation and is S-nitrosylated in amyotrophic lateral sclerosis*. Brain, 2010. **133**(Pt 1): p. 105-16.
469. Bonifacino, J.S. and B.S. Glick, *The mechanisms of vesicle budding and fusion*. Cell, 2004. **116**(2): p. 153-66.
470. De Matteis, M.A. and A. Luini, *Exiting the Golgi complex*. Nat Rev Mol Cell Biol, 2008. **9**(4): p. 273-84.
471. Wei, J.H. and J. Seemann, *Unraveling the Golgi ribbon*. Traffic, 2010. **11**(11): p. 1391-400.
472. Wei, J.H. and J. Seemann, *Golgi ribbon disassembly during mitosis, differentiation and disease progression*. Curr Opin Cell Biol, 2017. **47**: p. 43-51.
473. Bexiga, M.G. and J.C. Simpson, *Human diseases associated with form and function of the Golgi complex*. Int J Mol Sci, 2013. **14**(9): p. 18670-81.
474. Bellouze, S., et al., *Stathmin 1/2-triggered microtubule loss mediates Golgi fragmentation in mutant SOD1 motor neurons*. Mol Neurodegener, 2016. **11**(1): p. 43.
475. Bellouze, S., et al., *Golgi fragmentation in pmn mice is due to a defective ARF1/TBCE cross-talk that coordinates COPI vesicle formation and tubulin polymerization*. Hum Mol Genet, 2014. **23**(22): p. 5961-75.
476. Dascher, C. and W.E. Balch, *Dominant inhibitory mutants of ARF1 block endoplasmic reticulum to Golgi transport and trigger disassembly of the Golgi apparatus*. J Biol Chem, 1994. **269**(2): p. 1437-48.
477. Liu, C., et al., *Loss of the golgin GM130 causes Golgi disruption, Purkinje neuron loss, and ataxia in mice*. Proc Natl Acad Sci U S A, 2017. **114**(2): p. 346-351.

478. van Dis, V., et al., *Golgi fragmentation precedes neuromuscular denervation and is associated with endosome abnormalities in SOD1-ALS mouse motor neurons*. Acta Neuropathol Commun, 2014. **2**: p. 38.
479. Valenzuela, J.I. and F. Perez, *Diversifying the secretory routes in neurons*. Front Neurosci, 2015. **9**: p. 358.
480. Fujita, Y., et al., *Fragmentation of the Golgi apparatus of Betz cells in patients with amyotrophic lateral sclerosis*. J Neurol Sci, 1999. **163**(1): p. 81-5.
481. Gonatas, N.K., et al., *Fragmentation of the Golgi apparatus of motor neurons in amyotrophic lateral sclerosis*. Am J Pathol, 1992. **140**(3): p. 731-7.
482. Fujita, Y., et al., *Anterior horn cells with abnormal TDP-43 immunoreactivities show fragmentation of the Golgi apparatus in ALS*. J Neurol Sci, 2008. **269**(1-2): p. 30-4.
483. Ito, H., et al., *Clinicopathologic study on an ALS family with a heterozygous E478G optineurin mutation*. Acta Neuropathol, 2011. **122**(2): p. 223-9.
484. Gonatas, N.K., A. Stieber, and J.O. Gonatas, *Fragmentation of the Golgi apparatus in neurodegenerative diseases and cell death*. J Neurol Sci, 2006. **246**(1-2): p. 21-30.
485. Mourelatos, Z., et al., *The Golgi apparatus of spinal cord motor neurons in transgenic mice expressing mutant Cu,Zn superoxide dismutase becomes fragmented in early, preclinical stages of the disease*. Proc Natl Acad Sci U S A, 1996. **93**(11): p. 5472-7.
486. Stieber, A., et al., *Disruption of the structure of the Golgi apparatus and the function of the secretory pathway by mutants G93A and G85R of Cu, Zn superoxide dismutase (SOD1) of familial amyotrophic lateral sclerosis*. J Neurol Sci, 2004. **219**(1-2): p. 45-53.
487. Tong, J., et al., *XBP1 depletion precedes ubiquitin aggregation and Golgi fragmentation in TDP-43 transgenic rats*. J Neurochem, 2012. **123**(3): p. 406-16.
488. Sundaramoorthy, V., et al., *Defects in optineurin- and myosin VI-mediated cellular trafficking in amyotrophic lateral sclerosis*. Hum Mol Genet, 2015. **24**(13): p. 3830-46.
489. Teuling, E., et al., *Motor neuron disease-associated mutant vesicle-associated membrane protein-associated protein (VAP) B recruits wild-type VAPs into endoplasmic reticulum-derived tubular aggregates*. J Neurosci, 2007. **27**(36): p. 9801-15.
490. Nakagomi, S., et al., *A Golgi fragmentation pathway in neurodegeneration*. Neurobiol Dis, 2008. **29**(2): p. 221-31.
491. Nassif, M., et al., *Amyotrophic lateral sclerosis pathogenesis: a journey through the secretory pathway*. Antioxid Redox Signal, 2010. **13**(12): p. 1955-89.
492. Lippincott-Schwartz, J., T.H. Roberts, and K. Hirschberg, *Secretory protein trafficking and organelle dynamics in living cells*. Annu Rev Cell Dev Biol, 2000. **16**: p. 557-89.
493. Brooks, B.R., *The role of axonal transport in neurodegenerative disease spread: a meta-analysis of experimental and clinical poliomyelitis compares with amyotrophic lateral sclerosis*. Can J Neurol Sci, 1991. **18**(3 Suppl): p. 435-8.
494. Ravits, J., et al., *Implications of ALS focality: rostral-caudal distribution of lower motor neuron loss postmortem*. Neurology, 2007. **68**(19): p. 1576-82.
495. Maniecka, Z. and M. Polymenidou, *From nucleation to widespread propagation: A prion-like concept for ALS*. Virus Res, 2015. **207**: p. 94-105.
496. Brundin, P., R. Melki, and R. Kopito, *Prion-like transmission of protein aggregates in neurodegenerative diseases*. Nat Rev Mol Cell Biol, 2010. **11**(4): p. 301-7.
497. Duyckaerts, C., *Neurodegenerative lesions: seeding and spreading*. Rev Neurol (Paris), 2013. **169**(10): p. 825-33.
498. Holmes, B.B. and M.I. Diamond, *Prion-like properties of Tau protein: the importance of extracellular Tau as a therapeutic target*. J Biol Chem, 2014. **289**(29): p. 19855-61.

499. Ugalde, C.L., et al., *Pathogenic mechanisms of prion protein, amyloid-beta and alpha-synuclein misfolding: the prion concept and neurotoxicity of protein oligomers*. J Neurochem, 2016. **139**(2): p. 162-180.
500. Soto, C., *Transmissible Proteins: Expanding the Prion Heresy*. Cell, 2012. **149**(5): p. 968-977.
501. Cushman, M., et al., *Prion-like disorders: blurring the divide between transmissibility and infectivity*. J Cell Sci, 2010. **123**(Pt 8): p. 1191-201.
502. Smethurst, P., et al., *In vitro prion-like behaviour of TDP-43 in ALS*. Neurobiol Dis, 2016. **96**: p. 236-247.
503. Furukawa, Y., et al., *A seeding reaction recapitulates intracellular formation of Sarkosyl-insoluble transactivation response element (TAR) DNA-binding protein-43 inclusions*. J Biol Chem, 2011. **286**(21): p. 18664-72.
504. Nonaka, T., et al., *Prion-like properties of pathological TDP-43 aggregates from diseased brains*. Cell Rep, 2013. **4**(1): p. 124-34.
505. Ding, X., et al., *Exposure to ALS-FTD-CSF generates TDP-43 aggregates in glioblastoma cells through exosomes and TNTs-like structure*. Oncotarget, 2015. **6**(27): p. 24178-91.
506. Grad, L.I., et al., *Intermolecular transmission of superoxide dismutase 1 misfolding in living cells*. Proc Natl Acad Sci U S A, 2011. **108**: p. 16398-16403.
507. Ayers, J.I., et al., *Prion-like propagation of mutant SOD1 misfolding and motor neuron disease spread along neuroanatomical pathways*. Acta Neuropathol, 2016. **131**(1): p. 103-14.
508. Feiler, M.S., et al., *TDP-43 is intercellularly transmitted across axon terminals*. J Cell Biol, 2015. **211**(4): p. 897-911.
509. Ayers, J.I., et al., *Experimental transmissibility of mutant SOD1 motor neuron disease*. Acta Neuropathol, 2014. **128**(6): p. 791-803.
510. Morohoshi, F., et al., *Genomic structure of the human RBP56/hTAFII68 and FUS/TLS genes*. Gene, 1998. **221**(2): p. 191-8.
511. Rabbitts, T.H., et al., *Fusion of the dominant negative transcription regulator CHOP with a novel gene FUS by translocation t(12;16) in malignant liposarcoma*. Nat Genet, 1993. **4**: p. 6.
512. Zhou, Y., et al., *ALS-associated FUS mutations result in compromised FUS alternative splicing and autoregulation*. PLoS Genet, 2013. **9**(10): p. e1003895.
513. Andersson, M.K., et al., *The multifunctional FUS, EWS and TAF15 proto-oncoproteins show cell type-specific expression patterns and involvement in cell spreading and stress response*. BMC Cell Biol, 2008. **9**: p. 37.
514. Zinszner, H., et al., *TLS (FUS) binds RNA in vivo and engages in nucleo-cytoplasmic shuttling*. Journal of Cell Science, 1997. **110**(15): p. 1741-1750.
515. Fujii, R., et al., *The RNA binding protein TLS is translocated to dendritic spines by mGluR5 activation and regulates spine morphology*. Curr Biol, 2005. **15**(6): p. 587-93.
516. Belly, A., et al., *Delocalization of the multifunctional RNA splicing factor TLS/FUS in hippocampal neurones: exclusion from the nucleus and accumulation in dendritic granules and spine heads*. Neurosci Lett, 2005. **379**(3): p. 152-7.
517. Baechtold, H., et al., *Human 75-kDa DNA-pairing protein is identical to the pro-oncoprotein TLS/FUS and is able to promote D-loop formation*. J Biol Chem, 1999. **274**(48): p. 34337-42.
518. March, Z.M., O.D. King, and J. Shorter, *Prion-like domains as epigenetic regulators, scaffolds for subcellular organization, and drivers of neurodegenerative disease*. Brain Res, 2016.
519. Alberti, S., et al., *A systematic survey identifies prions and illuminates sequence features of prionogenic proteins*. Cell, 2009. **137**(1): p. 146-58.

520. Huntley, M.A. and G.B. Golding, *Simple sequences are rare in the Protein Data Bank*. Proteins, 2002. **48**(1): p. 134-40.
521. Burke, Kathleen A., et al., *Residue-by-Residue View of In Vitro FUS Granules that Bind the C-Terminal Domain of RNA Polymerase II*. Molecular Cell, 2015. **60**(2): p. 231-241.
522. Lu, Y., L. Lim, and J. Song, *RRM domain of ALS/FTD-causing FUS characteristic of irreversible unfolding spontaneously self-assembles into amyloid fibrils*. Sci Rep, 2017. **7**(1): p. 1043.
523. Yang, L., et al., *Self-assembled FUS binds active chromatin and regulates gene transcription*. Proc Natl Acad Sci U S A, 2014. **111**(50): p. 17809-14.
524. Lin, Y., et al., *Formation and Maturation of Phase-Separated Liquid Droplets by RNA-Binding Proteins*. Mol Cell, 2015. **60**(2): p. 208-19.
525. Calvio, C., et al., *Identification of hnRNP P2 as TLS/FUS using electrospray mass spectrometry*. Rna, 1995. **1**(7): p. 724-33.
526. Allain, F.H.T., et al., *Molecular basis of sequence - specific recognition of pre - ribosomal RNA by nucleolin*. The EMBO Journal, 2000. **19**(24): p. 6870-6881.
527. Bertolotti, A., et al., *hTAF(II)68, a novel RNA/ssDNA-binding protein with homology to the pro-oncoproteins TLS/FUS and EWS is associated with both TFIID and RNA polymerase II*. Embo j, 1996. **15**(18): p. 5022-31.
528. Liu, X., et al., *The RRM domain of human fused in sarcoma protein reveals a non-canonical nucleic acid binding site*. Biochim Biophys Acta, 2013. **1832**(2): p. 375-85.
529. Schwartz, J.C., et al., *RNA seeds higher-order assembly of FUS protein*. Cell Rep, 2013. **5**(4): p. 918-25.
530. Crozat, A., et al., *Fusion of CHOP to a novel RNA-binding protein in human myxoid liposarcoma*. Nature, 1993. **363**(6430): p. 640-4.
531. Lerga, M.H., Laurent Delva, Christophe Orvain, Isabelle Gallais, Joelle Marie, Françoise Moreau-Gachelin, *Identification of an RNA binding specificity for the potential splicing factor TLS*. The Journal of biological Chemistry, 2001. **276**(9): p. 6807-6816.
532. Wang, X., J.C. Schwartz, and T.R. Cech, *Nucleic acid-binding specificity of human FUS protein*. Nucleic Acids Res, 2015. **43**(15): p. 7535-43.
533. Sun, Z., et al., *Molecular determinants and genetic modifiers of aggregation and toxicity for the ALS disease protein FUS/TLS*. PLoS Biol, 2011. **9**(4): p. e1000614.
534. Svetoni, F., P. Frisone, and M.P. Paronetto, *Role of FET proteins in neurodegenerative disorders*. RNA Biol, 2016: p. 1-14.
535. Kino, Y., et al., *Intracellular localization and splicing regulation of FUS/TLS are variably affected by amyotrophic lateral sclerosis-linked mutations*. Nucleic Acids Res, 2011. **39**(7): p. 2781-98.
536. Ederle, H., et al., *Nuclear egress of TDP-43 and FUS occurs independently of Exportin-1/CRM1*. Sci Rep, 2018. **8**(1): p. 7084.
537. Sloutsky, R. and K.M. Naegle, *Proteome-Level Analysis Indicates Global Mechanisms for Post-Translational Regulation of RRM Domains*. J Mol Biol, 2018. **430**(1): p. 41-44.
538. Malgieri, G., et al., *The prokaryotic zinc-finger: structure, function and comparison with the eukaryotic counterpart*. Febs j, 2015. **282**(23): p. 4480-96.
539. Iko, Y., et al., *Domain architectures and characterization of an RNA-binding protein, TLS*. J Biol Chem, 2004. **279**(43): p. 44834-40.
540. Bentmann, E., et al., *Requirements for stress granule recruitment of fused in sarcoma (FUS) and TAR DNA-binding protein of 43 kDa (TDP-43)*. J Biol Chem, 2012. **287**(27): p. 23079-94.
541. Gerstberger, S., M. Hafner, and T. Tuschl, *A census of human RNA-binding proteins*. Nat Rev Genet, 2014. **15**(12): p. 829-45.

542. Thandapani, P., et al., *Defining the RGG/RG motif*. Mol Cell, 2013. **50**(5): p. 613-23.
543. Ghisolfi, L., et al., *The glycine-rich domain of nucleolin has an unusual supersecondary structure responsible for its RNA-helix-destabilizing properties*. J Biol Chem, 1992. **267**(5): p. 2955-9.
544. Takahama, K. and T. Oyoshi, *Specific binding of modified RGG domain in TLS/FUS to G-quadruplex RNA: tyrosines in RGG domain recognize 2'-OH of the riboses of loops in G-quadruplex*. J Am Chem Soc, 2013. **135**(48): p. 18016-9.
545. Ozdilek, B.A., et al., *Intrinsically disordered RGG/RG domains mediate degenerate specificity in RNA binding*. Nucleic Acids Res, 2017. **45**(13): p. 7984-7996.
546. Fujii, R. and T. Takumi, *TLS facilitates transport of mRNA encoding an actin-stabilizing protein to dendritic spines*. J Cell Sci, 2005. **118**(Pt 24): p. 5755-65.
547. Lee, B.J., et al., *Rules for nuclear localization sequence recognition by karyopherin beta 2*. Cell, 2006. **126**(3): p. 543-58.
548. Dormann, D., et al., *ALS-associated fused in sarcoma (FUS) mutations disrupt Transportin-mediated nuclear import*. Embo J, 2010. **29**(16): p. 2841-57.
549. Dormann, D., et al., *Arginine methylation next to the PY-NLS modulates Transportin binding and nuclear import of FUS*. Embo j, 2012. **31**(22): p. 4258-75.
550. Chook, Y.M. and K.E. Süel, *Nuclear import by karyopherin-βs: Recognition and inhibition*. Biochimica et Biophysica Acta (BBA) - Molecular Cell Research, 2011. **1813**(9): p. 1593-1606.
551. Niu, C., et al., *FUS-NLS/Transportin 1 complex structure provides insights into the nuclear targeting mechanism of FUS and the implications in ALS*. PLoS One, 2012. **7**(10): p. e47056.
552. Zhang, Z.C. and Y.M. Chook, *Structural and energetic basis of ALS-causing mutations in the atypical proline-tyrosine nuclear localization signal of the Fused in Sarcoma protein (FUS)*. Proc Natl Acad Sci U S A, 2012. **109**(30): p. 12017-21.
553. Darovic, S., et al., *Phosphorylation of C-terminal tyrosine residue 526 in FUS impairs its nuclear import*. J Cell Sci, 2015. **128**(22): p. 4151-9.
554. Swetha, R.G., S. Ramaiah, and A. Anbarasu, *R521C and R521H mutations in FUS result in weak binding with Karyopherinbeta2 leading to Amyotrophic lateral sclerosis: a molecular docking and dynamics study*. J Biomol Struct Dyn, 2017. **35**(10): p. 2169-2185.
555. Minguez, P., et al., *Deciphering a global network of functionally associated post-translational modifications*. Mol Syst Biol, 2012. **8**: p. 599.
556. Guo, A., et al., *Immunoaffinity enrichment and mass spectrometry analysis of protein methylation*. Mol Cell Proteomics, 2014. **13**(1): p. 372-87.
557. Rappsilber, J., et al., *Detection of Arginine Dimethylated Peptides by Parallel Precursor Ion Scanning Mass Spectrometry in Positive Ion Mode*. Analytical Chemistry, 2003. **75**(13): p. 3107-3114.
558. Shen, E.C., et al., *Arginine methylation facilitates the nuclear export of hnRNP proteins*. Genes Dev, 1998. **12**(5): p. 679-91.
559. Du, K., et al., *TLS and PRMT1 synergistically coactivate transcription at the survivin promoter through TLS arginine methylation*. Biochem Biophys Res Commun, 2011. **404**(4): p. 991-6.
560. Yamaguchi, A. and K. Kitajo, *The effect of PRMT1-mediated arginine methylation on the subcellular localization, stress granules, and detergent-insoluble aggregates of FUS/TLS*. PLoS One, 2012. **7**(11): p. e49267.
561. Scaramuzzino, C., et al., *Protein arginine methyltransferase 1 and 8 interact with FUS to modify its sub-cellular distribution and toxicity in vitro and in vivo*. PLoS One, 2013. **8**(4): p. e61576.

562. Jackel, S., et al., *Nuclear import factor transportin and arginine methyltransferase 1 modify FUS neurotoxicity in Drosophila*. Neurobiol Dis, 2015. **74**: p. 76-88.
563. Suarez-Calvet, M., et al., *Monomethylated and unmethylated FUS exhibit increased binding to Transportin and distinguish FTL-D-FUS from ALS-FUS*. Acta Neuropathol, 2016. **131**(4): p. 587-604.
564. Fujii, S., et al., *Treatment with a Global Methyltransferase Inhibitor Induces the Intranuclear Aggregation of ALS-Linked FUS Mutant In Vitro*. Neurochem Res, 2016. **41**(4): p. 826-35.
565. Brelstaff, J., et al., *Transportin1: a marker of FTL-D-FUS*. Acta Neuropathol, 2011. **122**(5): p. 591-600.
566. Troakes, C., et al., *Transportin 1 colocalization with Fused in Sarcoma (FUS) inclusions is not characteristic for amyotrophic lateral sclerosis-FUS confirming disrupted nuclear import of mutant FUS and distinguishing it from frontotemporal lobar degeneration with FUS inclusions*. Neuropathol Appl Neurobiol, 2013. **39**(5): p. 553-61.
567. Neumann, M., et al., *FET proteins TAF15 and EWS are selective markers that distinguish FTL-D with FUS pathology from amyotrophic lateral sclerosis with FUS mutations*. Brain, 2011. **134**(Pt 9): p. 2595-609.
568. Urwin, H., et al., *FUS pathology defines the majority of tau- and TDP-43-negative frontotemporal lobar degeneration*. Acta Neuropathol, 2010. **120**(1): p. 33-41.
569. Neumann, M., et al., *A new subtype of frontotemporal lobar degeneration with FUS pathology*. Brain, 2009. **132**(Pt 11): p. 2922-31.
570. Lashley, T., et al., *A comparative clinical, pathological, biochemical and genetic study of fused in sarcoma proteinopathies*. Brain, 2011. **134**(Pt 9): p. 2548-64.
571. Hofweber, M., et al., *Phase Separation of FUS Is Suppressed by Its Nuclear Import Receptor and Arginine Methylation*. Cell, 2018. **173**(3): p. 706-719.e13.
572. Perrotti, D., et al., *BCR-ABL prevents c-jun-mediated and proteasome-dependent FUS (TLS) proteolysis through a protein kinase Cbeta11-dependent pathway*. Mol Cell Biol, 2000. **20**(16): p. 6159-69.
573. Gardiner, M., et al., *Identification and characterization of FUS/TLS as a new target of ATM*. Biochem J, 2008. **415**(2): p. 297-307.
574. Deng, Q., et al., *FUS is phosphorylated by DNA-PK and accumulates in the cytoplasm after DNA damage*. J Neurosci, 2014. **34**(23): p. 7802-13.
575. Naumann, M., et al., *Impaired DNA damage response signaling by FUS-NLS mutations leads to neurodegeneration and FUS aggregate formation*. Nat Commun, 2018. **9**(1): p. 335.
576. Monahan, Z., et al., *Phosphorylation of the FUS low-complexity domain disrupts phase separation, aggregation, and toxicity*. Embo j, 2017. **36**(20): p. 2951-2967.
577. Lin, Y., S.L. Currie, and M.K. Rosen, *Intrinsically disordered sequences enable modulation of protein phase separation through distributed tyrosine motifs*. J Biol Chem, 2017. **292**(46): p. 19110-19120.
578. Murray, D.T., et al., *Structure of FUS Protein Fibrils and Its Relevance to Self-Assembly and Phase Separation of Low-Complexity Domains*. Cell, 2017. **171**(3): p. 615-627.e16.
579. Luo, F., et al., *Atomic structures of FUS LC domain segments reveal bases for reversible amyloid fibril formation*. Nat Struct Mol Biol, 2018. **25**(4): p. 341-346.
580. Li, W. and Y. Ye, *Polyubiquitin chains: functions, structures, and mechanisms*. Cell Mol Life Sci, 2008. **65**(15): p. 2397-406.
581. Nedelsky, N.B., P.K. Todd, and J.P. Taylor, *Autophagy and the ubiquitin-proteasome system: collaborators in neuroprotection*. Biochim Biophys Acta, 2008. **1782**(12): p. 691-9.

582. Farrawell, N.E., et al., *Distinct partitioning of ALS associated TDP-43, FUS and SOD1 mutants into cellular inclusions*. Sci Rep, 2015. **5**: p. 13416.
583. Murayama, S., *[Clinical and pathological characteristics of FUS/TLS-associated amyotrophic lateral sclerosis (ALS)]*. Rinsho Shinkeigaku, 2010. **50**(11): p. 948-50.
584. Rhoads, S.N., et al., *The Role of Post-Translational Modifications on Prion-Like Aggregation and Liquid-Phase Separation of FUS*. Int J Mol Sci, 2018. **19**(3).
585. Kim, W., et al., *Systematic and quantitative assessment of the ubiquitin-modified proteome*. Mol Cell, 2011. **44**(2): p. 325-40.
586. Povlsen, L.K., et al., *Systems-wide analysis of ubiquitylation dynamics reveals a key role for PAF15 ubiquitylation in DNA-damage bypass*. Nat Cell Biol, 2012. **14**(10): p. 1089-98.
587. Wagner, S.A., et al., *A proteome-wide, quantitative survey of in vivo ubiquitylation sites reveals widespread regulatory roles*. Mol Cell Proteomics, 2011. **10**(10): p. M111.013284.
588. Mertins, P., et al., *Integrated proteomic analysis of post-translational modifications by serial enrichment*. Nat Methods, 2013. **10**(7): p. 634-7.
589. Oh, S.M., et al., *Ebp1 sumoylation, regulated by TLS/FUS E3 ligase, is required for its anti-proliferative activity*. Oncogene, 2010. **29**(7): p. 1017-30.
590. Liebelt, F. and A.C. Vertegaal, *Ubiquitin-dependent and independent roles of SUMO in proteostasis*. Am J Physiol Cell Physiol, 2016. **311**(2): p. C284-96.
591. Steentoft, C., et al., *Precision mapping of the human α -GalNAc glycoproteome through SimpleCell technology*. The EMBO Journal, 2013. **32**(10): p. 1478-1488.
592. Kamemura, K., *O-GlcNAc glycosylation stoichiometry of the FET protein family: only EWS is glycosylated with a high stoichiometry*. Biosci Biotechnol Biochem, 2017. **81**(3): p. 541-546.
593. Lee, A., et al., *Combined Antibody/Lectin Enrichment Identifies Extensive Changes in the O-GlcNAc Sub-proteome upon Oxidative Stress*. J Proteome Res, 2016. **15**(12): p. 4318-4336.
594. Cook, C., et al., *Acetylation of the KXGS motifs in tau is a critical determinant in modulation of tau aggregation and clearance*. Hum Mol Genet, 2014. **23**(1): p. 104-16.
595. Ayyadevara, S., et al., *Aspirin-Mediated Acetylation Protects Against Multiple Neurodegenerative Pathologies by Impeding Protein Aggregation*. Antioxid Redox Signal, 2017. **27**(17): p. 1383-1396.
596. Liu, D., et al., *Proteomic analysis reveals differentially regulated protein acetylation in human amyotrophic lateral sclerosis spinal cord*. PLoS One, 2013. **8**(12): p. e80779.
597. Catherman, A.D., et al., *Large-scale top-down proteomics of the human proteome: membrane proteins, mitochondria, and senescence*. Mol Cell Proteomics, 2013. **12**(12): p. 3465-73.
598. Hornbeck, P.V., et al., *PhosphoSitePlus, 2014: mutations, PTMs and recalibrations*. Nucleic Acids Res, 2015. **43**(Database issue): p. D512-20.
599. Guo, W., et al., *HDAC6 inhibition reverses axonal transport defects in motor neurons derived from FUS-ALS patients*. Nat Commun, 2017. **8**(1): p. 861.
600. Kuroda, M., et al., *Male sterility and enhanced radiation sensitivity in TLS(-/-) mice*. Embo j, 2000. **19**(3): p. 453-62.
601. Hicks, G.G., et al., *Fus deficiency in mice results in defective B-lymphocyte development and activation, high levels of chromosomal instability and perinatal death*. Nat Genet, 2000. **24**: p. 5.

602. Bertrand, P., et al., *Human POMp75 is identified as the pro-oncoprotein TLS/FUS: both POMp75 and POMp100 DNA homologous pairing activities are associated to cell proliferation*. *Oncogene*, 1999. **18**(31): p. 4515-21.
603. Akhmedov, A.T., et al., *Characterization of two nuclear mammalian homologous DNA-pairing activities that do not require associated exonuclease activity*. *Proc Natl Acad Sci U S A*, 1995. **92**(5): p. 1729-33.
604. Wang, W.Y., et al., *Interaction of FUS and HDAC1 regulates DNA damage response and repair in neurons*. *Nat Neurosci*, 2013. **16**(10): p. 1383-91.
605. Rulten, S.L., et al., *PARP-1 dependent recruitment of the amyotrophic lateral sclerosis-associated protein FUS/TLS to sites of oxidative DNA damage*. *Nucleic Acids Res*, 2014. **42**(1): p. 307-14.
606. Gong, J., et al., *RBM45 competes with HDAC1 for binding to FUS in response to DNA damage*. *Nucleic Acids Res*, 2017. **45**(22): p. 12862-12876.
607. Hill, S.J., et al., *Two familial ALS proteins function in prevention/repair of transcription-associated DNA damage*. *Proc Natl Acad Sci U S A*, 2016. **113**(48): p. E7701-e7709.
608. Takahama, K., et al., *Regulation of telomere length by G-quadruplex telomere DNA- and TERRA-binding protein TLS/FUS*. *Chem Biol*, 2013. **20**(3): p. 341-50.
609. Kondo, K., et al., *Plastic roles of phenylalanine and tyrosine residues of TLS/FUS in complex formation with the G-quadruplexes of telomeric DNA and TERRA*. *Sci Rep*, 2018. **8**(1): p. 2864.
610. Schwartz, J.C., et al., *FUS binds the CTD of RNA polymerase II and regulates its phosphorylation at Ser2*. *Genes Dev*, 2012. **26**(24): p. 2690-5.
611. Kwon, I., et al., *Phosphorylation-regulated binding of RNA polymerase II to fibrous polymers of low-complexity domains*. *Cell*, 2013. **155**(5): p. 1049-60.
612. Schwartz, J.C., et al., *FUS is sequestered in nuclear aggregates in ALS patient fibroblasts*. *Mol Biol Cell*, 2014. **25**(17): p. 2571-8.
613. Errichelli, L., et al., *FUS affects circular RNA expression in murine embryonic stem cell-derived motor neurons*. *Nat Commun*, 2017. **8**: p. 14741.
614. Tan, A.Y. and J.L. Manley, *TLS inhibits RNA polymerase III transcription*. *Mol Cell Biol*, 2010. **30**(1): p. 186-96.
615. Dhar, S.K., et al., *FUsed in sarcoma is a novel regulator of manganese superoxide dismutase gene transcription*. *Antioxid Redox Signal*, 2014. **20**(10): p. 1550-66.
616. Convertini, P., et al., *Genome wide array analysis indicates that an amyotrophic lateral sclerosis mutation of FUS causes an early increase of CAMK2N2 in vitro*. *Biochim Biophys Acta*, 2013. **1832**(8): p. 1129-35.
617. Raczynska, K.D., et al., *FUS/TLS contributes to replication-dependent histone gene expression by interaction with U7 snRNPs and histone-specific transcription factors*. *Nucleic Acids Res*, 2015. **43**(20): p. 9711-28.
618. Hallier, M., et al., *The transcription factor Spi-1/PU.1 interacts with the potential splicing factor TLS*. *J Biol Chem*, 1998. **273**(9): p. 4838-42.
619. Yamaguchi, A. and K. Takanashi, *FUS interacts with nuclear matrix-associated protein SAFB1 as well as Matrin3 to regulate splicing and ligand-mediated transcription*. *Sci Rep*, 2016. **6**: p. 35195.
620. Ishigaki, S., et al., *Position-dependent FUS-RNA interactions regulate alternative splicing events and transcriptions*. *Sci Rep*, 2012. **2**: p. 529.
621. Ray, D., et al., *A compendium of RNA-binding motifs for decoding gene regulation*. *Nature*, 2013. **499**(7457): p. 172-7.
622. Rogelj, B., et al., *Widespread binding of FUS along nascent RNA regulates alternative splicing in the brain*. *Sci Rep*, 2012. **2**: p. 603.

623. Lagier-Tourenne, C., et al., *Divergent roles of ALS-linked proteins FUS/TLS and TDP-43 intersect in processing long pre-mRNAs*. Nat Neurosci, 2012. **15**(11): p. 1488-97.
624. Masuda, A., et al., *Position-specific binding of FUS to nascent RNA regulates mRNA length*. Genes Dev, 2015. **29**(10): p. 1045-57.
625. Takeda, J.-i., A. Masuda, and K. Ohno, *Six GU-rich (6GUR) FUS-binding motifs detected by normalization of CLIP-seq by Nascent-seq*. Gene, 2017. **618**: p. 57-64.
626. Kapeli, K., et al., *Distinct and shared functions of ALS-associated proteins TDP-43, FUS and TAF15 revealed by multisystem analyses*. Nat Commun, 2016. **7**: p. 12143.
627. Machamer, J.B., S.E. Collins, and T.E. Lloyd, *The ALS gene FUS regulates synaptic transmission at the Drosophila neuromuscular junction*. Hum Mol Genet, 2014. **23**(14): p. 3810-22.
628. Reber, S., et al., *Minor intron splicing is regulated by FUS and affected by ALS-associated FUS mutants*. Embo j, 2016. **35**(14): p. 1504-21.
629. Kameoka, S., P. Duque, and M.M. Konarska, *p54(nrb) associates with the 5' splice site within large transcription/splicing complexes*. Embo j, 2004. **23**(8): p. 1782-91.
630. Kamelgarn, M., et al., *Proteomic analysis of FUS interacting proteins provides insights into FUS function and its role in ALS*. Biochimica et Biophysica Acta (BBA) - Molecular Basis of Disease, 2016. **1862**(10): p. 2004-2014.
631. Sun, S., et al., *ALS-causative mutations in FUS/TLS confer gain and loss of function by altered association with SMN and U1-snRNP*. Nat Commun, 2015. **6**: p. 6171.
632. Meissner, M., et al., *Proto-oncoprotein TLS/FUS is associated to the nuclear matrix and complexed with splicing factors PTB, SRm160, and SR proteins*. Exp Cell Res, 2003. **283**(2): p. 184-95.
633. Mirra, A., et al., *Functional interaction between FUS and SMN underlies SMA-like splicing changes in wild-type hFUS mice*. Sci Rep, 2017. **7**(1): p. 2033.
634. Yamazaki, T., et al., *FUS-SMN protein interactions link the motor neuron diseases ALS and SMA*. Cell Rep, 2012. **2**(4): p. 799-806.
635. Gregory, R.I., et al., *The Microprocessor complex mediates the genesis of microRNAs*. Nature, 2004. **432**(7014): p. 235-40.
636. Morlando, M., et al., *FUS stimulates microRNA biogenesis by facilitating co-transcriptional Drosha recruitment*. Embo j, 2012. **31**(24): p. 4502-10.
637. Zhang, T., et al., *FUS Regulates Activity of MicroRNA-Mediated Gene Silencing*. Mol Cell, 2018. **69**(5): p. 787-801.e8.
638. Emde, A., et al., *Dysregulated miRNA biogenesis downstream of cellular stress and ALS-causing mutations: a new mechanism for ALS*. Embo j, 2015. **34**(21): p. 2633-51.
639. Dini Modigliani, S., et al., *An ALS-associated mutation in the FUS 3'-UTR disrupts a microRNA-FUS regulatory circuitry*. Nat Commun, 2014. **5**: p. 4335.
640. Ishigaki, S., et al., *Altered Tau Isoform Ratio Caused by Loss of FUS and SFPQ Function Leads to FTL-like Phenotypes*. Cell Rep, 2017. **18**(5): p. 1118-1131.
641. Orozco, D., et al., *Loss of fused in sarcoma (FUS) promotes pathological Tau splicing*. EMBO Rep, 2012. **13**(8): p. 759-64.
642. Yoshimura, A., et al., *Myosin-Va facilitates the accumulation of mRNA/protein complex in dendritic spines*. Curr Biol, 2006. **16**(23): p. 2345-51.
643. Takarada, T., et al., *A protein-protein interaction of stress-responsive myosin VI endowed to inhibit neural progenitor self-replication with RNA binding protein, TLS, in murine hippocampus*. J Neurochem, 2009. **110**(5): p. 1457-68.
644. Kanai, Y., N. Dohmae, and N. Hirokawa, *Kinesin transports RNA: isolation and characterization of an RNA-transporting granule*. Neuron, 2004. **43**(4): p. 513-25.
645. Fujii, R., et al., *TLS-GFP cannot rescue mRNP formation near spines and spine phenotype in TLS-KO*. Neuroreport, 2009. **20**(1): p. 57-61.

646. Yasuda, K., et al., *The RNA-binding protein Fus directs translation of localized mRNAs in APC-RNP granules*. J Cell Biol, 2013. **203**(5): p. 737-46.
647. Udagawa, T., et al., *FUS regulates AMPA receptor function and FTL/ALS-associated behaviour via GluA1 mRNA stabilization*. Nat Commun, 2015. **6**: p. 7098.
648. So, E., et al., *Mitochondrial abnormalities and disruption of the neuromuscular junction precede the clinical phenotype and motor neuron loss in hFUSWT transgenic mice*. Hum Mol Genet, 2018. **27**(3): p. 463-474.
649. Schoen, M., et al., *Super-Resolution Microscopy Reveals Presynaptic Localization of the ALS/FTD Related Protein FUS in Hippocampal Neurons*. Front Cell Neurosci, 2015. **9**: p. 496.
650. Reschke, M., et al., *Characterization and analysis of the composition and dynamics of the mammalian riboproteome*. Cell Rep, 2013. **4**(6): p. 1276-87.
651. Millicamps, S., et al., *Phenotype difference between ALS patients with expanded repeats in *C9ORF72* and patients with mutations in other ALS-related genes*. Journal of Medical Genetics, 2012. **49**(4): p. 258-263.
652. Shang, Y. and E.J. Huang, *Mechanisms of FUS mutations in familial amyotrophic lateral sclerosis*. Brain Res, 2016.
653. Deng, H., K. Gao, and J. Jankovic, *The role of FUS gene variants in neurodegenerative diseases*. Nat Rev Neurol, 2014. **10**(6): p. 337-48.
654. Lattante, S., et al., *Defining the genetic connection linking amyotrophic lateral sclerosis (ALS) with frontotemporal dementia (FTD)*. Trends Genet, 2015. **31**(5): p. 263-73.
655. Kim, Y.E., et al., *De novo FUS mutations in 2 Korean patients with sporadic amyotrophic lateral sclerosis*. Neurobiol Aging, 2015. **36**(3): p. 1604.e17-9.
656. Belzil, V.V., et al., *Mutations in FUS cause FALS and SALS in French and French Canadian populations*. Neurology, 2009. **73**(15): p. 1176-9.
657. Yan, J., et al., *Frameshift and novel mutations in FUS in familial amyotrophic lateral sclerosis and ALS/dementia*. Neurology, 2010. **75**(9): p. 807-14.
658. van Blitterswijk, M., et al., *Evidence for an oligogenic basis of amyotrophic lateral sclerosis*. Hum Mol Genet, 2012. **21**(17): p. 3776-84.
659. Rademakers, R., et al., *Fus gene mutations in familial and sporadic amyotrophic lateral sclerosis*. Muscle Nerve, 2010. **42**(2): p. 170-6.
660. Lattante, S., et al., *Contribution of major amyotrophic lateral sclerosis genes to the etiology of sporadic disease*. Neurology, 2012. **79**(1): p. 66-72.
661. Kwon, M.J., et al., *Screening of the SOD1, FUS, TARDBP, ANG, and OPTN mutations in Korean patients with familial and sporadic ALS*. Neurobiol Aging, 2012. **33**(5): p. 1017.e17-23.
662. Tarlarini, C., et al., *Novel FUS mutations identified through molecular screening in a large cohort of familial and sporadic amyotrophic lateral sclerosis*. Eur J Neurol, 2015.
663. DeJesus-Hernandez, M., et al., *De novo truncating FUS gene mutation as a cause of sporadic amyotrophic lateral sclerosis*. Hum Mutat, 2010. **31**(5): p. E1377-89.
664. Groen, E.J., et al., *FUS mutations in familial amyotrophic lateral sclerosis in the Netherlands*. Arch Neurol, 2010. **67**(2): p. 224-30.
665. Nagayama, S., et al., *Novel FUS mutation in patients with sporadic amyotrophic lateral sclerosis and corticobasal degeneration*. J Clin Neurosci, 2012. **19**(12): p. 1738-9.
666. Hara, M., et al., *Lower motor neuron disease caused by a novel FUS/TLS gene frameshift mutation*. J Neurol, 2012. **259**(10): p. 2237-9.
667. Zou, Z.Y., et al., *Identification of a novel missense mutation in angiogenin in a Chinese amyotrophic lateral sclerosis cohort*. Amyotroph Lateral Scler, 2012. **13**(3): p. 270-5.
668. Hewitt, C., et al., *Novel FUS/TLS mutations and pathology in familial and sporadic amyotrophic lateral sclerosis*. Arch Neurol, 2010. **67**(4): p. 455-61.

669. Waibel, S., et al., *Novel missense and truncating mutations in FUS/TLS in familial ALS*. *Neurology*, 2010. **75**(9): p. 815-7.
670. Suzuki, N., et al., *FALS with FUS mutation in Japan, with early onset, rapid progress and basophilic inclusion*. *J Hum Genet*, 2010. **55**(4): p. 252-4.
671. Robertson, J., et al., *A novel double mutation in FUS gene causing sporadic ALS*. *Neurobiol Aging*, 2011. **32**(3): p. 553.e27-30.
672. Sproviero, W., et al., *FUS mutations in sporadic amyotrophic lateral sclerosis: clinical and genetic analysis*. *Neurobiol Aging*, 2012. **33**(4): p. 837.e1-5.
673. Van Langenhove, T., et al., *Genetic contribution of FUS to frontotemporal lobar degeneration*. *Neurology*, 2010. **74**(5): p. 366-71.
674. Broustal, O., et al., *FUS mutations in frontotemporal lobar degeneration with amyotrophic lateral sclerosis*. *J Alzheimers Dis*, 2010. **22**(3): p. 765-9.
675. Chio, A., et al., *Phenotypic heterogeneity of amyotrophic lateral sclerosis: a population based study*. *J Neurol Neurosurg Psychiatry*, 2011. **82**(7): p. 740-6.
676. Kuang, L., et al., *Clinical and experimental studies of a novel P525R FUS mutation in amyotrophic lateral sclerosis*. *Neurol Genet*, 2017. **3**(4): p. e172.
677. Qiu, H., et al., *ALS-associated mutation FUS-R521C causes DNA damage and RNA splicing defects*. *J Clin Invest*, 2014. **124**(3): p. 981-99.
678. Lenzi, J., et al., *ALS mutant FUS proteins are recruited into stress granules in induced pluripotent stem cell-derived motoneurons*. *Dis Model Mech*, 2015. **8**(7): p. 755-66.
679. Blechingberg, J., et al., *Gene expression responses to FUS, EWS, and TAF15 reduction and stress granule sequestration analyses identifies FET-protein non-redundant functions*. *PLoS One*, 2012. **7**(9): p. e46251.
680. Lo Bello, M., et al., *ALS-Related Mutant FUS Protein Is Mislocalized to Cytoplasm and Is Recruited into Stress Granules of Fibroblasts from Asymptomatic FUS P525L Mutation Carriers*. *Neurodegener Dis*, 2017. **17**(6): p. 292-303.
681. Sama, R.R., et al., *FUS/TLS assembles into stress granules and is a prosurvival factor during hyperosmolar stress*. *J Cell Physiol*, 2013. **228**(11): p. 2222-31.
682. Schwartz, J.C., T.R. Cech, and R.R. Parker, *Biochemical Properties and Biological Functions of FET Proteins*. *Annu Rev Biochem*, 2015. **84**: p. 355-79.
683. Yoshizawa, T., et al., *Nuclear Import Receptor Inhibits Phase Separation of FUS through Binding to Multiple Sites*. *Cell*, 2018. **173**(3): p. 693-705.e22.
684. Takanashi, K. and A. Yamaguchi, *Aggregation of ALS-linked FUS mutant sequesters RNA binding proteins and impairs RNA granules formation*. *Biochem Biophys Res Commun*, 2014. **452**(3): p. 600-7.
685. Higelin, J., et al., *FUS Mislocalization and Vulnerability to DNA Damage in ALS Patients Derived hiPSCs and Aging Motoneurons*. *Front Cell Neurosci*, 2016. **10**: p. 290.
686. Biscarini, S., et al., *Characterization of the lncRNA transcriptome in mESC-derived motor neurons: Implications for FUS-ALS*. *Stem Cell Res*, 2018. **27**: p. 172-179.
687. Colombrita, C., et al., *From transcriptomic to protein level changes in TDP-43 and FUS loss-of-function cell models*. *Biochim Biophys Acta*, 2015. **1849**(12): p. 1398-410.
688. Coady, T.H. and J.L. Manley, *ALS mutations in TLS/FUS disrupt target gene expression*. *Genes Dev*, 2015. **29**(16): p. 1696-706.
689. Capauto, D., et al., *A Regulatory Circuitry Between Gria2, miR-409, and miR-495 Is Affected by ALS FUS Mutation in ESC-Derived Motor Neurons*. *Mol Neurobiol*, 2018.
690. Suzuki, H. and M. Matsuoka, *Overexpression of nuclear FUS induces neuronal cell death*. *Neuroscience*, 2015. **287**: p. 113-24.
691. Shelkovnikova, T.A., et al., *Compromised paraspeckle formation as a pathogenic factor in FUSopathies*. *Hum Mol Genet*, 2014. **23**(9): p. 2298-312.
692. Naganuma, T., et al., *Alternative 3'-end processing of long noncoding RNA initiates construction of nuclear paraspeckles*. *Embo j*, 2012. **31**(20): p. 4020-34.

693. Yu, Y., et al., *U1 snRNP is mislocalized in ALS patient fibroblasts bearing NLS mutations in FUS and is required for motor neuron outgrowth in zebrafish*. Nucleic Acids Res, 2015. **43**(6): p. 3208-18.
694. Yadav, S.P., et al., *The transcription-splicing protein NonO/p54nrb and three NonO-interacting proteins bind to distal enhancer region and augment rhodopsin expression*. Hum Mol Genet, 2014. **23**(8): p. 2132-44.
695. Wang, E.T., et al., *Alternative isoform regulation in human tissue transcriptomes*. Nature, 2008. **456**(7221): p. 470-6.
696. Kim, M.S., et al., *A draft map of the human proteome*. Nature, 2014. **509**(7502): p. 575-81.
697. Goodson, M.L., B.A. Jonas, and M.L. Privalsky, *Alternative mRNA splicing of SMRT creates functional diversity by generating corepressor isoforms with different affinities for different nuclear receptors*. J Biol Chem, 2005. **280**(9): p. 7493-503.
698. Asselin-Mullen, P., et al., *Protein interaction network of alternatively spliced NudCD1 isoforms*. Sci Rep, 2017. **7**(1): p. 12987.
699. Gowravaram, M., et al., *A conserved structural element in the RNA helicase UPF1 regulates its catalytic activity in an isoform-specific manner*. Nucleic Acids Res, 2018.
700. Yan, Y., et al., *ERalpha36, a variant of estrogen receptor alpha, is predominantly localized in mitochondria of human uterine smooth muscle and leiomyoma cells*. PLoS One, 2017. **12**(10): p. e0186078.
701. Patounas, O., et al., *A novel splicing isoform of protein arginine methyltransferase 1 (PRMT1) that lacks the dimerization arm and correlates with cellular malignancy*. J Cell Biochem, 2018. **119**(2): p. 2110-2123.
702. Behzadnia, N., et al., *Composition and three-dimensional EM structure of double affinity-purified, human prespliceosomal A complexes*. Embo j, 2007. **26**(6): p. 1737-48.
703. Lin, S. and X.D. Fu, *SR proteins and related factors in alternative splicing*. Adv Exp Med Biol, 2007. **623**: p. 107-22.
704. Sharp, P.A., *Split genes and RNA splicing*. Cell, 1994. **77**(6): p. 805-15.
705. Martinez-Contreras, R., et al., *hnRNP proteins and splicing control*. Adv Exp Med Biol, 2007. **623**: p. 123-47.
706. Fredericks, A.M., et al., *RNA-Binding Proteins: Splicing Factors and Disease*. Biomolecules, 2015. **5**(2): p. 893-909.
707. Wang, Y., et al., *Mechanism of alternative splicing and its regulation*. Biomed Rep, 2015. **3**(2): p. 152-158.
708. Sanchez, L., *Sex-determining mechanisms in insects*. Int J Dev Biol, 2008. **52**(7): p. 837-56.
709. Makeyev, E.V., et al., *The MicroRNA miR-124 promotes neuronal differentiation by triggering brain-specific alternative pre-mRNA splicing*. Mol Cell, 2007. **27**(3): p. 435-48.
710. Boutz, P.L., et al., *A post-transcriptional regulatory switch in polypyrimidine tract-binding proteins reprograms alternative splicing in developing neurons*. Genes Dev, 2007. **21**(13): p. 1636-52.
711. Goncalves, V., J.F.S. Pereira, and P. Jordan, *Signaling Pathways Driving Aberrant Splicing in Cancer Cells*. Genes (Basel), 2017. **9**(1).
712. Yeo, G., et al., *Variation in alternative splicing across human tissues*. Genome Biol, 2004. **5**(10): p. R74.
713. Su, C.H., D. D, and W.Y. Tarn, *Alternative Splicing in Neurogenesis and Brain Development*. Front Mol Biosci, 2018. **5**: p. 12.
714. Vuong, C.K., D.L. Black, and S. Zheng, *The neurogenetics of alternative splicing*. Nat Rev Neurosci, 2016. **17**(5): p. 265-81.

715. Hakim, N.H., et al., *Neuron-specific splicing*. Biosci Trends, 2017. **11**(1): p. 16-22.
716. Chabot, B. and L. Shkreta, *Defective control of pre-messenger RNA splicing in human disease*. J Cell Biol, 2016. **212**(1): p. 13-27.
717. Gámez-Valero, A. and K. Beyer, *Alternative Splicing of Alpha- and Beta-Synuclein Genes Plays Differential Roles in Synucleinopathies*. Genes, 2018. **9**(2): p. 63.
718. Niblock, M. and J.-M. Gallo, *Tau alternative splicing in familial and sporadic tauopathies*. Biochemical Society Transactions, 2012. **40**(4): p. 677-680.
719. Hutton, M., et al., *Association of missense and 5'-splice-site mutations in tau with the inherited dementia FTDP-17*. Nature, 1998. **393**(6686): p. 702-5.
720. Lacovich, V., et al., *Tau Isoforms Imbalance Impairs the Axonal Transport of the Amyloid Precursor Protein in Human Neurons*. J Neurosci, 2017. **37**(1): p. 58-69.
721. Gu, J., et al., *Transactive response DNA-binding protein 43 (TDP-43) regulates alternative splicing of tau exon 10: Implications for the pathogenesis of tauopathies*. J Biol Chem, 2017. **292**(25): p. 10600-10612.
722. Honda, D., et al., *The ALS/FTLD-related RNA-binding proteins TDP-43 and FUS have common downstream RNA targets in cortical neurons*. FEBS Open Bio, 2013. **4**: p. 1-10.
723. D'Alton, S., M. Altshuler, and J. Lewis, *Studies of alternative isoforms provide insight into TDP-43 autoregulation and pathogenesis*. Rna, 2015. **21**(8): p. 1419-32.
724. Pons, M., et al., *Splicing factors act as genetic modulators of TDP-43 production in a new autoregulatory TDP-43 Drosophila model*. Hum Mol Genet, 2017. **26**(17): p. 3396-3408.
725. Da Cruz, S. and D.W. Cleveland, *Understanding the role of TDP-43 and FUS/TLS in ALS and beyond*. Curr Opin Neurobiol, 2011. **21**(6): p. 904-19.
726. White, M.A., et al., *TDP-43 gains function due to perturbed autoregulation in a Tardbp knock-in mouse model of ALS-FTD*. Nat Neurosci, 2018. **21**(4): p. 552-563.
727. D'Erchia, A.M., et al., *Massive transcriptome sequencing of human spinal cord tissues provides new insights into motor neuron degeneration in ALS*. Sci Rep, 2017. **7**(1): p. 10046.
728. Rabin, S.J., et al., *Sporadic ALS has compartment-specific aberrant exon splicing and altered cell-matrix adhesion biology*. Hum Mol Genet, 2010. **19**(2): p. 313-28.
729. Prudencio, M., et al., *Distinct brain transcriptome profiles in C9orf72-associated and sporadic ALS*. Nat Neurosci, 2015. **18**(8): p. 1175-82.
730. Theodoratos, A., et al., *Splice variants of the condensin II gene Ncap2 include alternative reading frame translations of exon 1*. Febs j, 2012. **279**(8): p. 1422-32.
731. Wilson, L.O., et al., *A novel splicing outcome reveals more than 2000 new mammalian protein isoforms*. Bioinformatics, 2014. **30**(2): p. 151-6.
732. Karousis, E.D. and D.C. Sideris, *A subtle alternative splicing event gives rise to a widely expressed human RNase k isoform*. PLoS One, 2014. **9**(5): p. e96557.
733. Soares, L., et al., *Two isoforms of otubain 1 regulate T cell anergy via GRAIL*. Nat Immunol, 2004. **5**(1): p. 45-54.
734. Yin, S., et al., *Evidence that C9ORF72 Dipeptide Repeat Proteins Associate with U2 snRNP to Cause Mis-splicing in ALS/FTD Patients*. Cell Rep, 2017. **19**(11): p. 2244-2256.
735. Masuda, A., J. Takeda, and K. Ohno, *FUS-mediated regulation of alternative RNA processing in neurons: insights from global transcriptome analysis*. Wiley Interdiscip Rev RNA, 2016. **7**(3): p. 330-40.
736. Tollervey, J.R., et al., *Characterizing the RNA targets and position-dependent splicing regulation by TDP-43*. Nat Neurosci, 2011. **14**(4): p. 452-8.
737. Weskamp, K. and S.J. Barmada, *TDP43 and RNA instability in amyotrophic lateral sclerosis*. Brain Res, 2018.

738. Highley, J.R., et al., *Loss of nuclear TDP-43 in amyotrophic lateral sclerosis (ALS) causes altered expression of splicing machinery and widespread dysregulation of RNA splicing in motor neurones*. *Neuropathol Appl Neurobiol*, 2014. **40**(6): p. 670-85.
739. Horton, P., et al., *WoLF PSORT: protein localization predictor*. *Nucleic Acids Res*, 2007. **35**(Web Server issue): p. W585-7.
740. Palade, G., *Intracellular aspects of the process of protein synthesis*. *Science*, 1975. **189**(4206): p. 867.
741. Mothes, W., et al., *Molecular mechanism of membrane protein integration into the endoplasmic reticulum*. *Cell*, 1997. **89**(4): p. 523-33.
742. Ng, D.T., J.D. Brown, and P. Walter, *Signal sequences specify the targeting route to the endoplasmic reticulum membrane*. *J Cell Biol*, 1996. **134**(2): p. 269-78.
743. Zalucki, Y.M. and M.P. Jennings, *Signal peptidase I processed secretory signal sequences: Selection for and against specific amino acids at the second position of mature protein*. *Biochem Biophys Res Commun*, 2017. **483**(3): p. 972-977.
744. Borgese, N., *Getting membrane proteins on and off the shuttle bus between the endoplasmic reticulum and the Golgi complex*. *J Cell Sci*, 2016. **129**(8): p. 1537-45.
745. Appenzeller-Herzog, C. and H.P. Hauri, *The ER-Golgi intermediate compartment (ERGIC): in search of its identity and function*. *J Cell Sci*, 2006. **119**(Pt 11): p. 2173-83.
746. Rabouille, C., *Pathways of Unconventional Protein Secretion*. *Trends Cell Biol*, 2017. **27**(3): p. 230-240.
747. Adamczyk, M., et al., *P2X7 receptor activation regulates rapid unconventional export of transglutaminase-2*. *Journal of Cell Science*, 2015. **128**(24): p. 4615-4628.
748. Ktistakis, N.T. and S.A. Tooze, *Digesting the Expanding Mechanisms of Autophagy*. *Trends in Cell Biology*, 2016. **26**(8): p. 624-635.
749. Grieve, A.G. and C. Rabouille, *Golgi bypass: skirting around the heart of classical secretion*. *Cold Spring Harb Perspect Biol*, 2011. **3**(4).
750. Petersen, T.N., et al., *SignalP 4.0: discriminating signal peptides from transmembrane regions*. *Nat Methods*, 2011. **8**(10): p. 785-6.
751. Krogh, A., et al., *Predicting transmembrane protein topology with a hidden Markov model: application to complete genomes*. *J Mol Biol*, 2001. **305**(3): p. 567-80.
752. Tsirigos, K.D., et al., *The TOPCONS web server for consensus prediction of membrane protein topology and signal peptides*. *Nucleic Acids Res*, 2015. **43**(W1): p. W401-7.
753. Viklund, H. and A. Elofsson, *OCTOPUS: improving topology prediction by two-track ANN-based preference scores and an extended topological grammar*. *Bioinformatics*, 2008. **24**(15): p. 1662-8.
754. Reynolds, S.M., et al., *Transmembrane topology and signal peptide prediction using dynamic bayesian networks*. *PLoS Comput Biol*, 2008. **4**(11): p. e1000213.
755. Kall, L., A. Krogh, and E.L. Sonnhammer, *Advantages of combined transmembrane topology and signal peptide prediction--the Phobius web server*. *Nucleic Acids Res*, 2007. **35**(Web Server issue): p. W429-32.
756. Peters, C., et al., *Improved topology prediction using the terminal hydrophobic helices rule*. *Bioinformatics*, 2016. **32**(8): p. 1158-62.
757. Viklund, H., et al., *SPOCTOPUS: a combined predictor of signal peptides and membrane protein topology*. *Bioinformatics*, 2008. **24**(24): p. 2928-9.
758. Satoh, T., et al., *Tat-binding protein-1 (TBP-1), an ATPase of 19S regulatory particles of the 26S proteasome, enhances androgen receptor function in cooperation with TBP-1-interacting protein/Hop2*. *Endocrinology*, 2009. **150**(7): p. 3283-90.
759. Danshina, P.V., et al., *Phosphoglycerate kinase 2 (PGK2) is essential for sperm function and male fertility in mice*. *Biol Reprod*, 2010. **82**(1): p. 136-45.
760. Rabilloud, T. and C. Lelong, *Two-dimensional gel electrophoresis in proteomics: A tutorial*. *Journal of Proteomics*, 2011. **74**(10): p. 1829-1841.

761. Srivastava, R., M.J. Murphy, and J. Jeffery, *Cerebrospinal fluid: the role of biochemical analysis*. Br J Hosp Med (Lond), 2008. **69**(4): p. 218-21.
762. Ogata, Y., M.C. Charlesworth, and D.C. Muddiman, *Evaluation of protein depletion methods for the analysis of total-, phospho- and glycoproteins in lumbar cerebrospinal fluid*. J Proteome Res, 2005. **4**(3): p. 837-45.
763. Huang, T., et al., *Fractionation of Fab glycosylated immunoglobulin G with concanavalin A chromatography unveils new structural properties of the molecule*. Oncotarget, 2016. **7**(21): p. 31166-76.
764. Uhlen, M., et al., *A proposal for validation of antibodies*. Nat Methods, 2016. **13**(10): p. 823-7.
765. Revest, J.M., L. DeMoerlooze, and C. Dickson, *Fibroblast growth factor 9 secretion is mediated by a non-cleaved amino-terminal signal sequence*. J Biol Chem, 2000. **275**(11): p. 8083-90.
766. Itoh, N., *The Fgf families in humans, mice, and zebrafish: their evolutionary processes and roles in development, metabolism, and disease*. Biol Pharm Bull, 2007. **30**(10): p. 1819-25.
767. Miyakawa, K. and T. Imamura, *Secretion of FGF-16 requires an uncleaved bipartite signal sequence*. J Biol Chem, 2003. **278**(37): p. 35718-24.
768. Miyakawa, K., et al., *A hydrophobic region locating at the center of fibroblast growth factor-9 is crucial for its secretion*. J Biol Chem, 1999. **274**(41): p. 29352-7.
769. Biron, D.G., et al., *The pitfalls of proteomics experiments without the correct use of bioinformatics tools*. Proteomics, 2006. **6**(20): p. 5577-96.
770. Xu, N. and B. Dahlback, *A novel human apolipoprotein (apoM)*. J Biol Chem, 1999. **274**(44): p. 31286-90.
771. von Heijne, G., et al., *The efficiency of the uncleaved secretion signal in the plasminogen activator inhibitor type 2 protein can be enhanced by point mutations that increase its hydrophobicity*. J Biol Chem, 1991. **266**(23): p. 15240-3.
772. Shanthalingam, S. and S. Srikumaran, *Intact signal peptide of CD18, the beta-subunit of beta2-integrins, renders ruminants susceptible to Mannheimia haemolytica leukotoxin*. Proc Natl Acad Sci U S A, 2009. **106**(36): p. 15448-53.
773. Harrington, J.M., et al., *A retained secretory signal peptide mediates high density lipoprotein (HDL) assembly and function of haptoglobin-related protein*. J Biol Chem, 2014. **289**(36): p. 24811-20.
774. Liu, M., et al., *Uncleaved ApoM signal peptide is required for formation of large ApoM/sphingosine 1-phosphate (S1P)-enriched HDL particles*. J Biol Chem, 2015. **290**(12): p. 7861-70.
775. Wang, J., et al., *Comparative Secretome Analysis Reveals Perturbation of Host Secretion Pathways by a Hypovirus*. Sci Rep, 2016. **6**: p. 34308.
776. Falgarone, G. and G. Chiocchia, *Chapter 8: Clusterin: A multifacet protein at the crossroad of inflammation and autoimmunity*. Adv Cancer Res, 2009. **104**: p. 139-70.
777. Leskov, K.S., et al., *Synthesis and functional analyses of nuclear clusterin, a cell death protein*. J Biol Chem, 2003. **278**(13): p. 11590-600.
778. Bae, C.H., et al., *Clusterin Induces MUC5AC Expression via Activation of NF-kappaB in Human Airway Epithelial Cells*. Clin Exp Otorhinolaryngol, 2018.
779. Jacobsson, J., et al., *Superoxide dismutase in CSF from amyotrophic lateral sclerosis patients with and without CuZn-superoxide dismutase mutations*. Brain, 2001. **124**(Pt 7): p. 1461-6.
780. Basso, M., et al., *Mutant copper-zinc superoxide dismutase (SOD1) induces protein secretion pathway alterations and exosome release in astrocytes: implications for disease spreading and motor neuron pathology in amyotrophic lateral sclerosis*. J Biol Chem, 2013. **288**(22): p. 15699-711.

781. Mondola, P., et al., *Evidence for secretion of cytosolic CuZn superoxide dismutase by Hep G2 cells and human fibroblasts*. Int J Biochem Cell Biol, 1996. **28**(6): p. 677-81.
782. Grad, L.I., et al., *Intercellular propagated misfolding of wild-type Cu/Zn superoxide dismutase occurs via exosome-dependent and -independent mechanisms*. Proc Natl Acad Sci U S A, 2014. **111**(9): p. 3620-5.
783. Gomes, C., et al., *Evidence for secretion of Cu,Zn superoxide dismutase via exosomes from a cell model of amyotrophic lateral sclerosis*. Neurosci Lett, 2007. **428**(1): p. 43-6.
784. Silverman, J.M., et al., *Disease Mechanisms in ALS: Misfolded SOD1 Transferred Through Exosome-Dependent and Exosome-Independent Pathways*. Cell Mol Neurobiol, 2016. **36**(3): p. 377-81.
785. Guo, J.L. and V.M. Lee, *Cell-to-cell transmission of pathogenic proteins in neurodegenerative diseases*. Nat Med, 2014. **20**(2): p. 130-8.
786. Grad, L.I., et al., *Exosome-dependent and independent mechanisms are involved in prion-like transmission of propagated Cu/Zn superoxide dismutase misfolding*. Prion, 2014. **8**(5): p. 331-5.
787. Steinacker, P., et al., *TDP-43 in cerebrospinal fluid of patients with frontotemporal lobar degeneration and amyotrophic lateral sclerosis*. Arch Neurol, 2008. **65**(11): p. 1481-7.
788. Melot, T., et al., *Characterization of a new brain-specific isoform of the EWS oncoprotein*. Eur J Biochem, 2001. **268**(12): p. 3483-9.
789. Barel, M. and A. Charbit, *Role of Glycosylation/Deglycosylation Processes in Francisella tularensis Pathogenesis*. Front Cell Infect Microbiol, 2017. **7**: p. 71.
790. Nguyen, A.T., et al., *Organelle Specific O-Glycosylation Drives MMP14 Activation, Tumor Growth, and Metastasis*. Cancer Cell, 2017. **32**(5): p. 639-653.e6.
791. Jacquemin, M., et al., *Variable region heavy chain glycosylation determines the anticoagulant activity of a factor VIII antibody*. J Thromb Haemost, 2006. **4**(5): p. 1047-55.
792. Sumer-Bayraktar, Z., et al., *Asn347 Glycosylation of Corticosteroid-binding Globulin Fine-tunes the Host Immune Response by Modulating Proteolysis by Pseudomonas aeruginosa and Neutrophil Elastase*. J Biol Chem, 2016. **291**(34): p. 17727-42.
793. Yi, W., et al., *Phosphofructokinase 1 glycosylation regulates cell growth and metabolism*. Science, 2012. **337**(6097): p. 975-80.
794. Freeze, H.H., et al., *Neurology of inherited glycosylation disorders*. Lancet Neurol, 2012. **11**(5): p. 453-66.
795. Scott, H. and V.M. Panin, *The role of protein N-glycosylation in neural transmission*. Glycobiology, 2014. **24**(5): p. 407-17.
796. Schwetz, T.A., et al., *Sialic acids attached to O-glycans modulate voltage-gated potassium channel gating*. J Biol Chem, 2011. **286**(6): p. 4123-32.
797. Scott, H. and V.M. Panin, *N-Glycosylation in Regulation of the Nervous System*, in *Glycobiology of the Nervous System*, R.K. Yu and C.-L. Schengrund, Editors. 2014, Springer New York: New York, NY. p. 367-394.
798. Moremen, K.W., M. Tiemeyer, and A.V. Nairn, *Vertebrate protein glycosylation: diversity, synthesis and function*. Nat Rev Mol Cell Biol, 2012. **13**(7): p. 448-62.
799. Van den Steen, P., et al., *Concepts and principles of O-linked glycosylation*. Crit Rev Biochem Mol Biol, 1998. **33**(3): p. 151-208.
800. Kamemura, K. and G.W. Hart, *Dynamic Interplay between O-Glycosylation and O-Phosphorylation of Nucleocytoplasmic Proteins: A New Paradigm for Metabolic Control of Signal Transduction and Transcription*, in *Progress in Nucleic Acid Research and Molecular Biology*. 2003, Academic Press. p. 107-136.
801. Hanisch, F.G., *O-glycosylation of the mucin type*. Biol Chem, 2001. **382**(2): p. 143-9.

802. Bause, E. and H. Hettkamp, *Primary structural requirements for N-glycosylation of peptides in rat liver*. FEBS Lett, 1979. **108**(2): p. 341-4.
803. Marshall, R.D., *The nature and metabolism of the carbohydrate-peptide linkages of glycoproteins*. Biochem Soc Symp, 1974(40): p. 17-26.
804. Aepli, M., *N-linked protein glycosylation in the ER*. Biochim Biophys Acta, 2013. **1833**(11): p. 2430-7.
805. Bickel, T., et al., *Biosynthesis of lipid-linked oligosaccharides in Saccharomyces cerevisiae: Alg13p and Alg14p form a complex required for the formation of GlcNAc(2)-PP-dolichol*. J Biol Chem, 2005. **280**(41): p. 34500-6.
806. Noffz, C., S. Keppler-Ross, and N. Dean, *Hetero-oligomeric interactions between early glycosyltransferases of the dolichol cycle*. Glycobiology, 2009. **19**(5): p. 472-8.
807. Elbein, A.D., *Inhibitors of the biosynthesis and processing of N-linked oligosaccharides*. CRC Crit Rev Biochem, 1984. **16**(1): p. 21-49.
808. Gao, X.D., A. Nishikawa, and N. Dean, *Physical interactions between the Alg1, Alg2, and Alg11 mannosyltransferases of the endoplasmic reticulum*. Glycobiology, 2004. **14**(6): p. 559-70.
809. Cipollo, J.F., et al., *The yeast ALG11 gene specifies addition of the terminal alpha 1,2-Man to the Man5GlcNAc2-PP-dolichol N-glycosylation intermediate formed on the cytosolic side of the endoplasmic reticulum*. J Biol Chem, 2001. **276**(24): p. 21828-40.
810. Sanyal, S. and A.K. Menon, *Flipping lipids: why an' what's the reason for?* ACS Chem Biol, 2009. **4**(11): p. 895-909.
811. Lairson, L.L., et al., *Glycosyltransferases: structures, functions, and mechanisms*. Annu Rev Biochem, 2008. **77**: p. 521-55.
812. Kornfeld, R. and S. Kornfeld, *Assembly of asparagine-linked oligosaccharides*. Annu Rev Biochem, 1985. **54**: p. 631-64.
813. Mohorko, E., R. Glockshuber, and M. Aepli, *Oligosaccharyltransferase: the central enzyme of N-linked protein glycosylation*. J Inherit Metab Dis, 2011. **34**(4): p. 869-78.
814. Zielinska, D.F., et al., *Precision mapping of an in vivo N-glycoproteome reveals rigid topological and sequence constraints*. Cell, 2010. **141**(5): p. 897-907.
815. Apweiler, R., H. Hermjakob, and N. Sharon, *On the frequency of protein glycosylation, as deduced from analysis of the SWISS-PROT database*. Biochim Biophys Acta, 1999. **1473**(1): p. 4-8.
816. Hubbard, S.C. and P.W. Robbins, *Synthesis and processing of protein-linked oligosaccharides in vivo*. J Biol Chem, 1979. **254**(11): p. 4568-76.
817. Ferris, S.P., V.K. Kodali, and R.J. Kaufman, *Glycoprotein folding and quality-control mechanisms in protein-folding diseases*. Dis Model Mech, 2014. **7**(3): p. 331-41.
818. Galli, C., et al., *Malectin participates in a backup glycoprotein quality control pathway in the mammalian ER*. PLoS One, 2011. **6**(1): p. e16304.
819. Rutkevich, L.A. and D.B. Williams, *Participation of lectin chaperones and thiol oxidoreductases in protein folding within the endoplasmic reticulum*. Curr Opin Cell Biol, 2011. **23**(2): p. 157-66.
820. Caramelo, J.J. and A.J. Parodi, *A sweet code for glycoprotein folding*. FEBS Lett, 2015. **589**(22): p. 3379-87.
821. Helenius, A., *How N-linked oligosaccharides affect glycoprotein folding in the endoplasmic reticulum*. Mol Biol Cell, 1994. **5**(3): p. 253-65.
822. Zapun, A., et al., *Enhanced catalysis of ribonuclease B folding by the interaction of calnexin or calreticulin with ERp57*. J Biol Chem, 1998. **273**(11): p. 6009-12.
823. Appenzeller, C., et al., *The lectin ERGIC-53 is a cargo transport receptor for glycoproteins*. Nat Cell Biol, 1999. **1**(6): p. 330-4.
824. Roth, J. and C. Zuber, *Quality control of glycoprotein folding and ERAD: the role of N-glycan handling, EDEM1 and OS-9*. Histochem Cell Biol, 2017. **147**(2): p. 269-284.

825. Cali, T., et al., *Segregation and rapid turnover of EDEM1 by an autophagy-like mechanism modulates standard ERAD and folding activities*. Biochem Biophys Res Commun, 2008. **371**(3): p. 405-10.
826. Benyair, R., N. Ogen-Shtern, and G.Z. Lederkremer, *Glycan regulation of ER-associated degradation through compartmentalization*. Semin Cell Dev Biol, 2015. **41**: p. 99-109.
827. Arvan, P., et al., *Secretory pathway quality control operating in Golgi, plasmalemmal, and endosomal systems*. Traffic, 2002. **3**(11): p. 771-80.
828. Saito, F., K. Yanagisawa, and T. Miyatake, *Soluble derivatives of beta/A4 amyloid protein precursor in human cerebrospinal fluid are both N- and O-glycosylated*. Brain Res Mol Brain Res, 1993. **19**(1-2): p. 171-4.
829. Yazaki, M., et al., *Mutation of potential N-linked glycosylation sites in the Alzheimer's disease amyloid precursor protein (APP)*. Neurosci Lett, 1996. **221**(1): p. 57-60.
830. Pahlsson, P. and S.L. Spitalnik, *The role of glycosylation in synthesis and secretion of beta-amyloid precursor protein by Chinese hamster ovary cells*. Arch Biochem Biophys, 1996. **331**(2): p. 177-86.
831. Nizynski, B., W. Dzwolak, and K. Nieznanski, *Amyloidogenesis of Tau protein*. Protein Sci, 2017. **26**(11): p. 2126-2150.
832. Liu, F., et al., *Involvement of aberrant glycosylation in phosphorylation of tau by cdk5 and GSK-3beta*. FEBS Lett, 2002. **530**(1-3): p. 209-14.
833. Frenkel-Pinter, M., et al., *Interplay between protein glycosylation pathways in Alzheimer's disease*. Sci Adv, 2017. **3**(9): p. e1601576.
834. Palmigiano, A., et al., *CSF N-glycoproteomics for early diagnosis in Alzheimer's disease*. J Proteomics, 2016. **131**: p. 29-37.
835. Fodero, L.R., et al., *Wheat germ agglutinin-binding glycoproteins are decreased in Alzheimer's disease cerebrospinal fluid*. J Neurochem, 2001. **79**(5): p. 1022-6.
836. Taniguchi, M., et al., *Sugar chains of cerebrospinal fluid transferrin as a new biological marker of Alzheimer's disease*. Dement Geriatr Cogn Disord, 2008. **26**(2): p. 117-22.
837. Edri-Brami, M., et al., *Glycans in sera of amyotrophic lateral sclerosis patients and their role in killing neuronal cells*. PLoS One, 2012. **7**(5): p. e35772.
838. Gonçalves, M., et al., *Phosphoneurofilament heavy chain and N-glycomics from the cerebrospinal fluid in amyotrophic lateral sclerosis*. Clinica Chimica Acta, 2015. **438**: p. 342-349.
839. Shan, X., D.J. Vocadlo, and C. Krieger, *Reduced protein O-glycosylation in the nervous system of the mutant SOD1 transgenic mouse model of amyotrophic lateral sclerosis*. Neurosci Lett, 2012. **516**(2): p. 296-301.
840. Roy, S., F.H. Hochberg, and P.S. Jones, *Extracellular vesicles: the growth as diagnostics and therapeutics; a survey*. J Extracell Vesicles, 2018. **7**(1): p. 1438720.
841. Zaborowski, M.P., et al., *Extracellular Vesicles: Composition, Biological Relevance, and Methods of Study*. Bioscience, 2015. **65**(8): p. 783-797.
842. Witwer, K.W., et al., *Standardization of sample collection, isolation and analysis methods in extracellular vesicle research*. J Extracell Vesicles, 2013. **2**.
843. Akers, J.C., et al., *Biogenesis of extracellular vesicles (EV): exosomes, microvesicles, retrovirus-like vesicles, and apoptotic bodies*. J Neurooncol, 2013. **113**(1): p. 1-11.
844. Colombo, M., G. Raposo, and C. Thery, *Biogenesis, secretion, and intercellular interactions of exosomes and other extracellular vesicles*. Annu Rev Cell Dev Biol, 2014. **30**: p. 255-89.
845. Hanson, P.I. and A. Cashikar, *Multivesicular body morphogenesis*. Annu Rev Cell Dev Biol, 2012. **28**: p. 337-62.

846. Thery, C., et al., *Proteomic analysis of dendritic cell-derived exosomes: a secreted subcellular compartment distinct from apoptotic vesicles*. J Immunol, 2001. **166**(12): p. 7309-18.
847. Hessvik, N.P. and A. Llorente, *Current knowledge on exosome biogenesis and release*. Cell Mol Life Sci, 2018. **75**(2): p. 193-208.
848. McMahon, H.T. and E. Boucrot, *Membrane curvature at a glance*. J Cell Sci, 2015. **128**(6): p. 1065-70.
849. Moreno-Gonzalo, O., C. Villarroja-Beltri, and F. Sanchez-Madrid, *Post-translational modifications of exosomal proteins*. Front Immunol, 2014. **5**: p. 383.
850. Liang, Y., et al., *Complex N-linked glycans serve as a determinant for exosome/microvesicle cargo recruitment*. J Biol Chem, 2014. **289**(47): p. 32526-37.
851. Jaiswal, J.K., N.W. Andrews, and S.M. Simon, *Membrane proximal lysosomes are the major vesicles responsible for calcium-dependent exocytosis in nonsecretory cells*. J Cell Biol, 2002. **159**(4): p. 625-35.
852. McKelvey, K.J., et al., *Exosomes: Mechanisms of Uptake*. J Circ Biomark, 2015. **4**: p. 7.
853. Camussi, G., et al., *Exosomes/microvesicles as a mechanism of cell-to-cell communication*. Kidney International, 2010. **78**(9): p. 838-848.
854. Holdt, L.M., A. Kohlmaier, and D. Teupser, *Molecular roles and function of circular RNAs in eukaryotic cells*. Cell Mol Life Sci, 2018. **75**(6): p. 1071-1098.
855. Lamparski, H.G., et al., *Production and characterization of clinical grade exosomes derived from dendritic cells*. J Immunol Methods, 2002. **270**(2): p. 211-26.
856. Tan, S.S., et al., *Therapeutic MSC exosomes are derived from lipid raft microdomains in the plasma membrane*. J Extracell Vesicles, 2013. **2**.
857. Sarko, D.K. and C.E. McKinney, *Exosomes: Origins and Therapeutic Potential for Neurodegenerative Disease*. Front Neurosci, 2017. **11**: p. 82.
858. Bonafede, R. and R. Mariotti, *ALS Pathogenesis and Therapeutic Approaches: The Role of Mesenchymal Stem Cells and Extracellular Vesicles*. Front Cell Neurosci, 2017. **11**: p. 80.
859. Fevrier, B., et al., *Cells release prions in association with exosomes*. Proc Natl Acad Sci U S A, 2004. **101**(26): p. 9683-8.
860. Pan, I., N. Roitenberg, and E. Cohen, *Vesicle-mediated secretion of misfolded prion protein molecules from cyclosporin A-treated cells*. Faseb j, 2018. **32**(3): p. 1479-1492.
861. Vella, L.J., et al., *Packaging of prions into exosomes is associated with a novel pathway of PrP processing*. J Pathol, 2007. **211**(5): p. 582-90.
862. Guo, B.B., S.A. Bellingham, and A.F. Hill, *Stimulating the Release of Exosomes Increases the Intercellular Transfer of Prions*. J Biol Chem, 2016. **291**(10): p. 5128-37.
863. Cervenakova, L., et al., *Are prions transported by plasma exosomes?* Transfus Apher Sci, 2016. **55**(1): p. 70-83.
864. Yim, Y.I., et al., *The multivesicular body is the major internal site of prion conversion*. J Cell Sci, 2015. **128**(7): p. 1434-43.
865. Pinto, S., et al., *Exosomes from NSC-34 Cells Transfected with hSOD1-G93A Are Enriched in miR-124 and Drive Alterations in Microglia Phenotype*. Front Neurosci, 2017. **11**: p. 273.
866. Zondler, L., et al., *Impaired activation of ALS monocytes by exosomes*. Immunol Cell Biol, 2017. **95**(2): p. 207-214.
867. Jensen, P.H., et al., *Structural analysis of N- and O-glycans released from glycoproteins*. Nat Protoc, 2012. **7**(7): p. 1299-310.
868. Ashwood, C., et al., *Discrimination of Isomers of Released N- and O-Glycans Using Diagnostic Product Ions in Negative Ion PGC-LC-ESI-MS/MS*. J Am Soc Mass Spectrom, 2018.

869. Ito, D., et al., *Nuclear transport impairment of amyotrophic lateral sclerosis-linked mutations in FUS/TLS*. *Ann Neurol*, 2011. **69**(1): p. 152-62.
870. Snapp, E., *Design and use of fluorescent fusion proteins in cell biology*. *Curr Protoc Cell Biol*, 2005. **Chapter 21**: p. Unit 21.4.
871. Tanudji, M., S. Hevi, and S.L. Chuck, *Improperly folded green fluorescent protein is secreted via a non-classical pathway*. *J Cell Sci*, 2002. **115**(Pt 19): p. 3849-57.
872. Reynard, O., et al., *Unconventional secretion of Ebola virus matrix protein VP40*. *J Infect Dis*, 2011. **204 Suppl 3**: p. S833-9.
873. Kenny, P.A., T. Enver, and A. Ashworth, *Receptor and secreted targets of Wnt-1/beta-catenin signalling in mouse mammary epithelial cells*. *BMC Cancer*, 2005. **5**: p. 3.
874. Blom, N., et al., *Prediction of post-translational glycosylation and phosphorylation of proteins from the amino acid sequence*. *Proteomics*, 2004. **4**(6): p. 1633-49.
875. Palmisano, G., et al., *Chemical deamidation: a common pitfall in large-scale N-linked glycoproteomic mass spectrometry-based analyses*. *J Proteome Res*, 2012. **11**(3): p. 1949-57.
876. Oda, T., et al., *Distinct mechanism of cell death is responsible for tunicamycin-induced ER stress in SK-N-SH and SH-SY5Y cells*. *Neuroscience Research*, 2008. **60**(1): p. 29-39.
877. Wang, P., et al., *Evolution of protein N-glycosylation process in Golgi apparatus which shapes diversity of protein N-glycan structures in plants, animals and fungi*. *Sci Rep*, 2017. **7**: p. 40301.
878. Ota, F., et al., *N-Glycosylation is essential for the secretion of extracellular superoxide dismutase*. *FEBS Lett*, 2016. **590**(19): p. 3357-3367.
879. Mondola, P., et al., *The Cu,Zn superoxide dismutase in neuroblastoma SK-N-BE cells is exported by a microvesicles dependent pathway*. *Brain Res Mol Brain Res*, 2003. **110**(1): p. 45-51.
880. Farg, M.A., et al., *Mutant FUS induces endoplasmic reticulum stress in amyotrophic lateral sclerosis and interacts with protein disulfide-isomerase*. *Neurobiology of Aging*, 2012. **33**(12): p. 2855-2868.
881. Wiesman, K.C., et al., *CCN5, a secreted protein, localizes to the nucleus*. *J Cell Commun Signal*, 2010. **4**(2): p. 91-8.
882. Kryndushkin, D., R.B. Wickner, and F. Shewmaker, *FUS/TLS forms cytoplasmic aggregates, inhibits cell growth and interacts with TDP-43 in a yeast model of amyotrophic lateral sclerosis*. *Protein Cell*, 2011. **2**(3): p. 223-36.
883. Nomura, T., et al., *Intranuclear aggregation of mutant FUS/TLS as a molecular pathomechanism of amyotrophic lateral sclerosis*. *J Biol Chem*, 2014. **289**(2): p. 1192-202.
884. Shelkovernikova, T.A., et al., *Multistep process of FUS aggregation in the cell cytoplasm involves RNA-dependent and RNA-independent mechanisms*. *Hum Mol Genet*, 2014. **23**(19): p. 5211-26.
885. Yang, L., et al., *Subcellular localization and RNAs determine FUS architecture in different cellular compartments*. *Hum Mol Genet*, 2015. **24**(18): p. 5174-83.
886. Suzuki, H., K. Lee, and M. Matsuoka, *TDP-43-induced death is associated with altered regulation of BIM and Bcl-xL and attenuated by caspase-mediated TDP-43 cleavage*. *J Biol Chem*, 2011. **286**(15): p. 13171-83.
887. Vogt, M.A., et al., *TDP-43 induces p53-mediated cell death of cortical progenitors and immature neurons*. *Sci Rep*, 2018. **8**(1): p. 8097.
888. Ederle, H. and D. Dormann, *TDP-43 and FUS en route from the nucleus to the cytoplasm*. *FEBS Lett*, 2017. **591**(11): p. 1489-1507.

889. Kim, S.H., et al., *Amyotrophic lateral sclerosis-associated proteins TDP-43 and FUS/TLS function in a common biochemical complex to co-regulate HDAC6 mRNA*. J Biol Chem, 2010. **285**(44): p. 34097-105.
890. Tada, M., et al., *Matrin 3 Is a Component of Neuronal Cytoplasmic Inclusions of Motor Neurons in Sporadic Amyotrophic Lateral Sclerosis*. Am J Pathol, 2018. **188**(2): p. 507-514.
891. Lasser, C., et al., *Two distinct extracellular RNA signatures released by a single cell type identified by microarray and next-generation sequencing*. RNA Biol, 2017. **14**(1): p. 58-72.
892. Arroyo, J.D., et al., *Argonaute2 complexes carry a population of circulating microRNAs independent of vesicles in human plasma*. Proc Natl Acad Sci U S A, 2011. **108**(12): p. 5003-8.
893. Patton, J.G., et al., *Biogenesis, delivery, and function of extracellular RNA*. J Extracell Vesicles, 2015. **4**: p. 27494.
894. Hurwitz, S.N., et al., *Proteomic profiling of NCI-60 extracellular vesicles uncovers common protein cargo and cancer type-specific biomarkers*. Oncotarget, 2016. **7**(52): p. 86999-87015.
895. Marimpietri, D., et al., *Proteome profiling of neuroblastoma-derived exosomes reveal the expression of proteins potentially involved in tumor progression*. PLoS One, 2013. **8**(9): p. e75054.
896. Kopito, R.R., *Aggresomes, inclusion bodies and protein aggregation*. Trends Cell Biol, 2000. **10**(12): p. 524-30.
897. Ohtsubo, K. and J.D. Marth, *Glycosylation in cellular mechanisms of health and disease*. Cell, 2006. **126**(5): p. 855-67.
898. Halbgebauer, S., et al., *Modified serpinA1 as risk marker for Parkinson's disease dementia: Analysis of baseline data*. Sci Rep, 2016. **6**: p. 26145.
899. Vlug, A.S., et al., *ATF3 expression precedes death of spinal motoneurons in amyotrophic lateral sclerosis-SOD1 transgenic mice and correlates with c-Jun phosphorylation, CHOP expression, somato-dendritic ubiquitination and Golgi fragmentation*. Eur J Neurosci, 2005. **22**(8): p. 1881-94.
900. Jucker, M. and L.C. Walker, *Self-propagation of pathogenic protein aggregates in neurodegenerative diseases*. Nature, 2013. **501**(7465): p. 45-51.
901. Mackenzie, I.R., R. Rademakers, and M. Neumann, *TDP-43 and FUS in amyotrophic lateral sclerosis and frontotemporal dementia*. Lancet Neurol, 2010. **9**(10): p. 995-1007.
902. Ishigaki, S. and G. Sobue, *Importance of Functional Loss of FUS in FTL/ALS*. Front Mol Biosci, 2018. **5**: p. 44.
903. Ward, C.L., et al., *A loss of FUS/TLS function leads to impaired cellular proliferation*. Cell Death Dis, 2014. **5**: p. e1572.
904. Shiihashi, G., et al., *Mislocated FUS is sufficient for gain-of-toxic-function amyotrophic lateral sclerosis phenotypes in mice*. Brain, 2016. **139**(9): p. 2380-2394.
905. Scekcic-Zahirovic, J., et al., *Toxic gain of function from mutant FUS protein is crucial to trigger cell autonomous motor neuron loss*. Embo j, 2016. **35**(10): p. 1077-97.
906. Farg, M.A., et al., *Ataxin-2 interacts with FUS and intermediate-length polyglutamine expansions enhance FUS-related pathology in amyotrophic lateral sclerosis*. Hum Mol Genet, 2013. **22**(4): p. 717-28.
907. Huang, C., et al., *Entorhinal cortical neurons are the primary targets of FUS mislocalization and ubiquitin aggregation in FUS transgenic rats*. Hum Mol Genet, 2012. **21**(21): p. 4602-14.

908. Urushitani, M., et al., *The endoplasmic reticulum-Golgi pathway is a target for translocation and aggregation of mutant superoxide dismutase linked to ALS*. *FASEB J*, 2008. **22**(7): p. 2476-87.
909. Zhong, Z., et al., *Prion-like protein aggregates exploit the RHO GTPase to cofilin-1 signaling pathway to enter cells*. *EMBO J*, 2018. **37**(6).
910. Polymenidou, M. and D.W. Cleveland, *The seeds of neurodegeneration: prion-like spreading in ALS*. *Cell*, 2011. **147**(3): p. 498-508.
911. Feuillette, S., et al., *Neuron-to-Neuron Transfer of FUS in Drosophila Primary Neuronal Culture Is Enhanced by ALS-Associated Mutations*. *Journal of Molecular Neuroscience*, 2017: p. 1-9.
912. Pokrishevsky, E., L.I. Grad, and N.R. Cashman, *TDP-43 or FUS-induced misfolded human wild-type SOD1 can propagate intercellularly in a prion-like fashion*. *Sci Rep*, 2016. **6**: p. 22155.
913. Leblond, C.S., et al., *De novo FUS P525L mutation in Juvenile amyotrophic lateral sclerosis with dysphonia and diplopia*. *Neurol Genet*, 2016. **2**(2): p. e63.
914. Soo, K.Y., et al., *Recruitment of mitochondria into apoptotic signaling correlates with the presence of inclusions formed by amyotrophic lateral sclerosis-associated SOD1 mutations*. *J Neurochem*, 2009. **108**(3): p. 578-90.
915. Oliveros, J., *VENNY. An interactive tool for comparing lists with Venn diagrams*. BioinfoGP, CNB-CSIC, 2007-2015.
916. Mi, H., et al., *PANTHER version 11: expanded annotation data from Gene Ontology and Reactome pathways, and data analysis tool enhancements*. *Nucleic Acids Res*, 2017. **45**(D1): p. D183-d189.
917. Jung, J., M. Michalak, and L.B. Agellon, *Endoplasmic Reticulum Malfunction in the Nervous System*. *Frontiers in Neuroscience*, 2017. **11**(220).
918. Lamriben, L., et al., *N-Glycan-based ER Molecular Chaperone and Protein Quality Control System: The Calnexin Binding Cycle*. *Traffic*, 2016. **17**(4): p. 308-26.
919. Coe, H. and M. Michalak, *ERp57, a multifunctional endoplasmic reticulum resident oxidoreductase*. *Int J Biochem Cell Biol*, 2010. **42**(6): p. 796-9.
920. Sivadasan, R., et al., *C9ORF72 interaction with cofilin modulates actin dynamics in motor neurons*. *Nat Neurosci*, 2016. **19**(12): p. 1610-1618.
921. Tourrière, H., et al., *The RasGAP-associated endoribonuclease G3BP assembles stress granules*. *The Journal of Cell Biology*, 2003. **160**(6): p. 823-831.
922. Shen, M., et al., *A novel endoplasmic reticulum stress-induced apoptosis model using tunicamycin in primary cultured neonatal rat cardiomyocytes*. *Mol Med Rep*, 2015. **12**(4): p. 5149-54.
923. Wada, I., et al., *SSR alpha and associated calnexin are major calcium binding proteins of the endoplasmic reticulum membrane*. *J Biol Chem*, 1991. **266**(29): p. 19599-610.
924. Martin, L.J., *Neuronal death in amyotrophic lateral sclerosis is apoptosis: possible contribution of a programmed cell death mechanism*. *J Neuropathol Exp Neurol*, 1999. **58**(5): p. 459-71.
925. Sathasivam, S., P.G. Ince, and P.J. Shaw, *Apoptosis in amyotrophic lateral sclerosis: a review of the evidence*. *Neuropathol Appl Neurobiol*, 2001. **27**(4): p. 257-74.
926. Guegan, C. and S. Przedborski, *Programmed cell death in amyotrophic lateral sclerosis*. *J Clin Invest*, 2003. **111**(2): p. 153-61.
927. Zeineddine, R., et al., *Flow cytometric measurement of the cellular propagation of TDP-43 aggregation*. *Prion*, 2017. **11**(3): p. 195-204.
928. Ishii, T., et al., *Formation and spreading of TDP-43 aggregates in cultured neuronal and glial cells demonstrated by time-lapse imaging*. *PLoS One*, 2017. **12**(6): p. e0179375.

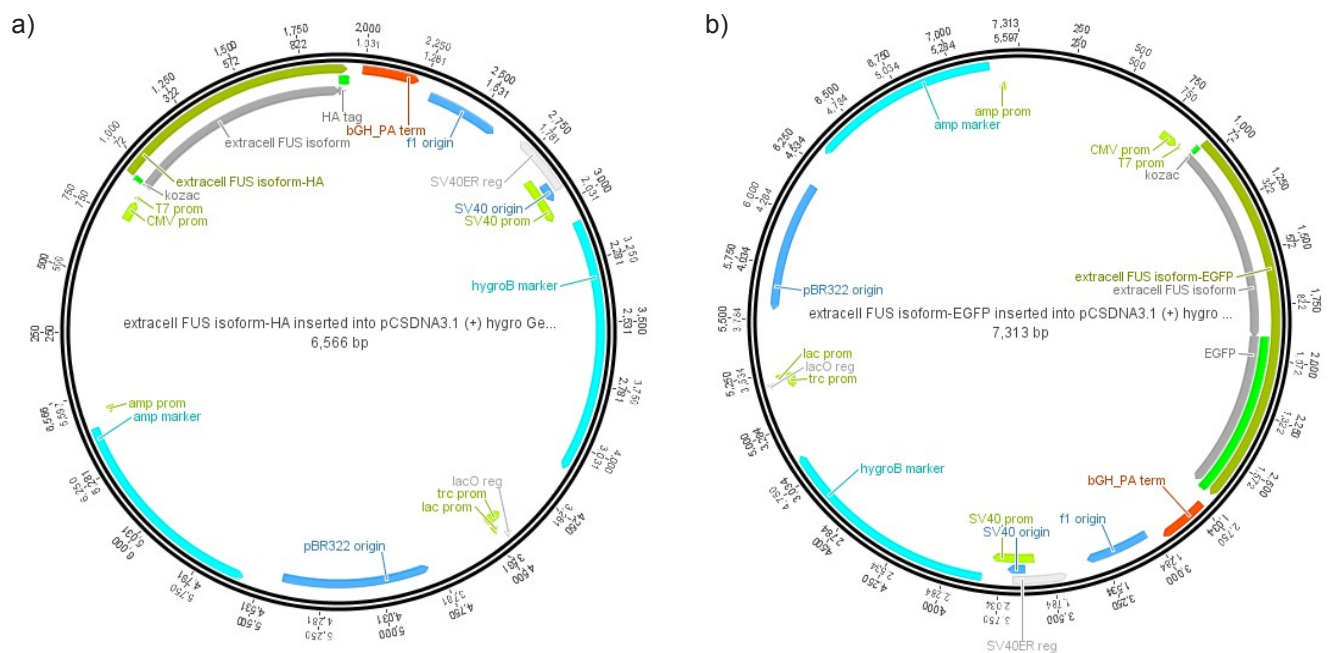
929. Yasuda, K., et al., *FUS inclusions disrupt RNA localization by sequestering kinesin-1 and inhibiting microtubule deetyrosination*. J Cell Biol, 2017. **216**(4): p. 1015-1034.
930. Arnold, E.S., et al., *ALS-linked TDP-43 mutations produce aberrant RNA splicing and adult-onset motor neuron disease without aggregation or loss of nuclear TDP-43*. Proc Natl Acad Sci U S A, 2013. **110**(8): p. E736-45.
931. Stieber, A., J.O. Gonatas, and N.K. Gonatas, *Aggregates of mutant protein appear progressively in dendrites, in periaxonal processes of oligodendrocytes, and in neuronal and astrocytic perikarya of mice expressing the SOD1(G93A) mutation of familial amyotrophic lateral sclerosis*. J Neurol Sci, 2000. **177**(2): p. 114-23.
932. Moriconi, C., et al., *Interactions between N-linked glycosylation and polymerisation of neuroserpin within the endoplasmic reticulum*. Febs j, 2015. **282**(23): p. 4565-79.
933. Bosques, C.J. and B. Imperiali, *The interplay of glycosylation and disulfide formation influences fibrillization in a prion protein fragment*. Proc Natl Acad Sci U S A, 2003. **100**(13): p. 7593-8.
934. Lee, H.S., Y. Qi, and W. Im, *Effects of N-glycosylation on protein conformation and dynamics: Protein Data Bank analysis and molecular dynamics simulation study*. Sci Rep, 2015. **5**: p. 8926.
935. Samandari, T. and J.L. Brown, *A study of the effects of altering the sites for N-glycosylation in alpha-1-proteinase inhibitor variants M and S*. Protein Sci, 1993. **2**(9): p. 1400-10.
936. Araman, C., et al., *Semisynthetic prion protein (PrP) variants carrying glycan mimics at position 181 and 197 do not form fibrils*. Chem Sci, 2017. **8**(9): p. 6626-6632.
937. Lawson, V.A., et al., *Prion protein glycosylation*. J Neurochem, 2005. **93**(4): p. 793-801.
938. Piro, J.R., et al., *Prion protein glycosylation is not required for strain-specific neurotropism*. J Virol, 2009. **83**(11): p. 5321-8.
939. Yuzwa, S.A., et al., *Increasing O-GlcNAc slows neurodegeneration and stabilizes tau against aggregation*. Nat Chem Biol, 2012. **8**(4): p. 393-9.
940. Guerin, R., et al., *Calnexin is involved in apoptosis induced by endoplasmic reticulum stress in the fission yeast*. Mol Biol Cell, 2008. **19**(10): p. 4404-20.
941. Gagnon, E., et al., *Endoplasmic reticulum-mediated phagocytosis is a mechanism of entry into macrophages*. Cell, 2002. **110**(1): p. 119-31.
942. Gonzalez-Perez, P., et al., *Identification of rare protein disulfide isomerase gene variants in amyotrophic lateral sclerosis patients*. Gene, 2015. **566**(2): p. 158-65.
943. Torres, M., et al., *The Protein-disulfide Isomerase ERp57 Regulates the Steady-state Levels of the Prion Protein*. J Biol Chem, 2015. **290**(39): p. 23631-45.
944. Holtz, W.A. and K.L. O'Malley, *Parkinsonian mimetics induce aspects of unfolded protein response in death of dopaminergic neurons*. J Biol Chem, 2003. **278**(21): p. 19367-77.
945. Honjo, Y., et al., *Protein disulfide isomerase-immunopositive inclusions in patients with amyotrophic lateral sclerosis*. Amyotroph Lateral Scler, 2011. **12**(6): p. 444-50.
946. Wang, T., et al., *Interaction of amyotrophic lateral sclerosis/frontotemporal lobar degeneration-associated fused-in-sarcoma with proteins involved in metabolic and protein degradation pathways*. Neurobiol Aging, 2015. **36**(1): p. 527-35.
947. Gal, J., et al., *Nuclear localization sequence of FUS and induction of stress granules by ALS mutants*. Neurobiol. Aging, 2011. **32**: p. 2323-2340.
948. Buchan, J.R., et al., *Eukaryotic stress granules are cleared by autophagy and Cdc48/VCP function*. Cell, 2013. **153**(7): p. 1461-74.

949. Sriburi, R., et al., *Coordinate regulation of phospholipid biosynthesis and secretory pathway gene expression in XBP-1(S)-induced endoplasmic reticulum biogenesis*. J Biol Chem, 2007. **282**(10): p. 7024-34.
950. Mitchell, J.C., et al., *Overexpression of human wild-type FUS causes progressive motor neuron degeneration in an age- and dose-dependent fashion*. Acta Neuropathol, 2013. **125**(2): p. 273-88.
951. Huang, C., et al., *FUS transgenic rats develop the phenotypes of amyotrophic lateral sclerosis and frontotemporal lobar degeneration*. PLoS Genet, 2011. **7**(3): p. e1002011.
952. Wang, X., et al., *Activation of ER Stress and Autophagy Induced by TDP-43 A315T as Pathogenic Mechanism and the Corresponding Histological Changes in Skin as Potential Biomarker for ALS with the Mutation*. Int J Biol Sci, 2015. **11**(10): p. 1140-9.
953. Xu, Y., et al., *DNAJC5 facilitates USP19-dependent unconventional secretion of misfolded cytosolic proteins*. Cell Discov, 2018. **4**: p. 11.
954. Fontaine, S.N., et al., *DnaJ/Hsc70 chaperone complexes control the extracellular release of neurodegenerative-associated proteins*. Embo j, 2016. **35**(14): p. 1537-49.
955. Mohamed, N.V., A. Desjardins, and N. Leclerc, *Tau secretion is correlated to an increase of Golgi dynamics*. PLoS One, 2017. **12**(5): p. e0178288.
956. Miyawaki, A., et al., *Dynamic and quantitative Ca²⁺ measurements using improved cameleons*. Proc Natl Acad Sci U S A, 1999. **96**(5): p. 2135-40.
957. Iradi, M.C.G., et al., *Characterization of gene regulation and protein interaction networks for Matrin 3 encoding mutations linked to amyotrophic lateral sclerosis and myopathy*. Sci Rep, 2018. **8**(1): p. 4049.
958. Altmeyer, M., et al., *Liquid demixing of intrinsically disordered proteins is seeded by poly(ADP-ribose)*. Nat Commun, 2015. **6**: p. 8088.
959. Hong, B.S., et al., *Colorectal cancer cell-derived microvesicles are enriched in cell cycle-related mRNAs that promote proliferation of endothelial cells*. BMC Genomics, 2009. **10**: p. 556.
960. Kowal, J., et al., *Proteomic comparison defines novel markers to characterize heterogeneous populations of extracellular vesicle subtypes*. Proc Natl Acad Sci U S A, 2016. **113**(8): p. E968-77.
961. Konig, J., et al., *iCLIP reveals the function of hnRNP particles in splicing at individual nucleotide resolution*. Nat Struct Mol Biol, 2010. **17**(7): p. 909-15.
962. Martin, G. and M. Zavolan, *Redesigning CLIP for efficiency, accuracy and speed*. Nature Methods, 2016. **13**: p. 482.
963. Haase, G. and C. Rabouille, *Golgi Fragmentation in ALS Motor Neurons. New Mechanisms Targeting Microtubules, Tethers, and Transport Vesicles*. Front Neurosci, 2015. **9**: p. 448.
964. Gitler, A.D. and J. Shorter, *RNA-binding proteins with prion-like domains in ALS and FTLD-U*. Prion, 2011. **5**(3): p. 179-87.
965. Machamer, J.B., et al., *FUS causes synaptic hyperexcitability in Drosophila dendritic arborization neurons*. Brain Res, 2018.
966. Maziuk, B., H.I. Ballance, and B. Wolozin, *Dysregulation of RNA Binding Protein Aggregation in Neurodegenerative Disorders*. Front Mol Neurosci, 2017. **10**: p. 89.
967. Taylor, J.P., et al., *OptoGranules reveal the evolution of stress granules to ALS-FTD pathology*. bioRxiv, 2018.
968. Aulas, A., S. Stabile, and C. Vande Velde, *Endogenous TDP-43, but not FUS, contributes to stress granule assembly via G3BP*. Mol Neurodegener, 2012. **7**: p. 54.
969. Gal, J., et al., *ALS mutant SOD1 interacts with G3BP1 and affects stress granule dynamics*. Acta Neuropathologica, 2016. **132**(4): p. 563-576.

970. Yamanaka, K., et al., *Astrocytes as determinants of disease progression in inherited amyotrophic lateral sclerosis*. Nat Neurosci, 2008. **11**(3): p. 251-3.
971. Yamanaka, K., et al., *Mutant SOD1 in cell types other than motor neurons and oligodendrocytes accelerates onset of disease in ALS mice*. Proc Natl Acad Sci U S A, 2008. **105**(21): p. 7594-9.
972. Suzuki, N., et al., *FUS/TLS-immunoreactive neuronal and glial cell inclusions increase with disease duration in familial amyotrophic lateral sclerosis with an R521C FUS/TLS mutation*. J Neuropathol Exp Neurol, 2012. **71**(9): p. 779-88.
973. Dinger, M.E., T.R. Mercer, and J.S. Mattick, *RNAs as extracellular signaling molecules*. J Mol Endocrinol, 2008. **40**(4): p. 151-9.

8. ■ Appendix

8.1. HA-FUS^{EC} and GFP-FUS^{EC} vector map



8.2. GFP-FUS^{EC} plasmid sequence

gacggatcggggagatctcccgatcccctatggtgcactctcagtaacaatctgctctgatgccgcatagttaagccagtatct
gctccctgcttggtgtgttggaggctgctgagtagtgccgagcaaaatttaagctacaacaaggcaaggcttgaccgaca
attgcatgaagaatctgcttaggggttaggcgttttgcgctgcttcgcgatgtacgggcccagatatacgcgttgacattgatta
ttgactagttattaatagtaatcaattacggggcttagtgctatagcccataatatggagttccgcgttacataacttacggta
aatggcccgctggctgaccgcccacgacccccgccattgacgtcaataatgacgtatgttcccatagtaacgcccaata
gggactttccattgacgtcaatgggtggagtattacggtaaaactgccacttggcagtacatcaagtgtatcatatgccaa
gtacgccccctattgacgtcaatgacggtaaattggcccgctggcattatgccagtacatgaccttatgggactttcctac
ttggcagtacatctacgtattagtcctgctattaccatgggtgatgcggttttggcagtacatcaatgggcgtggatagcgggt
ttgactcacggggatttccaagtctccacccattgacgtcaatgggagtttgttttggcaccaaaatcaacgggactttcc
aaaatgtcgtaaacaactccgccccattgacgcaaatgggcggtaggcgtgtacgggtgggaggtctatataagcagagctc
tctggctaactagagaaccctgcttactggcttatcgaaattaatacgaactactatagggagacccaagctggctagc
gtttaaacttaagcttggtaccgagctcggatccacatggccatcaagaccagagtgggtggaagtggccgccgtggcca
tggatagcagaacagttgaagctgctgctggcgtggcagtggttgcgtgctgccgctgctgcagtggttggttacaacagctg
ctgtggtggccatgaatcccaggttggtcgaagtggcgtggaagccgaagttgcttggggccctagagatcagggcagc
agacacgatagcgagcaggacaacagcgacaacaacaccatcttctgtgaaggcctgggcgagaacgtgaccattgag
agcgtggccgactacttcaagcagatcggcatcatcaagacgaacaagaaaaccgggcagcccatgatcaacctgtaca
ccgacagagagacaggcaagctgaaggcggaagccaccgtgtccttcgacgatcctccatctgccaaggccgccatcga
ttggttcgacggcaaaagagttcagcggcaaccctcatcaaggtgtcctttgccaccagacgggcccacttcaatagaggcg
gcggaaatggtagaggcgggacgtggaagaggtggccctatgggaagaggcggtatggtggcggaggatctggcgga
ggtggcagaggcggttttctagcggaggtggtggcggcggaggacaacaacagagctggcgattggaagtgcccaatc
ctacctgcgagaacatgaacttcagctggcggaacgagtgcaaccagtgaaggctcctaagcctgatggaccaggtgg
cggacctggcggatctcacatgggaggaaattacggcgacgatcggagaggtggacgcggcggttatgacagaggcgg
ctatagaggacgcggaggcgatcgcgaggattcagaggtggaagaggcggcggagatagaggcggatttggccctgg
caagatggactctagaggcgagcaccggcaggacagacgggaaagaccttcatgtgtcctaaaggcgagggaactgtt
caccggcgtggtgccattctggtggaactggacggggatgtgaacggccacaagtttagcgttagcggcgaaggcgaa
ggggatgccacatacggaaagctgacctgaagtttatctgcaccaccggcaagctgcccgcttggcctacactgtg

accacactgacctacggcgtgcagtgccttcagcagataccccgacctatgaagcagcacgacttcttcaagagcgccat
gcctgagggctacgtgcaagagcggacctcttctttaaggacgacggcaactacaagaccagggccgaagtgaagttc
gagggcgacacctgggtcaaccggatcgagctgaaaggcatcgatttcaaagaggacggcaacatcctgggccacaag
ctcgagtacaactacaactcccacaacgtgtacatcatggccgacaagcagaaaaacggcatcaaagtgaacttcaaga
tccggcacaacatcgaggacggctctgtgcagctggccgatcactaccagcagaacacacccatcggagatggccctgtc
ctgtgcctgacaaccactacgtgagcacacagagcgccctgagcaaggaccccaacgagaagagggatcacatgggtg
ctgtggaattctgtaccgccgtggcatcacactcggcatggacgaactgtacaaaaggcggaggcagaagcggcaact
ccagacctctggaaccactggatagcgctgccctctaagatatccagcacagtggcggccgctcgagtctagagggccc
tttaaaccgctgatcagcctcgactgtgccttctagttgccagccatctgttgttggccctccccctgccttccttgacct
ggaaggtgccactcccactgtcctttcctaataaaatgaggaaattgcacgcattgtctgagtaggtgtcatttctattctgg
ggggtggggtggggcaggacagcaagggggaggattgggaagacaatagcaggcatgctggggatcggtggggtct
atggcttctgaggcgaaagaaccagctggggctctagggggtatccccacgcgcctgtagcggcgcatthaagcgcg
cgggtgtgggtgttacgcgcagcgtgaccgctacacttgccagcgccctagcgcccgtcctttcgttcttcccttcttct
tcgccacgttcgccggctttccccgtcaagctctaaatcgggggctcccttaggggttcgatttagtgctttacggcacctc
gaccccaaaaaacttgattagggtaggttacgttagtggccatcgccctgatagacgggttttcgcccttgacgttg
agtccacgttctttaatagtgactctgttccaaactggaacaacactcaaccctatctcggtctattcttttgattataag
ggattttgccgatttcggcctattgggttaaaaaatgagctgatttaacaaaaatttaacgcgaattaattctgtggaatgtg
gtcagttagggtgtgaaagtccccaggctccccagcaggcagaagtatgcaaagcatgcatctcaattagtcagcaaccatagtc
aggtgtggaagtccccaggctccccagcaggcagaagtatgcaaagcatgcatctcaattagtcagcaaccatagtc
gcccctaactccgccatcccccttaactccgccagttccgccattctccgcccatggctgactaatttttttatttat
gcagaggccgagggcgctctgcctctgagctattccagaagtagtgaggaggtttttggaggcctaggcttttgc
aagctccgggagcttgcctatccatttccgatctgatcagcacgtgatgaaaaagcctgaactaccgcgacgtctgtc
gagaagttctgatcgaaggttcgacagcgtctccgacctgatgcagctctcgaggggcgaagaatctcgtgctttcagc
ttcgatgtaggagggcggtgatatgtctgcgggtaaatagctgcgccgatggtttctacaaagatcgttatgtttatcggc
actttgcatcgccgcgctccgattccggaagtgcctgacattggggaattcagcgagagcctgacctattgcatctccg
ccgtgcacaggggtgtcagttgcaagacctgcctgaaaccgaactgcccgctgttctgcagccggtcgcggaggccatgg
atgcgatcgctgcggccgatcttagccagacgagcgggttcggccattccggaccgaaggatcggtcaatacactaca
tggcgtgattcatatgcgcgattgctgatccccatgtgtatcactggcaactgtgatggacgacaccgtcagtcgctccg
tcgcgcaggctctcgatgagctgatgctttgggcccaggactgcccgaagtccggcacctcgtgcacgcggatttcggct
ccaacaatgtctgcaggacaatggccgcataacagcggctcattgactggagcgaggcgatgttcggggattccaatac
gaggtcgccaacatcttcttggaggccgtgggttgctgtatggagcagcagacgcgctacttcgagcggaggcatccg
gagcttgacggatcgccgggctccggcgatatgtccgcattggcttgaccaactctatcagagcttggtgacggca
atttcgatgatgcagcttgggcgagggtcgatgcgacgcaatcgccgatccggagccgggactgtcgggctacacaa
atcgcccgcagaagcgcgccgtctggaccgatggctgtgtagaagtactcgccgatagtgaaaccgacgcccagca
ctcgtccgagggcgaaggaatagcagtgctacgagatttcgattccaccgcccgttctatgaaagggtgggttcggaa
tcgttttcgggacgcgggctggatgatctccagcgcggggatctcatgctggagttcttcgccaccccaactgtttatt
gcagcttataatggttacaataaagcaatagcatcacaatttcacaataaagcattttttcactgcattctagttgtgg
ttgtccaaactcatcaatgtatcttatcatgtctgtataccgtcgacctctagctagagcttggtgtaacatggtcatagct
gttctctgtgtgaaattgttatccgctcacaattccacacacatacagccggaagcataaagtgtaaagcctgggggtc
ctaattgagtgcgtaactcacattaattgcgttgcgctcactgcccgttccagtcgggaaacctgtcgtgccagctgcatt
aatgaatcggccaacgcgcggggagaggcggtttgcgtattgggcgtcttccgcttctcgtcactgactcgtgcgt
cggtcgttcgggtcggcgagcggtatcagctcactcaaaggcggttaatacggttatccacagaatcaggggataacgca
ggaaagaacatgtgagcaaaaggccagcaaaaggccaggaaccgtaaaaaggccggttgctggcggttttccatagg
ctccgccccctgacgagcatcacaataatcgacgtcaagtcagaggtggcgaaaccgacaggactataaagatacc
aggcggttccccctggaagctccctcgtgcgtctcctgttccgacctgcccgttaccggatacctgtccgcttttccctt
cgggaagcgtggcgcttctcatagctcacgctgtaggtatctcagttcggtgtaggtcggtcgtccaagctggggtgtgt
gcacgaacccccgttcagccgacctgctgccttatccggtaactatcgtcttgagccaacccggttaagacacgactt
atcgccactggcagcagccactggtaacaggattagcagagcgaggtatgtaggcgggtgtacagagttctgaagtgtg
ggcctaactacggctacactagaagaacagtattggatctgcgctcgtgaagccagttaccttcggaaaaagagttg

gtagctcttgatccggcaaacaaccacgctggtagcggtttttgttgcaagcagcagattacgcgcagaaaaaag
gatctcaagaagatcctttgatctttctacggggtctgacgctcagtggaacgaaaactcacgttaagggattttggcat
gagattatcaaaaaggatcttcacctagatccttttaattaaaaatgaagtttaaatcaatctaaagtatatatgagtaa
acttggcttgacagttaccaatgcttaatcagtgaggcacctatctcagcgatctgtctatttcgttcatccatagttgcctga
ctccccgtcgttagataactacgatacgggaggggttaccatctggccccagtgctgcaatgataccgcgagaccacg
ctcaccggctccagatttatcagcaataaaccagccagccggaagggccgagcgcagaagtggctcctgcaactttatccg
cctccatccagcttattaattgttgccgggaagctagagtaagtagttcgccagttaatagtttgcgcaacgttgttgcatt
gctacaggcatcgtggtgtcacgctcgtcgtttggtatggcttcattcagctccggttccaacgatcaaggcgagtacat
gatccccatgttgtgcaaaaaagcggttagctccttcggtcctccgatcgttgtcagaagtaagttggccgcagtggtatc
actcatgggtatggcagcactgcataattctcttactgtcatgccatccgtaagatgcttttctgtgactggtgagtactcaac
caagtcattctgagaatagtgtatgctggcgaccgagttgctcttgccggcgtcaatacgggataataccgcgccacatag
cagaactttaaaagtgtcatcattggaaaacgttcttcggggcgaaaactctcaaggatcttaccgctgttgagatccagt
tcgatgtaaccactcgtgcacccaactgatcttcagcatcttttactttaccagcgtttctgggtgagcaaaaacaggaa
ggcaaaatgccgcaaaaaaggaataagggcgacacggaaatgttgaatactcatactcttcttttcaatattattgaa
gcatttatcagggttattgtctcatgagcggatacatatttgaatgtatttagaaaaataaacaataaggggttccgcgcac
attccccgaaaagtgccacctgacgtc

8.3. HA-FUSEC plasmid sequence

gacggatcgggagatctcccgatcccctatgggtgactctcagtacaatctgctctgatgccgcatagttaagccagtatctgctc
cctgcttggtgtgttgagggtcgctgagtagtgcgcgagcaaaatttaagctacaacaaggcaaggcttgaccgacaattgcatg
aagaatctgcttaggggttaggcgttttgcgctgcttcgcatgtacgggcccagatatagcggttgacattgattattgactagttat
taatagtaatacaattacgggggtcattagttcatagcccatatatggagttccgcgttacataacttacggtaaatggcccgcctgg
ctgaccgccaacgacccccgcccattgacgtcaataatgacgtatgttcccatagtaacgccaatagggactttccattgacgt
caatgggtggagtagttacggtaaaactgcccacttggcagtagcatcaagtgtatcatatgccaaagtacgccccctattgacgtca
atgacggtaaatggcccgcctggcattatgccagtagacgttatgggactttcctacttggcagtagcatctacgtattagtc
atcgctattaccatggtgatgcggttttggcagtagcatcaatgggcgtggatagcggttgactcacggggatttccaagtctcca
ccccattgacgtcaatgggagtttgttttggcaccaaaaatcaacgggactttccaaaatgtcgttaacaactccgccccattgacg
caaatgggtaggtaggcgtgtacgggtgggaggtctatataagcagagctctctggctaactagagaacccactgcttactggctt
atcgaaattaatacactcactatagggagacccaagctggctagcggttaacttaagcttggtagcgagctcgatccacca
tggccatcaagaccagagtggtggaagtggccgctggccatggatagcagaacagttgaagctgctgctggcgtggcagt
gggtgctgctgcgctgctgcagtggtggttacaacagctgctgtggtggccatgaatcccaggtggtcgaagttgccgtgga
agccgaagttgcttggggccctagagatcagggcagcagacacgatagcgagcaggacaacagcgacaacaacaccatcttc
gtgcaaggcctgggagagaacgtgaccattgagagcgtggccgactacttcaagcagatcggcacatcaagacgaacaaga
aaaccgggcagcccatgatcaacctgtacaccgacagagagacaggcaagctgaagggcgaagccaccgtgtccttcgacg
atcctccatctgccaaggccgcatcgattggttcgacggcaagagttcagcggaaccccatcaaggtgtcctttgccacca
gacgggcccacttcaatagaggcggcggaatggtagaggcggacgtggaagaggtggccctatgggaagaggcggatag
gtggcggaggatctggcggaggtggcagaggcggttttctagcggaggtggtggcggcggaggacaacaacagctggcg
attggaagtgcaccaatcctactgagagaacatgaacttcagctggcgaacagatgcaaccagtgaaggctcctaagcct
gatggaccaggtggcggacctggcggatctcatatgggaggaaattacggcgacgatcgagaggtggacgcggcggttatg
acagaggcggctatagaggacgcggaggcgtatcgcgaggattcagaggtggaagaggcggcggagatagaggcggattt
ggccttggaagatggactctagaggcgagcaccggcaggacagaagagagaggccttactaccctacgacgtgcccatt
acgcctgagatatccagcacagtggcggcgtcagcttagaggggccgtttaaacccgctgatcagcctcactgtgccttc
tagttgccagccatctgttgttgccttccccctgccttcttgacctggaaggtgccactcccactgtccttctcctaataaaat
gaggaaattgcatcgattgtctgagtaggtgtcattctatctggggggtgggggtggggcaggacagcaagggggaggattg
ggaagacaatagcaggcatgctggggatgcggtgggctctatggcttctgaggcggaaagaaccagctggggctctaggggg
tatccccacgcgcctgtagcggcgattaagcgcggcggtgtggtggttacgcgcagcgtgaccgtacacttgccagcgcc
ctagcggcgctcctttcgtttcttcccttcttctcgcacgttcgcccgtttccccgtcaagctctaatacgggggtccttt
agggttccgatttagtgctttacggcacctcgaccccaaaaacttgattagggtgatggttcacgtagtgggcatcgccctga
tagacggtttttcgccccttgacgttggagtccagttctttaatagtgactcttgttccaaactggaacaacactcaaccctatc
tcggtctattcttttgatttataagggattttgccgatttcggcctattggttaaaaaatgagctgatttaaaaaaatttaacgga
attaattctgtggaatgtgtgtcagttagggtgtggaagtcccaggctcccagcaggcagaagtagcaagcatgcatct
caattagtcagcaaccaggtgtggaagtcccaggctcccagcaggcagaagtagcaagcatgcatctcaattagtcag
caaccatagtcggcccttaactccgcccattccgcccactccgcccatttccgccccatggctgactaatt
tttttatttatgcagaggccgagggcgcctctgcctctgagctattccagaagtagtgaggaggctttttggaggcctaggcttt
tgcaaaaagctcccgggagcttgatatccatttccgatctgatcagcacgtgatgaaaaagcctgaactcaccgcgacgtctg
tcgagaagtttctgatgaaaagttcgacagcgtctccgacgtgatgcagctctcgaggggcgaagaatctcgtgctttcagctt
cgatgtaggagggcggtgatatgtcctgcgggtaaatagctgcgccgatggtttctacaaagatcggttatgtttatcggcactttg
catcgccgcgctcccattccggaagtgttgacattggggaattcagcgagagcctgacctattgcatctccgcccgtgcac
agggtgtcagttgcaagacctgcctgaaaccgaactcccgtgttctgcagccggtcgcgaggccatggatgcgatcgctg
cgccgatcttagccagacgagcgggttcggccattcggaccgcaaggaatcggtaatacactacatggcgtgatttcatat
gcgcgattgtgatccccatgttatcactggcaactgtgatggacgacaccgtcagtgctcgtcgcgaggtctcgatg
agctgatgctttgggcccaggactccccgaagtccggcacctctgtcacgcggatttcggctccaacaatgtcctgacggaca
atggccgcataacagcgggtcattgactggagcagggcgatgttcggggattccaatacagaggtcgccaacatcttcttctgga

ggccgtggttggttgatggagcagcagacgcgctacttcgagcggaggcatccggagcttgaggatcgccgaggctccgg
gcgtatatgctccgcattggctcttgaccaactctatcagagcttggttgacggcaatttcgatgatgcagcttgggcgcagggctc
atgcgacgcaatcgtccgatccggagccgggactgtcgggcgtacacaaatcgccgcagaagcgcggccgtctggaccgat
ggctgtgtagaagtactcgcgatagtggaacacgcgccccagcactcgtccgagggcaaaggaatgcacgtgctacgag
atttcgattccaccgcccgttctatgaaagggtgggcttcggaatcgtttccgggacgcgggctggatgctccagcgcgg
ggatctcatgctggagttcttcgcccacccaactgtttattgcagcttataatgggtacaaataaagcaatagcatcacaattt
cacaataaagcattttttcactgcattctagttgtggtttgtccaaactcatcaatgtatcttatcatgtctgtataccgtcgacct
ctagctagagcttggcgtaatcatggctcatagctgtttcctgtgtgaaattgttatccgctcacaattccacacaacatacagacc
ggaagcataaagtgtaaagcctggggtgcctaataagtgagtgtaactcacattaattgcgttgcgctcactgcccgtttccagt
cgggaaacctgtcgtgccagctgcattaatgaatcggccaaacgcgcggggagaggcggtttgcgtattgggcgctcttccgctt
cctcgtcactgactcgtcgcctcggctcgttcggctcggcgagcgggtatcagctcactcaaaggcggtataacggttatccac
agaatcaggggataacgcaggaagaacatgtgagcaaaaggccagcaaaaggccaggaaccgtaaaaaggccggttgc
tggcggttttccataggctccgccccctgacgagcatcacaataatcgacgctcaagtcagaggtggcgaaacccgacagga
ctataagataaccaggcggtttccccctggaagctccctcgtcgcctctcctgttccgacctgccgcttaccggatacctgtccgc
ctttctcccttcgggaagcgtggcgctttctcatagctcacgctgtaggtatctcagttcgggtgtaggtcgttcgctccaagctggg
ctgtgtgcacgaacccccgttcagcccagccgtcgcgcttatccggttaactatcgtcttgagtccaacccggttaagacacgac
ttatcgccactggcagcagccactggtaacaggattagcagagcgaggtatgtaggcggtgctacagagttcttgaagtgggtg
cctaactacggctacactagaagaacagtatttggatctcgcctctgctgaagccagttaccttcggaataaagagttggtagct
cttgatccggcaaaacaaaccacgctggtagcgggtttttgttgcaagcagcagattacgcgcagaaaaaaaggatctcaag
aagatcctttgatctttctacggggtcgtacgctcagtggaacgaaaactcacgttaagggttttggctatgagattatcaaaa
aggatcttcacctagatccttttaataaaaaatgaagttttaaatacaatctaaagtatatagtaaacttggctgacagttac
caatgcttaatcagtgaggcacctatctcagcgatctgtctatttcgttcatccatagttgcctgactccccgtcgtgtagataact
acgatacgggaggggcttaccatctggccccagtgctgcaatgataccgcgagaccacgctcaccgggtccagatttatcagca
ataaaccagccagccggaaggccgagcgcagaaagtggtcctgcaactttatccgctccatccagtctattaattgttgccgg
gaagctagagtaagtagttcgccagttaatagtttgcgcaacgttgttgccattgctacaggcatcgtggtgtcacgctcgtcgtt
tggtatgggttcattcagctccggttccaacgatcaaggcgagttacatgatccccatgttggtgcaaaaaagcggttagctcct
tcggctcctccgatcgttgcagaagtaagttggccgcagtggtatcactcatggttatggcagcactgcataattcttactgtca
tgccatccgtaagatgcttttctgtgactggtgagtactcaaccaagtcattctgagaatagtgtatgcggcgaccgagttgctct
tgccggcgctcaatacgggataataccgcgccacatagcagaactttaaagtgctcatcattggaaaacgttcttcggggcga
aaactctcaaggatcttaccgctgttgagatccagttcgatgtaaccactcgtgcaccaactgatcttcagcatctttactttc
accagcgtttctgggtgagcaaaaacaggaaggcaaaatgccgcaaaaaagggaataaggcgacacggaaatgttgaata
ctcactcttcttttcaatattattgaagcatttatcagggttattgtctcatgagcggatacatatttgaatgtatttagaaaa
taaacaatatgggggtccgcgcacattccccgaaaagtgccacctgacg

8.4. Uncropped western blots

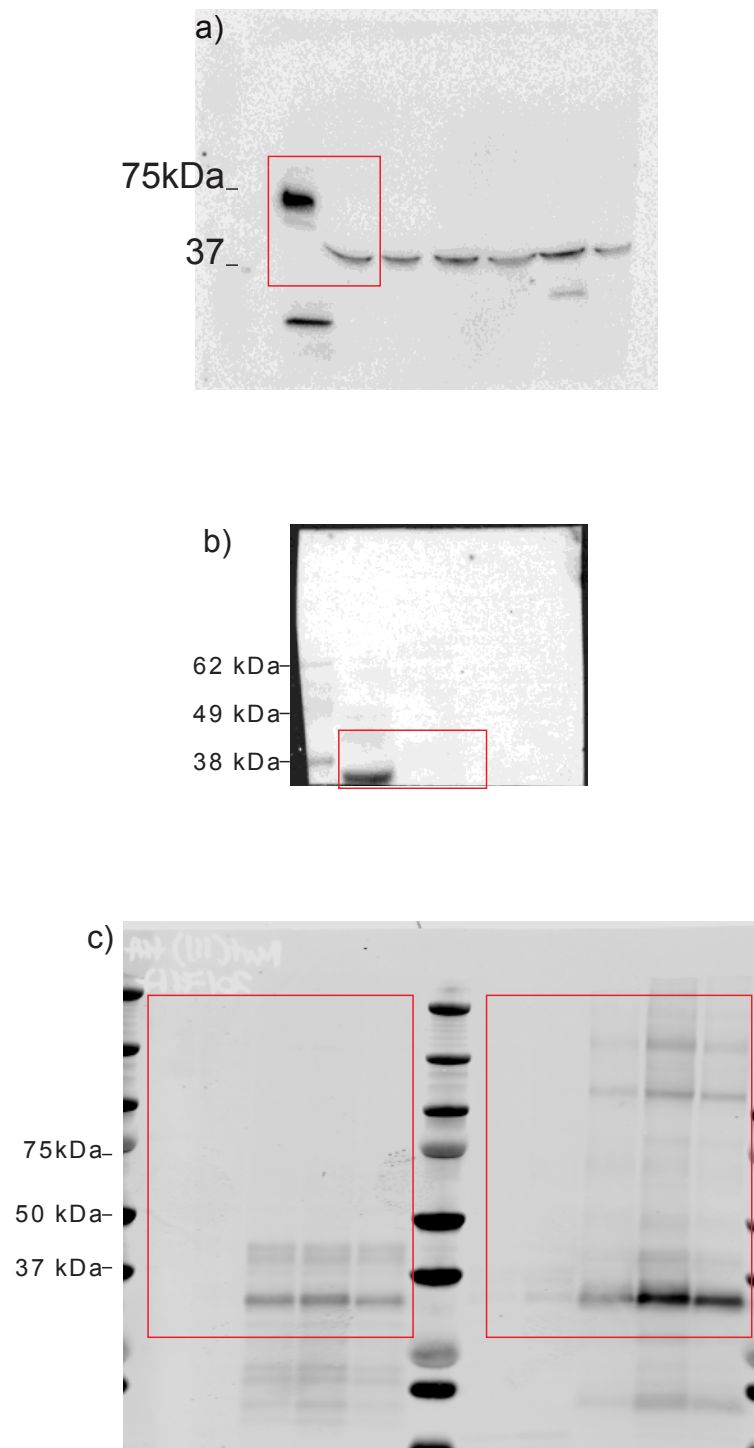


Figure 3 Uncropped wester blots Uncropped western blots from figure 3.5b (a), 4.9b (b) and 5.2a and 5.2c (c).

8.5. Mass spectrometry results for binding partners (Chapter 4 and 5)

Accession	Sum PEP Score	Coverage [%]	# Unique Peptides	Entrez Gene ID	Gene Symbol	LYSATE 1			MEDIA1			LYSATE 2			MEDIA2		
						WT	R316G	P320	WT	R316G	P320	WT	R316G	P320	WT	R316G	P320
P78527	401.811	29	110	5591	PRKDC	NF	High	High	High	NF	High	High	High	High	NF	NF	High
P49327	378.796	36	72	2194	FASN	NF	High	High	High	High	High	High	High	High	High	NF	High
P08670	350.098	80	48	7431	VIM	High	High	High	High	High	High	High	High	High	High	High	High
P04264	319.027	61	35	3848	KRT1	High	High	High	High	High	High	High	High	High	High	High	High
Q14204	314.772	20	79	1778	DYNC1H1	NF	High	High	High	NF	High	NF	High	High	NF	NF	NF
P13645	288.918	58	29	3858	KRT10	High	High	High	High	High	High	High	High	High	High	High	High
P08238	285.933	60	29	3326	HSP90AB1	NF	High	High	High	High	High	High	High	High	High	High	High
P0DMV8	275.456	61	26	3303; 3304	HSPA1A; HSPA1B	High	High	High	High	High	High	High	High	High	High	High	High
P07437	274.974	68	4	203068	TUBB	High	High	High	High	High	High	High	High	High	High	NF	High
P35580-3	259.487	33	43	4628	MYH10	NF	High	High	High	NF	High	NF	High	High	High	NF	NF
P10809	258.46	68	33	3329	HSPD1	NF	High	High	High	NF	High	High	High	High	NF	NF	High
P68371	250.452	68	2	10383	TUBB4B	NF	High	High	High	NF	High	High	High	High	NF	NF	NF
Q00610-1	247.174	35	48	1213	CLTC	NF	High	High	High	NF	High	High	High	High	High	NF	NF
P13639	244.567	60	43	1938	EEF2	NF	High	High	High	High	High	High	High	High	High	NF	High
Q08211	239.334	38	41	1660	DHX9	NF	High	High	High	NF	High	NF	High	High	High	NF	High
P35908	235.51	76	30	3849	KRT2	High	High	High	High	High	High	High	High	High	High	High	High
Q9BVA1	234.357	61	1	347733	TUBB2B	NF	NF	NF	NF	NF	NF	NF	High	NF	NF	NF	NF
Q13885	234.181	61	1	7280	TUBB2A	NF	NF	NF	High	NF	High	NF	High	NF	NF	NF	NF

O75643-1	207.463	25	45	23020	SNRNP200	NF	High	High	High	NF	High	NF	High	High	NF	NF	High
P21333	203.688	27	47	2316	FLNA	NF	High	High	High	NF	High	NF	High	High	NF	NF	NF
P09874	197.542	43	32	142	PARP1	NF	High	High	High	NF	High	High	High	High	High	NF	High
P60709	195.946	61	7	60	ACTB	High	High	High	High	NF	High	High	High	High	High	NF	High
Q71U36	192.729	58	1	7846	TUBA1A	NF	High	High	High	NF	High	NF	High	NF	NF	NF	NF
Q13813	190.446	20	40	6709	SPTAN1	NF	High	High	High	NF	High	NF	High	High	NF	NF	NF
Q9BQE3	177.858	53	1	84790	TUBA1C	NF	NF	NF	NF	NF	High	NF	NF	NF	NF	NF	NF
P19338	177.077	35	28	4691	NCL	NF	High	High	High	NF	High	High	High	High	High	NF	High
P05023	170.344	37	30	476	ATP1A1	NF	High	High	High	NF	High	High	High	High	NF	NF	NF
P68366	167.686	50	2	7277	TUBA4A	High	High	High	High	NF	High	NF	High	NF	High	NF	NF
P25705-1	163.507	56	27	498	ATP5A1	NF	High	High	High	NF	High	High	High	High	High	NF	High
Q00839	162.418	35	30	3192	HNRNPU	NF	High	High	High	NF	High	High	High	High	High	High	High
P22314	158.743	36	26	7317	UBA1	NF	High	High	High	NF	High	NF	High	High	NF	NF	NF
Q13509	157.793	40	3	10381	TUBB3	NF	High	High	High	NF	High	NF	High	NF	NF	NF	NF
Q6P2Q9	153.088	20	41	10594	PRPF8	NF	High	High	High	NF	High	High	High	High	NF	NF	NF
P53396-1	150.131	43	37	47	ACLY	NF	High	High	High	NF	High	High	High	High	NF	NF	High
P68104	148.093	71	20	1915	EEF1A1	High	High	High	High	High	High	High	High	High	High	High	High
P17987	146.435	74	31	6950	TCP1	NF	High	High	High	NF	High	High	High	High	NF	NF	High
P11021	143.881	45	25	3309	HSPA5	NF	High	High	High	NF	High	NF	High	NF	NF	NF	NF
P52272	139.704	41	28	4670	HNRNPM	NF	High	High	High	NF	High	High	High	High	NF	NF	NF
P78371-1	138.639	61	22	10576	CCT2	NF	High	High	High	NF	High	High	High	High	NF	NF	NF
P49411	136.618	54	23	7284	TUFM	NF	High	High	High	NF	High	High	High	High	High	NF	High
Q01082-1	135.234	17	32	6711	SPTBN1	NF	High	High	High	NF	High	NF	High	NF	NF	NF	NF
P38646	134.697	44	24	3313	HSPA9	NF	High	High	High	NF	High	High	High	High	NF	NF	NF
Q99873	133.453	52	19	3276	PRMT1	High	High	High	High	NF	High	High	High	High	High	NF	NF
P35637-1	132.772	26	13	2521	FUS	High	High	High	High	High	High	High	High	High	High	High	High
P14618	132.576	56	24	5315	PKM	NF	High	High	High	NF	High	High	High	High	High	NF	NF
P42704	129.017	26	31	10128	LRPPRC	NF	High	High	High	NF	High	High	High	High	NF	NF	NF
Q7L2E3-2	122.15	29	30	22907	DHX30	NF	High	High	High	NF	High	NF	High	NF	NF	NF	High

P11940-1	121.506	39	17	26986	PABPC1	NF	High	High	High	NF	High	NF	High	High	NF	NF	NF
Q9NR30-1	120.996	37	21	9188	DDX21	NF	High	High	High	NF	High	NF	High	High	NF	NF	NF
P06576	120.564	60	20	506	ATP5B	NF	High	High	High	NF	High	High	High	High	NF	NF	NF
Q99832	120.238	50	21	10574	CCT7	NF	High	High	High	NF	High	High	High	High	NF	NF	NF
P26599-3	118.444	38	13	5725	PTBP1	NF	High	High	High	NF	High	NF	High	High	NF	NF	High
P04843	112.469	49	24	6184	RPN1	NF	High	High	High	NF	High	High	High	High	NF	NF	High
P07814	112.463	21	26	2058	EPRS	NF	High	High	High	NF	High	High	High	High	NF	NF	NF
Q9BQG0-2	111.505	29	30	10514	MYBBP1A	NF	High	High	High	NF	High	NF	High	NF	NF	NF	NF
P46940	110.851	19	25	8826	IQGAP1	NF	High	High	High	High	High	High	High	High	NF	NF	NF
P33993-1	110.651	41	24	4176	MCM7	NF	High	High	High	NF	High	High	High	High	NF	NF	NF
Q9UJS0-2	108.016	44	15	10165	SLC25A13	NF	High	High	High	NF	High	NF	High	High	NF	NF	NF
P36578	106.192	43	18	6124	RPL4	High	High	High	High	High	High	High	High	High	High	NF	NF
P17844	105.665	44	19	1655	DDX5	NF	High	High	High	NF	High	High	High	High	NF	NF	NF
P27708	104.477	17	32	790	CAD	NF	High	High	High	NF	High	High	High	High	NF	NF	NF
P60842	103.33	62	11	1973	EIF4A1	NF	High	High	High	NF	High	NF	High	High	NF	NF	NF
P50991	101.665	48	20	10575	CCT4	NF	High	High	High	NF	High	High	High	High	NF	NF	NF
P06737-1	100.774	36	22	5836	PYGL	NF	High	High	High	NF	High	NF	High	NF	NF	NF	High
P39023	100.044	46	17	6122	RPL3	High	High	High	High	High	High	High	High	High	High	NF	NF
P08779	99.603	46	8	3868	KRT16	High	NF	High	NF	High	High	NF	High	High	High	NF	NF
P14625	98.99	28	19	7184	HSP90B1	NF	High	High	High	NF	High	High	High	NF	NF	NF	NF
Q15149-1	98.8	9	35	5339	PLEC	NF	NF	High	High	NF	High	NF	High	NF	NF	NF	NF
P02533	98.63	45	5	3861	KRT14	High	High	High	High	High	High	High	High	High	High	High	High
P02538	98.231	35	2	3853	KRT6A	High	High	High	High	NF	NF	NF	NF	High	High	NF	NF
Q15029	96.253	30	21	9343	EFTUD2	NF	High	High	High	NF	High	NF	High	High	NF	NF	NF
O75369-8	96.123	17	29	2317	FLNB	NF	High	High	High	NF	High	NF	High	High	NF	NF	NF
P53621-1	96.089	26	28	1314	COPA	NF	High	High	High	NF	High	NF	High	High	NF	NF	NF
P13647	96.065	34	12	3852	KRT5	High	High	High	High	High	High	High	High	High	High	High	High
P04075-2	95.549	55	16	226	ALDOA	NF	High	High	High	NF	High	NF	High	High	High	NF	NF
P61978-2	94.87	46	19	3190	HNRNPK	NF	High	High	High	NF	High	High	High	High	High	NF	NF

Q9BUF5	94.821	30	4	84617	TUBB6	NF	High	High	High	NF	High	NF	High	NF	NF	NF	NF
P04259	94.363	33	2	3854	KRT6B	High	High	NF	NF	NF	NF	NF	NF	High	High	NF	NF
P41252	92.506	23	24	3376	IARS	NF	High	High	High	NF	High	NF	High	NF	NF	NF	NF
P31943	91.918	41	9	3187	HNRNPH1	NF	High	High	High	NF	High	High	High	High	NF	NF	NF
P13010	91.457	42	24	7520	XRCC5	NF	High	High	High	NF	High	High	High	High	NF	NF	NF
P07195	90.703	46	12	3945	LDHB	NF	High	High	High	NF	High	High	High	High	NF	NF	NF
P43243	90.08	30	20	9782	MATR3	NF	High	High	High	NF	High	High	High	High	NF	NF	High
Q86VP6-1	90.059	23	24	55832	CAND1	NF	High	High	High	NF	High	NF	High	NF	NF	NF	NF
P68032	89.857	47	5	70	ACTC1	NF	High	High	High	NF	High	NF	High	High	NF	NF	High
P55060-1	89.743	30	23	1434	CSE1L	NF	High	High	High	NF	High	NF	High	High	NF	NF	NF
Q12905	89.681	58	15	3608	ILF2	NF	High	High	High	NF	High	High	High	High	NF	NF	High
P62701	89.265	66	19	6191	RPS4X	High	High	High	High	High	High	High	High	High	High	High	High
Q92841	89.246	33	14	10521	DDX17	NF	High	High	High	NF	High	NF	High	High	NF	NF	NF
P12956	89.041	39	20	2547	XRCC6	NF	High	High	High	NF	High	High	High	High	NF	NF	NF
P17066	87.669	21	3	3310	HSPA6	NF	High	High	NF	NF	High	NF	High	High	NF	NF	High
Q9H0A0	87.013	27	23	55226	NAT10	NF	High	High	High	NF	High	High	High	High	NF	NF	NF
P63244	86.489	67	15	10399	GNB2L1; RACK1	NF	High	High	High	High	High	High	High	High	NF	NF	NF
P60174	84.988	69	15	7167	TPI1	High	High	High	High	High	High	NF	High	High	High	NF	NF
Q9Y490	84.868	12	19	7094	TLN1	NF	High	High	High	NF	High	NF	High	NF	NF	NF	NF
Q14566	83.285	30	22	4175	MCM6	NF	High	High	High	NF	High	NF	High	NF	NF	NF	NF
Q14697-1	81.927	24	20	23193	GANAB	NF	High	High	High	NF	High	NF	High	NF	NF	NF	NF
P55072	81.75	23	15	7415	VCP	NF	High	High	High	NF	High	NF	High	High	NF	NF	NF
O00571	81.656	33	19	1654	DDX3X	NF	High	High	High	NF	High	High	High	High	NF	NF	High
Q14498-2	81.608	41	15	9584	RBM39	NF	High	High	High	High	High	High	High	High	NF	NF	NF
O43143	81.117	30	19	1665	DHX15	NF	High	High	High	NF	High	NF	High	NF	NF	NF	NF
Q9BVP2	80.785	28	15	26354	GNL3	NF	High	High	High	NF	High	High	High	NF	NF	NF	High
P04406	80.486	55	15	2597	GAPDH	NF	High	High	High	High	High	NF	High	High	High	NF	NF
P23396	79.924	77	21	6188	RPS3	NF	High	High	High	High	High	High	High	High	NF	High	High
P12277	79.793	31	10	1152	CKB	NF	High	High	High	NF	High	NF	High	High	NF	NF	NF

[illegible]

P54136-1	67.056	32	18	5917	RARS	NF	High	High	High	NF	High	NF	High	NF	NF	NF	NF
P13646	66.914	34	12	3860	KRT13	NF	NF	High	High	NF	NF	NF	NF	NF	High	NF	NF
P62753	66.641	38	12	6194	RPS6	High	High	High	High	High	High	High	High	High	High	High	High
O43390-2	66.572	26	10	10236	HNRNPR	NF	High	High	High	NF	High	High	High	NF	NF	NF	High
P00558	66.293	40	12	5230	PGK1	NF	High	High	NF	NF	High	NF	High	NF	NF	NF	NF
P16615	66.204	20	17	488	ATP2A2	NF	High	High	High	NF	High	NF	High	NF	NF	NF	NF
O43242	64.948	38	18	5709	PSMD3	NF	High	High	High	NF	High	NF	High	NF	NF	NF	NF
P07355-2	64.767	39	10	302	ANXA2	NF	High	High	High	High	High	High	High	High	High	NF	NF
P30153	64.358	25	12	5518	PPP2R1A	NF	High	High	High	NF	High	NF	High	NF	NF	NF	NF
P41250	64.343	22	13	2617	GARS	NF	High	High	High	NF	High	NF	High	High	NF	NF	NF
P14868	64.308	41	18	1615	DARS	NF	High	High	High	NF	High	NF	High	NF	NF	NF	NF
P33991	63.685	22	15	4173	MCM4	NF	High	High	High	NF	High	High	High	High	NF	NF	NF
P26641-2	63.208	32	15	1937	EEF1G	NF	High	High	High	High	High	High	High	High	NF	NF	NF
P46777	63.165	42	13	6125	RPL5	High	High	High	High	High	High	High	High	High	High	High	NF
Q15366-2	62.974	31	5	5094	PCBP2	NF	High	High	High	NF	High	High	High	High	NF	NF	NF
Q5JTH9-1	62.428	17	19	23223	RRP12	NF	High	High	High	NF	High	NF	High	High	NF	NF	NF
P15880	61.732	52	15	6187	RPS2	High	High	High	High	High	High	High	High	High	NF	NF	NF
O60506	61.714	31	12	10492	SYNCRIP	NF	High	High	High	NF	High	NF	High	High	NF	NF	NF
P05141	61.347	38	5	292	SLC25A5	NF	High	High	High	NF	High	High	High	High	High	NF	NF
P12235	61.134	41	1	291	SLC25A4	NF	NF	NF	NF	NF	High	NF	NF	NF	NF	NF	NF
Q02878	60.28	42	12	6128	RPL6	NF	High	High	High	High	High	NF	High	High	NF	NF	High
P05388	60.257	43	9	6175	RPLP0	NF	High	High	High	NF	High	High	High	High	NF	NF	NF
Q92945	59.985	24	14	8570	KHSRP	NF	High	High	High	NF	High	NF	High	High	NF	NF	NF
P18124	59.365	49	14	6129	RPL7	High	High	High	High	High	High	High	High	High	High	NF	High
Q15393-1	59.026	16	17	23450	SF3B3	NF	High	High	High	NF	High	NF	High	NF	NF	NF	NF
P29401-2	58.998	26	13	7086	TKT	NF	High	High	High	NF	High	NF	High	High	NF	NF	NF
P08708	58.957	53	7	6218	RPS17; RPS17L	NF	High	High	High	High	High	High	High	High	NF	NF	High
Q07157-2	58.824	10	14	7082	TJP1	NF	NF	NF	High	NF	NF	NF	NF	NF	NF	NF	NF
P13797	58.798	28	14	5358	PLS3	NF	High	High	High	NF	High	NF	High	NF	NF	NF	NF

Q13263	58.718	17	12	10155	TRIM28	NF	High	High	High	NF	High	NF	High	NF	NF	NF	NF
Q99714-1	58.554	59	9	3028	HSD17B10	NF	High	High	High	NF	High	NF	High	NF	NF	NF	NF
Q14654	58.534	18	16	8471	IRS4	NF	High	High	High	NF	High	NF	High	NF	NF	NF	NF
Q9UQ35	58.482	8	17	23524	SRRM2	NF	High	High	High	NF	High	NF	High	NF	NF	NF	NF
Q07065	58.303	25	11	10970	CKAP4	NF	High	High	High	NF	NF	NF	High	High	NF	NF	NF
Q16891	58.238	27	15	10989	IMMT	NF	High	High	High	NF	High	NF	High	NF	NF	High	NF
P06748	58.09	32	7	4869	NPM1	NF	High	High	High	High	High	NF	High	High	NF	High	High
P20700	57.911	28	15	4001	LMNB1	NF	High	High	NF	NF	High	NF	High	NF	NF	NF	NF
P62269	57.211	63	15	6222	RPS18	High	High	High	High	High	High	High	High	High	High	High	NF
Q92616	56.908	8	16	10985	GCN1L1; GCN1	NF	High	High	High	NF	High	NF	High	NF	NF	NF	NF
P07237	56.741	33	12	5034	P4HB	NF	High	High	NF	NF	High	NF	High	High	NF	NF	NF
Q9Y678	56.543	17	8	22820	COPG1	NF	High	High	High	NF	High	NF	High	NF	NF	NF	NF
P15924-1	56.477	7	20	1832	DSP	High	High	High	High	High	High	High	High	High	High	NF	NF
P40227-1	56.397	32	12	908	CCT6A	NF	High	High	High	NF	High	NF	High	High	NF	NF	NF
Q14240-2	56.173	29	1	1974	EIF4A2	NF	High	NF	High	NF	High	NF	High	NF	NF	NF	NF
P17812	55.857	30	15	1503	CTPS1	NF	High	High	High	NF	High	NF	High	High	High	NF	NF
P18621-3	55.657	33	9	100526842; 6139	RPL17- C18ORF32; RPL17	NF	High	High	High	NF	High	High	High	High	NF	NF	NF
P12270	55.475	6	14	7175	TPR	NF	High	High	NF	NF	High	NF	High	High	NF	NF	NF
Q13838-2	55.25	31	6	7919	DDX39B	NF	High	High	NF	NF	High	NF	High	High	NF	NF	NF
Q9H9B4	54.934	47	10	94081	SFXN1	NF	High	High	High	NF	High	NF	High	High	NF	NF	NF
P63104	54.284	51	9	7534	YWHAZ	NF	High	High	High	NF	High	NF	High	High	NF	NF	NF
Q9P2E9-1	53.913	9	10	6238	RRBP1	NF	High	High	High	NF	High	NF	High	NF	NF	NF	NF
Q14980	53.296	19	16	7514	XPO1	NF	High	High	High	NF	High	NF	High	NF	NF	NF	NF
O95831-1	53.295	30	12	9131	AIFM1	NF	High	High	High	NF	High	NF	High	High	NF	NF	NF
P11387	53.172	23	17	7150	TOP1	NF	High	High	High	NF	High	NF	High	NF	NF	NF	NF
Q9HCE1	53.1	19	18	4343	MOV10	NF	High	High	High	NF	High	NF	High	NF	NF	NF	NF
P22102-1	52.926	20	14	2618	GART	NF	High	High	High	NF	High	NF	High	High	NF	NF	NF
P49736	52.593	15	11	4171	MCM2	NF	High	High	High	NF	High	NF	High	High	NF	NF	NF

Q14152	52.505	13	18	8661	EIF3A	NF	High	High	High	NF	High	NF	High	High	NF	NF	NF
Q99623	52.332	53	13	11331	PHB2	NF	High	High	High	NF	High	High	High	High	NF	NF	NF
Q9UHX1-1	52.22	27	9	22827	PUF60	NF	High	High	High	NF	High	High	High	NF	NF	NF	NF
Q9Y383	52.129	32	7	51631	LUC7L2	High	High	High	High	High	High	NF	High	High	High	NF	NF
P19013	51.94	30	10	3851	KRT4	NF	NF	High	High	NF	NF	NF	NF	NF	High	NF	NF
Q9NXF1	51.832	18	12	54881	TEX10	NF	High	High	High	NF	High	NF	High	High	NF	NF	NF
P62263	51.067	43	9	6208	RPS14	High	High	High	High	High	High	High	High	High	High	High	NF
P34932	50.564	17	10	3308	HSPA4	NF	High	High	NF	NF	High	NF	High	NF	NF	NF	NF
P78386	50.497	32	7	3891	KRT85	High	High	NF	NF	NF	NF	NF	NF	NF	NF	NF	NF
P48047	50.203	59	9	539	ATP5O	NF	High	High	High	NF	High	NF	High	High	NF	NF	NF
Q02978	50.022	38	11	8402	SLC25A11	NF	High	High	High	NF	High	NF	High	High	NF	NF	NF
P45880-1	49.393	48	11	7417	VDAC2	NF	High	High	High	NF	High	NF	High	NF	NF	NF	NF
P46781	49.297	46	15	6203	RPS9	High	High	High	High	High	High	High	High	High	High	High	NF
P04844-1	49.099	26	11	6185	RPN2	NF	High	High	High	NF	High	NF	High	High	NF	NF	NF
Q15323	48.674	32	5	3881	KRT31	NF	High	NF	NF	NF	NF	NF	NF	NF	NF	NF	NF
P40939	48.647	22	10	3030	HADHA	NF	High	High	NF	NF	High	NF	High	NF	NF	NF	NF
Q15233	48.628	33	11	4841	NONO	NF	High	High	High	NF	High	NF	High	NF	NF	NF	NF
Q92598-4	48.433	18	10	10808	HSPH1	NF	High	High	High	NF	High	High	High	NF	NF	NF	NF
Q15758-1	48.259	26	10	6510	SLC1A5	NF	High	High	High	NF	High	High	High	NF	NF	NF	NF
O00410-3	47.988	13	10	3843	IPO5	NF	High	High	High	NF	High	NF	High	NF	NF	NF	NF
Q9Y5M8	47.853	39	8	58477	SRPRB	NF	High	High	High	NF	High	NF	High	NF	NF	NF	NF
P30101	47.571	36	14	2923	PDIA3	NF	High	High	NF	NF	High	NF	High	High	NF	NF	NF
P62979	46.925	51	6	6233	RPS27A	High	High	High	High	High	High	High	High	High	High	High	NF
Q9UHB9	46.599	19	9	6730	SRP68	NF	High	High	High	High	High	NF	High	High	NF	NF	NF
P62081	46.518	44	10	6201	RPS7	High	High	High	High	High	High	High	High	High	High	High	High
P15311	46.382	21	9	7430	EZR	NF	High	High	NF	NF	High	NF	High	High	NF	NF	NF
Q04695	45.998	24	4	3872	KRT17	NF	NF	High	High	NF	High	NF	NF	High	High	NF	NF
Q13162	45.734	41	7	10549	PRDX4	NF	High	High	High	NF	High	NF	High	NF	NF	NF	NF
P22695	45.375	30	9	7385	UQCRC2	NF	High	High	High	NF	High	High	High	NF	NF	NF	NF

P46060	45.245	23	10	5905	RANGAP1	NF	High	High	High	NF	High	NF	High	NF	NF	NF	NF
Q7KZF4	45.121	17	13	27044	SND1	NF	High	High	NF	NF	High	NF	High	High	NF	NF	NF
Q9BXJ9	44.757	17	15	80155	NAA15	NF	High	High	High	NF	High	NF	High	NF	NF	NF	NF
P61221	44.617	28	12	6059	ABCE1	NF	High	High	High	NF	High	NF	High	NF	NF	NF	NF
P00505	44.423	27	9	2806	GOT2	NF	High	High	NF	NF	High	NF	High	High	NF	NF	NF
Q9NVI7	44.341	22	5	55210	ATAD3A	NF	High	High	High	NF	High	NF	High	High	NF	NF	NF
O43491-1	44.264	12	11	2037	EPB41L2	NF	High	High	High	High	High	High	High	NF	NF	NF	NF
P51659-1	44.215	17	10	3295	HSD17B4	NF	High	High	High	NF	High	NF	High	NF	NF	NF	NF
Q8N1F7-1	43.784	20	14	9688	NUP93	NF	High	High	High	NF	High	High	High	High	NF	NF	NF
P47897	43.711	21	14	5859	QARS	NF	High	High	High	NF	High	NF	High	NF	NF	NF	NF
P27348	43.316	42	8	10971	YWHAQ	NF	High	High	High	NF	High	NF	High	NF	NF	NF	NF
Q06830	43.316	52	9	5052	PRDX1	NF	High	High	High	High	High	NF	High	High	NF	NF	NF
P62280	43.297	57	11	6205	RPS11	High	High	High	High	High	High	High	High	High	High	NF	NF
P13804-1	43.278	36	9	2108	ETFA	NF	High	High	High	NF	High	NF	High	High	NF	NF	NF
Q07020	43.137	39	10	6141	RPL18	NF	High	High	High	High	High	High	High	High	High	NF	High
Q99798	43.128	20	11	50	ACO2	NF	High	High	NF	NF	NF	NF	High	NF	NF	NF	NF
P31930	43.041	26	8	7384	UQCRC1	NF	High	High	High	NF	High	High	High	NF	NF	NF	NF
P42766	43.01	30	5	11224	RPL35	High	High	High	High	High	High	High	High	High	High	NF	NF
Q7Z6Z7	42.818	3	10	10075	HUWE1	NF	NF	High	High	NF	High	NF	High	NF	NF	NF	NF
P08195-4	42.78	16	9	6520	SLC3A2	NF	High	High	High	NF	High	High	High	NF	NF	NF	NF
P30050-1	42.62	55	6	6136	RPL12	NF	High	High	High	NF	High	High	High	High	NF	NF	NF
P27797	42.265	24	8	811	CALR	NF	NF	High	NF	NF	High	NF	High	NF	NF	NF	NF
Q7Z406-2	42.264	6	4	79784	MYH14	NF	NF	NF	High	NF	NF	NF	High	NF	NF	NF	NF
Q9Y262	41.974	24	11	51386	EIF3L	NF	High	High	High	NF	High	NF	High	NF	NF	NF	NF
P62258-1	41.526	55	11	7531	YWHAЕ	NF	High	High	High	NF	High	NF	High	NF	NF	NF	NF
P11177	41.074	37	9	5162	PDHB	NF	High	High	High	NF	High	NF	High	NF	NF	NF	NF
Q9BUQ8	41.025	17	14	9416	DDX23	NF	High	High	High	NF	High	NF	High	NF	NF	NF	NF
Q14525	40.928	27	2	3884	KRT33B	NF	High	NF	NF	NF	NF	NF	NF	NF	NF	NF	NF
B5ME19	40.442	16	14	728689	EIF3CL	NF	High	High	High	NF	High	High	High	High	NF	NF	NF

[illegible]

P31040	36.846	15	7	6389	SDHA	NF	High	High	High	NF	High	NF	High	High	NF	NF	NF
P36873-2	36.807	25	2	5501	PPP1CC	NF	High	High	NF	NF	NF	NF	High	NF	NF	NF	NF
Q13435	36.788	14	12	10992	SF3B2	NF	High	High	High	NF	High	NF	High	NF	NF	NF	NF
P62140	36.608	26	2	5500	PPP1CB	NF	High	High	NF	NF	High	NF	NF	NF	NF	NF	NF
P08243-1	36.589	19	9	440	ASNS	NF	High	High	High	NF	High	NF	High	High	NF	NF	NF
P07197	36.353	13	10	4741	NEFM	NF	High	High	High	NF	High	High	NF	NF	NF	NF	NF
P02786	36.226	18	12	7037	TFRC	NF	High	High	High	NF	High	NF	High	NF	NF	NF	NF
P14866	35.927	20	10	3191	HNRNPL	NF	High	High	High	NF	High	NF	High	High	NF	NF	NF
Q9UMS4	35.918	22	8	27339	PRPF19	NF	High	High	High	NF	High	NF	High	NF	NF	NF	NF
Q9Y2L1-1	35.886	14	10	22894	DIS3	NF	High	High	High	NF	High	NF	High	NF	NF	NF	NF
O00303	35.473	27	7	8665	EIF3F	NF	High	High	High	NF	High	NF	High	High	NF	NF	NF
P12035	35.309	11	1	3850	KRT3	NF	NF	NF	NF	NF	NF	NF	NF	NF	High	NF	NF
P42285	35.114	13	10	23517	SKIV2L2	NF	High	High	NF	NF	High	NF	High	High	NF	NF	NF
O94906-1	35.093	12	10	24148	PRPF6	NF	High	High	High	NF	High	NF	High	NF	NF	NF	NF
Q16531	35.085	10	9	1642	DDB1	NF	High	High	NF	NF	High	NF	High	NF	NF	NF	NF
P07910-1	35.027	35	11	3183	HNRNPC	High	High	High	High	NF	High	High	High	High	NF	NF	NF
P62917	34.912	32	10	6132	RPL8	High	High	High	High	High	High	High	High	High	High	High	NF
Q8TDD1-2	34.888	15	9	79039	DDX54	NF	High	High	NF	NF	High	NF	High	NF	NF	NF	NF
Q9UBU9-1	34.278	16	7	10482	NXF1	NF	High	High	High	NF	High	NF	NF	NF	NF	NF	NF
P23526-1	34.258	25	10	191	AHCY	NF	High	High	High	NF	High	NF	High	High	NF	NF	NF
O76094	34.076	17	8	6731	SRP72	NF	High	High	High	High	High	NF	High	High	NF	NF	NF
Q14103	33.645	26	6	3184	HNRNPD	NF	High	High	NF	NF	High	NF	High	NF	NF	NF	NF
Q9P258	33.645	28	13	55920	RCC2	NF	High	High	High	High	High	NF	High	NF	NF	NF	NF
Q00325-2	33.611	30	9	5250	SLC25A3	NF	High	High	High	NF	High	High	High	NF	NF	NF	NF
P38919	33.53	25	6	9775	EIF4A3	NF	NF	High	NF	NF	High	NF	High	High	NF	NF	NF
Q02543	33.194	42	8	6142	RPL18A	NF	High	High	High	NF	High	High	High	High	NF	NF	NF
P26373-1	33.144	37	10	6137	RPL13	High	High	High	High	High	High	High	High	High	High	NF	NF
P54577	33.091	21	11	8565	YARS	NF	High	High	NF	NF	High	NF	High	NF	NF	NF	NF
P02751-15	33.044	5	9	2335	FN1	NF	NF	NF	NF	NF	NF	NF	NF	High	NF	NF	NF

P22626	33.01	27	9	3181	HNRNPA2B1	NF	High	High	High	NF	High	NF	High	High	NF	NF	NF
P28288	32.986	19	10	5825	ABCD3	NF	High	High	High	NF	High	NF	High	High	NF	NF	NF
P08754	32.841	24	3	2773	GNAI3	NF	NF	High	High	NF	NF	NF	High	NF	NF	NF	NF
P08133-1	32.719	17	11	309	ANXA6	NF	NF	High	NF	NF	NF	NF	High	NF	NF	NF	NF
P62937	32.488	64	9	5478	PPIA	NF	High	High	NF	NF	High	NF	High	NF	NF	NF	NF
Q9NVP1	32.384	14	8	8886	DDX18	NF	High	High	High	NF	High	NF	High	NF	NF	NF	NF
P46782	32.31	32	6	6193	RPS5	High	High	High	High	High	High	High	High	High	High	NF	High
Q9Y265	32.304	22	8	8607	RUVBL1	NF	High	High	High	NF	High	NF	High	NF	NF	NF	NF
P17858-2	32.234	13	6	5211	PFKL	NF	NF	High	High	NF	High	NF	High	NF	NF	NF	NF
P49915	32.017	13	7	8833	GMPS	NF	High	High	NF	NF	High	NF	High	NF	NF	NF	NF
P62826	31.928	39	7	5901	RAN	High	High	High	High	High	High	High	High	High	NF	High	NF
P27824-2	31.735	12	7	821	CANX	NF	High	High	NF	NF	High	NF	High	High	NF	NF	NF
O00425	31.731	19	6	10643	IGF2BP3	NF	High	High	High	NF	High	NF	High	NF	NF	NF	NF
P21796	31.705	37	6	7416	VDAC1	NF	High	High	High	NF	High	NF	High	NF	NF	NF	NF
O75534-4	31.691	15	10	7812	CSDE1	NF	High	High	High	NF	High	NF	High	NF	NF	NF	NF
Q92900	31.65	13	13	5976	UPF1	NF	High	High	NF	NF	High	NF	High	NF	NF	NF	NF
P06744-2	31.607	18	8	2821	GPI	NF	High	High	NF	NF	High	NF	High	NF	NF	NF	NF
P51991-1	31.173	21	6	220988	HNRNPA3	NF	NF	High	NF	NF	High	NF	High	NF	NF	NF	NF
Q96EY7-1	31.112	15	7	55037	PTCD3	NF	High	High	High	NF	High	NF	High	NF	NF	NF	NF
P27635	30.949	29	7	6134	RPL10	NF	High	High	High	NF	High	High	High	High	NF	High	NF
P67809	30.946	36	7	4904	YBX1	High	High	High	High	High	High	NF	High	High	NF	High	NF
Q9BQ39	30.928	14	5	79009	DDX50	NF	High	High	NF	NF	High	NF	High	NF	NF	NF	NF
P62277	30.924	38	7	6207	RPS13	NF	High	High	NF	High	High	NF	High	High	NF	NF	NF
Q99459	30.626	13	9	988	CDC5L	NF	High	High	NF	NF	High	High	High	NF	NF	NF	NF
Q6UB35-1	30.581	9	8	25902	MTHFD1L	NF	High	High	NF	NF	NF	NF	High	NF	NF	NF	NF
P31689	30.423	27	8	3301	DNAJA1	NF	High	High	NF	NF	High	NF	High	NF	NF	NF	NF
P50402	30.283	33	7	2010	EMD	NF	High	High	High	NF	High	High	High	NF	NF	NF	NF
Q9Y617-1	30.266	29	10	29968	PSAT1	NF	High	High	NF	NF	High	NF	High	NF	NF	NF	NF
P41091	30.171	22	8	1968	EIF2S3	NF	High	High	High	NF	High	NF	High	High	NF	NF	NF

Q7Z794	30.167	11	4	374454	KRT77	NF	High	NF	NF	NF	NF	NF	NF	NF	NF	NF	NF
P30084	30.046	19	3	1892	ECHS1	NF	NF	High	NF	NF	NF	NF	High	High	NF	NF	NF
Q9UJV9	30.043	18	10	51428	DDX41	NF	High	High	High	NF	High	NF	High	NF	NF	NF	NF
Q16630-2	30.015	11	5	11052	CPSF6	NF	High	High	High	NF	High	NF	High	NF	NF	NF	NF
P27816-1	29.983	8	7	4134	MAP4	NF	High	High	High	NF	High	NF	High	NF	NF	NF	NF
O75694	29.735	8	9	9631	NUP155	NF	High	High	NF	NF	High	NF	High	NF	NF	NF	NF
Q5T9A4	29.657	16	2	83858	ATAD3B	NF	High	High	NF	NF	High	NF	NF	NF	NF	NF	NF
O00148	29.559	18	1	10212	DDX39A	NF	High	NF	NF	NF	NF	NF	High	NF	NF	NF	NF
P32119	29.463	34	8	7001	PRDX2	NF	High	High	High	NF	High	NF	High	High	NF	NF	NF
P36542-1	29.38	29	8	509	ATP5C1	NF	High	High	High	NF	High	NF	High	NF	NF	NF	NF
Q03252	29.325	14	7	84823	LMNB2	NF	High	High	NF	NF	High	NF	High	NF	NF	NF	NF
P78347	29.197	12	10	2969	GTF2I	NF	High	High	NF	NF	High	NF	High	NF	NF	NF	NF
P07737	29.102	57	7	5216	PFN1	NF	High	High	NF	NF	High	NF	High	NF	NF	NF	NF
O43290	29.062	11	9	9092	SART1	NF	High	High	High	NF	High	NF	High	NF	NF	NF	NF
P00367	29.004	16	7	2746	GLUD1	NF	High	High	NF	NF	NF	NF	High	NF	NF	NF	NF
P11216	28.968	12	4	5834	PYGB	NF	NF	NF	NF	NF	High	NF	High	NF	NF	NF	NF
P50454	28.929	18	5	871	SERPINH1	NF	High	High	High	NF	High	NF	High	High	NF	NF	High
Q9UG63-2	28.849	15	9	10061	ABCF2	NF	High	High	High	NF	High	NF	High	NF	NF	NF	NF
P35606	28.82	12	9	9276	COPB2	NF	High	High	High	NF	High	NF	High	NF	NF	NF	NF
Q9NSE4	28.809	7	5	55699	IARS2	NF	High	High	NF	NF	High	NF	High	NF	NF	NF	NF
P12532	28.789	20	6	1159; 548596	CKMT1B; CKMT1A	NF	High	High	NF	NF	High	NF	High	NF	NF	NF	NF
Q8WUM4-2	28.577	14	9	10015	PDCD6IP	NF	High	High	High	NF	High	NF	High	NF	NF	NF	NF
Q7RTS7	28.522	10	2	121391	KRT74	High	High	NF	High	NF	High	NF	NF	NF	NF	NF	High
Q13148-1	28.48	27	6	23435	TARDBP	High	High	High	High	NF	High	NF	High	High	NF	NF	NF
P52292	28.407	26	8	3838	KPNA2	NF	High	High	NF	NF	High	High	High	NF	NF	NF	High
P13489	28.23	19	6	6050	RNH1	NF	High	High	High	NF	High	NF	High	NF	NF	NF	NF
Q86UP2-1	28.176	6	9	3895	KTN1	NF	High	High	High	NF	NF	NF	High	NF	NF	NF	NF
P62829	28.106	44	5	9349	RPL23	NF	High	High	High	NF	High	High	High	High	High	NF	NF

Q01780	28.101	10	7	5394	EXOSC10	NF	High	High	High	NF	High	NF	High	NF	NF	NF	NF
P49792	28.057	4	8	5903	RANBP2	NF	High	High	High	NF	High	NF	High	NF	NF	NF	NF
P09622	27.768	17	7	1738	DLD	NF	High	High	NF	NF	High	NF	High	NF	NF	NF	NF
Q6PKG0-1	27.765	7	9	23367	LARP1	NF	High	High	High	NF	High	NF	NF	NF	NF	NF	High
Q8TEX9-2	27.75	9	7	79711	IPO4	NF	NF	High	High	High	High	NF	High	High	NF	NF	NF
O95573	27.232	13	7	2181	ACSL3	NF	High	High	High	NF	High	NF	High	NF	NF	NF	NF
P18085	27.219	36	3	378	ARF4	NF	High	High	High	NF	High	High	High	High	NF	NF	NF
Q92621	27.177	6	8	23165	NUP205	NF	High	High	High	NF	High	NF	High	NF	NF	NF	NF
P62750	27.15	44	8	6147	RPL23A	High	High	High	High	High	High	High	High	High	High	High	NF
P48681	27.141	5	8	10763	NES	NF	NF	High	High	NF	NF	NF	NF	NF	NF	NF	NF
O75306	26.894	22	7	4720	NDUFS2	NF	High	High	NF	NF	High	NF	High	High	NF	NF	NF
Q93008-3	26.867	4	9	8239	USP9X	High	High	NF	High	NF	High	NF	High	High	NF	NF	NF
P49588-2	26.797	9	7	16	AARS	NF	High	High	NF	NF	High	NF	High	NF	NF	NF	NF
P62906	26.68	41	8	4736	RPL10A	NF	High	High	High	High	High	High	High	High	NF	NF	NF
O75131	26.65	16	6	8895	CPNE3	NF	NF	High	NF	NF	NF	NF	High	NF	NF	NF	NF
Q06210-1	26.604	17	9	2673	GFPT1	NF	NF	NF	High	NF	High	NF	High	NF	NF	NF	NF
P62910	26.326	33	5	6161	RPL32	NF	High	High	High	High	High	NF	High	NF	NF	NF	NF
Q8IY37	26.307	7	7	57647	DHX37	NF	High	High	NF	NF	High	NF	High	NF	NF	NF	NF
O43592	26.297	10	7	11260	XPOT	NF	NF	NF	High	NF	High	NF	High	NF	NF	NF	NF
P62266	26.257	43	5	6228	RPS23	High	High	High	High	High	High	High	High	High	High	NF	High
P30048	26.203	34	5	10935	PRDX3	NF	High	High	NF	NF	NF	NF	High	NF	NF	NF	NF
P30041	26.084	35	7	9588	PRDX6	NF	High	High	High	NF	High	NF	High	NF	NF	NF	NF
P08758	25.997	25	8	308	ANXA5	NF	High	High	NF	NF	High	NF	High	NF	NF	NF	NF
P50914	25.945	21	4	9045	RPL14	NF	High	High	High	NF	High	High	High	High	NF	NF	High
P51114-1	25.852	11	6	8087	FXR1	NF	High	High	High	NF	High	NF	High	NF	NF	NF	NF
Q16836-2	25.788	20	6	3033	HADH	NF	High	High	High	NF	High	NF	High	High	NF	NF	NF
Q96AG4	25.733	31	7	55379	LRRC59	NF	High	High	High	NF	High	High	High	High	NF	NF	NF
Q9BSD7	25.627	30	4	84284	NTPCR	NF	NF	High	High	NF	High	NF	High	High	NF	NF	NF
P26038	25.307	15	4	4478	MSN	NF	High	High	NF	NF	High	NF	High	NF	NF	NF	NF

Q13724	25.154	13	9	7841	MOGS	NF	High	High	High	NF	High	NF	High	NF	NF	NF	NF
P46776	24.929	31	6	6157	RPL27A	NF	High	High	High	High	High	High	High	High	NF	NF	NF
O75746	24.917	14	3	8604	SLC25A12	NF	High	High	High	NF	NF	NF	High	NF	NF	NF	NF
Q9P035	24.822	15	6	51495	PTPLAD1; HACD3	NF	High	High	High	NF	High	NF	High	High	NF	NF	NF
P02768-1	24.659	8	6	213	ALB	High	High	High	High	High	High	High	High	High	High	High	High
Q14694-2	24.632	11	8	9100	USP10	NF	High	High	High	NF	High	NF	High	NF	NF	NF	NF
Q9NU22	24.628	2	8	23195	MDN1	NF	High	High	NF	NF	NF	NF	High	NF	NF	NF	NF
P33176	24.527	12	8	3799	KIF5B	NF	High	NF	High	NF	High	NF	High	NF	NF	NF	NF
P55196-5	24.495	5	8	4301	MLLT4; AFDN	NF	High	High	High	NF	High	NF	High	NF	NF	NF	NF
P47756-2	24.466	32	6	832	CAPZB	NF	High	High	High	NF	High	NF	High	NF	NF	NF	NF
P55884-2	24.295	10	8	8662	EIF3B	NF	High	High	High	NF	High	NF	High	NF	NF	NF	NF
O15371	24.292	16	7	8664	EIF3D	NF	High	High	High	NF	High	NF	High	NF	NF	NF	NF
P31939	24.156	17	9	471	ATIC	NF	NF	High	NF	NF	High	NF	High	NF	NF	NF	NF
P84098	24.069	18	5	6143	RPL19	High	High	High	High	High	High	High	High	High	High	NF	NF
P04899-4	24.031	23	2	2771	GNAI2	NF	NF	NF	High	NF	NF	NF	NF	NF	NF	NF	NF
O76021	23.941	15	6	26156	RSL1D1	NF	High	High	High	High	High	NF	High	NF	NF	NF	High
Q9H857-2	23.902	17	8	64943	NT5DC2	NF	High	High	NF	NF	High	NF	High	NF	NF	NF	NF
P28074-1	23.889	26	6	5693	PSMB5	NF	High	High	NF	NF	High	NF	High	NF	NF	NF	NF
P60891	23.851	22	6	5631	PRPS1	NF	High	High	High	NF	High	NF	High	NF	NF	NF	NF
P11413-2	23.82	15	8	2539	G6PD	NF	High	High	NF	NF	High	NF	High	NF	NF	NF	NF
P42167	23.803	19	6	7112	TMPO	NF	High	High	High	NF	High	NF	High	NF	NF	NF	NF
Q10567	23.768	10	4	162	AP1B1	NF	High	High	High	NF	NF	NF	High	High	NF	NF	NF
P53985	23.755	13	3	6566	SLC16A1	NF	High	High	NF	NF	High	NF	High	High	NF	NF	NF
P46778	23.743	26	4	6144	RPL21	NF	High	High	High	NF	High	NF	High	NF	NF	NF	NF
Q9UQ80	23.559	22	9	5036	PA2G4	NF	High	High	NF	NF	High	NF	High	NF	NF	NF	NF
P62913	23.558	33	6	6135	RPL11	NF	High	High	High	High	High	High	High	High	NF	NF	NF
Q14008-3	23.541	5	8	9793	CKAP5	NF	High	High	High	NF	High	NF	High	NF	NF	NF	NF
P29692-2	23.445	9	4	1936	EEF1D	NF	NF	High	NF	NF	NF	NF	High	NF	NF	NF	NF
O43684	23.422	19	6	9184	BUB3	NF	High	High	High	High	High	NF	High	High	NF	NF	NF

P49756-1	23.393	10	6	58517	RBM25	NF	High	High	High	NF	High	NF	High	NF	NF	NF	NF
Q9UBF2	23.254	11	5	26958	COPG2	NF	NF	High	NF	NF	High	NF	High	NF	NF	NF	NF
Q14929	22.96	14	4	8520	HAT1	NF	High	High	High	NF	NF	NF	High	NF	NF	NF	NF
Q9NYF8-1	22.951	8	6	9774	BCLAF1	NF	High	High	High	NF	High	NF	High	NF	NF	NF	NF
Q9UBX3-2	22.921	23	6	1468	SLC25A10	NF	High	High	High	NF	High	NF	High	NF	NF	NF	NF
Q99729-2	22.877	19	5	3182	HNRNPAB	NF	High	High	NF	NF	High	NF	High	NF	NF	NF	NF
Q9Y277	22.723	19	4	7419	VDAC3	NF	NF	High	High	NF	High	NF	High	NF	NF	NF	NF
Q99460	22.685	8	6	5707	PSMD1	NF	High	High	High	NF	High	NF	High	NF	NF	NF	NF
O75390	22.666	18	8	1431	CS	NF	High	High	NF	NF	High	NF	High	NF	NF	NF	NF
P39656	22.622	18	6	1650	DDOST	NF	High	High	NF	NF	High	NF	High	NF	NF	NF	NF
Q16352	22.608	16	7	9118	INA	NF	NF	NF	High	NF	NF	NF	NF	NF	NF	NF	NF
P18669	22.483	26	4	5223; 643576	PGAM1; LOC643576	NF	High	High	NF	NF	NF	NF	High	NF	NF	NF	NF
Q8IY81	22.454	11	7	117246	FTSJ3	NF	High	High	NF	NF	High	NF	High	NF	NF	NF	NF
O95757	22.393	8	3	22824	HSPA4L	NF	NF	High	NF	NF	High	NF	High	NF	NF	NF	NF
P38159-1	22.259	19	7	27316	RBMX	NF	High	High	High	NF	High	NF	High	NF	NF	NF	NF
P61204	22.238	29	1	377	ARF3	NF	NF	High	NF	NF	NF	NF	High	NF	NF	NF	NF
Q9NSD9	22.178	14	8	10056	FARSB	NF	High	High	High	NF	High	NF	High	NF	NF	NF	NF
Q8TCJ2	22.16	7	5	201595	STT3B	NF	High	High	High	NF	High	NF	High	NF	NF	NF	NF
O00541-1	22.095	15	8	23481	PES1	NF	High	High	NF	NF	High	NF	High	NF	NF	NF	NF
P32322-3	21.972	21	4	5831	PYCR1	NF	High	High	High	NF	NF	NF	High	NF	NF	NF	NF
Q92499	21.954	11	5	1653	DDX1	NF	High	High	High	NF	High	NF	High	NF	NF	NF	NF
Q86XK2-5	21.931	9	7	80204	FBXO11	NF	High	High	NF	NF	High	NF	NF	NF	NF	NF	NF
P15531-2	21.918	34	1	4830	NME1	NF	NF	NF	NF	NF	NF	NF	High	NF	NF	NF	NF
Q9P2J5	21.903	6	6	51520	LARS	NF	NF	High	High	NF	High	NF	High	NF	NF	NF	NF
Q8N163-1	21.887	9	8	57805	KIAA1967; CCAR2	NF	High	High	NF	NF	High	NF	NF	NF	NF	NF	NF
P84085	21.852	27	1	381	ARF5	NF	High	NF	NF	NF	High	NF	NF	NF	NF	NF	NF
Q13247	21.826	17	4	6431	SRSF6	NF	High	High	High	NF	High	NF	High	NF	NF	NF	NF
P56192	21.656	10	7	4141	MARS	NF	High	High	High	NF	High	NF	High	NF	NF	NF	NF

P11717	21.458	3	7	3482	IGF2R	NF	High	High	High	NF	NF	NF	High	NF	NF	NF	NF
Q06787	21.409	9	5	2332	FMR1	NF	High	NF	High	NF	High	NF	High	NF	NF	NF	NF
Q07955-1	21.39	30	6	6426	SRSF1	NF	High	High	High	NF	NF	NF	High	High	NF	NF	NF
Q9Y285	21.307	14	7	2193	FARSA	NF	High	High	High	NF	High	NF	High	High	NF	NF	NF
P83731	21.229	34	7	6152	RPL24	NF	High	High	High	NF	High	NF	High	High	NF	NF	NF
P35613	21.189	17	5	682	BSG	NF	NF	High	NF	NF	NF	NF	High	NF	NF	NF	NF
Q5C9Z4	21.16	8	6	64434	NOM1	NF	NF	High	NF	NF	High	NF	NF	NF	NF	NF	NF
Q6P158-1	21.154	6	6	90957	DHX57	NF	High	High	NF	NF	High	NF	NF	NF	NF	NF	NF
P62851	21.076	31	6	6230	RPS25	High	High	High	High	High	High	High	High	High	High	High	NF
P22392-2	20.99	43	2	654364; 4830; 4831	NME1-NME2; NME1; NME2	NF	High	NF	NF	NF	NF	NF	High	NF	NF	NF	NF
Q53GS9	20.961	12	4	10713	USP39	NF	High	High	High	NF	High	NF	High	NF	NF	NF	NF
P62995	20.925	24	5	6434	TRA2B	NF	High	High	High	NF	High	NF	High	NF	NF	NF	NF
P46779-3	20.828	28	7	6158	RPL28	High	High	High	High	High	High	High	High	High	NF	NF	NF
P10515	20.769	10	5	1737	DLAT	NF	High	High	NF	NF	NF	NF	High	NF	NF	NF	NF
Q99615-1	20.764	14	6	7266	DNAJC7	NF	High	High	NF	NF	High	NF	High	NF	NF	NF	NF
Q9BSJ8-2	20.547	4	4	23344	ESYT1	NF	High	High	NF	NF	High	NF	High	NF	NF	NF	NF
P25398	20.517	54	6	6206	RPS12	NF	High	High	High	NF	High	NF	High	NF	NF	NF	NF
P50395-1	20.511	10	1	2665	GDI2	NF	NF	High	NF	NF	High	NF	High	NF	NF	NF	NF
Q15003	20.495	10	6	23397	NCAPH	NF	NF	High	High	NF	High	NF	High	NF	NF	NF	NF
O15042	20.49	6	5	23350	U2SURP	NF	High	High	NF	NF	NF	NF	High	NF	NF	NF	NF
O60763-2	20.463	7	6	8615	USO1	NF	High	High	High	NF	High	NF	High	NF	NF	NF	NF
O94826	20.449	12	6	9868	TOMM70A; TOMM70	NF	High	High	High	NF	NF	NF	High	High	NF	NF	NF
P23528	20.403	39	5	1072	CFL1	NF	High	High	High	NF	High	NF	High	High	NF	NF	NF
P26368	20.327	16	6	11338	U2AF2	NF	High	High	High	High	High	NF	High	NF	NF	NF	NF
Q14684	20.276	11	7	23076	RRP1B	NF	High	High	High	NF	High	NF	High	NF	NF	NF	NF
P63010-2	20.225	10	4	163	AP2B1	NF	High	NF	High	NF	High	NF	High	NF	NF	NF	NF
Q9UN86	20.144	12	5	9908	G3BP2	NF	High	High	High	NF	High	NF	High	NF	NF	NF	NF
O14744	20.095	11	7	10419	PRMT5	High	High	NF	NF	High	High	High	High	NF	High	NF	NF

P62888	20.028	48	4	6156	RPL30	NF	High	High	High	NF	NF	NF	High	High	NF	NF	NF
Q12769	20.009	4	5	23279	NUP160	NF	NF	High	NF	NF	High	NF	High	NF	NF	NF	NF
P31150	19.991	10	1	2664	GDI1	NF	NF	High	NF	NF	NF	NF	NF	NF	NF	NF	NF
Q9GZR7	19.974	6	4	57062	DDX24	NF	High	High	NF	NF	High	NF	High	High	NF	NF	NF
P84103	19.829	29	3	6428	SRSF3	NF	High	High	High	NF	High	NF	High	High	NF	NF	NF
Q9Y4L1	19.778	6	4	10525	HYOU1	NF	High	High	NF	NF	NF	NF	High	NF	NF	NF	NF
Q8N684-3	19.697	14	5	79869	CPSF7	NF	High	High	NF	NF	NF	NF	High	NF	NF	NF	NF
Q9NNW5	19.666	8	6	11180	WDR6	NF	NF	High	High	NF	High	NF	NF	NF	NF	NF	NF
Q15459	19.643	7	4	10291	SF3A1	NF	High	High	NF	NF	High	NF	High	NF	NF	NF	NF
P38117	19.621	29	7	2109	ETFB	NF	High	High	High	NF	NF	NF	High	NF	NF	NF	NF
Q9HAV4	19.569	6	7	57510	XPO5	NF	NF	High	High	NF	High	NF	High	NF	NF	NF	NF
P24539	19.559	32	6	515	ATP5F1	NF	High	High	NF	NF	High	NF	High	NF	NF	NF	NF
Q7Z2W4	19.436	8	5	56829	ZC3HAV1	NF	High	NF	NF	NF	High	NF	High	NF	NF	NF	NF
P49321-3	19.403	9	6	4678	NASP	NF	High	High	High	NF	High	NF	High	NF	NF	NF	NF
O95433	19.059	18	5	10598	AHSA1	NF	High	NF	High	NF	High	NF	High	NF	NF	NF	NF
O60762	19.053	28	5	8813	DPM1	NF	High	High	NF	NF	High	NF	High	High	NF	NF	NF
Q96AE4-2	18.971	11	6	8880	FUBP1	NF	High	High	NF	NF	High	NF	High	NF	NF	NF	NF
P48444	18.895	10	6	372	ARCN1	NF	High	High	High	NF	High	NF	High	NF	NF	NF	NF
P46977	18.672	10	6	3703	STT3A	NF	NF	High	NF	NF	High	NF	High	NF	NF	NF	NF
O43660-1	18.661	11	5	5356	PLRG1	NF	High	High	NF	NF	High	NF	High	NF	NF	NF	NF
P30837	18.604	12	5	219	ALDH1B1	NF	High	High	High	NF	High	NF	High	NF	NF	NF	NF
P08559-4	18.443	16	7	5160	PDHA1	NF	High	High	High	NF	NF	NF	High	NF	NF	NF	NF
Q9H4A4	18.406	12	7	6051	RNPEP	NF	NF	High	High	NF	High	NF	High	NF	NF	NF	NF
Q16629	18.34	21	4	6432	SRSF7	NF	High	High	High	NF	High	NF	NF	NF	NF	NF	NF
Q02790	18.263	16	6	2288	FKBP4	NF	High	High	NF	NF	NF	NF	High	NF	NF	NF	NF
Q13620	18.246	6	5	8450	CUL4B	NF	High	High	High	NF	High	NF	High	NF	NF	NF	NF
P61313-1	18.214	24	5	6138	RPL15	NF	High	High	High	High	High	High	High	High	NF	NF	NF
Q9P2R7	18.12	14	7	8803	SUCLA2	NF	High	High	High	NF	High	NF	High	NF	NF	NF	NF
O95232-1	18.065	9	3	51747	LUC7L3	NF	NF	High	High	NF	High	NF	High	NF	NF	NF	NF

O00567	17.982	9	5	10528	NOP56	NF	High	High	High	NF	High	NF	High	NF	NF	NF	NF
Q2NL82	17.947	9	5	55720	TSR1	NF	High	High	High	NF	High	NF	NF	NF	NF	NF	NF
Q9BXS5-2	17.929	15	6	8907	AP1M1	NF	High	High	NF	NF	High	NF	High	NF	NF	NF	NF
P00492	17.927	27	5	3251	HPRT1	NF	High	High	High	NF	High	NF	High	NF	NF	NF	NF
P28331-2	17.855	11	6	4719	NDUFS1	NF	High	High	High	NF	High	NF	High	NF	NF	High	NF
Q5T4S7-2	17.853	2	5	23352	UBR4	NF	NF	NF	High	NF	High	NF	High	NF	NF	NF	NF
Q7Z7H8-2	17.849	11	2	124995	MRPL10	NF	High	High	NF	NF	High	NF	High	NF	NF	NF	NF
Q9BXP5	17.8	7	6	51593	SRRT	NF	High	High	High	NF	High	NF	High	NF	NF	NF	NF
P63173	17.772	50	5	6169	RPL38	NF	High	High	NF	NF	High	NF	High	High	NF	NF	NF
P60866-2	17.662	24	4	6224	RPS20	NF	High	High	High	NF	High	High	High	High	NF	NF	NF
O60610-1	17.651	5	5	1729	DIAPH1	NF	High	NF	High	NF	High	NF	High	NF	NF	NF	NF
Q9BRT6	17.648	29	3	84298	LLPH	NF	NF	NF	High	NF	High	NF	High	NF	NF	NF	NF
Q15046-2	17.594	9	5	3735	KARS	NF	High	High	NF	NF	High	NF	High	NF	NF	NF	NF
Q14444-1	17.567	8	5	4076	CAPRIN1	NF	High	High	NF	NF	High	NF	High	NF	NF	NF	NF
P35998	17.499	14	5	5701	PSMC2	NF	High	High	High	NF	High	NF	High	NF	NF	NF	NF
Q8TEQ6	17.397	4	5	25929	GEMIN5	NF	High	NF	High	NF	High	NF	High	NF	NF	NF	NF
Q5JTZ9	17.391	8	6	57505	AARS2	NF	High	High	High	NF	High	NF	High	NF	NF	NF	NF
P54819	17.379	20	4	204	AK2	NF	High	High	NF	NF	NF	NF	High	NF	NF	NF	NF
P62314	17.298	37	3	6632	SNRPD1	NF	NF	High	NF	NF	NF	NF	High	NF	NF	NF	NF
P62244	17.28	44	6	6210	RPS15A	NF	High	High	High	High	High	NF	High	High	NF	NF	NF
Q9Y6M1	17.209	9	2	10644	IGF2BP2	NF	High	High	High	NF	High	NF	High	NF	NF	NF	NF
Q15717-2	17.184	14	4	1994	ELAVL1	NF	High	High	High	NF	High	NF	High	NF	NF	NF	NF
P62805	17.151	39	4	8359; 8361; 8360; 8363; 8365; 8364; 121504; 554313; 8367; 8294; 8366; 8370; 8362; 8368	HIST1H4A; HIST1H4F; HIST1H4D; HIST1H4J; HIST1H4H; HIST1H4C; HIST4H4; HIST2H4B; HIST1H4E;	High	High	High	High	High	NF	High	High	High	High	High	NF

					HIST1H4I; HIST1H4B; HIST2H4A; HIST1H4K; HIST1H4L												
Q9BZZ5-4	17.15	11	5	8539	API5	NF	NF	High	NF	NF	High	NF	High	High	NF	NF	NF
Q8N766-1	17.058	5	4	23065	EMC1	NF	High	High	NF	NF	NF	NF	High	NF	NF	NF	NF
P01861	17.002	23	6	3503	IGHG4	High	NF	NF	NF	High	NF	High	NF	High	High	High	NF
P61619	17.002	16	6	29927	SEC61A1	NF	High	High	High	NF	High	High	High	NF	NF	NF	NF
P62854	16.936	31	3	6231; 728937; 101929876	RPS26; RPS26P25; LOC101929876	NF	High	High	High	High	High	High	High	High	NF	High	High
Q5SRE5	16.919	3	5	23511	NUP188	NF	High	High	NF	NF	High	NF	High	NF	NF	NF	NF
P05455	16.82	13	5	6741	SSB	NF	High	High	High	NF	High	NF	High	High	NF	NF	NF
P55209	16.769	14	4	4673	NAP1L1	NF	High	High	High	NF	High	NF	High	NF	NF	NF	NF
P27695	16.743	16	4	328	APEX1	NF	High	High	NF	NF	NF	NF	High	NF	NF	NF	NF
P61981	16.657	17	3	7532	YWHAG	NF	High	High	NF	NF	NF	NF	High	NF	NF	NF	NF
P61026	16.643	23	2	10890	RAB10	NF	NF	High	NF	NF	High	NF	High	NF	NF	NF	NF
P05198	16.515	18	6	1965	EIF2S1	High	High	High	High	High	High	NF	High	High	NF	NF	NF
P36776	16.423	7	5	9361	LONP1	NF	High	High	High	NF	High	NF	High	NF	NF	NF	NF
P46459	16.419	7	5	4905	NSF	NF	High	High	High	NF	High	NF	High	NF	NF	NF	NF
P61224-1	16.252	27	5	5908	RAP1B	NF	NF	High	NF	NF	High	NF	High	NF	NF	NF	NF
P26639-2	16.244	8	6	6897	TARS	NF	High	High	High	NF	High	NF	High	NF	NF	NF	NF
Q3ZCQ8-2	16.214	9	3	92609	TIMM50	NF	High	High	NF	NF	High	NF	High	NF	NF	NF	NF
O00178	16.189	9	4	9567	GTPBP1	NF	NF	High	NF	NF	High	NF	High	NF	NF	NF	NF
Q08J23	16.186	11	7	54888	NSUN2	NF	High	High	High	High	High	High	High	NF	NF	NF	NF
Q9BWD1-2	16.143	17	4	39	ACAT2	NF	NF	High	NF	NF	High	NF	High	NF	NF	NF	NF
P30566	16.115	11	5	158	ADSL	NF	High	High	High	NF	High	NF	High	NF	NF	NF	NF
Q92973-1	16.097	5	3	3842	TNPO1	NF	NF	High	High	NF	High	NF	High	NF	NF	NF	NF
Q16795	16.054	14	4	4704	NDUFA9	NF	NF	High	NF	NF	NF	NF	High	NF	NF	NF	NF
O00203-1	16.009	4	4	8546	AP3B1	NF	NF	NF	High	NF	High	NF	High	NF	NF	NF	NF

O95347-1	15.994	5	5	10592	SMC2	NF	NF	NF	High	NF	High	NF	High	NF	NF	NF	NF
P40938	15.957	14	4	5983	RFC3	NF	NF	High	High	NF	NF	NF	High	NF	NF	NF	NF
O43615	15.927	15	6	10469	TIMM44	NF	High	High	NF	NF	High	NF	High	NF	NF	NF	NF
Q14690	15.922	3	6	22984	PDCD11	NF	NF	NF	NF	NF	High	NF	NF	NF	NF	NF	NF
P31948-2	15.889	10	6	10963	STIP1	NF	High	NF	High	NF	High	NF	High	NF	NF	NF	NF
P06753-2	15.804	23	4	7170	TPM3	NF	High	High	NF	NF	NF	NF	High	NF	NF	NF	NF
O95373	15.777	6	5	10527	IPO7	NF	High	High	High	NF	High	NF	High	High	NF	NF	NF
Q00341-1	15.776	4	5	3069	HDLBP	NF	High	High	NF	NF	High	NF	High	NF	NF	NF	NF
Q8IX01-1	15.729	6	4	10147	SUGP2	NF	High	High	NF	NF	High	NF	High	NF	NF	NF	NF
P43686	15.675	12	4	5704	PSMC4	NF	High	High	High	NF	High	NF	High	High	NF	NF	NF
P40429	15.598	29	6	23521	RPL13A	NF	High	High	High	NF	High	NF	High	NF	NF	NF	NF
Q9Y2W1	15.586	5	4	9967	THRAP3	NF	High	High	High	NF	High	NF	High	NF	NF	NF	NF
P50502	15.551	12	4	6767	ST13	NF	High	High	NF	NF	High	NF	High	NF	NF	NF	NF
P60953	15.484	26	3	998	CDC42	NF	High	High	NF	NF	NF	NF	High	NF	NF	NF	NF
O94905-1	15.455	13	4	11160	ERLIN2	NF	High	High	High	NF	High	High	High	NF	NF	NF	NF
O14617-5	15.385	4	3	8943	AP3D1	NF	High	High	High	NF	High	NF	High	NF	NF	NF	NF
P35241-5	15.382	9	1	5962	RDX	NF	NF	NF	NF	NF	NF	NF	High	NF	NF	NF	NF
P16435	15.305	9	5	5447	POR	NF	High	High	NF	NF	NF	NF	High	NF	NF	NF	NF
Q96S52	15.298	4	1	94005	PIGS	NF	NF	High	NF	NF	NF	NF	High	NF	NF	NF	NF
P62495	15.295	15	5	2107	ETF1	NF	NF	High	High	NF	High	NF	High	NF	NF	NF	NF
P62820	15.249	22	2	5861	RAB1A	NF	High	NF	NF	NF	High	NF	High	NF	NF	NF	NF
P14923	15.241	8	6	3728	JUP	High	High	High	High	NF	High	NF	High	High	High	NF	NF
P14324	15.237	12	4	2224	FDPS	NF	High	High	High	NF	High	NF	High	NF	NF	NF	NF
Q969V3	15.191	10	5	56926	NCLN	NF	High	High	NF	NF	NF	NF	High	NF	NF	NF	NF
Q8WVM8	15.178	6	2	23256	SCFD1	NF	High	High	NF	NF	NF	NF	High	NF	NF	NF	NF
Q9H0D6-1	15.054	6	4	22803	XRN2	NF	NF	High	NF	NF	High	NF	High	NF	NF	NF	NF
Q9BVI4	15.049	10	4	79050	NOC4L	NF	NF	High	High	NF	High	NF	High	NF	NF	NF	NF
Q5JPE7	15.036	5	5	283820	NOMO2	NF	NF	High	NF	NF	NF	NF	High	NF	NF	NF	NF
P18754-2	15.021	12	4	1104	RCC1	NF	High	High	NF	NF	High	NF	NF	NF	NF	NF	NF

Q96I99-1	14.981	13	5	8801	SUCLG2	NF	High	High	High	NF	High	NF	High	NF	NF	NF	NF
Q15637-5	14.944	7	4	7536	SF1	NF	High	High	High	NF	High	NF	High	NF	NF	NF	NF
O95299-2	14.881	11	4	4705	NDUFA10	NF	High	High	High	NF	High	NF	High	High	NF	NF	NF
O60264	14.786	5	5	8467	SMARCA5	NF	High	NF	NF	NF	High	NF	NF	NF	NF	NF	NF
Q9H0S4	14.722	7	2	51202	DDX47	NF	NF	High	NF	NF	High	NF	High	NF	NF	NF	NF
P62195-1	14.691	12	4	5705	PSMC5	NF	High	High	High	NF	High	NF	High	NF	NF	NF	NF
P07339	14.682	21	7	1509	CTSD	High	High	High	NF	NF	High	NF	High	High	NF	NF	NF
Q9BZE1	14.611	13	5	51253	MRPL37	NF	NF	High	High	NF	NF	NF	High	NF	NF	NF	NF
P07196	14.596	9	3	4747	NEFL	NF	High	High	High	NF	NF	NF	High	NF	NF	NF	NF
Q9UKF6	14.53	8	5	51692	CPSF3	NF	High	High	High	NF	High	NF	High	NF	NF	NF	NF
Q8NC51-1	14.476	9	3	26135	SERBP1	NF	High	NF	NF	NF	NF	NF	High	NF	NF	NF	NF
P52294	14.472	7	2	3836	KPNA1	NF	High	NF	NF	NF	High	NF	NF	NF	NF	NF	NF
P22087	14.446	13	3	2091	FBL	NF	NF	High	NF	NF	High	NF	NF	NF	NF	NF	NF
P13667	14.41	9	4	9601	PDIA4	NF	NF	High	NF	NF	High	NF	High	NF	NF	NF	NF
P28066-1	14.378	17	3	5686	PSMA5	NF	NF	High	NF	NF	NF	NF	High	NF	NF	NF	NF
Q5QNW6-2	14.364	38	5	440689	HIST2H2BF	High	High	High	High	High	NF	High	High	High	High	High	High
P54709	14.351	14	3	483	ATP1B3	NF	High	High	NF	NF	NF	NF	High	NF	NF	NF	NF
P46087-4	14.31	5	3	4839	NOP2	NF	High	NF	NF	NF	High	NF	High	NF	NF	NF	NF
Q99497	14.255	24	4	11315	PARK7	NF	NF	High	NF	NF	NF	NF	High	NF	NF	NF	NF
P35268	14.214	36	5	6146	RPL22	NF	High	High	High	NF	High	NF	High	NF	NF	NF	NF
P62847-4	14.175	13	3	6229	RPS24	NF	High	High	High	High	High	High	High	NF	NF	High	High
P23921	14.118	8	3	6240	RRM1	NF	NF	High	NF	NF	NF	NF	High	NF	NF	NF	NF
Q7L014	14.077	6	6	9879	DDX46	NF	NF	NF	High	NF	NF	NF	High	NF	NF	NF	NF
Q9NX63	14.075	18	4	54927	CHCHD3	NF	NF	High	High	NF	High	NF	NF	NF	NF	NF	NF
Q01650	14.015	8	3	8140	SLC7A5	NF	High	High	NF	NF	High	NF	High	NF	NF	NF	NF
Q9NWB6	13.982	14	5	55082	ARGLU1	NF	High	High	High	High	High	High	High	High	High	NF	NF
Q6L8Q7-1	13.926	8	4	201626	PDE12	NF	High	High	High	NF	High	NF	High	NF	NF	NF	NF
Q9Y5Q9	13.921	7	6	9330	GTF3C3	NF	NF	High	NF	NF	High	NF	High	NF	NF	NF	NF
Q15417	13.904	14	4	1266	CNN3	NF	High	High	NF	NF	NF	NF	High	NF	NF	NF	NF

P25786-2	13.887	16	3	5682	PSMA1	NF	High	High	NF	NF	NF	NF	High	NF	NF	NF	NF
P09211	13.883	17	2	2950	GSTP1	NF	High	High	NF	NF	High	NF	High	High	NF	NF	NF
P09960-1	13.859	10	5	4048	LTA4H	NF	High	NF	High	NF	High	NF	High	NF	NF	NF	NF
Q9UBE0-1	13.844	10	2	10055	SAE1	NF	NF	NF	NF	NF	High	NF	High	NF	NF	NF	NF
P49189	13.806	9	4	223	ALDH9A1	NF	High	High	NF	NF	High	NF	High	High	NF	NF	NF
P63151-2	13.801	8	3	5520	PPP2R2A	NF	High	High	High	NF	High	NF	High	NF	NF	NF	NF
Q53H12	13.773	11	3	55750	AGK	NF	High	High	High	NF	High	NF	High	High	NF	NF	NF
Q96CS3	13.738	12	3	23197	FAF2	NF	High	High	High	NF	High	NF	NF	NF	NF	NF	NF
Q96T37-1	13.649	5	4	64783	RBM15	NF	NF	High	NF	NF	High	NF	High	NF	NF	NF	NF
P47914	13.635	15	3	6159	RPL29	NF	High	High	High	High	High	High	High	High	High	High	NF
P31946	13.603	17	2	7529	YWHAB	NF	High	High	NF	NF	NF	NF	High	NF	NF	NF	NF
Q9UBM7	13.603	11	5	1717	DHCR7	NF	High	High	High	NF	High	NF	High	NF	NF	NF	NF
Q9Y4P3	13.524	9	3	26608	TBL2	NF	High	High	NF	NF	NF	NF	High	NF	NF	NF	NF
Q9NTK5-1	13.444	9	3	29789	OLA1	NF	High	High	NF	NF	High	NF	High	High	NF	NF	NF
Q96GQ7	13.434	7	5	55661	DDX27	NF	High	High	NF	NF	High	NF	NF	NF	NF	NF	NF
P35520-2	13.357	9	3	875; 102724560	CBS; LOC102724560; CBSL	NF	High	High	NF	NF	High	NF	NF	NF	NF	NF	NF
Q9Y6G9	13.266	10	4	51143	DYNC1LI1	NF	NF	NF	NF	NF	High	NF	High	NF	NF	NF	NF
O60832-1	13.241	8	3	1736	DKC1	NF	NF	NF	NF	NF	High	NF	NF	NF	NF	NF	NF
Q9NZ01-1	13.225	15	5	9524	TECR	NF	High	High	High	NF	High	NF	NF	NF	NF	NF	NF
O00232-1	13.16	13	5	5718	PSMD12	NF	High	High	NF	NF	NF	NF	High	NF	NF	NF	NF
Q10713	13.114	7	3	23203	PMPCA	NF	NF	High	NF	NF	NF	NF	NF	High	NF	NF	NF
P36871-1	13.104	8	3	5236	PGM1	NF	NF	NF	NF	NF	NF	NF	High	NF	NF	NF	NF
O75439	13.098	8	3	9512	PMPCB	NF	High	High	High	NF	NF	NF	High	NF	NF	NF	NF
Q9Y4W6	13.055	6	5	10939	AFG3L2	NF	High	High	High	NF	NF	NF	High	NF	NF	NF	NF
P55265-4	13.029	4	4	103	ADAR	NF	High	High	High	NF	High	NF	High	NF	NF	NF	NF
Q96I24-1	13.019	9	5	8939	FUBP3	NF	High	High	High	NF	NF	NF	High	NF	NF	NF	NF
O00159-1	13.016	5	4	4641	MYO1C	NF	NF	NF	High	NF	NF	NF	NF	NF	NF	NF	NF
Q96P70	12.999	5	3	55705	IPO9	NF	High	High	High	NF	High	NF	High	NF	NF	NF	NF

Q8WXF1	12.999	11	4	55269	PSPC1	NF	High	High	High	NF	High	NF	High	High	NF	NF	NF
Q14966-1	12.993	2	3	27332	ZNF638	NF	NF	High	NF	NF	NF	NF	NF	NF	NF	NF	NF
P01834	12.985	50	3	3514	IGKC	High	NF	NF	NF	High	NF	NF	NF	High	NF	High	NF
P61254	12.962	27	6	6154	RPL26	High	High	High	High	High	High	High	High	High	High	High	NF
Q7L576-1	12.876	3	3	23191	CYFIP1	NF	High	High	High	NF	High	NF	High	NF	NF	NF	NF
P20042	12.834	11	4	8894	EIF2S2	NF	NF	High	NF	NF	High	NF	High	NF	NF	NF	NF
A1L0T0	12.804	7	3	10994	ILVBL	NF	High	High	High	NF	High	NF	High	NF	NF	NF	NF
P61289-2	12.762	18	4	10197	PSME3	NF	High	High	NF	NF	NF	NF	High	NF	NF	NF	NF
O94813	12.675	3	4	9353	SLIT2	NF	NF	High	NF	High	High	NF	NF	High	NF	NF	NF
P07954	12.667	6	2	2271	FH	NF	NF	High	NF	NF	NF	NF	High	NF	NF	NF	NF
Q10570	12.665	3	5	29894	CPSF1	NF	High	High	High	NF	High	NF	NF	NF	NF	NF	NF
P13611	12.664	1	4	1462	VCAN	NF	NF	NF	NF	NF	NF	NF	NF	High	NF	NF	NF
P56945-6	12.623	5	4	9564	BCAR1	NF	NF	NF	High	NF	NF	High	NF	NF	NF	NF	NF
P21127-1	12.62	6	5	984	CDK11B	NF	High	NF	High	NF	NF	NF	High	NF	NF	NF	NF
P82933	12.618	11	4	64965	MRPS9	NF	NF	High	NF	NF	High	NF	High	NF	NF	NF	NF
P37837	12.614	13	4	6888	TALDO1	NF	High	High	NF	NF	NF	NF	High	NF	NF	NF	NF
Q15181	12.599	14	2	5464	PPA1	NF	High	High	High	NF	NF	NF	High	NF	NF	NF	NF
Q96HS1-1	12.553	17	5	192111	PGAM5	NF	High	High	High	NF	High	High	High	NF	NF	NF	NF
Q9UHD8-1	12.527	8	4	10801	SEPT9	NF	NF	High	NF	NF	NF	NF	High	NF	NF	NF	NF
P52209	12.507	8	3	5226	PGD	NF	NF	High	NF	NF	High	NF	High	NF	NF	NF	NF
P19367-3	12.495	5	3	3098	HK1	NF	High	High	High	NF	High	NF	NF	NF	NF	NF	NF
P61077-3	12.492	23	2	7323	UBE2D3	NF	NF	High	NF	NF	NF	NF	High	NF	NF	NF	NF
P51116	12.442	5	2	9513	FXR2	NF	High	NF	High	NF	High	NF	High	NF	NF	NF	NF
Q5T749	12.417	8	5	448834	KPRP	NF	High	High	High	High	High	NF	NF	High	High	High	NF
Q9BZI7-1	12.401	8	4	65109	UPF3B	NF	NF	High	High	NF	High	NF	High	NF	NF	NF	NF
Q1KMD3	12.388	7	5	221092	HNRNPUL2	NF	High	High	NF	NF	High	NF	High	NF	NF	NF	NF
Q14160-3	12.312	4	4	23513	SCRIB	NF	NF	High	High	NF	NF	NF	NF	NF	NF	NF	NF
Q9UJZ1	12.305	12	2	30968	STOML2	NF	High	High	High	NF	High	NF	High	NF	NF	NF	NF
Q9BZE4	12.287	7	4	23560	GTPBP4	NF	NF	NF	NF	NF	High	NF	NF	NF	NF	NF	NF

Q9BWF3-1	12.221	9	3	5936	RBM4	NF	High	High	High	NF	NF	NF	High	NF	NF	NF	NF
O94925-1	12.136	5	2	2744	GLS	NF	NF	High	NF	NF	NF	NF	NF	NF	NF	NF	NF
P23284	12.113	19	4	5479	PPIB	NF	High	High	NF	NF	NF	NF	High	NF	NF	NF	NF
Q9Y4W2	12.092	5	3	81887	LAS1L	NF	NF	High	NF	NF	NF	NF	NF	NF	NF	NF	NF
P07305	12.072	16	3	3005	H1F0	NF	High	High	High	NF	High	High	High	NF	NF	NF	NF
Q96C36	12.031	19	3	29920	PYCR2	NF	NF	High	NF	NF	NF	NF	High	NF	NF	NF	NF
Q13084	12.02	20	3	10573	MRPL28	NF	NF	High	NF	NF	NF	NF	High	NF	NF	NF	NF
O75874	11.99	8	2	3417	IDH1	NF	NF	NF	NF	NF	NF	NF	High	NF	NF	NF	NF
Q9BYD6	11.927	11	2	65008	MRPL1	NF	High	High	NF	NF	NF	NF	High	NF	NF	NF	NF
O60684	11.896	7	2	23633	KPNA6	NF	High	NF	NF	NF	High	NF	NF	NF	NF	NF	NF
Q9Y276	11.87	5	1	617	BCS1L	NF	NF	High	NF	NF	NF	NF	NF	NF	NF	NF	NF
Q16850-1	11.763	10	3	1595	CYP51A1	NF	NF	High	NF	NF	NF	NF	High	NF	NF	NF	NF
P61160-2	11.729	10	3	10097	ACTR2	NF	NF	High	NF	NF	High	NF	High	NF	NF	NF	NF
Q8NBS9-1	11.663	6	2	81567	TXNDC5	NF	NF	NF	NF	NF	NF	NF	High	NF	NF	NF	NF
P60900	11.653	14	3	5687	PSMA6	NF	High	High	NF	NF	High	NF	High	NF	NF	NF	NF
Q53GQ0	11.589	15	3	51144	HSD17B12	NF	High	High	High	NF	High	NF	High	High	NF	NF	NF
P26196	11.567	10	3	1656	DDX6	NF	NF	High	High	NF	NF	NF	High	NF	NF	NF	NF
Q99575	11.563	6	6	10940	POP1	NF	NF	NF	NF	High	High	NF	High	NF	NF	NF	NF
P61353	11.549	36	4	6155	RPL27	High	High	High	High	High	High	NF	High	NF	NF	NF	NF
P35658-5	11.547	2	2	8021	NUP214	NF	NF	High	NF	NF	NF	NF	High	NF	NF	NF	NF
P02545	11.514	5	2	4000	LMNA	NF	NF	High	NF	NF	NF	NF	NF	NF	NF	NF	NF
P51571	11.502	17	2	6748	SSR4	NF	High	High	NF	NF	High	NF	High	NF	NF	NF	NF
Q92688	11.479	18	3	10541	ANP32B	NF	NF	High	NF	NF	NF	NF	NF	NF	NF	NF	NF
Q04917	11.473	19	2	7533	YWHAH	NF	High	NF	NF	NF	NF	NF	High	NF	NF	NF	NF
Q8IYB3	11.465	6	2	10250	SRRM1	NF	NF	High	NF	NF	NF	NF	NF	NF	NF	NF	NF
Q9NRN7	11.461	13	3	60496	AASDHPPT	NF	NF	High	NF	NF	NF	NF	High	NF	NF	NF	NF
Q6YN16	11.445	10	3	84263	HSDL2	NF	High	High	NF	NF	NF	NF	High	NF	NF	NF	NF
P63241-2	11.44	26	3	1984	EIF5A	NF	NF	High	NF	NF	High	NF	NF	NF	NF	NF	NF
P55084	11.404	9	4	3032	HADHB	NF	High	High	NF	NF	High	NF	NF	High	NF	NF	NF

P42677	11.352	39	3	6232	RPS27	NF	High	High	High	High	High	High	High	High	NF	NF	NF
Q9H2U1	11.335	5	4	170506	DHX36	NF	High	High	NF	NF	High	NF	High	NF	NF	NF	NF
O75475-1	11.315	7	3	11168	PSIP1	NF	NF	NF	NF	NF	High	NF	NF	NF	NF	NF	NF
Q9BQ67	11.27	9	3	83743	GRWD1	NF	NF	NF	NF	NF	High	NF	High	NF	NF	NF	NF
Q14318-2	11.21	7	2	23770	FKBP8	NF	NF	High	NF	NF	NF	NF	High	NF	NF	NF	NF
P20020-3	11.161	4	4	490	ATP2B1	NF	High	High	High	NF	High	NF	High	High	NF	NF	NF
P08574	11.122	9	2	1537	CYC1	NF	NF	High	NF	NF	NF	NF	NF	NF	NF	NF	NF
Q01844-5	11.118	4	2	2130	EWSR1	NF	High	High	High	NF	High	High	High	NF	NF	NF	NF
O43747-2	11.074	6	5	164	AP1G1	NF	NF	High	NF	NF	High	NF	High	NF	NF	NF	NF
Q9Y520-7	11.055	1	4	23215	PRRC2C	NF	NF	NF	NF	NF	NF	High	High	NF	NF	NF	NF
P48735	10.968	9	3	3418	IDH2	NF	High	High	High	NF	NF	NF	High	NF	NF	NF	NF
P57088	10.964	11	3	55161	TMEM33	NF	High	High	High	NF	High	NF	High	NF	NF	NF	NF
P26640	10.789	3	3	7407; 57176	VAR5; VAR52	NF	High	High	NF	NF	NF	NF	NF	NF	NF	NF	NF
P61513	10.786	28	2	6168	RPL37A	NF	High	High	High	High	NF	High	High	High	NF	NF	NF
O75400	10.717	3	3	55660	PRPF40A	NF	High	High	High	NF	High	NF	High	NF	NF	NF	NF
P81605-2	10.705	21	3	117159	DCD	High	High	High	High	NF	High	NF	High	High	NF	High	NF
P05091	10.695	6	2	217	ALDH2	NF	High	High	NF	NF	NF	NF	High	NF	NF	NF	NF
P61586	10.631	18	2	387	RHOA	NF	NF	High	NF	NF	NF	NF	High	NF	NF	NF	NF
P53007	10.628	13	4	6576	SLC25A1	NF	NF	High	High	NF	High	NF	High	NF	NF	NF	NF
A5YKK6	10.596	2	5	23019	CNOT1	NF	High	NF	High	NF	NF	NF	High	NF	NF	NF	NF
P28838	10.571	6	3	51056	LAP3	NF	High	High	NF	NF	NF	NF	High	NF	NF	NF	NF
Q14126	10.497	3	4	1829	DSG2	NF	NF	NF	High	NF	NF	NF	NF	NF	NF	NF	NF
Q8WWY3	10.457	7	3	26121	PRPF31	NF	High	High	High	NF	High	NF	High	NF	NF	NF	NF
Q7L0Y3	10.424	9	4	54931	TRMT10C	NF	High	High	NF	NF	High	NF	High	NF	NF	NF	NF
P57678	10.387	3	3	50628	GEMIN4	NF	NF	NF	High	NF	High	NF	High	NF	NF	NF	NF
Q15031	10.379	4	4	23395	LARS2	NF	NF	High	NF	NF	NF	NF	High	NF	NF	NF	NF
Q5TFE4	10.372	12	3	221294	NT5DC1	NF	High	High	High	NF	High	NF	High	NF	NF	NF	NF
P08621-1	10.319	9	4	6625	SNRNP70	NF	High	High	NF	High	High	NF	High	High	High	NF	NF
Q8NI27-1	10.275	3	4	57187	THOC2	NF	High	High	NF	NF	High	NF	NF	NF	NF	NF	NF

Q9BU76-1	10.26	14	3	79169	C1orf35	NF	High	High	High	NF	High	NF	High	NF	NF	NF	NF
Q9UJX3-1	10.251	5	2	51434	ANAPC7	NF	NF	High	NF	NF	High	NF	High	NF	NF	NF	NF
Q9Y5B9	10.229	3	3	11198	SUPT16H	NF	High	High	NF	NF	High	NF	High	NF	NF	NF	NF
Q8WUM0	10.223	5	5	55746	NUP133	NF	High	High	High	NF	High	NF	NF	NF	NF	NF	NF
P28072	10.206	13	3	5694	PSMB6	NF	High	High	NF	NF	High	NF	High	NF	NF	NF	NF
O14979-1	10.182	10	2	9987	HNRNPDL; HNRPDL	NF	NF	High	NF	NF	High	NF	High	NF	NF	NF	NF
O00186	10.174	6	3	6814	STXBP3	NF	NF	High	NF	NF	NF	NF	NF	NF	NF	NF	NF
P27694	10.133	13	5	6117	RPA1	NF	NF	High	High	NF	NF	NF	High	NF	NF	NF	NF
Q92769	10.131	8	3	3066	HDAC2	NF	High	High	NF	NF	High	NF	High	NF	NF	NF	NF
P13861	10.122	9	3	5576	PRKAR2A	NF	High	High	High	NF	High	NF	High	NF	NF	NF	NF
O75396	10.065	16	3	9554	SEC22B	NF	NF	High	NF	NF	NF	NF	High	NF	NF	NF	NF
P60660	10.046	21	3	4637	MYL6	NF	High	High	High	NF	High	NF	High	NF	NF	NF	NF
O00231-2	10.041	8	3	5717	PSMD11	NF	High	High	NF	NF	NF	NF	High	NF	NF	NF	NF
Q96FW1	10.035	9	2	55611	OTUB1	NF	High	High	High	NF	High	NF	High	NF	NF	NF	NF
E9PAV3	10.006	1	2	4666	NACA	NF	NF	High	High	NF	NF	NF	High	NF	NF	NF	NF
Q04760-1	10.005	18	3	2739	GLO1	NF	High	High	NF	NF	NF	NF	High	High	NF	NF	NF
P23381	9.992	9	3	7453	WARS	NF	NF	NF	NF	NF	High	NF	High	NF	NF	NF	NF
P04908	9.978	22	2	8335; 3012	HIST1H2AB; HIST1H2AE	High	High	High	High	High	NF	High	High	High	High	High	High
Q5SY16	9.978	6	3	79707	NOL9	NF	NF	High	NF	NF	High	NF	NF	NF	NF	NF	NF
Q07666	9.978	6	2	10657	KHDRBS1	NF	High	High	NF	NF	NF	NF	High	NF	NF	NF	NF
Q9P2I0	9.954	4	3	53981	CPSF2	NF	High	High	High	NF	High	NF	High	NF	NF	NF	NF
Q14203	9.922	2	3	1639	DCTN1	NF	NF	High	NF	NF	High	NF	High	NF	NF	NF	NF
Q5T3I0-3	9.89	6	2	54865	GPATCH4	NF	NF	High	NF	NF	High	NF	High	NF	NF	NF	NF
O00629	9.88	7	2	3840	KPNA4	NF	NF	High	NF	NF	High	NF	High	NF	NF	NF	NF
P40925-3	9.875	11	3	4190	MDH1	NF	High	High	NF	NF	NF	NF	High	NF	NF	NF	NF
P10155-1	9.871	7	4	6738	TROVE2	NF	NF	NF	High	NF	High	NF	High	NF	NF	NF	NF
P14314	9.864	8	4	5589	PRKCSH	NF	NF	High	NF	NF	NF	NF	High	NF	NF	NF	NF
Q08170	9.836	7	1	6429	SRSF4	NF	High	High	High	NF	High	NF	High	NF	NF	NF	NF

Q5JTV8-3	9.829	7	3	26092	TOR1AIP1	NF	High	High	NF	NF	NF	NF	High	NF	NF	NF	NF
P38606	9.803	7	3	523	ATP6V1A	NF	NF	High	NF	NF	NF	NF	High	NF	NF	High	NF
Q8N1G4	9.788	8	4	57470	LRRC47	NF	NF	High	NF	NF	NF	NF	High	NF	NF	NF	NF
P52701	9.727	2	3	2956	MSH6	NF	High	High	High	NF	High	NF	High	NF	NF	NF	NF
O94874-1	9.681	5	4	23376	UFL1	NF	High	High	NF	NF	NF	NF	High	NF	NF	NF	NF
Q7Z478	9.68	3	2	54505	DHX29	NF	High	High	High	NF	NF	NF	High	NF	NF	NF	NF
P60228	9.666	9	4	3646	EIF3E	NF	NF	High	High	NF	High	NF	High	NF	NF	NF	NF
Q9HB71	9.591	13	3	27101	CACYBP	NF	NF	NF	NF	NF	High	NF	High	NF	NF	NF	NF
P43246-1	9.577	5	4	4436	MSH2	NF	High	High	High	NF	High	NF	High	NF	NF	NF	NF
Q9P2M7-1	9.565	3	3	57530	CGN	NF	NF	NF	High	NF	NF	NF	NF	NF	NF	NF	NF
P51398-1	9.538	8	2	7818	DAP3	NF	High	High	NF	NF	NF	NF	High	NF	NF	NF	NF
P25789	9.496	11	4	5685	PSMA4	NF	High	High	High	NF	High	NF	High	NF	NF	NF	NF
P08240-1	9.492	7	4	6734	SRPR; SRPRA	NF	High	High	High	NF	NF	NF	High	NF	NF	NF	NF
Q9UHI6	9.469	3	2	11218	DDX20	NF	High	NF	High	NF	High	NF	NF	NF	NF	NF	NF
Q9NP92	9.449	7	2	10884	MRPS30	NF	High	High	NF	NF	NF	NF	NF	NF	NF	NF	NF
Q9Y5A9-1	9.368	5	3	51441	YTHDF2	NF	High	High	High	NF	High	NF	High	NF	NF	NF	NF
P31153	9.361	7	2	4144	MAT2A	NF	NF	High	NF	NF	High	NF	High	NF	NF	NF	NF
Q5D862	9.352	1	2	388698	FLG2	High	High	NF	High	High	High	NF	NF	High	High	High	NF
A0FGR8-2	9.314	5	3	57488	ESYT2	NF	NF	High	NF	NF	High	NF	High	NF	NF	NF	NF
O75494-1	9.254	11	2	10772	SRSF10; LOC100996657	NF	NF	High	NF	NF	High	NF	NF	NF	NF	NF	NF
Q9UI10-2	9.247	9	3	8890	EIF2B4	NF	NF	High	NF	NF	High	NF	High	NF	NF	NF	NF
P02765	9.237	5	3	197	AHSG	High	NF	NF	NF	High	NF	NF	NF	High	High	High	NF
Q71RC2-4	9.167	4	2	113251	LARP4	NF	High	NF	NF	NF	NF	NF	High	NF	NF	NF	NF
Q96HE7	9.148	5	2	30001	ERO1L; ERO1A	NF	NF	High	NF	NF	NF	NF	High	NF	NF	NF	NF
P49591	9.138	4	2	6301	SARS	NF	NF	NF	NF	NF	High	NF	High	NF	NF	NF	NF
Q9Y2X3	9.128	7	3	51602	NOP58	NF	NF	High	NF	NF	High	NF	NF	NF	NF	NF	NF
P13995	9.091	9	3	10797	MTHFD2	NF	High	High	NF	NF	High	NF	High	NF	NF	NF	NF
O15269	9.091	5	2	10558	SPTLC1	NF	NF	High	High	NF	NF	NF	High	NF	NF	NF	NF
Q9NX20	9.048	11	3	54948	MRPL16	NF	High	High	High	NF	High	NF	NF	NF	NF	NF	NF

Q14683	9.046	3	3	8243	SMC1A	NF	High	NF	High	NF	High	NF	High	NF	NF	NF	NF
P52907	9.029	9	1	829	CAPZA1	NF	NF	NF	NF	NF	NF	NF	High	NF	NF	NF	NF
Q01081	9.023	11	2	7307; 102724594	U2AF1; LOC102724594; U2AF1L5	NF	High	High	High	NF	High	NF	High	NF	NF	NF	NF
P04637	8.986	8	3	7157	TP53	NF	NF	High	High	NF	NF	NF	High	NF	NF	NF	NF
Q12996-1	8.968	4	2	1479	CSTF3	NF	NF	High	NF	NF	NF	NF	NF	NF	NF	NF	NF
Q8NF37	8.945	5	2	79888	LPCAT1	NF	High	High	High	NF	High	NF	High	NF	NF	NF	NF
O00264	8.905	16	2	10857	PGRMC1	NF	High	High	NF	NF	NF	NF	High	NF	NF	NF	NF
Q15020	8.899	4	5	9733	SART3	NF	NF	High	NF	NF	High	NF	High	NF	NF	NF	NF
Q9Y2J2	8.871	2	2	23136	EPB41L3	NF	NF	High	High	NF	NF	NF	High	NF	NF	NF	NF
Q9H936	8.864	11	3	79751	SLC25A22	NF	NF	High	High	NF	NF	NF	High	NF	NF	NF	NF
Q12849	8.835	9	3	2926	GRSF1	NF	High	High	NF	NF	High	NF	High	NF	NF	NF	NF
P51148-2	8.834	10	2	5878	RAB5C	NF	High	High	NF	NF	NF	NF	High	NF	NF	NF	NF
Q13595-1	8.825	8	2	29896	TRA2A	NF	NF	High	NF	NF	High	NF	High	NF	NF	NF	NF
P50213-1	8.816	5	2	3419	IDH3A	NF	NF	High	NF	NF	High	NF	High	NF	NF	NF	NF
P56182	8.777	5	2	8568	RRP1	NF	High	High	High	NF	High	NF	High	NF	NF	NF	NF
P62191	8.748	8	2	5700	PSMC1	NF	High	NF	High	NF	High	NF	High	NF	NF	NF	NF
Q49A26-1	8.74	6	2	84656	GLYR1	NF	NF	High	NF	NF	High	NF	NF	NF	NF	NF	NF
Q01518-1	8.709	9	3	10487	CAP1	NF	NF	High	NF	NF	NF	NF	High	NF	NF	NF	NF
Q12789-2	8.688	2	3	2975	GTF3C1	NF	NF	High	High	NF	NF	NF	NF	NF	NF	NF	NF
P61019-1	8.679	12	2	5862	RAB2A	NF	NF	High	NF	NF	NF	NF	NF	NF	NF	NF	NF
Q13243-1	8.673	9	1	6430	SRSF5	NF	NF	High	NF	NF	NF	NF	NF	NF	NF	NF	NF
P78417	8.671	17	4	9446	GSTO1	NF	NF	High	NF	NF	NF	NF	High	NF	NF	NF	NF
P35250-1	8.658	8	2	5982	RFC2	NF	NF	High	NF	NF	NF	NF	High	NF	NF	NF	NF
P68036-3	8.632	16	2	7332	UBE2L3	NF	NF	High	High	NF	NF	NF	High	NF	NF	NF	NF
Q96GA3	8.626	7	2	84946	LTV1	NF	NF	High	High	NF	High	NF	NF	NF	NF	NF	NF
P36915-1	8.585	9	3	2794	GNL1	NF	High	NF	High	NF	NF	NF	High	NF	NF	NF	NF
P35659-1	8.575	8	3	7913	DEK	NF	High	High	NF	NF	NF	NF	High	NF	NF	NF	NF
P63000-2	8.527	14	2	5879	RAC1	NF	High	High	High	NF	NF	NF	High	NF	NF	NF	NF

Q9NWU5	8.517	16	3	29093	MRPL22	NF	High	High	High	NF	NF	NF	High	NF	NF	NF	NF
Q14562	8.511	5	3	1659	DHX8	NF	NF	High	High	High	NF	NF	NF	NF	NF	NF	NF
O00116	8.491	5	2	8540	AGPS	NF	NF	High	NF	NF	NF	NF	High	NF	NF	NF	NF
O43776	8.482	5	4	4677	NARS	NF	High	NF	High	NF	High	NF	High	NF	NF	NF	NF
O60841	8.453	4	4	9669	EIF5B	NF	NF	High	NF	NF	High	NF	High	NF	NF	NF	NF
Q15021	8.42	3	3	9918	NCAPD2	NF	NF	NF	High	NF	NF	NF	High	NF	NF	NF	NF
P39019	8.389	26	4	6223	RPS19	NF	High	High	High	NF	High	NF	High	High	NF	NF	NF
Q9BYG3	8.382	8	2	84365	MKI67IP; NIFK	NF	High	High	NF	NF	NF	High	High	NF	NF	NF	NF
Q9NQC3	8.372	2	2	57142	RTN4	NF	NF	High	NF	NF	NF	NF	High	NF	NF	NF	NF
P09972	8.344	16	1	230	ALDOC	NF	NF	NF	NF	NF	NF	NF	High	NF	NF	NF	NF
P49419	8.318	5	2	501	ALDH7A1	NF	NF	High	NF	NF	NF	NF	High	NF	NF	NF	NF
O14802	8.305	3	3	11128	POLR3A	NF	High	NF	NF	NF	High	NF	High	NF	NF	NF	NF
Q8N1N4	8.298	4	1	196374	KRT78	NF	High	NF	NF	NF	NF	NF	NF	NF	NF	NF	NF
Q92974	8.292	3	2	9181	ARHGEF2	NF	High	High	NF	NF	NF	NF	NF	NF	NF	NF	NF
O00429-6	8.26	7	2	10059	DNM1L	NF	High	NF	NF	NF	NF	NF	High	NF	NF	NF	NF
Q969N2	8.234	4	2	51604	PIGT	NF	NF	High	NF	NF	NF	NF	NF	NF	NF	NF	NF
P37802-2	8.23	10	2	8407	TAGLN2	NF	NF	High	NF	NF	NF	NF	High	NF	NF	NF	NF
Q8TAA3-1	8.216	10	2	143471	PSMA8	NF	NF	High	NF	NF	NF	NF	High	NF	NF	NF	NF
O00299	8.207	12	3	1192	CLIC1	NF	High	NF	NF	NF	NF	NF	High	NF	NF	NF	NF
Q8IZ83	8.192	4	3	126133	ALDH16A1	NF	NF	High	NF	NF	NF	NF	High	NF	NF	NF	NF
Q96QK1	8.182	4	3	55737	VPS35	NF	High	High	High	NF	High	NF	High	NF	NF	NF	NF
Q9NZB2-6	8.17	5	4	23196	FAM120A	NF	NF	NF	NF	NF	High	NF	High	NF	NF	NF	NF
Q08945	8.167	7	4	6749	SSRP1	NF	NF	High	NF	NF	High	NF	High	High	NF	NF	NF
P51610-4	8.146	1	2	3054	HCFC1	NF	NF	High	NF	NF	NF	NF	NF	NF	NF	NF	NF
Q15738	8.131	9	2	50814	NSDHL	NF	High	High	NF	NF	NF	NF	NF	NF	NF	NF	NF
P21912	8.12	8	2	6390	SDHB	NF	High	High	NF	NF	NF	NF	NF	NF	NF	NF	NF
P40937-1	8.095	11	3	5985	RFC5	NF	NF	High	High	NF	High	NF	NF	NF	NF	NF	NF
Q13573	8.037	6	3	22938	SNW1	NF	NF	NF	NF	NF	High	NF	High	NF	NF	NF	NF
P35221-2	7.978	4	3	1495	CTNNA1	NF	NF	NF	High	NF	NF	NF	High	NF	NF	NF	NF

P07741-1	7.975	13	2	353	APRT	NF	High	High	NF	NF	NF	NF	High	NF	NF	NF	NF
O15294	7.941	2	1	8473	OGT	NF	NF	High	NF	NF	NF	NF	High	NF	NF	NF	NF
Q9BW72	7.933	24	1	192286	HIGD2A	NF	NF	High	NF	NF	NF	NF	NF	NF	NF	NF	NF
Q5T8P6	7.915	3	2	64062	RBM26	NF	NF	High	High	NF	NF	NF	NF	NF	NF	NF	NF
Q53EL6-1	7.907	6	2	27250	PDCD4	NF	NF	NF	High	NF	NF	High	NF	NF	NF	NF	NF
Q86X55	7.886	4	2	10498	CARM1	NF	NF	NF	NF	NF	High	NF	High	NF	NF	NF	NF
Q8IWX8	7.874	2	2	10523	CHERP	NF	NF	High	NF	NF	High	NF	NF	NF	NF	NF	NF
P78344-1	7.85	3	3	1982	EIF4G2	NF	High	High	High	NF	NF	NF	High	NF	NF	NF	NF
P05109	7.801	31	3	6279	S100A8	NF	High	High	High	High	High	NF	High	NF	NF	NF	NF
Q13868	7.8	8	2	23404	EXOSC2	NF	High	High	NF	NF	NF	NF	High	NF	NF	NF	NF
Q9NQ55-3	7.723	5	2	692312; 56342	PPAN-P2RY11; PPAN	NF	NF	High	NF	NF	High	NF	NF	NF	NF	NF	NF
Q6PD62	7.721	2	2	9646	CTR9	NF	NF	High	NF	NF	NF	NF	NF	NF	NF	NF	NF
P83881	7.715	21	2	6173	RPL36A	High	High	High	High	High	High	High	High	High	NF	High	NF
Q96DV4	7.7	7	3	64978	MRPL38	NF	High	High	NF	NF	NF	NF	NF	NF	NF	NF	NF
Q92552-2	7.668	8	4	23107	MRPS27	NF	NF	High	High	NF	High	NF	High	NF	NF	NF	NF
Q969Y2-2	7.654	4	1	84705	GTPBP3	NF	NF	High	NF	NF	NF	NF	NF	NF	NF	NF	NF
Q8WUQ7-2	7.626	3	2	58509	CACTIN	NF	NF	NF	High	NF	NF	NF	NF	NF	NF	NF	NF
Q9UM00-1	7.601	12	2	54499	TMCO1	NF	High	High	NF	NF	High	NF	NF	NF	NF	NF	NF
O14828	7.601	8	2	10067	SCAMP3	NF	NF	High	NF	NF	NF	NF	High	NF	NF	NF	NF
Q7Z6E9	7.593	1	2	5930	RBBP6	NF	NF	High	NF	NF	High	NF	NF	NF	NF	NF	NF
Q9H1I8-1	7.581	5	2	84164	ASCC2	NF	High	High	NF	NF	NF	NF	NF	NF	NF	NF	NF
Q9H3U1	7.557	3	3	55898	UNC45A	NF	NF	High	NF	NF	High	NF	High	NF	NF	NF	NF
Q96T76-8	7.551	4	3	64210	MMS19	NF	NF	NF	NF	NF	High	NF	High	NF	NF	NF	NF
Q9BV20-1	7.549	6	2	84245	MRI1	NF	High	High	NF	NF	High	NF	High	NF	NF	NF	NF
Q13616	7.531	5	4	8454	CUL1	NF	High	High	High	NF	High	NF	High	NF	NF	NF	NF
P17980	7.531	7	2	5702	PSMC3	NF	High	High	NF	NF	NF	NF	NF	NF	NF	NF	NF
P61106	7.53	9	1	51552	RAB14	NF	NF	High	NF	NF	NF	NF	High	NF	NF	NF	NF
P17655-1	7.493	4	2	824	CAPN2	NF	NF	NF	NF	NF	High	NF	NF	NF	NF	NF	NF

P62873	7.471	7	2	2782	GNB1	NF	NF	High	NF	NF	NF	NF	High	NF	NF	NF	NF
Q96GD0	7.462	8	2	57026	PDXP	NF	High	NF	High	NF	High	NF	High	NF	NF	NF	NF
P19784	7.42	11	3	1459	CSNK2A2	NF	NF	High	NF	NF	NF	NF	High	NF	NF	NF	NF
Q12788	7.406	5	2	10607	TBL3	NF	High	High	High	NF	NF	NF	NF	NF	NF	NF	NF
Q9H3N1	7.378	7	2	81542	TMX1	NF	High	High	NF	NF	NF	NF	High	NF	NF	NF	NF
O75955	7.363	5	2	10211	FLOT1	NF	NF	NF	High	NF	NF	NF	High	NF	NF	NF	NF
Q09028	7.322	6	1	5928	RBBP4	NF	NF	High	NF	NF	High	NF	High	NF	NF	NF	NF
P10768	7.316	9	2	2098	ESD	NF	High	High	NF	NF	NF	NF	High	NF	NF	NF	NF
Q9BQA1	7.309	6	2	79084	WDR77	NF	High	NF	NF	NF	High	NF	NF	NF	NF	NF	NF
Q6PI48	7.267	5	3	55157	DARS2	NF	NF	High	NF	NF	High	NF	NF	NF	NF	NF	NF
O75083	7.264	4	2	9948	WDR1	NF	High	NF	NF	NF	NF	NF	High	NF	NF	NF	NF
Q6PJT7-1	7.261	3	2	79882	ZC3H14	NF	High	High	NF	NF	NF	NF	NF	NF	NF	NF	NF
Q8NFW8	7.26	6	2	55907	CMAS	NF	High	High	High	NF	High	High	High	NF	NF	NF	NF
P09429	7.242	13	2	3146	HMGB1	NF	NF	High	NF	NF	NF	NF	High	NF	NF	NF	NF
P18583-9	7.201	1	3	6651	SON	NF	NF	High	NF	NF	NF	NF	High	NF	NF	NF	NF
Q9H845	7.179	5	3	28976	ACAD9	NF	NF	High	NF	NF	NF	NF	High	NF	NF	NF	NF
Q5JXB2	7.162	14	2	389898	UBE2NL	NF	High	High	NF	NF	NF	NF	High	NF	NF	NF	NF
Q709F0-1	7.154	3	2	84129	ACAD11	NF	High	NF	High	NF	High	NF	High	NF	NF	NF	NF
O95197	7.151	2	2	10313	RTN3	NF	High	High	NF	NF	High	NF	High	NF	NF	NF	NF
Q8WVM0	7.145	7	2	51106	TFB1M	NF	High	High	High	NF	NF	NF	High	NF	NF	NF	NF
Q9Y696	7.141	6	1	25932	CLIC4	NF	NF	NF	NF	NF	NF	NF	High	NF	NF	NF	NF
O14776-1	7.068	2	3	10915	TCERG1	NF	NF	High	NF	NF	High	NF	High	NF	NF	NF	NF
Q6P2E9-1	7.066	3	3	23644	EDC4	NF	High	High	High	NF	High	NF	High	NF	NF	NF	NF
Q9NY93	7.016	3	1	54606	DDX56	NF	High	High	NF	NF	NF	NF	High	NF	NF	NF	NF
Q9H0U3	7.01	5	2	84061	MAGT1	NF	NF	High	NF	NF	High	NF	High	NF	NF	NF	NF
Q96KR1	7.002	3	3	51663	ZFR	NF	High	High	NF	NF	High	NF	NF	NF	NF	NF	NF
P62899-2	6.974	18	2	6160	RPL31	High	High	High	High	High	High	High	High	High	High	NF	NF
Q8IZL8	6.964	4	3	27043	PELP1	NF	NF	High	NF	NF	High	NF	High	NF	NF	NF	NF
Q9NX58	6.925	4	1	55646	LYAR	NF	NF	NF	NF	NF	High	NF	NF	NF	NF	NF	NF

P62861	6.919	20	3	2197	FAU	NF	High	High	High	NF	NF	High	High	High	NF	NF	NF
Q16658	6.886	6	2	6624	FSCN1	NF	NF	High	NF	NF	NF	NF	High	NF	NF	NF	NF
P53597	6.879	7	2	8802	SUCLG1	NF	High	High	NF	NF	NF	NF	NF	NF	NF	NF	NF
Q8WWM7-3	6.848	3	4	11273	ATXN2L	NF	NF	NF	High	NF	High	NF	High	NF	NF	NF	NF
Q15006	6.846	10	2	9694	EMC2	NF	High	High	NF	NF	NF	NF	High	NF	NF	NF	NF
P27144	6.817	10	2	205	AK4; LOC100507855	NF	NF	NF	NF	NF	NF	NF	High	NF	NF	NF	NF
P46783	6.817	15	2	6204	RPS10	NF	High	High	High	NF	High	NF	High	NF	NF	NF	NF
Q29RF7-1	6.81	2	2	23244	PDS5A	NF	High	NF	NF	NF	NF	NF	NF	NF	NF	NF	NF
P07384	6.785	4	3	823	CAPN1	NF	NF	NF	NF	NF	High	NF	High	NF	NF	NF	NF
P55036-1	6.764	7	2	5710	PSMD4	NF	NF	High	NF	NF	NF	NF	High	NF	NF	NF	NF
O00483	6.74	27	2	4697	NDUFA4	NF	High	High	NF	NF	NF	NF	High	NF	NF	NF	NF
Q9P2N5	6.726	4	3	54439	RBM27	NF	High	High	NF	NF	High	NF	High	NF	NF	NF	NF
O95782	6.715	5	2	160	AP2A1	NF	NF	High	High	NF	NF	NF	NF	NF	NF	NF	NF
Q9BW27	6.701	5	3	79902	NUP85	NF	NF	High	NF	NF	High	NF	NF	NF	NF	NF	NF
Q08554-1	6.701	2	1	1823	DSC1	NF	NF	NF	High	NF	NF	NF	NF	NF	NF	NF	NF
Q9NUL7	6.701	3	1	55794	DDX28	NF	High	High	NF	NF	NF	NF	NF	NF	NF	NF	NF
P21741	6.684	12	2	4192	MDK	High	NF	NF	High	High	High	High	NF	High	High	High	NF
Q8IX12	6.678	2	3	55749	CCAR1	NF	NF	High	NF	NF	NF	NF	High	NF	NF	NF	NF
E9PRG8	6.662	16	1	102288414	LOC102288414; C11orf98	NF	High	High	High	NF	High	High	High	NF	NF	NF	NF
Q13347	6.662	6	2	8668	EIF3I	NF	High	High	NF	NF	NF	NF	High	NF	NF	NF	NF
Q02218	6.655	3	2	4967	OGDH	NF	NF	High	NF	NF	NF	NF	NF	NF	NF	NF	NF
Q15477	6.643	1	1	6499	SKIV2L	NF	NF	NF	High	NF	NF	NF	High	NF	NF	NF	NF
P11310-2	6.635	4	1	34	ACADM	NF	NF	High	NF	NF	NF	NF	NF	NF	NF	NF	NF
Q86YZ3	6.584	1	2	388697	HRNR	NF	NF	NF	NF	High	NF	NF	NF	NF	High	NF	NF
P15170-3	6.553	5	3	2935	GSPT1	NF	High	High	High	NF	NF	NF	High	NF	NF	NF	NF
O43809	6.526	9	2	11051	NUDT21	NF	High	High	NF	NF	NF	NF	NF	NF	NF	NF	NF
P35251-1	6.513	2	2	5981	RFC1	NF	NF	High	NF	NF	High	NF	NF	NF	NF	NF	NF

[illegible]

P25788-1	6.073	12	3	5684	PSMA3	NF	High	NF	NF	NF	High	NF	High	NF	NF	NF	NF
Q13363-1	6.06	4	2	1487	CTBP1	NF	High	NF	High	NF	NF	NF	NF	NF	NF	NF	NF
Q7L1Q6-3	6.024	6	1	9689	BZW1	NF	NF	NF	NF	NF	NF	NF	High	NF	NF	NF	NF
Q9HDC9	6.02	5	2	57136	APMAP	NF	NF	High	NF	NF	NF	NF	High	NF	NF	NF	NF
Q9H7E9-2	6.017	7	1	65265	C8orf33	NF	NF	NF	NF	NF	High	NF	NF	NF	NF	NF	NF
Q13155	5.993	7	2	7965	AIMP2	NF	High	NF	NF	NF	NF	NF	High	NF	NF	NF	NF
O60783	5.974	12	1	63931	MRPS14	NF	NF	NF	NF	NF	NF	NF	High	NF	NF	NF	NF
Q9NYK5-2	5.965	9	3	54148	MRPL39	NF	High	High	NF	NF	NF	NF	High	NF	NF	NF	NF
P31937	5.959	9	2	11112	HIBADH	NF	NF	High	NF	NF	NF	NF	NF	NF	NF	NF	NF
Q9NQX3-2	5.947	2	1	10243	GPHN	NF	NF	NF	NF	NF	NF	NF	High	NF	NF	NF	NF
Q9BVK6	5.925	5	1	54732	TMED9	NF	High	High	NF	NF	NF	NF	High	NF	NF	NF	NF
P07477	5.901	8	1	5644	PRSS1	High	High	NF	NF	High	High	High	High	High	High	High	NF
O75821	5.882	6	2	8666	EIF3G	NF	NF	High	NF	NF	NF	NF	High	NF	NF	NF	NF
Q9UID3-1	5.878	3	1	738	VPS51	NF	NF	NF	NF	NF	High	NF	NF	NF	NF	NF	NF
A6NHR9-1	5.87	2	3	23347	SMCHD1	NF	NF	High	NF	NF	NF	NF	NF	NF	NF	NF	NF
Q9UHD1	5.864	5	1	26973	CHORDC1	NF	NF	High	NF	NF	High	NF	NF	NF	NF	NF	NF
Q9HCC0-1	5.846	4	1	64087	MCCC2	NF	NF	High	NF	NF	NF	NF	NF	NF	NF	NF	NF
Q7L2J0-1	5.835	3	1	56257	MEPCE	NF	NF	NF	NF	NF	High	NF	NF	NF	NF	NF	NF
Q9Y5J1	5.823	5	1	51096	UTP18	NF	NF	High	NF	NF	NF	NF	High	NF	NF	NF	NF
Q16576-2	5.805	6	1	5931	RBBP7	NF	NF	NF	NF	NF	High	NF	NF	NF	NF	NF	NF
P08631-1	5.803	3	1	3055	HCK	NF	NF	NF	High	NF	NF	NF	NF	NF	NF	NF	NF
P35249	5.785	8	3	5984	RFC4	NF	High	NF	NF	NF	NF	NF	High	NF	NF	NF	NF
P62318	5.774	15	2	6634	SNRPD3	NF	High	High	High	NF	High	NF	High	NF	NF	NF	NF
P30040-1	5.769	10	2	10961	ERP29	NF	NF	NF	NF	NF	NF	NF	High	NF	NF	NF	NF
Q8WU90	5.767	3	1	55854	ZC3H15	NF	NF	High	NF	NF	NF	NF	High	NF	NF	NF	NF
O95202-1	5.74	2	1	3954	LETM1	NF	High	High	NF	NF	NF	NF	High	NF	NF	NF	NF
O15144	5.735	7	2	10109	ARPC2	NF	NF	NF	NF	NF	NF	NF	High	NF	NF	NF	NF
Q9Y295	5.725	6	2	4733	DRG1	NF	High	High	NF	NF	High	NF	High	NF	NF	NF	NF
Q86VI3	5.704	3	2	128239	IQGAP3	NF	NF	High	High	NF	NF	NF	NF	NF	NF	NF	NF

[illegible]

[illegible]

Q96AC1-3	4.984	3	1	10979	FERMT2	NF	High	NF	NF	NF	High	NF	High	NF	NF	NF	NF
Q9UM54-3	4.981	2	2	4646	MYO6	NF	NF	NF	High	NF	NF	NF	NF	NF	NF	NF	NF
P51648-2	4.973	5	2	224	ALDH3A2	NF	NF	NF	NF	NF	NF	NF	High	NF	NF	NF	NF
O60716-1	4.952	3	3	1500	CTNND1	NF	High	High	High	NF	NF	NF	High	NF	NF	NF	NF
Q9Y2Z0-1	4.943	6	1	10910	SUGT1	NF	NF	High	NF	NF	NF	NF	NF	NF	NF	NF	NF
Q96CW1	4.937	6	3	1173	AP2M1	NF	High	NF	High	NF	High	NF	High	NF	NF	NF	NF
O43432-3	4.931	2	1	8672	EIF4G3	NF	NF	NF	NF	NF	NF	NF	High	NF	NF	NF	NF
Q9Y5Q8-3	4.928	4	2	9328	GTF3C5	NF	NF	NF	High	NF	NF	NF	High	NF	NF	NF	NF
Q9NTZ6	4.917	2	2	10137	RBM12	NF	High	High	High	NF	NF	NF	High	NF	NF	NF	NF
Q9GZL7	4.916	6	1	55759	WDR12	NF	NF	NF	NF	NF	NF	NF	High	NF	NF	NF	NF
Q6NUK1	4.91	3	1	29957	SLC25A24	NF	High	NF	NF	NF	High	NF	High	NF	NF	NF	NF
Q9Y3U8	4.904	18	2	25873	RPL36	NF	High	NF	High	NF	High	NF	High	High	NF	NF	NF
Q9UDY2-7	4.901	3	3	9414	TJP2	NF	High	NF	High	NF	NF	NF	NF	NF	NF	NF	NF
O15020	4.879	1	2	6712	SPTBN2	NF	NF	NF	High	NF	NF	NF	NF	High	High	NF	NF
P48651	4.87	5	2	9791	PTDSS1	NF	High	High	High	NF	NF	NF	NF	NF	NF	NF	NF
Q9H6R4-1	4.868	1	1	65083	NOL6	NF	NF	NF	NF	NF	High	NF	NF	NF	NF	NF	NF
Q9BXW7	4.859	6	2	27440	CECR5; HDHD5	NF	High	NF	High	NF	NF	NF	High	NF	NF	NF	NF
Q12907	4.856	3	1	10960	LMAN2	NF	NF	High	NF	NF	NF	NF	NF	NF	NF	NF	NF
Q9UGY1	4.853	13	1	79159	NOL12	NF	NF	NF	NF	NF	High	NF	NF	NF	NF	NF	NF
Q14331	4.836	5	1	2483	FRG1	NF	NF	NF	NF	NF	High	NF	High	NF	NF	NF	NF
P06730-2	4.825	6	1	1977	EIF4E	NF	High	NF	NF	NF	NF	NF	High	NF	NF	NF	NF
Q14151	4.82	2	2	9667	SAFB2	NF	NF	High	NF	NF	High	NF	High	NF	NF	NF	NF
Q13011	4.82	5	1	1891	ECH1	NF	NF	NF	NF	NF	NF	NF	High	NF	NF	NF	NF
Q8WYA6	4.813	3	1	56259	CTNBL1	NF	NF	High	NF	NF	NF	NF	NF	NF	NF	NF	NF
O43719	4.813	4	3	27336	HTATSF1	NF	NF	High	NF	NF	High	NF	NF	NF	NF	NF	NF
Q9H583	4.781	2	2	55127	HEATR1	NF	NF	High	NF	NF	NF	NF	High	NF	NF	NF	NF
Q5MIZ7-1	4.777	2	2	57223	SMEK2; PPP4R3B	NF	High	High	High	NF	High	NF	High	NF	NF	NF	NF
Q15388	4.754	13	2	9804	TOMM20	NF	High	High	High	NF	High	High	NF	NF	NF	NF	NF
P08572	4.752	1	2	1284	COL4A2	NF	NF	NF	NF	NF	NF	NF	NF	High	NF	NF	NF

P36551	4.742	4	2	1371	CPOX	NF	NF	High	NF	NF	NF	NF	NF	NF	NF	NF	NF
Q9Y388	4.74	7	2	51634	RBMX2	NF	NF	High	NF	NF	High	NF	High	NF	NF	NF	NF
P56134	4.731	14	1	9551	ATP5J2	NF	NF	High	NF	NF	High	NF	High	NF	NF	NF	NF
Q99426	4.724	5	1	1155	TBCB	NF	NF	NF	NF	NF	NF	NF	High	NF	NF	NF	NF
Q14254	4.717	5	2	2319	FLOT2	NF	NF	NF	High	NF	NF	NF	NF	NF	NF	NF	NF
Q15631-1	4.717	7	1	7247	TSN	NF	NF	High	NF	NF	NF	NF	NF	NF	NF	NF	NF
Q86UK7-1	4.704	1	1	90850	ZNF598	NF	NF	NF	NF	NF	NF	NF	High	NF	NF	NF	NF
Q9BT22	4.7	3	1	56052	ALG1	NF	NF	High	NF	NF	NF	NF	NF	NF	NF	NF	NF
Q9NRG9-1	4.668	6	2	8086	AAAS	NF	NF	High	NF	NF	NF	NF	High	NF	NF	NF	NF
P11172	4.654	6	2	7372	UMPS	NF	NF	NF	High	NF	NF	NF	High	NF	NF	NF	NF
P52789	4.653	2	1	3099	HK2	NF	NF	NF	NF	NF	NF	NF	High	NF	NF	NF	NF
Q9NVH0	4.647	2	1	55218	EXD2	NF	High	High	NF	NF	NF	NF	NF	NF	NF	NF	NF
P61158	4.635	3	1	10096	ACTR3	NF	High	High	High	NF	High	NF	High	High	NF	NF	NF
P19623	4.632	7	2	6723	SRM	NF	High	High	NF	NF	High	NF	High	NF	NF	NF	NF
Q9UBQ0-2	4.627	5	1	51699	VPS29	NF	High	High	High	NF	NF	NF	NF	NF	NF	NF	NF
Q16643-3	4.619	2	1	1627	DBN1	NF	NF	NF	High	NF	NF	NF	NF	NF	NF	NF	NF
P62745	4.606	12	1	388	RHOB	NF	NF	NF	NF	NF	NF	NF	NF	High	NF	NF	NF
Q15269	4.602	2	1	5822; 102724159	PWP2; LOC102724159	NF	High	NF	NF	NF	NF	NF	NF	NF	NF	NF	NF
Q93009	4.598	2	2	7874	USP7	NF	NF	High	NF	NF	High	NF	High	NF	NF	NF	NF
P50570-1	4.591	3	3	1785	DNM2	NF	NF	High	High	NF	High	NF	High	NF	NF	NF	NF
O95168-1	4.586	17	2	4710	NDUFB4	NF	High	High	High	NF	NF	NF	NF	NF	NF	NF	NF
Q09161	4.586	1	1	4686	NCBP1	NF	NF	NF	High	NF	High	NF	NF	NF	NF	NF	NF
Q13098-6	4.577	3	2	2873	GPS1	NF	High	High	High	NF	NF	NF	High	NF	NF	NF	NF
O75122-3	4.571	1	2	23122	CLASP2	NF	NF	NF	High	NF	NF	NF	High	NF	NF	NF	NF
P19525	4.558	2	1	5610	EIF2AK2	NF	NF	NF	NF	NF	High	NF	NF	NF	NF	NF	NF
O14880	4.537	10	1	4259	MGST3	NF	NF	High	NF	NF	High	NF	NF	NF	NF	NF	NF
Q14789-2	4.534	1	2	2804	GOLGB1	NF	High	NF	NF	NF	NF	NF	NF	NF	NF	NF	NF
Q96RQ3	4.532	3	2	56922	MCCC1	NF	High	NF	NF	NF	NF	NF	High	NF	NF	NF	NF
Q9NZM5	4.529	3	1	29997	GLTSCR2;	NF	NF	NF	NF	NF	High	NF	NF	NF	NF	NF	NF

					NOP53												
P30042-1	4.516	4	1	8209; 102724023	C21orf33; LOC102724023	NF	NF	High	NF	NF	NF	NF	High	NF	NF	NF	NF
P82930	4.512	10	3	65993	MRPS34	NF	High	High	High	NF	High	NF	NF	NF	NF	NF	NF
Q9H490	4.507	4	1	128869	PIGU	NF	NF	High	NF	NF	NF	NF	NF	NF	NF	NF	NF
Q9NRL2	4.506	1	1	11177	BAZ1A	NF	NF	NF	NF	NF	High	NF	NF	NF	NF	NF	NF
P49069	4.501	7	1	819	CAMLG	NF	NF	High	NF	NF	NF	NF	NF	NF	NF	NF	NF
Q13610	4.472	4	2	11137	PWP1	NF	NF	NF	NF	NF	High	NF	NF	NF	NF	NF	NF
Q9BQ86-1	4.467	8	1	79001	VKORC1	NF	NF	NF	NF	NF	NF	NF	High	NF	NF	NF	NF
Q15050	4.463	3	1	23212	RRS1	NF	High	High	NF	NF	High	NF	High	NF	NF	NF	NF
Q9HD45	4.46	4	2	56889	TM9SF3	NF	NF	High	NF	NF	High	NF	NF	NF	NF	NF	NF
P62891	4.456	20	1	6170; 285785	RPL39; RPL39P3	NF	High	High	High	NF	High	NF	High	NF	NF	NF	NF
Q14C86-6	4.451	1	1	26130	GAPVD1	NF	NF	NF	NF	NF	NF	NF	High	NF	NF	NF	NF
Q8NFF5	4.418	4	1	80308	FLAD1	NF	High	NF	NF	NF	NF	NF	NF	NF	NF	NF	NF
O15260-1	4.401	5	1	6836	SURF4	NF	NF	NF	High	NF	High	NF	NF	NF	NF	NF	NF
Q04323-2	4.391	4	1	51035	UBXN1	NF	NF	NF	NF	NF	NF	NF	High	NF	NF	NF	NF
P46379-3	4.389	1	1	7917	BAG6	NF	NF	High	NF	NF	NF	NF	NF	NF	NF	NF	NF
P13473-3	4.373	4	2	3920	LAMP2	NF	NF	High	NF	NF	NF	NF	NF	NF	NF	NF	NF
P04004	4.355	3	1	7448	VTN	High	NF	NF	NF	High	NF	NF	NF	NF	High	NF	NF
Q9NTJ3-1	4.351	2	2	10051	SMC4	NF	NF	NF	High	NF	NF	NF	High	NF	NF	NF	NF
Q9H3G5	4.349	6	2	54504	CPVL	NF	NF	High	NF	NF	NF	NF	High	NF	NF	NF	NF
Q13642	4.348	4	1	2273	FHL1	NF	High	High	NF	NF	High	NF	High	NF	NF	NF	NF
Q5SSJ5-1	4.348	4	2	50809	HP1BP3	NF	NF	High	NF	NF	High	NF	NF	NF	NF	NF	NF
Q15645	4.335	3	1	9319	TRIP13	NF	NF	NF	NF	NF	NF	NF	High	NF	NF	NF	NF
P47755	4.311	6	1	830	CAPZA2	NF	High	NF	NF	NF	NF	NF	NF	NF	NF	NF	NF
Q9Y512	4.309	4	2	25813	SAMM50	NF	NF	NF	High	NF	NF	NF	NF	NF	NF	NF	NF
Q13601	4.27	4	1	11103	KRR1	NF	NF	NF	NF	NF	High	NF	NF	NF	NF	NF	NF
Q8N9T8	4.265	4	2	65095	KRI1	NF	NF	High	NF	NF	High	NF	NF	NF	NF	NF	NF
Q96ME7	4.235	2	1	84450	ZNF512	NF	NF	NF	NF	NF	High	NF	NF	NF	NF	NF	NF

P04632	4.221	6	1	826	CAPNS1	NF	NF	High	NF	NF	NF	NF	NF	NF	NF	NF	NF
Q8TCT9-2	4.213	3	1	81502	HM13	NF	NF	High	NF	NF	High	NF	NF	NF	NF	NF	NF
Q9NQZ2	4.212	3	1	57050	UTP3	NF	NF	NF	NF	NF	High	NF	NF	NF	NF	NF	NF
P30520	4.208	2	1	159	ADSS	NF	NF	NF	NF	NF	High	NF	High	NF	NF	NF	NF
Q9NYV4-1	4.207	1	1	51755	CDK12	NF	NF	NF	NF	NF	NF	NF	High	NF	NF	NF	NF
P55809	4.206	2	1	5019	OXCT1	NF	NF	NF	NF	NF	NF	NF	High	NF	NF	NF	NF
Q13523	4.189	2	2	8899	PRPF4B	NF	NF	High	NF	NF	High	NF	NF	NF	NF	NF	NF
Q9BTW9-4	4.185	1	1	6904	TBCD	NF	NF	NF	NF	NF	NF	NF	High	NF	NF	NF	NF
Q95604	4.182	4	1	3107	HLA-C	NF	NF	High	NF	NF	NF	NF	NF	NF	NF	NF	NF
P61163	4.18	7	2	10121	ACTR1A	NF	NF	High	NF	NF	High	NF	High	NF	NF	NF	NF
P24468	4.178	4	2	7026	NR2F2	NF	High	High	NF	NF	NF	NF	High	NF	NF	NF	NF
O00767	4.174	4	1	6319	SCD	NF	NF	High	NF	NF	High	NF	NF	NF	NF	NF	NF
O60884	4.156	4	2	10294	DNAJA2	NF	NF	High	NF	NF	NF	NF	High	NF	NF	NF	NF
Q92797-1	4.152	1	1	8189	SYMPK	NF	NF	High	NF	NF	NF	NF	NF	NF	NF	NF	NF
O14981	4.15	1	1	9044	BTAF1	NF	NF	NF	NF	NF	NF	NF	High	NF	NF	NF	NF
Q9UPN3	4.139	0	1	23499	MACF1	NF	NF	NF	NF	NF	NF	NF	High	NF	NF	NF	NF
Q13428-4	4.139	1	2	6949	TCOF1	NF	High	High	NF	NF	High	NF	High	NF	NF	NF	NF
Q96EY1-1	4.135	3	1	9093	DNAJA3	NF	NF	High	NF	NF	High	NF	NF	NF	NF	NF	NF
P21399	4.135	2	1	48	ACO1	NF	NF	NF	NF	NF	NF	NF	High	NF	NF	NF	NF
Q9BVC6	4.131	5	1	79073	TMEM109	NF	NF	High	NF	NF	NF	NF	NF	NF	NF	NF	NF
O75150	4.094	2	1	9810	RNF40	NF	High	High	High	NF	High	NF	High	NF	NF	NF	NF
Q5JVF3-4	4.088	4	1	55795	PCID2	NF	NF	High	NF	NF	High	NF	NF	NF	NF	NF	NF
Q9UNM6-2	4.063	5	2	5719	PSMD13	NF	High	High	NF	NF	High	NF	High	NF	NF	NF	NF
Q9NW13-1	4.038	3	2	55131	RBM28	NF	NF	NF	NF	NF	High	NF	High	NF	NF	NF	NF
P49821	4.036	4	2	4723	NDUFV1	NF	NF	High	NF	NF	NF	NF	High	NF	NF	NF	NF
Q5SW79-1	4.031	1	1	9859	CEP170	NF	High	NF	High	NF	NF	NF	NF	NF	NF	NF	NF
Q86V81	4.024	4	1	10189	ALYREF	NF	High	NF	NF	NF	NF	NF	NF	NF	NF	NF	NF
P54105	3.976	5	1	1207	CLNS1A	NF	NF	High	NF	NF	NF	NF	NF	NF	NF	NF	NF
O60701	3.976	4	2	7358	UGDH	NF	NF	High	NF	NF	NF	NF	High	NF	NF	NF	NF

Q9H2U2-2	3.973	5	1	27068	PPA2	NF	High	High	NF	NF	NF	NF	High	NF	NF	NF	NF
Q02241-1	3.971	2	1	9493	KIF23	NF	NF	NF	NF	NF	High	NF	NF	NF	NF	NF	NF
P60981-1	3.969	7	1	11034	DSTN	NF	NF	NF	NF	NF	NF	NF	High	NF	NF	NF	NF
P15121	3.963	6	2	231	AKR1B1	NF	High	High	NF	NF	NF	NF	High	NF	NF	NF	NF
Q9BYD2	3.961	9	2	65005	MRPL9	NF	NF	High	High	NF	High	NF	High	NF	NF	NF	NF
Q3SY69-1	3.958	3	1	160428	ALDH1L2	NF	NF	NF	NF	NF	NF	NF	High	NF	NF	NF	NF
P30044-1	3.957	7	1	25824	PRDX5	NF	NF	High	NF	NF	NF	NF	NF	NF	NF	NF	NF
Q08257	3.944	4	1	1429	CRYZ	NF	NF	High	NF	NF	NF	NF	NF	NF	NF	NF	NF
Q9Y3Z3	3.934	3	2	25939	SAMHD1	NF	High	NF	NF	NF	High	NF	High	NF	NF	NF	NF
Q8WWK9-1	3.924	2	1	26586	CKAP2	NF	NF	NF	NF	NF	High	NF	NF	NF	NF	NF	NF
Q8N3C0	3.919	1	1	10973	ASCC3	NF	NF	NF	High	NF	High	NF	NF	NF	NF	NF	NF
P99999	3.915	10	1	54205	CYCS	NF	NF	High	NF	NF	NF	NF	NF	NF	NF	NF	NF
Q9UNF1	3.913	3	2	10916	MAGED2	NF	NF	NF	NF	NF	High	NF	High	NF	NF	NF	NF
P57740	3.911	2	2	57122	NUP107	NF	NF	High	NF	NF	High	NF	NF	NF	NF	NF	NF
P59998-3	3.902	10	2	10093	ARPC4	NF	NF	High	NF	NF	High	NF	High	NF	NF	NF	NF
Q92542-1	3.889	3	2	23385	NCSTN	NF	NF	High	NF	NF	NF	NF	NF	NF	NF	NF	NF
Q9Y3Y2-3	3.881	5	1	26097	CHTOP	NF	High	High	NF	NF	NF	NF	NF	NF	NF	NF	NF
Q9BTE3-1	3.88	3	2	79892	MCMBP	NF	High	High	NF	NF	NF	NF	High	NF	NF	NF	NF
O15027-5	3.858	0	1	9919	SEC16A	NF	NF	NF	NF	NF	NF	NF	High	NF	NF	NF	NF
P14678-3	3.858	5	2	6628	SNRPB	NF	High	High	NF	High	High	NF	High	NF	NF	NF	NF
Q12923-4	3.835	1	2	5783	PTPN13	NF	NF	NF	High	NF	NF	NF	High	NF	NF	NF	NF
Q92538	3.833	1	1	8729	GBF1	NF	NF	NF	High	NF	NF	NF	High	NF	NF	NF	NF
Q9H5H4	3.825	2	1	79724	ZNF768	NF	NF	NF	NF	NF	NF	NF	High	NF	NF	NF	NF
P56545-2	3.818	1	1	1488	CTBP2	NF	NF	High	NF	NF	NF	NF	NF	NF	NF	NF	NF
P20930	3.806	0	1	2312	FLG	High	NF	High	NF	High	NF	NF	NF	High	High	NF	NF
O75489	3.774	12	2	4722	NDUFS3	NF	High	High	NF	NF	NF	NF	NF	NF	NF	NF	NF
P54578	3.768	3	1	9097	USP14	NF	NF	NF	NF	NF	High	NF	NF	NF	NF	NF	NF
Q13769	3.756	2	2	8563	THOC5	NF	NF	High	NF	NF	High	NF	NF	NF	NF	NF	NF
Q9P0L0-2	3.745	4	1	9218	VAPA	NF	NF	High	NF	NF	NF	NF	High	NF	NF	NF	NF

Q96SB4-3	3.742	1	1	6732	SRPK1	NF	NF	NF	NF	NF	High	NF	High	NF	NF	NF	NF
Q5JRX3-2	3.735	1	1	10531	PITRM1	NF	NF	High	NF	NF	NF	NF	NF	NF	NF	NF	NF
O43663-1	3.73	2	1	9055	PRC1	NF	NF	NF	High	NF	NF	NF	NF	NF	NF	NF	NF
P49720	3.722	9	1	5691	PSMB3	NF	High	NF	NF	NF	NF	NF	NF	NF	NF	NF	NF
O15226-2	3.708	3	2	55922	NKRF	NF	High	NF	NF	NF	NF	NF	NF	NF	NF	NF	NF
O15228	3.7	1	1	8443	GNPAT	NF	NF	NF	High	NF	NF	NF	NF	NF	NF	NF	NF
P33240	3.675	4	2	1478	CSTF2	NF	NF	High	NF	NF	NF	NF	NF	NF	NF	NF	NF
Q5T160	3.667	2	1	57038	RARS2	NF	High	High	NF	NF	NF	NF	NF	NF	NF	NF	NF
Q9BV38	3.658	3	1	57418	WDR18	NF	NF	High	NF	NF	NF	NF	High	NF	NF	NF	NF
Q13823	3.644	2	1	29889	GNL2	NF	NF	NF	NF	NF	High	NF	NF	NF	NF	NF	NF
O00139-4	3.62	1	1	3796	KIF2A	NF	High	High	NF	NF	NF	NF	High	NF	NF	NF	NF
Q9UBT2	3.618	4	2	10054	UBA2	NF	NF	High	NF	NF	NF	NF	High	NF	NF	NF	NF
P31350-2	3.604	2	1	6241	RRM2	NF	NF	NF	NF	NF	NF	NF	High	NF	NF	NF	NF
P49406	3.601	4	1	9801	MRPL19	NF	High	High	NF	NF	NF	NF	High	NF	NF	NF	NF
Q9Y570-4	3.6	5	1	51400	PPME1	NF	NF	NF	NF	NF	NF	NF	High	NF	NF	NF	NF
Q9BRL6-1	3.598	5	2	10929	SRSF8	High	NF	High	NF	High	High	NF	NF	NF	NF	NF	NF
Q9NVU0	3.574	1	1	55718; 101060521	POLR3E; LOC101060521	NF	High	NF	NF	NF	NF	NF	High	NF	NF	NF	NF
Q8ND56	3.561	2	1	26065	LSM14A	NF	High	High	NF	NF	NF	NF	High	NF	NF	NF	NF
P29372	3.543	5	1	4350	MPG	NF	High	NF	NF	NF	NF	NF	NF	NF	NF	NF	NF
P02462	3.54	1	1	1282	COL4A1	NF	NF	NF	NF	NF	NF	NF	NF	High	NF	NF	NF
P49207	3.528	13	2	6164	RPL34	High	High	High	High	NF	High	NF	High	High	NF	NF	NF
Q9Y676	3.525	4	1	28973	MRPS18B	NF	NF	High	NF	NF	NF	NF	NF	NF	NF	NF	NF
P16152	3.511	4	1	873; 54093	CBR1; SETD4	NF	High	High	NF	NF	NF	NF	NF	NF	NF	NF	NF
Q8IWS0-1	3.501	6	2	84295	PHF6	NF	NF	High	NF	NF	High	NF	NF	NF	NF	NF	NF
Q9H7B2	3.494	5	2	84154	RPF2	NF	NF	NF	NF	NF	High	NF	High	NF	NF	NF	NF
P22033	3.491	2	1	4594	MUT	NF	NF	High	NF	NF	NF	NF	NF	NF	NF	NF	NF
O75027-2	3.491	2	1	22	ABCB7	NF	NF	High	NF	NF	NF	NF	NF	NF	NF	NF	NF
P31942	3.491	6	1	3189	HNRNPH3	NF	NF	NF	NF	NF	NF	NF	High	NF	NF	NF	NF
Q8WVV9	3.478	3	1	92906	HNRNPPL;	NF	NF	High	NF	NF	NF	NF	High	NF	NF	NF	NF

					HNRPLL												
P33316-3	3.474	4	1	1854	DUT	NF	High	High	NF	NF	NF	NF	NF	NF	NF	NF	NF
A6NDG6	3.472	7	2	283871	PGP	NF	High	NF	NF	NF	NF	NF	High	NF	NF	NF	NF
Q00059	3.461	4	1	7019	TFAM	NF	NF	High	NF	NF	NF	NF	High	NF	NF	NF	NF
Q96G03	3.447	4	1	55276	PGM2	NF	NF	NF	NF	NF	NF	NF	High	NF	NF	NF	NF
Q9BW92	3.447	1	1	80222	TARS2	NF	NF	High	NF	NF	NF	NF	NF	NF	NF	NF	NF
Q5RKV6	3.445	6	1	118460	EXOSC6	NF	NF	High	NF	NF	NF	NF	High	NF	NF	NF	NF
Q9UKV3-1	3.438	2	2	22985	ACIN1	NF	NF	High	NF	NF	High	NF	NF	NF	NF	NF	NF
O43795	3.437	2	2	4430	MYO1B	NF	NF	NF	High	NF	NF	NF	NF	NF	NF	NF	NF
Q04727-3	3.399	1	1	7091	TLE4	NF	NF	NF	NF	NF	NF	NF	High	NF	NF	NF	NF
Q9BTX1	3.398	2	1	55706	NDC1; TMEM48	NF	NF	NF	NF	NF	NF	NF	High	NF	NF	NF	NF
Q13464	3.395	1	1	6093	ROCK1	NF	NF	High	NF	NF	NF	NF	High	NF	NF	NF	NF
P00387-3	3.372	3	1	1727	CYB5R3	NF	NF	High	NF	NF	NF	NF	High	NF	NF	NF	NF
Q9BY77	3.37	3	1	84271	POLDIP3	NF	NF	High	NF	NF	NF	NF	NF	NF	NF	NF	NF
P67775	3.362	4	1	5515	PPP2CA	NF	NF	High	NF	NF	NF	NF	NF	NF	NF	NF	NF
P49354	3.358	5	1	2339	FNTA	NF	NF	NF	NF	NF	NF	NF	High	NF	NF	NF	NF
P0C7P4	3.353	8	2	100128525	UQCRFS1P1	NF	High	High	NF	NF	High	NF	NF	NF	NF	NF	NF
Q5TDH0-3	3.345	2	1	84301	DDI2	NF	High	High	NF	NF	NF	NF	High	NF	NF	NF	NF
Q9BZX2-1	3.344	5	1	7371	UCK2	NF	NF	NF	NF	NF	NF	NF	High	NF	NF	NF	NF
P40616	3.338	6	1	400	ARL1	NF	NF	NF	NF	NF	High	NF	NF	NF	NF	NF	NF
P02746	3.335	6	1	713	C1QB	NF	NF	NF	High	NF	NF	NF	High	NF	NF	NF	NF
P62333	3.334	4	1	5706	PSMC6	NF	High	NF	NF	NF	NF	NF	NF	NF	NF	NF	NF
Q00577	3.333	3	1	5813	PURA	NF	High	High	High	NF	High	NF	High	NF	NF	NF	NF
P24534	3.33	6	1	1933	EEF1B2	NF	High	NF	NF	NF	NF	NF	NF	NF	NF	NF	NF
P35611-3	3.322	1	1	118	ADD1	NF	NF	High	NF	NF	NF	NF	NF	NF	NF	NF	NF
Q9NUQ2	3.314	3	1	55326	AGPAT5	NF	NF	NF	NF	NF	NF	NF	High	NF	NF	NF	NF
Q8TC12	3.306	4	1	51109	RDH11	NF	NF	NF	NF	NF	NF	NF	High	NF	NF	NF	NF
Q7Z434	3.304	3	1	57506	MAVS	NF	NF	High	NF	NF	NF	NF	NF	NF	NF	NF	NF
P53004	3.303	3	1	644	BLVRA	NF	NF	NF	High	NF	NF	NF	NF	NF	NF	NF	NF

Q9Y2A7-2	3.299	1	1	10787	NCKAP1	NF	NF	High	NF	NF	NF	NF	High	NF	NF	NF	NF
Q9NVI1-3	3.299	2	2	55215	FANCI	NF	NF	NF	High	NF	NF	NF	High	NF	NF	NF	NF
Q15126	3.288	6	1	10654	PMVK	NF	NF	NF	NF	NF	NF	NF	High	NF	NF	NF	NF
P09012	3.279	6	2	6626	SNRPA	High	High	High	NF	NF	High	NF	High	NF	NF	High	NF
P31944	3.278	4	1	23581	CASP14	NF	NF	NF	NF	High	NF	NF	NF	High	High	NF	NF
Q9BTE7	3.274	4	1	84259	DCUN1D5	NF	NF	NF	NF	NF	NF	NF	High	NF	NF	NF	NF
Q15291-1	3.265	2	1	5929	RBBP5	NF	NF	NF	NF	NF	NF	NF	High	NF	NF	NF	NF
O95602	3.245	1	1	25885	POLR1A	NF	NF	High	NF	NF	High	NF	NF	NF	NF	NF	NF
Q8WUA4-1	3.232	2	2	2976	GTF3C2	NF	NF	NF	NF	NF	High	NF	High	NF	NF	NF	NF
Q92734	3.231	3	1	10342	TFG	NF	High	NF	High	NF	High	NF	High	NF	NF	NF	NF
Q9Y450-1	3.213	3	2	10767	HBS1L	NF	NF	NF	NF	NF	High	NF	High	NF	NF	NF	NF
Q02040-1	3.209	2	1	8227	AKAP17A	NF	NF	High	NF	NF	High	NF	NF	NF	NF	NF	NF
Q9BTV4	3.208	3	1	79188	TMEM43	NF	NF	NF	NF	NF	NF	NF	High	NF	NF	NF	NF
Q99567	3.206	2	1	4927	NUP88	NF	High	High	NF	NF	NF	NF	NF	NF	NF	NF	NF
O15173-2	3.174	7	1	10424	PGRMC2	NF	NF	High	NF	NF	NF	NF	NF	NF	NF	NF	NF
P62304	3.173	12	1	6635	SNRPE	NF	NF	High	NF	NF	NF	NF	NF	NF	NF	NF	NF
Q5BKZ1	3.166	2	1	284695	ZNF326	NF	NF	High	NF	NF	NF	NF	NF	NF	NF	NF	NF
Q15907	3.146	5	1	9230	RAB11B	NF	High	High	NF	NF	NF	NF	High	NF	NF	NF	NF
Q99436	3.145	7	2	5695	PSMB7	NF	NF	High	NF	NF	NF	NF	High	NF	NF	NF	NF
Q9BT78	3.14	5	1	51138	COPS4	NF	NF	High	NF	NF	NF	NF	NF	NF	NF	NF	NF
Q16543	3.136	2	1	11140	CDC37	NF	High	High	NF	NF	High	NF	NF	NF	NF	NF	NF
P53701	3.129	4	1	3052	HCCS	NF	NF	NF	NF	NF	NF	NF	High	NF	NF	NF	NF
P62070-4	3.127	6	1	22800	RRAS2	NF	NF	High	NF	NF	NF	NF	NF	NF	NF	NF	NF
Q92947-1	3.114	3	1	2639	GCDH	NF	High	NF	NF	NF	NF	NF	NF	NF	NF	NF	NF
P37108	3.098	7	1	6727	SRP14	NF	NF	High	NF	NF	NF	NF	NF	NF	NF	NF	NF
O43670-4	3.092	3	1	7756	ZNF207	NF	NF	High	NF	NF	NF	NF	High	NF	NF	NF	NF
Q8WVX9	3.091	3	1	84188	FAR1	NF	NF	High	NF	NF	High	NF	NF	NF	NF	NF	NF
O96008	3.091	3	1	10452	TOMM40	NF	NF	NF	NF	NF	High	NF	NF	NF	NF	NF	NF
Q02413	3.086	1	1	1828	DSG1	High	NF	NF	High	High	NF	NF	NF	High	NF	NF	NF

P60468	3.081	10	1	10952	SEC61B	NF	High	NF	NF	NF	High	NF	NF	NF	NF	NF	NF
O95819-3	3.076	1	1	9448	MAP4K4	NF	NF	NF	NF	NF	NF	NF	High	NF	NF	NF	NF
P42696	3.074	2	1	23029	RBM34	NF	NF	NF	NF	NF	High	NF	NF	NF	NF	NF	NF
P49711-1	3.066	1	1	10664	CTCF	NF	NF	NF	NF	NF	High	NF	NF	NF	NF	NF	NF
P54920	3.059	3	1	8775	NAPA	NF	High	High	NF	NF	NF	NF	NF	NF	NF	NF	NF
Q9GZT3	3.053	9	1	81892	SLIRP	NF	High	High	High	NF	NF	NF	High	NF	NF	NF	NF
O95707	3.05	5	1	10775	POP4	NF	NF	NF	NF	NF	High	NF	NF	NF	NF	NF	NF
O15355	3.048	2	1	5496	PPM1G	NF	High	NF	NF	NF	High	NF	NF	NF	NF	NF	NF
O75608	3.023	5	1	10434	LYPLA1	NF	NF	NF	NF	NF	NF	NF	High	NF	NF	NF	NF
P30260-2	3.02	1	1	996	CDC27	NF	NF	NF	NF	NF	High	NF	NF	NF	NF	NF	NF
P30046	3.011	9	1	1652	DDT	NF	High	NF	NF	NF	NF	NF	NF	NF	NF	NF	NF
Q5HYI8	3	5	1	285282	RABL3	NF	NF	NF	NF	NF	NF	NF	High	NF	NF	NF	NF
O94973-2	2.991	2	1	161	AP2A2	NF	NF	NF	NF	NF	High	NF	NF	NF	NF	NF	NF
O43824	2.985	2	1	8225	GTPBP6	NF	High	High	NF	NF	NF	NF	High	NF	NF	NF	NF
Q9H9A6	2.976	3	2	55631	LRRC40	NF	NF	High	NF	NF	NF	NF	High	NF	NF	NF	NF
Q96AA3	2.973	3	2	91869	RFT1	NF	High	NF	NF	NF	NF	NF	NF	NF	NF	NF	NF
P19388	2.969	5	1	5434	POLR2E	NF	NF	NF	NF	NF	NF	NF	High	NF	NF	NF	NF
Q8IX18	2.949	2	1	79665	DHX40	NF	NF	High	NF	NF	NF	NF	NF	NF	NF	NF	NF
P62841	2.949	8	1	6209	RPS15	NF	NF	High	High	High	High	High	High	NF	NF	High	NF
Q96P63-2	2.941	4	2	89777	SERPINB12	NF	NF	NF	NF	NF	NF	NF	NF	High	NF	NF	NF
Q96TA2-1	2.94	1	1	10730	YME1L1	NF	NF	High	NF	NF	NF	NF	NF	NF	NF	NF	NF
Q13325	2.93	2	1	24138	IFIT5	NF	NF	NF	NF	NF	High	NF	NF	NF	NF	NF	NF
Q6DKI1	2.926	4	1	285855	RPL7L1	NF	NF	High	NF	NF	High	NF	High	NF	NF	NF	NF
Q9BPW8	2.901	3	1	8508	NIPSNAP1	NF	High	NF	NF	NF	NF	NF	NF	NF	NF	NF	NF
Q5T280	2.893	2	1	51490	C9orf114; SPOUT1	NF	NF	NF	NF	NF	High	NF	NF	NF	NF	NF	NF
Q9UHG3	2.887	2	1	51449	PCYOX1	NF	High	NF	NF	NF	NF	NF	High	NF	NF	NF	NF
Q7KZI7-1	2.882	1	1	2011	MARK2	NF	NF	NF	NF	NF	NF	NF	High	NF	NF	NF	NF
Q92979	2.851	8	1	10436	EMG1	NF	NF	High	NF	NF	NF	NF	NF	NF	NF	NF	NF
Q9HCS7	2.847	2	2	56949	XAB2	NF	NF	High	NF	NF	High	NF	NF	NF	NF	NF	NF

P45954	2.831	2	1	36	ACADSB	NF	NF	NF	NF	NF	NF	NF	High	NF	NF	NF	NF
Q9UBQ7	2.829	3	1	9380	GRHPR	NF	High	High	NF	NF	NF	NF	NF	NF	NF	NF	NF
Q9P2X0-2	2.801	8	1	54344	DPM3	NF	NF	NF	NF	NF	NF	NF	High	NF	NF	NF	NF
Q9Y679-1	2.789	3	1	550	AUP1	NF	NF	NF	NF	NF	NF	NF	High	NF	NF	NF	NF
Q969X5	2.789	3	1	57222	ERGIC1	NF	NF	NF	NF	NF	NF	NF	High	NF	NF	NF	NF
P63167	2.783	12	1	8655	DYNLL1	NF	NF	NF	NF	NF	NF	NF	High	NF	NF	NF	NF
P68431	2.774	10	2	8968; 8352; 8351; 8355; 8357; 8358; 8350; 8353; 8354; 8356	HIST1H3F; HIST1H3C; HIST1H3D; HIST1H3G; HIST1H3H; HIST1H3B; HIST1H3A; HIST1H3E; HIST1H3I; HIST1H3J	High	High	High	High	NF	NF	NF	High	High	NF	NF	NF
Q9UL46	2.766	9	1	5721	PSME2	NF	NF	NF	NF	NF	NF	NF	High	NF	NF	NF	NF
Q8TCS8	2.758	2	2	87178	PNPT1	NF	NF	High	NF	NF	NF	NF	High	NF	NF	NF	NF
Q96A65	2.74	2	2	60412	EXOC4	NF	NF	NF	NF	NF	High	NF	High	NF	NF	NF	NF
P61086	2.735	14	1	3093	UBE2K	NF	NF	NF	NF	NF	NF	NF	High	NF	NF	NF	NF
Q6P1X5	2.716	2	2	6873	TAF2	NF	NF	High	NF	NF	NF	NF	NF	NF	NF	NF	NF
P09496-1	2.695	4	1	1211	CLTA	NF	High	NF	NF	NF	NF	NF	High	NF	NF	NF	NF
P48556	2.693	5	2	5714	PSMD8	NF	High	NF	NF	NF	NF	NF	High	NF	NF	NF	NF
P23588	2.691	4	2	1975	EIF4B	NF	NF	NF	NF	NF	NF	NF	High	NF	NF	NF	NF
P00491	2.69	3	1	4860	PNP	NF	NF	High	NF	NF	NF	NF	NF	NF	NF	NF	NF
Q969Z0-1	2.689	3	1	9238	TBRG4	NF	NF	High	NF	NF	NF	NF	NF	NF	NF	NF	NF
Q8NBM4-1	2.687	3	1	337867	UBAC2	NF	NF	NF	High	NF	NF	NF	NF	NF	NF	NF	NF
P28340	2.681	2	2	5424	POLD1	NF	NF	High	NF	NF	NF	NF	High	NF	NF	NF	NF
P30419	2.678	3	1	4836	NMT1	NF	NF	High	NF	NF	NF	NF	NF	NF	NF	NF	NF
P61009	2.674	5	1	60559	SPCS3	NF	High	High	High	NF	High	NF	High	NF	NF	NF	NF
Q12894-2	2.665	3	1	7866	IFRD2	NF	NF	High	NF	NF	High	NF	NF	NF	NF	NF	NF

[illegible]

Q9H9Y6-3	2.474	1	1	84172	POLR1B	NF	NF	NF	NF	NF	High	NF	NF	NF	NF	NF	NF
Q92620	2.471	1	1	9785	DHX38	NF	NF	NF	NF	NF	High	NF	High	NF	NF	NF	NF
Q9H1A4	2.454	1	1	64682	ANAPC1	NF	NF	NF	NF	NF	High	NF	NF	NF	NF	NF	NF
O75165	2.449	1	1	23317	DNAJC13	NF	NF	NF	High	NF	High	NF	NF	NF	NF	NF	NF
O75348	2.441	12	1	9550	ATP6V1G1	NF	NF	NF	NF	NF	NF	NF	High	NF	NF	NF	NF
O15145	2.441	7	1	10094	ARPC3	NF	NF	High	NF	NF	NF	NF	NF	NF	NF	NF	NF
Q92615	2.435	1	1	23185	LARP4B	NF	NF	NF	NF	NF	NF	NF	High	NF	NF	NF	NF
Q92506	2.435	6	1	7923	HSD17B8	NF	NF	High	NF	NF	NF	NF	NF	NF	NF	NF	NF
O96011-1	2.431	4	1	8799	LOC101060567; PEX11B	NF	NF	NF	NF	NF	High	NF	NF	NF	NF	NF	NF
Q9NVU7	2.416	1	1	55153	SDAD1	NF	High	High	NF	NF	High	NF	High	NF	NF	NF	NF
O94832	2.414	2	2	4642	MYO1D	NF	NF	NF	High	NF	NF	NF	NF	NF	NF	NF	NF
O15143	2.412	3	1	10095	ARPC1B	NF	NF	High	NF	NF	NF	NF	NF	NF	NF	NF	NF
Q9Y4A5	2.404	0	1	8295	TRRAP	NF	NF	High	NF	NF	NF	NF	NF	NF	NF	NF	NF
Q8IZ81	2.399	3	1	255520	ELMOD2	NF	NF	NF	High	NF	NF	NF	NF	NF	NF	NF	NF
P0CG43	2.395	7	1	100996541	FAM157C; LOC100132055; LOC100996541	High	NF	NF	NF	NF	NF	NF	NF	NF	NF	NF	NF
P37198	2.381	2	1	23636	NUP62	NF	NF	High	NF	NF	NF	NF	NF	NF	NF	NF	NF
P36957	2.38	3	1	1743	DLST	NF	High	High	NF	NF	NF	NF	High	NF	NF	NF	NF
P52434-4	2.376	7	1	5437	POLR2H	NF	NF	High	NF	NF	NF	NF	NF	NF	NF	NF	NF
O60831	2.371	6	1	11230	PRAF2	NF	High	High	High	NF	NF	NF	High	NF	NF	NF	NF
P43003	2.354	2	1	6507	SLC1A3	NF	High	NF	NF	NF	High	NF	NF	NF	NF	NF	NF
Q9UKZ9	2.347	3	1	26577	PCOLCE2	High	NF	NF	NF	NF	NF	NF	NF	NF	NF	NF	NF
Q9H4L4	2.338	2	1	26168	SENP3	NF	High	High	NF	NF	High	NF	NF	NF	NF	NF	NF
Q13085-4	2.335	1	1	31	ACACA	NF	NF	NF	NF	NF	NF	NF	High	NF	NF	NF	NF
O96019-1	2.331	2	1	86	ACTL6A	NF	NF	NF	NF	NF	High	NF	NF	NF	NF	NF	NF
Q9Y6C9	2.325	4	1	23788	MTCH2	NF	High	NF	NF	NF	High	NF	NF	NF	NF	NF	NF
Q70UQ0-4	2.32	2	1	121457	IKBIP	NF	NF	High	NF	NF	NF	NF	NF	NF	NF	NF	NF
Q9Y6A5	2.315	2	1	10460	TACC3	NF	NF	NF	NF	NF	NF	NF	High	NF	NF	NF	NF

Q8IXI1	2.315	2	1	89941	RHOT2	NF	NF	High	NF	NF	High	NF	NF	NF	NF	NF	NF
P98175-1	2.312	1	1	8241	RBM10	NF	NF	NF	NF	NF	High	NF	High	NF	NF	NF	NF
Q9UQE7	2.311	1	1	9126	SMC3	NF	NF	NF	NF	NF	NF	NF	High	NF	NF	NF	NF
P11498	2.31	1	1	5091	PC	NF	High	High	NF	NF	NF	NF	NF	NF	NF	NF	NF
Q5T750	2.292	3	1	100129271	C1orf68	NF	NF	NF	NF	NF	NF	NF	NF	High	NF	NF	NF
Q9C0J8	2.29	1	1	55339	WDR33	NF	NF	High	NF	NF	NF	NF	NF	NF	NF	NF	NF
Q92572	2.28	6	1	1176	AP3S1	NF	High	NF	NF	NF	High	NF	NF	NF	NF	NF	NF
P12955	2.267	2	1	5184	PEPD	NF	NF	High	NF	NF	NF	NF	NF	NF	NF	NF	NF
O43709-3	2.259	4	1	114049	WBSCR22; BUD23	NF	NF	NF	High	NF	NF	NF	High	NF	NF	NF	NF
Q6WCQ1-2	2.259	1	1	23164	MPRIP	NF	NF	NF	High	NF	NF	NF	NF	NF	NF	NF	NF
Q14232	2.255	3	1	1967	EIF2B1	NF	High	High	NF	NF	High	NF	High	NF	NF	NF	NF
Q15154-1	2.253	1	1	5108	PCM1	NF	NF	High	NF	NF	NF	NF	NF	NF	NF	NF	NF
Q13907-2	2.247	3	1	3422	IDI1	NF	NF	High	NF	NF	NF	NF	NF	NF	NF	NF	NF
Q99700-1	2.245	1	1	6311	ATXN2	NF	High	NF	NF	NF	NF	NF	NF	NF	NF	NF	NF
Q3MHD2-2	2.244	7	1	124801	LSM12	NF	NF	High	NF	NF	NF	NF	NF	NF	NF	NF	NF
Q9Y5L0-2	2.225	2	1	23534	TNPO3	NF	NF	NF	NF	NF	High	NF	NF	NF	NF	NF	NF
Q14247-2	2.223	2	1	2017	CTTN	NF	NF	NF	NF	NF	NF	NF	High	NF	NF	NF	NF
Q14671-3	2.191	1	1	9698	PUM1	NF	NF	NF	High	NF	NF	NF	NF	NF	NF	NF	NF
Q13561-2	2.187	2	1	10540	DCTN2	NF	NF	NF	NF	NF	NF	NF	High	NF	NF	NF	NF
Q9UPW6	2.162	1	1	23314	SATB2	NF	NF	NF	High	NF	NF	NF	NF	NF	NF	NF	NF
Q9BRP1	2.161	3	1	84306	PDCD2L	NF	NF	NF	NF	NF	NF	NF	High	NF	NF	NF	NF
Q8TB61	2.161	3	1	347734	SLC35B2	NF	NF	High	NF	NF	NF	NF	High	NF	NF	NF	NF
O75616-1	2.158	3	1	26284	ERAL1	NF	NF	High	NF	NF	NF	NF	High	NF	NF	NF	NF
P21266	2.157	4	1	2947	GSTM3	NF	High	NF	NF	NF	NF	NF	High	NF	NF	NF	NF
Q9NQI8	2.153	1	1	23303	KIF13B	NF	NF	NF	NF	NF	High	NF	NF	NF	NF	NF	NF
O95071	2.139	0	1	51366	UBR5	NF	NF	High	NF	NF	NF	NF	NF	NF	NF	NF	NF
O43657	2.128	3	1	7105	TSPAN6	NF	NF	High	NF	NF	NF	NF	High	NF	NF	NF	NF
Q9P2R3-4	2.124	1	1	51479	ANKFY1	NF	NF	High	NF	NF	NF	NF	NF	NF	NF	NF	NF
Q8IUF8	2.119	3	1	84864	MINA; RIOX2	NF	NF	NF	NF	NF	High	NF	NF	NF	NF	NF	NF

Q13423	2.118	1	1	23530	NNT	NF	NF	NF	NF	NF	NF	NF	High	NF	NF	NF	NF
Q00796	2.115	3	1	6652	SORD	NF	High	NF	High	NF	NF	NF	High	NF	NF	NF	NF
P55081	2.108	2	1	4236	MFAP1	NF	NF	NF	NF	NF	NF	NF	High	NF	NF	NF	NF
Q9UNS2	2.108	3	1	8533	COPS3	NF	NF	NF	NF	NF	NF	NF	High	NF	NF	NF	NF
Q92820	2.104	3	1	8836	GGH	NF	NF	NF	NF	NF	NF	NF	High	NF	NF	NF	NF
P30086	2.098	4	1	5037	PEBP1	NF	High	High	NF	NF	NF	NF	High	NF	NF	NF	NF
Q9HC38	2.096	3	1	51031	GLOD4	NF	NF	High	NF	NF	NF	NF	NF	NF	NF	NF	NF
P53677	2.094	2	1	10947	AP3M2	NF	NF	NF	NF	NF	High	NF	NF	NF	NF	NF	NF
P39687	2.091	4	1	8125	ANP32A	NF	NF	NF	NF	NF	NF	NF	High	NF	NF	NF	NF
O15160	2.085	3	1	9533	POLR1C	NF	High	NF	NF	NF	NF	NF	NF	NF	NF	NF	NF
Q96RP9-2	2.077	1	1	85476	GFM1	NF	High	High	NF	NF	High	NF	NF	NF	NF	NF	NF
Q8NBJ5	2.07	1	1	79709	COLGALT1; GLT25D1	NF	NF	High	NF	NF	NF	NF	NF	NF	NF	NF	NF
P52732	2.065	1	1	3832	KIF11	NF	NF	NF	NF	NF	NF	NF	High	NF	NF	NF	NF
P0DOX8	2.06	7	1			NF	NF	NF	NF	NF	NF	NF	NF	High	NF	NF	NF
Q16637	2.055	4	1	6606; 6607	SMN1; SMN2	NF	NF	NF	NF	NF	High	NF	NF	NF	NF	NF	NF
Q8TAF3-1	2.053	2	1	57599	WDR48	NF	NF	High	NF	NF	NF	NF	NF	NF	NF	NF	NF
Q9H269	2.039	1	1	64601	VPS16	NF	NF	NF	NF	NF	High	NF	NF	NF	NF	NF	NF
Q96I25	2.038	2	1	84991	RBM17	NF	NF	High	NF	NF	NF	NF	NF	NF	NF	NF	NF
Q14728	2.03	3	1	10227	MFSD10	NF	High	High	NF	NF	NF	NF	NF	NF	NF	NF	NF
Q9Y5K5-1	2.012	2	1	51377	UCHL5	NF	NF	NF	NF	NF	NF	NF	High	NF	NF	NF	NF
Q9NTJ5	2.002	2	1	22908	SACM1L	NF	NF	NF	NF	NF	High	NF	High	NF	NF	NF	NF
Q92504	2	3	1	7922	SLC39A7	NF	NF	High	NF	NF	NF	NF	NF	NF	NF	NF	NF
Q8N1F8	1.983	1	1	114790	STK11IP	NF	NF	High	NF	NF	NF	NF	NF	NF	NF	NF	NF
O95793	1.982	2	1	6780	STAU1	NF	NF	NF	NF	NF	High	NF	NF	NF	NF	NF	NF
O14561	1.978	6	1	4706	NDUFAB1	NF	NF	High	NF	NF	NF	NF	NF	NF	NF	NF	NF
P35916	1.978	1	1	2324	FLT4	NF	NF	NF	NF	NF	NF	NF	High	NF	NF	NF	NF
Q13123	1.976	2	1	3550	IK	NF	NF	High	NF	NF	NF	NF	NF	NF	NF	NF	NF
Q9UI26-2	1.959	1	1	51194	IPO11	NF	NF	NF	NF	NF	NF	NF	High	NF	NF	NF	NF
Q96KP1	1.939	1	1	55770	EXOC2	NF	NF	NF	NF	NF	High	NF	NF	NF	NF	NF	NF

O75947-1	1.937	6	1	10476	ATP5H	NF	NF	High	NF	NF	NF	NF	NF	NF	NF	NF	NF
O00471	1.934	2	1	10640	EXOC5	NF	NF	High	NF	NF	NF	NF	NF	NF	NF	NF	NF
Q9UDR5	1.93	2	1	10157	AASS	NF	NF	NF	NF	NF	High	NF	NF	NF	NF	NF	NF
P07942	1.924	0	1	3912	LAMB1	NF	NF	NF	NF	NF	NF	NF	NF	High	NF	NF	NF
Q9UHQ9	1.915	4	1	51706	CYB5R1	NF	NF	High	NF	NF	NF	NF	NF	NF	NF	NF	NF
Q8N8S7	1.902	2	1	55740	ENAH	NF	NF	High	NF	NF	NF	NF	NF	NF	NF	NF	NF
Q05086	1.897	1	1	7337	UBE3A	NF	NF	NF	NF	NF	High	NF	NF	NF	NF	NF	NF
P78346-2	1.891	3	1	10556	RPP30	NF	NF	NF	NF	NF	High	NF	NF	NF	NF	NF	NF
P82675	1.88	4	1	64969	MRPS5	NF	NF	High	NF	NF	NF	NF	NF	NF	NF	NF	NF
Q96B26	1.872	4	1	11340	EXOSC8	NF	High	NF	NF	NF	NF	NF	NF	NF	NF	NF	NF
O75914-3	1.865	2	1	5063	PAK3	NF	NF	NF	NF	NF	NF	NF	High	NF	NF	NF	NF
Q14112-1	1.863	1	1	22795	NID2	NF	NF	NF	NF	NF	NF	NF	NF	High	NF	NF	NF
Q99961	1.862	3	1	6455	SH3GL1	NF	High	NF	NF	NF	NF	NF	NF	NF	NF	NF	NF
O95470	1.859	3	1	8879	SGPL1	NF	NF	NF	NF	NF	High	NF	NF	NF	NF	NF	NF
Q9Y6V7	1.831	2	1	54555	DDX49	NF	High	NF	NF	NF	High	NF	NF	NF	NF	NF	NF
Q9NSI2-1	1.827	6	1	85395	FAM207A	NF	NF	NF	NF	NF	High	NF	NF	NF	NF	NF	NF
Q9NVN8	1.815	2	1	54552	GNL3L	NF	High	NF	NF	NF	High	NF	NF	NF	NF	NF	NF
O60637	1.804	3	1	10099	TSPAN3	NF	High	High	NF	NF	NF	NF	NF	NF	NF	NF	NF
O95631	1.803	1	1	9423	NTN1	NF	NF	NF	NF	High	NF	NF	NF	NF	NF	NF	NF
P05089-2	1.796	3	1	383	ARG1	NF	NF	NF	NF	High	NF	NF	NF	NF	NF	NF	NF
P46939-2	1.786	0	1	7402	UTRN	NF	NF	NF	High	NF	NF	NF	NF	NF	NF	NF	NF
Q8N9C0-2	1.785	1	1	283284	IGSF22	High	High	NF	High	NF	NF	High	NF	NF	NF	NF	NF
Q01581	1.777	2	1	3157	HMGCS1	NF	NF	NF	NF	NF	NF	NF	High	NF	NF	NF	NF
Q9Y399	1.773	3	1	51116	MRPS2	NF	NF	High	NF	NF	NF	NF	NF	NF	NF	NF	NF
Q15436	1.768	2	1	10484	SEC23A	NF	NF	NF	NF	NF	NF	NF	High	NF	NF	NF	NF
P45974-1	1.765	1	1	8078	USP5	NF	NF	NF	NF	NF	NF	NF	High	NF	NF	NF	NF
Q8NI60-1	1.761	2	1	56997	ADCK3; COQ8A	NF	NF	High	NF	NF	High	NF	High	NF	NF	NF	NF
Q9H2G2-1	1.749	1	1	9748	SLK	NF	NF	NF	High	NF	NF	NF	NF	NF	NF	NF	NF
Q9Y394	1.747	2	1	51635	DHRS7	NF	NF	High	NF	NF	NF	NF	High	NF	NF	NF	NF

P21281	1.745	2	1	526	ATP6V1B2	NF	NF	NF	NF	NF	NF	NF	NF	NF	NF	High	NF
P42126	1.736	2	1	1632	ECI1	NF	NF	High	NF	NF	NF	NF	NF	NF	NF	NF	NF
Q06265-2	1.735	2	1	5393	EXOSC9	NF	High	NF	NF	NF	NF	NF	NF	NF	NF	NF	NF
Q2TAY7	1.735	2	1	55234	SMU1	NF	NF	High	NF	NF	High	NF	NF	NF	NF	NF	NF
Q8IV08	1.722	2	1	23646	PLD3	NF	NF	High	NF	NF	NF	NF	NF	NF	NF	NF	NF
Q9BYE4	1.721	12	1	6706	SPRR2G	NF	NF	NF	NF	High	NF	High	NF	NF	High	High	NF
Q9NVH1-1	1.716	2	1	55735	DNAJC11	NF	NF	NF	NF	NF	High	NF	NF	NF	NF	NF	NF
Q9HD20	1.707	1	1	57130	ATP13A1	NF	NF	High	NF	NF	NF	NF	High	NF	NF	NF	NF
P56381	1.703	16	1	514	ATP5E	NF	NF	High	NF	NF	NF	NF	NF	NF	NF	NF	NF
P35610	1.7	2	1	6646	SOAT1	NF	NF	High	NF	NF	NF	NF	NF	NF	NF	NF	NF
Q9UNX4	1.693	2	1	10885	WDR3	NF	NF	NF	NF	NF	High	NF	NF	NF	NF	NF	NF
Q96T58	1.691	0	1	23013	SPEN	NF	NF	NF	NF	NF	High	NF	NF	NF	NF	NF	NF
P61962	1.69	4	1	10238	DCAF7	NF	NF	NF	High	NF	NF	NF	High	NF	NF	NF	NF
Q8TAD8	1.687	2	1	79753	SNIP1	NF	NF	NF	High	NF	NF	NF	NF	NF	NF	NF	NF
P56270-2	1.687	2	1	4150	MAZ	NF	NF	High	NF	NF	NF	NF	NF	NF	NF	NF	NF
P61970	1.679	6	1	10204	NUTF2	NF	High	High	NF	NF	NF	NF	High	NF	NF	NF	NF
Q5JPH6-2	1.674	3	1	124454	EARS2	NF	NF	High	NF	NF	NF	NF	NF	NF	NF	NF	NF
Q9NRL3-3	1.671	1	1	29888	STRN4	NF	NF	High	NF	NF	NF	NF	NF	NF	NF	NF	NF
P61964	1.668	4	1	11091	WDR5	NF	NF	NF	NF	NF	NF	NF	High	NF	NF	NF	NF
Q86XI2-2	1.662	1	1	54892	NCAPG2	NF	NF	High	NF	NF	High	NF	High	NF	NF	NF	NF
Q9Y2R9	1.662	5	1	51081	MRPS7	NF	NF	High	NF	NF	NF	NF	NF	NF	NF	NF	NF
O60256-1	1.661	2	1	5636	PRPSAP2	NF	NF	NF	NF	NF	NF	NF	High	NF	NF	NF	NF
P02788	1.644	1	1	4057	LTF	High	NF	NF	NF	NF	NF	NF	NF	High	NF	NF	NF
Q9UKM9-1	1.644	3	1	22913	RALY	NF	NF	NF	NF	NF	NF	NF	High	NF	NF	NF	NF
Q9BTD8-1	1.635	2	1	79171	RBM42	NF	NF	NF	NF	NF	High	NF	NF	NF	NF	NF	NF
Q16698	1.633	4	1	1666	DECR1	NF	NF	High	NF	NF	NF	NF	High	NF	NF	NF	NF
P04040	1.631	2	1	847	CAT	NF	NF	NF	NF	NF	NF	NF	NF	NF	High	NF	NF
Q5JSL3	1.626	1	1	139818	DOCK11	NF	NF	NF	NF	NF	NF	NF	High	NF	NF	NF	NF
Q9BQ75	1.61	4	1	84319	CMSS1	NF	NF	NF	NF	NF	High	NF	NF	NF	NF	NF	NF

[illegible]

8.6. Flow cytometry results, Chapter 5

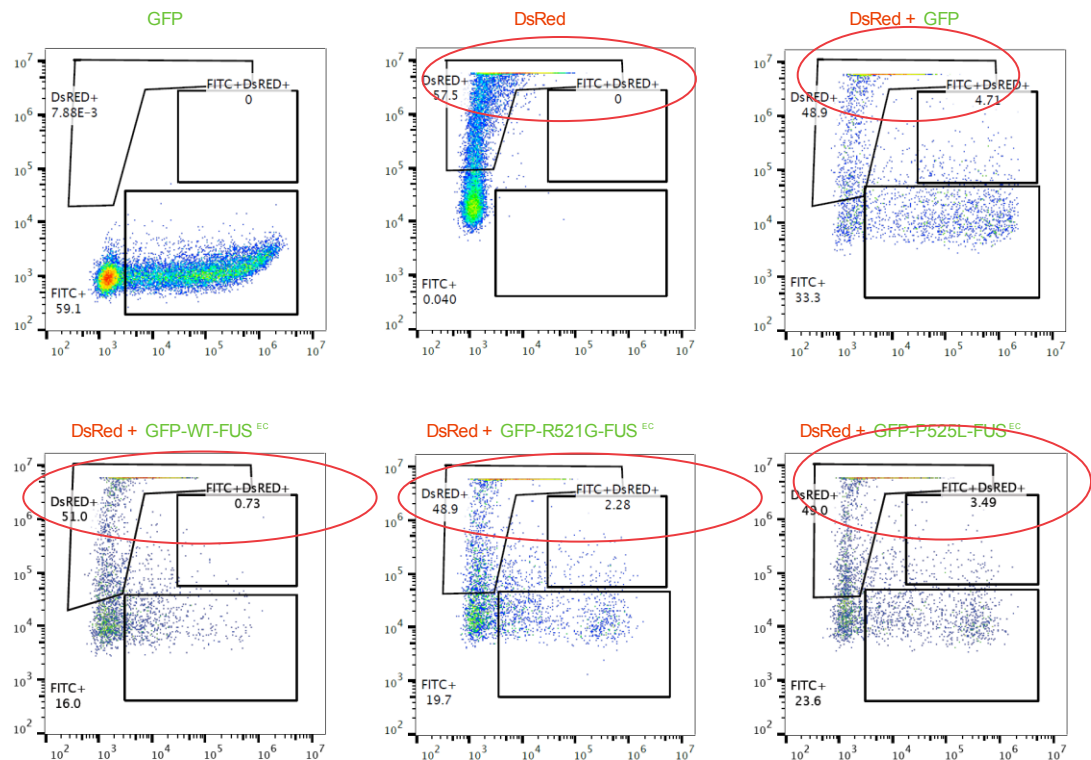


Fig. 1 Flow cytometry plots with the population outside the plot highlighted in red

8.7. Ethics

1. Ethics application for Human tissue samples

Appendix 8.7 of this thesis has been removed as it may contain sensitive/confidential content